HYDRAULIC TURBINES

Design, Erection and Operation

By

Hermod Brekke

Endringsdato: Juni 2001

CONTENTS

PREFACE.

This book is based on the authors experience working with development, research and production of hydraulic turbines and control systems at the turbine manufacturer KVAERNER from 1959 until he was appointed professor at the Norwegian University of Science and Technology in 1987.
During his time as professor from 1987 to 2003 he worked part time with research for KVAERNER, especially in development of turbine runners and control systems.

1. INTRODUCTION

1.1. Historical review of the development of hydraulic machinery for electricity production in Norway.

The geographical location, climate and topography of Norway are ideal for Hydro Power development. The basis is the Golfstream sweeping moist air from the west along our 2000 km long coast. This wind meets the mountainous country with peaks above 2000 m and a highland in the south west at 1000 - 1500 m. level. The result is an annual rainfall of 2000 mm with peaks up to 5000 mm in local places on the west side of the mountains. The south east and middle of our country have a rainfall of 750 - 800 mm. The rainfall accumulated as snow during the winter fills the lakes in the spring when the snow smelts. These lakes form natural reservoirs for numerous hydro power plants.
The river water is in general clean because the soft rock and gravel have been swept away by the glaciers 10 000 years ago. The hard ground rock consisting mainly of gneiss, felt spat and quartzite is very resistant to abrasion and only little soil and gravel are observed even in flood times of the rivers in the high land in the west. However, in reservoirs close to the glaciers, the reservoirs contain hard sediments which cause problems at low water level, since the last outgoing water is sand laden.

The first knowledge of hydro power development recorded in Norwegian history is a small water wheel driving a flour mill built by the Cistercienser monks in a small river where the capital Oslo is located today. It has been documented that this mill existed in 1160 - 1170 i.e. just after the Viking period.
Later man power to driven saw mills were substituted by water wheel driven saw mills. During the beginning of the 19th century a large number of paper mills were also built and driven by hydropower as a result of the invention of water turbines and electro-hydraulic power developement.

The first known hydroelectric power station in Norway was built at a farm in 1877 at Lisleby Brug in southern Norway producing approximately 200 Watt. Later in 1890 the worlds most northerly town, Hammerfest, at 70^{o} north in Northern Norway got electricity supply for street lightening driven by a hydro electric power plant. The street lightening was important because of 24 hours nights with darkness in winter time.

Up to the 20th century the electricity production for industry and private consumption in Norway increased to approximately 100 MW in total. The largest power plant in Oslo was Hammeren with an installed power of 1800 kW and Hafslund power plant south east of Oslo with 5200 kW. It is also of interest to know that 4 vertical Francis turbines in another plant built in 1905 were still in operation during the flood season as late as the year 2000. The power of each of the 4 turbines in this power station was 600 kW.
However, the first boom in developing hydro power came in 1907-1916 when the development of electrochemical and metallurgical industry started in Norway. The two Norwegians, Birkeland and Eyde started the nitrogen fertilizer production in 1908 by an electro chemical process producing 25000 tons of "Norges saltpeter" containing 13% N. These men then planned to produce 300000 tons per year and the demand for hydro electric power was estimated to be 360 MW. With a total installation of 200 MW in Norway at that time, this industrial demand was a great challenge.

To meet this challenge Vemork power plant was built and put into operation in 1910 and then Såheim power plant was built and put into operation in 1916.

In addition to the electrochemical industry the mechanical industry grew up to meet the demand for turbo machinery for hydropower production in general.

The Technical University of Norway* was built in 1910 and The Water power laboratory at this University was finished in 1917 starting its research work for the Norwegian industrial companies Kværner and Myren (Myren was later bought by Kværner). In the first period of the hydropower development the high head turbines for Vemork and Rjukan were imported. Later the Norwegian industry specialized on development of high head turbines to meet the demand for such turbines in Norway. The development of high head turbines in Norway may be illustrated by the following table: (* Name changed to "the Norwegian University of Science and Technology" January 1st. 1996)

	Name of plant	Net head m	Output MW	Speed RPM
1930	Nygaard	225	8.5	750
1940	Skjerka	325	17	600
1946	Nedre Vinstra	420	50	500
1957	Hemsil	510	36	750
1982	Kvilldal	520	315	333
1984	Oevre Otta	610	154	500
1985	Svartisen	543	350	333

In 1955 the total capacity of the Norwegian Hydro Electric power production was 6000 MW. Up to 1990, the electro hydraulic power production increased to nearly 27000 MW and 105 TWh annual energy production.
In the mid 70's the development of a new generation of Pelton turbines started in Norway by Kværner in order to meet the demand of large Pelton turbines for new projects at the west coast. The following table gives an illustration of this development:

Year of commission	Name of Plant	Net head m	Out-put MW	Speed RPM	* Type and No. of jets
1965	Skjaak	638	31	500	H 2
1967	Uvdal I	540	50	500	V 4
1968	Evanger	765	110	500	V 6
1970	Aurland I	840	245	375	V 6
1980	Lang Sima	1028/1136	260/300	428	V 5
1981	Sy Sima	885	315	300	V 5

*V = vertical shaft, H = horizontal shaft

In the early 70's the Norwegian development of Bulb turbines and Reversible pump turbines also started at Kværner.

The first intalled Bulb turbines were:

Year of commission	Name of plant	Net head m	Output MW	Speed RPM	No of units
1972	Funnefoss	10,3	20	100	2
1973	Kongsvinger	9,16	19,1	93,75	2
1975	Bingsfoss	5,0	10,8	71,4	3

The most important Reversible pump turbines built by Kvaerner and installed in Norway are:

Year of commission	Name of plant	Net head (m) Turbine	Pump	Power MW	Speed (RPM)	No of units
1972	Øljusjøen	220	230	50,5	428	1
1974	Duge	215	220	100	375	2
1975	Aurland 3	400	420	150	500	2
1981	Saurdal	390	440	160	428	2

Also Kaplan turbines have been installed in Norway. The largest were installed in the river Glomma south east of Oslo. These turbines were produced in Sweden by the Swedish companies NOHAB and KMW which was bought by Kvaerner Energy a.s. in the peroid from 1970 to 1980 (Kvaerner Energy was Earlier named Kvaerner Brug a.s).

The most important Kaplan turbines installed in Norway but produced in Sweeden are:

Year of commission	Name of plant	Net head m	Output MW	Speed	No of units
1970	Vamma	27,2	110	100	1
1974	Sarp	19,6	82,7	93,8	1
1980	Rånåsfoss	12,3	44,8	75	1
1982	Solbergfoss	20	104,9	78,9	1

Only a few large low head Francis turbines made by Kvaerner have been installed in Norway.
The largest of these turbines are installed in Hylen power plant on the west coast of Norway. The technical data for the two turbines in this power plant are:

Year of commission	Name of plant	Net head m	Output MW	Speed RPM	No of units
1976	Hylen	66	81,6	136	2

Following conclusion may be drawn of the historical development of water turbines in Norway until the end of the 19th century:

High head turbines must be regarded to be a speciality for Norway.
However, as with all Scandinavian turbine industry joint in one company expertise in low head turbine technology was also covered.

It should also be emphasized that the most important development for low head and medium head turbines was made in Norway, resulting in the patented X blade runners for the for the Three Gorges Power plant in China.
The runner was developed in collaboration between the author as professor of Hydraulic machinery at The Norwegian University of Science and Technology and the hydraulic engineers at Kværner Energy in 1996.
The main advantage with the X-Blade design is a flat efficiency curve with very stable operation over a whole range of flow and with a head variation from 61 m to 113 m.
A detailed description of this design will be given later in this book.

1.2. The research on hydraulic turbines and power plant design.

The goals in the development of an optimal water turbine with high efficiency in general may be listed as follows:

- no rotation of the flow from the runner outlet at best efficiency point of operation.
- an even distribution of energy across the outlet cross section at best efficiency point.
- no areas with decelerating velocities and cross flow leading to separation inside the runner during operation around the best efficiency
- a widest possible range of operation without unacceptable cross flow and cavitation.

The main task will be to calculate the flow field and pressure distribution through the runner. Long time before computer programs were developed for this purpose, analytical-graphical methods for both high head Francis runners and Pelton runners were developed around 1918-1920 at the Water Power Laboratory at The Technical University of Norway. Later these methodes were used in practice at Kvarner Brug in the design of turbines listed in the tables in the previous chapter.
The analytical equations used for a study of the influence from the design parameters, like the blade lean angles of reaction turbines described in chapter 7.4 and curvature in Pelton buckets, were based on these methods and will be briefly described later in this book.
For Francis turbines the analytical methods are still used together with a final CFD analysis in order to obtain a more detailed optimisation when designing a new runner. The X-BLADE runner for Three Gorges Power Plant was designed similarly as described later in this book.

The reason for the early use of analytical-graphical methods was that high head turbines of the Francis type are very well suited for such methods because of the long blades. However, this method is also very efficient during the design study of the influence from blade angles in flow direction and in particular from the blade lean angles. For Pelton turbines no other methods than the analytical graphical method were used by Kvaener before 1970. Tests in laboratory and efficiency measurements at site have proven a high standard of turbines developed by these methods.

The content on this book will be concentrated on the design of Francis and Pelton turbines and turbine control systems based on experience from Norwegian production and testing of mechanical equipment for Electro Hydraulic Power plants.
Examples of turbine control systems and analysis of governing stability for some of the most important high head and low head power plants with turbines built in Norway, will be described.

A speciality in hydro power plant design in Norway has been the development of cavern power houses with high pressure tunnel systems. In order to obtain stable governing systems the air cushion surge chambers have been introduced for these plants.

Typical plant conditions for turbine and control equipment delivery to a Norwegian
Power plant, to day, will be as follows:

Head range:	100 - 1100 m
Type of plant:	Underground powerplant in rock.
Water quality:	Normally low content of solids. Acid water with ph-value down to 4 in extreme cases may occure in the South West of Norway due to acid rain fall caused by industry in western Europe and no limestone rock to neutralize the acidity in Norwegian rock.

Long branched tunnel system connected to one or more reservoirs and several drainage shafts connected to the tunnels in order to collect water from small streams. Such systems leads to complex governing problems because of the requirement for stable operation on isolated resistive load from local electrochemical industry. Such load conditions occur in cases of break down of the transmission power lines connected to the main grid systems which may happen during winter storms.

In the following chapters the design, the erection work, maintenance and operation of turbines and mechanical equipment for hydro power plant will be discussed. Also the governing problems will be described.

2. DESCRIPTION OF TYPICAL POWER PLANTS

2.1 Lay-out of a high head plant

Fig. 2.1 shows the main elements of the water conduit system of a traditional Norwegian high head power plant for high head Francis turbines. Downstream from the upstream reservoir we find the coarse trash rack, intake gate, inlet tunnel, surge shaft, sand trap, fine trash rack, penstock isolating valve with air inlet valve, pressure shaft, spherical valve turbine, draft tube, draft tube gate, outlet surge shaft and outlet tunnel.

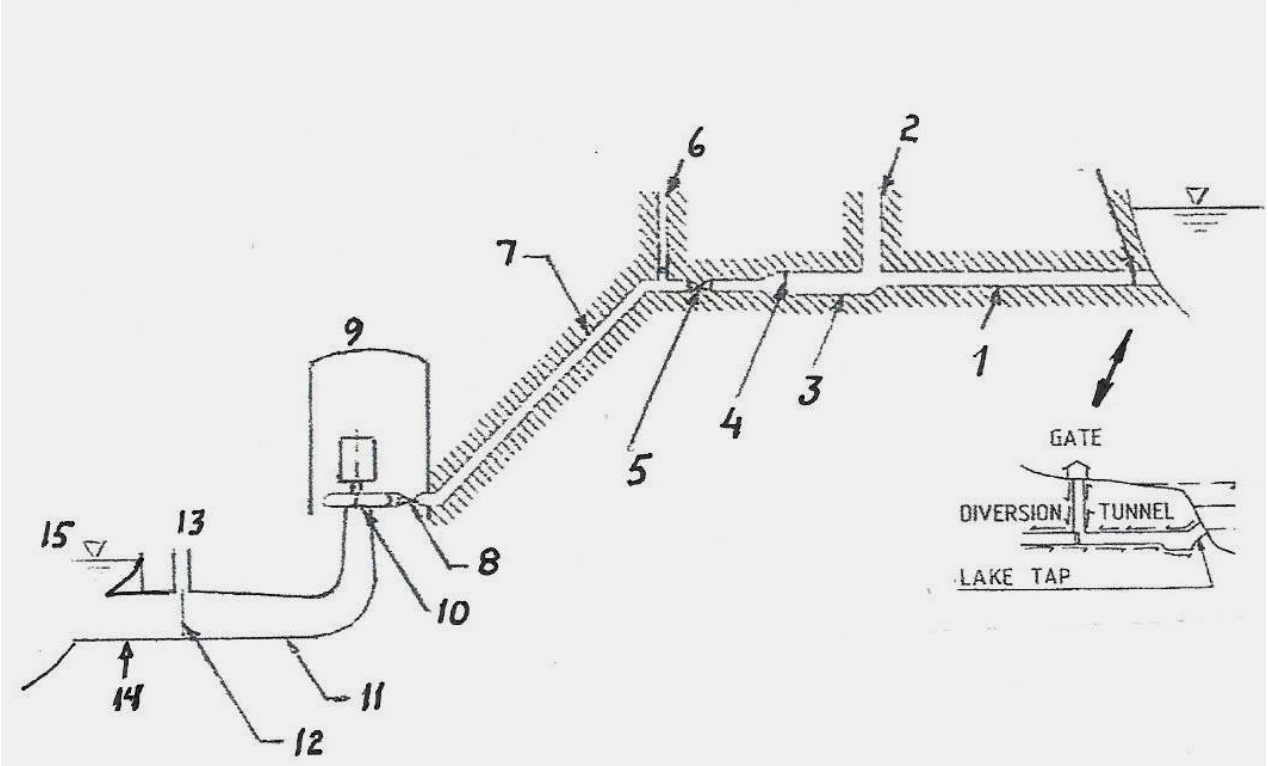

Fig. 2.1 The sketch is showing the water conduits in principle. Upstream reservoir and intake gate as well as the stone trap is illusrated in the detailed figure. Further, (1) Head race tunnel, (2) Surge shaft, (3) Sand trap, (4) Fine trash rack, (5) Penstock isolating valve, (6) Air inlet valve to prevent vacum when draining the penstock, (7) Penstock, (8) Turbine inlet valve (9) Power house (excavated in rock), (10) Turbine, (11) Draft tube, (12) Draft tube gate, (13) Outlet surge shaft, (14) Outlet tunnel, (15)Downstream reservoir.

The function of each element is described as follows:

The Stone Trap prevents larger objects such as stones and pieces of rocks to enter the inlet tunnel. This is to prevent blocking of the closure of the intake gate and clogging of the fine track rack. (A Coarse Trash Rack is normally installed if the intake setting is shallow in the reservoir allowing gravel and floating wood to enter the intake.).

The Intake Gate
The intake gate shall allow water (often through a small by pass gate) to fill the inlet tunnel and pressure shaft. The gate is also used to shut off the water during maintenance and inspections of the inlet tunnel and the surge shaft.

The Head Race Tunnel
The head race tunnel serves as the water conduit from the intake to the pressure shaft and must be dimensioned for optimum economy (price of production loss caused by friction loss versus price of pay down of invested capital). Further the Thoma stability criterion must be fulfilled (see chapter 12).

The Surge Shaft
The surge shaft reduces the water hammer pressure variations in the water conduits in front of the turbine by reducing the distance from the turbine to the nearest free water level. It must be large enough to fulfil the regulating stability criterion (Thoma criterion) and reduce the maximum surge pressure in the tunnel to an acceptable level. (For air cushion surge chambers the air volume must be large enough to fulfil the Thoma criterion).

The Sand Trap
The sand trap is, in principle, a part of the inlet tunnel, but with a widened cross-section to allow for sand sedimentation. It is located at the downstream end of the tunnel. The sand trap is shaped as a rectangular basin, immediately upstream of the fine trash rack and the penstock isolating valve. The reduced water velocity in the sand trap, allows sedimentation of sand that can be collected and transported out of this basin via a transport tunnel through the connecting gates. In this way, the coarse sand that is sedimented and the erosion of the mechanical components on valves and turbines will be reduced. The basin should be emptied of collected sediments at certain intervals because a sand filled up basin will cause bypassing of sand. The intervals are depending upon the sand content in the water, and should be coordinated with the plant's operation and maintenance program.

The Fine Trash Rack
For high head plants, a fine trash rack is installed downstream of the sand trap in front of the steel lined intake and the isolating valve on the penstock. This trash rack prevents floating objects exceeding a certain size to pass through to the turbine. Rock pieces and metal objects are also of primary concern if there is no sand trap or the sand trap is filled up. The fine trash rack bars have a considerably smaller spacing than the bars in the coarse trash rack at the inlet of the tunnel in cases where such trash rack is installed. The bars should be dimensioned to withstand a completely clogged trash rack. The natural frequency of the bars must be different from the Von Karmans vortex frequency to avoid resonance problems and fatigue fractures of the bars. (Strohals number will be 0.19-0.20 for such analysis.).

The Penstock Isolating Valve
The penstock isolating valve is normally of the butterfly type, and shall close automatically if the water velocity exceeds a certain limit, normally approximately 1.25 times the water velocity at full

power output of the plant. This is in order to reduce the damages in case of rupture of non-embedded parts of the penstocks or a turbine spiral casing. It should, however, also be mentioned that in some cases of presently built plants with short tunnels shut-off devices have not been installed for embedded penstocks in solid rock. This depends on the length of the head race tunnel. (Draining a long tunnel is inconvenient for inspection and maintenance of pressure shaft lining and inlet valve.)

The pressure shaft

The pressure shaft is steel lined from top to bottom if the quality of rock is poor. In good rock the main part may be unlined and only the lower part in a length of 50 - 200 m will be lined depending on the pressure.

The turbine inlet valve

The turbine inlet valve is located in front of the turbine. For high pressure turbines spherical valves are normally used. The valve seal must be drop tight for high pressure turbines in order to avoid cavitation damage of the valve seal. On the upstream side a manually operated maintenance seal is located. This seal is closed during inspection and repair of the main seal on the downstream side.

The turbine

For heads between 50 m and 650 m (and up to 700 m) Francis turbines are normally used. Turbines in underground powerhouses are normally of vertical type and also large units will be of vertical type even for low head turbines in above ground power houses.

The draft tube

The draft tube forms the downstream part of the turbine. The purpose of the draft tube is to convert the high kinetic energy at the runner outlet to pressure energy at the draft tube outlet by a gradually increased cross section towards the outlet.

The draft tube gate

The draft tube gate is used for isolating the draft tube and turbine for inspection. During operation of the turbine the draft tube gate is normally locked and secured or storred outside the gate opening in order to prevent closure during operation of the turbine.

The outlet surge shaft

If the power plant has an outlet tunnel a surge shaft is located downstream of the draft tube gate. This arrangement reduces a low pressure wave to separate the water column underneath the runner during shut down of the turbine. The draft tube surge shaft should also be dimensioned to avoid the maximum surge level to flood the power house during shut down of the turbines, followed by start at the worst point of time ragarding the surge time of the outlet tunnel system. If that requirement is not fulfilled, restriction on the start sequences after a shut down must be set.

The outlet tunnel

The outlet tunnel is normally designed with the same criteria as for the head race tunnel. Economic optimum and maximum and minimum allowable surges and also with fulfilment of the Thoma stability criterion (see chapter 12.)

2.2 Lay out of a low pressure power plant

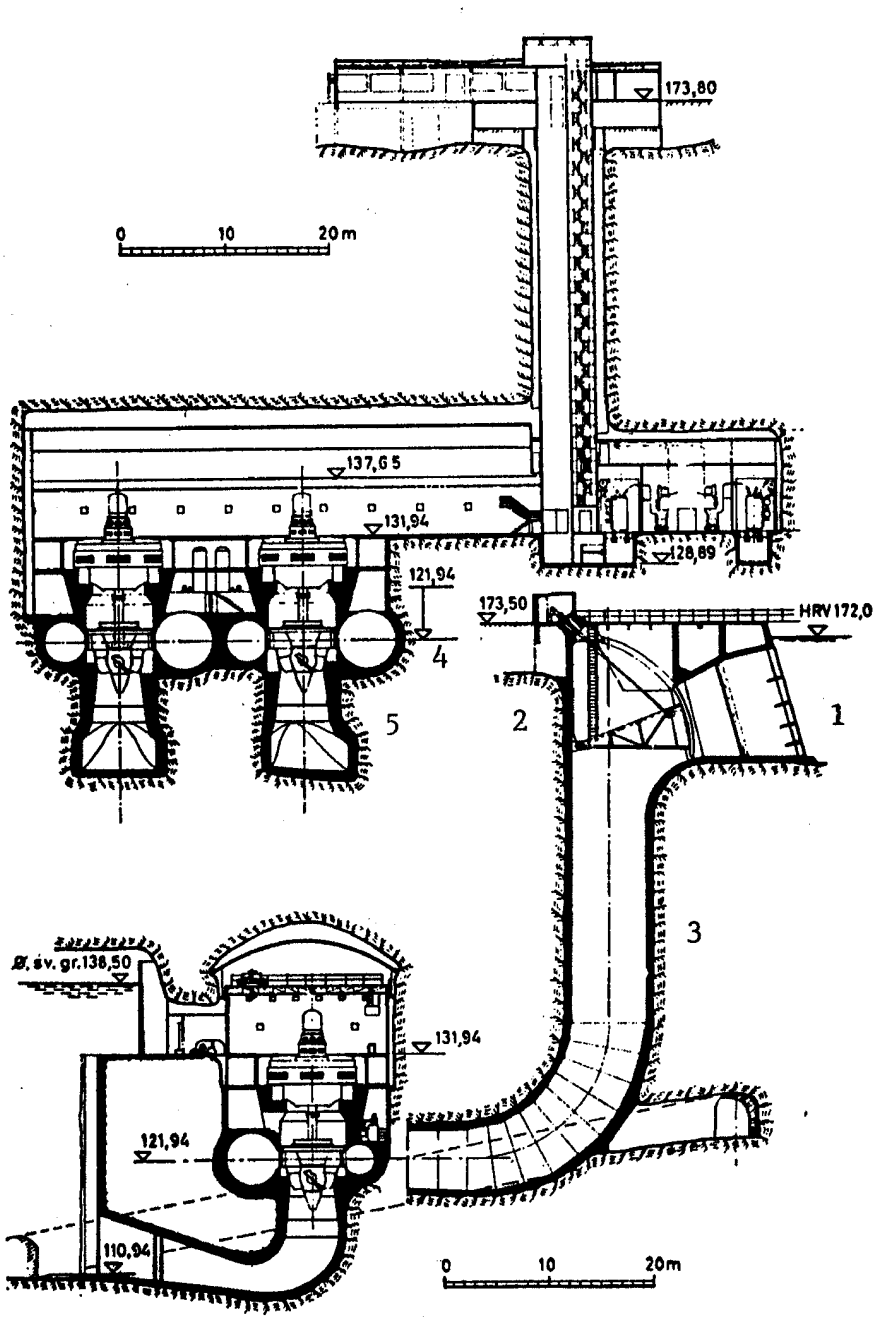

Fig. 2.2 Example of a low head power plant with Kaplan turbine in rock. Hunderfossen Kaplan power plant near Lillehammer, Norway.

Low pressure power plants in Norway are often excavated in the rock on the river bed beside the dam if the head is more than 20 m. Fig. 2.2 shows the power plant Hunderfossen as an example of this design. The different components of the water conduit system are described below with reference to fig.2.2. (For low heads, below 15 m Kaplan Bulb turbines are normally located in the dam).

1. Trash rack
   The trash rack is of the fine grid type in order to prevent trash floating in the river reaching the turbine. The trash rack is designed to carry full water pressure in case it is clogged by wood, timber or ice.

2. The intake gate
   The intake gate is of the segment type supported by two trunion bearings and is operated by two servomotors.

3. The pressure shaft
   The pressure shaft is excavated and lined with concrete on the upper part and has a steel lining in the lower part through the bend that is connected to the spiral casing of the turbine.

4. Turbine
   The turbine is in this case a Kaplan turbine with a steel lined spiral casing connected to the pressure shaft by welding. The head cover is bolted to the stay ring and supports the bearing. The runner can be removed upwards after the generator is dismantled, but there is access to repair the blades through the runner stainless steel chamber.

5. The draft tube
   The draft tube is steel lined through the bend and has no pier in the middle of the outlet part.

6. The draft tube gate
   The draft tube gate is of the sliding type and is operated only during the maintenance and inspection of the turbine in order to dewater the wetted parts.

3. ENERGY CONVERSION IN HYDRO POWER PLANTS

The energy conversion in Hydro Power Plants is illustrated in Fig. 3.1 and described below.

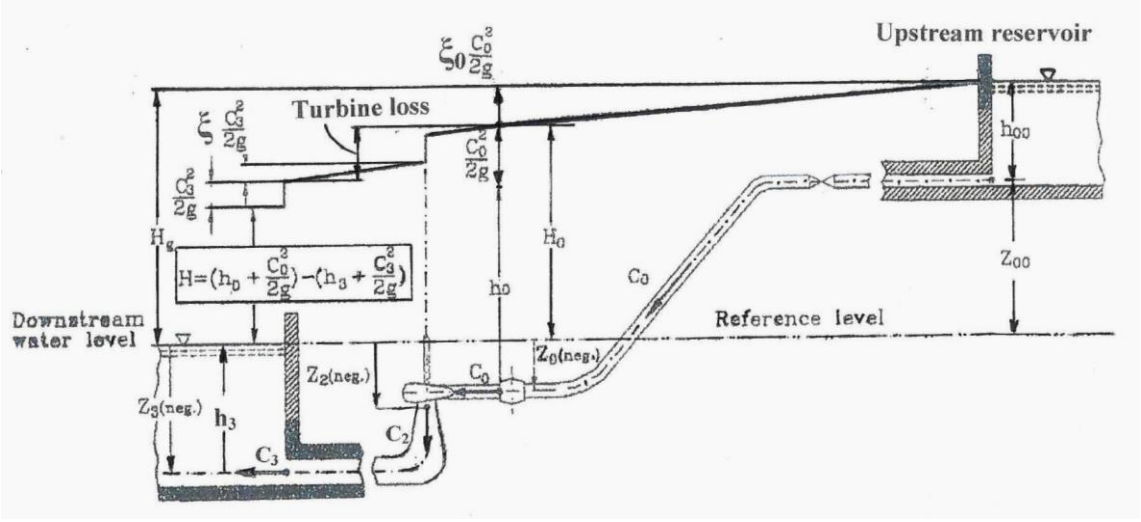

Denotations:

00	Inlet from reservoir
0	Turbine inlet
1	Runner inlet (not shown in fig.)
2	Runner outlet
3	Draft tube outlet

Fig. 3.1 Energy conversion in a Hydro Electric Power Plant.

Considering the available specific energy E = gH [(m^2/s^2) = (Joule/kg) where H is head in m (W.C.)] between the upstream side of the turbine and downstream of the turbine at the draft tube outlet. This leads to the definition of the net head across the turbine as deascribed in eq. (3.1) according to the IEC41 code were the draft tube outlet loss is regarded to be a power plant loss and not a turbine loss.

Note: $c_3 = c_{m3} = Q/A_3$ where A_3 is the cross section of draft tube outlet. (c_{m3} = the mean meridional velocity in eq. 3.1.

$$E = gH = \left(gh_0 + \frac{c_0^2}{2} + gZ_0 \right) - \left(gh_3 + \frac{c_3^2}{2} + gZ_3 \right) \quad \text{(Joule/kg)} \qquad (3.1)$$

The gross head H_g is defined as the net head plus the head loss in the conduits from the intake to the turbine and from the turbine draft tube outlet to the reservoir at the downstream side of the turbine (Note in fig. 3.1, there is no downstream tunnel and no head loss at downstream side except for the draft tube outlet loss $c_3^2/2g$).

From fig. 3.1 we can establish the following equation:

$$H_g = h_0 + \frac{c_0^2}{2g} + Z_0 + \xi_0 \frac{c_0^2}{2g} - \left(h_3 + Z_3\right) = H + \xi_0 \frac{c_0^2}{2g} + \frac{c_3^2}{2g} \qquad (3.2)$$

Here $_0$ denotes the turbine inlet, and $_3$ draft tube outlet. (Note that in chapter 4 the inlet and outlet of the runner are denoted $_1$ and $_2$ respectively).

(Note: that the loss $\xi_0 \frac{c_0^2}{2g}$ from the intake to the turbine is a plant loss while the loss in the inlet valve and spiral case and the loss inside the draft tube $J = \xi_2 \frac{c_2^2}{2g}$ are parts of the turbine losses (see fig. (3.1)). The draft tube outlet energy $\frac{c_3^2}{2g}$ is, as described earlier, not regarded to be part of the turbine loss according to the IEC41 norm).

The net head is the theoretical energy of which the majority will be utilized and transformed to mechanical energy by the turbine. The rest of the energy will be converted to losses i.e. mainly increased heat energy in the water and a very small negligible part as a heat flux to the surroundings.

The available power for the turbines in a powerplant project depends on the available flow Q m^3/s and is defined by:

$$P = EQ\rho \quad \left[(Joule/kg)(m^3/s)(kg/m^3) = Joule/s = W\right] \tag{3.3}$$

ρ is the density of water [approximately 10^3 (kg/m^3)]

For a river with a flow Q = 100 (m^3/s) and a net head H = 50 m, the following available power is utilised by the turbine. For H = 50 m and Q = 100 (m^2/s) we get the turbine power as follows.

$$P = Hg\ Q\rho = 50 \cdot 9.81 \cdot 100 \cdot 10^3 = 49.05 \cdot 10^6\ W = 49.05\ MW$$

The available energy stored in a reservoir is determined by multiplying the mass of water (i.e. the stored volume of water multiplied by the density) with the net head.

The equation for stored energy of a volume V and head H i.e. E = gH yields:

$$W = V\ \rho \cdot E \qquad \left[m^3 \cdot (kg/m^3)(Joule/kg) = Joule = Ws\right] \tag{3.4}$$

Note: Joule = Ws = $1/\left(3600 \cdot 10^3\right)$ kWh.

For a reservoir with a volume of $V = 500 \cdot 10^6\ m^3$ and a head of H = 400 m the following available storage of energy which can be utilised by the turbine when ignoring head losses in tunnels and the losses in turbines and generators:

$$W = 1000 \cdot 10^6 \cdot 10^3 \cdot 400 \cdot 9.81/(3600 \cdot 10^3) = 10.9 \cdot 10^8\, kWh = 1.09\ TWh$$

Note: 1 TWh = 10^{12} Wh = 10^9 kWh = 10^3 GWh.

In the Norwegian reservoirs the total energy storage is approximately 80.4 TWh. In addition, run of the river power is added to a total production of 124.4 TWh. (Data from 2010). As an example one of the largest reservoirs, Blåsjø has a storage capacity of 3105 m^3 and a mean production of 7 759 TWh.

The power production for consume will be smaller than the available storage energy because of losses in the water conduit system, turbine and generator, transformers and power lines.

The total efficiency for a modern Francis turbine is 94 - 96% depending on size and operational head with best efficiency for large turbines operating at around 100 m net head. The generator efficiency is 98 - 99% so the total net energy will be reduced to 95 * 98.5 = 93.5% of the available energy at best operational point. At part load and overload the efficiency will drop.

The hydraulic efficiency of a turbine excludes friction losses on the outside of the runner, leakage loss of water that does not pass through the runner blades and mechanical friction losses. The hydraulic efficiency of a well-designed turbine is 98-99% and can be developed as shown in the following description.

The specific hydraulic energy utilized by the turbine runner can be described mathematically by the well known Euler turbine equation expressing the hydraulic efficiency (see chapter 5). The difference in specific hydraulic energy from inlet to outlet of the runner can be expressed by $E_1 - E_2 = E = gH$ as shown in eq. (3.5) where:

$E = gh + \frac{c^2}{2} + gZ$ (See also fig. 3.1 for description of Z).

Note: In the Euler equation the runner inlet is denoted by index $_1$ and the outlet by index $_2$.

$$\eta_h = \frac{E_1 - E_2 - J_R}{gH} = \frac{E_1 - (E_2 + J_R)}{E} \tag{3.5}$$

where E_1 and E_2 are the specific energy upstream and downstream of the runner respectively and J_R is the hydraulic loss of energy (Joule/kg) in the runner.

Then: Eq. (3.5) may also be written as follows: see fig. (3.1)

$$\eta_h = \frac{(gh_1 + \frac{c_1^2}{2} + g\,Z_1) - (gh_2 + \frac{c_2^2}{2} + gZ_2 + J_R)}{gH} \tag{3.6}$$

The hydraulic efficiency according to this equation is the ratio between the specific energy transferred to the runner = $E_1 - E_2 - J_R$ and the difference in specific hydraulic energy from upstream to downstream side of the turbine, gH. The energy transferred by the runner to the turbine shaft will be $E_1 - E_2$ minus the hydraulic energy loss in runner (J_R), the mechanical loss, labyrinth leakage loss and disk friction losses.
The hydraulic efficiency $\eta_h = (E_1 - E_2 - J_R) / (gH)$ may also be expressed by the following equation recognised as the EULER turbine equation:

$$\eta_h = (u_1 c_{u1} - u_2 c_{u2}) / E \tag{3.7}$$

This equation is the well known Euler turbine equation which will be developed and discussed in eq. (5.7) and eq. (5.54) in chapter 5.

4. CLASSIFICATION AND DESCRIPTION OF DIFFERENT TURBINE TYPES

4.1. Classification of turbine types

The turbine types can be divided in two main groups.

1. THE REACTION type where there is a pressure difference from inlet to outlet of the runner.

   At the runner inlet of this type of turbine part the specific energy is pressure energy. The specific energy converted to mechanical energy by the flow through the runner is partly converted from the drop in pressure - this is the reaction part of the energy conversion. The other part is converted from the impulse forces from changes in the direction of the relative velocity vectors. The reaction ratio may be denoted by $(h_1-h_2)/H_n$ where $\rho g h_1=p_1$ is the hydraulic pressure at the runner inlet and $\rho g h_2=p_2$ is the hydraulic pressure at the outlet.

   Among the reaction turbines the Francis turbines and the Kaplan and Kaplan Bulb turbines are the most commonly used turbines today. For low heads also Propeller turbines with fixed guide vanes or runner blades are used for mini turbines and for best efficiency point operation in plants with many units. Reversible Francis type pump turbines installed for energy accumulation have been installed also in Norway where the electricity production is 99.8% hydropower. (These unit operates for season pumping in the spring and power generating in the winter and not for peak power operation. In the future more Reversible Pump Turbines may also be installed in Norway for peak load operation only without a net production from a catchment area.).

2. THE IMPULSE types where there is no pressure difference between the inlet and the outlet of the runner.

   The specific energy is completely converted to kinetic energy at the runner inlet of this turbine type. Because of this the specific energy converted to mechanical energy comes only from the impulse forces created by the changes of direction of the velocity vectors.

   The most commonly used IMPULSE TURBINE today is the PELTON TURBINE. The TURGO TURBINE, which is an axial type impulse turbine has only rarely been used for small units and will not be described in this book. The CROSS FLOW TURBINE is a two stage impulse turbine used for small units only and a description of this type is also not described in this book. The efficiency of the cross flow turbine has been measured in laboratory to be around 80% while efficiency of the Turgo Turbine has been reported to be close to 90%.

4.2. Description of the different types of turbines used for electricity production.

Pelton turbines

In this chapter some typical turbines installed in Norway are described as examples for a general turbine design.

For the highest heads Pelton turbines will be the only choice. Such turbines have been designed for heads up to 1886 m at Biedron Power Plant in Switzerland. The Pelton turbine is an impulse turbine where all the energy is converted to kinetic energy in front of the runner. There is then no pressure

drop from the inlet to the outlet of the runner. In Norway the worlds most powerful Pelton turbines at that time were installed at Sy Sima power plant in 1981 with two units of 315 MW rated output and 350 MW maximum power for a net head of 885m at speed n = 330 rpm*. Two more units were installed in the same power house connected to two different reservoires at 1065 m and 1152 m net head respectively. The rated power of these turbines were P = 260 MW with speed n = 428.rpm. All turbines in this powerhøuse were 5 jet vertical Pelton turbines.

* The 3 Pelton turbines in the high head plant BIEDRON in SWITZERLAND designed for 1886 m net head were in operation again in 2010 after the rupture of the steel lined penstock in 2000. BIEDRIN is a power plant in the GRANDE DIXENCE power system. The output of the 5 jet vertical turbines are 400 MW and thus these units break the world record in power per unit for Pelton turbines.

However, the traditional Pelton turbine was the horizontal type and in fig. 4.1 a turbine of this type installed in Skjaak power plant is shown.

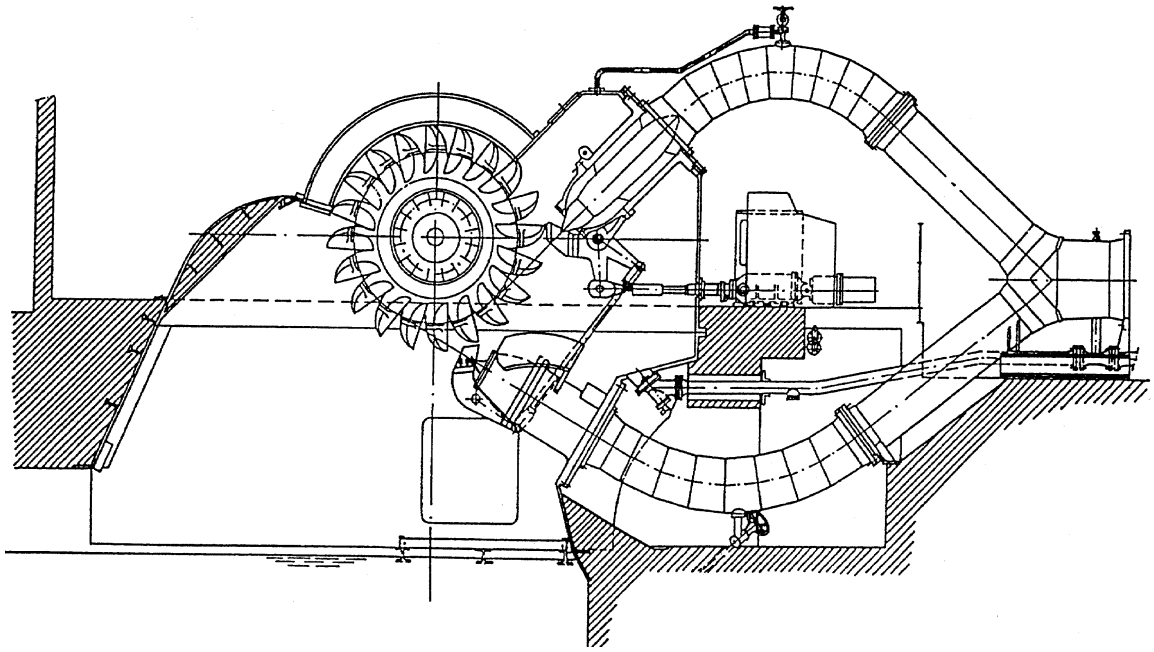

Fig. 4.1 Horizontal Pelton turbine for Skjaak power plant. Power, net head and speed are P=31,47 MW, H_n=638 m, n=500 rpm.

Even if the Skjaak turbine was installed in 1965 it still represents a modern version of the horizontal type of Pelton turbine with a single monacast runner, two straight flow injectors and welded bifurcation and inlet bends.

The regulating mechanism of Pelton turbines consists of series coupled deflectors and needle system linked through the oil hydraulic system.

Such system is suitable for operation on isolated load because partial load drops can be controlled by combined the fast deflector movement and the slower needle movement within acceptable frequency and voltage deviations.
A deflector system of the "on-off" type, which does not take active part in speed control at partial shut down cannot be used for operation on isolated load

.

In fig. 4.2 one of the two vertical 350 MW turbines for Sy Sima Power Plant is shown.

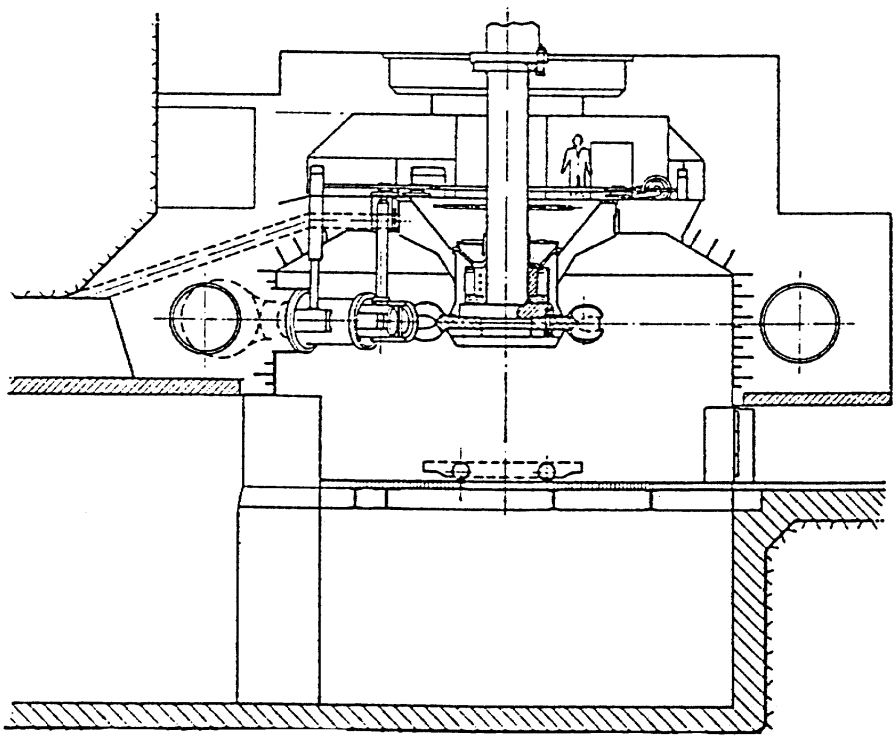

Fig. 4.2 One of the 5 jet vertical Pelton turbine for Sy Sima power plant. P=315 MW, H=885 m, n=300 rpm.

The turbines for Sy Sima still represent the modern vertical multi-nozzle Pelton turbines with combined deflector-needle control and straight flow injectors. For new turbines the turbine governors are based on Programmable Logic Systems (PLS) while the governors delivered before 1985 normally were of the analogue type.

The modern vertical units are also furnished with automatic selection of number of needles in operation controlled by the output of the turbine in order to obtain the highest possible efficiency at part load with a single jet or a reduced number of jets in operation. An efficiency curve for a turbine with automatic selection of number of jets in operation is shown in fig. 4.3. The turbines for Sy Sima also have such system which have been successfully in operation since 1981.

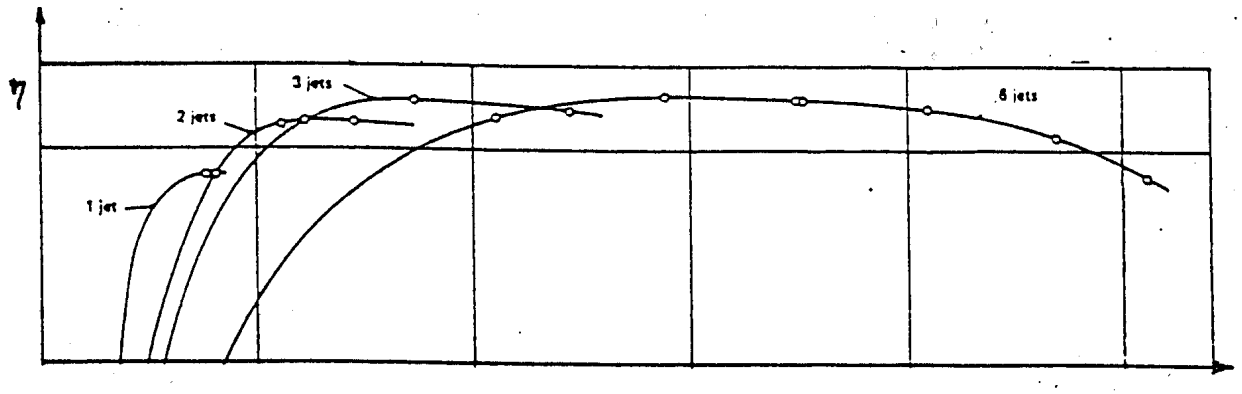

Fig. 4.3. Efficiency for a 6 jet Pelton turbine with automatic selection of number of nozzles operation.

Francis turbines

Francis turbines, which are the most commonly used turbine for head ranges between 50 and 650 m (max head 750 m) as well as the Kaplan turbines, are of the reaction type where the specific energy in front of the runner consists of partly pressure energy (gH) and partly kinetic energy ($c^2/2$). For the high head Francis turbine approximately 50% of the energy is converted into kinetic energy at the runner inlet, and there is a pressure drop through the runner of approximately 50% of the total energy. [For a Kaplan turbine the drop in pressure energy from inlet of the runner is relatively larger than for a Francis turbine (see chapter 6.4)]. In fig. 4.4 the design of a modern high head Francis turbine for Svartisen Power Plant is shown.

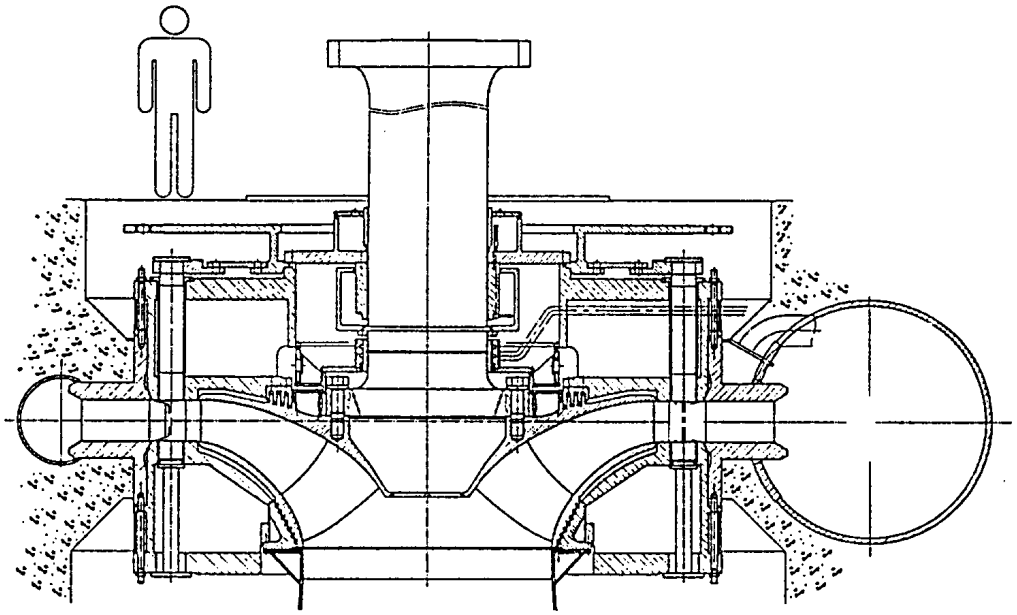

Fig. 4.4 Francis turbine for Svartisen Power Plant.

The technical data for the two Francis turbines for Svartisen Power Plant is H=543 m, Q_n=71.5 m^3/sec. P=350 MW and n=333 rpm. The first turbine was put into operation in 1992. The turbine for Svartisen is the largest Francis turbine installed in Norway and represents one of the largest Francis units in the world operating at net heads exceeding 500 m.

Fig. 4.4 indicates that the components in the turbine (except for the casted crown and band of the runner) have been fabricated from plates with thickness up to 200 mm. A special plate quality with Toughness Through Thickness (TTT) has been used where forces are transferred through the thickness of the plates. Such parts must be used in the stay ring and head and bottom covers. In fig. 4.4 the outlet edge of the splitter blades is also shown indicating the special high head runner design which has been used by Kvaerner since the 1930's.

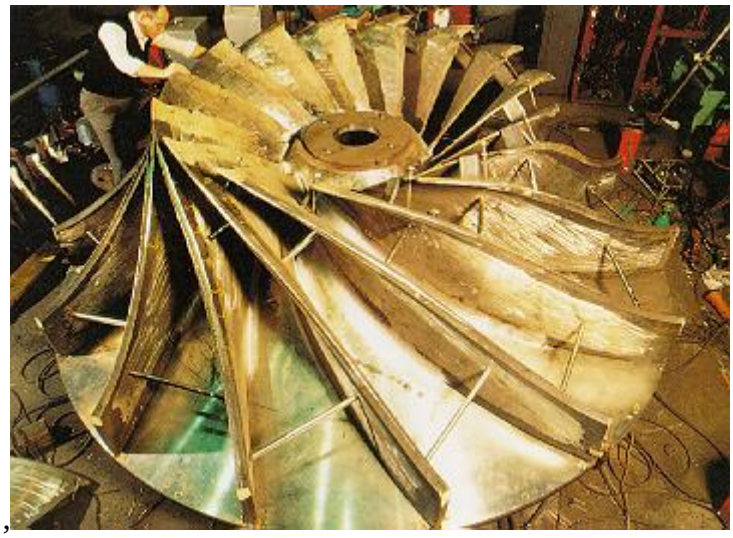

Fig. 4.5. Fabrication of a runner with splitter blades in the workshop at Kværner Energy A.S. Note: Only the full length blades are welded in the picture of the runner. (See also fig. 10.7 chapter 10 where all the splitter blades are also welded to the crown of the runner.)

Fig. 4.5 shows a high head runner in the workshop at Kværner Energy A.S. For a Francis turbine designed for high head as shown in fig. 4.4 traditional Teflon lubricated regulating ring driven by two servo-motors forms the main part of the regulating mechanism. All bearings on the guide vanes are of the self-lubricated DU type. The connection to the regulating ring is of the conventual lever/link type. It should be noted that no shear pins or fracture linkage have been used in the guide vane regulating ring mechanisms. For high head turbines with deep submerged intakes in reservoirs, shear pins or other remedies will not be necessary to prevent destruction by hard objects stuck in between the guide vanes. From the experiences in Norway it is possible to conclude that no problems have occurred with this design. Accidents by "chain reaction" caused by broken shear pins have been avoided with this design. However, the guide vane levers have also been fixed by frictional couplings of every second guide vane for turbines where a large amount of solids in the water is expected. For very large low head turbines one servomotor on each guide vane have also been used. The governor for the Svartisen turbines are of the PLS type furnished with a modern pressure feed back algorithms in order to obtain stable governing on isolated load in a tunnel system with no surge chamber.

Kaplan turbines

Kaplan turbines are normally used for heads below 50 m and in extreme cases up to 75 m head. In Norway only a few large Kaplan turbines have been installed. These turbines are in operation in the South East of the country where the largest rivers with low head power plants are located.

In fig. 4.6 the Kaplan turbine for Solbergfoss is shown. The turbine has been produced by Kværner Turbin A.B. in Sweden and it has following technical specification.
P=104.9 MW H_n=20.0 m n=78.9 RPM

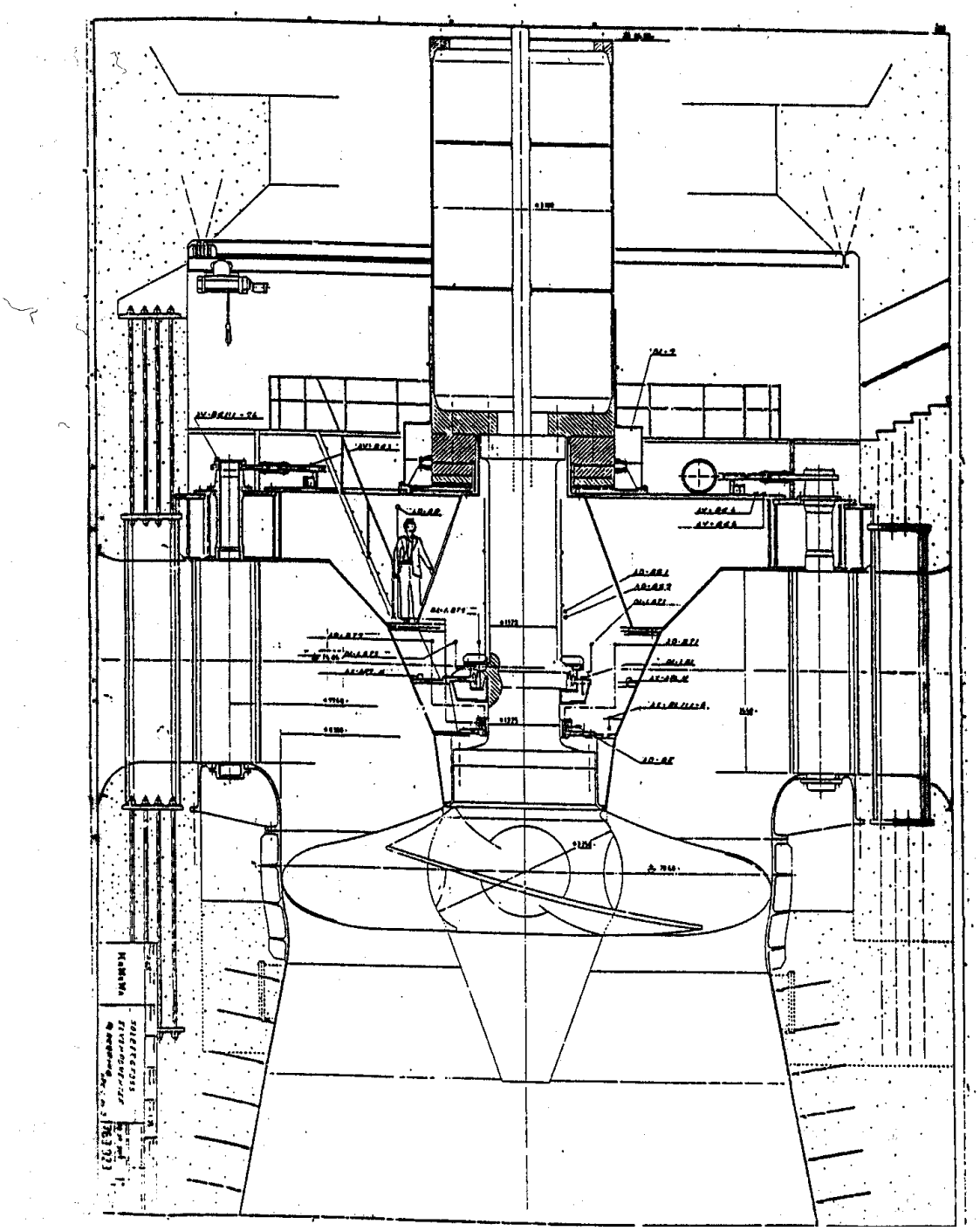

Fig. 4.6. The Kaplan turbine for Solbergfoss Norway

For this turbine the runner blades are made of the 13% Cr 6% Ni type cast steel. The guide vanes and the steel structure are fabricated of fine grade carbon steel plates and castings.

The thrust bearing is located on the turbine cover and guide bearings are located on the generator top and above the runner hub respectively.

The runner blade servomotor is located in the hub and the oil supply and feed back mechanisms are transferred via the top of the hollow shaft to the turbine governor. The governor is of the electronic type with parallel control of guide vanes and runner blades. The guide vanes are controlled by one servomotor on each guide vane, connected to a mechanical control system. In such system no friction slip or shear pin system on the guide vane lever system will be necessary because the regulating force from one guide vane servomotor is too small to damage the guide vane even if the guide vane is blocked by solids jammed in between two guide vanes.

Kaplan Bulb turbines

Kaplan bulb turbines are normally used for heads below 15 m because of the increased price of the bulb and structural supports for higher heads. In fig. 4.7 one of the three Kaplan Bulb turbines for Kongsvinger Power Plant is shown. The technical data for the turbines are: P=19.1 MW , H=9.16m, n=93.75RPM

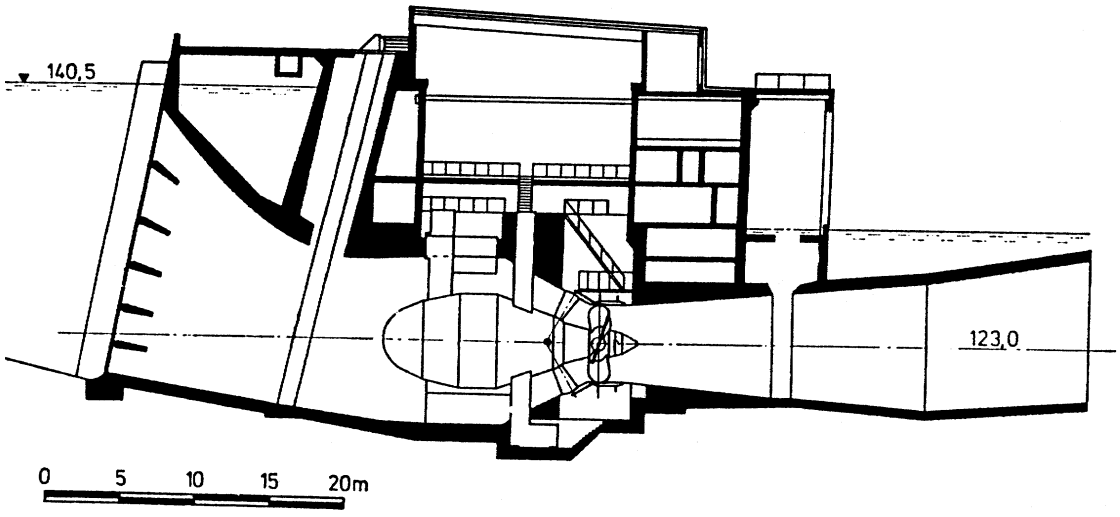

Fig. 4.7 The Kaplan Bulb turbine for Kongsvinger power plant.

The Kongsvinger Kaplan Bulb turbine is equipped with roller gates upstream of the turbine for shut down of the units. The turbine regulating system consists of separately controlled guide vane servomotors connected to the oil pressure system.
Further a manual separated operation of each guide vane servomotor will be possible in such systems in order to open a single guide vane for flushing away possible solids jammed in between two guide vanes. Because of the separate guide vane servo system the maximum force on a guide vane is limitted if solids are jammed between two guide vanes. This system then prevents damage on the guide vanes or leverage system.

The runner blade servomotor is located on the down stream side of the blades in the hub allowing for maintenance work of the servo-system without dismantling of the shaft coupling and blades. The guide-vane/runner-blade position system is compensated for variation in the head.

Reversible Pump turbines

Reversible pump turbines have been installed in Norway for the purpose of pumping flooding water from a downstream catchment area up to the main reservoir in the spring. During the winter the machines are running only in turbine mode.

By means of the pumping operation, cheap summer electricity may be used for extending the catchment area and increasing the electricity production during the winter when the price of electricity is high. [In the future daily peak production may also be delivered for peak load exchange of electricity between Norway and continental countries like Denmark and Germany, where the electricity production is based on thermal energy which will increase the pollution in peaking operation.]

The main difference between a Francis turbine and a Reversible pump turbine can clearly been seen in the larger diameter of the runner on the pressure side of a Pump turbine due to the higher kinetic energy needed in pumping mode.
In fig. 4.8 one of the reversible pump turbines for Saurdal Power plant is shown. In this power plant two reversible pump turbines and two ordinary Francis turbines are installed. The technical data for the Reversible Pump Turbines, which were commissioned in 1983, are:

Turbine mode: P=160 MW Hn=390 m n=428 RPM
Pumping mode: Q=38 m^3/sec Hn=440 m n=-428 RPM

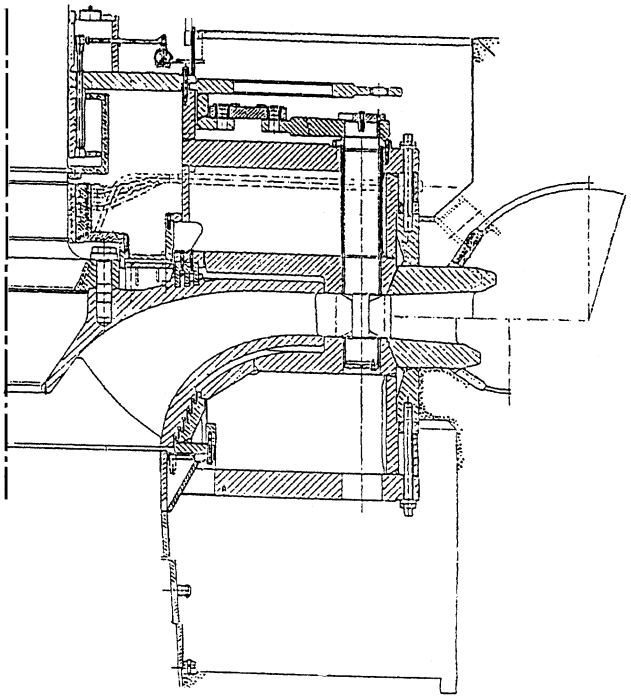

Fig. 4.8 Cross Section of a Reversible Pump Turbine for Saurdal Power Plant.

5 CHOICE OF TURBINE TYPES WITH DISCUSSION OF PARAMETERS AND CALCULATION OF MAIN DIMENSIONS

5.1 Choice of turbine types

In chapter 4.1 the turbine types were divided into two main groups, namely REACTION TYPES (Kaplan and Francis types) and IMPULSE TYPES (among which the Pelton turbines is the dominating type in use today).

In addition to the net head the limitation for reaction turbines is the necessary "setting" or submergence which can be determined as a function of the speed of the outlet blade tip or rim speed of the runner band. For physical reasons the rim speed must be limited to avoid noise, vibration and fatigue problems of the runner even if it is possible to avoid cavitation by a deep submergence.

For Francis turbines there will be an increasing difference between the inlet diameter and outlet diameter for increasing net head. This is because of a necessary increase of the inlet velocity and a limited outlet velocity of the blades due to a practical limit of submergence of the runner. The outlet/inlet diameter ratio can be expressed by the low speed number, see eq. (9.4) and eq. (9.5), chapter 9.1 and 9.2.

For a Kaplan turbine, an increasing length of the blades or decreasing distance between the blades (by increasing the number of blades) will be necessary for increasing operation head. This is because increasing energy difference between inlet and outlet requires longer blades in order to avoid too high blade loading. (A higher number of blades for a given length gives the similar result as longer blades for a given number of blades). For movable blades of a Kaplan turbine the blade length is limited due to geometry limitation for the spherical part on hub and runner chamber. Due to limited space for the mechanism in the hub, an increase in number of blades is also limited. Maximum number of blades will be 7 or 8. These restrictions limit the maximum head for Kaplan turbines to approximately 75 m.

For Pelton turbines the (runner diameter/bucket width) ratio must be increased for increasing head in order to avoid cavitation pitting on the back side of the bucket inlets, i.e. the speed number must be decreased for increasing head. The maximum head for a Pelton turbine is approximately 2000 m with the technology of today.

The operating range for the different types of turbines chosen for operation in Norway at present time is shown in fig. 5.1.

In the future the DC power lines from Norway to the Continent will lead to an exchange of energy with peak load exported from Norwegian hydropower during the day time and thermal base load imported back to Norway from the continent during the night.
In countries where peak load operation and spinning reserve power production is needed and paid for by a high price, the borderline for head between Pelton- and Francis turbines may be as low as 300m even for large units. This is because of the low minimum flow of a Pelton turbine that have a water consume of only 1% at no load operation and an efficiency of 90% at 10-12% load for operation with one jet of a 6 jets unit. Even if a Franci turbine has around 3% higher peak efficiency compared to a Pelton turbine, a Francis turbine drops normally below 90% efficiency at 45-50% load with a no load water consume of around 8-10 %. This will be described in this chapter 8. (see also [Ref 4]).

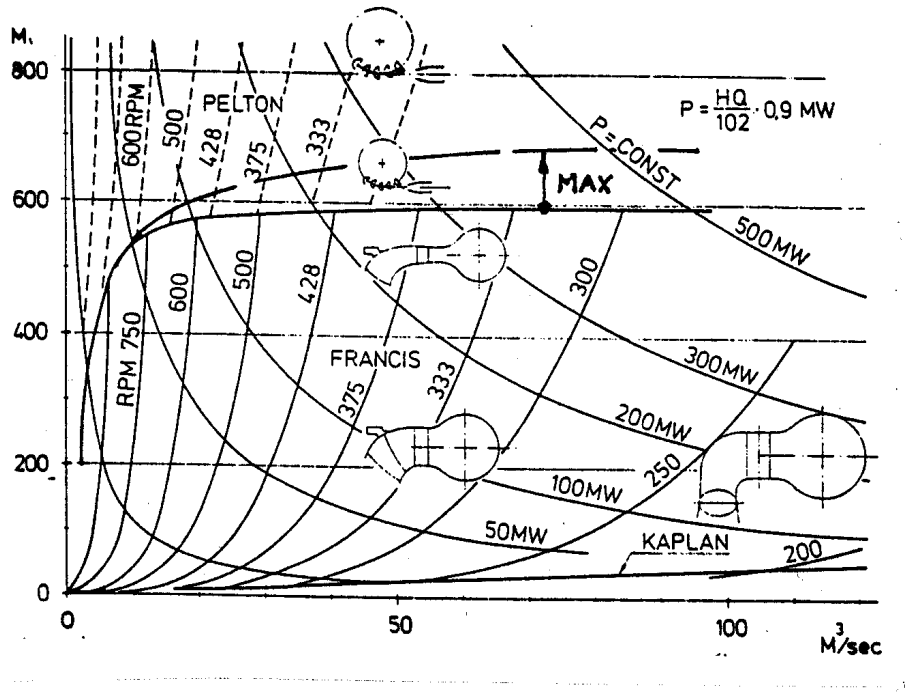

Fig. 5.1. Range of operation for different types of turbines.

For the choice of turbine type following parameters are given:

Net head = H
Total flow in the power plant = ΣQ
Expected load over time and expected efficiency over the range of output or flow.
Unit price
Water quality

For a given head the choice of turbine type will depend on the flow capacity of the unit as shown in fig. 5.1.

However, the expected load over time may influence the size and number of units of the plant.

If the plant is operated as a peak power plant with load variation from e.g. 10% of the total flow and up, a higher number of smaller units or units with "flat" efficiency curves will be chosen instead of a low number of units with a higher efficiency caused by bigger size and somtimes higher spesific speed. Such choice will be economic even if one or few large units have a higher peak efficiency. This is explained by lower efficiency at part load.

Turbines with flat efficiency curves are Pelton turbines for the high head range and a Kaplan turbines in the low head range due to the movable runner blades.

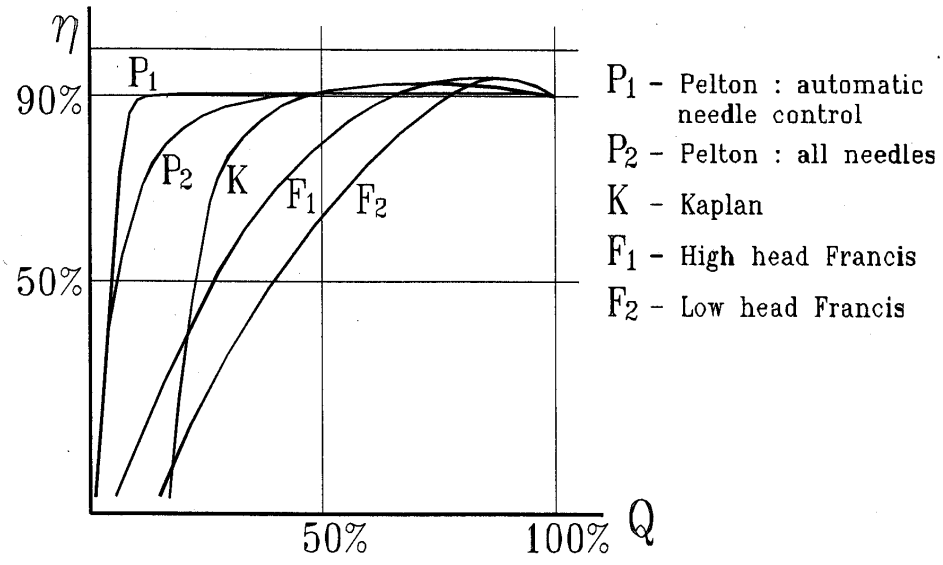

Fig. 5.2. Comparison of efficiency of different turbine types.

In fig. 5.3 a comparison is made for plant efficiency for an alternative with three units compared with one large unit.

Even if the efficiency for one large unit is higher than the efficiency for three units with one third the size, the smaller units give higher efficiency for plant operation below 50% load.

The choice of number of units is then depending on the way of operation of the power plant, as well as price and transport possibilities to the power house.
The higher efficiency of one unit is caused by lower friction losses which gives a so called scale effect with increasing efficiency when increasing the size from smaller to bigger units.

However, in some cases the operational conditions of head and flow will be in the domain where either Pelton turbines or Francis turbines can be chosen outside the border lines given in fig. 5.1 [Ref. 4].

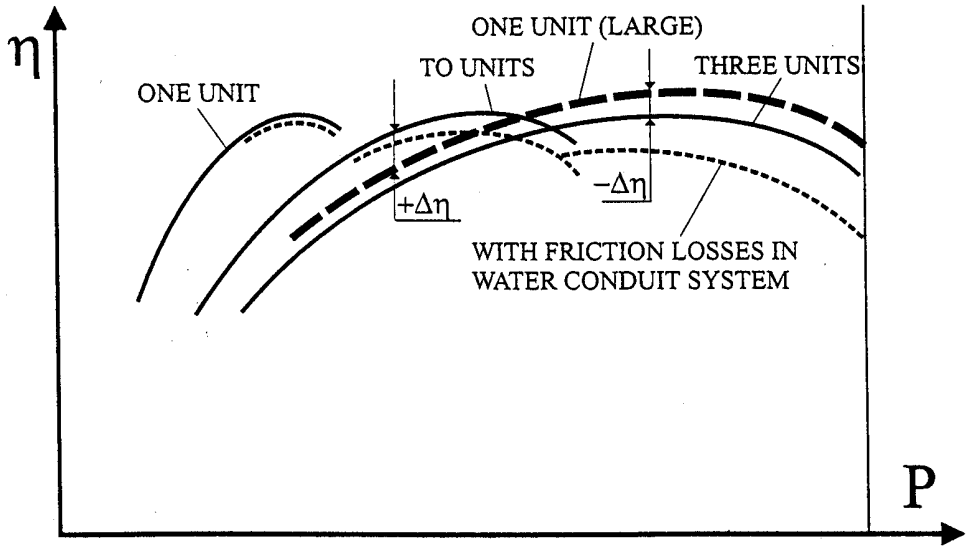

Fig. 5.3. Difference in efficiency of one big Francis turbine versus 3 smaller units with 1/3 of the output of the big unit.

The choice of Pelton versus Francis turbines is normally based upon 3 factors.

- The price of the unit. (must include cost of excavation and concrete works).
- The difference in efficiency (way of operation must be taken into consideration).
- The reliability and availability or risk for unplanned stops and time for repair especially for operation in sand laden water.

The choice based upon the price of the unit may be illustrated as shown in fig. 5.4 where the unit price NOK/KW or US$/kW is chosen as a relative price index.

Such diagram will be somewhat different for turbines from different manufacturers and must be regarded to be qualitative information only.

From the diagram Pelton turbines are found to be cheaper than Francis turbines for decreasing capacity (flow) and increasing head. The practical limit for building conventional Francis turbines will be for a head of 750 m. The reason for the head limit will be problems with guide vane clearance losses and blunt very thick stay vanes which will decrease the efficiency, cause material and welding problems because of the increasing material thickness in the stay ring.

By studying fig.5.4 it is clear that Pelton turbines are the most economical turbines for high head and a low capacity flow when looking at the investment.

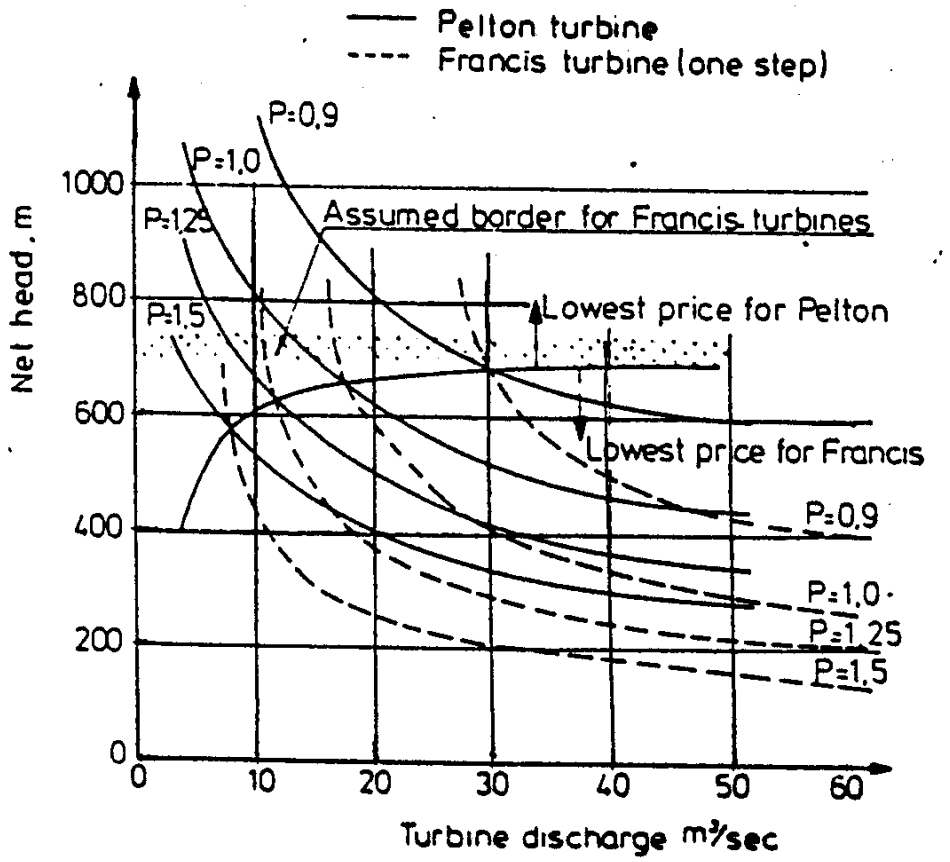

Fig.5.4. Price index for Pelton and Francis turbines as function of head and discharge flow.

The diagrams in fig. 5.5 and 5.6, illustrate a comparison based on the loss in production due to the variation in turbine efficiency versus output of the turbine (MW). In fig. 5.5 is shown a comparison of a 50 MW Francis turbine and a Pelton turbine designed for 470 m net head. At best efficiency point the Francis turbine is the best choice as well as for operation from 50 % load up to full load. However, the Pelton

turbine will be the best choice if a typical peaking operation is wanted with operation equally distributed over the whole range of power including also very low load. The favour of Pelton turbines increases if an automatic selection of number of needles in operation is chosen due to increased efficiency at part load with operation down to one jet operation.

By integrating the loss of energy production due to loss in efficiency over the turbine output, it is quite clear as illustrated at the bottom of fig. 5.5 that the Pelton turbine is the best choice if the time in operation is equally distributed from zero load to full load. However if operation is avoided below 30 % load the Francis turbine will be the best choice for the example shown in fig.5.5.

By comparing different sizes of turbines for different heads, a similar comparison as shown in fig. 5.5 may be made. Then a boundary selection curve between Pelton and Francis turbine may be drawn for different kind of operation as illustrated in fig. 5.6. The zig zag lines illustrates the different range of operation as follows: Zig zag illustration for peaking operation from 0 to 100% load, at the bottom in fig. 5.6 illustrated by "zig zag" curves for "amplitudes" from 0% to 100%. Further 25%-100% load variation and 50%-100% load variation and finally best efficiency point operation plus minus 10% load variation are illustrated by amplitudes from 25% to 100%, 50% to 100% and best point ± 10% respectively.

In Norway, daily peaking operation has not been needed up to 1995 because the electricity production has been 98.8% hydropower, and the choice between Pelton and Francis turbines has been the alternative curve in fig. 5.6 for no operation below 50% load (see also fig 5.1).

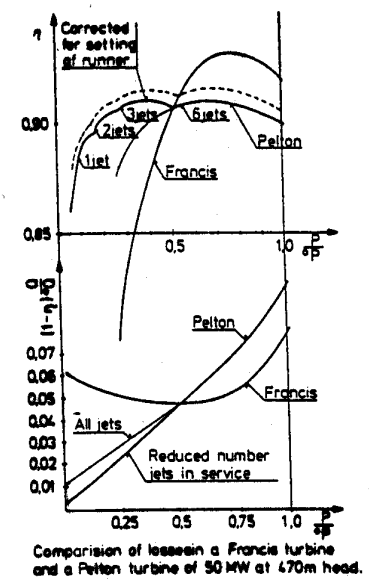

Fig. 5.5 Efficiency and total loss of 50 MW Pelton turbine compared with a Francis turbine both for 470 m net head

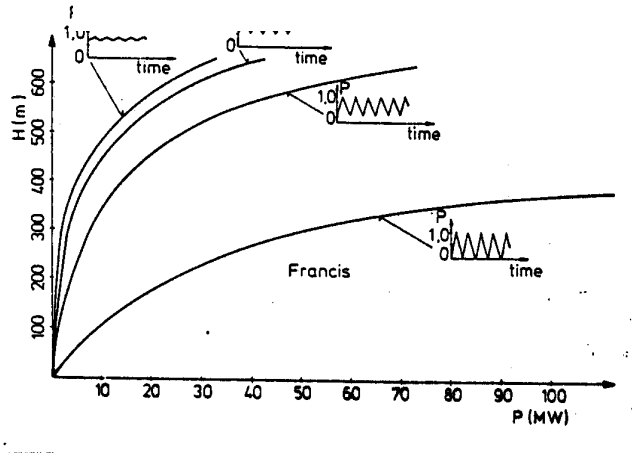

Fig. 5.6 Boundary curves between a Francis turbine based on loss analyses for different kind of operation

The third criteria for the choice between Francis versus Pelton turbine is the down time for repair which is normally related to sand erosion if cavitation and fatigue problems are solved. This is because a well designed turbine will be in operation at least in 10 years without any repair if the water is clean. In sand laden water turbine repair may be necessary each year in order to avoid loss of production caused by decreased efficiency.

Sand erosion

The most exposed areas with respect to sand erosion will be surfaces where the water velocity and/or the acceleration is high.

Such areas are:

For Pelton turbines:	- Nozzles
	- Needles
	- Runner buckets
For Francis turbines:	- Guide vanes and guide vane facing plates
	- Runner inlet and outlet
	- Labyrinth seals

It should be mentioned that high head Francis runners with splitter blades have a lower erosion in sand laden water than ordinary runners without splitter blades. This is because the flow is more uniform and the double number of blades is located at the low velocity region i.e. at the runner inlet. At the outlet of the runner where the velocity is high, the number of blades is normally lower than in an ordinary runner without splitter blades, but also in this place the velocity distribution is very uniform because of the splitter blades.

Since dismantling and assembly of sand eroded parts take considerably shorter time for Pelton than for Francis turbines, Pelton turbines will normally be preferred where severe sand erosion is expected. However, this is depending on the plant's operation schedule. If one or more turbines are stopped for a long period of e.g. one or two months per year, Francis turbines may be chosen even if the water has a high sand content because there will be enough time for an annual repair.

The choice between Francis turbines and Kaplan turbines

The choice between Francis turbines and Kaplan turbines can be made in a similar way as for Francis and Pelton turbines, but the parameters are somewhat different. In general, the Kaplan turbines are chosen below 40 m. Occasionally Kaplan turbines have been used for net head and up to about 75 m due to a wider efficiency curve compared to the efficiency curve for a low head Francis turbine (see fig. 5.7). However, the main advantage of a Kaplan turbine may be that the blades also can be adjusted for variations in head. In this way pressure pulsations and cavitation can be avoided over the total range of variation in flow and head. For low head Francis turbines, part load operation at higher head than the design head is a general problem which can be avoided by using Kaplan turbines. (It should be noted that the new X blade runner design has an improved part load operation at high head.(Ref. Kværner). Further, a larger capacity of a turbine with smaller dimensions and higher speed is an additional advantage for Kaplan turbines. Especially for large machines where capacities of 200-500 m^3/sec is wanted, the Kaplan turbine is chosen because such capacity can be handled by one big high speed unit allowing for a cheaper power house than for the alternative with more Francis turbines or one big Francis turbine with a low speed.

In fig. 5.8 typical efficiency curves for the two types of turbines around the borderline are drawn. It can be seen that the efficiency curve of the Francis turbine has a more narrow shape with a higher peak than the curve for the Kaplan turbine.The reason for the latter is because the Kaplan turbine has adjustable runner blades where the blade angles can be adjusted also for a large variation in head. As shown in the figure, each position of the runner blades gives a new efficiency curve, while the envelope curve gives the total efficiency curve for the turbine. This implies that the Kaplan turbine is more favourable if the turbine runs on part load and the efficiency is the deciding criteria.

In fig. 5.8 the efficiency hill diagram from model turbine tests is illustrated qualitatively for use for a prototype turbine with variation of guide vane angles α and runner blade angles φ. By using reduced flow $Q/\sqrt{2gH}$, speed $n/\sqrt{2gH}$ and dimensionless ratios relative to best efficiency, the diagram can be used to determine the best combination of α and φ as illustrated.

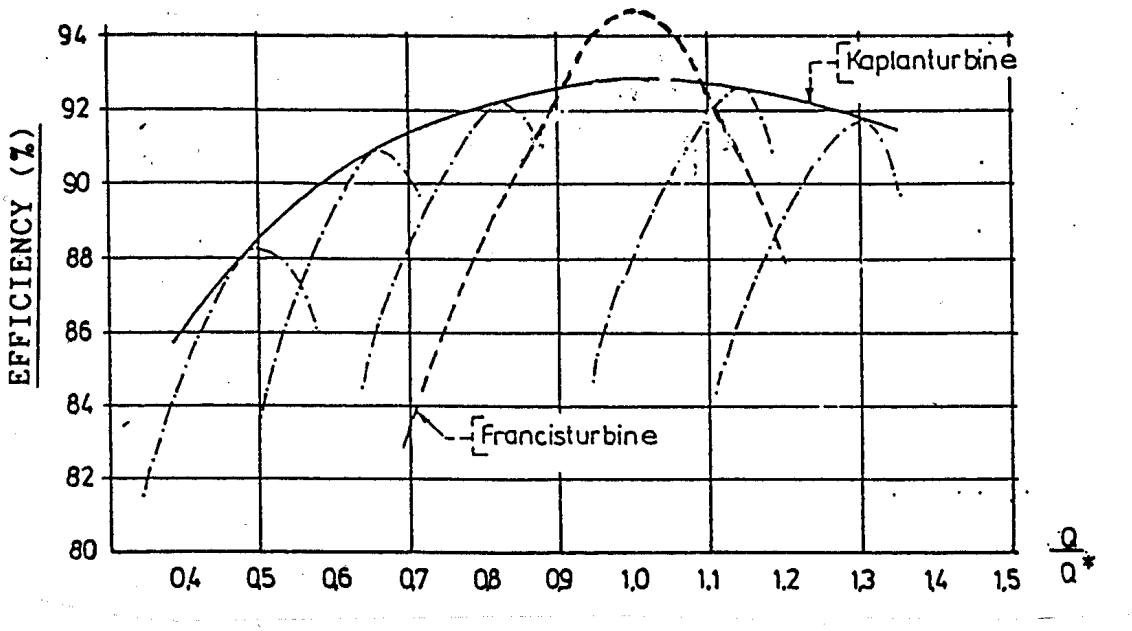

Fig. 5.7 Comparison of efficiency curves for Kaplan and Francis turbines.

The upper economic/practical limit of head for Kaplan turbines is in the range up to 70 m, but in extreme cases Kaplan turbines have been built also for 75-80 m head. The head limit is caused by mechanical strength problems in hub and blades.

Choice between vertical Kaplan turbines and Bulb turbines

Where the head is low, Bulb turbines will be an alternative to the Kaplan.

The advantage of Bulb turbines is clearly seen where the powerhouse is built inside the dam.
In fig. 5.9 a, it is illustrated that the space required for Bulb turbines is much smaller than for the spiral casings of Kaplan units. Further, the necessary depth of the draft tube of a Kaplan turbine is a disadvantage for this turbine type (see fig. 5.9b). However, if the powerhouse is excavated in rock on the riverbed besides the dam, Kaplan turbines will have an advantage because the necessary width of the excavated powerhouse is less than for a Bulb turbine powerhouse due to the vertical orientation of the shaft.

There will be an upper limit of head for a Bulb turbine because of the concentrated hydraulic load on the concrete foundation through the stress carrying ribs connecting the bulb and the concrete. The net head will normally be limited to 15 m for this reason.

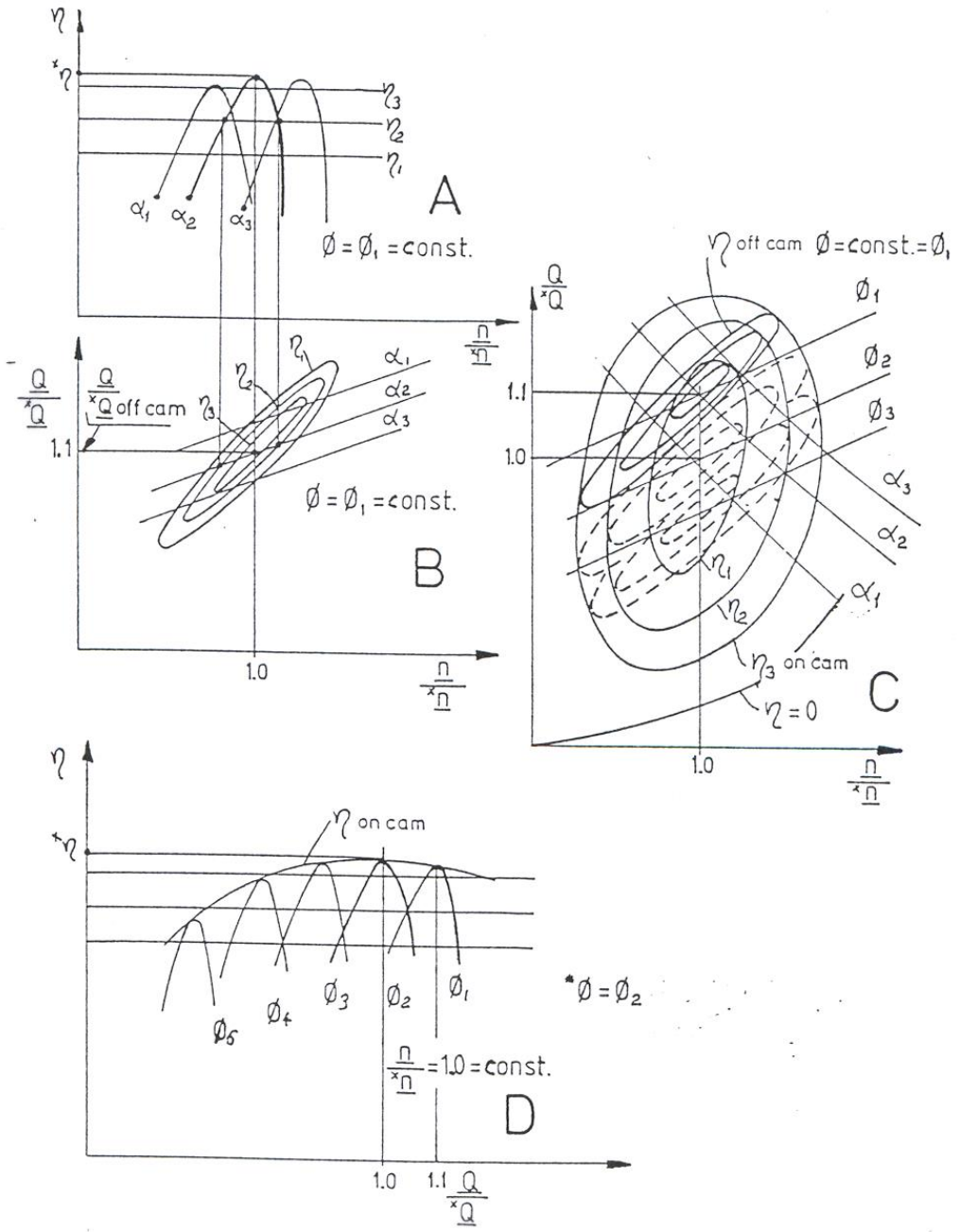

Fig. 5.8 Illustration of the build up of the efficiency hill diagram for variation in flow and speed of a Kaplan turbine based on model tests.

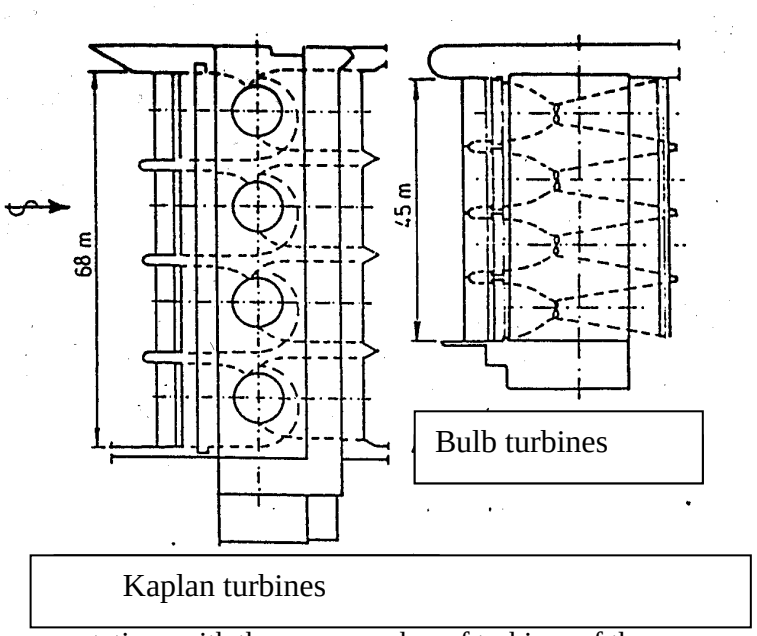

Fig. 5.9a Two German power stations with the same number of turbines of the same capacity and 7.25 m head in both cases..

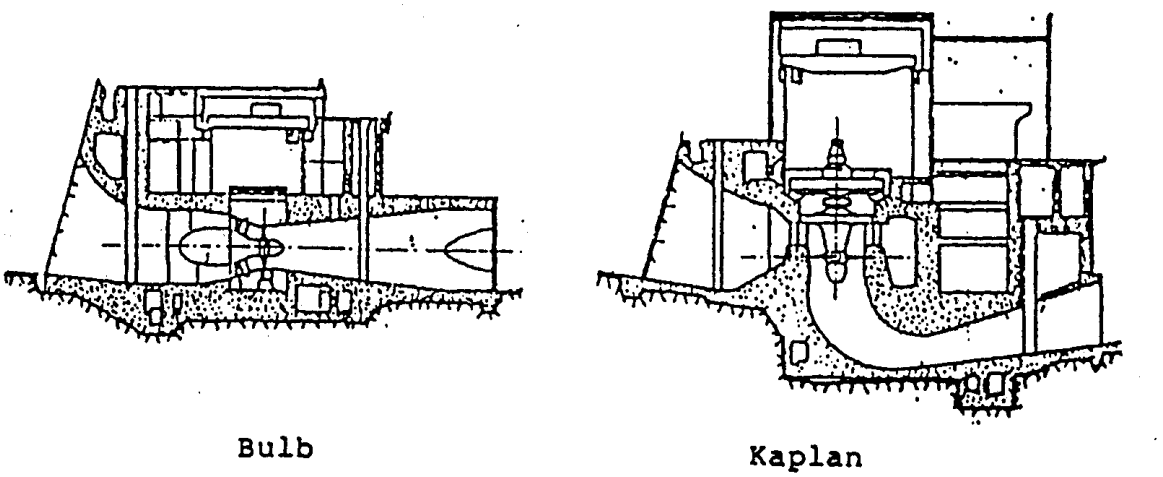

Fig. 5.9b Comparison of a Bulb turbine and a Kaplan turbine.

5.2. Definition of parameters required for determining types and sizes of turbines

In order to determine the size and shape of a turbine, it is convenient to use dimensionless relative values. The dimensionless so called reduced values of velocity, flow and speed number, have been used in Norway since 1916 in order to establish suitable parameters for turbine design. [The speed number is dimensionless and is proportional to the speed factor as defined by the new IEC code published in 1995. (See also [Ref.5])]. The reduced velocity is the velocity in question (absolute or relative velocity) divided by the absolute highest possible velocity which is obtained if the total net head is transferred to kinetic energy.

The reduced values denoted by underlined letters, are defined in chapter 10.3 and in the following page.

The absolute velocity

$$\underline{c} = c / \sqrt{2gH} \qquad (5.1)$$

In the same way the relative velocity yields

$$\underline{w} = w / \sqrt{2gH} \qquad (5.1)$$

and the circumferential speed

$$\underline{u} = u / \sqrt{2gH} \qquad (5.1c)$$

Also the angular velocity may be treated in the same way, but this value will not be dimensionless $\omega = n \cdot \pi / 30$ where: (n = rotational speed RPM).

$$\underline{\omega} = \omega / \sqrt{2gH} \quad [1/m] \qquad (5.2)$$

For the turbine capacity of the unit the turbine flow may also be treated as a reduced, but not dimensionless value i.e.

$$\underline{Q} = Q / \sqrt{2gH} \quad [m^2] \qquad (5.3)$$

The capacity has the dimension m^2 and will then be proportional to the outlet cross section of the turbine. In other words $\underline{Q}$ is a measure of the cross section of the turbine outlet.

If we combine the reduced angular velocity of the turbine multiplied with a radius we get the dimensionless circumferential speed. Then it is convenient to use the square root of the capacity $\underline{Q}$ which will be proportional to the outlet radius and to use this dimensionless circumferential speed as a speed number.

Traditionally, the capital Greek letter Ω has been used for the speed number and the equation yields: (see chapter 6.1)

$$\Omega = \underline{\omega} \sqrt{\rho} = \omega \sqrt{Q} / (2E)^{0.75} \qquad (5.4)$$

The advantage of using the speed number is that it is dimensionless. (In the IEC code [Ref. 5] a new **specific speed** has been introduced which also is dimensionless $\mathbf{N_{QE} = nQ_1^{0.5}/E^{0.75}}$ where n = Cycles/sec and Q_1 is the discharge flow through the the high pressure reference section and E is the net head of the turbine. This is also a dimensionless number, but the explanation of Ω has a better physical meaning and in this book Ω will be used.)

For dimensioning of turbines the flow, head and speed at best efficiency point are normally used denoted by asterix i.e. *Q = flow *ω = angular speed (rad/sec) Then the following expression for the CAPACITY or size of the turbine is obtained from eq (5.3).

$$^{*}\underline{Q} = {}^{*}Q/\sqrt{2gH} = \underline{C}_{m2}\,\pi D_2^2/4\sqrt{2gH} \quad (m^3) \quad \text{where } D_2 = \text{outlet diameter} \tag{5.5}$$

In addition, the speed number that shows the shape and type of turbine is given by:

$$^{*}\Omega = {}^{*}\omega\sqrt{{}^{*}Q}/(2E)^{0.75} = \sqrt{\pi}\;\underline{u}_2^{1.5}\;\sqrt{\tan(\pi - \beta_2)} \tag{5.6}$$

where E = gH, $\underline{u}_2 = u_2/\sqrt{2E}$ and β_2 is the blade outlet angle. See also chapt. 9.1 eq. (9.4).

The conventional scaled flow, speed and output

Traditionally the capacity has been expressed by the unit flow i.e. the flow for a turbine with 1 m outlet diameter operating at 1 m net head:

Further the value for unit speed has been the speed of a turbine with one m diameter operating at 1 m net head. In the same way the unit output may be defined.

Then the following expressions for unit flow, speed and output yields:

Unit flow	$Q_{11} = Q/(D_2^2 \cdot H^{0.5})$	(5.7)
Unit speed	$n_{11} = n\,D_2/H^{0.5}$	(5.8)
Unit output	$P_{11} = P/(D_2^2 \cdot H^{1.5})$	(5.9)

These values are not dimensionless unless multiplied by D=1 m and H=1 m to compensate for D_2 and H in the three expressions above. Then, the best known traditionally used parameters for determining the shape and size of a turbine or pump may be the specific speed.

The new version of specific speed in the IEC code referes as mentioned above to nominal flow and head and will not be used in this book for dimensioning of turbines:

$$\mathbf{N_{QE} = nQ_1^{0.5}/E^{0.75}} \tag{5.10}$$

This expression for the specific speed is proportional to the speed number when substituting for E = g*H and Q_1 = nominal flow (m^3/s). However, the formula has no physical meening in the same way as the speed number and also Q_{11} and n_{11} and P_{11}.

The old version in the IEC formula for **specific speed** was not dimensionless and is not used in this book but shown as a back ground for comparision when studying the litterature: The equation for specific speed yields:

$$n_s = n\sqrt{P}/H^{1.25} \tag{5.11}$$

(Where $P = \rho\, gQH\eta\, 10^{-3}$ kW and n = RPM)

The old version includes the efficiency and for this reason it will not be recommended.
In addition to the described parameters, the flow coefficient and pressure coefficient has been commonly used especially for reversible pump turbines and pumps.
These parameters are:

The flow coefficient

$$\phi = c_m / u \qquad (5.12)$$

where c_m is the inlet meridional velocity and u is the circumferential speed at the turbine runner inlet (or outlet for a pump impeller).

The pressure coefficient

$$\psi = H/(u^2/g) \qquad (5.13)$$

Here H is the pressure head across the turbine or pump.

As described above, it should again be noted that in the **new IEC** code [Ref. 5] for hydraulic turbines, the pressure water head has been substituted by the specific energy. **E=gH** and the units for speed **n (RPM)** has been substituted by revolutions per **sec (RPS).** Then the Norwegian parametres will be mainly used when studying turbine design in this book.)

5.3. Main dimensions and hydraulic design

General philosophy

The basic data for the hydraulic dimensions are:

- Nominal flow Q_n (m^3/sec) (or output P(kW)).
- Nominal head H (m) (also called net head).
- Proposed turbine setting H_s (m) [i.e. the distance from the turbine runner reference point (according to the IEC code) to the tail water level. H_s is negative if the turbine center or reference point is below the tail race level. For some turbine types the IEC reference point is different from the turbine center)[Ref. 5]].

The hydraulic design of a water turbine normally starts with the suction side. The important geometrical parameters here are the outlet angle of the blade at the maximum diameter and the circumferential speed i.e. the angular velocity multiplied by the outlet radius of the runner.

In order to avoid cavitation i.e. vapour bubble formation caused by low pressure which is depending on the velocity of the flow, the local velocity must be limited so the pressure stays above vapour pressure. Due to this a limit has to be set on the circumferential speed of the runner as well as the meridional velocity component of the flow. This limitation depends also on the outlet angle of the blades, the number of blades and the curvature of the blades and if rotation of the draft tube flow is accepted at best efficiency flow (see chapter 10).

The inlet conditions of a runner for a reaction turbine will be based on how big fraction of the specific energy should be converted into kinetic energy (velocity head) at the inlet of the runner. By means of the Euler's turbine equation the tangential component of the absolute velocity = c_{u1} can be found and then the chosen meridional velocity at the blades inlet together with c_{u1} gives the inlet velocity (see chapter 8).

Example of design of a runner for a Francis turbine

The parameters used will be different for different manufacturers and in this chapter only a general guideline will be given.

Cavitation limits and choice of blade angles

The cavitation limit is based on the absolute pressure at the runner outlet according to Bernoulli's equation expressed in eq.(5.14) including the draft tube friction loss and bend loss. (See also chapters 9.2 and 10.3). Note that h_2 is the absolute pressure in m W.C. and that h_3 includes the barometric pressure = h_b in m W.C when calculating cavitation conditions at the runner outlet. (Note that point 2 in fig 5.10 should refere to the runner outlet for large turbines.)

$$h_2 + c_2^2/(2g) + Z_2 = h_3 + c_3^2/(2g) + J_3 + Z_3 \qquad (5.14)$$

In this equation the specific kinetic outlet energy head ($c_3^2/2g$) is normally less than 0.5 [mWC].
The following expression is obtained by regarding fig 5.10 where Z_3 will be the vertical distance from the draft tube outlet (point 3) to the reference level. Normally the distance between the level at the runner outlet (for large turbines) 2 and the water level outside the draft tube is denoted as the suction head = H_s, as shown in fig. 5.10.
By studying fig. 5.10 and using absolute outlet pressure including the barometric pressure h_b, we can be substituted for h_3 in eq.(5.14) by $\mathbf{h_3 = Z_2 - Z_3 - H_s + h_b}$ in eq. 5.14 remembering that H_s has a negative value if point (2) is below the water level outside the draft tube.
Then we find following equation:

$$h_2 = -H_s + h_b + \frac{c_3^2}{2g} + J_3 - \frac{c_2^2}{2g} \qquad (5.15)$$

$J_3 = \zeta_3 c_3^2/(2g)$ is the draft tube friction loss and bend loss. This equation shows that if the outlet velocity c_2 is too high, the pressure h_2 may be too far below atmospheric pressure so "boiling" or cavitation occurs. Then the following equation for the acceptable absolute pressure = h_2 may be established by the requirement that h_2 shall be higher than the vapour pressure = h_{va}.

$$h_2 = -H_s + h_b - \left(\frac{c_2^2}{2g} - \frac{c_3^2}{2g} - J_3 \right) > h_{va}$$

Then, after rearranging the equation the following requirement is obtained in order to determine the value of the turbine setting H_s and define the available NOMINAL POSITIVE SUCTION HEAD = $NPSH_A$:

$$-H_s + h_b - h_{va} = NPSH_A > \frac{c_2^2}{2g} - \frac{c_3^2}{2g} - J \qquad (5.16)$$

Here the right hand side, THE POSITIVE SUCTION HEAD required = $[c_2^2/(2g) - c_3^2/(2g) - J] = NPSH_R$ is depending on the turbine parameters and is a requirement for the turbine design also denoted as the required NET POSITIVE SUCTION HEAD for the turbine. The left hand side is the available suction head $NPSH_A$ of the power plant, including the necessary submergence of the runner ($-H_s$) the barometric pressure (h_b) and the vapour pressure (h_{va}) which depends on the water temperature.

The relationship between the velocity head below a runner and the cavitation performance of a runner denotes a complex problem that can finally be determined after the prototype has been put into operation. However, by means of a cavitation test of a model turbine that is homologous to the prototype the value of NPSH where cavitation occurs (i.e. the critical value of $NPSH_{cr}$) for the prototype can be calculated from the Thoma cavitation number σ = NPSH/H measured on the model.

The outlet velocity and local low pressure zones in the runner have the main influence on the cavitation behaviour. Since the test head of the model normally is lower than for the prototype, the $NPSH_{cr}$ value of

the prototype must be found indirectly calculated from the Thoma cavitation number as mentioned above by running the model in a closed test loop and decreasing the pressure at the draft tube outlet until cavitation occurs.
The critical value of the net positive suction head i.e. $NPSH_{cr}$ found by model test must be less than the required value $NPSH_R$ described in the turbine contract where a safety margin between $NPSH_A$ and $NPSH_R$ must be included.

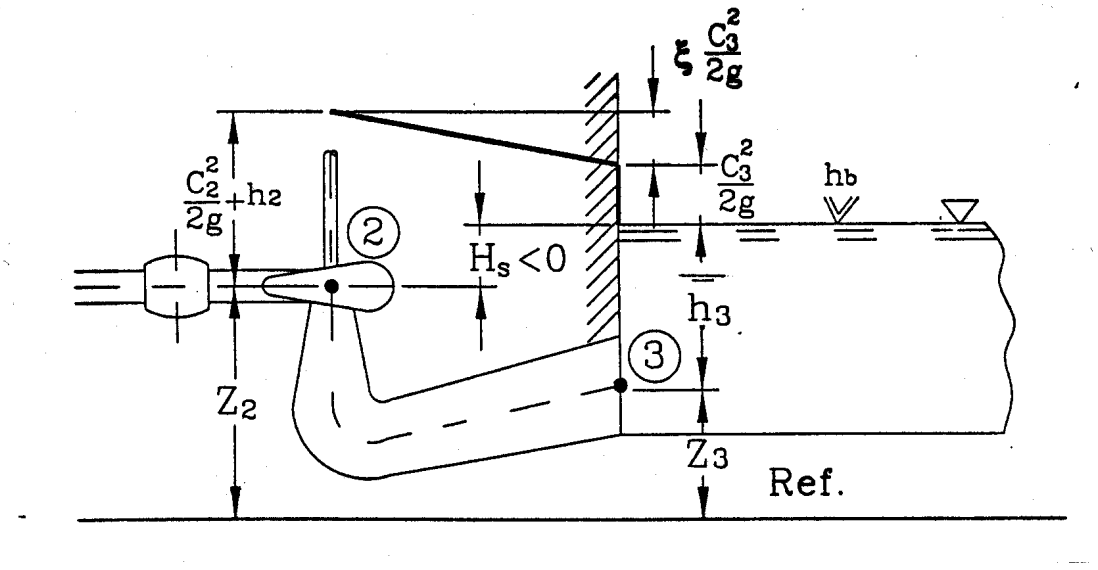

Fig. 5.10 The specific energy at runner outlet and draft tube outlet

The definition of the Thoma cavitation number is as mentioned above:

$$\sigma = \frac{(NPSH)}{H} \tag{5.17}$$

The nominal positive suction head for the turbine may also be found as a turbine parameter empirically determined from experience by the turbine manufacturer. The critical value of the cavitation is found by means of the pressure where the efficiency due to cavitation, drops below the value for cavitation-free operation.

For this value $\sigma=\sigma_{cr}$ is expressed by the following equation. (See fig. 5.11)

$$\sigma_{cr} = \frac{(NPSH)_{cr}}{H} \tag{5.18}$$

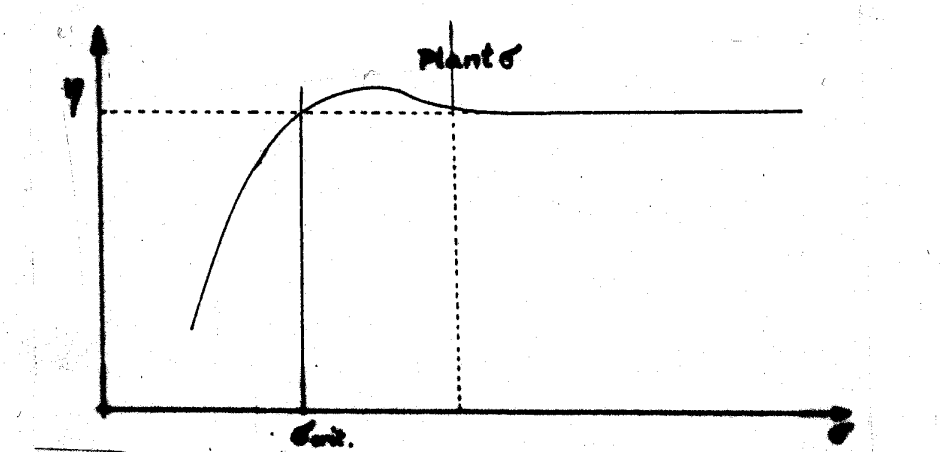

Fig. 5.11 Illustration of the critical value of $\sigma=\sigma_{crit}$ and example of cavitation for the choice of σ plant for a Francis turbine.

Further explanation may be found in the IEC code [Ref. 5]. (Note: In the new code 995 NPSE is used instead of NPSH i.e. E = gH = specific energy Joule/kg instead of m WC). From experiences, turbine manufacturers normally have established formulas in order to find the critical value of the required $NPSH_{cr}$ for use in contract negotiations. Such a formula has been introduced in chapter 9, eq. 9.6 and in chapter 10 eq. 10.16 which yields:

$$NPSH_R = a\, c_{m2}^2/(2g) + b\, u_2^2/(2g) \qquad (5.9)$$

The constants a and b are given and discussed in chapter 9, eq. (9.6), and the constant a and in particulary b is depending on the specific speed and shape of the runner.

Example of a dimensioning procedure of a high head Francis turbine runner

As an example, nominal data for flow and net head may be given: $Q_n=36$ m^3/sec, H=400 m. Choice of best efficiency point parameter may be $\kappa=1.2$ (*denotes best efficiency point).
$Q_n=1.2^*Q$ - for $\kappa=1.2$
i.e. $^*Q=30$ m^3/sec

Theoretical flow angle at maximum outlet diameter D_2 may be chosen to $(\pi-\beta_2)=17.5^o$ (Normal range $13^o < (\pi-\beta_2) < 19^o$). The outlet flow angle is 1-2^o larger than the blade angle depending on the shape and number of blades.

Choosing max rim speed
$u_2 = 41$ m/sec for a moderate setting. (40 m/sec $< u_2 <$ 45 m/sec. for high head turbines). Also higher values have been used, but the noice and vibrations increases with the speed and $u_2 >$ 45 m/s is not recommended.

The meridional velocity $c_{m2} = 41 \cdot \tan 17.5^0$ at the outlet of runner at best efficiency with no rotation in draft tube will get a normal value in this case. (See the outlet velocity vector diagram in fig. 5.12.)

If a higher value of u_2 is chosen, the blade outlet angle should be reduced.

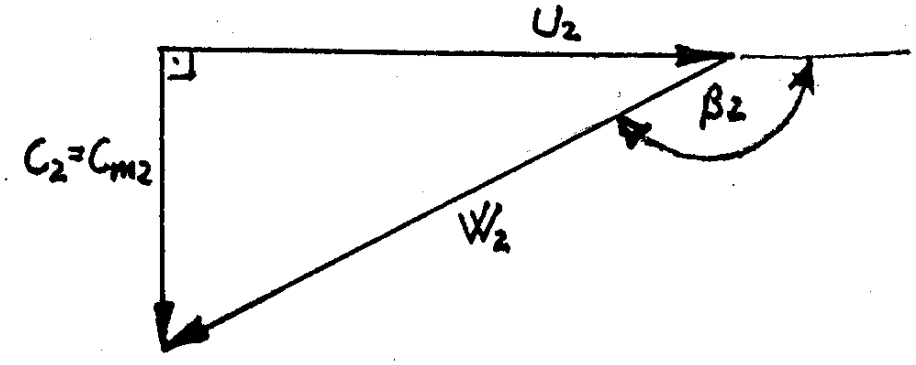

Fig. 5.12 Outlet velocity diagram

Then the following meridional velocity will be obtained::
$c_{m2} = u_2 \tan(\pi - \beta_2) = 41 \cdot \tan 17.5 = 12.93$ m/sec

The outlet diameter may now be found by assuming c_{m2} to be constant across the outlet area.

$$\underline{D_2 = \sqrt{4 * Q/(\pi\, c_{m2})}} = 1.719\, m$$

The speed of the turbine will then be according to the chosen values of u_2 and β_2
$D(n \cdot \pi/60) = u_2$

$n = 60u_2/(\pi D_2) = 60 \cdot 41/(\pi \cdot 1.719) = 455.5$ RPM

This will not normally be a synchronous speed and an adjustment of the speed has to be made by adjusting the circumferential speed u_2 and the diameter. The outlet angle β_2 may also be adjusted, but for a turbine manufacturer the geometry must normally be homologous to an existing model turbine i.e. there are restrictions on the outlet angles of the blades if not a new or modified runner shall be made.

In order not to increase the necessary submergence of the turbine, the speed should be <u>reduced</u> to nearest synchronous speed. The synchronous speed is found by checking the formula

$n = 3000/Z$ (5.20)

where Z=number of pairs of poles in the generator for an electric grid with f=50 Hz. Choosing Z=7 gives n=428.6 RPM.

If the outlet angle β_2 shall be unchanged as well as the best efficiency flow $^*Q$, the velocity vector diagram will be homologous and the following equations will be valid.

$$\frac{\pi D_2^2}{4} c_m = {}^*Q$$

1. $D_2^2\, c_{m2} = \text{const.} = 38.21$
2. $c_{m2}/u_2 = \text{const..} = 0.315$
3. $u_2 = n\, \pi\, D_2/60$

Now by eliminating c_{m2} and u_2 one finds $D_2 = f(n)$ i.e. $D_2^2 = 38.21/(c_{m2}/u_2)u_2$

1 and 2 $D_2^{2} = 38.21/0.315\ u_2 = 121.3 \cdot u_2$ i.e. $u_2 = D_2^2/121.3$

1-2 and 3 $121.3/D_2^2 = n\pi D_2/60$

$D_2 = (121.3 \cdot 60/(\pi \cdot n))^{1/3}$ and n=428.6 RPM

Then

$\underline{D_2 = 1.755 \text{ m}}$

and

$\underline{u_2 = 39.38 \text{ m/sec}}$

$\underline{c_{m2} = 12.42}$

(Control $^{*}Q = c_{m2} \cdot \pi D_2^2/4 = 30.04 \text{ m}^3/\text{sec}$.)

The inlet dimensions may now be found by means of the Euler turbine equation which is identical to eq. (8.55), see chapter 8.4)). This equation proves that the energy converted by the runner will be:

$E_1 - E_2 = u_1 c_{u1} - u_2 c_{u2} = gH \eta_h$

The hydraulic efficiency η_h is as described earlier in this book, the ratio of the available energy which is transferred to (and converted to mechanical energy) by the runner divided by the net energy drop from the upstream to downstream side of the turbine = gH . (Mechanical loss disk friction loss and leakage loss is not taken into consideration in the hydraulic efficiency.)

That is:

$$\eta_h = \frac{u_1 c_{u1} - u_2 c_{u2}}{gH} \tag{5.21}$$

By using dimensionless reduced velocities as explained in chapter 8 eq. (8.55) and chapter 10 eq. (10.2) the following equation is obtained:

$$\eta_h = 2(\underline{u_1}\,\underline{c_{u1}} - \underline{u_2}\,\underline{c_{u2}})$$

For the design of the turbine it has been assumed that we have the best efficiency where there is no rotation in the draft tube i.e. $c_{u2}=0$. Further an hydraulic efficiency of 96% is assumed and that approximately 50% of the energy in front of the runner is converted to kinetic energy.

I.e. $c_1^2/(2g) = 0.5\ H$ or $c_1^2/(2gH) = 0.5$ or $\underline{c_1} \approx 0.7$.

The inlet velocity vector diagram is drawn in order to try to obtain the stagnation point on the blade inlet tip and the inlet angle so the relative velocity does not lead to separation and possible inlet cavitation (especially for low head turbines) (see fig. 5.13).

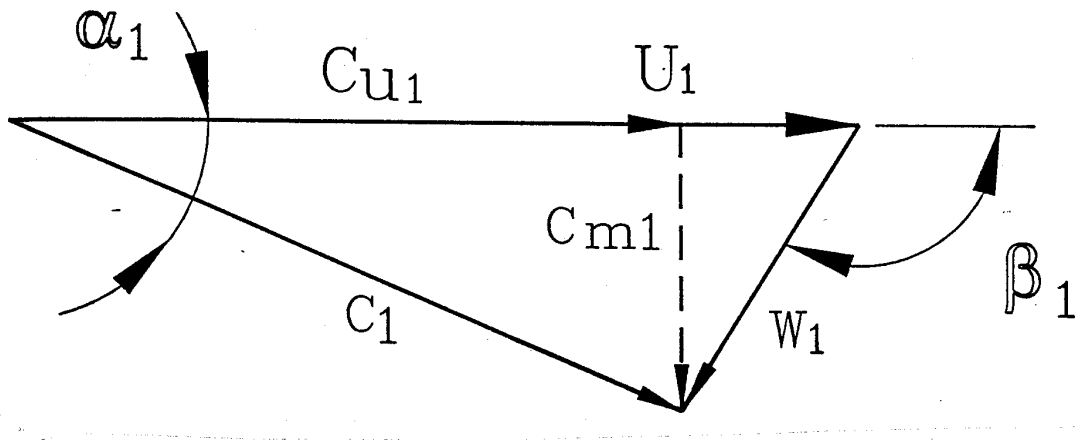

Fig. 5.13 The inlet velocity diagram

Besides the assumption that $\underline{c}_1 \approx 0.7$ eq. (5.22) is also used when assuming the hydraulic efficiency $\eta_h = 0.96$ and assuming $c_{u2} = 0$. Then following equation yields:

$\underline{u}_1 \, \underline{c}_{u1} = 0.48$

The inlet velocity diagram clearly illustrates that the smallest variation of the inlet flow angle with variation in the guide vane angle is obtained if the angle between the absolute and relative velocity in close to 90° at best efficiency point of operation. The reduced dimensionless circumferential speed of the blade inlet then from experience may be chosen to 0.72 for a low specific speed runner and then $\underline{c}_{u1} = 0.48/0.72 = 0.67$.

The inlet diameter of the runner can now be found by the absolute value of u_1:

$$u_1 = 0.72\sqrt{2gH} = 0.72\sqrt{2 \bullet 9.81 \bullet 400} = \underline{63.78 m/\sec}$$

The inlet diameter of the runner will then be

$D_1 = u_1 \cdot 60/(n \cdot \pi) = 63.78 \cdot 60/(428.6 \cdot \pi) = 2.842$ m

The meridional velocity at the inlet may from experience be chosen approximately 10% lower than at the outlet of the runner in order to obtain a slight acceleration of the meridional flow. (However, this choice will be different for different manufacturers due to the philosophy of blade shape etc.)
Choosing: $c_{m1} = 0.9 \cdot c_{m2} = 0.9 \cdot 12.42 = 11.18$ m/sec

Then the height of the blade at the inlet=B, can now be found by means of the equation of continuity as follows.

$B_1 = *Q/(\pi D_1 c_{m1}) = 30/(\pi \cdot 2.842 \cdot 11.18) = \underline{0.300 \text{ m}}$

(Note: In this preliminary calculation the displacement of the blades thickness which may be (approx) 10%, has been neglected. By taking the blade thickness into consideration the blade angles must be corrected due to the increased relative velocity or meridional velocity c_m).

A drawing of the meridional section of the runner, the guide vanes, stay ring and spiral case is shown in fig. 5.14. The main dimensioning parameters are marked with arrows.

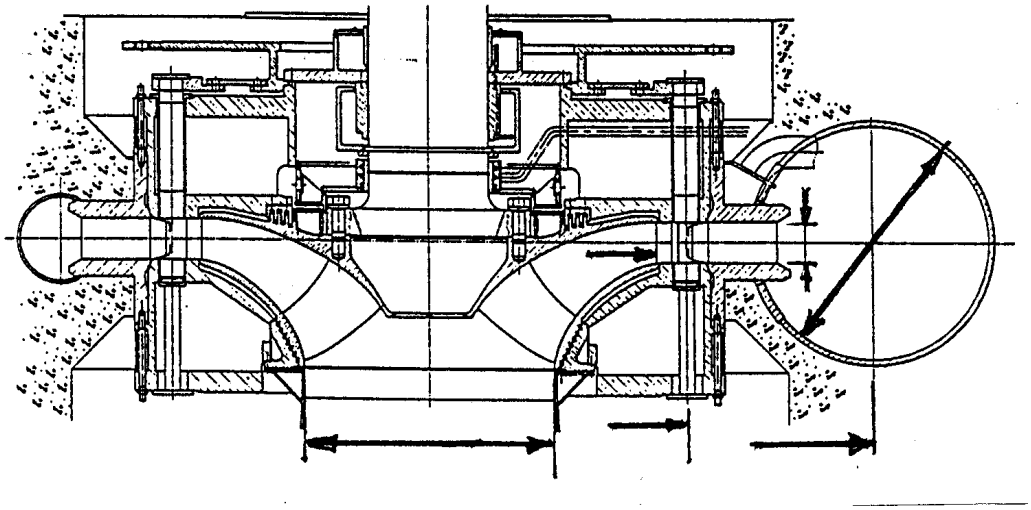

Fig. 5.14 Main dimensions of a high head Francis turbine.

The cross section area of the inlet of the spiral case may be chosen to be close to the cross section area of the runner outlet.

However, different manufacturers will use a different cross sections of the spiral casing inlet. A variation of the inlet velocity versus the runner outlet velocity will also be a function of the specific speed of the turbine.

The Kaplan turbines

The design of Kaplan turbines is based on the foil cascade theory during the dimensioning stage. In this book example of the dimensioning of the runner will only be given in principle form.

An example such formula may be as follows:

$$D_i=(0.85+0.3\cdot^{*}\Omega)D_2 \qquad (5.23)$$

This leads to a somewhat smaller inlet diameter of the spiral case versus the outlet diameter for a high head turbine (low specific speed) where the outlet energy from the runner is a small part of the total energy.

Main dimensions of a Pelton runner

A Pelton turbine is an impulse turbine and not a reaction turbine and the total energy is converted totally to kinetic energy at the runner inlet (see chapter 5).

The Euler equation eq. (5.22) then gives if $\eta_h=0.96$ and $\underline{c}_{u1}=1.0$ and $\underline{c}_{u2}=0$

$\underline{u}_1\underline{c}_{u1} = 0.48$ and $\underline{u}_1 = 0.48$

Then the pitch diameter can easily be found. The bucket width may be determined as function of the jet diameter as follows. [Note: smaller buckets than the formulas given below will be used by some turbine manufacturers].

1-2 jet turbine	$B=3.0\ d_j - 3.3\ d_j$ - where d_j=jet diameter
4-6 Jet turbine	$B=3.3\ d_j - 3.4\ d_j$

The shape of the buckets must be made so the relative flow angle of a particle on the jet surface and the backside of the buckets inlet at the first touch of the jet in the middle does not exceed 3-6^o for high head turbines and 10^o for low head machines. This guide line is given in order to avoid cavitation or droplet pitting. For further information see [Ref. 6] and [Ref. 7].

The diameter of the runner pit lining for a vertical turbine may be roughly calculated by following formula:

$$D_L = D_R + K \cdot B \qquad (5.24)$$

Here D_R = runner pitch diameter, D_L = diameter of pit liner, B = bucket width and the constant K will have value $8<K<9$ with increasing value for increasing number of jets. However, larger diameter of D_L gives less problem with splashing and loss of performance. (It should also be noted that pit liners with hexagonal shape for 6 jet turbines pentagonal shape for 5 jet turbines and quadratic shape for 4 jet turbines have been used).

The height from the center line of the runner to the ceiling of the runner pit will be 2 – 2.5 times the inside bucket width B. For horizontal Pelton turbines the width of the turbine pit should be approximately 4 times the inside bucket width.In general the hydraulic forces on a Kaplan turbine blade can be found as lift and drag vectorforce components on a single profile and corrected for the effect of the cascade according to the traditional wing theory.
The lift (L) and drag (D) is normally calculated from the simple formulae along a length 1 at constant radius=r with a width dr (see fig. 5.16) (ρ=density of water)

$$L = C_L\ \rho \frac{1}{2} C_\infty^2\ l\ dr$$

$$D = C_D\ \ \rho \frac{1}{2} C_\infty^2\ l\ dr$$

The constants C_L and C_D may be found from tables or diagrams available from NACA or GÖTTINGEN foil profiles corrected for the cascade effect. The optimum angle of the relative inflow direction = δ as a parameter may be found from C_L - C_D diagrams as indicated in fig. 5.17 by choosing the minimum ratio of C_D/C_L which will be the tangent to the curve shown in fig. 5.17. In the diagram the constant $C_L = 0.85$ for a GÖTTINGEN profile for the optimum value of $\delta = \delta_{opt}$.

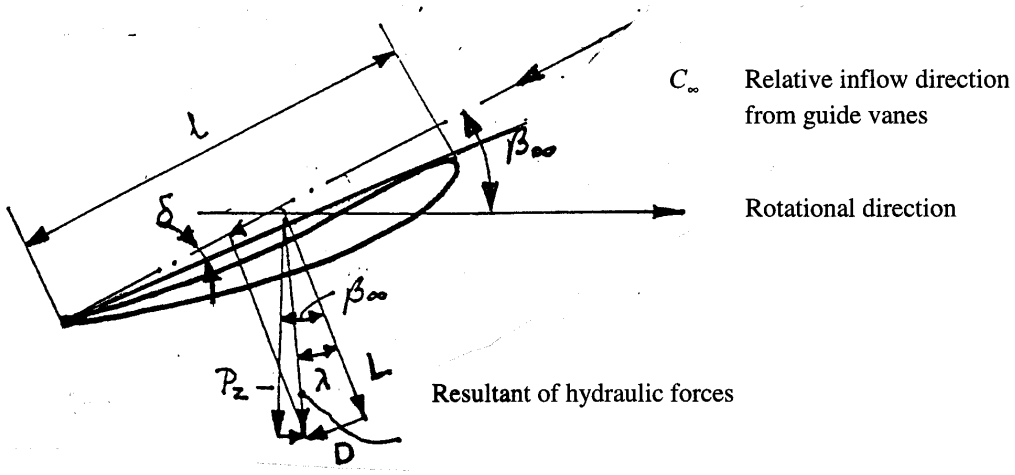

Fig. 5.16 Illustration of lift = L and drag = D forces on a profile with length l in the middle section of a Kaplan blade. Radial stretch = Δr = 10% of the blade length i.e. 5-10 various profiles with increasing thickness must be chosen for the preliminary design.

In fig. 5.16 the lift and drag forces for a profile are shown schematically. By studying the vectors representing L and D, the very large axial forces component compared with the tangential forces component is clearly illustrated especially for a small opening of the runner blades.

For the first layout of a runner the middle section of the profile is normally chosen and the inflow angle will increase towards the hub (and the profile will be thicker for structural reasons). On the contrary the blade angles will decrease towards the tip of the blade due to higher circumferential speed.

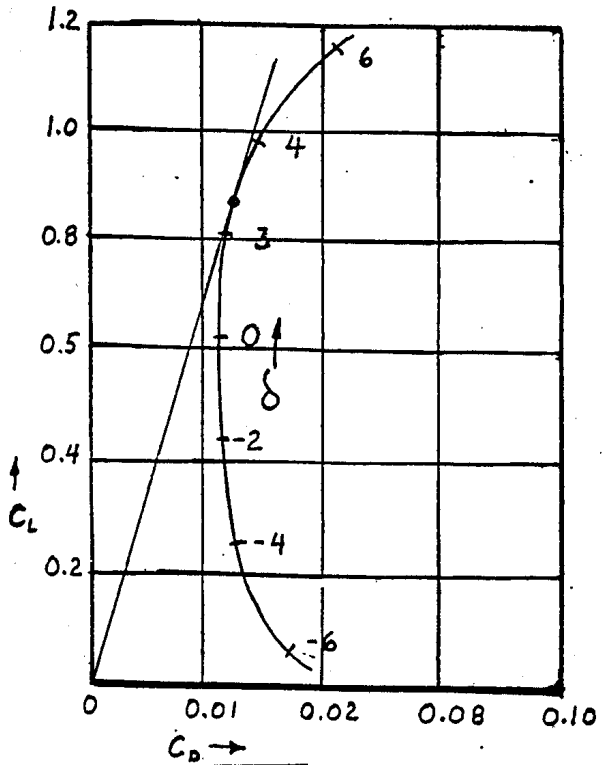

Fig. 5.17 C_L as functions of C_D for Göttingen 480 aerofoil profiles.

A typical Kaplan blade is shown in fig. 5.18. The number of blades will be normally between 4 and 7. However, also 3 blades have been used for extremely low and high heads and 8 blades have also been used for very high heads exceeding 70m. The minimum specific speed of a turbine will depend on the number of blades. The maximum blades stress is found in the fillet in the bolt connection to the pivot. The hub is weakened by the high number of holes for the blade pivots for the lowest specific speeds and the hub stresses limits the maximum number of blades to a maximum of 8.

As the blades are movable the inflow conditions on the runner blades will be adjusted for optimum lift conditions based on the lift and drag components which gives the optimum torque on the turbine shaft and maximum efficiency over a large range of flow and head in operation as was shown in fig. 5.8.

The hydraulic force on a Kaplan blade is found by integrating the values of the resultant vector of lift (L) and drag (D) from the minimum diameter to the maximum diameter.

However, by studying the resultant force it is obvious that a Kaplan runner gives a very large axial force compared to the tangential force, which gives the torque and power of the turbine. Specially at low load the ratio (axial force)/ (tangential force) is unfavourable. Because of the large axial the design of the thrust bearing is important and the increased bearing loss from the hydraulic load from the runner should be subtracted from the turbine efficiency. The thrust bearing is also often a part of the turbine contract and the bearing is located on the head cover of the turbine to avoid transfer of large forces through the generator structure.

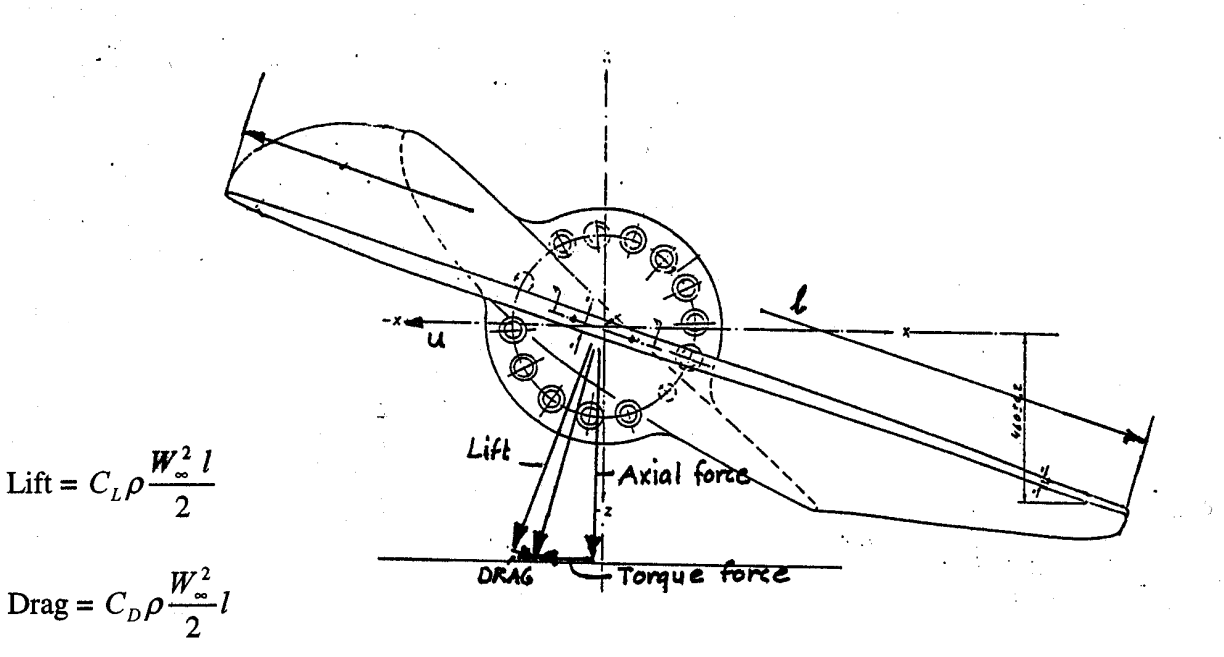

Fig. 5.18 Hydraulic Forces on Kaplan bl

6. TURBINE DESIGN WITH ERECTION AND DISMANTLING PROCEDURES FOR MAINTENANCE WORK

6.1. Introduction

Development of hydraulic turbines during the last 30 years has been concentrated in the following main area:

* Increasing size of the machines, which are designed for higher heads with improved efficiency for a given specific speed.

* With the environmentalist´s protection of rivers by avoiding big dams in industrialised countries, a new trend in the turbine design has also occurred:

* The development of mini turbines with simplified designs and low cost without sacrificing reliability and with acceptable efficiency when operating off the design point.

The reason for building the largest possible units is to lower the kW price or weight/kW ratio and increase the efficiency and thus produce electricity in the cheapest possible way.

The mini turbines are for small rivers and creeks where the environmental requirements demand a minimum of dams and tunnels.

The development of mini turbines is theoretically based upon the hydraulic knowledge from the development of large units and the developing work has been mainly on the production side by simplifying the design with a certain loss in efficiency. It should also be emphasised that experience is needed to carry out a simplification of the structural design.

Inexperienced work shops will have difficulties in producing small hydro turbines with success without having access to laboratories and experts in hydraulic design, structural design and production of hydro turbines. Design of mini turbines is not described in books because the theory and design criteria are based on the knowledge from development of large turbines for which design criteria and production methods are described.

The efficiency of hydro turbines has been constantly improved. Today more than 92 per cent efficiency for low specific speed Pelton turbines and 96 per cent for large Francis turbines has been obtained for prototype turbines made by skilled manufacturers.

6.2. Pelton turbines

General description

The introduction of the vertical multi-nozzle turbines has increased the output of Pelton turbines. (Ref. 21), (Ref. 22).
The most powerful Pelton turbines in operation in Norway are the two 5 nozzles 315 MW turbines operating at 885 m net head and a speed of 300 RPM in Sima Power plant put in to opreration in 1976. With today's technology it will be possible to build reliable Pelton turbines

with a unit output of 700 MW for 1500 m net head and with outputs exceeding 1000 MW per unit for heads up to 2000 m if the water is clean. (Low sand or silt content.)

The development of Pelton turbines has mainly been based upon model tests. However, theoretical analyses of the flow in Pelton buckets have also been carried out. By combining theoretical analysis with high-speed video techniques the knowledge of non-stationary flow over Pelton buckets has increased resulting in an improved efficiency.

Measurement of the velocity distribution in the jets' cross section, which is highly affected by the inlet conditions in bifurcations and nozzles, gives also valuable information for the designer. The shape of the bucket's entrance must be optimised to fit the velocity distribution across the jet. An increase in efficiency depends on an improved solution to this complex problem.

The problem of fatigue in Pelton runners has been under continuous study. Today reliable runners with a lifetime 10^{11} cycles, or more than 50 years, of operation may be built if the alternating peak-to-peak stress amplitudes in the buckets is limited to approximately 45 MPa and the runner is a high quality casting or build with a combined forged/welded method. It sould however be noted that when passing 10^{11} cycles an infinite life time is expcted if no welding and grinding on the buckets are made. This is because such maintenance work introduces local high stresses that may lead to fatigue cracking if defects above critical sizes occurs.

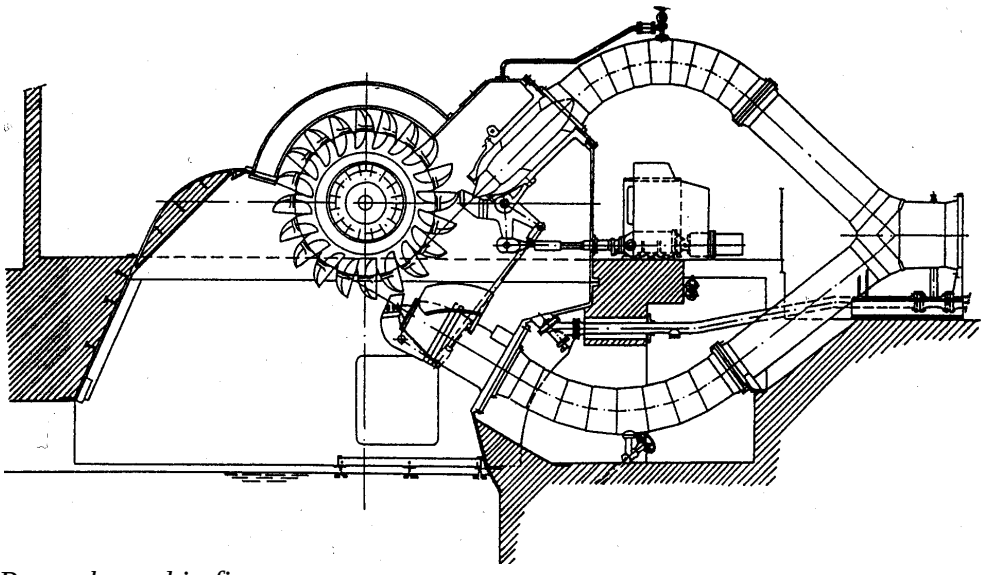

Parts showed in fig.:
Pelton runner, Turbine housing, Deflector mechanism, Inlet bend Wheel hatch cover, Governor cabinet, Inlet bend, Ispection platform with man door, Bifurcafion, Air outlet valve, Bifurcation, Drainage valve, Brake jet pipe.

Fig. 6.1a Horizontal Pelton turbine delivered by Kværner for Skjaak Power Plant in Norway, P=31.5 MW H=638m n=500 RPM.

The relatively modern design of a horizontal 2 jets Pelton turbine is shown in fig. 6.1.
.The power plant where this turbine has been installed is Skjaak Power Plant in Norway. The year of commissioning was 1965, but the design represents still a modern turbine with straight flow injectors and fabricated structure.

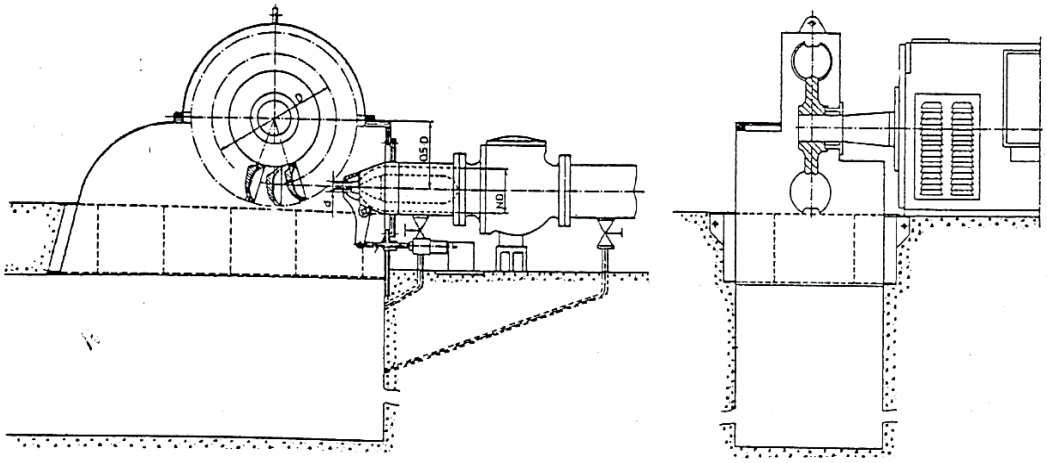

Fig 6.1 b, Horizontal one jet small Pelton turbine operating at around 300 m net head.

The turbine illustrated in fig 61 b, is a typical small hydro which is conected to the main grid, For operation on isolated load a fly wheel is normally required if the turbine is connected to a long penstock.

However, the most commonly used Pelton turbines today are the multi-nozzle vertical units and in fig. 6.2, the 5 jet 288 MW units operating at 1130 m net head for Jostedal Power Plant in Norway is shown.

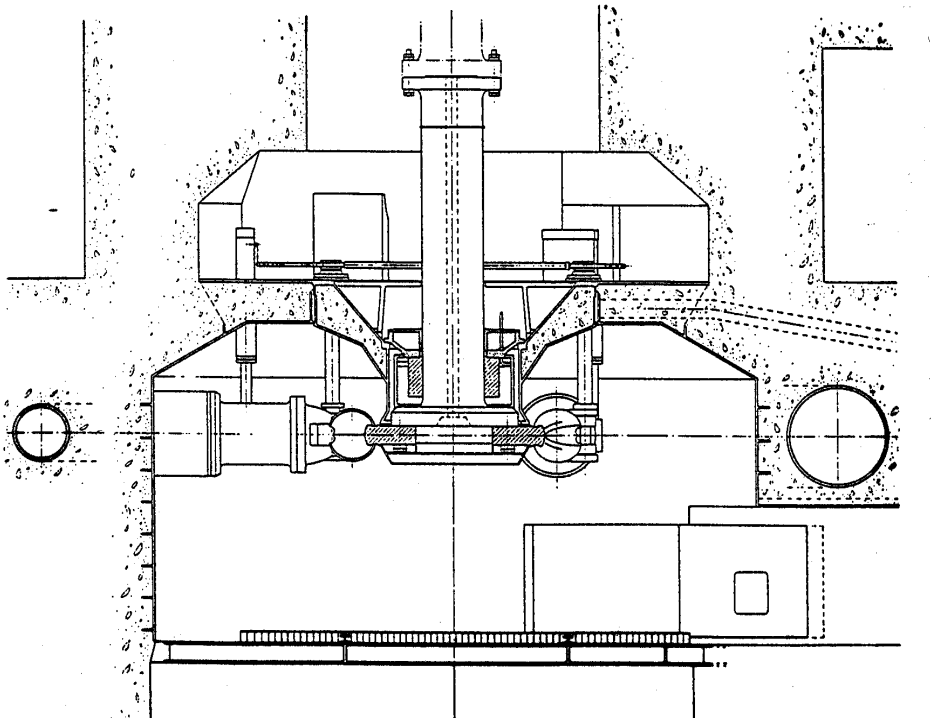

Fig. 6.2 Pelton Turbine for JOSTEDAL POWER PLANT
P=288 MW H_n=1130m n=428.6 RPM

Due to the combination of large dimensions and high pressure the plate thickness will be a critical dimension for such units. High tensile strength fine grain steel materials have been used. In fig. 6.2 the general design of a vertical Pelton turbine is shown. The advantage of a vertical multi-jet Pelton turbine compared with a Francis turbine is the easy access for inspection and maintenance and the simple way of exchanging damaged or eroded components.

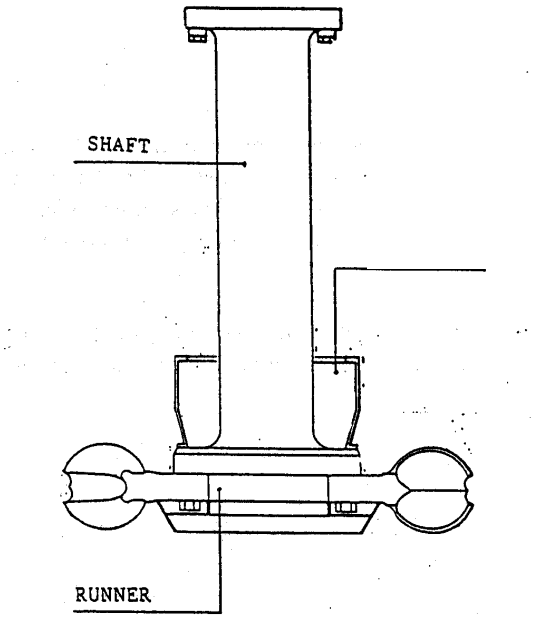

Fig. 6.3 The rotating part of a vertical Pelton turbine (courtesy Kværner)

The design consists of the rotating parts shown in fig. 6.3 i.e. the turbine shaft, the rotating lower oil reservoir for the radial turbine bearing and the Pelton runner.
The rotating energy of the oil in the lower reservoir is utilized to lift the oil up to the upper oil reservoir. A scoop pipe anchored in the bottom of the upper stationary reservoir and reaching down to the outer wall of the rotating reservoir utilizes the rotational energy of the oil and thus "pumps" the oil up to the upper reservoir "through a cooler if necessary". (see fig. 6.4)

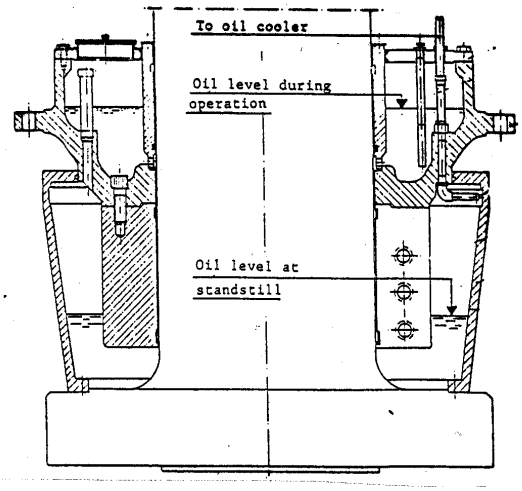

Fig. 6.4 Details of the self lubricated air-cooled bearing of a vertical Pelton turbine made by Kværner.

The upper part and the bearing pad cylinder are split in two halves for erection and dismantling. From the upper reservoir the oil flows through the four rigid, but specially machined bearing pads and down to the lower reservoir again. By locating the scoop close to the wall near the top of the rotating slightly conically shaped reservoir a thin oil film is obtained. (see fig. 6.4) For cooling purposes, cooled air from the tailrace tunnel is flushing the outside of the rotational reservoir. The cooled air is sucked from the tail race tunnel by the low pressure in the centre of the runner pit. There is no need for shaft seal in a vertical Pelton turbine unless the turbine is working with back pressure.

In fig. 6.5 the vertical Pelton unit for Tafjord 5 Power Plant in Norway is shown. This turbine is working with up to 12 m back pressure with maximum tail race water level.

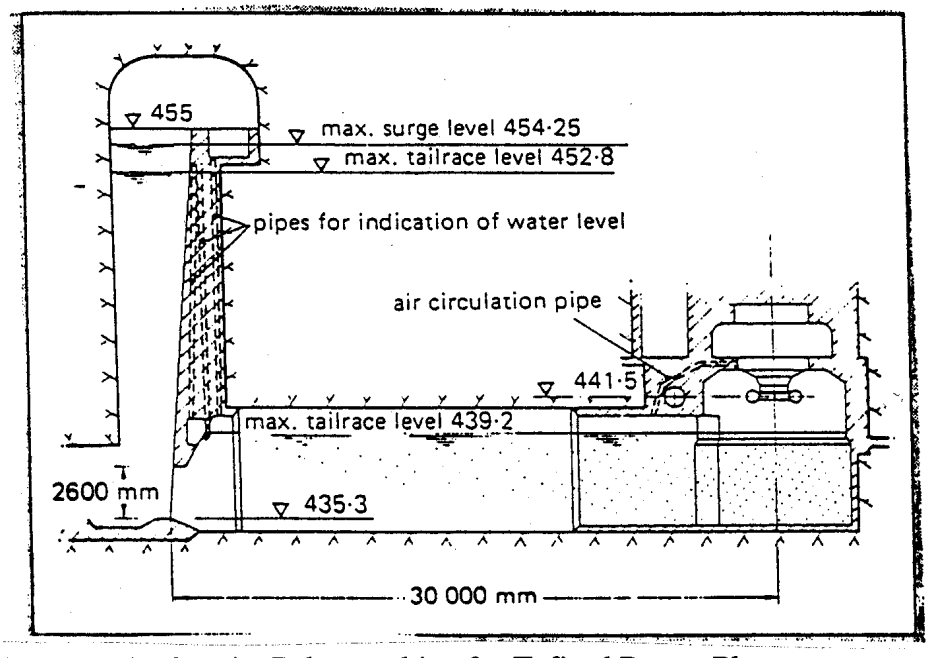

Fig. 6.5 The four jet Pelton turbine for Tafjord Power Plant
P=80MW H=660m to H=810m and n= 500 RPM

Surging of the water level of the surge chamber of the tail race tunnel outside the turbine will also be reduced underneath the runner by a factor of approximately 1:10 due to compression of the trapped air in the runner pit inside the concrete baffle as shown in fig. 6.5. A non-touching labyrinth type shaft seal (locked with 20 m-pressure water) has been used to prevent air leakage from the runner pit.

The turbine bearing for the Tafjord turbine is not located near the flange as shown in fig. 6.4, but above the seal and it is not primary air cooled as for the case shown in fig. 6.4. The Tafjord bearing type is normally used for Francis turbines designed by KVÆRNER. The advantage with the labyrinth shaft seal is that it is running dry without water when the unit is not submerged and the compressor for depressing the water level is not running. It is also important to note that the air leakage through a dry seal is so small that the turbine can operate also without pressure water in the seal. However, energy will be lost by increased air supply from the compressors. As illustrated in fig. 6.5 a baffle located approximately 10 runner diameters downstream of the turbine pit forms an air lock at high tail race level. A long distance from the runner centre to the baffle reduces the amount of air bubbles to escape from

the runner pit. This reduces the compressor capacity which may be designed for approximately 3% air/water flow (Nm^3/s)/(m^3/s) to compensate for possible leakages in the concrete.

For the vertical Pelton turbines the design of the straight flow injectors with internal servosystem and balancing of the hydraulic forces on the needle is the most complicated part of the turbine besides the Pelton runner and the manifold.

In fig. 6.6 an injector made by Kværner is shown. For this injector the hydraulic balancing is obtained by a combination of a hydraulic seal between the needle base and the guidance cylinder (pos. 11) together with a disk spring column. (Note the injector is shown in closed position in the lower half below the centre line in fig. 6.6)

The different parts of the injector are as listed in fig. 6.6. Because competition simplified versions of injectors have been made on order to reduce production cost. The injector shown in fig. 6.6 however, have been produced in a number close to 200 and the first one of this design has been in operation since 1965 with no maintenance work at all. Except for minor production errors no maintenance has been necessary for these injectors except for exchange of the balancing gasket and needle/nozzle units due to sand erosion. In a few cases fractures of disk springs has occurred if the preloading to introduce compression at the inner diameter of the disks.

All parts exposed to abrasion or wear are made of stainless 13% Cr 4% Ni or 16% Cr 5%Ni coated with hard wear resistant material. For clean water the needle tip and nozzle are normally hardened to 300 HB with no hard surface coating.

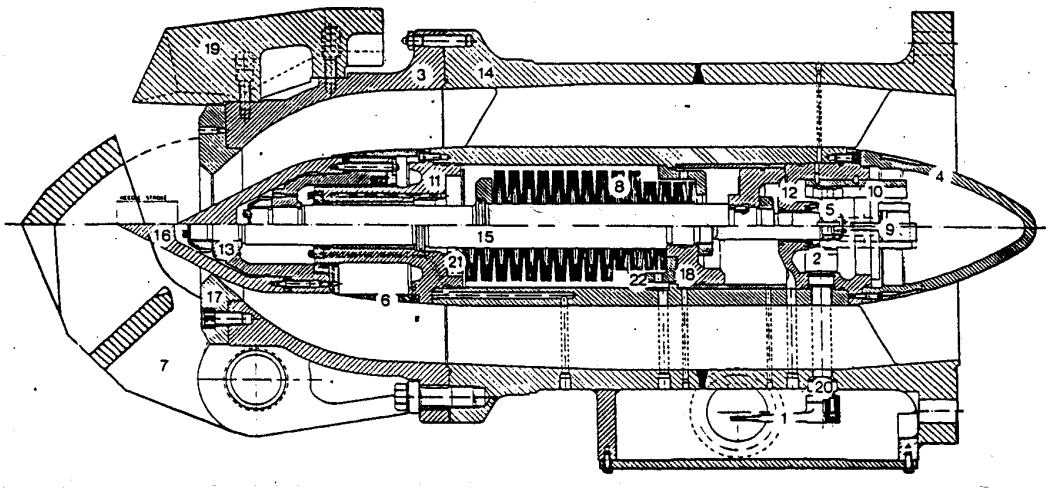

Fig. 6.6. Straight flow injector of Kværner design (1970-1995)

3,14 Injector nozzle section, main body with inner guidance straighteners welded to servomotor cylinder body.

1,2,5,9,10,20 Levers, Links, guidance and shaft for mechanical feed back system.

8,15,18,21,22 Disk spring column, needle rod, servomotor piston, and lining in cast iron, and disk spring support rings.

11,12 Needle guidance cylinder with hydraulic balancing seals, upstream end cover.

4,6,13,16 Servomotor inlet flow bulk head, streamlined flow guidance cylinder, needle tip base and needle tip.

17,7,19 Nozzle ring, deflector and nozzle splash baffle.

[Note, the chamber for the leverage system is filled with oil for rust protection. The bored conduit from the closed chamber behind the needle base (pos. 13) serves as leakage conduit for observing eventual oil or water leakage caused by e.g. sand in the seals.]

Fig. 6.6 For operation in sand laden water hard surface coating on ceramic basis or other types have been developed for protection of needle and nozzles. Also turbine runners may be coated, but not only with success because a minor loss in efficiency.

For a further description of the design of vertical Pelton turbines it is convenient to follow the erection procedure step by step describing the different parts.

Erection procedure

In fig. 6.6 a, b, c, d, e, f the erection procedure is illustrated part by part, step by step. For a study of design, erection and concrete foundation procedure of the different turbine parts it is convenient to look also on the figs. 6.2 and 6.3 where completed vertical turbines are shown. (Courtesy of Kværner)

Erection of a vertical Pelton turbine in cavern power houses starts on concrete foundations integrated in the concreted lower part of the runner pit and outlet channel leading to the tail race tunnel.

The first part to be erected is the combined inspection and working platform with rails for the dismantling cart for the Pelton runner. (see fig. 6.6a)

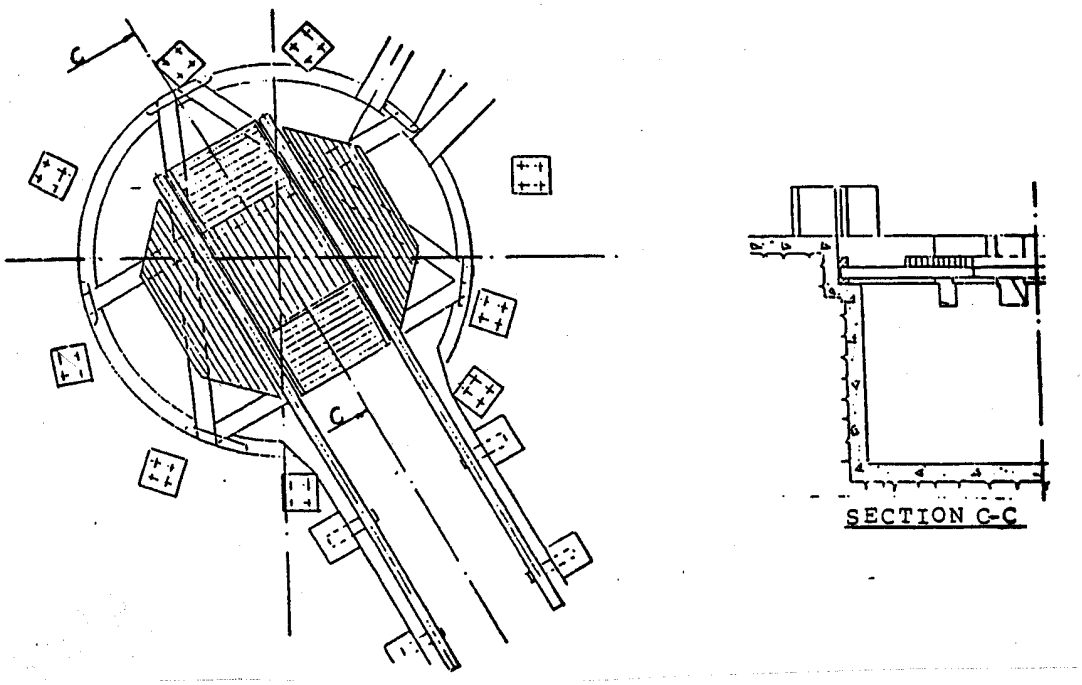

Fig. 6.6 a Concrete foundations for a vertical Pelton turbine

The next stage in the erection is to install the lower part of the runner pit liner (8-16 mm plate thickness depending on turbine size). The liner is reinforced by outside ribs and furnished with anchoring bars to avoid buckling during concreting, and avoid loosing contact to the concrete during operation.

Then the manifold sections are placed in position on the steel plate anchors on top of the concrete foundations shown in fig. 6.6b. The manifold sections will then be welded together, heat treated, and pressure tested after examination of the welds. An accurate positioning and anchoring of the manifold is made. The manifold is then ready for embedment in concrete after the turbine housing top cover including the upper part of the runner pit liner is mounted.

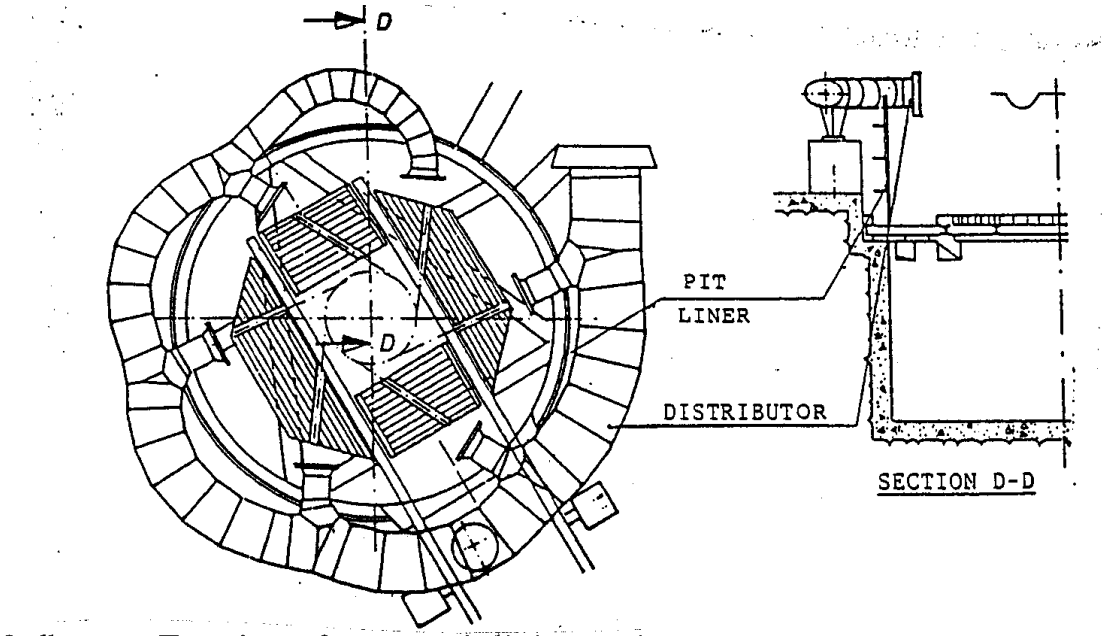

Fig. 6.6b Erection of runner pit lining and manifold

The top section of the turbine housing with cover are welded together and then welded to the lower part of the liner and joined to horizontal plate cylinders connecting the outlet flanges of the manifold and the turbine housing. (see fig. 9.6b and fig. 9.6c). It is important to control the correct level and secure anchorage of the top sections during embedment in concrete.

Finally the central cone with the machined turbine bearing support flage is welded to the turbine cover with a special procedure to keep the bearing support flange in level within an accuracy of 4/100 mm per m. (fig. 6.6c). (The flange for the turbine bearing must be continously controlled during the welding if the accuracy of 4/100 mm pr m shall be obtained by welding on two sides at the same time with controlled heat input.)

The final erection before concreting of the embedded parts is shown in fig. 6.6c. [Note the water jet braking pipe shown in fig. 6.6c and the reinforcement bars]

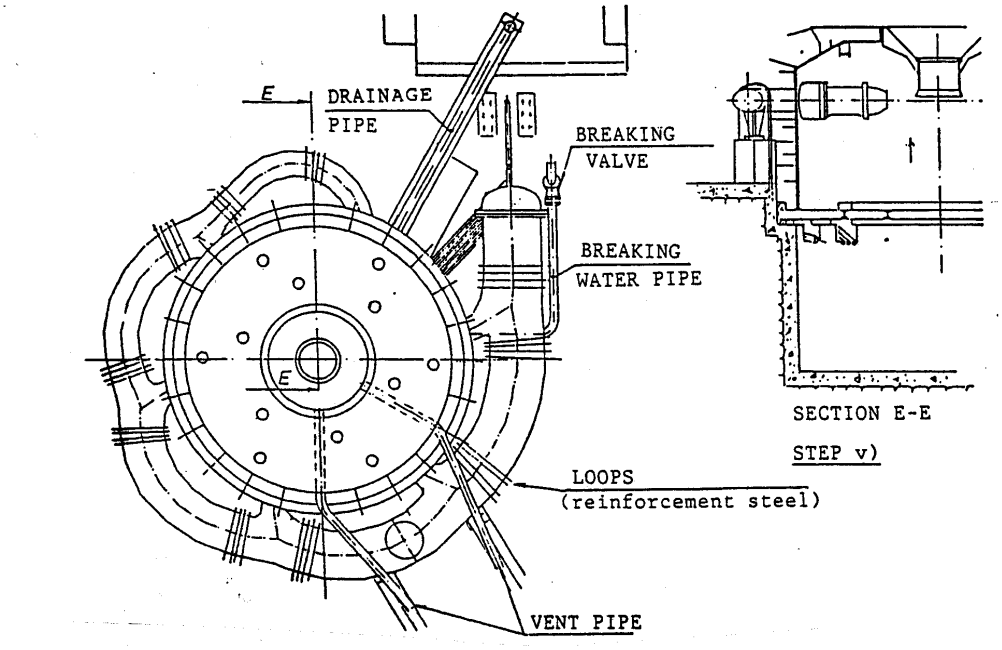

Fig. 6.6c Final erection before concreting of turbine

In fig. 6.6d the completed concreted turbine is shown with the continued concreting of the generator foundation shown to the left. The turbine erection work will continue with positioning of the turbine shaft, installing the governor equipment and inlet valve including connection of piping systems.[Note: the oil sump and governor foundation as well as the foundation for the inlet value is concentrated together with the turbine].

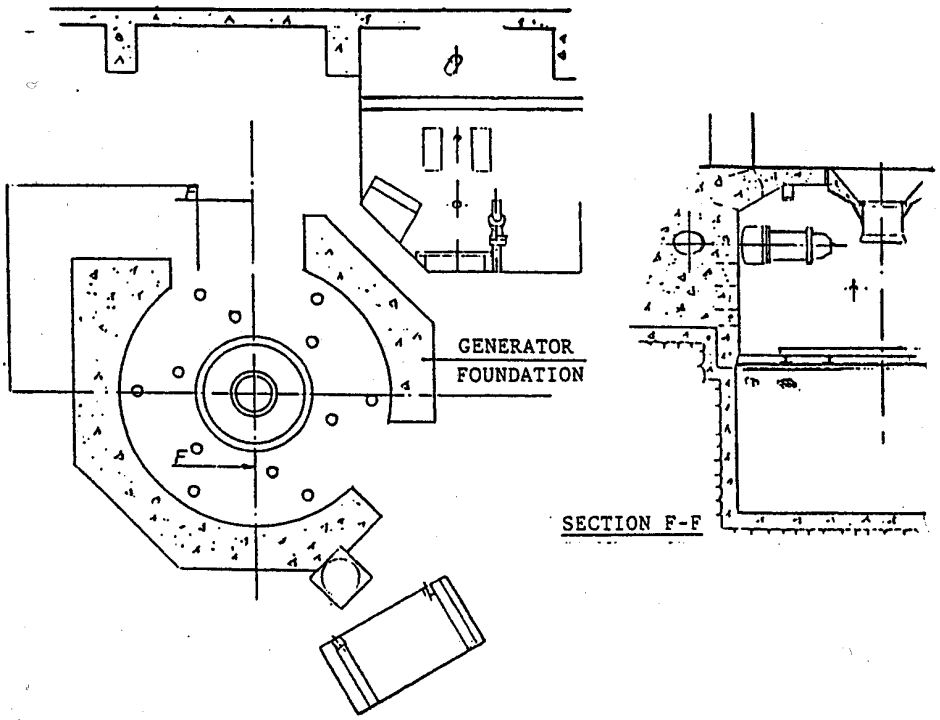

Fig. 6.6d Concrete work finished. Turbine ready for final erection work.

The turbine installation before starting the erection of the generator is shown in fig.6.6e after the deflector mechanism the governor system and inlet valves have been installed. The turbine shaft is positioned in a correct centred vertical position approximately 20 mm below the final level ready for connection to the generator shaft flange (fig. 6.6e to the right).

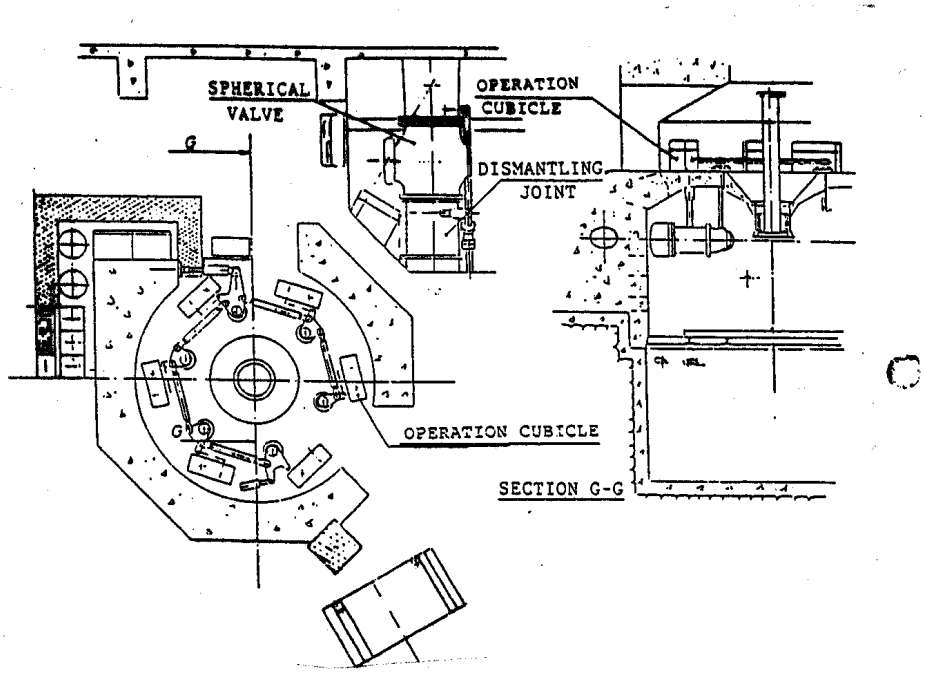

Fig. 6.6e Final erection of turbine before coupling to the generator

[Note that before governor cabinets and the oil hydraulic components are installed the concrete surfaces should be cleaned and coated with paint to avoid dust pollution of the oil hydraulic parts].

Before the last stage of turbine erection can be made, the erection of the generator stator, rotor and thrust bearing must be finished.

The first stage in the last part of the turbine erection is to connect the generator and turbine shaft.
After the flange bolts in the turbine generator coupling have been prestressed the complete turbine generator shaft will be rotated with the lower generator bearing and the turbine bearing dismantled. This is for control of the straightness by turning the the shaft and and reading the radial positions for each 90 degree at each guide bearing position and above and below the flange coupling for possible eccentricity.

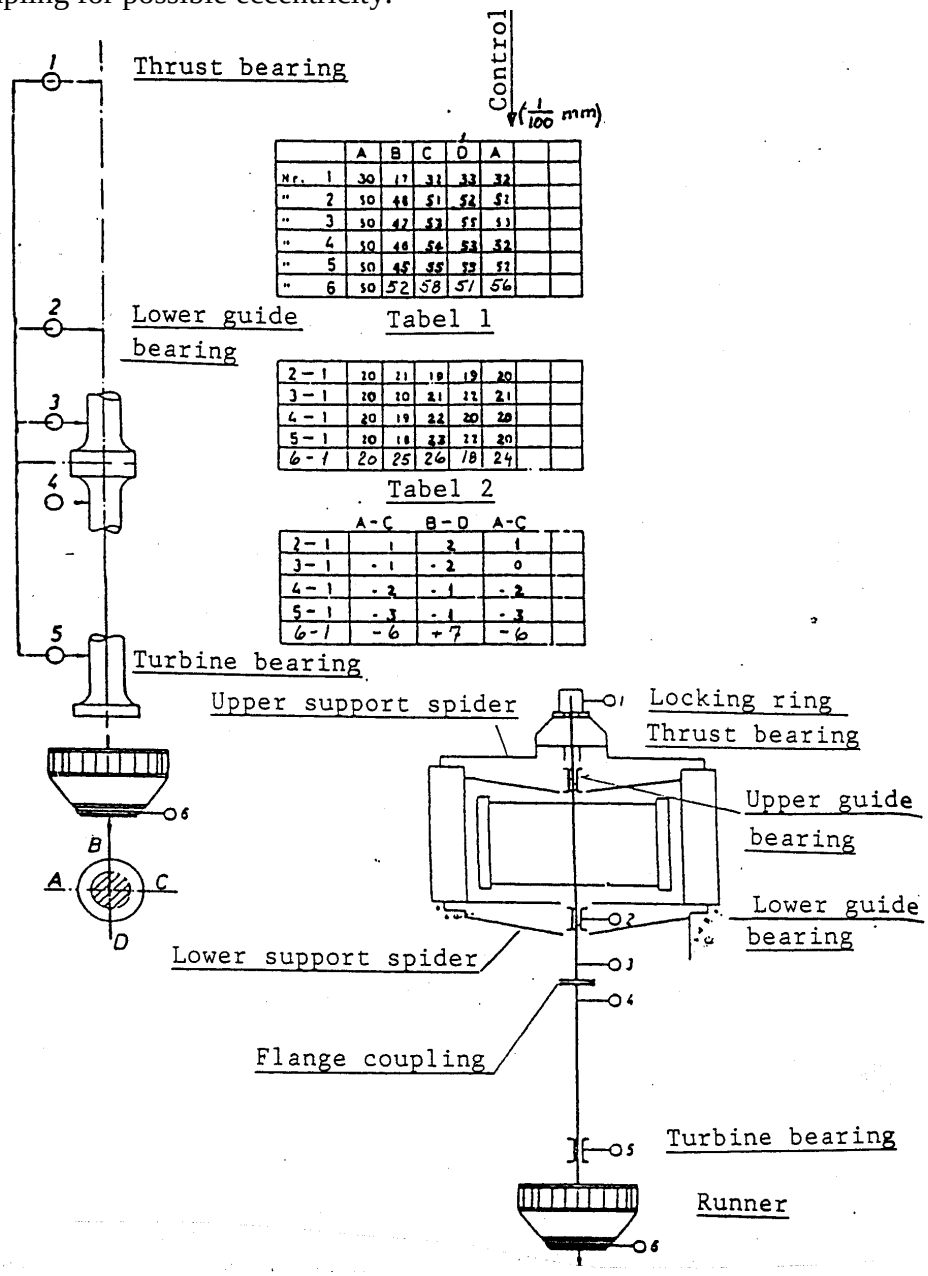

Fig. 6.6f Control of the straightness of the generator shaft and turbine shaft at site by rotating the shaft and reading the positions every 90 degree.

The procedure is illustrated in fig. 6.6f showing the readings in (1/100) mm. For each 90^{o} turning of the shaft in positions 1-5. If any bend of the shaft in the coupling is observed a straightening may be made by tightening the bolts further on convex side of the bend in the coupling.

The example of the control procedure shown in fig. 6.6f is valid for both a Pelton turbine and a Francis turbine, where also the runout of the lower runner labyrinth is included. For a Pelton turbine the procedure is made without the runner, but with a possible control of the runout of the male flange which will be coupled to the runner.

The last and final part of the turbine erection is mantling of the Pelton runner, normally by means of a hydraulic lifting cylinder and the runner cart on which the runner is brought in position below the shaft flange. The procedure is illustrated in fig. 6.6g.

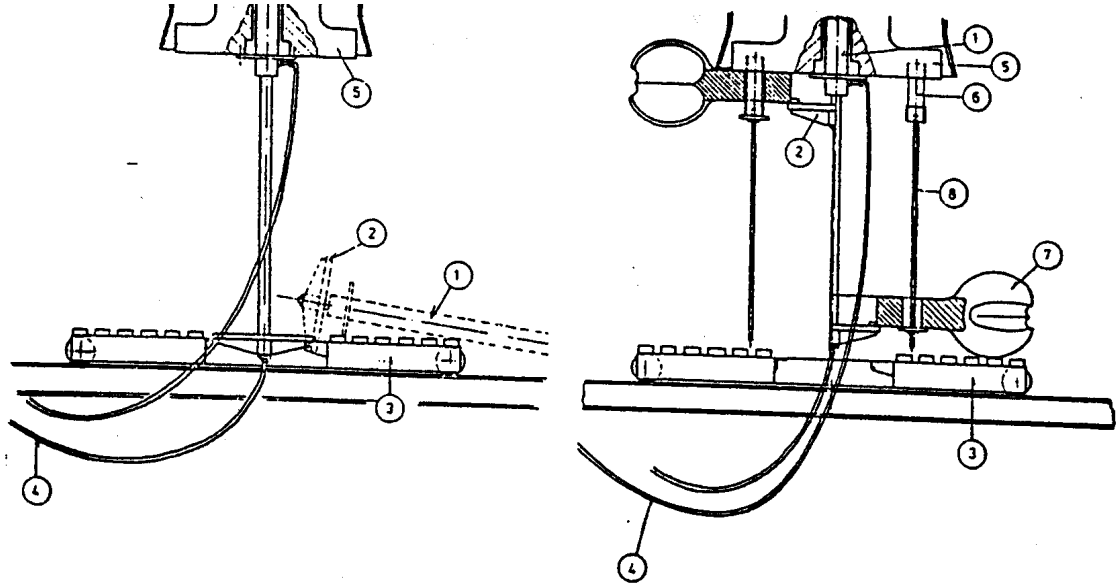

Parts shown in the fig. are.
1. Cylinder, 2. Lifting fixture, 3. Cart, 4. Hydraulic cylinder and flexible oil supply pipes. .
5. Shaft flange. 6. Friction bolts. 7. Runner. 8 Safety bars (threaded with nut.)

Fig. 6.6g Erection of Pelton runner

The straight flow injectors and deflectors are normally erected by lifting pulleys attached to eyebolts fixed in threaded holes in the turbine housing cover located in convenient places in the sealing above the injectors. The dismantling procedure for the turbine runner is just the opposite way of the erection procedure.

Exchange of needles and nozzles or complete injectors is also made with convenient lifting tools with access from the dismantling and inspection platform. Minor repair work such as grinding of the runner due to minor erosion damages may be done without dismantling of the runner

The access to the governor and inlet valve is from the outside and will be similar to that for Francis turbines. The Pelton turbine bearing shown earlier in this book in fig. 6.4 is split in two halves and may be dismantled in the opposite way as shown in the erection procedure.

6.3. Francis turbines

General comments with description of some special high head turbine design

Francis turbines are the most commonly used turbines today. These turbines cover a wide range of heads from 20-30 m up to 700 m and even higher in special cases.
Exept for small hydro Francis turbines are of the vertical shaft type .
In fig. 6.7a a horizontal small hydro Francis turbine is shown which normally can be used up to 300m head.

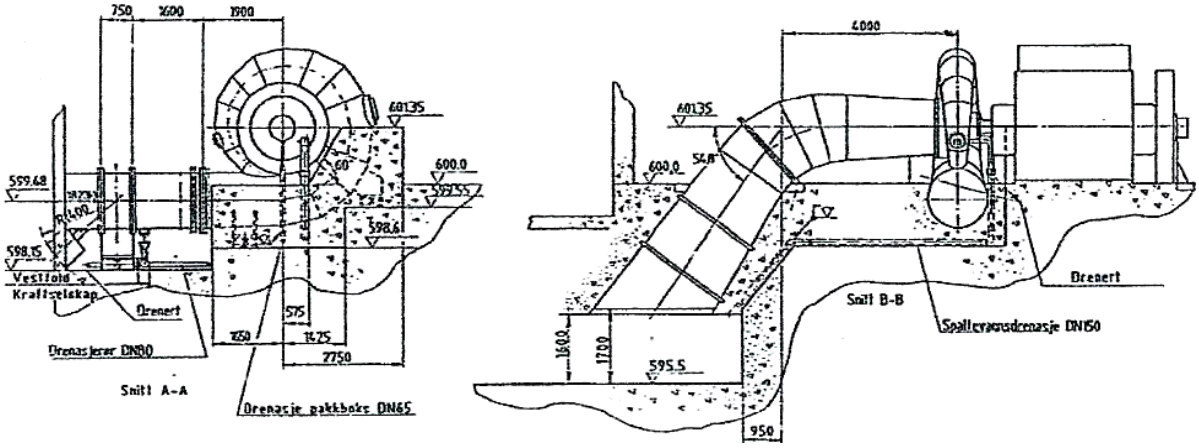

Fig. 6.7a A typical small hydro Francis unit with horizontal shaft.

Of the large Francis turbines installed in Norway before year 2000 the turbines for Svartisen power plant should be mentioned.
The first turbine for Svartisen Power Plant was commissioned in 1993 and was at that time the most powerful turbine operating at head above 500 m to the author´s knowledge.
The output of this turbines is 350 MW operating at a net head 543 m and with a speed of 333.3 RPM. The worlds largest Francis turbine including the whole range of heads was at that time the turbines for ITAIPU at the border between Brazil and Paraguay. The output of these machines are 740 MW operating at a net head 118.4 m with a speed of 90.9 RPM and 92.3 RPM, for 50 and 60 Hz production respectively.

At present time the turbines for Three Gorges Powerplant in China are the most powerful turbines with design head of 757 MW at a net head of 80.6 m. (Ref. 29).
However, in China even more powerful turbines operating at higher head, will be installed in the future.
In this chapter the design and erection of typical high head units will be described.
However, the design philosophy and the research work for development of Francis turbines will in general be valid for all types of units. Also the erection procedure for high head turbines will be similar unless the fact that the very large low- and medium head units must have a larger portion of the fabrication at site, and in some cases also the runners must be fabricated at site or even bolted together at site because of transport limitations.

The development of Francis turbines has been based on an extensive use of model testing internationally. However, for high head machines with long blades graphical methods of flow analysis have been used as early as in the late twenties.
In Norway Professor Sundby at the Norwegian Institute of Technology started an extended use of graphical flow analysis of runners during world war I. Later Chief eng. Christie and Chief eng. Sømming at KVÆRNER developed this method further for practical use in industry, and

after World war II remarkable high efficiency was obtained for high head turbines without use of model tests. Thermodynamic efficiency tests at site on these machines today proved an efficiency on the same level which can be achieved with modern numerical programs and laboratory test facilities at present time for high head turbines.

In the Appendix is presented a further development of the theoretical background for the graphical method focused on the blade lean parameter θ which is important for low head turbines. The philosophy of the blade lean influence was used when shaping the low and medium runners at Kværner which started late in 1995. In this development the blade shaping was followed by a fine tuning of inlet and outlet by CFD analysis.
Theoretical flow analysis of incompressible steady state flow for high head Francis turbines is far advanced and commonly based on Euler's equations computed by CFD programmes. For the final analysis including part load and overload operation the Baldwin Lomax and partly the K, ε model for viscid turbulent flow have normally been used. However, the flow in the runner is of a non-steady nature due to the wakes trailing behind the guide vanes.

In the future advanced mathematical turbulence models for non-steady flow analysis may be developed and commonly used for study of the non-stationary turbulent flow in the runners. The disturbance from vortex cores formed by leakage in the guide vanes clearance gaps are studied at the Norwegian Institute of Technology and will hopefully also give a valuable contribution to the solution of this problem.
Detailed measurements of pressure on the runner blades are necessary to fix the boundary conditions for the theoretical analysis. Then an improved understanding of the behaviour of the runner flow can be achieved. Advanced velocity measurements using high speed video and laser Doppler techniques and further advanced computer studies of unsteady flow including turbulence and boundary layers, will help improve the efficiency and cavitation performance of the turbines.

Another special area of study is operation of the turbine away from the design point. Off design operation of Francis turbines will be very important for peak load production from hydro power plants. Of importance is the recently started research work on balancing the blade lean angle of the blade with a twisted blade design recognised as X blade runners in order to decrease the cross flow swirl in the blade channels. Model tests have so far proven an exceptional stable operation at part load for these pressure balanced X blade runners.

On the structural side the increased size of machines has in the same way as for Pelton turbines led to an extended use of high tensile strength steel. The expression LEAKAGE BEFORE RUPTURE, which limits the allowable stress level of big machines, will be an important design criterion for large machines.
Another important design criterion is to make compromises between the optimum hydraulic design and the structural requirements to avoid stress peaks and blade cracking in runners. The dynamic load from blade passing frequencies and pressure pulsation in the draft tube are also important in the study of blade cracking problems.

In fig. 6.7 b a 3D drawing of a low specific speed Francis turbine is shown. A description of the different parts is listed in the fig. 6.7 b. The function and design of the different parts will be described in the erection procedure and the dismantling procedure for maintenance work. The turbine design represents the KVÆRNER design. Other different designs of Francis turbines made by other manufacturers are not described in this book.

The erection procedure for Francis turbines follows a similar procedure as shown in the previous chapter for Pelton turbines with pressure testing at site after the final welding of the spiral casing for large turbines with split spiral cases. For smaller units with the spiral casing in one piece the pressure testing is normally made in the work shop, but a repeated test may be made at site if required to seek if any leakage occurs in the seals between stay ring and the covers. [Not necessarily with full test pressure, but with max operational pressure].

A Francis turbine may be divided in following main sub structures:

1. The rotating parts
2. The head and bottom cover included the guide vane system
3. The bearing and shaft seals
4. The spiral casing with stay ring
5. The draft tube

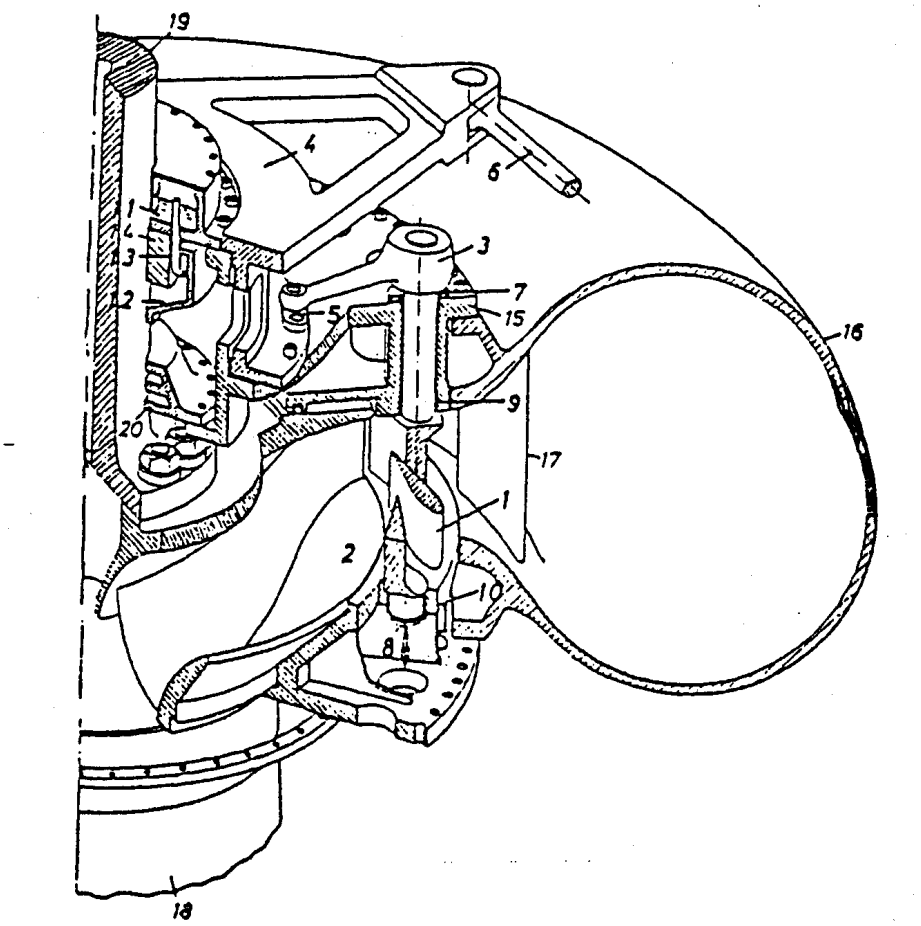

1.	Guide vanes	12.	Lower rotating reservoir
2.	Runner	13.	Oil scoop pipe for oil circulation
3.	Guide vane liver	14.	Bearing pad supporting cylinder
4.	Regulating ring	15.	Head cover
5.	Guide vane link	16.	Spiral casing
6.	Servomotor rod	17.	Stay vanes
7,8,9	Guide vane bushings	18.	Draft tube cone
10.	Bottom cover		
11.	Bearing hodsing with upper oil reservoir		

Fig. 6.7 b 3 D view of a high head Francis turbine (Courtesy of KVÆRNER)

In this chapter a description of the main parts including some items of a special design, made by the Norwegian turbine manufacturer KVÆRNER is presented.

In fig. 6.8 the assembled rotating parts of a Francis turbine is shown. The rotating assembly includes the turbine shaft with the lower rotating oil reservoir for the turbine bearing and the runner connected to the turbine shaft by a pure frictional connection. The bolts are prestressed up to 560 MPa by heating or by means of a hydraulic prestressing tool.

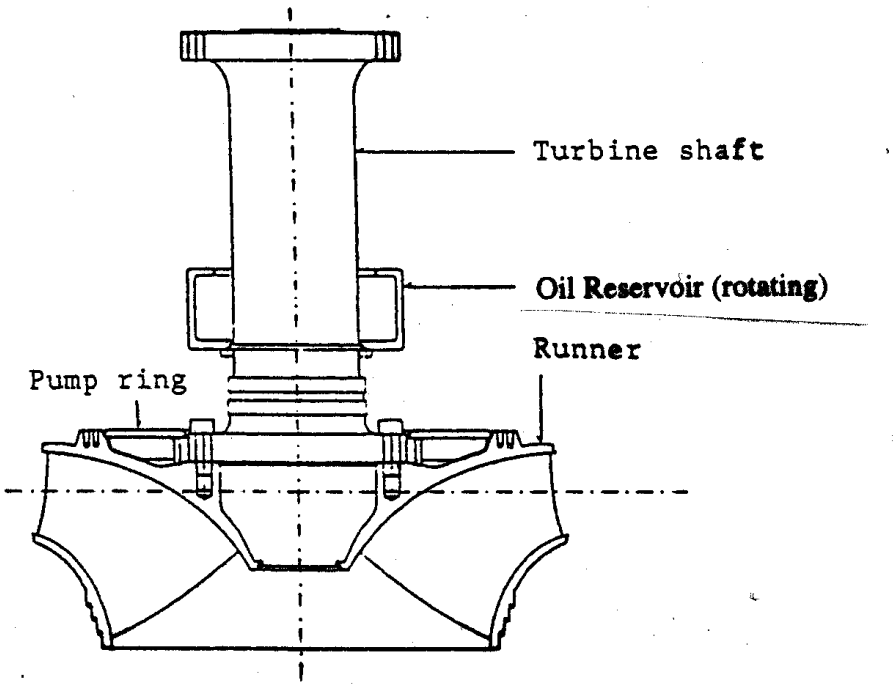

Fig. 6.8 Rotating parts. Including lower rotating oil reservoir of turbine bearing.

In fig. 6.9 the radial bearing for a Francis turbine is shown. The self-pumping system consisting of a scoop in the lower rotating oil reservoir is shown at the bottom of the reservoir. The reason for the location of the scoop different from that in a Pelton turbine bearing is because no air- cooling is used which excludes the necessity of a thin oil film along the wall of the rotating oil reservoir. Otherwise the oil circulation system of the bearing pads is the same as for the Pelton turbine bearing shown in chapter 6.2. Of special design is the split lower rotating oil reservoir consisting of two halves joint by a special oil tight bolt connection. [Not shown in fig. 6.9].

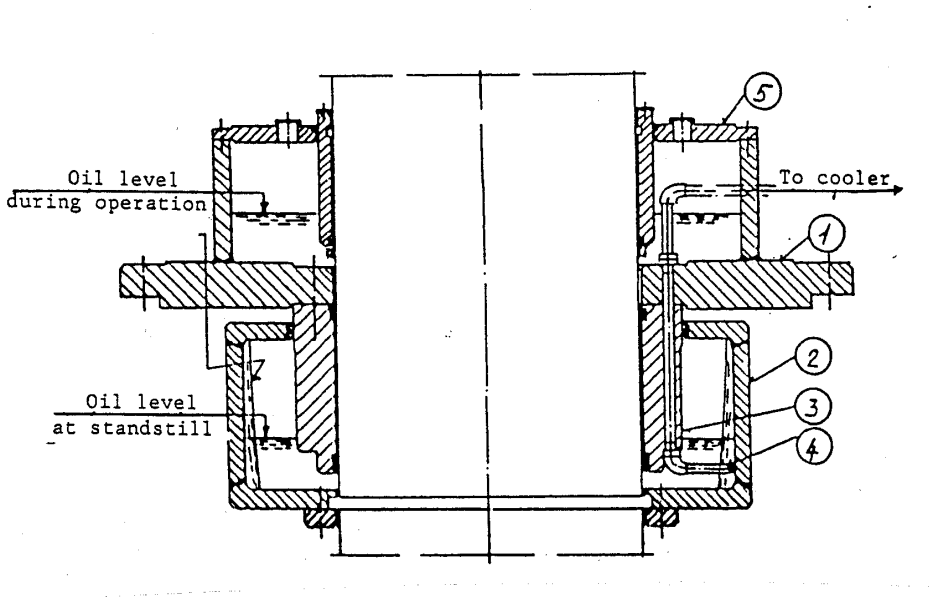

1. Bearing house
2. Rotating oil reservoir
3. Bearing support cylinder with 4 fired babit metal pads
4. Oil circulation scoop
5. Upper oil reservoir

Fig. 6.9 Francis turbine guide bearing.

In fig. 6.10 the non-touching labyrinth type shaft seal is shown. The seal consists of a 3 stage labyrinth system made of babit metal melted in a supporting stationary cylinder. The stationary babitlined labyrinth seal rings have a narrow clearance to a stainless sleeve on the shaft. The clearance is a little bit (1/10 mm) bigger or the same as the bearing clearance. However, after a few hours of operation the sharp noses of the soft babit metal labyrinths are flattened to a non- touching seal. The shaft seal is running dry during operation because the pumping plate system on top of the runner crown inside the runner seal ring keeps the water away from the shaft flange at normal rotating speed. This system will be described later (see fig. 6.11).

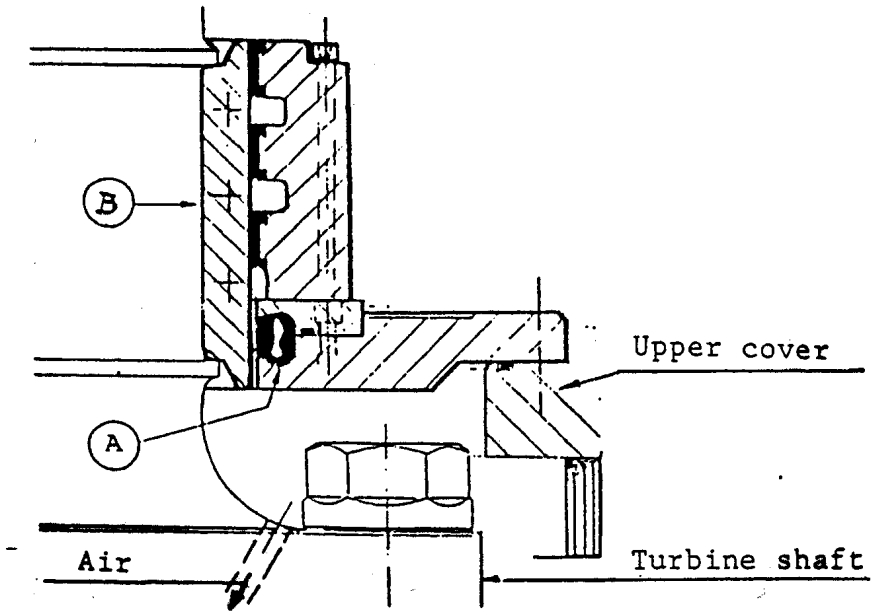

A = Inflatable rubber seal
B = Stainless sleeve on turbine shaft

Fig. 6.10 Labyrinth shaft seal with inflatable rubber seal for stand still of turbine. The rubber seal is used for turbines with deep submergence.

When the turbine is stopped the shaft seal is exposed to the draft tube pressure and is no longer dry. For stand still of the turbine an inflatable rubber seal is installed at the bottom of the labyrinth if the submergence of the turbine is deep (More than 20 m). The rubber seal is activated by air pressure when the turbine is stopped. For normal and low submergence no rubber seal is installed and the labyrinth seal is drained by siphoned pipes from the last two stages down to the pump sump of the powerhouse. The reliability of this type of seal is very good and it is suitable for turbines operation in sand-laden water, because it is running in air during normal operation and is not affected by the sand transport through the turbine. No leakage has been observed from the top of the seal during stand still even without a rubber seal when the siphon system is running. In case of clogging of the siphoned pipes for some reason an automatically controlled drainage pump system is located on the head cover outside of the seal to take care of possible leakage during stand still.

The pumping plate system on the runner is shown in fig. 6.11b.

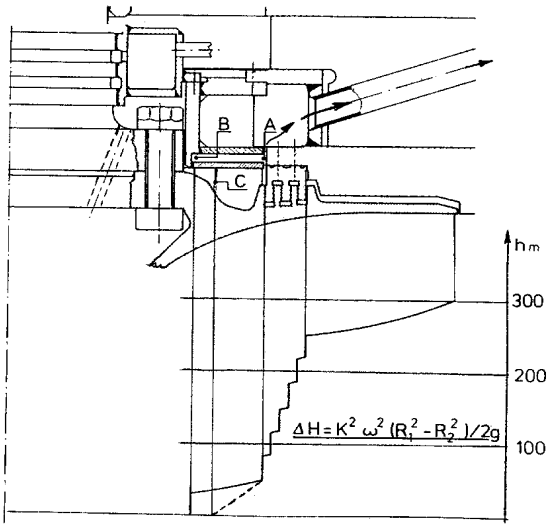

A. outer diameter of pumping plate
B. inner diameter of pumping plate
C. inner diameter of water surface atmospheric pressure

Fig. 6.11 The pumping plate arrangement

The pumping plate system is invented by KVÆRNER and the leakage water from the upper labyrinth seal is normally used for cooling water purposes. The system is illustrated in fig 6.11. The necessary cooling water pressure at point A in fig. 6.11 will then be the dimensioning parameter for the pumping plate system.
The system consists of a smooth stainless plate fixed with ribs on top of the runner crown inside the labyrinth seal. A similar smooth stainless plate is attached to the head cover ending in an axial cylinder forming a narrow vertical clearance on the inside of the pumping plate.

On the upper side of the rotating pumping plate the rotational speed of the water will be approximately 50% of the circumferential speed of the pumping plate while the water will have full rotation equal to the speed of the runner crown underneath the plate due to the radial ribs.
The pressure, equal to the cooling water pressure in the open space at the outer rim of the pumping plate will be the same above and underneath the plate. The pressure drops more towards the inner diameter underneath the plate with full rotation of the water than above the plate with lower rotational speed of the water. The pressure underneath the plate will drop enough to reach atmospheric pressure outside the inside diameter of the plate.

On the upper side of the pumping plate, however, there will be a certain water pressure at the inside diameter driving the water through the narrow clearance between the edge of the plate and the static cylinder inside the plate down to the atmospheric air pressure below. The rotating ribs on the lower side of the plate forces the air mixed water flow outwards to reach the parabolic surface of the water in between the rotating ribs underneath the plate.

The pressure drop on the topside of the pumping plate can be calculated by the following simplified formula

$$h_A - h_B = K^2 \frac{\omega^2}{2g}(R_A^2 - R_B^2)$$

Here K 0.5 and ω = angular velocity of the runner.
R_A and R_B is shown in fig. 9.11 and h_A = cooling water pressure.

[The real pressure distribution is more complex than shown in the equation above and 0.5 . Then a larger pressure drop gives a higher rotation than by using K obtained above as given in the equation. The rotation is depending of the flow velocity from outer to inner diameter and the rotation of the water at the rim of the runner crown.]
The power needed for the circulation of water can be found theoretically as shown in following equation:

$$P = \rho g q \, h_A/\eta_c \text{ kW}$$

where q = the leakage flow and h_A = the cooling water pressure, η_c = an assumed efficiency of ~ 50%.

However, the energy saved by obtaining that the coupling bolts are running in air saves more energy than used by the pumping plate system because the flow (=q m^3/s) is very small because of a narrow clearance on the inside of the pumping plate.

Erection procedure with a description of the main parts of a high head Francis turbine.

Before the erecting procedure is described it is convenient to take a look at fig. 6.12 showing a schematic drawing of a modern Francis turbine included inlet valve draft tube, draft tube gate and necessary drainage piping.

The erection procedure of a vertical Francis turbine produced by KVÆRNER can be described as shown in Fig. 6.13 a, b, c, d, e, f and g together with a brief description of the foundation works and the design of the different parts included the dismantling procedure for maintenance work (see following pages).

The erection procedure starts with the draft tube, which must be positioned and securely anchored against buoyancy in liquefied concrete. In addition it must be reinforced by removable stiffeners from the inside to avoid buckling during embedment in concrete. In fig. 6.13a the draft tube is shown after concreting with the concrete supports for the spiral casing which will be the next part for erection. Fig. 6.13b shows the spiral casing with stay ring (2), head and bottom covers (5), guide vanes (6), the pressure testing cylinder located on the inside of the guide vanes (7) ready for pressure testing. In fig. 6.13c the spiral casing with the draft tube cone (3) and the bulk head (4) are shown erected and securely anchored by welding to the anchoring plates on top of the concrete foundations.

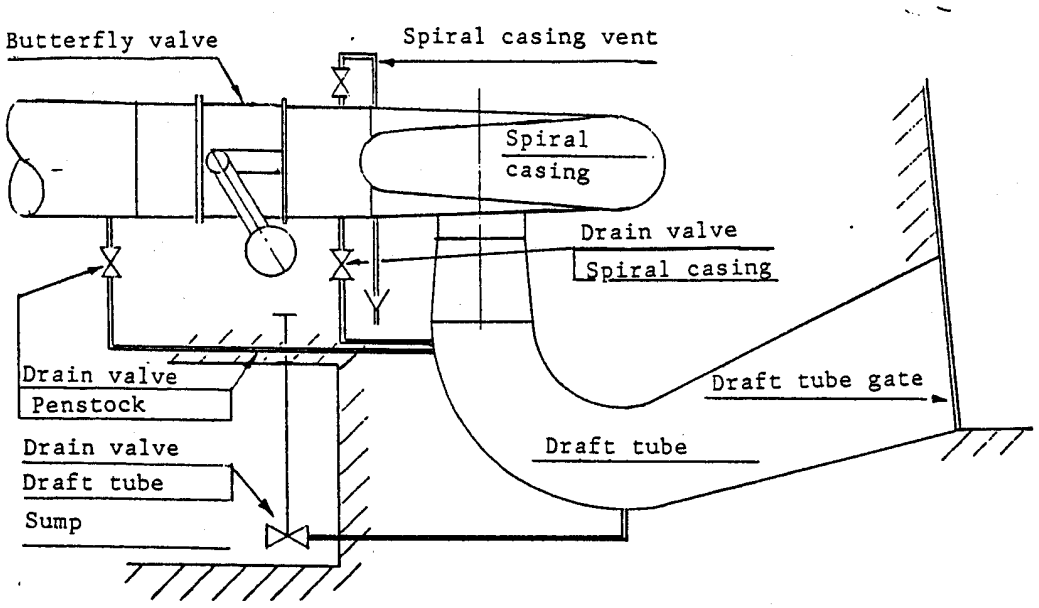

Fig. 6.12 Schematic drawing of a Francis turbine complete with inlet valve and draft tube

Before pressure testing of a not assembled spiral casing the parts must be assembled and welded by joining two or four sections if a split spiral casing design is used. Another and preferred solution for high head turbines of moderate dimensions is to cut off sections of the plates on the outer parts of the spiral casing for transport reason. Later these parts are welded back in place at site. The field welding is stress relieved by heat treatment for plates thicker than 40 mm depending on the carbon equivalent of the plates. Thinner plates are welded with preheating, but without thermal stress relieving. For a split design post weld heat-treating will be required if the plates are thick. However, for the low carbon fine grain steel, which is used to day welding on split spiral cases has been done without post weld heat treatment.

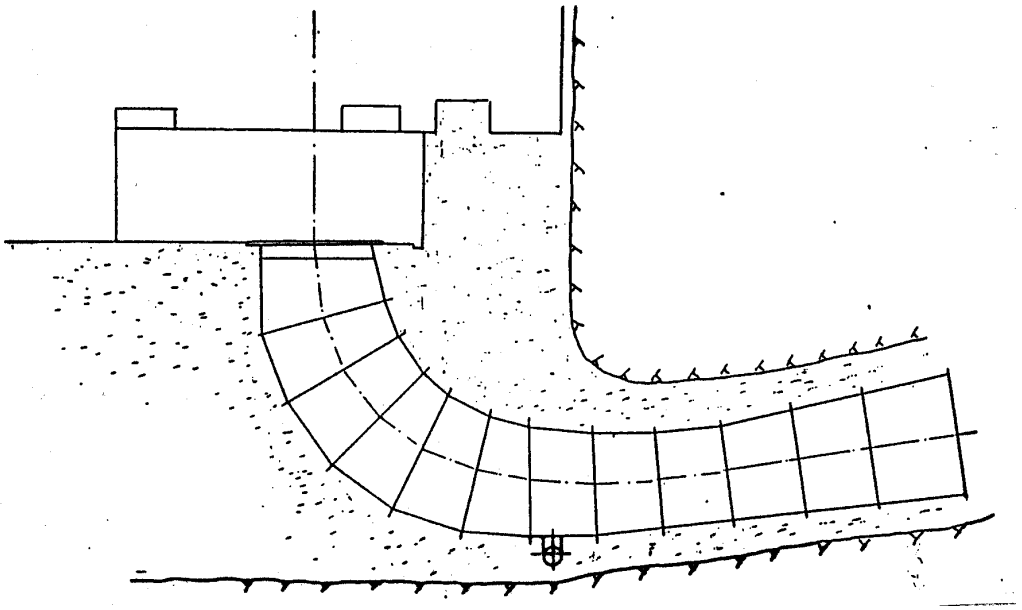

Fig. 6.13a Draft tube embedded in concrete

The concreting of the turbine up to the turbine floor is in Norway normally made without pressure in the spiral casing and no soft material is used between the steel plates and the concrete for high head machines. The experience is good with this method. The gap between the concrete and the steel plates in a depressurised spiral case caused by the shrinkage of the concrete will be reduced. This is an advantage concerning possible humidity and rust later during operation.

The finished concreting work continues from the turbine floor up to the generator floor including the generator support structure before the turbine erection work is continued. The draft tube cone is not embedded in concrete in Norwegian power plants, allowing for dismantling of the bottom cover, the guide vanes and the runner down and out underneath the spiral casing as shown in fig. 6.14a and 6.14 b later in this chapter.

In fig. 6.13d the runner and turbine shaft is erected and positioned for the generator erection supported on the draft tube cone. Before the generator erection is started the head cover, the regulating ring and regulating mechanisms are mounted as shown in fig. 6.13e.

Fig. 6.13f shows the complete turbine shaft and runner after the turbine shaft is connected to the generator shaft. In this position the complete shaft and runner is turned and measured in 5 positions along the shaft after each 90 turning to control the straightness as described for Pelton turbines (see fig. 6.6f). The runout of the lower runner labyrinth will also be controlled in this case. In case the shaft is not completely straight the straightness may be corrected within certain limits by an increased prestressing of the coupling bolts as described for Pelton turbines referring to fig 6.6 f. Such correction is acceptable and have been successfully carried out on many turbine-generator shafts also of large size machines.

The completion of the erection of the turbine and generator will be to mount the lower stationary labyrinth housing. This is made by locking the shaft in correct position concentric to the upper runner labyrinth ring of the runner and concentric to the upper generator bearing, and finally mount the lower generator- and turbine guide bearing and the labyrinth shaft seal and lower stationary runner labyrinth concentric to the shaft.

The last turbine part to be erected is the draft tube cone which will normally have a fixed rigid -flange connection to the lower turbine cover and a looser telescope connection to the draft tube top. (see fig. 6.13g).

The labyrinth seal and the turbine bearing, the guide vane lever system, the regulating ring connection to the servomotors as well as the installation of the spherical valve and connecting pipe between the valve and the spiral casing, will be the last heavy parts to be erected in the main turbine system. In addition all piping for draining the penstock cooling and oil piping will normally be part of the turbine system erection.

The height between the draft tube floor and the lower side of the bottom cover is chosen around 2.1 m to allow for working and walking with free overhead space for inspection and dismantling work.

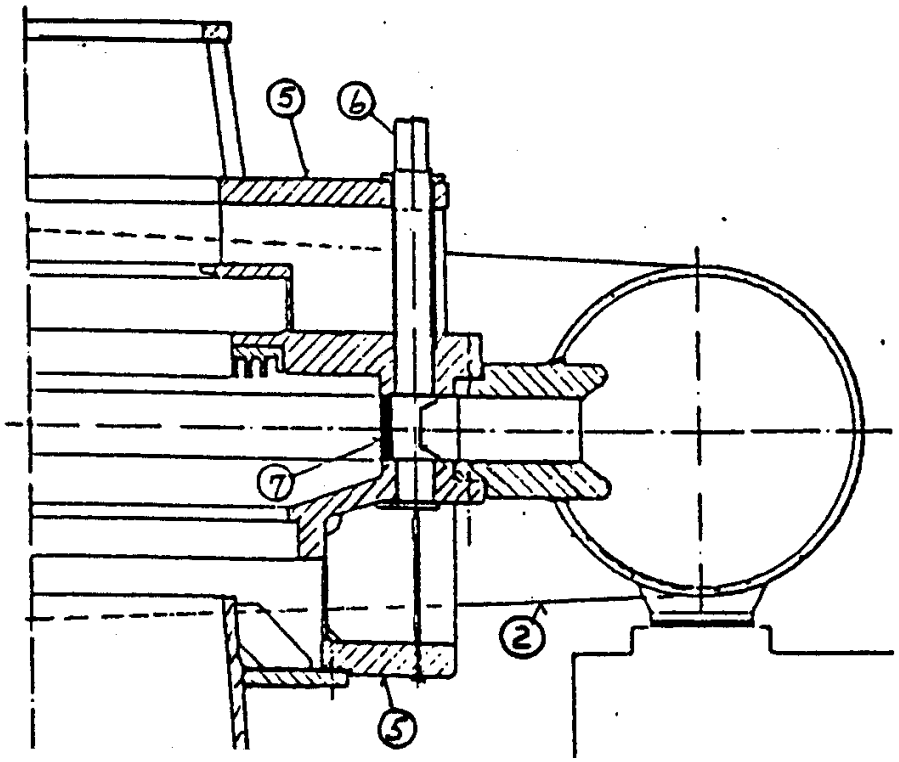

Fig. 6.13 b Francis turbine parts erected for concreting (5 heads and bottom cover, 6 guidevane, 7 pressure-testing cylinder)

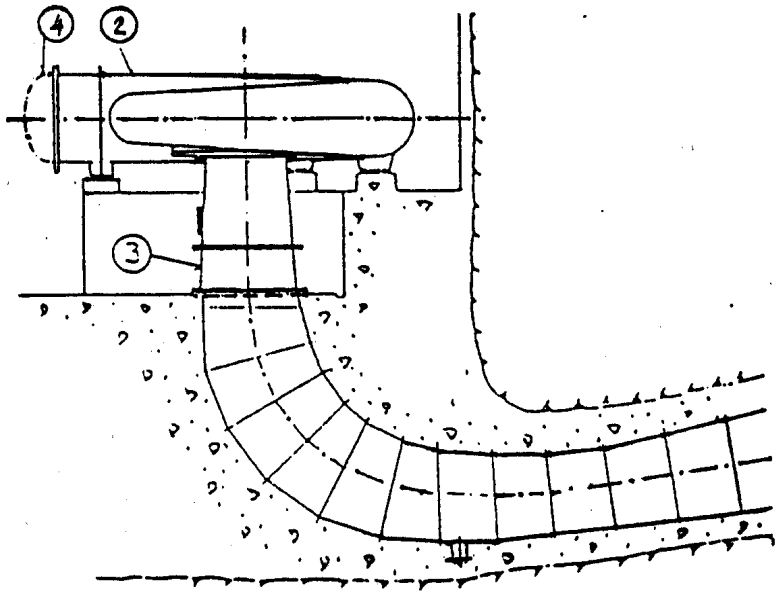

Fig. 6.13c Erection of spiral casing ready for concreting

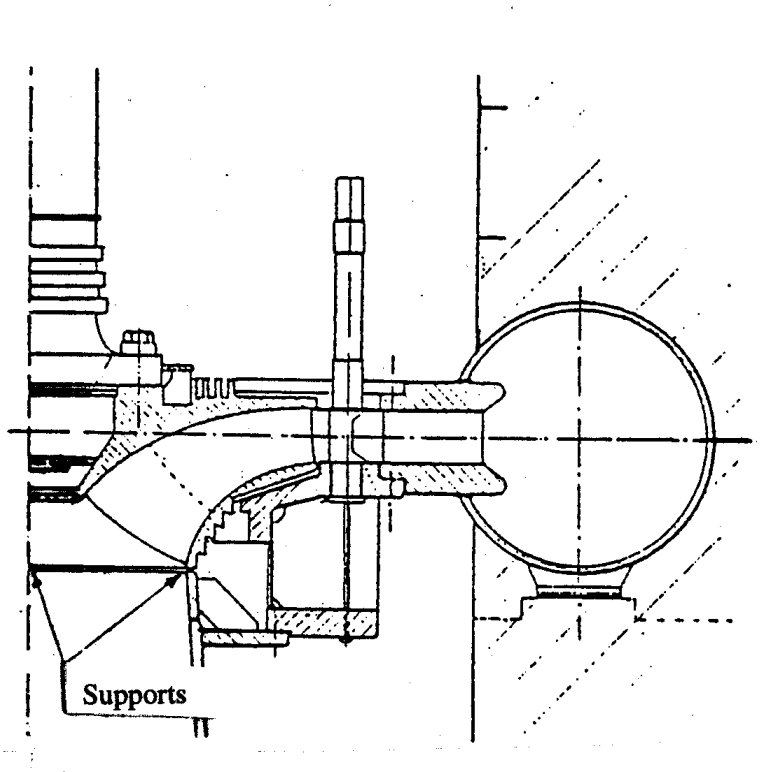

Fig. 6.13d Positioning of turbine shaft for generator erection.
Note the runner support on top of draft tube cone

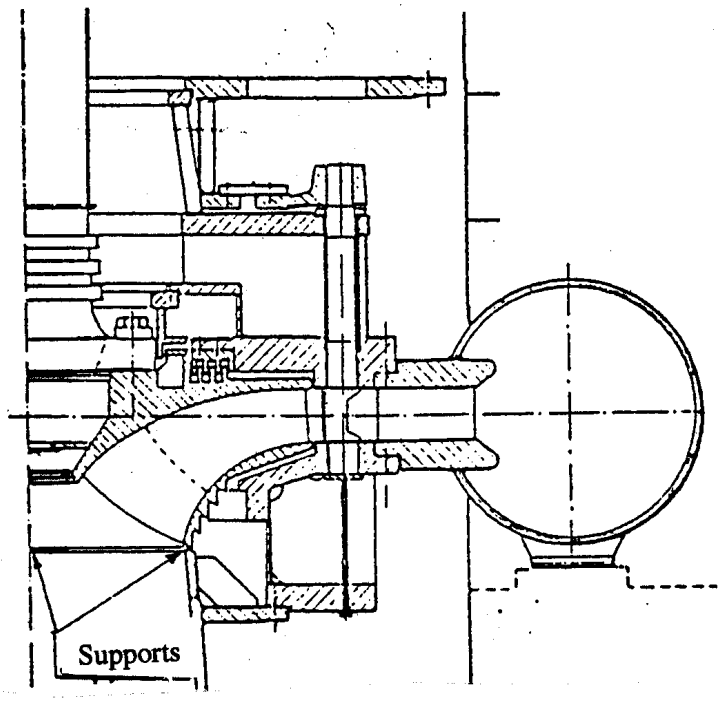

Fig. 6.13e Turbine erected ready for start of generator erection
Governor mechanisms are mounted during generator erection periods

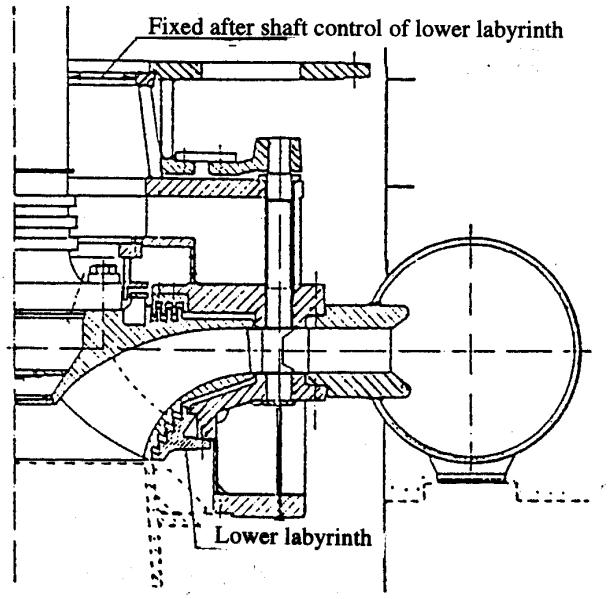

Fig. 6.13f Turbine shaft is connected to generator flange for control of turbine generator shaft straightness by rotating the shaft fixed in position by wedges in the lower labyrinth seal. The fixed straight shaft is used for positioning the radial bearing and the labyrinth shaft seal (see description in the text).

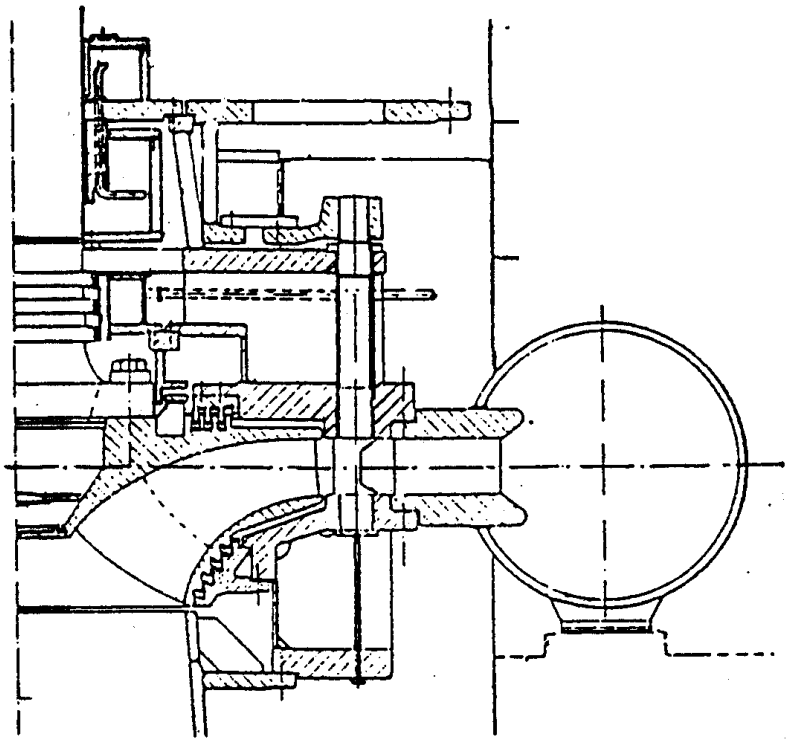

Fig. 6.13g Turbine erection completed

The dismantling procedure of the not embedded parts which are exposed to wear and thus needs maintenance work are normally the stationary seal rings and the guide vanes in addition to the guide vanes facing plates on bottom cover and upper cover for plants with sand erosion problems.

Except for the upper cover all the turbine main parts can be dismantled down and out which is an advantage due to less work compared with a dismantling procedure up and out for a turbine designed with an intermediate shaft between the turbine and generator flange. (If the head cover is furnished with a bolted facing plate this plate may also be dismantled down, depending on the way the plate is attached to the head cover).

In figures. 6.14a, b, c, d, e, f and g. the dismantling procedure for repair of the turbine is illustrated. It should be noted that the draft tube cone must be divided in a lower and upper part in order to move the cone out of the draft tube pit underneath the spiral casing. This is illustrated in fig. 6.14a and 6.14b.

In fig. 6.14c and 6.14d the bottom cover with the labyrinth are lowered down by means of hydraulic jacks fastened in 4 threaded bolt holes in the stay ring. In fig. 6.14e, 6.14f and 6.14g the removal of the guide vanes and runner is illustrated showing lowering of the turbine shaft by hydraulic jacks with guidance bars fastened in the generator coupling boltholes.

All parts are moved out of the draft tube pit by a cart on rails on the floor in the draft tube pit. The shown procedure is a quick and labour saving dismantling process. For small units the dismantled parts may be slid out on the floor on rails by a jack pulley.

The mantling process will be the same procedure but in opposite order.

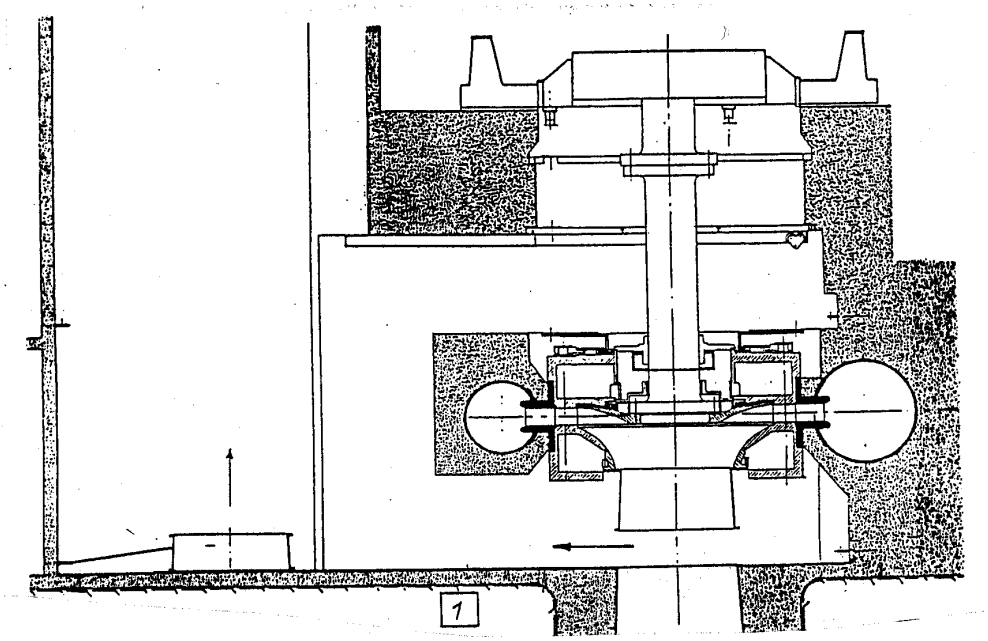

Fig. 6.14a Removal of lower draft tube cone section

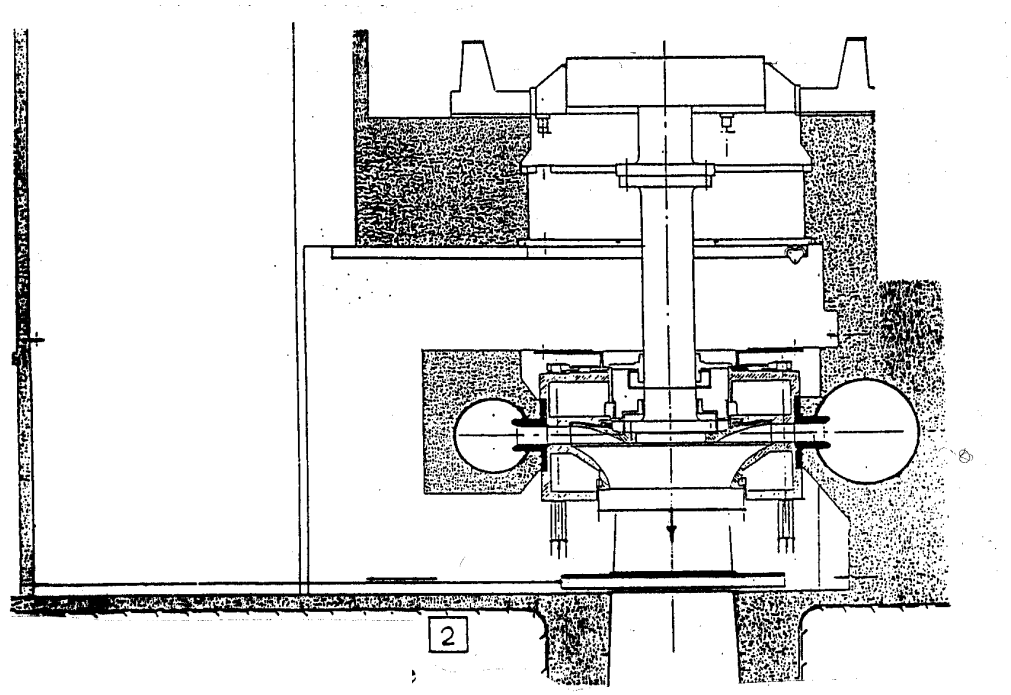

Fig. 6.14b Removal of upper draft tube cone

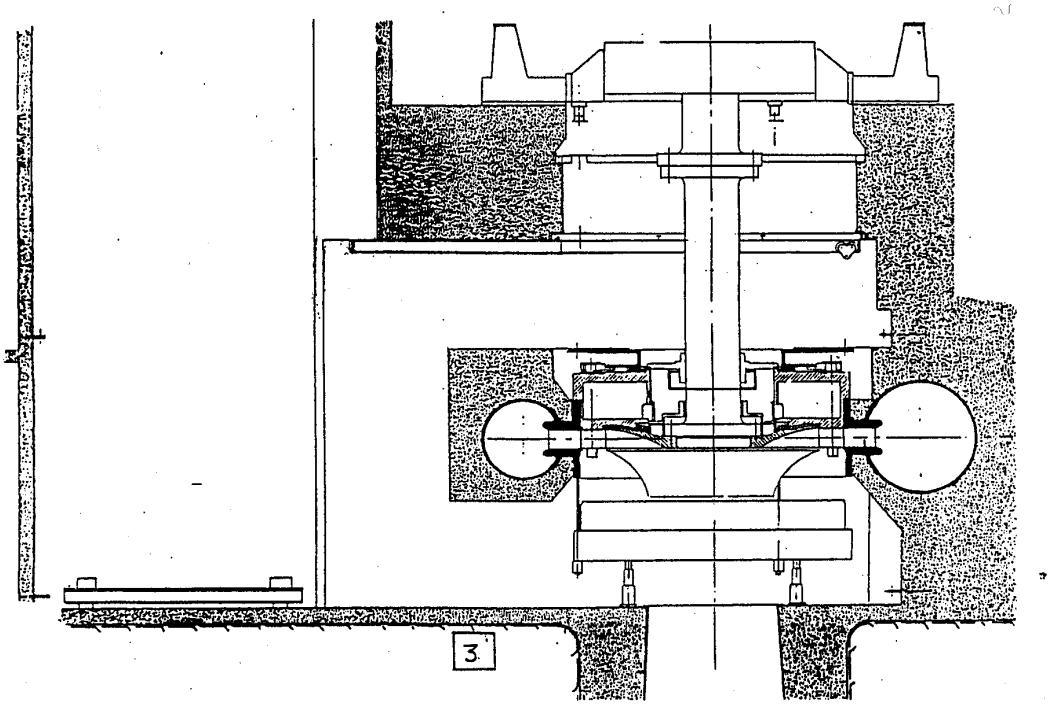

Fig. 6.14c Dismantling of bottom cover

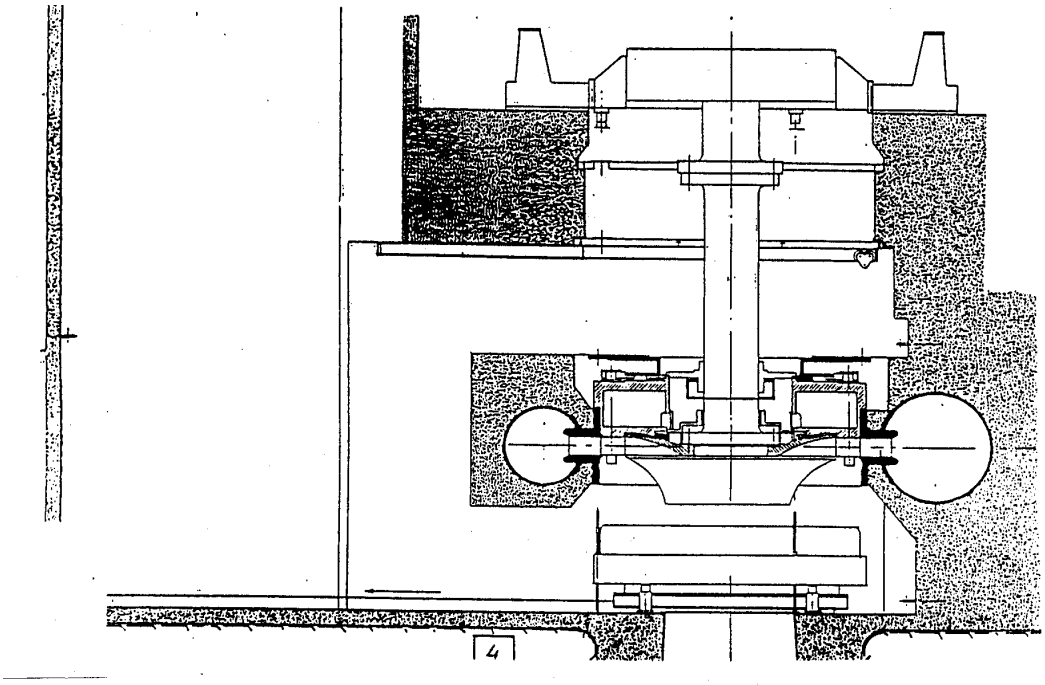

Fig. 6.14d Bottom cover ready for transport out of the draft tube pit on the transport cart.

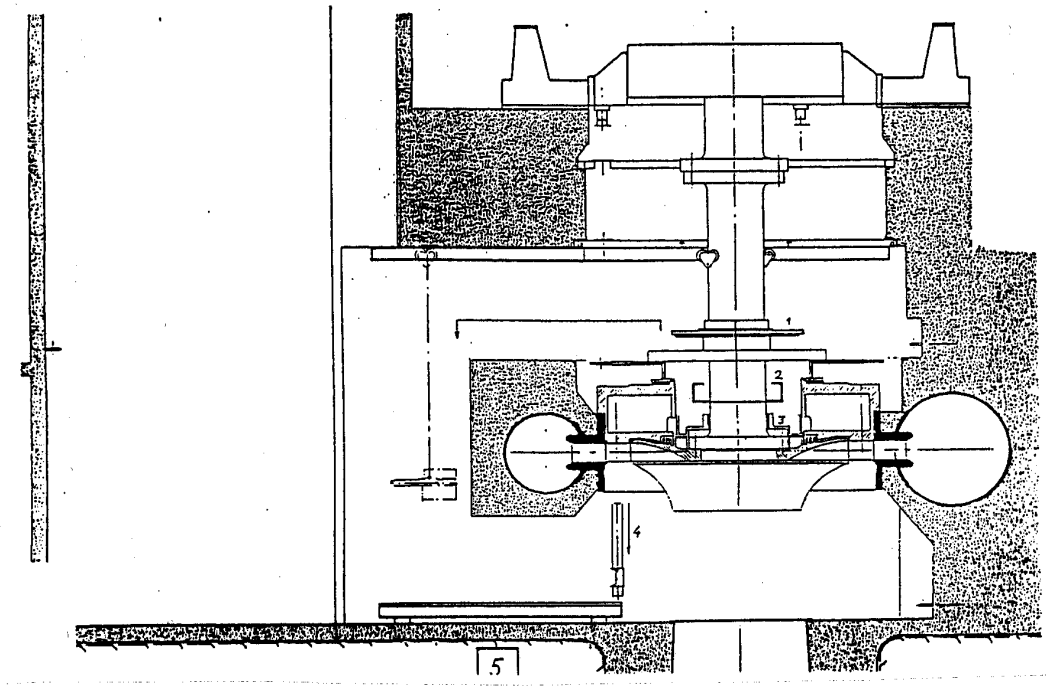

Fig. 6.14e Dismantling of guide vanes and guide vane levers.

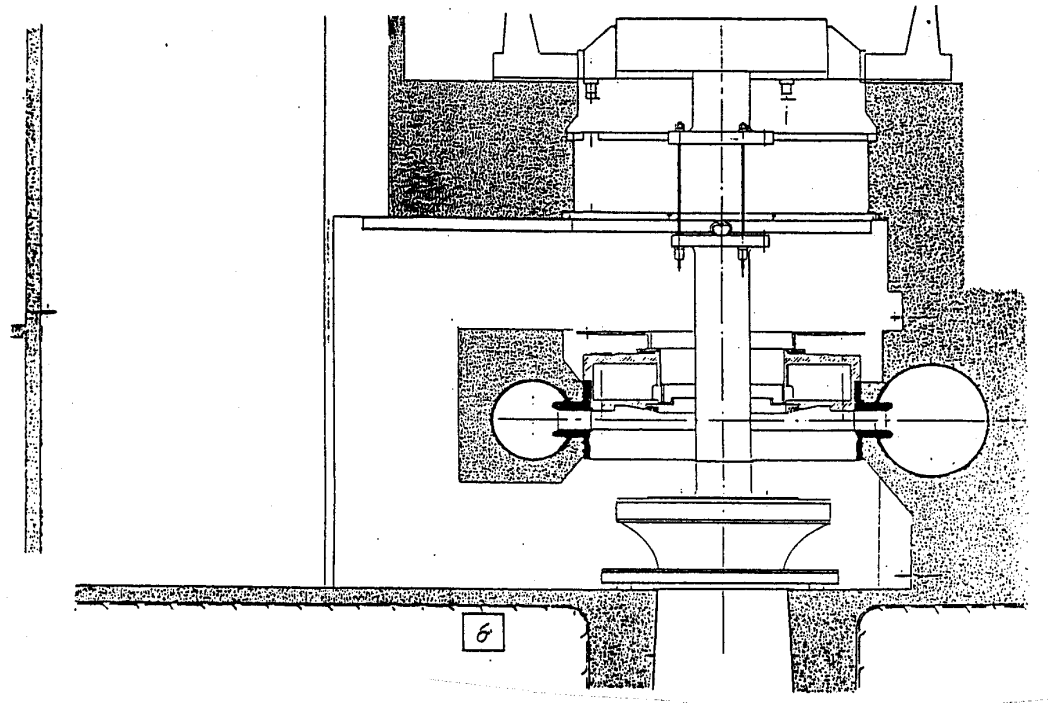

Fig 6.14f Lowering of shaft and runner

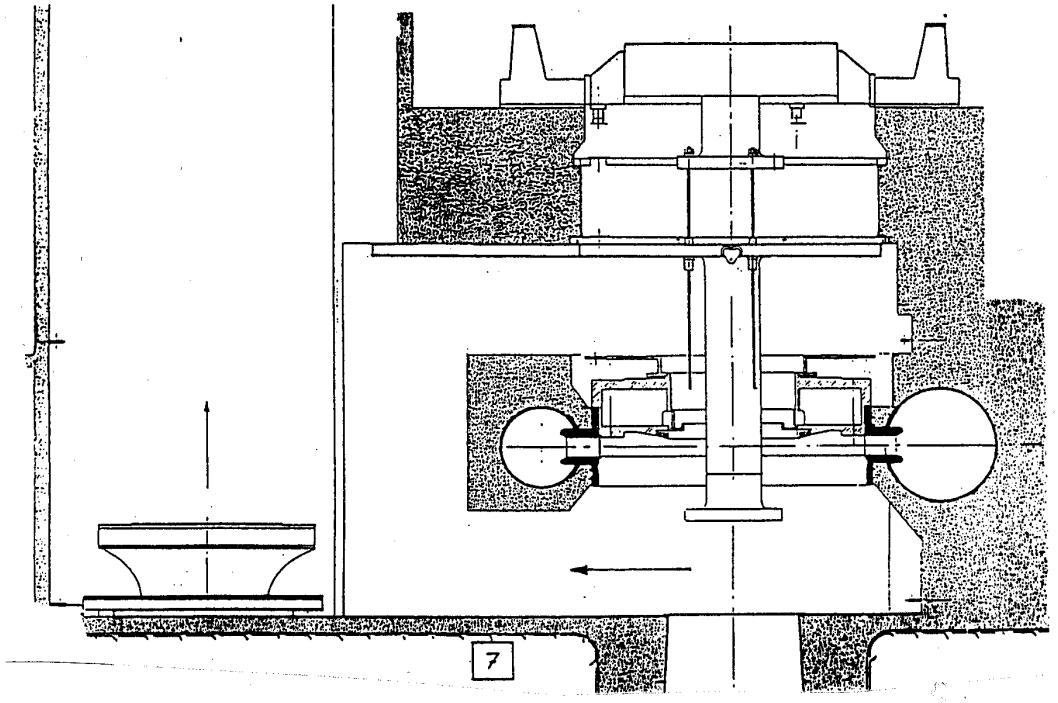

Fig. 6.14g Moving the runner out of the draft tube pit

6.4 Kaplan turbines

The development of Kaplan turbines has been towards larger units and also for increased head. For average size rivers which is the case in Norway the choice between one or a few large Kaplan units, or a higher number of smaller Francis turbines has favoured Kaplan units for heads up to 50 m due to poor off design performance of Francis turbines. However, it should be emphasised on the tip blade clearance problem of the Kaplan runner blades, which increases with size and with head. This represents a current area of research. (The competition between Kaplan and Francis turbine has also in some cases lead to the installation of one small and another twice as big Francis unit which allows for a widened operation of the turbines at high efficiency by an optimal operation of the two units. The best efficiency is then obtained at 1/3-2/3 and 3/3 of best efficiency point load of the two turbines together.)

The design of the control system with an individual servomotor for each guide vane has been successfully in operation for several large Kaplan units in southern Norway including 11 Bulb turbines.

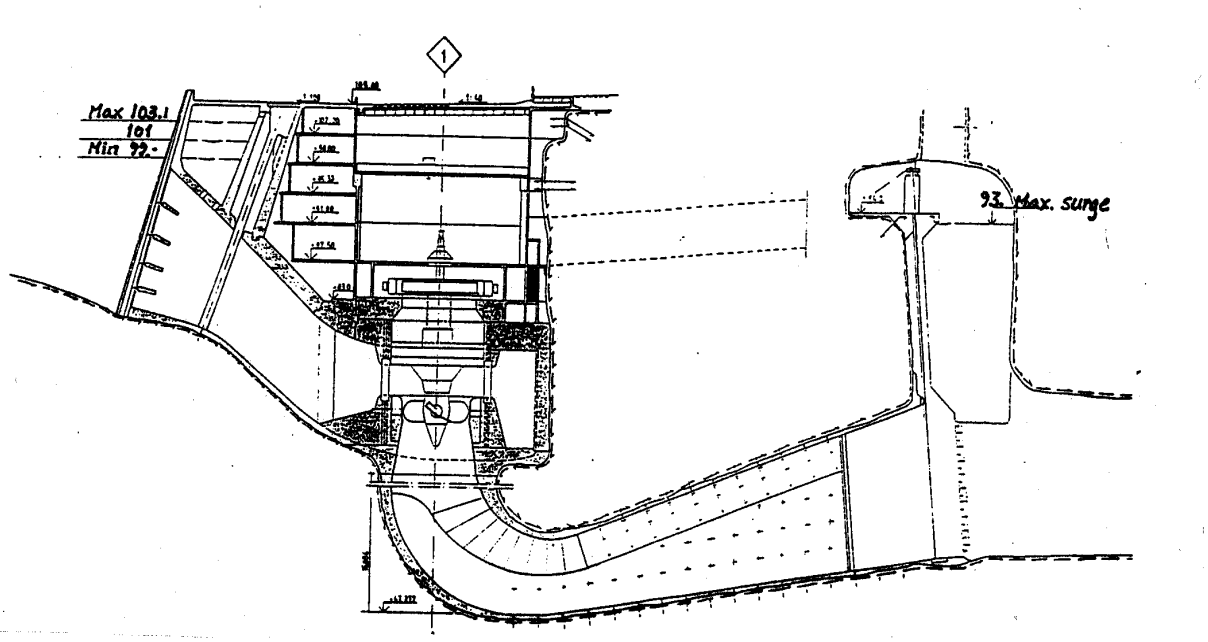

Fig. 6.15 Solbergfoss Kaplan turbine P=100 MW H=20 m n=79 RPM (courtesy Kværner)

In fig. 6.15 is shown the excavated powerhouse for Solbergfoss which has a big Kaplan turbine delivered by KVÆRNER. The turbine, which was described in fig. 4.6, has individual servomotors for the guide vanes. The unit has the thrust bearing located on the turbine head cover which reduces the relative vertical movement between runner and runner chamber. The max flow capacity is Q=500 m^3/sec.

In fig. 6.16 is shown the cross section of a traditional Kaplan turbine design with regulating ring and two or more servomotors connected to the ring from the inside. For smaller units the

regulating ring may be designed in the same way as for Francis turbines with the servomotors connected from the outside of the ring.

The advantage in the efficiency for Kaplan turbines is obtained by the double regulating system, which adjusts the runner blades in optimal position to the guide vanes position.

However, the double regulating system gives a complicated and expensive design.

On the other hand a higher specific speed of a Kaplan turbine compared with a Francis turbine is obtained without the disadvantage of a very narrow peak of high efficiency. This is because the efficiency of the double regulating on cam envelopes all peak efficiencies resulting in a wide range of high efficiency. This has earlier been illustrated in fig. 5.7 a in chapter 5.1 and the system allows for the possibility of having a higher specific speed than for a Francis turbine. Then the speed of the Kaplan turbine alternative will be higher than for a Francis turbine and the generator will be cheaper.

The runner blade guide vane combination is also governed by variation in the head leading to a two dimensional combination controlled by both flow and head (see fig 5.7 b chapter 5.1).

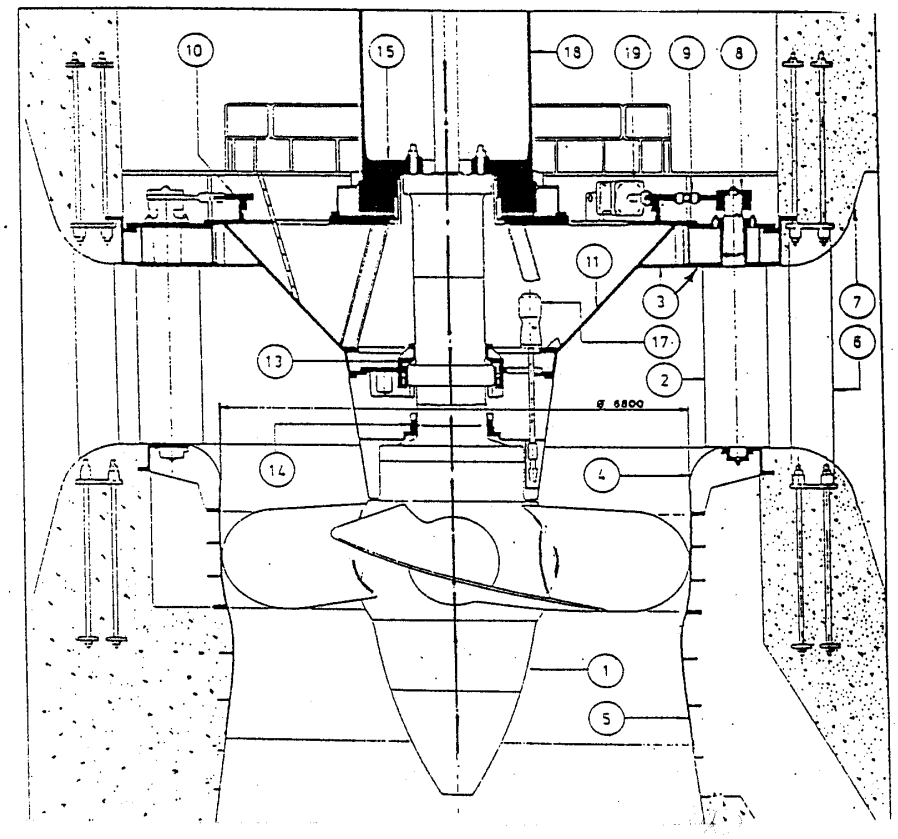

1. Runner
2. Guide vanes
3. Outer top cover
4. Bottom cover
5. Runner chamber
6. Stay ring
7. Spiral casing
8. Guide vane levers
9. Guide vane links
10. Regulating ring
11. Center top cover
12. Turbine shaft
13. Turbine bearing
14. Shaft seal
15. Trust bearing
16. Draft tube cone
17. Drainage pump
18. Intermediate shaft
19. Servomotors

Fig. 6.16 A general view of a traditional Kaplan turbine with regulating ring

Because of the large dimensions and the low pressure the main design criteria for the stationary parts of a Kaplan turbine will be deflections and clearances.

However, the most complicated part in a Kaplan turbine is the hub with the mechanism and servosystem for the runner blade control.

It is important to reduce the size of the turbine and get a high efficiency which may be obtained by making the hub as small as possible. The design criteria for the hub will be stresses besides acceptable deformation. The normal load will be the hydraulic forces during normal operation. However, the most extreme forces will occur during shut down and at maximum runaway speed with small runner blade openings and fully opened guide vanes with no load on the generator.

Such runaway shall never occur without serious failure in the guide vane/runner blade combination system and the (safety) margins for reaching the yield stress $\sigma_{0.2}$ is normally small both for turbine and generator.

For normal shut down of the generator load with runaway speed the runner blades shall close slowly from open position while the guide vanes shall close fast in order to avoid large guide vane opening combined with small runner blade opening. During fast opening at the guide vanes to gain load the runner blades should also open fast with the same speed as the guide vanes in order to follow the guide vanes in optimum efficiency position. Then a combination of large guide vane openings and small runner blade openings should be avoided if a sudden rejection of the generator load occurs.

One of the most difficult structural requirements to fulfil is to obtain a smallest possible gap between the runner blade tips and the runner chamber, due to deflections and roundness deviations of the large flexible runner chamber. Touching between blade tips and the runner chamber must be avoided, but large gaps decreases the efficiency. A mean value of clearance of 3-4 mm for a 5 m diameter should be obtained as a normal standard.

The different parts of a Kaplan turbine are illustrated in fig. 6.16.

In fig. 6.17 a traditional general lay out of a complete low load Kaplan turbine located in a dam with upstream and downstream gates is shown. The spiral casing is in this case an unlined concrete spiral because the turbine is designed for a very low head.

The most important assembly in a Kaplan turbine is as in a Francis turbine the rotating parts consisting of runner and shaft as shown in fig. 6.16. Note that the turbine guide bearing in fig. 6.16 is of the conventional type with a forged collar on the shaft and a non rotating lower oil reservoir. The oil circulation may be obtained by skewed grooves in front of the bearing pads or by means of an electric driven circulation pump.

The shaft seal may be of the carbon ring type or Teflon ring type because the seal is exposed to the pressure upstream of the runner and a pumping plate system with a labyrinth seal running dry in air cannot be used.

The hub may be of the same type as shown in detail for the Kaplan Bulb type turbine in fig. 6.21.

The erection of a Kaplan turbine starts as for a Francis turbine with concreting the draft tube lining (normally through the bend only) and making the foundation and anchoring plates for erection of the stay ring and spiral casing.

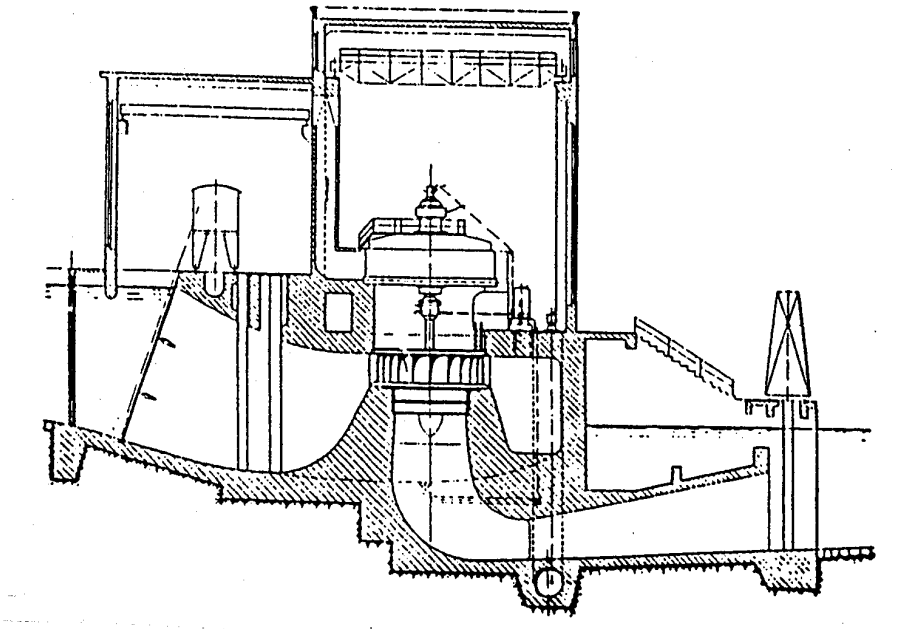

Fig. 6.17 A complete Kaplan turbine with gates for a low head power house in a dam

The first step in the erection of the stay ring pos 6 and 7 in fig. 6.16 will be concrete embedment of the long anchoring bolts for transfer of the hydraulic forces to the concrete. [For low head turbines the concrete and the weight of the generator help balancing the hydraulic forces. This is not possible for high head Francis turbines because the weight of generator and possible stress forces in the concrete cannot carry the very large hydraulic forces of a high head turbine.]

The concreting of the spiral casing and the runner chamber of a Kaplan turbine is normally continued to also include the generator foundations.

The next step after the concreting is to mount the guide vanes and the outer cover. The last erection work of the heavy main parts is to lower the complete set of shaft, runner and central top cover and position the runner in center ready for the generator shaft to be coupled after the generator stator is completed.

In the case as illustrated in fig. 6.16 in this chapter the thrust bearing is part of the turbine delivery and control of the straightness of the turbine generator shaft and the center positioning and run out of the rotating parts will be part of the turbine erection work.

For some turbines the runner blades may be removed through openings in the runner chamber while for other turbines the blades can only be removed from the hub after the runner is removed from the turbine.

Minor weld repair work on the runner blades may, however, be done without any dismantling. A modern Kaplan turbine is normally regarded to be a reliable turbine. The guide vane/runner

blade combination is not established by means of a mechanical cam transmission in a modern Kaplan turbine, but a double set of programmable logic control system feeding signals to hydraulic control valves for an individual control of guide vanes and runner blades after a programmed combination. Back up systems is in this case a necessary and important part of the system. Reliable systems of this type have been in operation for years and mechanical cam control is no more delivered for modern Kaplan turbines.

6.5 Kaplan Bulb turbines

The Kaplan Bulb turbines are as described in chapter 4.2, the horizontal version of the Kaplan turbines.

The design of these turbines is characterised by having both essential turbine parts and the generator inside a bulb, which have given the name of this turbine type. Further a horizontal shaft is characteristic for a Bulb turbine as well as a conical arrangement of the guide vanes and the straight horizontal draft tube.

By the locating of the generator in the bulb upstream of the turbine this part is forming the inlet conduit together with the outer steel liming of the concrete. The upstream bulb including the generator is normally delivered by the generator manufacturer.

In fig. 6.18 the design of a complete Kaplan Bulb unit is shown including generator, draft tube and inlet gate. The name of the power plant is Bingsfoss, which is located in Norway. The turbines are delivered by KVÆRNER.

For this plant there are no draft tube gate. Instead there is a stop log system for dewatering of the turbine if a main repair should be made. The reason for this is the individual servomotor system of the guide vanes with a back up pressure system. A speciality used in this case is that it is possible to open each one of the guide vanes individually by means of the individually controlled servomotors (one for each guide vanes). With this system it is possible to flush out pieces of wood or other objects which might be jammed in between the guide vanes without any disturbance of the power production. The generator brakes are also dimensioned for stopping the aggregates with two fully opened guide vanes.

The data for the turbines for Bingfoss power plant are P=10.8MW, H=5.0m and n=71.4RPM. The runner diameter is 6.05m.

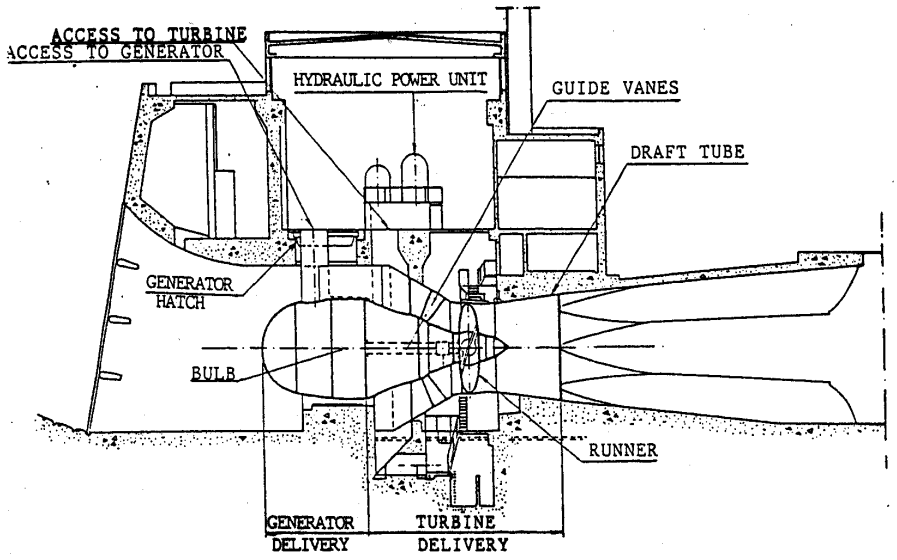

Fig. 6.18 The Kaplan Bulb turbine for Bingsfoss Power Plant

The main parts in a Kaplan Bulb turbine downstream of the generator, shown in fig. 6.19, includes the stress carrying parts transferring the axial- and radial forces from the downstream conical parts of the bulb (5) to the outer conical plate structure (6) through the struts (7) including the access to the turbine pit inside the bulb.

In fig. 6.20 the rotating parts including the generator shaft (3), the oil inlet box and the mechanical blade position indicator on the upstream side of the generator bearing is shown (9).

The runner hub is the most complicated part for a Kaplan or a Kaplan Bulb turbine and in fig. 6.21 a drawing of a modern design of a runner hub is shown. The main body of the hub (1) is normally casted, as shown in fig. 6.21, but this complicated part has also been fabricated from slabs (thick plates) in order to avoid casting defects. The stresses and deformations in such hubs must be carefully analysed by Finite Element Method (FEM) especially for high head Kaplan turbines where the number of blades may be as high as 8.

In Kaplan Bulb turbines the maximum head is normally below 15 m and the number of blades are normally limited to 4 due to the high specific speed.

Besides the main body of the hub (1) the blades pivots (2) with its support, the blades (4) with blade pivot connections and water seal for the blades are the most critical components. Also the runner blade levers with hubs (3) and connecting links (5) to the servomotor (6) are parts which are vital for the reliability of the turbine. Note that the servomotor cylinder is the movable part of the servomotor and the piston attached to the piston rod, is the stationary part in this case.

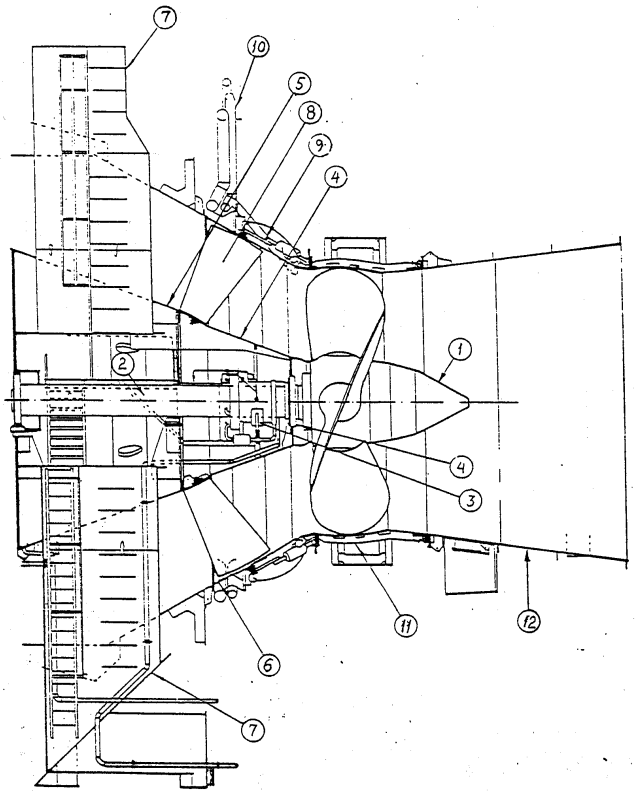

1. Runner
2. Turbine shaft
3. Turbine bearing
4. Shaft seal (Teflone type
5. Inner cone
6. Outer cone anchored in the conrete
7. Struts connecting (5) and (6) for transferring axial and radial forces

8,9,10. Guide vane with servomotor and pressure oil supply pipes
11. Runner chamber
12. Draft tube cone

Fig. 6.19 Details of the Kaplan Bulb turbine for Bingsfoss (courtesy KVÆRNER)

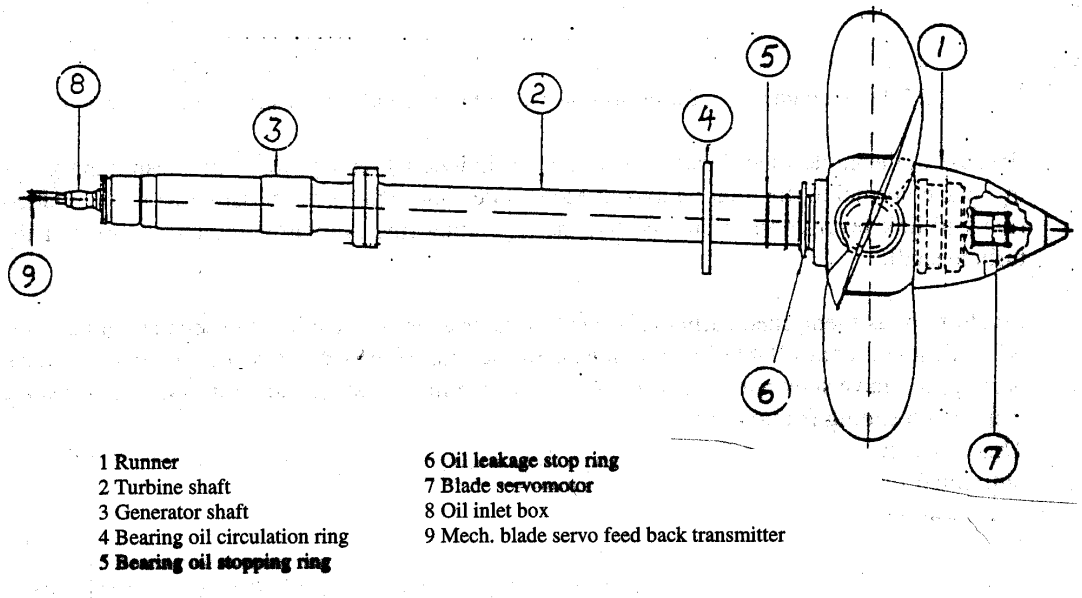

1 Runner
2 Turbine shaft
3 Generator shaft
4 Bearing oil circulation ring
5 Bearing oil stopping ring
6 Oil leakage stop ring
7 Blade servomotor
8 Oil inlet box
9 Mech. blade servo feed back transmitter

Fig. 6.20 Rotating parts for a Kaplan Bulb turbine

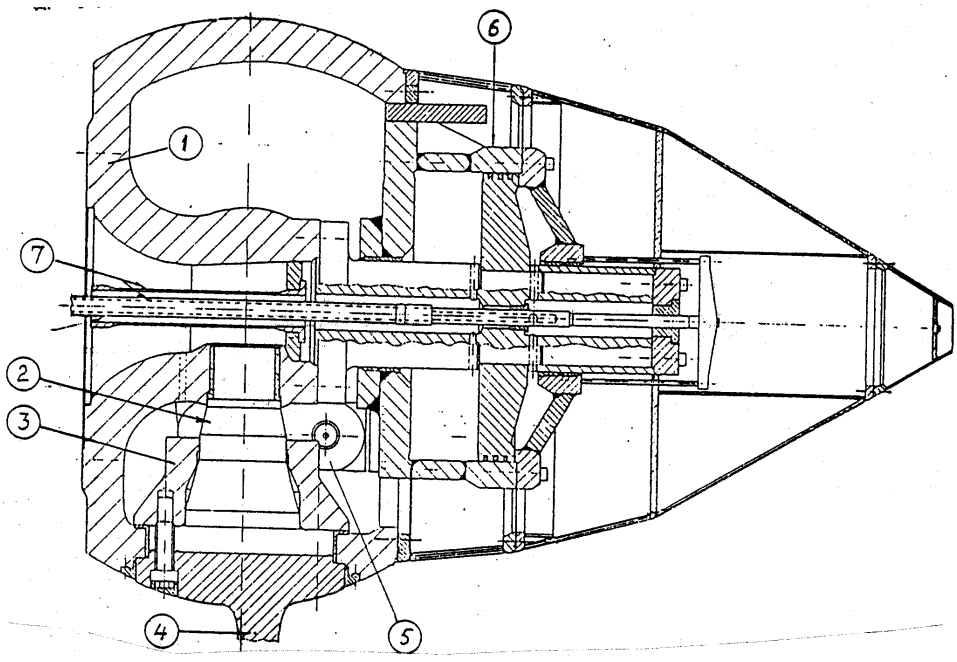

Fig. 6.21 Runner hub for a Kaplan Bulb turbine or a Kaplan turbine (courtesy KVÆRNER)

In fig. 6.22 the arrangement of a servomotor system with individual servomotor is shown.

Because of the guide vanes location on a cone the individual servomotors will transmit the forces in a plane normal to the rotating axis of each guide vane. This is not possible with a regulating ring and link lever connection, because the regulating ring is rotating around the axis of the turbine shaft.

In addition, as mentioned earlier it is possible to arrange for opening one separate guide vane with sufficient controllable force by means of the individual servo system. The two technical descriptions have shown the main advantages for the individual servomotor system besides the fact that no sliding friction or breakage link system of the guide vane connections is necessary. This because the closing force on one guide vane is limited to the force from one of the individual servomotors which cannot destroy the guide vane.

The different parts of the servo system are described in fig. 6.22.

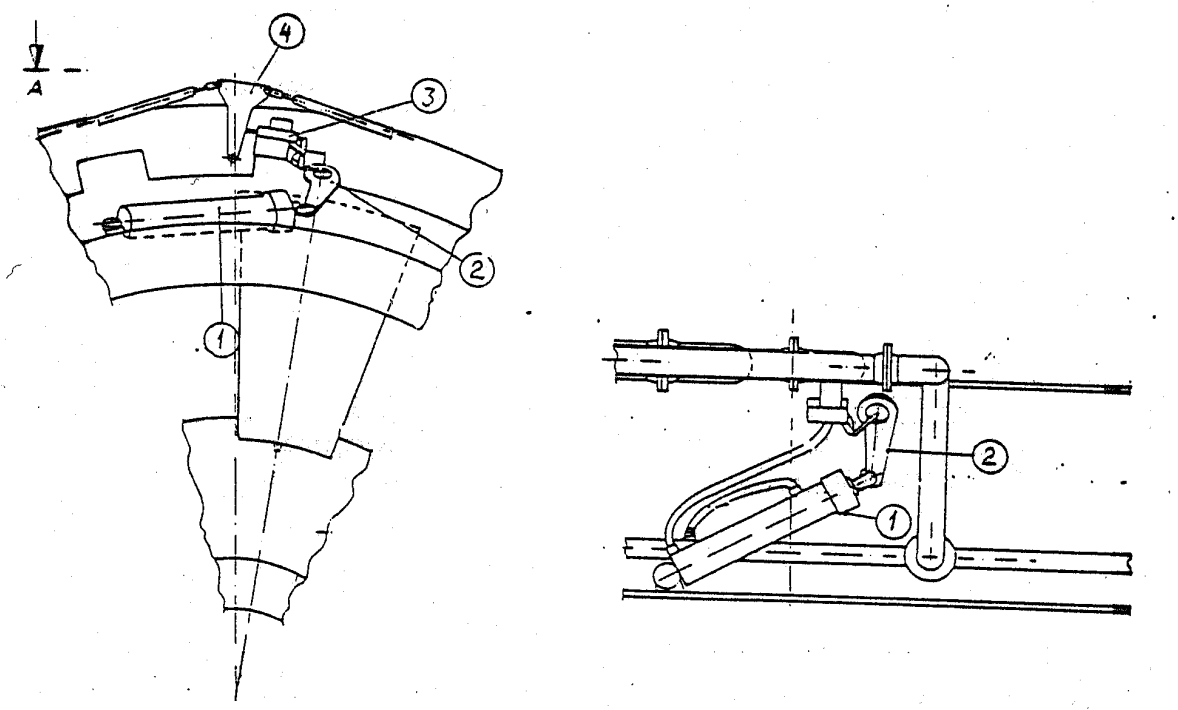

1. Servomotor
2 . Guide vane lever
3. Servo valve
4 . Mechanical forward signal to servo valve

Fig. 6.22 Arrangement of the individual guide vane servomotor system.

The limitation of head for using Kaplan Bulb turbines will be the axial forces from runner blades, guide vanes and bulb which must be transferred to the surrounding concrete via the struts (7) shown in fig. 6.19.

Another limitation is the safety of buckling for the generator bulb and the limitation of diameter which limits the available rotating inertia mass of the generator rotor which in turn increases the difficulty of obtaining stable speed control on isolated load.

In order to explain the design further it will be convenient to study the erection procedure which gives a good description of the design requirements as illustrated in figs. 6.23a, b, c, d and e.

The main structural part for embedment in concrete will be the outer cone connected to the inner down stream cone of the bulb by the struts (7) in fig. 6.18. These parts are welded together and positioned as shown in fig. 6.23a, where the first stage concrete work has been finished before turbine erection starts. (See pos. 1, 2, 3, 4, in fig. 6.23b)

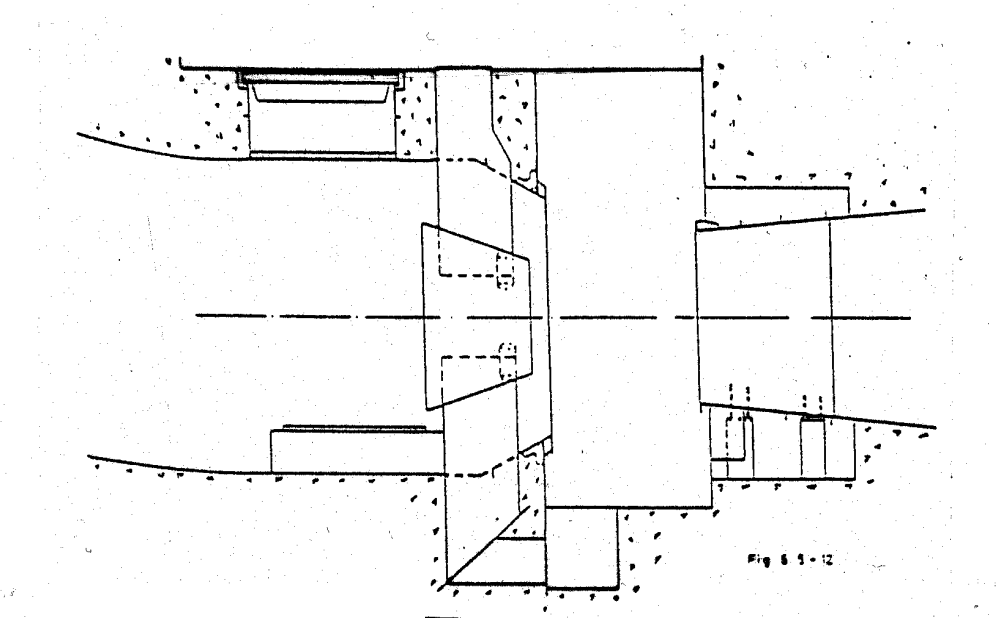

Fig. 6.23a Stress carrying parts embedded

Before the second stage of concreting shown in fig. 6.23b, the draft tube cone (5) and the access hatch for generator erection (with hatch cover for stiffening purpose) (6) is erected ready for embedment in concrete. Also the concrete foundations with anchoring plates for the generator bulb support are concreted together with the access hatch in the second stage. However, by regarding fig. 4.23c, showing the second stage concrete work finished we will find that the draft tube cone has not been embedded. This is because it is convenient to have the possibility of a final alignment in a later stage if the buoyancy of liquidized concrete has changed the position of the stress carrying parts and of the downstream bulb cone (7).

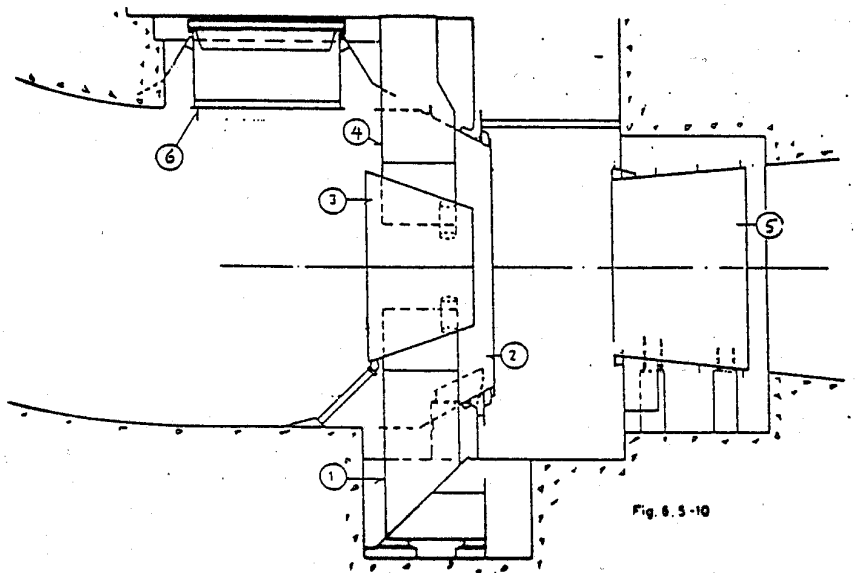

Fig. 6.23b Turbine and generator erection after the first stage of concreting before turbine erection

In fig. 6.23c the major erection work of the non embedded parts is illustrated. The inner cone (7) is bolted to the inner cone of the embedded site welded structure consisting of pos. 1, 2, 3

and 4 in fig. 6.23b. Then the horizontally split outer cone pos. (8) and the guide vanes are erected with bolt connection to the embedded outer cone [(2) in fig. 6.23b]

Finally fig. 6.23c shows the stainless steel runner chamber (10) erected in order to line the draft tube cone (5) in correct position to pos. (7) before being welded to the steel lining of the downstream part of the draft tube.

Now the turbine is ready for the final concreting including the draft tube cone (5) and the connection to the draft tube lining. (The concreting of the draft tube gate, which is done separately in connection to the draft tube concreting is not shown in this description).

The final turbine erection, before the beginning of the generator erection, starts with the turbine bearing (11) and a preliminary support at the upstream end of the shaft (see fig. 6.23d). Then the shaft is positioned and lined to fit the centerline of the draft tube and the bottom section of the runner chamber, which is fixed in its final position after the last concrete work. This is a very important part of the erection work. It should be noted that the buoyancy of the runner must be taken into consideration when adjusting for the theoretical tip clearances of the runner blades during the alignment of the turbine shaft.

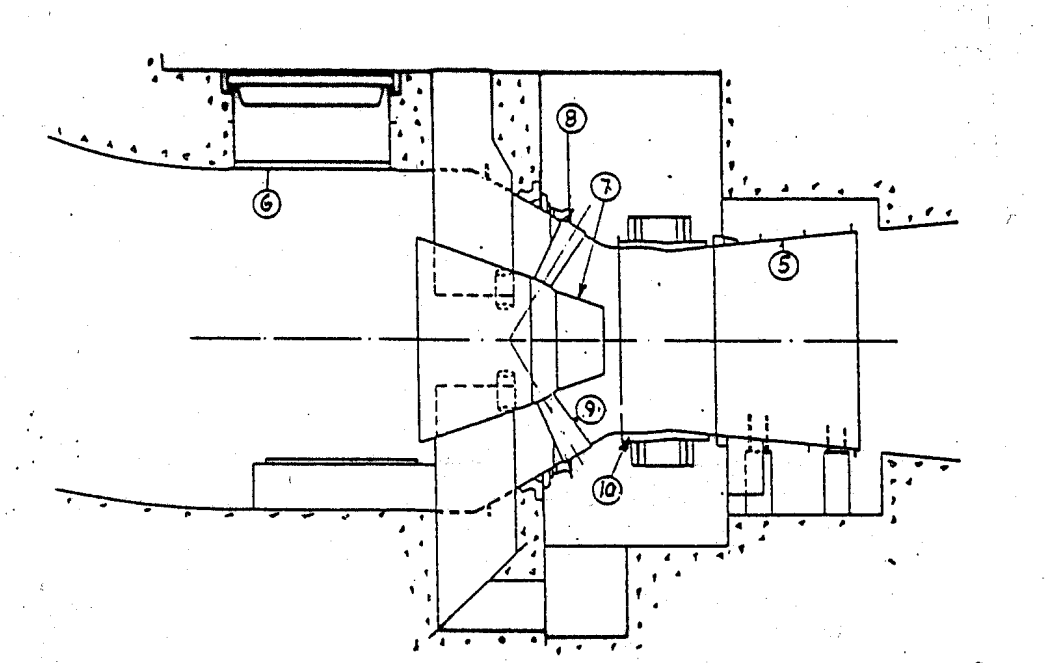

Fig. 6.23c Second stage of concreting

The last parts of the turbine to be erected is the runner and the shaft seal (14) and (13) respectively and finally the upper part of the runner chamber which has been removed during the
runner erection (see fig. 6.23d). The governor and the guide vane servo system and the generator erection work can now be started.

The mounting of servomotor system and other light weight part in the turbine and governor system where the heavy power house crane capacity is not needed may continue by means of light weight cranes during the erection work of the heavy generator parts. The joint between the turbine parts and the generator as well as the cover plates to form the support structure and access tubes to the turbine pit is also normally made by the turbine manufacturer in

collaboration with the generator manufacturer. These parts are shown in fig. 6.23e (15) where the completed Kaplan Bulb unit with generator is shown.

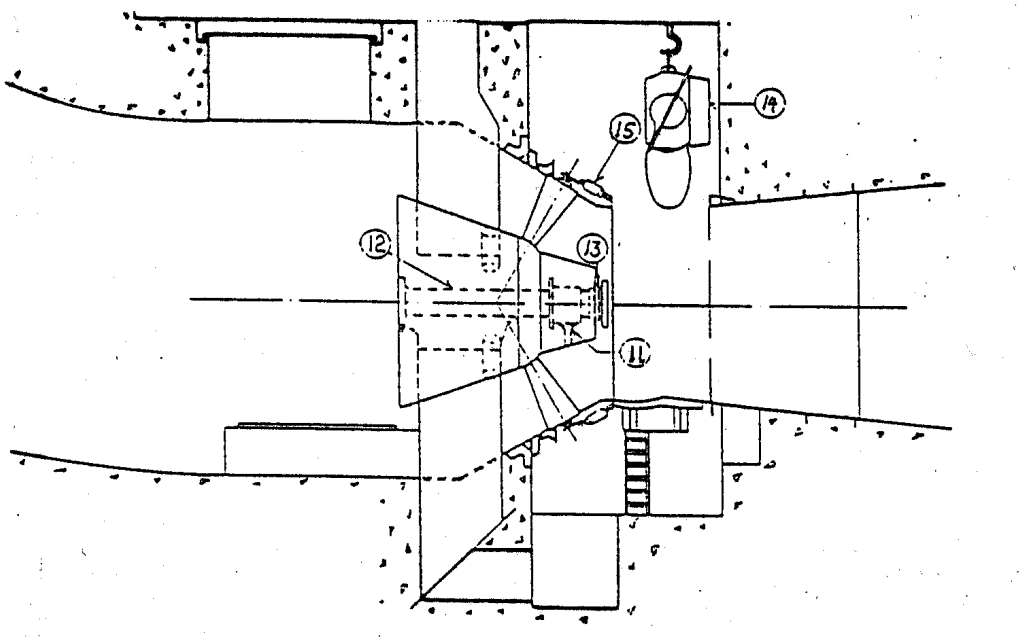

Fig.6.23d. Connection of runner to turbine shaft

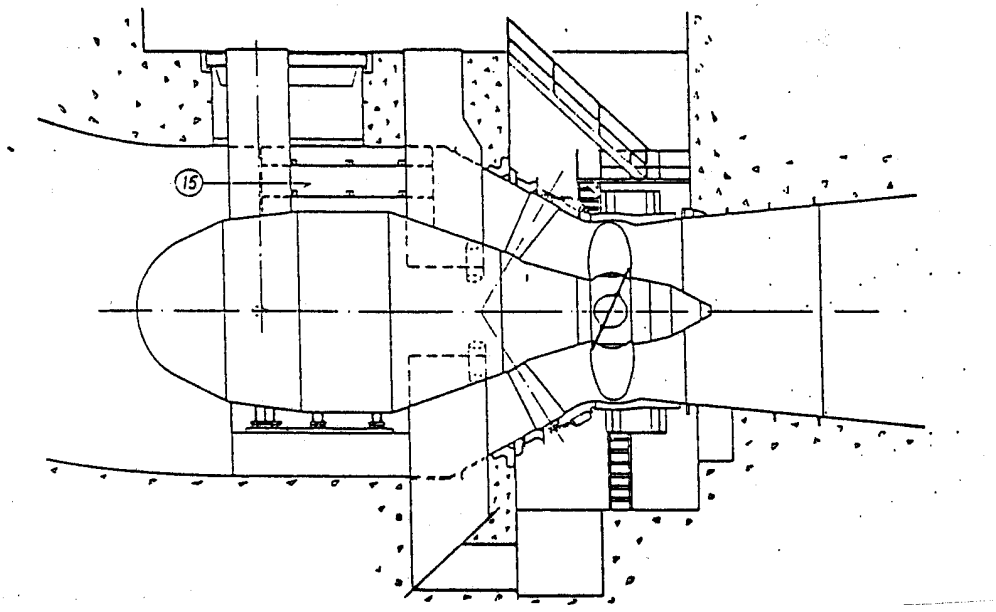

Fig. 6.23e Kaplan Bulb unit with generator bulb

6.6. Reversible Pump Turbines

The design and erection of reversible pump turbines will, except for the bearing, be similar to an ordinary Francis turbine and will not be repeated in this chapter (see chapter 6.3). It should also be noted that the bearings for a reversible pump turbine must be designed for rotation in both directions.

The most commonly used reversible pump turbine is the Francis type. However, the runner or impeller/runner is in shape closer to a pump impeller than an ordinary Francis runner.

Also reversible pump turbines of Kaplan Bulb, Kaplan or Deriaz turbines are used for high specific speed pump turbines with low head operation. These types of reversible pump turbines have so far not been installed in Norway and are not described in this book.

For the design of high head Francis type reversible pump turbines, special caution should be taken concerning design for reliable operation and long lifetime.

1. To avoid too low specific speed the maximum speed of the blades on the suction side of the runner may be as high as 55 m/sec* i.e. approximately 20% higher than for a Francis turbine. This requires deeper submergence and the designer must be more careful with shaft seal design. In addition the high back pressure gives a high cooling water pressure and possible leakage problems on the suction side requires high drainage pump energy consumption.

2. A practical problem for reversible pump turbines is the need for trash rack also on the suction side, and for extreme low setting (large submergence) the draft tube gate must be substituted by a valve in some cases.

   *Higher blade velocities on the suction side increase the danger of dynamic problems. Another problem is cavitation and pressure pulsation problems which will be more serious than for a Francis turbine due to the higher relative kinetic energy on both suction side and pressure side of the runner.

3. However, the most serious design problems the engineer will find on the pressure side of the turbine, because of the very high circumferential speed of the runner and the high relative velocities due to the back swept runner blades caused by the need for pumping against the same or normally higher pressure than for turbine operation.

   Because of the back swiped blades (similar to a low specific speed pump impeller) the number of blades are normally between 6 and 11 i.e. lower than for a Francis turbine. Together with high specific energy the lower number of blades compared with Francis runners creates high stresses in the joints between the blades and crown and shroud.

   In off design operation in turbine mode and especially during starting of the pump, the pressure fluctuations are much higher than for a Francis turbine and both the hydraulic designer and the structural designer must be very careful with both the runner design and the design of the guide vane system. Fatigue problems have been reported by many manufacturers.

4. Dynamic hydraulically induced radial forces require a careful design of the blades and of the labyrinth rings. Especially the lower labyrinth on the shroud must be made with care. These problems are also well known by pump manufacturers.

   A general advice may be to make the last labyrinth or last part of the labyrinth on the shroud with the smallest clearance. This is because it gives a stabilising tendency by increased pressure on the side of the runner which are moving towards the stationary seal ring. This pressure increase will push the runner back and thus stabilise the system. (However, the explained "spring" effect may also theoretically give a resonance frequency close to the running speed or other natural frequencies in the structures of the runner, but such effect has not been observed to the authors experience).

   The bearing of a reversible pump turbine must as mentioned earlier have bearing pads suitable for running in both directions. For rigid pads (not tilting) the bearing surface will be limited, but according to experiences from the Norwegian manufacturer KVÆRNER reversible pump turbines are operating satisfactory with this bearing with a design described in the chapter 6.2 of Francis turbines but with wider bearing pads skewed for oil entrance from both sides.

   The erection procedure and dismantling procedure with a free draft tube cone and dismantling of runner and lower cover down and out has been made for all reversible pump turbines delivered by KVÆRNER in Norway. No problems has been reported caused by this design for pump turbines operating at heads up to 450 m.

   For the erection and dismantling procedure see chapter 6.3 of Francis turbines, because the procedure will be identical to the procedure for high head Francis turbines.

7. DRAFT TUBE DESIGN AND SURGE PROBLEMS

GENERAL COMMENTS

The purpose of the draft tube is to convert the specific kinetic energy at the runner outlet to specific pressure energy by an increasing cross section of the draft tube towards the outlet.

Because the specific kinetic energy in off best point operation includes rotational energy, surging problems may occur in the draft tube which may lead to severe problems for the performance of the turbine.

7.1 The design of draft tubes

Except for Kaplan Bulb turbines the draft tubes are normally shaped with a bend.

The flow is decelerating through the draft tube in general, but in a bend decelerating flow may cause problems because of danger of separation and cavitation.

To reduce this problem the draft tube is normally shaped as a straight cone in the first section after the runner outlet in order to decrease the velocity in front of the bend as much as practical possible.

Through the bend the flow is normally slightly accelerated toward the outlet of the bend in order to avoid separation.

After the bend towards the outlet the cross sections is normally converted to a rectangular shape in front of the draft tube gate frame and the concrete structure which starts where the steel lining ends. Unlined concrete may be used up to a flow velocity of 6 [m/sec]. (Special concrete may allow for higher velocities without erosion damage).

In order to decrease the cost of excavation, the depth of the draft tube bend should be reduced as much as possible especially for low head machines with large dimensions. This is important especially for Kaplan turbines where the runner centre is located far below the centre of the spiral case. However, from chapter 8.4 and 8.5 we learned that the efficiency loss in the draft tube is a large portion of the total loss because the value of the kinetic energy $c^2_2/(2gH)$ is large compared with the total available energy gH for a low head Francis turbine and a Kaplan turbine. It is also important that as much as possible of the specific kinetic energy downstream of the runner is converted to pressure energy in the draft tube in low head turbine.

On the contrary the energy loss which occurs by removing the draft tube and loosing all specific kinetic energy of a high head Francis turbine may be less than 1% compared with the equivalent specific energy loss in a Kaplan Bulb turbine which may be more than 50% of the total specific energy for very low head.

For years intensive studies of draft tube losses have been made for Kaplan turbines and low head Francis turbines to improve the draft tube efficiency. Through this research work an optimal shape of the draft tube has been found by increasing the width of the tube through the bend and thus the height has been decreased accordingly.

It has also been obtained very good results of the kinetic energy conversion without acceleration through the bend, but acceleration through the bend is in general preferable in order to prevent separation at the bend's outlet.

The difference in the turbine power caused by the draft tube loss for an even velocity profile and an uneven velocity profile can be illustrated by the equation shown below.

Note that the outlet loss with an even velocity profile i.e. $c_{m3}=Q/A=$const over the cross section is not regarded to be a turbine loss, but a plant loss according to IEC code. However, the increase in power loss ΔP from variations in velocity over the cross section and any swirl flow loss is regarded to be a turbine loss.

The equation for the turbine loss from variations in the meridional outlet velocity yields:

$$\Delta P = \int\int_A c_{m3}\frac{c_{m3}^2}{2g}dA - \int\int_A \frac{Q}{A}\left(\frac{Q}{A}\right)^2/(2g)dA$$

$$\Delta P = \int\int_A \frac{c_{m3}}{2g}^3 dA - \int\int_A \left(\frac{Q}{A}\right)^3/(2g)dA$$

Here c_{m3} (m/s) is the meridional local velocity at draft tube outlet and A (m^2) is the cross section area of the draft tube outlet and Q (m^3/s) is flow.

In addition to this loss swirl flow from the runner will also be lost. However, a slight swirl flow may lead to a reduction of the meridional outlet loss because the meridional velocity distribution may be more even over the cross section. The reason for this is that separation at the outlet of the bend may be avoided by a slight swirl flow.

In fig. 7.1 and fig. 7.2 the cross sections through the draft tube bends of a high head Francis turbine and a Kaplan turbine respectively are shown.

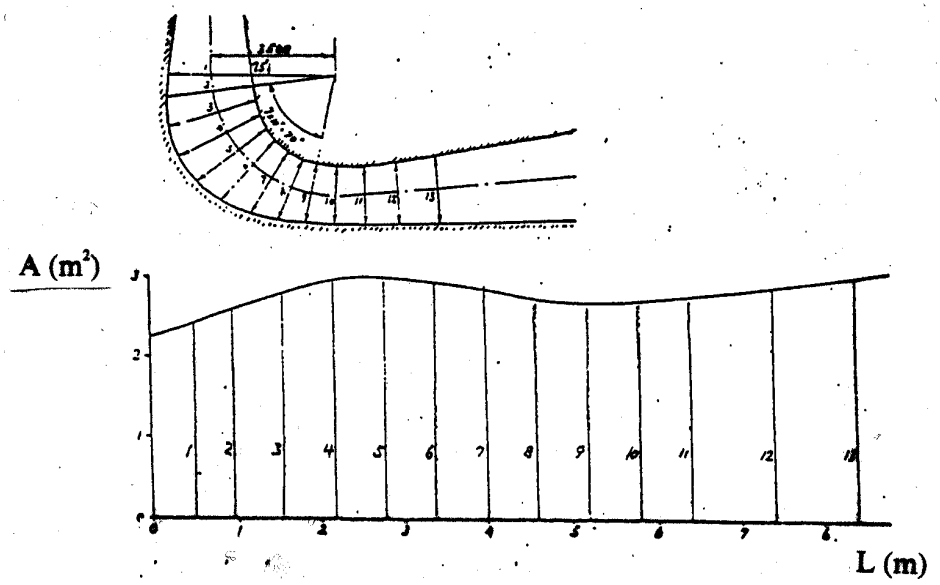

Fig. 7.1 Shape of draft tube bend of a Francis turbine P=36.7 MW, H=236 m, n= 428.7 RPM

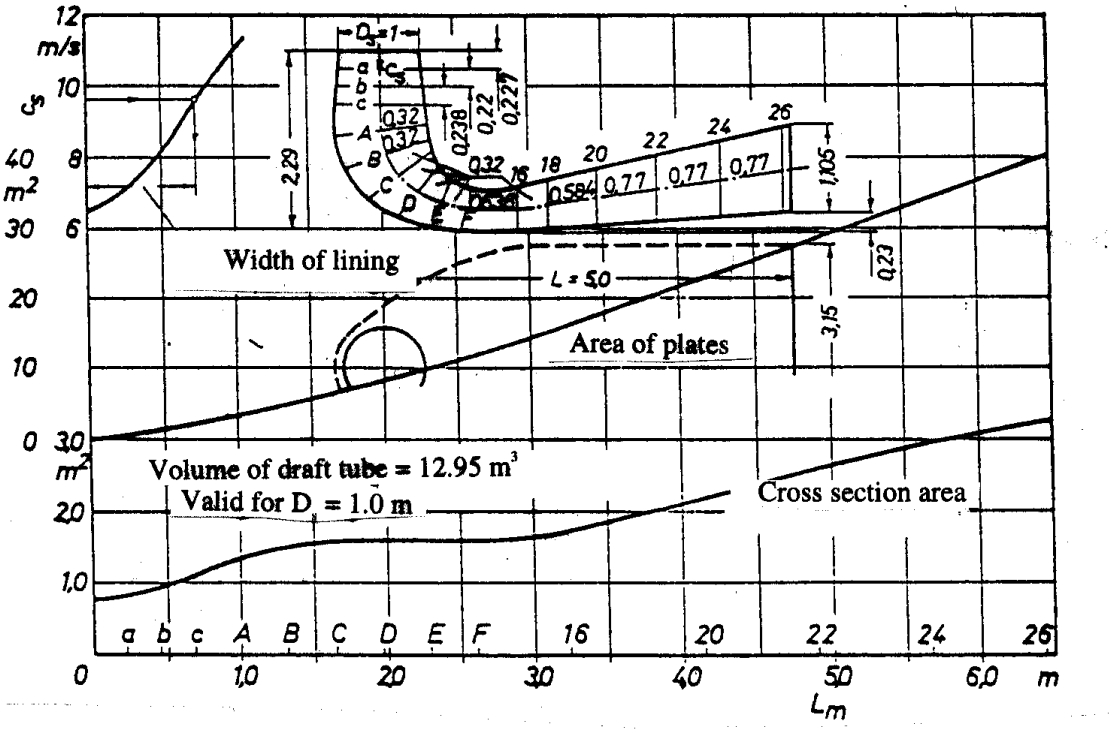

Fig. 7.2 Shape of a draft tube with inlet diameter D_s = 1.0 m for a Kaplan turbine (From Raabe)

7.2 Surge problems

The flow in the draft tube is complex because the turbine shall operate also outside best efficiency point. The first and best known surging problem is caused by the part load cork screw spiral which causes pressure surges at a load around 50% to 70% of best efficiency point for Francis turbines.

[For Kaplan turbines there are no stationary operation off cam, i.e. outside best efficiency point and part load surging problems similar to those of a Francis turbine does not normally occur]

The part load surging is recognised as the so-called Rheinganz frequency, which will have a frequency approximately like 1/3 of the rotational speed of the machine. However, the frequency and pressure amplitudes will depend of the geometry of the runner. So far no computer programs has been able to handle this phenomena properly.

In a model turbine the Rheinganz vortex core is visible at low σ values as a cork screw shaped void rotating in direction of the runner speed with frequency, as mentioned above, of approximately 1/3 of the shaft speed (see fig. 7.3). (A double corkscrew vortex core has also been observed, but a fully developed theory of the phenomena does not exist so far).

In addition to the unsteady behaviour at part load there has also been observed unsteady behaviour at operation above best efficiency at nominal full load and over load.

This surge phenomena at full load and above seems to have its root in a rotating symmetrical void stretching down from the centre of the hub as shown in fig. 7.3. If the air inlet in the centre of the bulb in a runner is blocked, unsteady behaviour may occur because of poor cushioning of the pressure surges without air in the voids at full load.

This symmetric full load centre core is rotating, towards the rotation of the runner and creates no rotating pressure pulsation on the draft tube wall similar to the cork screw vortex core which rotates in the same direction as the runner at part load. However, if pressure surges occur at full load pressure pulsation will be observed symmetrically around the draft tube cone without rotation. In fig. 10.3 the cork screw vortex and the full load void is illustrated schematically as a function of the load.

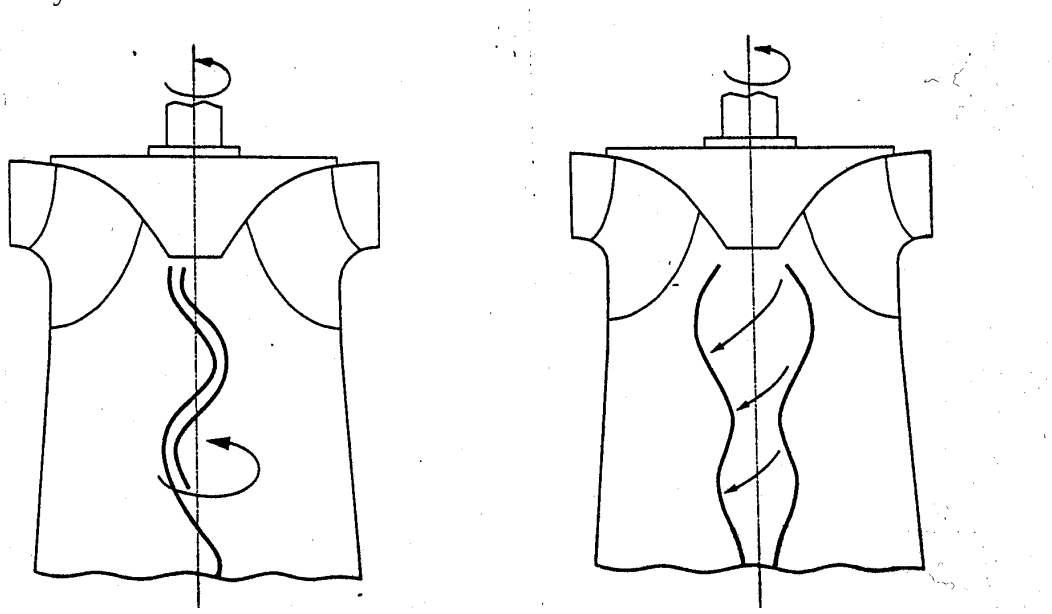

Fig. 7.3 Part load draft tube swirl and full load draft tube swirl in a Francis turbine

Analysis of the unsteady behaviour

The part load frequency has normally, as described earlier a rotational frequency of approximately 1/3 of the rotating speed of the turbine. Also the axis symmetrical void at full load and overload may cause pressure pulsation if the air and vapour cushion and the draft tube water column has a natural frequency in resonance with any driving frequencies in the system.

For example if this frequency is in resonance with the natural generator rotor frequency in the magnetic field of the stator or with the natural frequency of the hydraulic conduits, non-acceptable operational problems may occur.

The natural frequency of the generator rotor will be between 1 and 2 Hz depending on the load conditions and the voltage governor. For full load or overload condition a power and pressure oscillation with a natural frequency of draft tube surges may occur. By regarding the dynamic problem as a mass oscillation of the water in the draft tube against the elasticity of the air and vapour filled void below the runner hub, a simplified surge frequency formula may be established. The problem is illustrated in fig. 7.4.

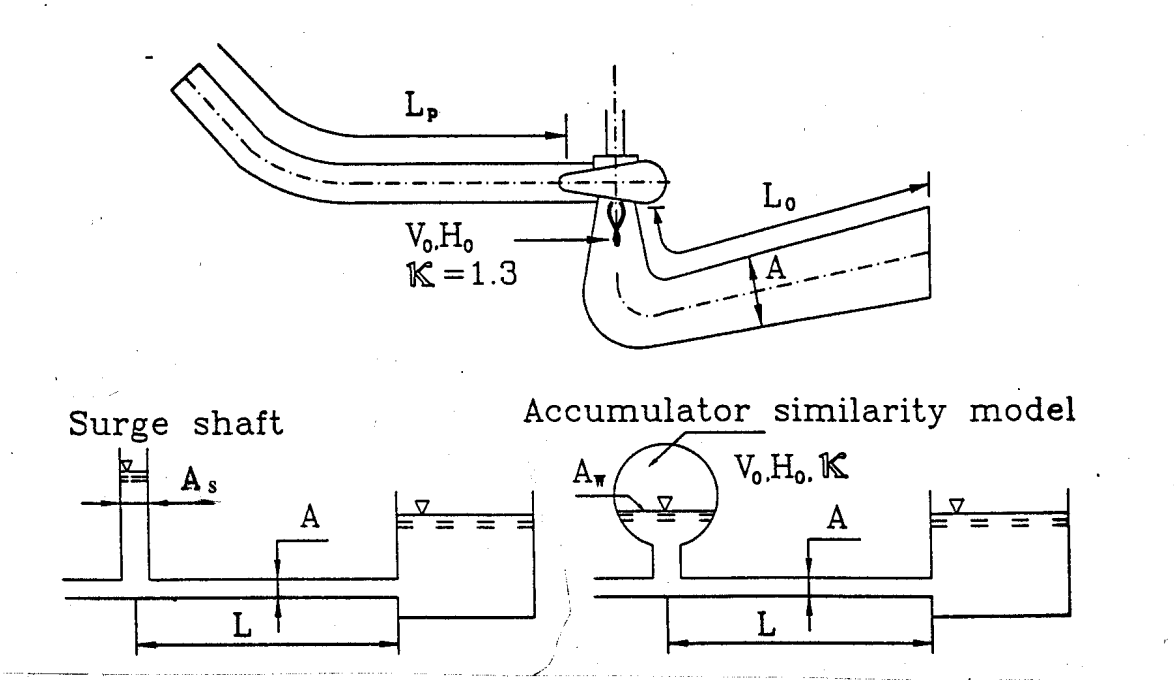

Fig. 7.4 Illustration for simplified calculation of possible resonance

For a similarity model shown in fig. 7.4, we can put up the natural frequency by the following well-known formula for a tunnel with surge shaft or air accumulator

$$f = [gA/(LA_s)]^{0.5}/(2\pi) = [gA/(LA_{eq})]^{0.5}/(2\pi) \quad [Hz] \tag{7.1}$$

Chapter 12.1 eq. 12.4c shows that $A_{eq} = V_o/(\kappa H_o)$, A = mean cross section of draft tube.

Where V_o = volume of the air and vapour in the void below the runner (m^3), H_o = the pressure in the void (mWC) and from experiences with air accumulator with vapour saturated air assuming the polytrophic exponent $\kappa = 1.3$. Further $H_o \supset$ NPSH + h_{va}.

Then the natural frequency of the draft tube surging can be found by following formula

$$f = [gA\kappa H_o/(L_o V_o)]^{0.5}/(2\pi) \quad [Hz] \tag{7.2}$$

In the draft tube-turbine-generator-penstock system shown in fig. 7.4 also has the natural frequency of the penstock (1. harmonic, 3. harmonic, 5.harmonic .....etc.)

$$f_p = a/4L, 3a/4L, 5a/4L \ldots\ldots[Hz] \tag{7.3}$$

In addition to these frequencies we know that the natural frequency of the generator rotor speed will be between 1 and 2 [Hz]. (Normally this frequency is around 1.5 [Hz] depending on the connection to other machines in the power house and the electric grid, as well as the of the voltage governor design). Let us assume the generator frequency to be

$$1.2 < f_g < 1.7 \text{ Hz}$$

[Formulas for calculating this frequency exists, but is not included in this book].

An example from Kvilldal power plant may be used for illustration of the problem.
In this power house 4 machines with power P = 315[MW] net head H = 520 [m] and speed n = 333.3 [RPM] are installed. By running simultaneously the two machines with the shortest penstocks with the two other machines stopped in Kvilldal, power surges and pressure surges occurred at full load. Power oscillations of 60[MW] was recorded. However, by switching off the voltage governor during testing the power swing and pressure oscillations stopped, but when the voltage governor was switched on again, the oscillations came back.

The frequency of the oscillations was between 1.4 [Hz] and 1.5 [Hz] in that case.

By using the data for the draft tube in this example we have:

V_o assumed to be ~ 0.5 [m^3] by studying the void from the model turbine tests.
H_o 5[m w.c.] abs. pressure
A = 5 [m^2)
L = 30 [m]
κ = 1.3 polytrophic exponent for water saturated air.

From equation (7.2) we get: f = 1.46 Hz which is very close to the measured frequency.

In addition the natural higher order frequencies for the penstock was close to the oscillating frequency.

The reason for the strong impact on the oscillations from the variation in the speed of the generator can be found in the turbine characteristics for such low specific speed machines.

Because of the negative slope of the constant guide vane characteristics in the turbine characteristic diagram the flow will decrease for an increase in speed during the speed variations of the generator caused by the rotor oscillations the magnetic field of the stator. The decreased flow will cause pressure surges which will give a positive feed-back by increasing the turbine speed, which in turn will increase the speed further if the pressure and speed oscillations have the same natural frequencies and are close in natural frequency.

This causes an unstable behaviour with increasing amplitudes which are limited only by frictional losses in the water conduits and turbine as well as from damping in the electrical system and the generator.

The natural mass oscillation illustrated in this chapter is depending on the submergence of the turbine, which will normally vary from time to time depending on the tailrace level, which will change the parameters V_o and H_o in eq. (7.2).

The given example shows that surging problems are very complex, and may be amplified if the natural frequencies of generator, penstock and draft tube are close.

High frequency pulsation in the draft tube from cavitation or hydraulic instability in the runner etc. may also cause problems. However, pressure variations in the draft tube should not cause serious radial forces on the runner by using a careful design of the labyrinth seal rings with the smallest clearance in the last labyrinth nearest to the suction side of the shroud. This is because when the last labyrinth clearance is dominating the throttling a centring force is established

because an increased pressure will build up a force on the runner shroud directing the runner back to a concentric position if the runner is moved out of its centre.

7.3 Basic theory of swirl flow in a draft tube cone

The power of the swirl flow leaving the runner is lost unless stationary guide vanes are transforming a torque to the stationary draft tube. However, it is of interest to make a theoretical analysis of the development of the swirl flow energy flux through a straight cone for non-viscous liquid in order to get a better physical understanding of the problem.

A physical understanding of the swirl flow in the draft tube cone may be obtained by an idealised swirl flow model as described in this chapter. The main purpose of the draft tube is to convert kinetic energy to pressure energy in the most efficient way.

In order to study these phenomena theoretically certain simplified boundary conditions must be made. The most important simplification is an assumption of a constant meridional velocity over the cross section both at inlet and outlet. (In a real flow the low pressure in the centre of the inlet may lead to a reversed meridional flow in the centre from outlet towards the inlet. In any case the assumption of constant meridional velocity c_m is doubtful.)

However, even if this assumption is incorrect a theoretical simplified study gives a basis for judging the result of CFD computations of these phenomena.

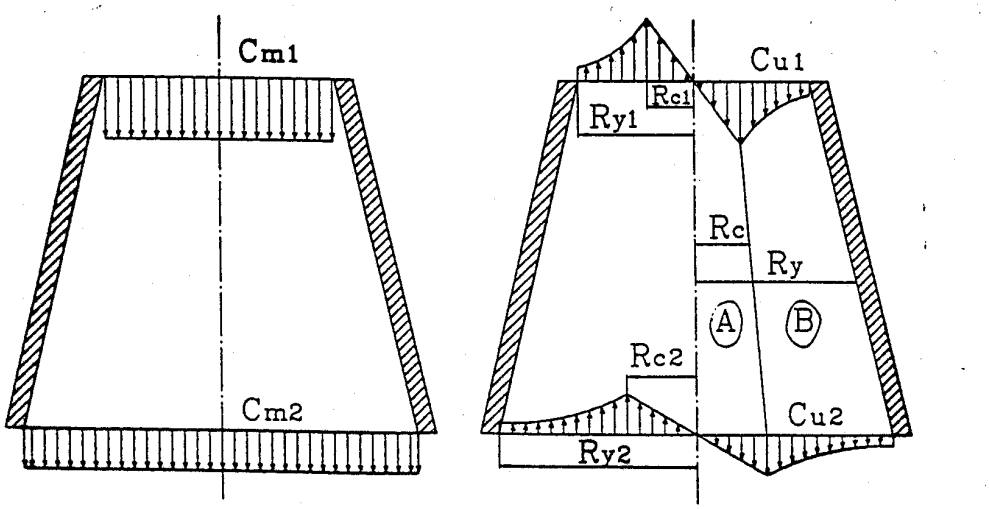

Fig.7.5 Simplified flow in a draft tube cone

The second simplification is that a swirl flow formation with a rigid-body motion or constant vorticity circulation core with c_{u1}/r_1 = constant and a vortex-free circulation with $r_1 c_{u1}$ = const from a given radius R_{c1} to the wall of the cone is established at the inlet of the draft tube cone.

The third assumption is that a similar swirl formation as at the inlet exist through the cone and at the outlet with (c_{u2}/r_2) = const from the centre to a radius R_{c2}.

It is also assumed that the equation of continuity yields for the meridian velocity through the cone and that the flow is incompressible.

The boundary conditions are illustrated in fig 7.5.

For the analysis of the problem the friction losses are ignored (i.e. the flow is inviscid).

Because there are no losses an no power conversion through the cone the power or the energy flux at the inlet and outlet of the draft tube must be the same = $W_1 = W_2 = W$. The equation for the energy flux for the described vortex yields:

$$W = \int_0^R 2\pi\left(\frac{p}{\rho} + \frac{c_u^2}{2} + \frac{c_m^2}{2} + \frac{c_r^2}{2}\right)\rho c_m r dr + \int_{r_c}^R 2\pi\left(\frac{p}{\rho} + \frac{c_u^2}{2} + \frac{c_m^2}{2} + \frac{c_r^2}{2}\right)\rho c_m r dr \qquad (7.4)$$

Because of the smallness of the cone angle the radial velocity component c_r will be ignored in the following equations.

The pressure p will be a function of the radius and the rotational component of the flow velocity = c_u.

Further c_u is a function of the radius which is different for ($0<r<R_c$) and ($R_c<r<R$).

For the inlet of the cone

Area A: $\varepsilon\ (0, R_c)$
$c_u/r = \text{const} = \omega_A = c_{uc1}/R_{c1}$

Area B: $\varepsilon\ (R_c, R_1)$
$rc_u = R_{c1}c_{uc1} = R_1c_{u1}$ i.e. $c_u = c_{u1}R_1/r$ and $c_{uc1} = c_{u1}R_1/R_{c1}$

On the border between area A and B (see fig. 7.5) i.e. for $r = R_{c1}$ the following expression for the angular velocity of the swirl flow is obtained:

$\omega_A = c_{uc1}/R_{c1}$ and $c_{uc1} = c_{u1}R_1/R_{c1}$

Then the expression for the angular velocity of the swirl in section A yields

$$\omega_A = c_{u1}R_1/R_{c1}^2 = c_u/r \text{ or } c_u = r\, c_{u1}R_1/R_c{}^2{}_1 \qquad (7.5)$$

In the outer section B, $r > R_{c1}$, $rc_u = \text{const}$

Then

$$c_u = R_1c_{u1}/r \qquad (7.6)$$

<u>The equation for the pressure in area A</u>

An equation for the pressure in section A can be established by regarding the equilibrium of forces in radial direction.

$$dp = \frac{\partial P}{\partial r} dr = \rho \frac{c_u^2}{r} dr$$

After integration:

$$\int_{p_{01}}^{p} dp = \rho \int_{0}^{r} \frac{c_u^2}{r} dr = \rho \int_{0}^{r} \left(\frac{c_{u1} R_1}{R_{c1}^2} \right)^2 r dr = \frac{1}{2} \rho \left(\frac{c_{u1} R_1}{R_{c1}^2} \right)^2 r^2$$

After rearrangement the equation for the pressure m are A yields:

$$p = p_{01} + \frac{1}{2} \rho \left(\frac{c_{u1} R_1}{R_{c1}^2} \right)^2 r^2 \qquad (7.7)$$

Then the pressure in area A [o<r<R_{1c}] can be found if the pressure in the centre p_o and the tangential velocity = c_{u1} at radius = R_1 is given and finally the radius R_{c1} must be given for the border between the core swirl and the vortex free swirl in area B i.e. rc_u = const.

The equation for the pressure in area B

In area B i.e. for R_{c1}<r<R_1 the equation (7.6) for the tangential velocity yields:

$$c_u = \frac{c_{u1} R_1}{r}$$

Then the pressure can be found by integrating the equation for the equilibrium of forces in the same way as for area A by substituting for c_u

$$\int_{p_{c1}}^{p} dp = \rho \int_{R_{c1}}^{r} \frac{c_u^2}{r} dr = \rho \int_{R_{c1}}^{r} \frac{(c_{u1} R_1)^2}{r^3} dr$$

After rearrangement we find:

$$p = p_{c1} + \frac{1}{2} \rho (c_{u1} R_1)^2 (1/R_{c1}^2 - 1/r^2) \qquad (7.8)$$

substituting for r = R_{c1} in eq. (7.7) the following expression for p_{c1} is obtained

$$p_{c1} = p_{o1} + \frac{1}{2}\rho\left(\frac{c_{u1}R_1}{R_{c1}}\right)^2 R_{c1} = p_{o1} + \frac{1}{2}\rho\left(\frac{c_{u1}R_1}{R_{c1}}\right)^2$$

Finally after substitution for p_{c1} in eq. (7.8) the following equation for the pressure p in area B, is obtained after some rearrangement

$$p = p_{o1} + \rho\left(\frac{c_{u1}R_1}{R_{c1}}\right)^2 - \frac{1}{2}\rho\left(\frac{c_{u1}R_1}{r^2}\right)^2 \qquad (7.9)$$

Now substitute for p in area A and area B in eq. (7.4) when neglecting the small term ($c_r^2/2$).

For area A the equation for the energy flux yields after substituting for p, rearranging and substituting for $c_m = Q/(\pi R_1)^2$:

$$W_1 = 2\rho\frac{Q}{R_1^2}\left[\int_o^{R_{c1}}\left[\frac{p_{o1}}{\rho} + \left(\frac{c_{u1}R_1}{R_{c1}^2}\right)^2 r^2 + \frac{1}{2}\left(\frac{Q}{\pi R_1^2}\right)^2\right)\right]rdr + \int_{R_{c1}}^{R_1}\left[\frac{p_{o1}}{\rho} + \left(\frac{c_{u1}R_1}{R_{c1}}\right)^2 + \frac{1}{2}\left(\frac{Q}{\pi R_1^2}\right)^2\right]rdr] \qquad (7.10)$$

For the outlet of the draft tube a similar equation can be established in the same way including the inner area $o<r<R_{c2}$ and an outer area $R_{c2}<r<R_2$. The equation for the energy flux = W_2 at the outlet then yields:

$$W_2 = 2\pi\rho\frac{Q}{R_2^2}\left[\int_o^{R_{c2}}\left[\frac{p_{o2}}{\rho} + \left(\frac{C_{u2}R_2}{R_{c2}^2}\right)^2 r^2 + \frac{1}{2}\left(\frac{Q}{\pi R_2^2}\right)^2\right]rdr + \int_{R_{c2}}^{R_2}\left[\frac{p_{o2}}{\rho} + \frac{1}{2}\left(\frac{c_{u2}R_2}{R_{c2}}\right)^2 + \frac{(c_{u2}R_2)^2}{r^2} + \frac{1}{2}\left(\frac{Q}{\pi R_2^2}\right)^2\right]rdr] \qquad (7.11)$$

Finally it is assumed that there is no loss or transfer of power between inlet and outlet and then the energy flux at inlet and outlet must be identical i.e.

$$W_1 = W_2 \qquad (7.12)$$

The swirl flow velocity c_{u2} can be found if the swirl flow at the inlet is given by assuming $R_1c_{u1} = R_2c_{u2}$ by calculating R_{c2} when R_{c1} and R_1c_{u1} is given.

On the other hand assuming a value for R_{c2}/R_{c1} and then calculate the value R_2c_{u2}. In this case R_2c_{u2} R_1c_{u1}.

A further calculation is not given in this chapter, but the reader of this book may find it interesting to study different variations of the development of swirl flow though a conical tube.

It should, however, be emphasised that the pressure p_{o2} cannot be below 100% vacuum. In a real case reversed flow will also occur in the centre of the cone for increasing rotational energy.

The meaning of including this study is as mentioned at the beginning to give the reader an analytical tool for judgement of computed results.

To the authors knowledge we have so far in 1997 no CFD code that is able to handle this phenomena correctly. However, an interesting Dr.ing. study have been made including interesting experimental results at the Norwegian University of Science and Technology in 1996-1997.

The best results of theoretical analyses have been obtained by using measured values as boundary conditions for swirl analyses.

Conclusion

The dynamic behaviour of the flow in a real draft tube with bend and rectangular outlet is not fully understood to day. Work is going on and even fractal theory with chaos has been used in order to try to solve the non-linear problem of the complex draft tube flow. However, a practical engineer may use simplified empirical analysis such as presented in this chapter, for the analysis of problems with pressure surges in hydraulic turbines.

In fig. 4.8, chapter 4.2, a cross section of the Saurdal Reversible Pump Turbine in western Norway is shown.

8. BASIC FLOW ANALYSIS AND ENERGY CONVERSION THROUGH DIFFERENT TYPES OF TURBINES.

8.1. The Euler turbine equation

In chapter 4 the hydraulic turbines was divided into two main groups; REACTION TURBINES and IMPULSE TURBINES.

In general, the total specific energy consists of partly pressure energy and partly kinetic energy formed by a swirl flow at the runner inlet for reaction turbines. For impulse turbines the total specific energy is converted to kinetic energy consisting of a flow with velocity in tangential direction at the runner inlet side.

The most important equation in the study of the basic turbine theory is the Euler turbine equation which is valid for both reaction turbines and impulse turbines. In this chapter a study of the Euler turbine equation is given. (A brief presentation of this equation was given in chapter 3).

The velocity vectors may now be analysed in three-dimensional coordinates with a meridional direction (m), and a rotational or tangential direction, (x) with a velocity u = dx/dt and finally a radial direction (r). This is illustrated in fig. 8.1 where a radial type and an axial type of reaction turbines are illustrated schematically.

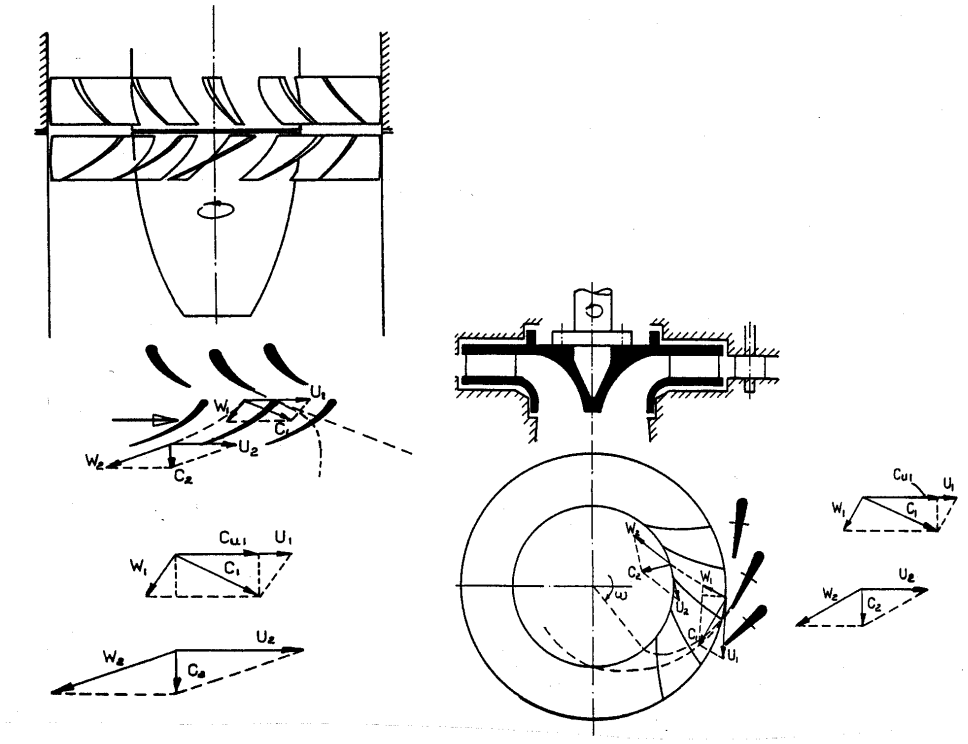

Fig. 8.1 Principles of blades and vector diagrams of radial- and axial turbines.

The Euler turbine equation for reaction turbines with radial inlets

The volume flow Q can be expressed as follows:

$$Q = c_{m1} 2\pi \, r_1 \, B_1 \qquad (8.1)$$

where B_1 = the height of the runner inlet, r_1 = the radius of the runner inlet and c_{m1} = the meridional velocity at the runner inlet.

The magnitude of the relative velocity in the direction along the stream lines on the blades equals w. The magnitude of the circumferential velocity is $u = r \cdot \omega$, the magnitude of the tangential or circumferential component of the absolute velocity c is c_u, and the meridional component of c is $c_m = w_m$. (Note: c_m will be in radial direction at the inlet and in axial direction at the outlet in a mixed flow turbine like a high head Francis turbine).

The swirl flow between radial type guide vanes and a radial runner inlet in a reaction turbine is recognized by the following equation if friction loss is ignored:

$$\vec{r} \bullet \vec{c} = \vec{r}_1 \bullet \vec{c}_1 = const. \qquad (8.2)$$

Here $_1$ denotes the runner blade inlet edge.

The equation for the force on a volume element dV in the runner yields:

$$d\vec{F} = \frac{\vec{D}c}{Dt} \rho dV$$

The momentum force for the control volume consisting of the blade channel from inlet to outlet yields: (see fig. 8.2)

$$\vec{F} = \int_v \int \int \frac{\vec{D}c}{Dt} \rho dV$$

The equation for the torque can be expressed as follows

$$\vec{M} = \iiint \frac{D}{Dt} (\vec{r} x \vec{c}) \, \rho dV \qquad (8.3)$$

The expression $D(\vec{r}x\vec{c})/Dt$ can be derived as follows:

$$\frac{D}{D_t} \left(\vec{r} x \vec{c} \right) = \frac{\partial \left(\vec{r} x \vec{c} \right)}{\partial t} + \left(\vec{c} \bullet \nabla \right) \left(\vec{r} x \vec{c} \right)$$

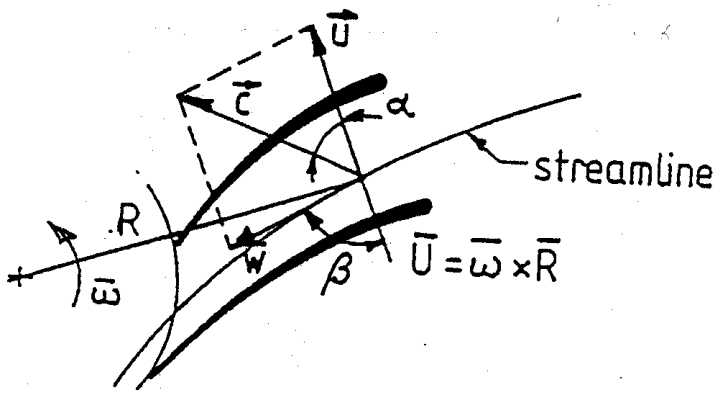

Fig. 8.2 Runner blades forming the control volume and velocity vectors.

For hydraulic turbines the flow is incompressible and for a reaction turbine the flow is basically regarded to be a steady state flow i.e. following therms are zero:

$$\nabla \bullet \vec{c} = 0 \quad and \quad \frac{\partial}{\partial t} = 0$$

Then following equation can be established after some mathematical manipulations [Ref 24]

$$\frac{D}{Dt}(\vec{r} x \vec{c}) = \nabla \bullet (\vec{c} \bullet (\vec{r} x \vec{c}))$$

and then

$$\vec{M} = \iiint_{v} \nabla \bullet (\vec{c} \bullet (\vec{r} x \vec{c})) \rho dV$$

By means of Gauss theorem we find:

$$\iiint_{V} \nabla \bullet (\vec{r} x \vec{c}) dV = \int_{A} \int (\vec{r} x \vec{c}) \bullet \vec{n} dA$$

where $\vec{n}$ is the unit normal vector.

Then:

$$\vec{M} = \int_{A} \int \vec{c} \bullet (\vec{r} x \vec{c}) \bullet \vec{n} q dA = \int_{A} \int (\vec{r} x \vec{c}) \bullet \vec{c} \bullet \vec{n} q dA \qquad (8.4)$$

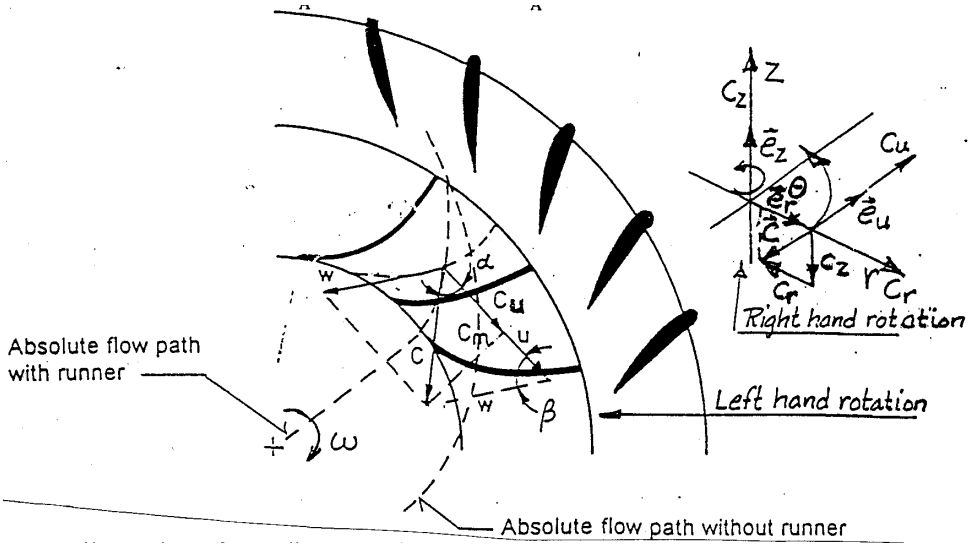

Fig. 8.3 Illustration of coordinates and vector directions.

Regarding a radial turbine or mixed flow (=radial/axial flow) turbine with r, u and z coordinates, $\vec{z}$ is in direction of the rotational axis and $\vec{u}$ is the tangential vector and $\vec{r}$ the radial vector i.e. (Note: in this case for a radial turbine c_r will be identical to the meridional velocity c_m used later for a so called "mixed flow" or radial inlet/axial outlet Francis turbine).

$$\vec{r} = [r \; o \; o]$$

Then

$$\vec{c} = [c_r \; c_u \; c_z]$$

$$\vec{r}x\vec{c} = \begin{bmatrix} \vec{e}_r & \vec{e}_u & \vec{e}_z \\ r & o & o \\ c_r & c_u & c_z \end{bmatrix}$$

and

$$\vec{r}x\vec{c} = -\vec{e}_u \bullet r\, c_z + \vec{e}_z \bullet r\, c_u$$

We now arrive at

$$\vec{M} = \int_A \int -\vec{e}_u \bullet r\, c_z \bullet \vec{c}\vec{n}\rho dA + \int_A \int \vec{e}_z \bullet r\, c_u \bullet \vec{c} \bullet \vec{n}\rho dA$$

Here the first term of the torque will try to bend the runner disk and thus this term will give no contribution to the shaft torque

Then the equation of the shaft torque yields:

$$\vec{M} = \int_A \int r\, c_u \bullet \vec{c} \bullet \vec{n}\rho dA \qquad (8.4)$$

By studying the control volume and knowing that the flow through the blades is zero, the surface of the control volume consists of the area from blade to blade at the inlet and the outlet.

The total mass flow in and out of all blade channels of a runner will be:

$$|\sum \dot{m}_{in}| = |\sum \dot{m}_{out}| = |\sum \vec{c} \bullet \vec{n} \rho dA| = \rho Q$$

Then the torque can be expressed by the following equation

$$\vec{M} = \sum (r\, c_u)_{in} \dot{m}_{in} - \sum (r\, c_u)_{out} \dot{m}_{out}$$

or

$$\vec{M} = \rho Q (r_1 c_{u1} - r_2 c_{u2}) \qquad (8.5)$$

where 1 denotes the inlet, and 2 the outlet of the runner.

The transfer of power and hydraulic efficiency expressed by the Euler turbine equation

The power transferred to the runner is easily found multiplying the torque by the angular speed = ω.

$$P_t = \vec{\omega} \bullet \vec{M}$$

or when substituting for $\vec{M}$ by eq. (5.5) and letting ωr = u :

$$P_t = \rho Q (u_1 c_{u1} - u_2 c_{u2}) \qquad (8.6)$$

The total available power is:

$$P_{AV} = \rho Q g H$$

Then the hydraulic efficiency η_h can be expressed by the well known Euler turbine equation as the ratio between the power transferred to the runner and the available power.

$$\eta_h = \frac{P_t}{P_{AV}} = \frac{u_1 c_{u1} - u_2 c_{u2}}{gH} \qquad (8.7)$$

Forces on the Pelton bucket and the development of the Euler equation based on the absolute impulse force

The equation for the turbine power P_t can also be established directly for impulse turbines by regarding the torque of the momentum from the inlet velocity vector and outlet velocity vectors multiplied by the angular speed ω taking into consideration the absolute mass flow ρQ.

A simplified study of the forces on one Pelton bucket and on a Pelton runner is presented here:

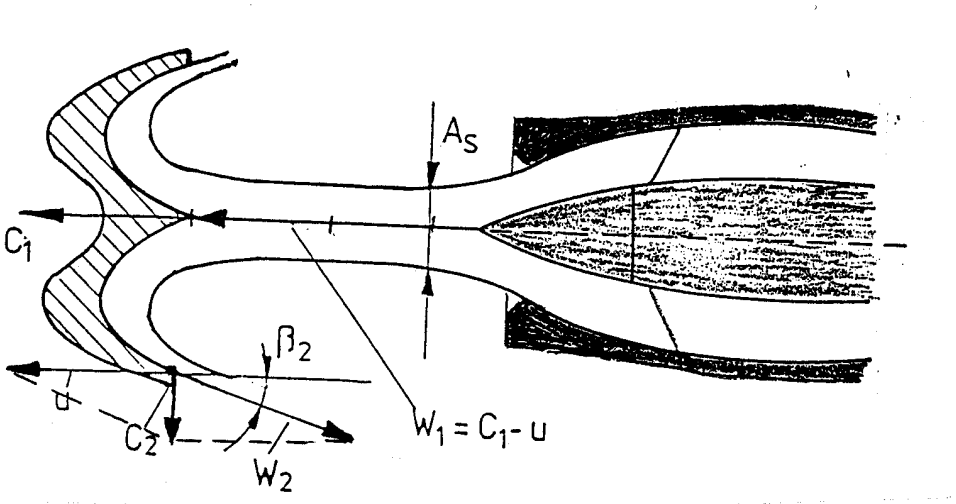

Fig. 8.4 Schematic illustration of nozzle and bucket in a Pelton turbine.

Relative force on one bucket = F_R (see fig. 8.4)

$$F_R = \rho Q_R (w_1 - w_2 \cos \beta_2) \tag{8.8}$$

For frictionless flow

$$w_2 \cos \beta_2 = w_{u2} \approx w_2 \quad and \quad w_1 = c_1 - u \quad and \quad w_2 = -w_1$$

If the cross section area of the jet is denoted A_j, then

$$Q_R = A_j (c_1 - u_1)$$

Therefore $$F_R = \rho A_j (c_1 - u_1)((c_1 - u_1) + (c_1 - u_1))$$

and

$$\boxed{F_R = \rho A_j 2(c_1 - u_1)^2} \tag{8.9}$$

The absolute force on the Pelton buckets on a Pelton runner is

$$F_A = \rho Q_A \left(c_{u1} - c_{u2}\right)$$

$$F_A = \rho A_j c_{u1} \left(c_{u1} - \left(2u - c_{u1}\right)\right)$$

and when $w_2 \cos\beta_2 \approx w_2$ and $u_2 = u_1 = u$:

$$c_{u2} = u_2 - w_{u2} \approx u_2 - w_2 = u_2 - (c_{u1} - u_1) = 2u - c_{u1}$$

The absolute jet flow is:

$$Q_A = A_j \cdot c_1$$

Therefore

$$\boxed{F_A = \rho A_j 2c_{u1}\left(c_{u1} - u_1\right)} \qquad (8.10)$$

The turbine power will be:

$$\boxed{P = F_A\ u_1 = \rho A_j 2c_{u1}\left(c_{u1}u_1 - u_1^2\right)} \qquad (8.11)$$

P max occurs theoretically for $\frac{\partial P}{\partial u} = 0$ i.e. $c_{u1} - 2u_1 = 0$ or $\underline{u_1 = \frac{1}{2}\ c_{u1}}$

At theoretical optimal speed the relative reaction force $F_R = 1/2\ F_A$ is given by following equations:

$$\boxed{F_R = \rho A_s c_1^2 / 2} \qquad \boxed{F_A = \rho\ A_S\ c_1^2} \qquad (8.12)$$

This can be explained by the fact that three or more buckets are loaded by water from the jet which gives a higher absolute force on the runner than the force on a single bucket.

(In a real Pelton turbine the optimal value for u will be between $0.48 \cdot c_1$ - $0.49 \cdot c_1$, because the bucket velocity is larger than the jet tangent radius at the maximum diameter and smaller at the minimum diameter of the outlet rim of the buckets and because of inlet losses and friction losses.

It should also be noted that a small runner diameter versus bucket size will be unfavourable, and the tangential velocity (u) will be in the lower range to avoid loss of water by the jet passing through the inlet cut out of the bucket.

The hydraulic efficiency η_h

The general equation for the absolute force on a Pelton runner according to eq. 8.10 can be written in following form:

$$F_A = \rho Q_A (c_{u1} - c_{u2})$$

The equation of the torque then yields:

$$M_A = \rho Q_A (r_1 c_{u1} - r_2 c_{u2})$$

Then the turbine power will be

$$P = \rho Q_A \omega (r_1 c_{u1} - r_2 c_{u2}) = \rho Q_A (u_1 c_{u1} - u_2 c_{u2})$$

The hydraulic efficiency will then be:

$$\eta_h = \frac{P}{\rho Q_A g H} = \frac{\rho Q_A (u_1 c_{u1} - u_2 c_{u2})}{\rho Q_A g H}$$

or

$$\eta_h = \frac{u_1 c_{u1} - u_2 c_{u2}}{g H} \qquad (8.13)$$

This equation is recognized as the general EULER turbine equation developed in the classical way.

8.2. Relative and absolute acceleration in a rotating system explained by a physical vector visualization

(Note: In this chapter R is the distance from the particle to the centre of rotation and r the radius of curvature of the runner vane)
In order to obtain a good understanding of the flow a physical explanation of the equations has been used instead of more abstract mathematical development. (Vector symbols have been used). (Ref. 23).

Consider a particle moving with a relative velocity w forced to follow a line formed by a vane on a rotating disk. At time point zero the particle is located at a point A with radius vector=R. The relative velocity = w. Relative displacement = S, and absolute displacement is shown by capital letters A-G in fig. 5.5. The relative acceleration is denoted a_r and the absolute acceleration a_{abs}.

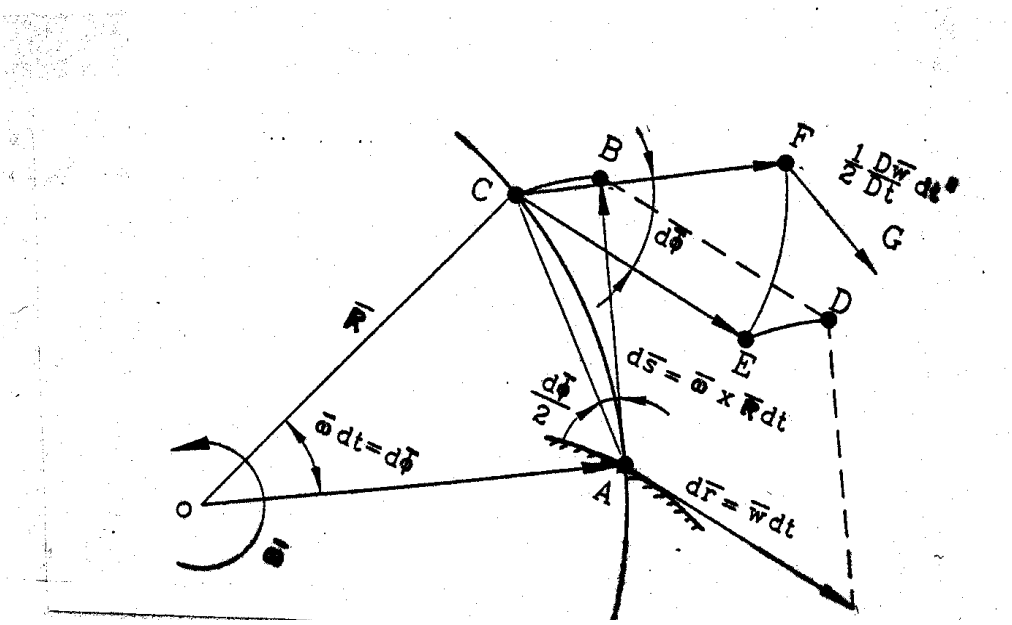

Fig. 8.5. Relative movement on a rotating disk.

The following relation between a particle displacement x, velocity C and acceleration may be established if terms of higher order smallness are neglected for decreasing dt.

$$|dx_{ac}| = \frac{1}{2} a\, dt^2$$

$$|dx| = c\,dt + \frac{1}{2} a\,dt^2 = dx_c + dx_a$$

(8.14)

Further the travelled distance on the rotating disk expressed by the relative velocity yields: (see fig. 5.5) (Note vector notations have been used in the following).

$$|\vec{AD}| = |\vec{CE}| = |\vec{CF}| = |d\vec{X}| = |\vec{w}\,dt| \quad \textit{relative movement} \qquad (8.15)$$

$$\vec{AB} = d\vec{S} = \vec{\omega} \times \vec{R} dt \quad \textit{tangential movement} \qquad (8.16)$$

Because of the rotation, the tangential displacement of the starting point A ends up in C instead of B which would be the end point with a linear movement of the starting point. Then the CENTRIPETAL ACCELERATION a_c caused by the rotation may be found as follows:

$$\vec{BC} = \frac{1}{2}\vec{a}_c\,dt^2 = \frac{1}{2} d\phi x d\vec{s} = \frac{1}{2}\vec{\omega} dt x (\vec{\omega} x \vec{R} dt) = \frac{1}{2}\vec{\omega} x (\vec{\omega} x \vec{R})\,dt^2$$

(8.17)

Further the relative velocity vector from the starting point-A-, which, after the time dt, has moved to point C ends up in F instead of E due to the rotation which changes the direction of the velocity vector.

The change of direction of the absolute velocity caused by a movement along a straight vane forcing the particle to follow a straight line on a rotating disk, can only occur if an absolute acceleration normal to the relative velocity vector occurs. This acceleration which is named CORIOLI'S ACCELERATION – and may be found by reference to fig. 8.5 as follows.

$$\vec{EF} = \frac{1}{2}\vec{a}_{cor}\,dt^2 = d\vec{\phi}x d\vec{s} = \vec{\omega}dtx\vec{w}dt = \vec{\omega}x\vec{w}\,dt^2 \qquad (8.18)$$

In addition a relative acceleration will be created by a curved vane causing an acceleration normal to the velocity vector and eventual changes in the cross section of the channel formed by the vanes which creates a relative acceleration component in direction of the velocity vector. This relative acceleration DW/Dt moves the particle from F to G and the equation for the relative movement yields:

$$\vec{FG} = \frac{1}{2}\frac{D\vec{w}}{Dt}dt^2 \quad (FG = 0 \text{ if } \vec{w} = const.) \qquad (8.19)$$

Further the equation for a relative acceleration yields:

$$\frac{D\vec{w}}{Dt} = \frac{\partial\vec{w}}{\partial t} + (\vec{w}\bullet\nabla)\vec{w}$$

For stationary relative flow: $\partial w/\partial t = 0$

$$i.e.\ \frac{D\vec{w}}{Dt} = (\vec{w}\bullet\nabla)\vec{w} \qquad (8.20)$$

The total absolute acceleration can be found by studying the particle moving on a rotational disk guided along a straight vane A-F or a curved vane A-G with a relative velocity w , and a relative acceleration Dw/Dt. Then the absolute acceleration = a_{abs} can be found by adding the relative acceleration, the Coriolis's acceleration and the centripetal acceleration.

The equation then yields:

$$\frac{1}{2}(\vec{a}_c + \vec{a}_{cor} + \frac{D\vec{w}}{Dt})dt^2 = \frac{1}{2}\vec{a}_{abs}\ dt^2$$

or

$$\vec{a}_{abs} = \vec{a}_c + \vec{a}_{cor} + \frac{D\vec{w}}{Dt} \qquad (8.21)$$

By substituting for a_c and a_{cor} by eq. (8.17) and eq. (8.18) respectively and the relative acceleration by eq. (5.20), the following equation for the absolute acceleration is obtained:

$$\vec{a}_{abs} = \frac{D\vec{c}}{Dt} = \vec{\omega}x(\vec{\omega}x\vec{R}) + 2(\vec{\omega}x\vec{w}) + (\vec{w} \bullet \nabla\_)\vec{w} \qquad (8.22)$$

i.e.

a_{abs} = centripetal - + Coriolis - + relative-accelerations

The direction of the centripetal acceleration will be towards to the centre of rotation and the direction of Coriolis acceleration will be normal to the relative velocity direction found by the right hand rule as shown in fig. 8.6.

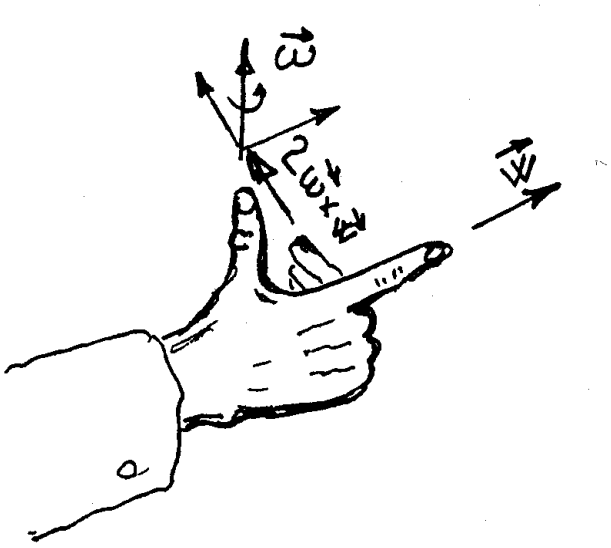

Fig. 8.6 Right hand rule for Corioli's acceleration

It should be emphasized that eq (8.22) is also valid for flow on a conical stream surface or for a mixed flow runner with radial inlet and axial outlet, i.e. partly axial partly radial direction. Then the vector component of the relative velocity w in radial direction will be $w_r = w \cdot \cos \delta$ where δ is the angle out of the radial direction in a meridional plane. If vector notations are not used the velocity component in radial direction for the Coriolis acceleration must then be corrected to $w_1 \cos \delta$. In the next chapter vector notations are not used and the Coriolis term must then be corrected if the turbine or pump is not a pure radial machine. (see also …… where a detailed complete study is made).

8.3. Flow analysis in a rotating blade channel of a turbine runner or a pump impeller

For stationary flow in a rotating conduit in a plane normal to the axis of rotation the absolute acceleration (in-s-direction) along a stream line may be found based on eq. (8.22). If vector notations are not used i.e. $(\vec{w} \bullet \_)\vec{w} \rightarrow w\partial w/\partial s$ and one dimensional stationary relative flow with velocity = w along the stream line is assumed, then $\partial w/\partial t = 0$ i.e. stationary flow.

Then by studying fig. 8.7, the following equation for the acceleration along a stream line in a rotating channel can be set up as follows: (As mentioned above vector symbols are not used in this chapter).

$$a_s = w\frac{\partial w}{\partial s} + \omega^2 R\cos\phi \qquad (8.23)$$

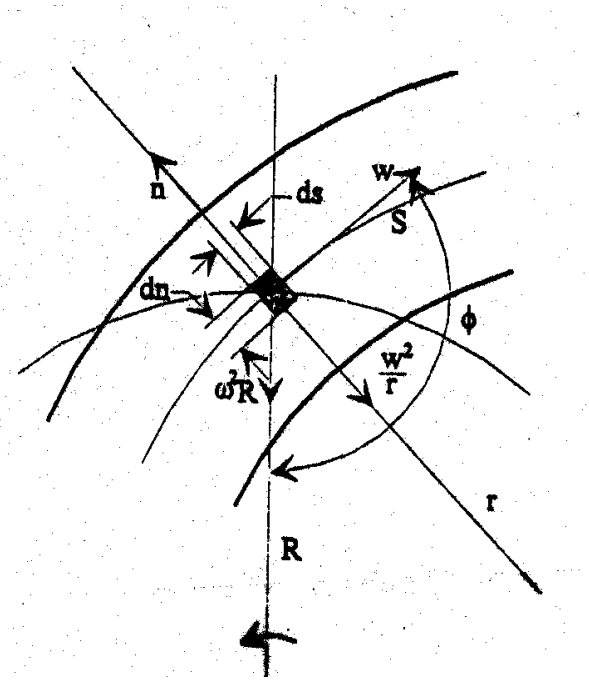

Fig. 8.7 Particle movement along a stream line in a rotating channel with height = b=const.

In the same way the equation for the absolute acceleration in the n direction normal to the stream lines yields:

$$a_n = -\frac{w^2}{r} - \omega^2 R\sin\phi + 2\omega w \qquad (8.24)$$

(Note $w\frac{\partial w}{\partial n} = -\frac{w^2}{r}$ *with the direction of axes as shown in fig. 5.7 and fig. 5.8)*

Equilibrium of forces along the stream line:

Pressure force (Note it is assumed that the height of the channel = b = constant and along a streamline
∂s = ds):

$$F_s = -\frac{\partial p}{\partial s}\, ds.\, dn\, b \quad (b = height = const.)$$

Newton's second law:

$$-\frac{\partial p}{\partial s}\, ds\, dn\, b = \rho\, dn\, ds\, b\, a_s \qquad (8.25)$$

Substituting for a_s from eq. (8.23)

$$-\frac{\partial p}{\partial s} = \rho(w\frac{\partial w}{\partial s} + \omega^2 R\cos\phi)$$

From fig. 8.7: cos φ · ds = -dR i.e. ds = -dR/cos φ.

Then by substituting for ds after multiplying by (ds/ρ):

$$\frac{1}{\rho}dp + wdw - \omega^2 RdR = 0$$

Then by integration along a stream line without friction the following equation for the relative specific stagnation energy, which is denoted as ROTHALPY, is obtained.

$$\frac{p}{\rho} + \frac{w^2}{2} - \frac{(\omega R)^2}{2} = const.$$

Substituting for ωR = u

$$\frac{p}{\rho} + \frac{w^2}{2} - \frac{u^2}{2} = const. \qquad (8.26)$$

This equation is a very useful and important equation for the preliminary design of runner blades. In this chapter it has been given a physical explanation which proves that the relative specific stagnation energy is constant along a stream line in a rotating runner. It should be emphasized that friction loss is neglected, but this error is negligible in the preliminary design stage when the basic blade design is made.

Equilibrium of forces normal to the stream line

The pressure forces are: (Note that the height is denoted b and ∂n = dn for analyses normal to a stream
line):

$$dF_n = -\frac{\partial p}{\partial n}\,dn\;ds\;\;b \qquad (8.25)$$

Newton's second law:

$$-\frac{\partial p}{\partial n}\,dn\;ds\;b = \rho\;dn\;ds\;b\;a_n \qquad (8.28)$$

Substituting for a_n from eq. (8.24) in eq. (8.28)

$$\frac{\partial p}{\partial n} = \rho\left(\frac{w^2}{r} + \omega^2 \; R\sin\phi - 2\omega w\right) \tag{8.29}$$

By differentiating the specific relative stagnation energy equation (ROTHALPY) (Eq. (8.26)) from stream line to stream line in (n) direction the following equation can be established if the relative specific hydraulic energy is constant over the cross section at the runner inlet (see fig. 8.7):

$$\frac{1}{\rho}\frac{\partial p}{\partial n} + w\frac{\partial w}{\partial n} - u\frac{\partial u}{\partial n} = 0$$

rearranging

$$\frac{\partial p}{\partial n} = \rho(u\frac{\partial u}{\partial n} - w\frac{\partial w}{\partial n})$$

By substituting for

$$\partial n = +\partial R/\sin\phi \;\; and \;\; u = \omega R \quad (\omega = const.)$$

then

$$u\frac{\partial u}{\partial n} = \omega R\frac{\partial(\omega R)}{\partial R}\sin\phi = \omega^2 R\sin\phi$$

and

$$\frac{\partial p}{\partial n} = \rho(+\omega^2 R\sin\phi - w\frac{\partial w}{\partial n}) \tag{8.30}$$

By substituting for $\partial p/\partial n$ from eq. (8.29), the following equation is obtained:

$$\frac{w^2}{r} - 2\omega w = -w\frac{\partial w}{\partial n} \tag{8.31}$$

Then the equation for the velocity variation normal to the stream lines in the rotating channel as illustrated in fig. 8.7 yields:

$$\frac{dw}{dn} = -\frac{w}{r} + 2\omega \tag{8.32}$$

Fig. 8.7 may be regarded to be an illustration of a radial-pump impeller and eqs. (8.26) and (8.32) will be valid for a radial centrifugal pump or a reversible pump turbine in pumping mode (normally $|2\omega| >> |w/r|$ for a pump). If both the rotational direction and flow

direction are changed, fig. 8.7 may illustrate a reversible pump turbine operating in turbine mode and eq. (8.31) is valid for this case if using negative values for w and ω. (see also fig. 8.8) Then eq. (8.32) will also be valid if it is derived from eq (8.31) with changed w and ω to negative values.

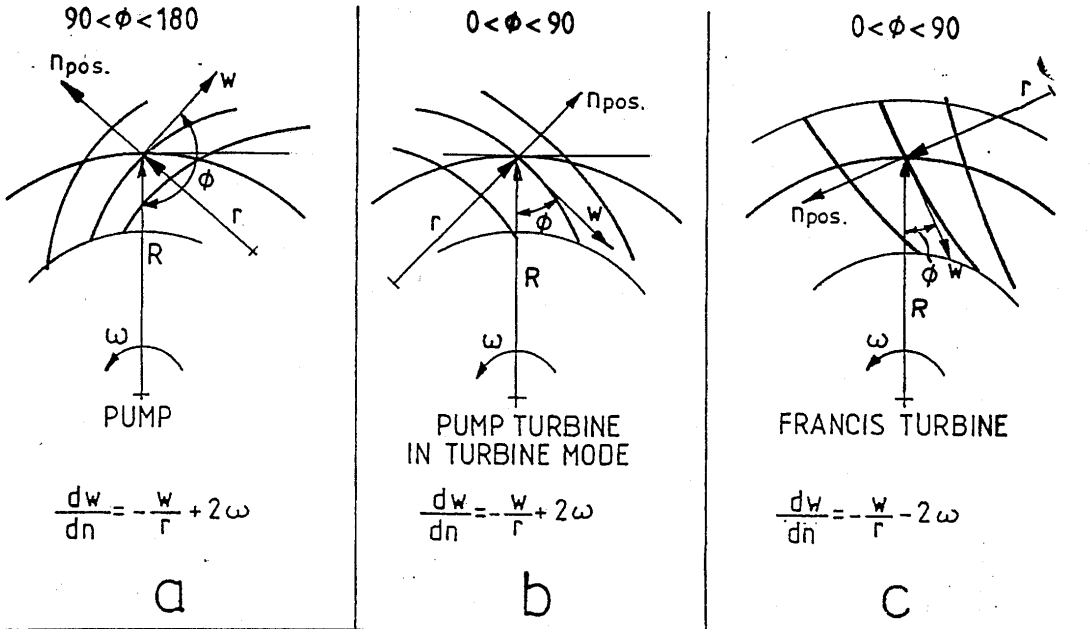

Fig. 8.8 Illustration of a pump (a), a pump turbine in turbine mode (b) and a Francis turbine (c)

For a normal Francis turbine the curvature of the stream line normally will change so the centre of the curvature radius will be located on the outside and the positive direction of n will be as shown in fig. 5.8. Then the last term in the right hand side of eq. (8.32) will be negative. The equation for a normal Francis turbine then will be as shown in eq. (8.33), if the positive n direction is chosen to be away from the centre of the radius of the curvature of the blade as shown in fig. 8.8.

The equation for a Francis turbine with geometry as shown in fig. 8.8c yield:

$$\frac{dw}{dn} = -\frac{w}{r} - 2\omega \qquad (8.33)$$

Equation (8.33) is very useful for a study of the velocity distribution from blade to blade in a radial turbine. However, eq. (8.31) can also be used for a combined radial/axial turbine (also called a mixed flow turbine) like a Francis turbine by multiplying the meridional component of the relative velocity w by cos δ in the last term on the left hand side.

(δ is the angle between the radial plane normal to the axis of rotation and the flow component in meridional direction in the rotational symmetric surface). (See …….. where a complete

physical analytical theory of the flow in a runner is explained. See also the theory used for the analysis of Pelton turbines).

8.4. Energy conversion in a turbine runner channel

In this analysis of flow, vectorial denotations have been used in the traditional way.

Equation of momentum (Newtons second law):

$$dm \ \vec{a}_{abs} = d\vec{F} \tag{8.34}$$

m = mass (kg), a = acceleration (m/s^2) F = force (N).

Further:

$$dm = \rho dV$$

ρ = density (kg/m^3), V = volume (m^3)

Substituting for

$$dm = \rho dV \text{ and for } d\vec{F} = d\vec{F}_s - \rho dV \nabla(gz)$$

$$\rho dV \bullet \vec{a}_{abs} = d\vec{F}_s - \rho dV \nabla (gz) \tag{8.35}$$

Here $\rho dV \nabla(gz)$ is the gravity force in vertical direction on the fluid inside the volume dV and dF_s is the sum of external forces acting on the surface of the volume, g is the gravity acceleration and z is the distance measured upward from a reference plane. (z is parallel to g, but opposite in direction).

Rearranging eq. (8.35)

$$\vec{a}_{abs} = \frac{d\vec{F}_s}{dV} \quad \frac{1}{\rho} - \nabla(gz) \tag{8.36}$$

Dividing F_s in pressure forces normal to the surface and friction forces (parallel to the surface) expressed in force per volume unit.

$$\frac{d\vec{F}_s}{dV} = \frac{d\vec{F}_f}{dV} - \nabla p \tag{8.37}$$

Then the equation for the acceleration yields:

$$\vec{a}_{abs} = \frac{d\vec{F}_f}{dV}\frac{1}{\rho} - \frac{\nabla p}{\rho} - \nabla(gz) \tag{8.38}$$

Further the friction forces expressed by classical theory for incompressible stationary flow by Navier Stoke's equation yields: [Ref. C. Hirch. Vol 2 pp. 654-655. Wiley & Sons 1990].

[For practical computation of viscous turbulent incompressible flow the Baldwin-Lomax model is normally used for flow analysis of runners. Also the K-ε model has been used by a correcting process because of Coriollis influence. Both methods are described in C. Hirch, Numerical Computation of Internal and External Flow. Vol 2. pp. 606-618. J. Wiley & Sons 1990 [Ref. 16]].

$$\frac{1}{\rho}\frac{d\vec{F}_f}{dV} = \mu\Delta\vec{c} = \vec{f} \qquad (8.39)$$

($\Delta = \nabla^2$ = Laplacian operator)

Here μ = coefficient of dynamic viscosity or the kinematic viscosity $\upsilon = \mu/\rho$, where ρ = density (kg/m^3). Then the final equation can be established by combining eqs. (8.38) and (8.39):

$$\vec{a}_{abs} = -\frac{\nabla P}{\rho} + \vec{f} - \nabla(gz) \qquad (8.40)$$

It is necessary to express the acceleration by differentiation of the velocities in order to analyze the flow in a turbine runner or pump impeller. The general equation for the absolute acceleration yields

$$\vec{a}_{abs} = \frac{\partial\vec{c}}{\partial t} + (\vec{c}\bullet\nabla)\vec{c} \qquad (8.41)$$

or when substituting for eq. (8.41) in eq. (8.40):

$$\vec{a}_{abs} = \frac{\partial\vec{c}}{\partial t} + (\vec{c}\bullet\nabla)\vec{c} = -\frac{\nabla p}{\rho} - \nabla(gz) + \vec{f} \qquad (8.42)$$

Here c = absolute velocity (m/sec).

It is possible to prove that:

$$(\vec{c}\bullet\nabla)\vec{c} = \nabla\left(\frac{c^2}{2}\right) - \vec{c}x(\nabla x\vec{c})$$

By substituting for $(\vec{c}\bullet\nabla)\vec{c}$ in eq (8.42), and assuming steady flow i.e. $\partial c/\partial t = 0$:

$$\vec{c}x(\nabla x\vec{c}) = \nabla\left(\frac{p}{\rho} + \frac{c^2}{2} + gz\right) - \vec{f} \qquad (8.43)$$

Note that the first term on the right hand side may be denoted ∇E where E is the absolute specific stagnation energy which is different at the inlet and outlet of the turbine $E_1 = gH_1$ and $E_2 = gH_2$ respectively, H = head (m). (See also Chapter 3).

$$E = \frac{p}{\rho} + \frac{c^2}{2} + gz \qquad (8.44)$$

Then the differentiated energy equation can be written:

$$\vec{c}x(\nabla x\vec{c}) = \nabla E - \vec{f} \qquad (8.45)$$

Equation (8.45) is expressed by absolute velocity vectors, but for analysis of flow between the blades in a rotating pump impeller or in a turbine runner it is more convenient to express the equation in pressure and relative velocities. It is convenient to work out this theory stepwise as follows:

In the same way as was proven for the absolute acceleration in eq. (8.43) the relative acceleration may
be expressed as follows:

$$a_R = (\vec{w} \bullet \nabla)\vec{w} = \nabla(\frac{w^2}{2}) - \vec{w}x(\nabla x\vec{w}) \qquad (8.46)$$

Then the absolute acceleration according to eq. (8.22), eq. (8.46) and eq. (8.42) may be established as follows:

$$a_{abs} = \nabla(\frac{w^2}{2}) - \vec{w}x(\nabla x\vec{w}) + 2\vec{\omega}x\vec{w} + \vec{\omega}x(\vec{\omega}x\vec{r}) = -\frac{\nabla p}{\rho} - \nabla(gz) + \vec{f} \qquad (8.47)$$

Now it is possible to modify equation (8.47) in order to explain the relative specific stagnation energy (ROTHALPY) in a runner compared with the absolute specific energy by introducing:

$$\vec{w}x(\nabla x\vec{w}) - 2\vec{\omega}x\vec{w} = \vec{w}x(\nabla x\vec{c})$$

Which is proven by the following derivation:

$$\vec{w}x(\nabla x\vec{c}) = \vec{w}x(\nabla x(\vec{w} + \vec{\omega}x\vec{r})) = \vec{w}x(\nabla x\vec{w}) + \vec{w}x(\nabla x\vec{\omega}x\vec{r})$$

where the following connection can be proven: (see Appendix)

$$\nabla x(\vec{\omega}x\vec{r}) = 2\vec{\omega}$$

Then

$$\vec{w}x(\nabla x\vec{c}) = \vec{w}x(\nabla x\vec{w}) + \vec{w}x2\vec{\omega}$$

and thus following equation is now proven:

$$\vec{w}x(\nabla x\vec{c}) = \vec{w}x(\nabla x\vec{w}) - 2\vec{\omega}x\vec{w} \qquad (8.48)$$

When substituting for $\vec{w}x(\nabla x\vec{c})$ by eq. (8.48) in eq. (8.47) and remembering that $\vec{\omega}x(\vec{\omega}x\vec{r}) = \nabla(\omega^2 r^2/2)$ the following convenient equation can be found.

$$\vec{w}x(\nabla x\vec{c}) = \frac{\nabla p}{\rho} + \nabla(\frac{w^2}{2}) - \nabla(\frac{\omega^2 r^2}{2}) + \nabla(gz) - \vec{f}$$

or when substituting for $\omega^2 r^2 = u^2$:

$$\vec{w}x(\nabla\vec{x}c) = \nabla(\frac{p}{\rho}\frac{w^2}{2} - \frac{u^2}{2} + gz) - \vec{f} \qquad (8.49)$$

Here the term in brackets on the right hand side is recognized in eq. (8.26) as the relative specific stagnation energy or ROTHALPY.

$$I = \frac{p}{\rho} + \frac{w^2}{2} - \frac{u^2}{2} + gz \qquad (8.50)$$

The last term (gz) in eq. (8.50) is normally ignored for flow analysis of runners because of its smallness.
As was shown earlier in eq. (8.26) we proved by a physical study that the ROTHALPY is constant along a stream line in a runner if the friction loss is neglected i.e. $\vec{f} = 0$. (It should also be noted that eq. (8.49) is valid for incompressible fluid only. However, by adding the term T∇S on the right hand side eq. (8.49) will also be valid for compressible flow.

The ROTHALPY is in fact the fraction of the total specific energy which is not transferred to the runner (i.e. the specific energy at the runner outlet) if the tangential absolute velocity component at the outlet $c_{u2} = 0$ i.e. best efficiency point. This can be proved by studying eq. (8.49) and by proving that

$w_2^2 = c_{m2}^2 + u_2^2$ if $c_{u2} = 0$ (see the velocity vector diagram)

Then by substituting for $w_2^2 = c_{m2}^2 + u_2^2$ in eq. (8.50)

$$\frac{p_2}{\rho} + \frac{w_2^2}{2} - \frac{u_2^2}{2} = \frac{p_2}{\rho} + c_m\frac{2^2}{2}$$

By studying the difference between the absolute specific stagnation energy - E - and the relative specific stagnation energy - I - the Euler turbine equation can be found. This can be done by means of the velocity vector diagram shown in fig. 8.9.

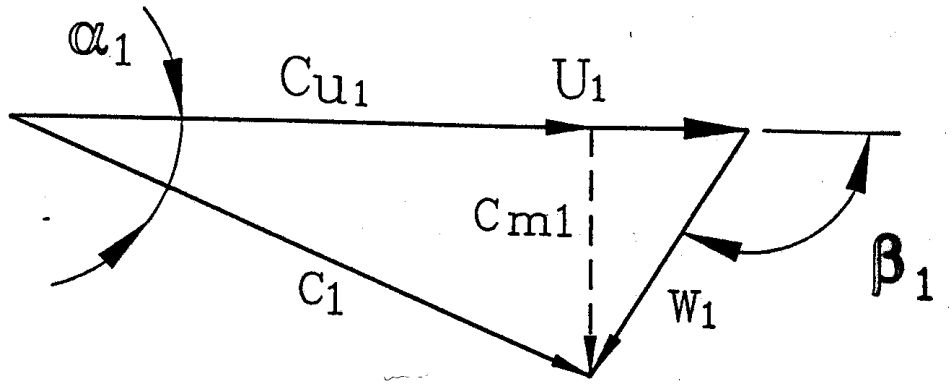

Fig. 8.9 Velocity vector diagram

By simply using the cosine law on the geometry of the velocity vector diagram we find:

$$w^2 = u^2 + c^2 - 2u\,c \quad \cos\alpha = u^2 + c^2 - \left|2\vec{u} \bullet \vec{c}\right|$$

Rearranged

$$\left|\vec{u} \bullet \vec{c}\right| = \frac{c^2}{2} - \frac{w^2}{2} + \frac{u^2}{2}$$

Then by combining eq (8.44) and eq. (8.50)

$$E - I = \frac{c^2}{2} - \frac{w^2}{2} + \frac{u^2}{2} = \left|\vec{u} \bullet \vec{c}\right| \qquad (8.51)$$

Further by not using vector symbols writing $\left|\vec{u} \bullet \vec{c}\right| = uc_u$ where c_u is the tangential component of c, we obtain a useful expression for friction free flow:

$$I = E - u\,c_u \qquad (8.52)$$

Then equation (8.51) can be used to develop the well known Euler equation if the energy in front of the runner is denoted by $_1$ and at the runner outlet denoted by $_2$.

$$(E_1 - I_1) - (E_2 - I_2) = u_1 c_{u1} - u_2 c_{u2} \qquad (8.53)$$

It has been proven earlier that the ROTHALPY is constant along a stream line through a runner if friction is ignored i.e. $I_1 = I_2$, and then the following important equation can be established.

$$E_1 - E_2 = u_1 c_{u1} - u_2 c_{u2} \qquad (8.54)$$

Equation (8.54) shows that (E_1 - E_2) is the energy transferred to the runner. Thus it is convenient to present the conversion of energy in a water turbine by the diagram illustrated in fig. 8.10 and fig. 8.11. In these figures the friction loss is neglected.*

However, it should be emphasised that the available net specific energy drop from inlet to outlet of a turbine is larger than the specific energy converted to specific mechanical energy by the runner. The equation for the total energy drop through the turbine yields: (see Chapter 3)

$$gH = E = E_0 - E_3 = (gh_0 + \frac{c_0^2}{2}) - (gh_3 + c_m \frac{3^2}{2}) \quad **$$

The ratio between the specific energy transferred by the runner and the total net specific energy from outlet to inlet of a turbine is denoted as hydraulic efficiency of the turbine. Note that in fig. 8.10 and fig. 8.11 the friction losses in the turbine are ignored.

The equation which describes the energy conversion through a turbine runner normally is named the EULER TURBINE EQUATION. As shown earlier in eq. (8.7) the EULER turbine equation was also proved by studying the reaction forces on the runner blades.
This equation yields:

$$gH_{\eta_h} = E_{\eta_h} = u_1 c_{u1} - u_2 c_{u2}$$

or

$$\eta_h = (u_1 c_{u1} - u_2 c_{u2})/(gH) \qquad (8.55)$$

The energy conversion through the turbine may be illustrated as shown in fig. 8.11 (next chapter) for a non rotating outlet flow i.e. $c_{u2} = 0$ with full line and an excample with $c_{u2} \neq 0$ with dotted lines.

* Notations to be remembered when studying fig. 8.10 (and Fig. 8.11 next chapter) 0 turbine inlet, 1 runner inlet, 2 runner outlet, 3 draft tube outlet.

** Note: According to the IEC norms the draft tube outlet loss $(Cm_3^2 / 2)$ is not regarded to be a turbine loss, but a plant loss if $c_{m3} = QA_3$. In this chapter $(Cm_3^2 / 2)$ is regarded as a turbine loss in order to get a physical understanding of the energy conversion through the turbine.

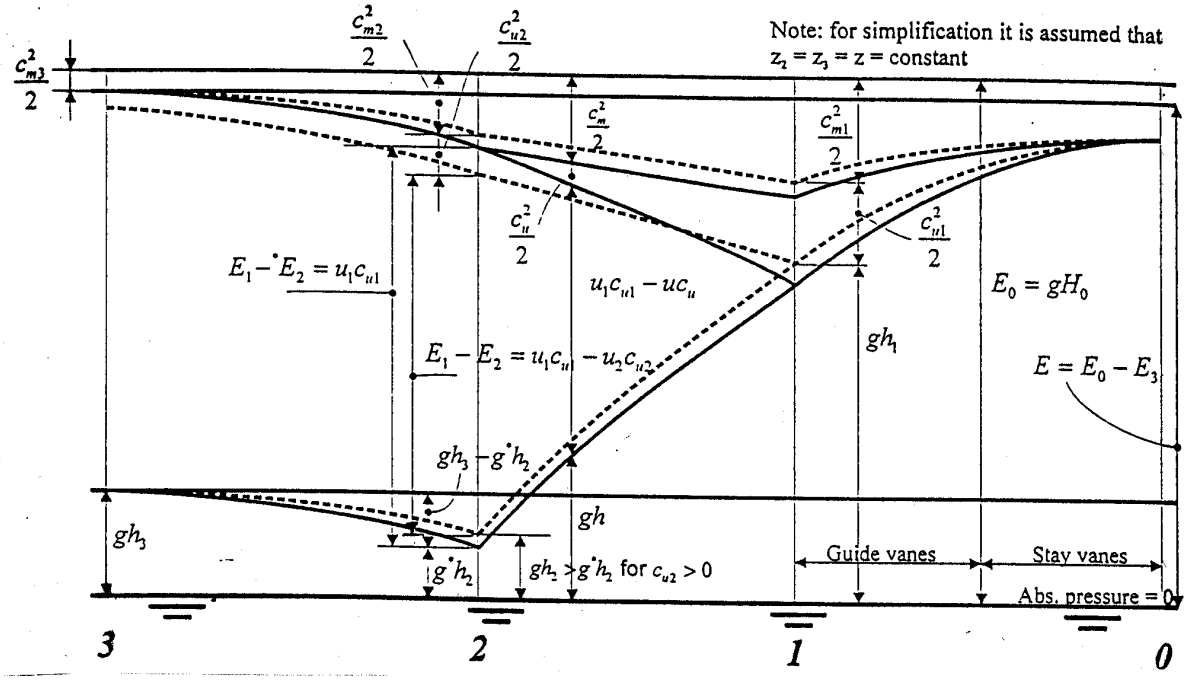

0 turbine inlet 2 runner outlet
1 runner inlet 3 draft tube outlet

Fig. 8.10 Energy conversion in a reaction turbine with frictionless flow at best efficiency (full lines) and flow below best efficiency (dotted lines).

8.5. Energy conversion through a Francis turbine.

Fig. 8.10, Section 8.4, showed the total absolute specific energy difference from the pressure side to the suction side of a turbine = E = gH. The friction losses are ignored. To the right hand side the available specific hydraulic energy at the inlet of the turbine is shown. The lower part of the diagram shows the pressure energy $p/\rho = gh$ and the upper part shows the kinetic energy $c^2/2 = c_u^2/2 + c_m^2/2$. ($c_u$ = the tangential component and c_m = the meridional component).

On the right hand side of fig. 8.10 the specific energy at the turbine inlet consists of approximately 95% pressure energy for Francis turbines with an increase of the kinetic energy towards the guide vane inlets where the swire flow is dominating.

Through the guide vane cascade the rotational energy increases to match the circumferential speed of the runner blades. Also the meridional velocity increases because the water is flowing towards a decreasing diameter. As a result the pressure energy decreases to approximately 50% of the total energy at the runner inlet.

From the runner inlet the energy is gradually converted to mechanical energy by the runner as shown by the term $E_1\text{-}E = u_1c_{u1}\text{-}uc_u$ in an arbitrarily chosen place on a stream line through the runner. Towards the outlet of the runner the absolute pressure decreases below the pressure outside the draft tube and the rotational kinetic energy decreases to zero at best efficiency theoretically. From the inlet to the outlet of the runner the specific energy has decreased by $E_1 - E_2 = u_1\, c_{u1} - u_2\, c_{u2}$.

At the runner outlet the pressure has normally decreased to a value below atmospherical pressure. However, the kinetic energy decreases from the runner outlet to the draft tube outlet where the pressure has increased to atmospheric pressure plus the pressure of the water level above the reference level.

The hydraulic energy loss will then be the kinetic outlet energy = $c_{m3}^2/2$ from the draft tube for an ideal frictionless flow through the turbine. (The kinetic outlet energy is not regarded to be a turbine loss but a head loss of the power plant according to the IEC norms).

Illustrating the specific energy conversion by the total absolute specific energy and the relative specific energy ROTHALPY as shown in fig. 8.11, makes an interesting study of the physical meaning of the ROTHALPY which will be described by the following equations.

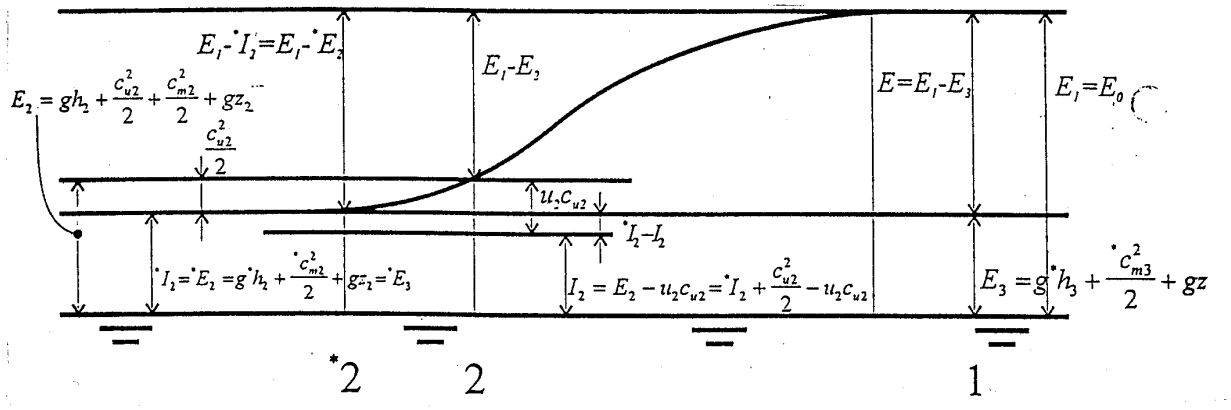

Fig. 8.11 Absolute specific energy and relative specific energy (ROTHALPY) when friction losses are ignored.

The equation for the specific energy at the runner inlet where * indicates the inlet condition at best efficiency with no swirl flow at the runner outlet i.e. for $c_{u2} = {}^*c_{u2} = 0$ yields

$$E_1 = {}^*E_1 \quad i.e. \quad gh_1 + \frac{c_1^2}{2} = g\,{}^*h_1 + \frac{{}^*c_1^2}{2}$$

and for friction free flow:

$${}^*I_1 = {}^*E_1 - {}^*u_1\,{}^*c_{u_1} = g\,{}^*h_1 + \frac{{}^*c_1^2}{2} - {}^*u_1\,{}^*c_{u1} = {}^*I_2$$

Using eq. (8.52) for the outlet condition of a runner and $gh = p/\rho$ gives:

$$I_2 = \frac{p_2}{\rho} + \frac{c_2^2}{2} - u_2 c_{u2} = E_2 - u_2 c_{u2} \qquad (8.56)$$

For a frictionless flow in a runner it has already been shown that $I = I_1 = I_2 = \text{const.}$

For $c_{u2} = 0$ (8.55) gives (Note * indicates best efficiency i.e. $c_{u2} = {}^*c_{u2} = 0$)

$$^{*}I_2 = {}^{*}E_2 = \frac{^{*}p_2}{\rho} + \frac{^{*}c_m 2^2}{2} = g\ {}^{*}h_2 + \frac{^{*}c_m 2^2}{2} = g\ {}^{*}h_3 + \frac{^{*}c_m 3^2}{2} = {}^{*}E_3$$

This shows that in a friction free flow the ROTHALPY is equal to the specific hydraulic energy at the draft tube outlet if $c_{u2} = 0$ (see fig. 8.11).

A simpler and more direct way to this conclusion is given by regarding the Euler turbine equation (eq. (8.53)) and letting $c_{u2} = 0$.

$$(E_1 - I_1) - (E_2 - I_2) = u_1 c_{u1} - u_2 c_{u2}$$

and for $c_{u2} = 0$:

$$^{*}E_2 - {}^{*}I_2 = {}^{*}u_2\ {}^{*}c_{u2} = 0$$

then:

$$^{*}E_2 = {}^{*}I_2 = {}^{*}I_1 = g\ {}^{*}h_2 + \frac{^{*}c_{m2}^{2}}{2} = g\ {}^{*}h_3 + \frac{^{*}c_{m3}^{2}}{2} = {}^{*}E_3 \qquad (8.57)$$

However, if any rotational energy exist at the runner outlet then

$$c_{u2} \neq 0 \text{ and } E_2 \neq 1_2 \neq {}^{*}E_3$$

It is then concluded that the ROTHALPY will be identical to the energy at the runner outlet if the rotational outlet velocity component is zero and there is frictionless flow when neglecting leakage flow and chock friction losses.

In this chapter a general theoretical evaluation of accelerations and energy conversion of the flow through the turbines has been made on a general basis.

Analysis of the energy conversion through a reaction turbine when changing outlet angles of the runner blades

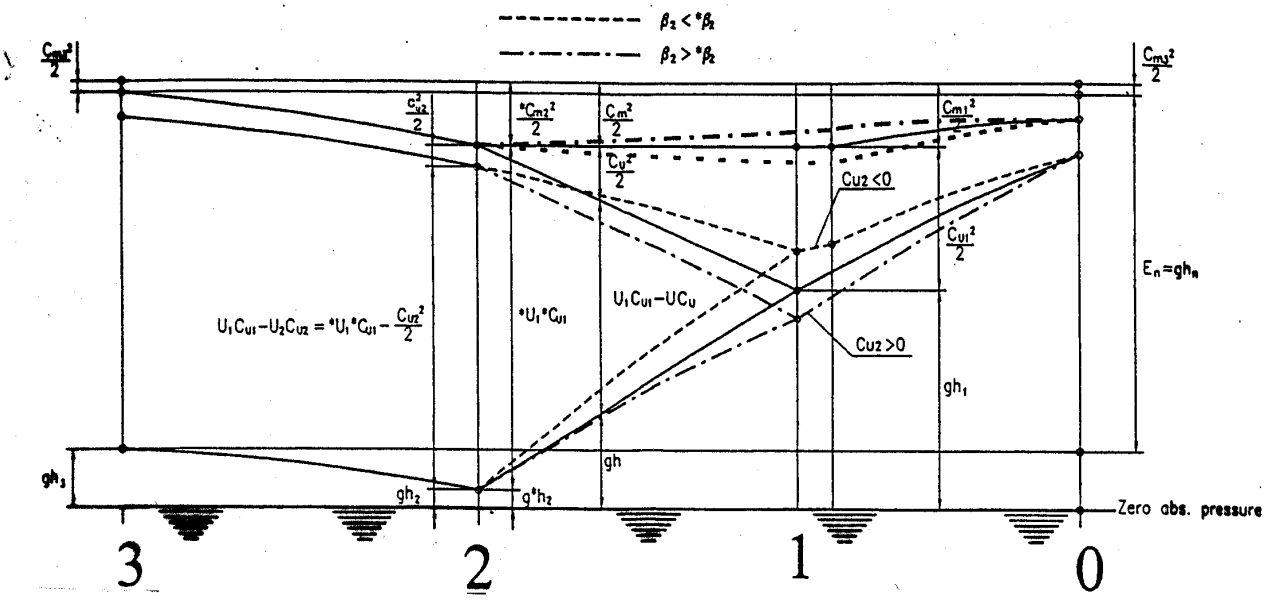

Fig. 8.12 Energy conversion through a Francis turbine with the effect of variation in the outlet angle β_2. (For simplification it has been assumed that $z_1 = z_2 = z_3 = 0$)

Assuming that the meridional inlet- and outlet velocities are equal i.e. $c_{m1} = c_{m2}$ = constant and defining the difference of the runner inlet energy and the draft tube outlet energy is given by eq (8.58) (Both a decreased and increased meridional velocity through a runner have been used by different turbine manufacturers, but for simplification constant meridional velocity is used in this explanation).

$$E_1 - E_3 = \left(gh_1 + \frac{c_1^2}{2} \right) - \left(gh_3 + \frac{c_{m3}^2}{2} \right) \qquad (8.58)$$

Here, E_3 is the outlet energy which cannot be utilized by the turbine and is equal to the Rothalpy at best efficiency.
Increased outlet angles of a runner operationg at best efficiency point where $c_{m2} = {}^*c_{m2}$ leads to an absolute tangential positive outlet velocity component = c_{u2} = 09. (By decreasing the outlet angle the tangential component of the outlet velocity will be negative i.e. $c_{u2} = 0$. (By decreasing the outlet angle the tangential component of the outlet velocity will be negative i.e. $c_{u2} < 0$ and the absolute inlet velocity = c_1 decreases at constant guide vane position).

It is now appropriate to study how the inlet conditions changes by increasing the outlet angle and obtaining $c_{u2} > 0$ assuming that $gh_2 = g{}^*h_2$ where $g\ {}^*h_2$ is the pressure energy at best efficiency point before the change.

Then the outlet ROTHALPY before and after the change is different i.e.: $I_2 \neq {}^*I_2$, but $I_1 = I_2$ after the changed outlet angle and ${}^*I_1 = {}^*I_2 = {}^*E_2$ before the change where ${}^*c_{u2} = 0$.

The following equation is obtained assuming constant flow i.e. Q = ‘Q and c_{m2} = *c_{m2} and u_2 = *u_2:

$$I_2 - {}^*I_2 = \left(gh_2 + \frac{w_2^2}{2} - \frac{u_2^2}{2} \right) - \left(g^* h_2 + \frac{{}^*w_2^2}{2} - \frac{{}^*u_2^2}{2} \right)$$

Substituting for

$$w_2^2 = \left(u_2 - c_{u2}\right)^2 + {}^*c_{m2}^2$$

and

$${}^*w_2^2 = {}^*u_2^2 + {}^*c_{m2}^2 \quad \left(for\ {}^*c_{u2} = 0 \right)$$

Then, because it has been assumed that h_2 = *h_2, *c_{m2} = c_{m2} and *u_2 = u_2 = constant:

$$I_2 - {}^*I_2 = gh_2 - u_2 c_{u2} + \frac{c_{u2}^2}{2} - g^* h_2 = -u_2 c_{u2} + \frac{c_{u2}^2}{2}$$

or

$$I_2 = {}^*I_2 - u_2 c_{u2} + \frac{c_{u2}^2}{2} \qquad (8.59)$$

Assuming that E_1 =*E_1 and substituting for I_2 by eq (8.59),

$$E_2 = I_2 + u_2 c_{u2} = {}^*I_2 - u_2 c_{u2} + \frac{c_{u2}^2}{2} + u_2 c_{u2}$$

$$i.e. \quad E_2 = {}^*I_2 + \frac{c_{u2}^2}{2} = {}^*E_2 + \frac{c_{u2}^2}{2} \qquad (8.60)$$

Because it was assumed that E_1 = *E_1, $^* I_1 = {}^*I_2$ *and* $I_1 = I_2$

Then

$$u_1 c_{u1} = {}^*u_1 {}^* c_{u1} + {}^*I_1 - I_1$$

Substituting for *I_1 – I_1 = *1_2 – I_2 by increasing eq (8.59 because *I_1 = *I_2 and I_1 = I_2:

$$u_1 c_{u1} = {}^*u_1 {}^* c_{u1} + u_2 c_{u2} - \frac{c_{u2}^2}{2} \qquad (8.61)$$

Assuming that no change in the inlet radius is made, i.e. u_1 = *u_1. Then the following equation yields:

$$c_{u1} = {}^*c_{u1} + c_{u2}\left(\frac{u_2}{u_1} - \frac{c_{u2}}{2u_1}\right) \qquad (8.62)$$

For normal operation $|c_{u2}| << |u_2|$ and for the majority of runners (medium and high head) $u_2 \le u_1$.

Then the inlet velocity diagram will be changed as shown qualitatively in fig. 8.13.

Loss in efficiency by rotation at outlet by increased outlet angles and assuming that $h_2 = {}^*h_2$.

$$\eta_h = \frac{{}^*E_1 - E_2}{E} = \frac{\left(g\,{}^*h_1 + \frac{{}^*c_{u1}^2}{2} + \frac{{}^*c_{m1}^2}{2}\right) - \left(g\,{}^*h_2 + \frac{c_{u2}^2}{2} + \frac{{}^*c_{m2}^2}{2}\right)}{E} = \frac{\left({}^*E_1 - {}^*E_2 - \frac{c_{u2}^2}{2}\right)}{E}$$

or by using eq. (8.53) and substituting for $u_1 c_{u1}$ by eq. (8.61):

$$\eta_h = \frac{u_1 c_{u1} - u_2 c_{u2}}{E} = \frac{{}^*u_1\,{}^*c_{u1} + u_2 c_{u2} - \frac{c_{u2}^2}{2} - u_2 c_{u2}}{E} = \frac{{}^*u_1\,{}^*c_{u1} - \frac{c_{u2}^2}{2}}{E}$$

Then by substituting for $E = {}^*u_1\,{}^*c_{u1}/{}^*\eta_h$ at best efficiency where ${}^*c_{u2} = 0$:

$$\frac{\eta_h}{{}^*\eta_h} = \frac{{}^*u_1\,{}^*c_{u1} - \frac{c_{u2}^2}{2}}{{}^*u_1\,{}^*c_{u1}} = 1 - \frac{1}{2}\frac{c_{u2}^2}{{}^*u_1\,{}^*c_{u1}} \qquad (8.63)$$

Calculation of necessary change of blade inlet angle if the outlet angle is increased in order to obtain increased flow at best efficiency

(Denotations to be remembered:
Blade inlet 1, blade outlet 2, draft tube outlet 3, tangential absolute velocity component c_u, absolute meridional velocity component c_m, relative velocity w and circumferential blade velocity u.)

Assumptions:

Inlet specific energy	= const. i.e. $E_1 = {}^*E_1$ = const.
Circumferential speed	= const. i.e. $u_1 = {}^*u_1$ and $u_2 = {}^*u_2$
Non rotating outlet flow	= $c_{u2} = {}^*c_{u2} = 0$
Friction ignored	= $I_1 = I_2 = {}^*I_2 = E_2 = {}^*E_2 = E_3 = {}^*E_3$
Draft tube outlet pressure constant	= $h_3 = {}^*h3$

* Denotes initial best efficiency point before change of outlet angle

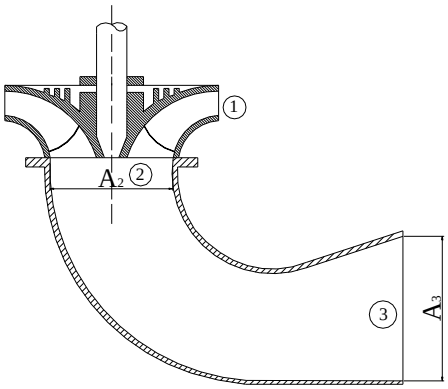

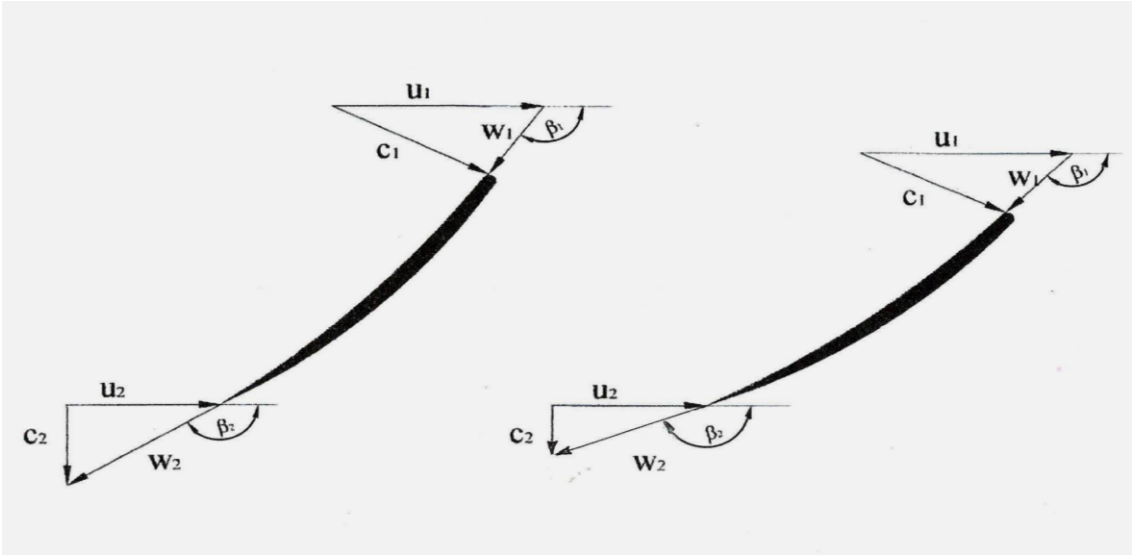

Fig. 8.13 Velocity diagrams at inlet and outlet of two blades with $c_{u2}=0$ with different outlet angels and constant specific energy and circumferential speed at the inlet.

The following equation can now be established if no rotation is assumed at the outlet and the available specific energy at the inlet is unchanged. (In this case the specific energy and velocities for the initial blade angles are denotet by asterix, but letters without the asterix are also denoting best efficiency with increased non rotating outlet flow on the blade to the left in Fig. 8.13.).
Then it is possible to write:

$$E_1 = {}^*E_1 \quad i.e. \quad \underline{gh_1 + \frac{c_1^2}{2} = g\,{}^*h_1 + \frac{{}^*c_1^2}{2}}$$

The further following equation is obtained for frictionless flow with non-rotating outlet flow from the runner: (see eq. (5.57))

$$E_1 = u_1 c_{u1} + I_1 = u_1 c_{u1} + I_2 = u_1 c_{u1} + E_3$$

Further, by introducing the runner outlet area by A_2 and the draft tube outlet area by A_3.

$$E_3 = gh_3 + \frac{c_{m3}^2}{2} = gh_3 + \left(\frac{A_2}{A_3}\right)^2 \frac{c_{m2}^2}{2} = gh_3 + \left(\frac{A_2}{A_3}\right)^2 \tan^2\beta_2 \left(\frac{u_2^2}{2}\right)$$

Then

$$E_1 = u_1 c_{u1} + g h_3 + \left(\frac{A_2}{A_3}\right)^2 \tan^2 \beta_2 \left(\frac{u_2^2}{2}\right)$$

Remembering the assumption that $E_1 = {}^*E_1$ and $h_3 = {}^*h_3$ and rearranging the equation:

$$u_1 c_{u1} = {}^*E_1 - \left(g {}^* h_3 + \left(\frac{A_2}{A_3}\right)^2 \tan^2 \beta_2 \left(\frac{u_2^2}{2}\right)\right)$$

When changing outlet angle from $^*\beta_2$ *to* β_2 we get $u_1c_{u1}/(^*u_1{}^*c_{u1}) = c_{u1}/{}^*c_{u1}$ because $u_1 = {}^*u_1$. Then following equation may be established: (note: $u_2 = {}^*u_2$)

$$\frac{c_{u1}}{{}^*c_{u1}} = \frac{{}^*E_1 - \left[g {}^* h_3 + \left(A_2/A_3\right)^2 \left({}^*u_2^2/2\right)\tan^2 \beta_2\right]}{{}^*E_1 - \left[g {}^* h_3 + \left(A_2/A_3\right)^2 \left({}^*u_2^2/2\right)\tan^2 {}^*\beta_2\right]} \quad (8.64)$$

(Note: normally $(A_2/A_3) \leq 0.2$ and then $c_{u1} \approx {}^*c_{u1}$, but always $c_{u1} < {}^*c_{u1}$ for $c_{m1} > {}^*c_{m1}$ and vice versa).

Further it is assumed that the meridional velocity component will increase at the inlet proportion to the meridional velocity at the outlet.

Then the following ratio normally yields:

$$\frac{c_{m1}}{{}^*c_{m1}} = \frac{c_{m2}}{{}^*c_{m2}} = \frac{u_2 \tan \beta_2}{{}^*u_2 \tan {}^*\beta_2} \quad (8.65)$$

The following relation is now obtained in order to determine the inlet blade angle as function of change in outlet angle remembering that $\tan \beta_1 = c_{m1}/\left(u_1 - c_{u1}\right)$ and substituting for $c_{m1}/{}^*c_{m1}$ by eq. (8.65) where $u_2 = {}^*u_2$:

$$\tan \beta_1 = \tan {}^* \beta_1 \frac{c_{m1}\left({}^*u_1 - {}^*c_{u1}\right)}{{}^*c_{m1}\left(u_1 - c_{u1}\right)} = \tan {}^* \beta_1 \frac{\tan \beta_2}{\tan {}^* \beta_2} \frac{\left({}^*u_1 - {}^*c_{u1}\right)}{\left({}^*u_1 - c_{u1}\right)} \quad (8.66)$$

Then by substituting for c_{u1} expressed by ${}^*c_{u1}$ by means of eq (8.64), $\tan \beta_1$, can be found by eq. (8.66). (Note: based on eq (8.64) it may be assumed that $c_{u1} \approx {}^*c_{u1}$ for small variations of the outlet angle and then $({}^*u_1 - {}^*c_{u1}) \approx (u_1 - c_{u1})$ as shown in eq (8.67).

The inlet diagram with changes of the guide vane angle is illustrated in fig. 8.14.

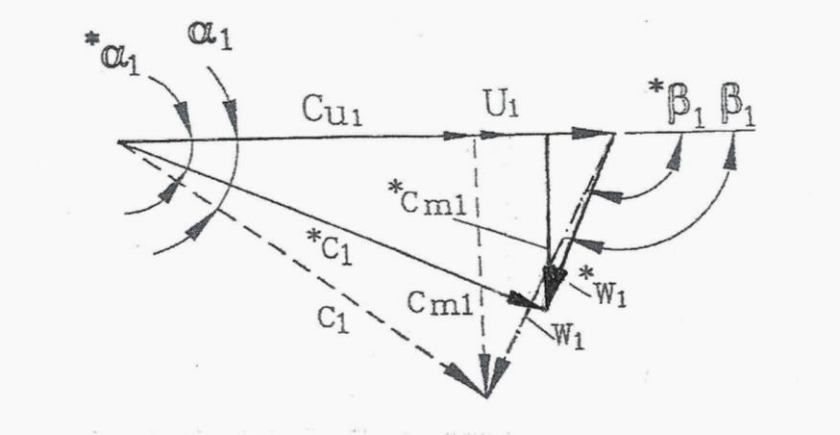

Fig. 8.14 Inlet diagram illustrating the variation in c_{u1} and c_{m1} and the inlet flow angle β_1, at increased guide vane angle $\alpha_1 > {}^*\alpha_1$ at constant blade outlet angle β_2

Example:
When letting $A_2 / A_3 = 0.2$ and ${}^*\beta_2 = 180^0 - 17^0$ i.e. $\tan^2 17 = 0.0093$,
then $(A_2 / A_3)^2 \tan^2 {}^*\beta_2 = 0.2^2 \cdot 0.093 = \underline{0.00372}$

By letting $\beta_2 = 180^0 - 19^0$ then $\tan^2(19) = 0.119$ and
$(A_2 / A_3)^2 \tan^2 \beta_2 = 0.2^2 \cdot 0.119 = 0.00476.$
*(Note: $180^0 - \beta_2 = 19^0$ is a large angle used for demonstration in this case).

Assuming as an example $h_3 = {}^*h_3 = 5$ m W.C. i.e. $g^*h \approx 50$ (Joule/kg) and $^*u_2 = 40$ m/sec i.e. $^*u^2/2 \approx 800$ Joule/kg)

Then

$g^*h_3 + (A_2/A_3)^2 \ {}^*u_2^2/2 \tan {}^*\beta_2 = 50 + 0.00372 \cdot 800 = 50 + 2.98 \approx 53.0$

and $g^*h_3 + (A_2/A_3)^2 {}^*u_2^2/2 \tan \beta_2 = 50 + 0.00476 \cdot 800 = 50 + 3.80 \approx 53.8$

Then

$c_{u1}/{}^*c_{u1} \approx 1$ according to eq. (8.64) because $E_1 >> g^*h_3$ and normally $g^*h_3 >> (A_2/A_3)^2 \cdot {}^*u_2^2/2 \tan\beta$

and thus:

$$\frac{(u_1 - {}^*c_{u1})}{(u_1 - c_{u1})} \approx 1$$

Simplifying eq (8.66) gives:

$$\tan\beta_1 \cong \tan {}^*\beta_1 \frac{c_{m1}}{{}^*c_{m1}} = \tan {}^*\beta_1 \frac{\tan\beta_2}{\tan {}^*\beta_2} \qquad (8.67)$$

8.6. Energy conversation through a Pelton turbine

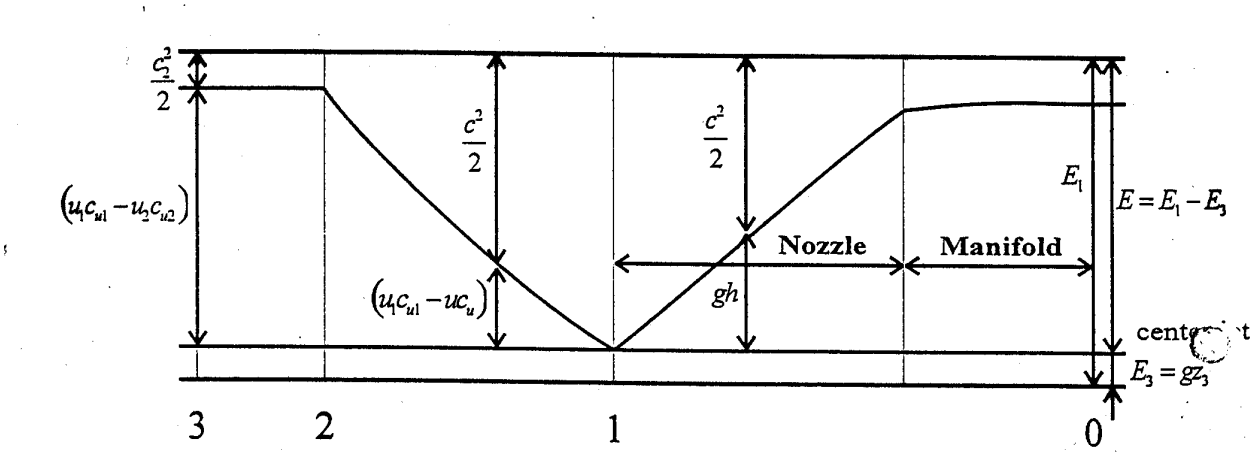

Fig. 8.15 Energy conversion diagram for a Pelton turbine (Impulse turbine)

In an impulse turbine the total specific inlet energy E_1 is converted to specific kinetic energy = $(c_1^2/2)$. The flow through the runner is converted to mechanical power by the impulse forces created by changes in the direction of the high velocity flow as explained by the Euler turbine equation. No reaction forces from pressure reduction through the blade channels is converted and no increase in the velocity occurs in the buckets of an impulse turbine and the spaces between the buckets are not filled with water. (For this reason an impulse turbine is also called a partial turbine.)

The flow is a non stationary free surface flow which is very difficult to analyse by CFD methods. However, research work is going on to solve this problem (by Dr ing work. (Ref. Paper by Dr.Ing.Stud. M.Hana, IAHR Singapore 1998) . A graphical method has been successfully used in Norway in order to study the flow. The method is based upon the fact that the acceleration vector of a water particle on the surface of the flow must be normal to the surface. A description is given later in the APPENDIX of this book.

Change in efficiency by change of outlet angles of an impulse turbine.

For an impulse turbine the absolute and relative inlet velocity will not be changed if the outlet angles of the buckets are changed.

Then following assumptions can be made for a simplified physical model where friction is ignored:

$h_1 = {}^*h_1 = h_2 = {}^*h_2 = \text{const.}$, $w_1 = w_2 = {}^*w_2$, $u_1 = u_2$ and $I_1 = {}^*I_1 = I_2 = {}^*I_2$.

The outlet velocity diagram shows that $w_2^2 = w_{u2}^2 + w_{m2}^2 = \text{const.}$, because

$$I_2 = gh_2 + \frac{w_2^2}{2} - \frac{u_2}{2} = {}^*I_2 .$$

Then $w_{u2}^2 + w_{m2}^2 = {}^*w_{u2}^2 + {}^*w_{m2}^2$ and $(w_{u2}^2 + w_{m2}^2)^{0.5} = c_1 - u_1 = \text{const.}$

Assuming that the outlet angle $^*\beta_2$ is an optimal angle and change this to β_2, the following equation is obtained:

$$w_{m2} / w_{u2} = \tan \beta_2$$

The following assumptions can be made when regarding the pitch diameter of a Pelton runner for simplification: (see also APPENDIX where a complete analysis of the flow on a Pelton bucket is shown).

Because:

$${}^*w_2 \cos {}^*\beta_2 \approx {}^*w_2 \text{ and } w_2 \cos \beta_2 \approx w_2 \text{ and } \sin \beta_2 \approx \beta_2$$

then:

$$c_2 \approx {}^*w_2 \sin \beta_2 \approx {}^*w_2 \beta_2 \text{ and } {}^*c_2 \approx {}^*w_2 \sin {}^*\beta_2 \approx {}^*w_2 {}^*\beta_2$$

and

$$c_2^2 - {}^*c_2^2 = {}^*w_2^2 (\beta_2^2 - {}^*\beta_2^2)$$

Note : β_2 is expressed in radians:

The change in specific outlet energy will then be: (note $^*h_2 = h_2 = 0$)

$$E_2 - {}^*E_2 = (g h_2 + \frac{c_2^2}{2}) - (g {}^*h_2 + \frac{{}^*c_2^2}{2}) \approx \frac{{}^*w_2^2}{2} (\beta_2^2 - {}^*\beta_2^2) \qquad (8.68)$$

Then the change in efficiency by increasing the outlet angle β_2 may be expressed by following equations when substituting for E_2 by eq. (5.68) in the efficiency equation:

$$\eta_h = \frac{{}^*E_1 - E_2}{E} = \frac{({}^*E_1 - {}^*E_2) - \frac{{}^*w_2^2}{2} (\beta_2^2 - {}^*\beta_2^2)}{E}$$

when substituting for $\frac{{}^*E_1 - {}^*E_2}{E} = {}^*\eta_h$

and according to eq. (3.1) chapter 3, where $z_0 = z_3$ according to the IEC norms where the outlet reference level is defined to be the jet centre for vertical units and E = gH and remembering that $^*h_1 = {}^*h_2 = 0$ we get following equation for friction free flow:

$$g * h_o + \frac{c_0^{\,2}}{2} = g * h_1 + \frac{{}^*c_1^2}{2} = E + g * h_2 = 0 \qquad \text{(for } {}^*h_2 = 0\text{)}$$

or $$E = g\ {}^* h_0 + \frac{{}^* c_0^{\,2}}{2} - g\ {}^* h_2 = \frac{{}^* c_1^{\,2}}{2} \qquad \text{(for } {}^*h_1 = 0 \text{ and } {}^*h_2 = 0\text{)}$$

The following expression is therefore obtained for the change in efficiency by changing the outlet angle from $^*\beta_2$ to β_2 by substituting for η_h by the equations shown above:

$$\boldsymbol{\eta_h = {}^*\eta - (^*w_2^2/{}^*c_1^2)\,(^*\beta_2^2 - \beta_2^2)} \qquad (8.69)$$

In a real turbine u_2 and β_2 are not constant along the outlet edge because u_2 is increasing proportionally to the radius and β_2 must vary to obtain clearance of the outlet water to the next bucket. The loss in efficiency is then highly influenced by the portion of the outlet flow which leaves the buckets at the inner and outer part of the outlet edge where $\mathbf{u_2 \neq {}^*u_2}$ and $\boldsymbol{\beta_2 \neq {}^*\beta_2}$.

The flow in a Pelton bucket can be analysed by an analytical -graphical method as described in the following.

Analysis of the flow the bucket of an Impulse turbine.

This is only a short chapter describing the available tools for analysis of the flow in Pelton turbines, but the procedure is also valid for other impulse turbines such as Turgo turbines and Cross flow turbines.

In the authors opinion it is a shame that too little effort has been made to analyze and optimize the Turgo turbines. The Turgo turbine should be used as vertical multi nozzle versions with a larger runner/jet-diameter ratio and a higher efficiency than the marketed units to day.

For the Cross flow turbines the water around and inside the runner will reduce the efficiency to a level that is of little interest for theoretical hydraulic research. The status for Pelton turbines is that an efficiency between 92 % and 93% has been obtained by model testing and careful analysis now also by CFD-VOF (Volume of fluid) methods.

However, the CFD-VOF analysis of the bucket flow does not give more information than was achieved by Graphical methods 40 years ago.

The reason for not using graphical methods is the work load of 3 months for one analysis. The main increase of the efficiency is found by a combination of theoretical analysis combined with model study of the turbine and the velocity distribution in jet , combined with pressure measurements in the buckets during model testing.

The week point in the CFD analyses is that the modelling of the velocity distribution in the jet is incorrect and thus the flow in the bucket is also incorrect.

The other most important study is the model testing of the outlet flow from the buckets in the runner pit.

It is also surprising to note that some customers requires a Froud's number similarity between model and prototype, while the main problem is the difference in the Weber number causing a quite different formation of water droplets air mixture in the prototype compared with the model.

This is leading to a quite different water circulation and windage loss especially in high head prototypes compared with a model operating at 100 m head.

In now way the water will fall down according to gravity according to Froud's law in the same way in model and prototype. Of interest might be to let the model and prototype operate at the same head and with the distance to the walls much larger than for practical economic limits. This will give an opportunity to study the effect of Froud's number.

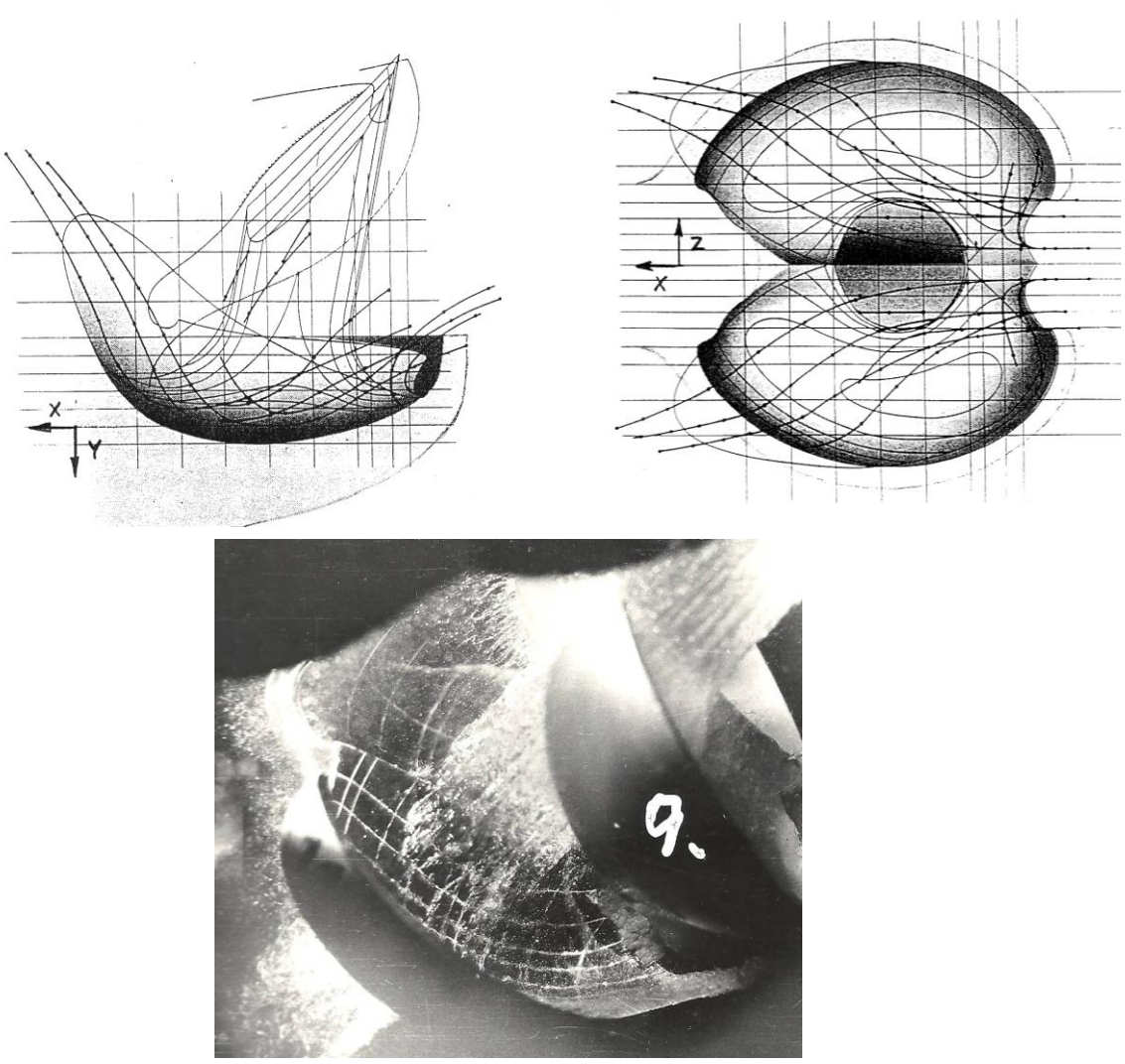

Fig. **8.16. Top:** Illustration the result of a graphical analysis based on the governing equations presented in this chapter for flow in a Pelton bucket. Bottom: High speed camera photo of the flow in the bucket for control of the graphical analysis. Note the edge flo the flow in the bucket for control of the graphical analysis.

The basis for the GRAPHICAL METHODE is that the resulting accelleration on a particle on the surface in the bucket must be normal to the surface of the moving water.

The analysis is based on a study of the path of a particle on the jet surface before the influence of the bucket occure and then following the particle path on the surface through the bucket where following equations are valid. Such analysis requires 2 months of work of a trained enginner, but the result is an excellent basis for the improvement of the bucket shape.

The acceleration in x, y and z direction will be as follows:

$$a_x = \frac{dx^2}{dt^2} + \omega^2 \cdot R \cdot \cos\phi + 2 \cdot \omega \cdot W_y$$

$$a_y = \frac{dy^2}{dt^2} + \omega^2 \cdot R \cdot \sin\phi + 2 \cdot \omega \cdot W_x \qquad a_z = \frac{dz^2}{dt^2}$$

To solve this task the assumed shape of the water in the bucket with the particle path must be drawn and the calculation of $\mathbf{a_x}$, $\mathbf{a_y}$ and $\mathbf{a_z}$ must be made.

If the resulting direction of the acceleration is not correct, the shape of the water surface and/or the particle path must be adjusted to fulfill the requirement that the acceleration must be normal (perpendicular) to the surface.

The methode is suitable for a combination with a stroboscopic picture from model tests and the graphical analysis.

With the graphical analysis 3 month work is needed, but the ingenier will get an excellent understanding of how to improve the bucket shape.

In the future there is a hope that the CFD - VOF methods will be able to give results that can be verified in model turbines and prototype. However, at the time being in 2012, we still to the author´s opinion, have to study the models of Pelton turbines and interpret the results to be valid for prototypes.

Analysis of the CFD-VOF method has been presented some years ago in a PhD work by **Morten Hana** at NTNU in Norway in 1999..

Further an other promising PhD work at NTNU in Norway was made by **Godtfred Berntsen** in 2003 on the free surface jet flow, proving the complicity of the velocity distribution in the jet depending on the distanve from the nozzle. His CFD analysie was confirmed by measurements in a 100 m head model. Such result is difficult to obtain in a prototype operating at 1000 m net head

9. CHARACTERISTIC PARAMETER

9.1 The speed number

The choice of turbine type is based upon the speed number or specific speed of the turbine.

The origin of the **speed number** which is described in chapter 5.1, is defined to be based on the best efficiency point (BEP) obtained at optimum angular speed *ω and the flow *Q. (* denotes BEP).

$$^{*}\Omega = {}^{*}\omega\sqrt{^{*}Q}/(2g*H)^{3/4} \qquad (9.1)$$

The **capacity** or size of a turbine can be expressed by the flow Q divided by the maximum theoretical velocity =

$$\sqrt{2gH}$$

The equation for the capacity yields:

$$\underline{Q} = Q/\sqrt{2gH} \quad (m^2) \qquad (9.2)$$

$$n_s = n\sqrt{Q_n}/H^{3/4}$$

The relation between the defined speed number and the specific speed will be when introducing K = (rated flow)/(BEP flow) = Q_n/*Q.

$$n_s = *\Omega\sqrt{K}(2g)^{3/4}30/\pi \qquad (9.3)$$

Because *Ω is a dimensionless parameter the speed number will be used in the following: The speed number may also be expressed as follows referring to the circumferential speed at the outlet diameter of the runner where (π - β_2) is the outlet blade angle, corrected for slip (see fig. 3.1), and $\underline{u}_2$ is the reduced circumferential blade speed.

$$*\Omega = \sqrt{\pi}\ \underline{u}_2^{3/2}\sqrt{\tan(\pi - \beta_2)} = \sqrt{\pi}\left(\frac{u_2^2 * \eta_n}{2 * u_1 * c_{u1}}\right)^{3/4}\sqrt{\tan(\pi - \beta_2)}$$

or

$$*\Omega = \sqrt{\pi}\left(\frac{\eta}{2}\right)^{3/4}\left(\frac{u_1}{c_{u1}}\right)^{3/4}\left(\frac{D_2}{D_1}\right)^{3/2}\sqrt{\tan(\pi - \beta_2)} \qquad (9.4)$$

where:

$$\underline{u}_2 = u_2/\sqrt{2gH} \quad and \quad 2gH = \frac{*u_1 * c_{u1}}{*\eta_n}$$

This equation shows that within the same speed number an increased outlet diameter and outlet circumferential speed may be compensated by a decreased outlet blade angle within a limited range of angles. Further an increased inlet diameter will decrease the speed number for a given outlet diameter. Then the blade angle must be increased because the ratio u_1/c_{u1} will also be increased.

9.2 Cavitation and net positive suction head NPSH

The required setting of a Francis turbine in order to avoid cavitation can be defined by means of the Net Positive Suction Head (NPSH) or the Thoma cavitation number σ = NPSH/H. The following formula may be established to find the required NPSH for a runner by expressing the reduced (dimensionless) circumferential runner outlet speed explicit by means of eq. (6.4):

$$\underline{u}_2 = {}^*\Omega^{2/3}\,(\pi\tan(\pi-\beta_2))^{1/3} \tag{9.5}$$

Then an empirical equation for $NPSH_R$ of a certain runner may be established as follows for Francis turbines:

$$NPSH_R = H\,\underline{u}_2^2[a\,K^2\tan^2(\pi-\beta_2)+b] = \frac{u_2^2}{2g}[\,aK^2\tan^2(\pi-\beta_2)+b] \tag{9.6}$$

Here $1 < a < 1.2$ and $0.05 < b < 0.11$ depending on the speed number and the blade geometry and number of blades (see also eq. (9.10) chapt 9.3).

For a Francis turbine (and also for a Kaplan turbine) the speed number *Ω and circumferential outlet velocity u_2 of the runner will then be limited due to the danger of cavitation for a given submergence of the turbine.

The necessary submergence must satisfy the value of $NPSH_R$ according to eq. (9.6) which is based on the circumferential velocity of the runners outlet rim and the blades outlet angles. On the contrary, for a given blade angle β_2 there is a limit of the absolute velocity of the outlet rim determined by the limited value of $NPSH_A$. Here $NPSH_A$ is the available value of the power plant in question, see chapt. 5.3.

9.3 The speed number covering Kaplan-Francis- and Pelton-turbines.

The cavitation value of $NPSH_A$ is based on the pressure at the runner outlet calculated on the basis of the pressure at the draft tube outlet according to Bernoulli's equation. (see fig. 5.10, chapt. 5.3)

$$h_2 + c_2^2/(2g) + Z_2 = h_3 + c_3^2/(2g) + J + Z_3 \tag{9.7.}$$

Here $J=\xi c_3^2/(2g)$ is the draft tube loss.

From this equation the available $NPSH_A$ for a turbine can be found as explained in chapt. 5.3 by substituting for $h_3 = Z_2 - Z_3 - H_s + h_b$ (see fig. 5.12, chapt. 5.3)

$$NPSH_A = -H_s + h_b - h_{va} > \frac{c_2^2}{2g} - \frac{c_3^2}{2g} - J$$

The definition of the Thoma cavitations number is the ratio between $NPSH_R$ and the net head for the turbine H.

$$\sigma = \frac{(NPSH)_R}{H} \qquad (9.8.)$$

The nominal positive suction head for the turbine may now be found as a turbine parameter determined from model tests with a smaller net head than for the prototype. The critical value of the cavitation is the value where the efficiency drops below the value for cavitation-free operation due to cavitation. For this value $\sigma=\sigma_{cr}$.

$$\sigma_{cr} = \frac{(NPSH)_{cr}}{H} \qquad (9.9.)$$

Further explanation may be found in the IEC code. (Note: In the new code 1991 NPSE is used instead of NPSH i.e. E = gH = specific energy Joule instead of m WC). From experiences the turbine manufacturers normally have established empirical formulas in order to find the critical value of the $NPSH_{cr}$. Such formula may be of the type as shown in eq. 9.6 or by using the meridian velocity c_{m2} and the circumferential speed of the band u_2 the equation may be as follows (see also eg (5.19) chapt. 5.3):

$NPSH_{turb} = a\, c_{m2}^2/(2g) + b\, u_2^2/(2g) < NPSH_A$ (9.10.)

where the values of a and b are the same values as given for eq. (9.6).

Because a safety margin is required $NPSH_{cr} < NPSH_R$ for a given turbine.

The speed number = $*\Omega$ for a Francis turbines will cover a range from 0.2 to approximately 1.2 referred to best efficiency overlapped by Kaplan turbines in the upper range.
This means that the Francis turbines may be used from very low head up to 750 m net head, and Kaplan turbines from the lowest head up to a head of 50-60 m, and in extreme cases 70-80 m with a speed number range from 1.0 and up only limited by the minimum economical net head which has been regarded to be approximately 4 m. For environmental reasons even lower heads may be utilized in the future.

The circumferential speed of an impulse turbine must fulfil the requirement $u_1/c_{u1} \leq 0.5$ which satisfies the requirement of zero reaction ratio (described later in this chapter). Further the inlet and outlet diameter for a Pelton turbine will be approximately the same and the ratio (runner diameter)/(jet diameter) = D/d_j is normally limited to $D/d_j \geq 10$ at rated output.

Then the maximum speed number referred to rated output for a Pelton turbine with one jet may be derived as follows when the expression for the theoretical jet velocity yields:

$$c_{u1} = \sqrt{2gH}$$

Then

$$\underline{u}_1 = u_1 / c_{u1} = u_1 / \sqrt{2gH} = 0.5$$

The equation connecting the jet diameter to the flow yields:

$$Q_n = (\pi d_j^2/4)\sqrt{2gH} \quad \text{i.e.} \quad \underline{Q}_n = d_j^2 \pi/4$$

Further the connections between the angular velocity and the runner diameter yields:

$$\omega = 2u_1/D = \sqrt{2gH}/D \quad \text{i.e.} \quad \underline{\omega} = \omega / \sqrt{2gH} = 1/D$$

then the maximum speed number for a Pelton turbine with one jet referred to nominal load and the assumed maximum ratio $D/d_j = 10$ will be if $\underline{u} = 0.5$ $\underline{C}_{u1} = 0.5$.

$$\Omega_n = \underline{\omega}_n \sqrt{\underline{Q}_n} = \frac{d_j}{D}\sqrt{\frac{\pi}{4}} \le \frac{1}{10}\sqrt{\frac{\pi}{4}} = 0.09$$

(The assumed minimum valve of D/dj≥10 is related to problems in 6 jets units)

For a 6 jet Pelton turbine the maximum speed number will then be:

$$\underline{\Omega_n = \sqrt{6}\ 0.09 = 0.22}$$

The speed number is then limited by the $D/d_j = 10$ ratio to $\Omega \le 0.22$ even for low heads if a reliable operation of a 6 jet turbine is wanted. For horizontal turbines and vertical turbines with less than 6 jets the D/dj ratio may be as low as 9.

On the other hand a Pelton turbine may be used up net head of approximately 2000 m, but with decreased speed number in order to avoid high stresses and fatigue problems and cavitation damage caused by too small runner diameter/jet diameter ratio = (D/d_j). See Appendix.

9.4 The reaction ratio.

Besides the specific speed the reaction ratio is a very important parameter for the blade loading and cavitation performance of a reaction turbine. The reaction ratio is describing the pressure drop from runner inlet to outlet divided by the total available net head at best efficiency flow for $c_{u2} = 0$.

By introducing the dimensionless expression for pressure h = h/H the reaction ratio yields:

$$\underline{h}_1 - \underline{h}_2 = \frac{h_1 - h_2}{H} \qquad (9.11.)$$

The relative specific stagnation energy is constant along a streamline through the runner if friction is ignored i.e. $I_1 = I_2$. The following equation can be established by combining the Euler turbine equation, the absolute specific energy equation (E) and the relative specific stagnation energy equation (ROTHALPY) (see eq. (5.26)):

$$gH\,\eta_h = u_1 c_{u1} - u_2 c_{u2} = (E_1 - I_1) - (E_2 - I_2) = E_1 - E_2 \qquad (9.12.)$$

$$gH\,\eta_h = E_1 - E_2 = (gh_1 + \frac{c_1^2}{2}) - (gh_2 + \frac{c_2^2}{2}) \qquad (9.13.)$$

then:

note: $\underline{c} = c/\sqrt{2g\,H_n}$ *and* $\underline{c}^2 = \underline{c}_u^2 + \underline{c}_m^2$

Here the difference in geodetic height from inlet to outlet is ignored. Introducing reduced variables , remembering that $c_{u2} = 0$ at best efficiency point (BEP) and assuming $\underline{c}_{m1} = \underline{c}_{m2}$ i.e. constant meridional cross section through the runner.

Then by combining eq. (9.12) and eq. (9.13) for $c_{u2} = 0$, remembering $gH\,\eta_h = u_1 c_{u1}$, the following equation can be established in order to find the reaction ratio:

$$(gh_1 + \frac{c_{u1}^2}{2} + \frac{c_{m1}^2}{2}) - (gh_2 + \frac{c_{m2}^2}{2}) = u_1 c_{u1}$$

Remembering the assumption that $c_{m1} \approx c_{m2}$

Then:

$$\underline{h}_1 - \underline{h}_2 = 2\,\underline{u}_1\underline{c}_{u1} - \underline{c}_{u1}^2 \qquad (9.14.)$$

Note that $c_{u1}=u_1+w_{u1}=u_1+c_{m1}/\tan\beta_1$ and $\tan\beta_1 < 0$ for $\beta_1 > 90°$.

Studying eq. (9.14) shows that an increasing pressure difference from inlet to outlet is obtained for increasing u_1/c_{u1} ratio if $\eta_h=u_1c_{u1}/(gH)=2\underline{u}_1\underline{c}_{u1}=$const. An illustration is given in fig. 9.1 of the influence on the reaction ratio for different blade shapes.

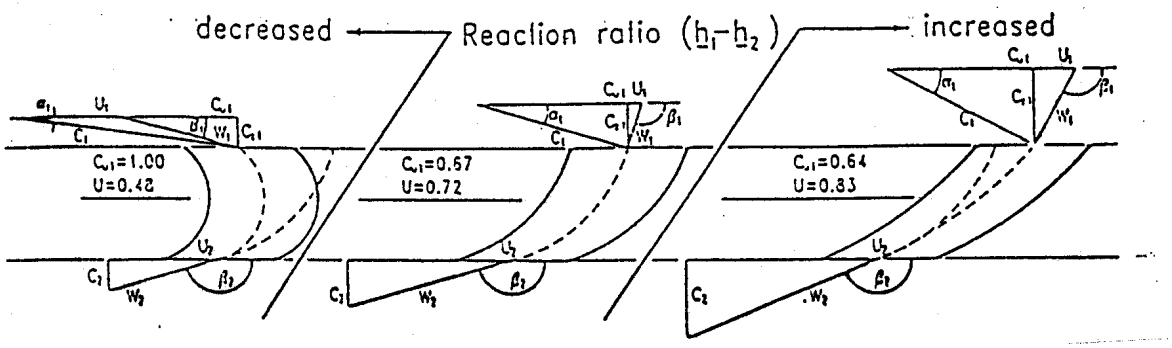

Fig. 9.1 Blade cascades and velocity vector diagrams for different reaction ratios for $c_{u2}=0$, and $\eta_h = u_1c_{u1}/(gH) =$ const.

Two examples illustrate differences in reaction ratio by using the Euler turbine equation for η_h = 0.98 and $c_{u2} = 0$:

For a high head turbine with splitter blades it may be assumed that $\underline{c}_{u1}$= 0.69 and $\underline{u}_1$ = 0.72:

Then:

$$\underline{h}_1 - \underline{h}_2 = 0.518.$$

For a low head turbine it may be assumed that $\underline{c}_{u1}$ = 0.6 and $\underline{u}_1$ = 0.83:

Then:

$$\underline{h}_1 - \underline{h}_2 = 0.636.$$

By studying fig. 6.1, and going to the blade shape to the left the decreasing reaction ratio is approaching the Pelton turbine when $u/c_u \rightarrow 0.5$ and $(\underline{h}_1\text{-}\underline{h}_2) \rightarrow 0$. By going to the right direction the blade shape is approaching a high specific speed Kaplan turbine with a small difference between inlet and outlet blade angles (β_1 and β_2) and thus a high value of the reaction ratio is obtained.

The reaction ratio is a very important parameter to be used in the design of reaction turbines when studying the blade loading in order to avoid cavitation at the inlet of the blades of low head turbines.

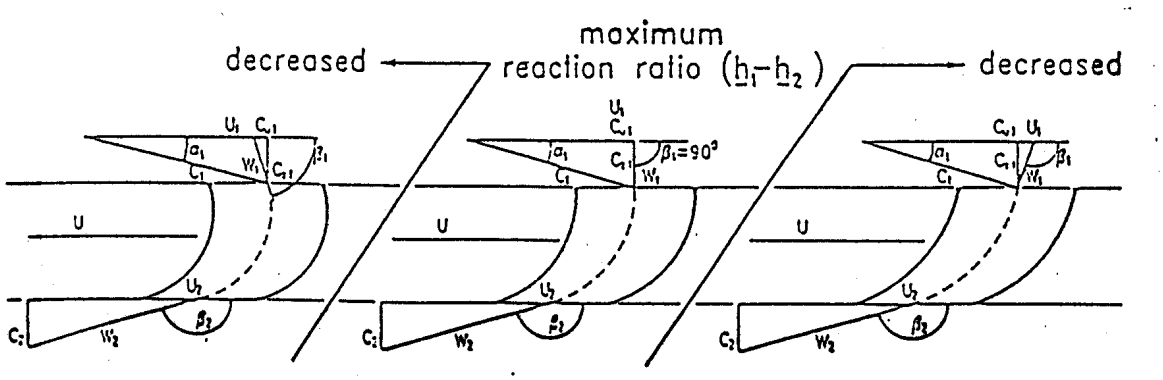

Fig. 9.2 Influence from blade inlet angle if u_1 = const. and $c_{u2} = 0$.

By studying eq. (9.14), letting u_1 = const. and $c_{u2} = 0$ it can be shown that the maximum reaction ratio i.e. (h_1-h_2) occurs for $\beta_1 = 90^o$. Thus a local increase of the inlet pressure can be obtained by bending the blade towards 90° for a constant value of u_1. Such local bending of the blade inlet at the shroud is often used. However, this often results in an unfavourable blade lean angle which reduces the pressure at the shroud as explained later in chapt. 10.

10 ANALYSIS FOR IMPROVEMENT OF HYDRAULIC DESIGN OF TURBINES TO AVOID CAVITATION.

Introduction

The development of hydraulic turbines is aimed towards two goals - to improve the efficiency and avoid cavitation damage with the highest possible circumferential speed and meridional velocity in the runner for the given submergence of the turbine. Because the problems will be different for turbines with regulated runner blades i.e. Kaplan turbines and impulse turbines this chapter will deal only with Francis turbines which are reaction turbines with fixed runner blades.

The challenge in modern design of hydraulic turbines in general is the demand for higher output and a design for higher heads with increasing specific speed which leads to a fast destruction of the machines if cavitation occurs.

In this chapter the design work on cavitation problems is described with a brief discussion of the influence from the non stationary flow in the runner caused by the wakes behind the guide vanes. Examples are also given of hydraulic design criteria and influence from parameters such as blade lean, blade angles and curvature as well as outlet and inlet diameters and speed. Special design to avoid separation and reversed flow at the inlet at best efficiency load will be described.

10.1. General design philosophy

The primary design of a runner in a Francis turbine is normally based upon following assumption

1. The absolute stagnation energy = E and relative stagnation energy ROTHALPY = I and the Euler turbine equation are valid for incompressible flow.

2. Uniform rotational symmetric flow field at inlet. (This is not correct because of the wakes behind the guide vanes, but for the shaping of the blades good results can be obtained by regarded the inlet flow to be uniform. Research work on the influence from the guide vanes valves is going on at The Norwegian Institute of Science and Technology in a special research programme.)

3. The influence of boundary layers and turbulence is ignored. Minor adjustment of blade shape are normally also made according to experiences.

During the initial stage of work the choice of inlet and outlet angels and blade lean and curvature are of great importance as well as the meridional cross section of the runner i.e. crown and shroud shape.

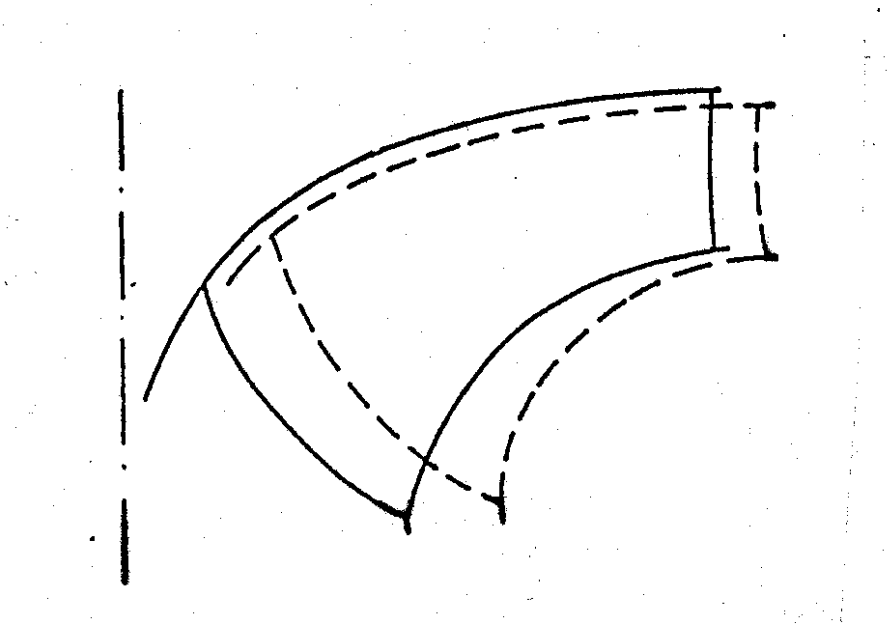

Fig. 10.1 Different shapes of high head Francis runners for the same specific speed i.e. same speed, output and head.

The blades outlet angles for example may have a variation from 162° to 167° and the inlet angle may have a variation 105° to 125° for a high head turbine. (Note definition of blade angle in fig. 8.13. Thus the shape of the meridional cross section may have a variation in shape as shown schematically in fig. 10.1.

For high head runners the cavitations problems occurs at the outlet section of the blades while also inlet cavitations often occurs on low head runners.

In order to study the cavitations a careful study of the blade loading must be done. For such study the curvature of shroud and crown as well as curvature of the blades, the blade angles and the blade leaning are important parameters.

10. 2 Influence from blade curvature along a stream line

When increasing the curvature (i.e. decreasing the radius of the curvature) of the runner blades in the portion where two blades are forming a duct the suction side of the blade will have increased velocity and decreased pressure which may lead to separation followed by cavitations on the outlet portion of the blade.

If the curvature is decreased in the duct portion of the blade and increased on the open suction side the separation point and cavitations will be moved downstream and for a successful runner. The bubble collapse of the cavitations may then occur in the water downstream of the blades. Cavitations damage of the blade may then be avoided. A comparison of the described curvatures is illustrated in fig. 10.2.

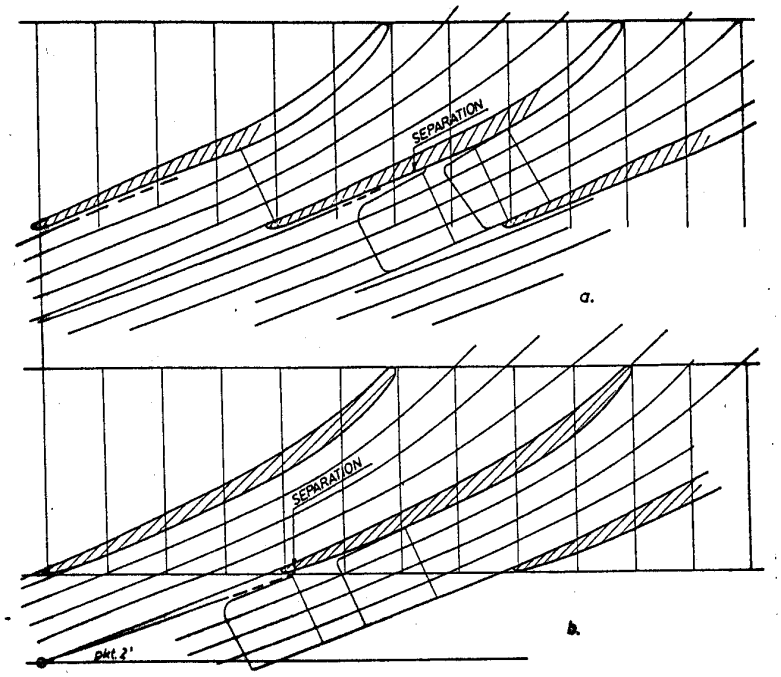

Fig. 10.2 Influence of blade curvature along a streamline

In the struggle of designing turbines for operation at increasing heads without sacrificing efficiency and increase the cost, the highest possible specific speed is chosen for Francis turbines. Because the specific speed is proportional to the maximum circumferential speed of the runner outlet in power of 1.5 divided by the net head in power of 0.75, the submergence of the turbines will increase with the circumferential speed for a given blade outlet angle.

10.3 Cavitation and balance of pressure energy and kinetic energy by means of the choice of inlet and outlet angles.

Severe cavitation may also occur at limited locations on a blade with high speed if small variations from the theoretical correct shape is found because of the high relative velocities and low pressure towards the outlet.

In order to obtain smaller submergence and/or obtain larger margin on cavitation pitting the relative outlet velocity should be reduced on the outer portion of the blades outlet close to the shroud.

The relative outlet velocity may be reduced in two ways i.e. by reducing the outlet diameter or allowing for a an absolute positive rotation of the outlet flow (rotation in the same direction as the blades). However, as shown below, a reduction of the diameter will decrease the ambient pressure below the runner.

In order to illustrate the problem Bernoullis' equation for the draft tube flow based on the meridional velocity c_m must be used and then we find the following relation: (see chapter 9.2 and 5.3).

Cavitation occurs if the pressure at the runner outlet is below the vapour pressure i.e. $h_2 \le h_{va}$ = vapour pressure in (m W.C.) and then following dissimilarity can be established if cavitation shall be avoided. [This equation is developed and discussed in chapt. 5.3]

$$h_2 = h_b - h_s - \frac{c_{m2}^2}{2g} - (\frac{c_{m3}^2}{2g} + J_{dr}) \ge h_{va}$$

$$\frac{c_{m2}^2}{2g} - (\frac{c_{m3}^2}{2g} + J_{dr}) = NPSH_R \le h_b - h_s - h_{va} \qquad (10.1)$$

Here the ambient absolute pressure at the draft tube outlet referred to the runner level (point 2) = (h_b - h_s) i.e. barometric pressure minus suction head referred to the location of the runner outlet. (The suction head h_s is the distance from the runner level (2) down to the water level outside the draft tube (3) i.e. h_s is negative if the water level is above runner level (2)).

This equation shows that an increased outlet diameter and a large outlet angle of the runner blades (as defined in fig. 10.2) combined with a decreased relative velocity, will be the right way to decrease the danger of cavitation on the blades near the shroud. However, this combination leads to positive rotation of the flow downstream of the runner.

By this design there is a danger of decreasing the pressure towards the centre of the runner outlet and also a danger of decreasing the pressure towards the inlet of the blades along the shroud as explained in the following.

When regarding the Euler turbine equation and the energy equation and for simplicity omitting friction losses and shock losses, the well known pressure energy conversion along a stream line through a turbine can be established.

The so called reduced dimensionless velocities are introduced as explained earlier:

$$\underline{c} = c/(2gH)^{0.5} = c/(2E)^{0.5} \text{ and } \underline{h} = h/H$$

The Eulers equation yields as illustrated in fig. 8.10 with friction loss ignored i.e. I_1=I_2:

$$\eta_h = 2(\underline{u}_1\underline{c}_{u1} - \underline{u}_2\underline{c}_{u2}) = \frac{(E_1 - I_1) - (E_2 - I_2)}{E} = \frac{E_1 - E_2}{E} \qquad 10.2)$$

Here E_1= gh_1+$c_1^2/2$ (= total specific energy above tail race level at the runner inlet). If losses in the draft tube and differences in geodetic height between runner outlet (2) and draft tube outlet are ignored (3) then $E = (gh_1 + c_1^2/_2) - (gh_3 + cm_3^2/_2)$ = the specific energy at runner outlet where $c_3^2/2$ is the kinetic energy at the draft tube outlet.

When ignoring losses in draft tube and substituting for in eq (10.2) and introducing dimensionless variables. [Note: According to the IEC codes the kinetic energy loss at the draft tube outlet is regarded not to be a part of the turbine loss, but part of the plant loss]

Then:

$$E\eta_h = E_1 - E_2 = (gh_1 + \frac{c_{m1}^2}{2} + \frac{c_{u1}^2}{2}) - (gh_2 + \frac{c_{m2}^2}{2} + \frac{c_{u2}^2}{2}) \qquad (10.3)$$

Further we assume that

$$c_{m1} = c_{m2} \quad \text{and} \quad gh_2 + \frac{c_{m2}^2}{2} = gh_3 + \frac{c_{m3}^2}{2}$$

Then:

$$\eta_h = \left(gh_1 + \frac{c_1^2}{2}\right) - \left(gh_3 + -\frac{c_{m3}^2}{2}\right) - \frac{c_{u2}^2}{2} / E = *\eta_h - \frac{\underline{c}_{u2}^2}{2E} = *\eta_h - \underline{c}_{u2}^2 \qquad (10.4)$$

This shows that for an ideal runner with friction loss ignored from runner inlet to draft tube outlet, the only turbine loss from runner inlet to draft tube outlet is the rotational energy at the runner outlet. Then if we have no outlet rotation the hydraulic efficiency $*\eta_h=1.0$ if friction flow losses are ignored also in spiral casing, stay vanes and guide vanes.

The energy conversion and the losses are illustrated in fig. 8.10, chapter 8. Fig. 8.10 also shows that the loss in efficiency by the rotation will be moderate in a high head turbine if $\underline{c}_{u2} \leq 0.05$. This will be discussed in detail in the following chapter.

10.4. Influence of the blade geometry both in stream line direction and normal to the stream lines in Francis runners in order to prevent cavitation.

Change of inlet and outlet blade angles for adjustment of the inlet pressure.

Referring to fig. 10.2, looking at the blade shape and the velocity vector diagrams at outlet and inlet of a runner blade the hydraulic efficiency, is given by means of the Euler equation if $\underline{c}_{u2}= 0$ as follows:

$$\eta_h = 2\underline{u}_1 \underline{c}_{u1} \qquad (10.5)$$

As an example assume that $*\eta_h=0.96$ and $*\underline{u}_1=0.72$, then $*\underline{c}_{u1}=0.67$ as the values for non rotating outlet flow.
Assuming a maximum reduced circumferential outlet blade speed of $\underline{u}_2=0.60$ i.e. $u_2=40$ m/sec for H=230 m. and deciding to redesign the turbine runner for positive rotation of the outlet flow where $\underline{c}_{u2}=0.1$ (10.4) shows the decrease in hydraulic efficiency to be $\underline{c}_{u2}^2 = 0.1^2 = 0.01$ or 1%.

However, by doing this the pressure at the runner outlet is increased towards the shroud and decreased towards the centre. The pressure at the outlet of the blade channel can be found by the ROTHALPY equation (8.26) because $\underline{w}_{u2}$ is decreased and by assuming that the meridional velocity and the outlet diameter and $w_{m2} = c_{m2}$ are assumed to be unchanged.

In the following equations the unchanged values equal to the values for non rotating outlet flow and best efficiency are denoted by asterix* ($*\eta=0.96$ where $*c_{u2} = 0$, and $u_2=*u_2$). Further

assuming that the outlet angles are decreased (see fig.10.2) and $c_{m2}=*c_{m2}=*w_{m2}=w_{m2}$ and $c_{u1}>0$.

Then following equation for friction free flow yields: [note: differences in geodetic heights are ignored in all energy equations in this chapter]

$$I_2 = gh_2 + \frac{w_2^2}{2} - \frac{*u_2^2}{2} = gh_2 + \frac{*w_{m2}^2}{2} + \frac{w_{u2}^2}{2} - \frac{*u_2^2}{2} \qquad (10.6)$$

By studying the velocity vector diagram, and substituting for $w_{u2}=u_2-c_{u2}$ and $w_{m2}=c_{m2}$ at following equation for the outlet ROTHALPY is obtained when remembering $E_1-u_1c_u=I_1$ and assuming that the absolute energy at the runner inlet $E_1=*E_1=$constant.

$$E_2 - u_2 c_{u2} = I_2 = gh_2 + \frac{c_{m2}^2}{2} + \frac{c_{u2}^2}{2} - u_2 c_{u2} = I_1 = E_1 - u_1 c_{u1} = *E_1 - *u_1 * c_{u1}$$

The increase of the pressure at the outlet of the blades ($h_2 - *h_2$) can be obtained:
Substituting for

$$E_1 = gh_1 + \frac{c_1^2}{2} = *E_1 = g * h_1 + \frac{*c_1^2}{2} \quad and \quad *I_2 = *E_2 = *I_1$$

Then:

$$I_2 = g\,h_2 + \frac{*c_{m2}^2}{2} + \frac{c_{u2}^2}{2} - u_2 c_{u2} = I_1 = g\,h_1 + \frac{*c_{m1}^2}{2} + \frac{c_{u1}^2}{2} - u_1 c_{u1}$$

and

$$*I_2 = *E_2 = g * h_2 + \frac{*c_{m2}^2}{2} = *I_1 = g * h_1 + \frac{*c_1^2}{2} - *u_1 * c_{u1}$$

Then

$$(I_2 - *I_2) = (g\,h_2 + \frac{*c_{m2}^2}{2} + \frac{c_{u2}^2}{2} - u_2 c_{u2}) - (g * h_2 + \frac{*c_{m2}^2}{2}) = (*E_1 - u_1 c_{u1}) - (E_1 - *u_1 * c_{u1})$$

After rearrangement remembering that $c_{m2}=*c_{m2}$ and $u_1=*u_1$ and $E_1=*E_1$

$$h_2 - *h_2 = \frac{*u_1 * c_{u1}}{g} - (\frac{u_1 c_{u1} - u_2 c_{u2}}{g}) - \frac{c_{u2}^2}{2g} = H\left[*\eta_h - (\eta_h + \underline{c}_{u2}^2)\right] \qquad (10.7)$$

Then from eq (10.4) and eq (10.7) the following surprising result is obtained if all flow losses are ignored;

$$h_2 - {}^{*}h_2 = 0$$

Examples of calculated values of the inlet pressure

By means of the Euler equation it can be shown that the inlet angle of the runner must also be corrected to obtain the efficiency which in this case will be 1% lower than the efficiency without rotation at the runner outlet because of the term $c_{u2}^2/(2gH) = 0.01$.

That is if $*\eta = 0.96$ eq (10.4) gives:

$$\eta_h = *\eta_h - 0.01 = 0.96 - 0.01 = 0.95 \qquad (10.8)$$

Then the difference in outlet pressure for H = 230 m as stated above yields

$$h_2 - *h_2 = 230\,[(0.96-0.95)-0.01] = 0$$

Assuming that $\underline{c}_{u2}=0.1$ for a decrease in efficiency of 1%.

Then

$$\eta_h = 2(\underline{u}_1\underline{c}_{u1} - \underline{u}_2\underline{c}_{u2})$$

$$2\underline{u}_1\underline{c}_{u1} = 0.95 + 2\cdot 0.6\cdot 0.1 = 1.07$$

with no change to the inlet diameter, $\underline{u}_1=0.72=*\underline{u}_1$. Then $\underline{c}_{u1}=0.535/0.72=0.743$.
now assuming that $\underline{c}_{m1}=\underline{c}_{m2}=0.25$.

Then $\underline{c}_1=(0.743^2+0.25^2)^{0.5}=0.78$. The hydraulic pressure at the inlet will, in this case, drop and the kinetic energy will increase compared with the case where $u_2c_{u2}=0$.

For comparison for $\underline{c}_{u2}=0$ and $\underline{c}_1=(0.67^2+0.25)^{0.5}=0.715$

Then

$$\frac{h_1}{H_1} + \frac{c_1^2}{2gH_1} = \frac{h_1}{H_1} + \underline{C}_1^2 = 1 \qquad (10.9)$$

$$\frac{h_1}{H_1} = \underline{0.489}$$

For comparison with the case where $\underline{c}_{u2}=0.1$

$$\frac{h_1}{H_1} + \frac{c_1^2}{2gH} = 1 \qquad (10.10)$$

$$\frac{h_1}{H} = 0.385$$

Here it is shown that the reduced inlet pressure energy drops from 0.489 to 0.385 or roughly 20%. By doing this the inlet angle β_1 must be decreased as defined in fig. 8.13 in chapt. 8.

From original values:

$$* \beta_1 = 180 - \cot^{-1}\left(\left(\underline{u}_1 - \underline{c}_{u1}\right)/\underline{c}_{m1}\right) = 101.3 \qquad (10.11)$$
$$for\ \underline{u}_1 = 0.72,\ \underline{c}_{u1} = 0.67\ and\ \underline{c}_{m1} = 0.25$$

to

$$\beta_1 = 84.75° \qquad (10.12)$$
$$for\ \ \underline{u}_1 = 0.72, \underline{c}_{u1} = 0.743\ \ and\ \ \underline{c}_{m1} = 0.25°$$

However, if the circumferential velocity is increased by increasing the inlet diameter and keeping c_{u1} unchanged the following values are obtained:

$\underline{c}_{u1} = 0.67$ $\underline{c}_{u2} = 0.1$ and then $\eta_h = 0.96 - 0.01 = 0.95$

From the Euler equation, for $\underline{u}_2$=0.6: $2u_1c_{u1} = 0.95 + 2 \cdot 0.6 \cdot 0.1 = 1.07$

$$2\underline{u}_1\underline{c}_{u1} = 1.07$$

i.e.

$$\underline{u}_1 = 0.799$$

Then the inlet angle will be $\beta_1 = 117.3°$

Conclusion:

The decrease of the inlet angle, as defined in fig. 8.13, is 101.3-84.75=16.55° if the inlet blade velocity is unchanged $\underline{u}_1 = 0.72$ which leads to an increased curvature of the inlet side of the blades.

The increased inlet angle, as defined in fig. 8.13, for $\underline{u}_1 = 0.799$ leads to a reduction of the curvature on the inlet side of the blades and reduced danger of cavitation and separation.

However, an increase of the inlet diameter of a mixed flow Francis runner of approximately 10% will increase the frictional disk losses of the crown and shroud and thus the total efficiency will be reduced (see also fig. 10.1).

The conclusion will be that by decreasing the danger of outlet cavitation by a slight positive outlet swirl we must sacrifice efficiency. In order to limit a further efficiency drop we must decrease the inlet angles of the blades and decrease the inlet pressure or increase the inlet diameter. (Note again definition of blade angles as shown in fig. 8.13).

For high specific speed machines the decrease in inlet pressure may also lead to inlet cavitation especially near the shroud. Inlet cavitation is normally formed by local separation close to the fillet along the shroud on the suction side of the blades.

Further the flow onto the runner contains wakes with vortices and pressure pulsations especially caused by the end gap leakage flow from the guide vane cascade. [Ref. 1] This will normally increase cavitation problems.

The most commonly used and efficient way to increase the pressure at the runner outlet will normally be to increase the outlet diameter of the runner and increase the outlet angles of the blades and thus increase the ambient pressure below the runner.

However, by doing this the relative velocity between the blades increases and the influence from waviness of the blade curvature increases the danger of local cavitation on the suction side of the blades. The danger of pressure pulsations and vibration will also increase with an increasd outlet velocity of the blades.

A combination of increased outlet diameter and increased blade angles on the outlet with a slight positive rotation by letting $\underline{c}_{u2} > 0$ may, however, be a useful and often used solution of outlet cavitation problems.

Care must be taken because by doing this inlet cavitation may occur if the positive outlet rotation is too high leading to a decrease of the pressure on the blade inlet to an unacceptable low level. (The explanation of this can be found by the Euler equation eq. (10.2) and the discussion followed after eq (10.10) and eq (10.11)).

Another important parameter to be used in the design is the blade lean angle θ which has a strong influence on the pressure distribution between crown and shroud.

Further the number of blades has a strong influence on the velocity- and pressure distribution from blade to blade. Specially for low specific turbines with large inlet diameters the distances between the blades may be large on the inlet and separation or back flow on the pressure side may occur.

To avoid this problem the blade curvature must be moderate on the inlet side of the runner. This leads to a higher blade loading towards the outlet.

The introduction of splitter blades on the inlet side has given a great contribution to solve this problem. A stronger curvature on the inlet section and a more uniform flow towards the outlet is obtained and the danger of local low pressure zones with cavitation decreases.

In the following examples of the influence from both the blade lean and splitter blades will be discussed.

The influence from blade lean angle Θ.

The blade lean is defined as the angle θ which is the blade angle normal to the streamlines as illustrated in fig. 7.4 and the pressure gradient in a stream surface may be calculated as shown by eq. (7.13) expressed by the reduced dimensionless meridional velocity $\underline{c}_m = c_m/(2gH)^{0.5}$. (A detail development of this theory is given in chapter 16).

$$\frac{dh}{dy} = 2\,[\,[(\frac{1}{R} - \frac{\cos\delta\cos^3\beta}{r})\frac{\underline{c}_m^2}{\sin^3\beta} - \frac{\underline{c}_m(\partial\,\underline{c}_m/\partial m)}{\tan\beta} + 2\underline{\omega}\cos\delta\,\underline{c}_m]\tan\theta$$

$$+(\frac{\sin\delta}{r\tan^2\beta} + \frac{1}{\rho})\underline{c}_m^2 + (2\underline{\omega}\frac{\sin\delta}{\tan\beta})c_m + \underline{\omega}^2 r\sin\delta\,] \qquad (10.13)$$

The relative reduced pressure = $\underline{h}$=h/H and the other parameters are defined in fig. 10.4.

Equation (10.13) is based upon the equilibrium of forces and is valid for a runner with infinite number of blades (i.e. potential theory). The theory is 2 dimensional only, but is still useful in order to design a preliminary blade shape followed by a full 3D CFD analysis for fine tuning of the blade outlet and inlet.

In addition to equation (10.13) the Euler-energy equation and the equation of continuity are also established as shown in eq. (14) and (15). (See chapter 16).

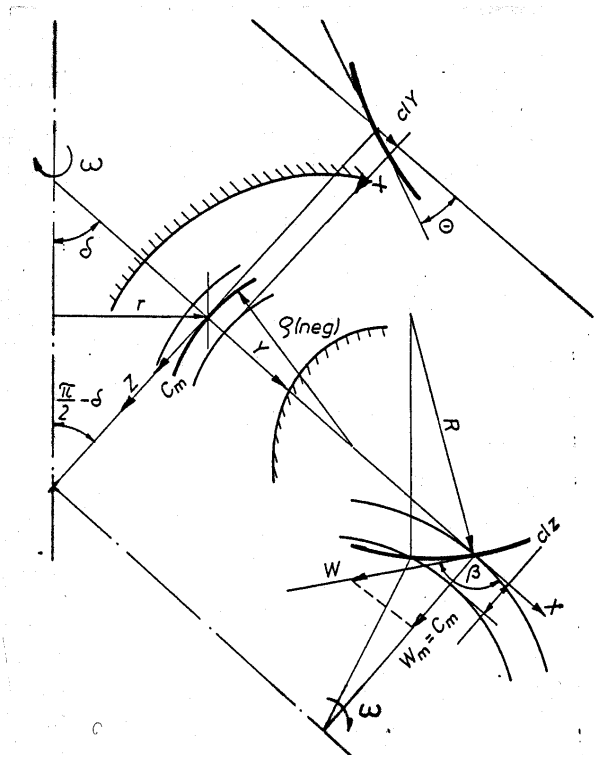

Fig. 10.4 Definition of blade lean and the blade geometry

$$\underline{h} = \underline{\omega}^2 r^2 - \underline{c}_m^2/\sin^2\beta + (1 - 2\underline{u}_1\underline{c}_{u1}) - J \qquad (10.14)$$

where J is the estimated losses along a stream line from inlet to the regarded point along the stream line. (See chapter 16).

Further the equation of continuity yields

$$c_m = \frac{Q/N}{2\pi r \Delta Y \phi} \qquad (10.15)$$

where φ = the decrease in cross section caused by the blade thickness in meridional direction, and N=number of blades and ΔY distance between the stream lines (see chapter 16).

An example of a CFD analysis of a low head runner, illustrated in fig. 10.5, showing the velocity distribution on the pressure side and suction side of the blade (fig. 10.5a) and pressure distribution between the blades (fig. 10.5b). In this example a strong curvature of the shroud together with a strong blade leaning angle towards the shroud leads to an unacceptable low inlet pressure on the suction side of the blades. This example is taken from the GAMM workshop runner where measurement has proved the computation.

For the GAMM workshop runner it can be proven that cavitation will occur near the inlet of the blades because of the unfavourable curvature and blade lean. In the case of a low head runner it is also not recommended to design for positive rotation at the outlet along the shroud because the pressure at the inlet will decrease. It should, however, be emphasized that during the design stage the pressure gradient dh/dy could be tuned by means of the blade lean angle in order to solve the inlet cavitation problem (see chapter 16). For high head runners with low specific speed, a slight positive rotation along the shroud may also be used successfully in order to avoid outlet cavitation.

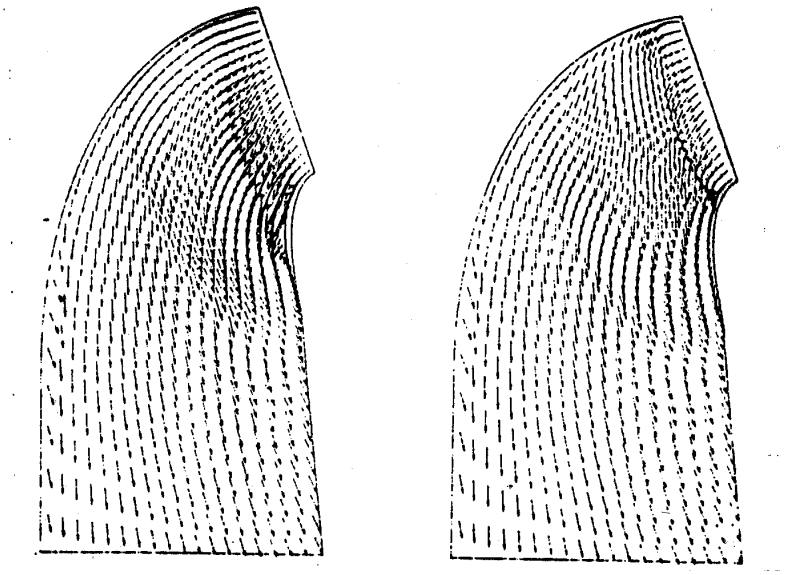

Fig. 10.5a Velocity vector plots. Suction side (left) and pressure side (right).

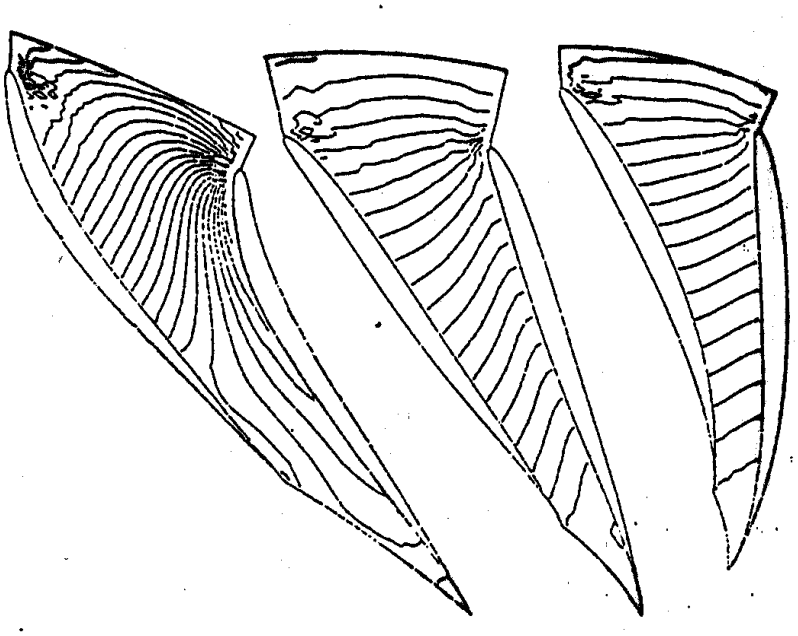

Fig. 10.5b Isobars. Equidistance 0.2 m. band (left), middle (middle), Crown (right).

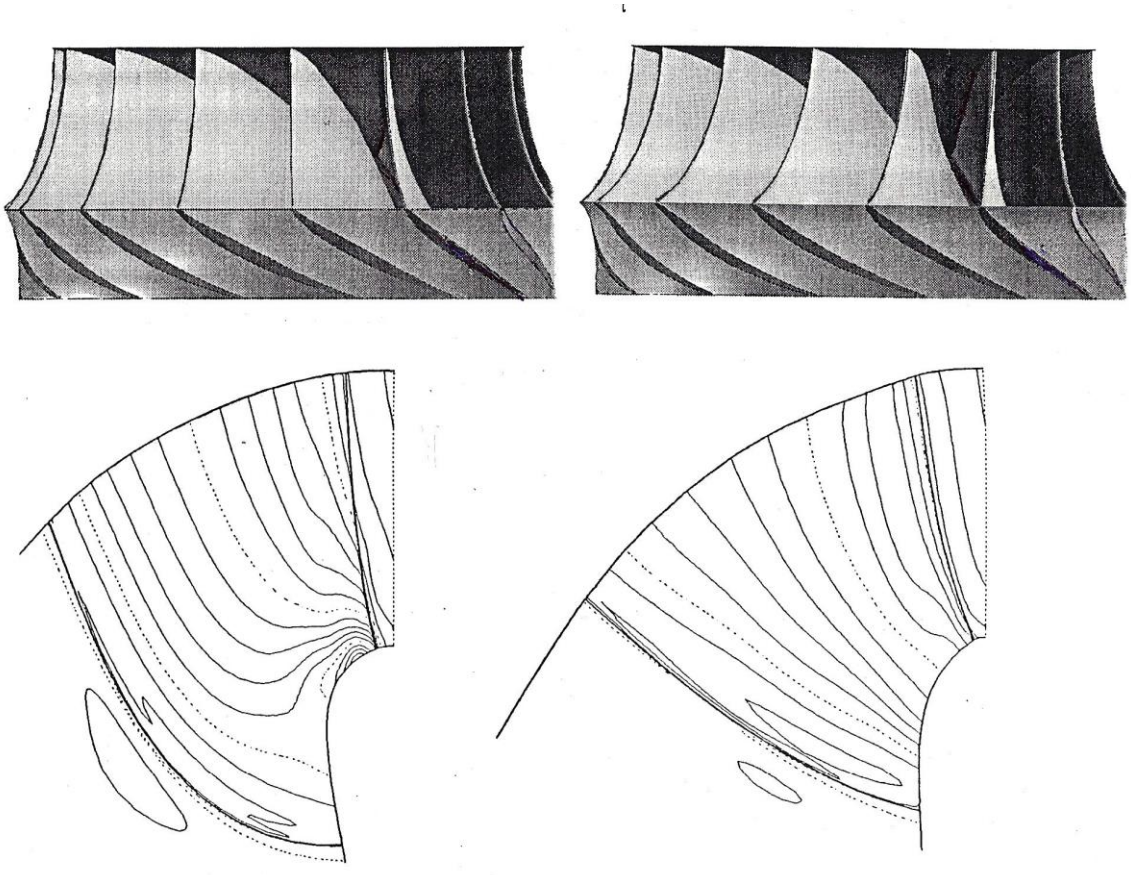

Fig. 10.5c Computed isobars for a modern X blade runner with balanced blade lean angles (right) compared with traditional well designed runner (left)

In fig. 10.5c an illustration is given of the computed isobars on suction side of the runner blades with balanced blade lean angles (right) compared with a traditional runner (left). A three dimensional picture of the two runners is shown at the top of the figure illustrating the so called X blade shape. A so called X blade runner with fully balanced blade lean angles from inlet to outlet combined with skewed blade outlets was for the first time designed and tested in Norway during a collaboration between the author and Kværner Energy in 1995-1996 for the Three Gorges project.

Examples of increasing the outlet cavitation performance by decreasing the blade outlet angles

As mentioned earlier in this chapter the cavitation performance will be improved by increasing the outlet diameter of the runner and increase the blade outlet angles of Francis turbines. Definition of blade angle is shown in Fig. 10.4 and Fig. 8.13

The disadvantage for an increased outlet diameter is that this often leads to deceleration of the meridional flow velocity through the runner and problems with off design operation may occur.

However, the danger of outlet cavitation will decrease with increased outlet diameter.

As an example the value of NPSH of a runner with outlet flow angle of β_2=180-17=163° and an alternative with β_2=180-13=167° and increased outlet diameter is shown for comparison. The value of NPSH may be calculated as a function of c_{m2} and u_2 depending on the curvature and number of blades at the outlet. A formula taking into consideration both c_{u2} and u_2 is shown in chapter 9 eq. (9.6) and chapter 5.3
eq. (5.19).

This formula may be written as follows:

$$NPSH_R = a\, c_{m2}^2/(2g) + b\ \ u_2^2/(2g) \qquad (10.16)$$

Here a and b are constants found empirically by model tests with range of values given in chapter 9 eq. (9.6). The constants a and b are depending on the runner design and will be different for different manufactorers and with change in design by the same manufacturer.

By using a formula as shown in eq (10.16) the following result has been calculated as an example.

Technical data of turbine				
Rated output		P = 143 MW		
Net head		H = 230 m		
Assumed full load efficiency		η = 0.93 (conservative)		
Speed		n = 300 RPM		
Outlet flow angle		alternatives	163°	167° [i.e. (u,_-β_2) 17°-13°]
Calculated NPSH		(m WC)	15.8	13.0
Outlet diameter D_2	(m)	2.470	2.710	

This brief calculation shows that the Nominal Positive Suction Head ($NPSH_R$) has a difference of 2.80 m by changing the blade outlet angle by 4° and increasing the diameter by 9.7%. (The given values may be a bit extreme, but illustrates the influence of D_2 and β_2).
In this case the inlet angles of the runner must also be adjusted as shown earlier in chapter 8.5, eq. 8.66, in order to optimize the efficiency in the best possible way.

However, it should be emphasized that for the smallest outlet angles the cavitation bubble collapse may occur behind the blades outlet while the larger outlet angles often lead to cavitation closer to the blades or on the blades if care is not taken due to increased relative velocity and less overlapping of the blade outlets and possible small waviness on the surface. (Note definition of outlet angles (see fig. 10.2))

It should be noted that if reversed flow or separation with strong vortices are formed, cavitation may occur also in the higher pressure region. Also the earlier described pressure pulsations caused by the wakes behind the guide vanes may lead to cavitation caused by the minimum values of the pressure waves and vortices travelling through the runner. A thorough study of the guide vane flow is described in [Ref 2].

The micro bubble collapse caused by the travelling high pressure wave following after the low pressure wave may also lead to severe damage especially if the collapse occurs in the high specific energy region of the runner. (The cavitation damage will be proportional to the velocity in a power higher than 3 which means that high energy cavitation is very dangerous).

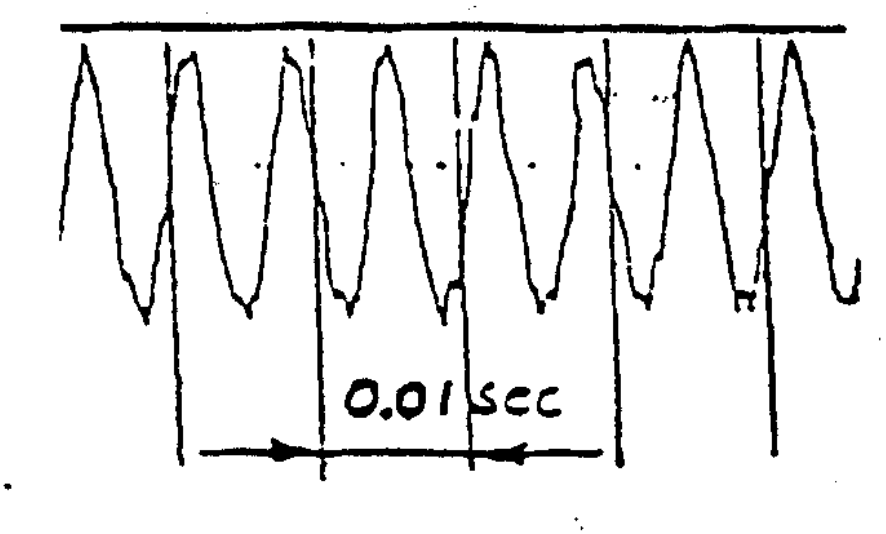

Fig. 10.6 Typical measured mechanical stress amplitudes of a blade outlet indicating pressure pulsations in a high head Francis turbine with speed 375 RPM and 24 guide vanes.

In fig.10.6 measurement of stress amplitudes caused by pressure shocks from the guide vane wakes on the outlet of a high head Francis runner is shown. The stress amplitudes indicate pressure amplitudes of the same magnitude as the hydraulic mean pressure.

Because of this it is important to establish a uniform flow with a balanced uniform pressure based on the steady state flow analyses over a widest possible range of operation for the turbine.

The introduction of splitter blades

In order to reduce the danger of destructive cavitation pitting on the blades in the outlet region the blade should be reduced. Then the blade loading must be increased in the inlet region.

However, for a traditional low specific speed runner without splitter blades the blade curvature at the inlet must be limited in order to avoid cavitation and reversed flow and separation at part load. Non uniform flow towards the outlet in general may be the result of incorrect blade loading at the inlet. This may cause vibrations and cavitation.
Because non uniform flow often leads to severe cavitation damage at off design operation, an improved design with splitter blades was introduced in Norway as early as before World War II. This design has been improved and has shown excellent performance both for cavitation and also for minimizing sand erosion. (Even in cases of severe damage of the guide vanes and facing plates, and labyrinths seals by sand erosion, only negligible repair of the runner has been necessary where splitter blades have been used).
The reason for this may be explained as follows:

1. Very uniform flow with low specific blade loading and no reversed flow in the inlet region over a wide range of operation.
2. Uniform flow combined with a reduced number of blades towards the outlet where the highest relative velocities occur.

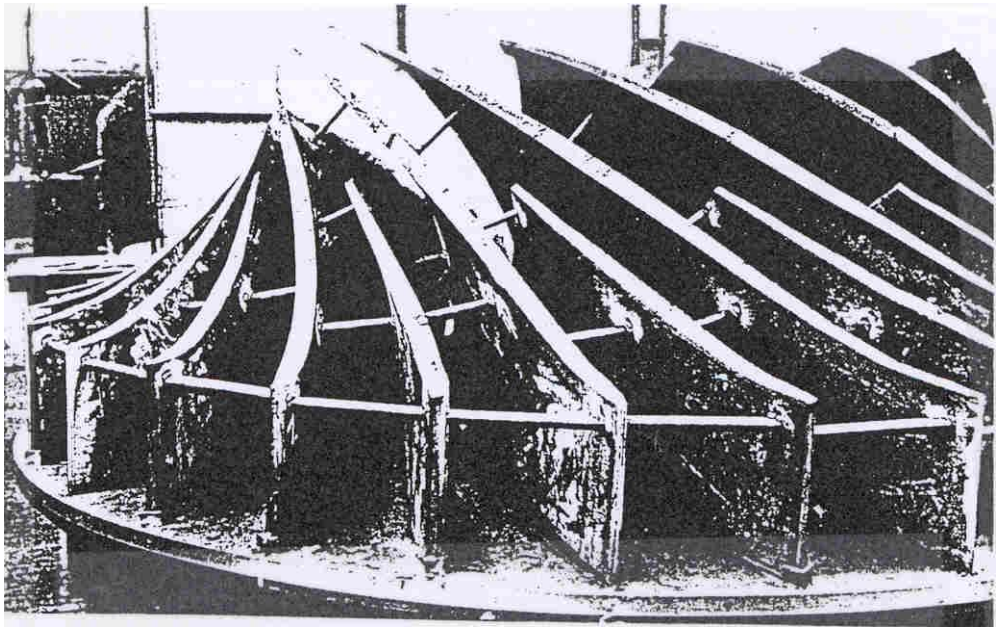

Fig. 10.7 A splitter blade runner in fabrication. (Courtesy Kværner)

In fig. 7.7 is shown a high head runner with splitter blades during fabrication in work shop of KVÆRNER Norway.

10.5 Conclusion of the influence of design parameters on Cavitation performance

In this chapter concluding remarks of main chapter 10 and in particular subchapters 10.3 and 10.4 which deals with a discussion of design parameters in order to avoid or decrease cavitation in Francis turbine runners.

The examples in chapter 10, only gives a brief guide line of a possible strategy for design. However, cavitation is a very complex phenomena often combined with sand erosion. Sand laden water forms waviness on the surface and the water may contain a high number of nuclei in such water quality because of the high number of particles. This leads to the need for a thorough study from the influence of the quality of the water on cavitation. The scale effect of cavitation from model test to prototype should include the influence from the nuclei content and air content in the water, but the scale effect is very complex and an IEC norm does not exist.

Therefore it is advisable for the reader to study a paper presented by prof. Henry and his colleagues form Switzerland in the IAHR Symposium Belgrade 1990. Ref. [3]

(The author wants to thank his former employer KVÆRNER ENERGY AS for allowing to publish the runner design with splitter blades which has been used so successfully by this company since before World War II for high head Francis runners. The first runner with splitter blades was installed in a Francis turbine for the Norwegian power plant Nygaardsanlegget. This turbine was put in operation in 1932 and had an output of 8456 KW operating at a net head of 225m with a speed of 750 RPM)

11. CHOICE OF MATERIALS, TESTING AND INSPECTION.

11.1. The choice of materials for different applications in turbine design.

The choice of materials for machine design is generally based upon criteria and requirements.

For hydraulic machinery such requirements and criteria may be as listed in the following table:

REQUIREMENTS TO BE FULFILLED	**CRITERIA FOR THE CHOICE OF MATERIALS**
1. OPERATIONAL CONDITION:	STATICAL LOAD, DYNAMICAL LOAD, TEMPERATURE, CORROSION, ABRASIVE WEAR ETC.
2. OPERATIONAL REQUIREMENTS:	RELIABILITY, AVAILABILITY (REPAIR TIME AND COST), LIFE TIME
3. PRODUCTION POSSIBILITY:	WELDABILITY, ACCESS POSSIBILITY, MACHINING POSSIBILITY
4. PRICE AND DELIVERY TIME:	MATERIAL COST / LABOUR COST (INTEREST) DIFFERENT QUALITY, DIFFERENT DELIVERY TIME

During the development of water turbines the material development has allowed for higher stresses, improved cavitation resistance and fatigue resistance for the most important rotating parts and parts exposed to high flow velocity. The improved material qualities have allowed for higher specific speed and increased size turbines with less weight per MW.

Sixty years ago cast iron was commonly used in water turbines. Later the cast iron was replaced by cast steel and riveted plates due to higher strength and toughness. Impact test was introduced as a requirement.

The cast steel has gradually been replaced by fabricated steel plate structures during the last 40 years when the weldability of plates improved and the fine grain steel quality was developed.

FRANCIS TURBINES

In fig. 4.4 chapter 4.2, a sectional view of a modern Francis turbine is shown and in fig. 6.7, chapter 6.3, 3 dimensional view of a Francis turbine with casted main parts is shown.

The pressurised static parts of a Francis turbine may be divided in the stress carrying parts consisting of the spiral casing, covers on the pressure side and the draft tube on the suction side.

Then moveable parts are the control parts represented by the guide vane system, and finally the rotating parts consisting of the shaft with the rotating oil reservoir and the runner with

labyrinth seal system against head and bottom covers. The guide bearing and the regulating ring and leverages represent the parts, which are not in contact with water.

For high head turbines the stress carrying parts are made of fine grain high tensile strength carbon steel (micro alloy steel)* in order to increase the stresses without increased danger of fracture. The maximum stress and number of cycles of pressurising will be the base for the dimensioning criteria for these parts. In order to allow for acceptable material and weld defects within realistic values for production, materials with yield point or $\sigma_{0.2}$ above 460 MPa is not recommended. (This will be explained later.)

The head and bottom covers are dimensioned for minimum deflections in order to minimise the clearance between the guide vane facings and the covers. The covers and the draft tube cone are made of low tensile stress fine grain steel with low carbon content in order to obtain a "problem free" welding.

Examples of choice of materials for a Norwegian built high Francis turbine:

The guide vanes and the runner with the rotating labyrinth seal rings exposed to high flow velocities with danger of cavitation or turbulence corrosion are made of stainless steel 13% Cr 4% Ni and 16% Cr 5% Ni respectively. The 16% Cr 5% Ni is normally used in fabricated high head runners due to good weldability without preheating. The upper part of the draft tube cone is also made of stainless steel 16% Cr 5% Ni in order to avoid corrosion and cavitation. The facing of the covers against the guide vane end faces are normally cladded by welded stainless steel of 16% Cr 5% Ni with a hardness of about 300 HB or 17% Cr 1% Ni with 350-400 HB. This is made so in order to obtain a difference in hardness between the guide vanes and the facing of the covers of 70 HB which in turn prevents galling of the surface when the guide vanes are moved.

The static labyrinth seals are made of Ni-Al bronze, which is different from the hardness of the rotating stainless steel ring surface in the 16% Cr 5% Ni material. The Ni-Al bronze has also a good resistance against turbulence erosion, cavitation and corrosion.

PELTON TURBINES

In fig. 4.2 chapter 4.2 is shown a vertical 5 jet vertical Pelton turbine under erection at site (see also fig. 6.2, chapter 6.2). The stress carrying parts, formed by the manifold for this type of turbines, may be exposed to pressure up to 2000 m. and fine grain high tensile strength steel plates are always used in the stress carrying fabricated parts in order to reduce the plate thickness.

In this case it should also be emphasised that the maximum Von Mieses stresses are limited to about 200 MPa and then $\sigma_{0.2}$ may be limited to 460 MPa with a safety to $\sigma_{0.2}$ of 2.5 for the nominal stress. The stress limitation is established in order to avoid unstable fracture before a growing crack by cyclic pressurising during stopping and starting has penetrated the plate and

*There are three basic qualities of fine grain steel. (1)Micro alloy steel where the chemical composition alone leads to the fine grain quality. (2) Quenched and Tempered (QT) steel where the heat treatment leads to a fine grain quality with less micro alloy additives.(3) Thermic Mechanic Controlled Process (TMCP) where a temperature controlled rolling during the cooling process is made in order to obtain a fine grain quality.

caused leakage. The reason for this is that a leakage will always be detected. This design criterion is denoted LEAKAGE BEFORE RUPTURE. (Also the allowable size of acceptable defects (that must be big enough to be detected in welds in a new turbine) puts a limit to the maximum stress in order to avoid dangerous fatigue propagation towards critical size during a lifetime of 50 years. This will be explained later.)

The turbine housing serves as a formwork for embedding the turbine in concrete and the steel lining of the wheel pit is formed as a rigid structure designed to withstand buckling during embedding.

The material used in the turbine housing is low carbon mild steel of fine grain quality to allow for welding at site without heat treatment because rigidity and not maximum stress will be the dimensioning criteria here.

The inlet pipes of the injectors are made of fine grain cast steel of medium strength because both rigidity and stress will be the design criteria in this case. (See fig. 6.6, chapter 6.2)

The parts exposed to high flow velocity such as needle tips and nozzles are made of hardened stainless steel of 13% Cr 4% Ni or 16% Cr 5% Ni steel. If severe sand erosion is expected a ceramic coating on the needle tip and the nozzle ring has been used successfully. However, this coating must be made in workshop with a special equipment and the needle tips and nozzles must be shipped to the work shop for repair in cases of severe sand erosion.

In the needle servomotor system stainless steel and hard chromium surface should be recommended for the needle stems and surfaces exposed to sliding seal rings against water pressure. (Hard chromium surfaces contain often micro cracks and corrosion problems may occur if the base material is not stainless. Therefore all surface coating with chromium should have stainless steel base materials).

The Pelton runner is today normally made of integrally cast 13% Cr 4% Ni steel. For high cycle fatigue reason heat treatment aiming for a lower $\sigma_{0.2}$ value should be recommended even if a harder surface has better resistance against sand erosion. [Ceramic coating of Pelton runners is under development, but so far a 100% successful process is not found].

Also welded Pelton runners have been made by using a forged disk and building the buckets by welded parts or building the buckets by a so called micro cast procedure on a forged disk with pre-machined buckets roots. (Ref. SULZER ENERGY).

For the base material it is important to keep the quantity of sulphur (S_2) and nitrogen (N_2) to a lowest possible value in order to minimise micro defects in the materials. (If possible $S_2 <$ 0.008% and $N_2 < 0.02\%$). The most dangerous defects are the flaws of MnS which may be reduced if the content of S_2 is very low.

11.2. Material development and weldability.

Before 1965 the high head Francis turbines were made mainly from cast steel. However, the cost of production of steel plates was reduced and fabrication of welded structure became more efficient compared with the more laborious casting procedure in foundries.

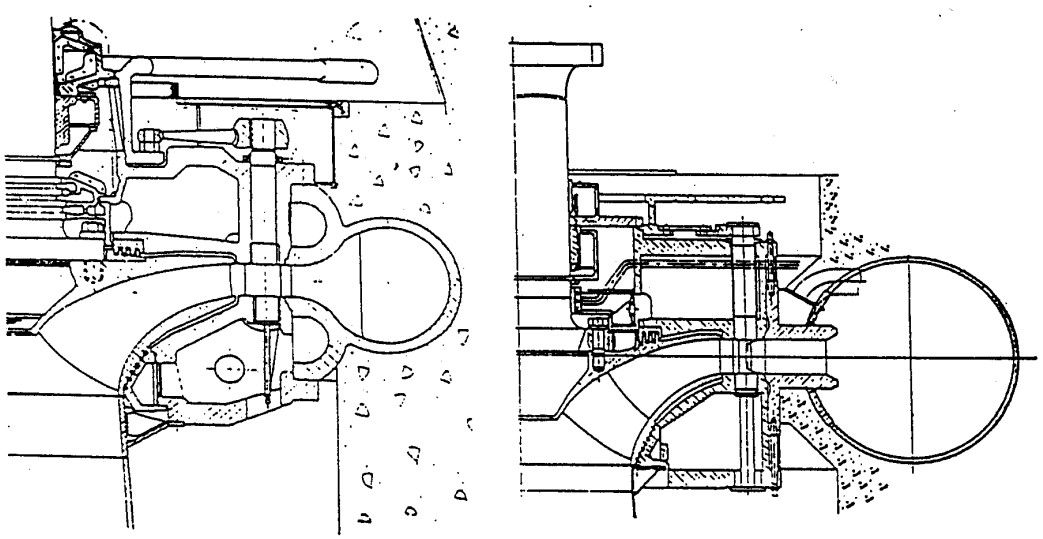

Fig. 11.1 A cast steel 1955 design compared with a fabricated 1992 design of a Francis turbine

In fig.11.1 a cast steel high head Francis turbine produced between 1950 and 1960 is compared with a welded modern Francis turbine produced in 1990-1992.

The presented content in this part deals with the most commonly used materials for turbines at present time. In the future other new materials and composites may be available based on new knowledge on fracture mechanics, corrosion and theory about cavitation.
New joining methods such as diffusion-.narrow gap and electric beam welding may change the design in a way similar to the change from the cast steel design which was replaced by the welded plate designe.
For the designing ingeneer it is important to adjust the design in accordance to available materials and welding methods.

The main development has mainly taken place the last 100 years.

During the last years development of new materials imprived the reciatance against cavitation and an increase in ductility. A higher stress level can be tolerated in pressure loaded parts due to improved fracture mechanic properties.
For materials used in rotating parts and pressure loaded parts exposed to high frequency stress variations the stress level must be reduced due to fatigue.
About 85 years ago cast iron was normally used. Later after the Second World War cast iron was substituted by cast steel and riveted plate structures.
Brittleness tested by impact tests was introduced and required for the choice of materials in Norway before World War 2. This requirement was earlier than in other countries in Europe.
Cast steel has gradually been graduallt been substituted by welded structures of steel plate structures mainly because a lower price increase of plates compared with the cost of labour.

The development is illustrated in fig. 11.2 showing the weight reduction per MW of spiral casings for high head Francis turbines produced from 1955 to 1990. The weight reduction is caused by increased stresses in the high tensile strength plate materials with increasing strength during the time period of 25 years.

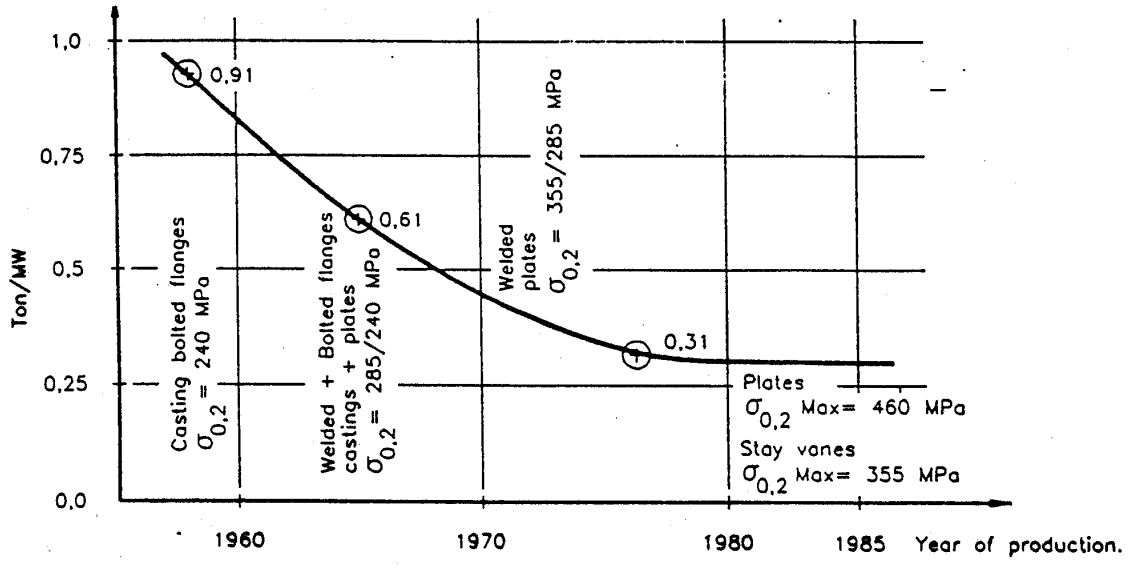

Fig. 11.2 Weight reduction of high head Francis turbine spiral casings

In addition to the development of materials a rationalization in mechanical welding process has been done. The new welding prcesses required less work houres, making the spiral casing cheaper. Further the higher ultimate stresses in plates leads to a lighter design as illustrated in Fig. 11.2.

The development of materials and design.

In 1945 the high head Francis turbines were mainly made by cast steel. By a comparison between the cost of materials and labour we will find that it was economical to use expansive materials in order to save labour cost.
Cast steel required a large amount of labour and at the same time the parts were produced in a low number. Production of steel plates required less labour and the improved welding technique has later reduced the the labour time in welding.
These factores has gradually transferred the turbine production towards a fully welded design. The evaluation is clearly illustrated in the weight reduction of spiral cases presented in fig.11.2.
In turbine and pump production is the plate thickness is an important parameter for carrying the hydraulic forces and the weight reduction of the plate design has pushed the production towards the light weight steel plate production.

The light weight plate design is based on fine grain steel plates which also can take care of forces in the thickness direction. At present time thicker plates which are also able to take care of forces in the thickness direction normallt defined as TTT plates i.e. Toughness Through Thickness Plates. (In some countries these plates are denoted as Z steel where Z defines the direction through the thickness of the plate)
The TTT quality has been obtained by getting a very low content of sulphure which is obtained by a ver low content of Suophure and by adding kalium in the melted steel which prevents layer of MnS in the plate during rolling.
Compared to bthe casted design the thickness and weight is reduced compared to the casted design.and further the design has an improved homogeneity.
For welding at site a low carbone content is required and in addition the content of V, Nb and S are reduced in order to avoid the so called Hydrogen brittleness.

In addition dried electrodes must be used as well as ciorrect preheating and correct temperature in the melted weld composite.

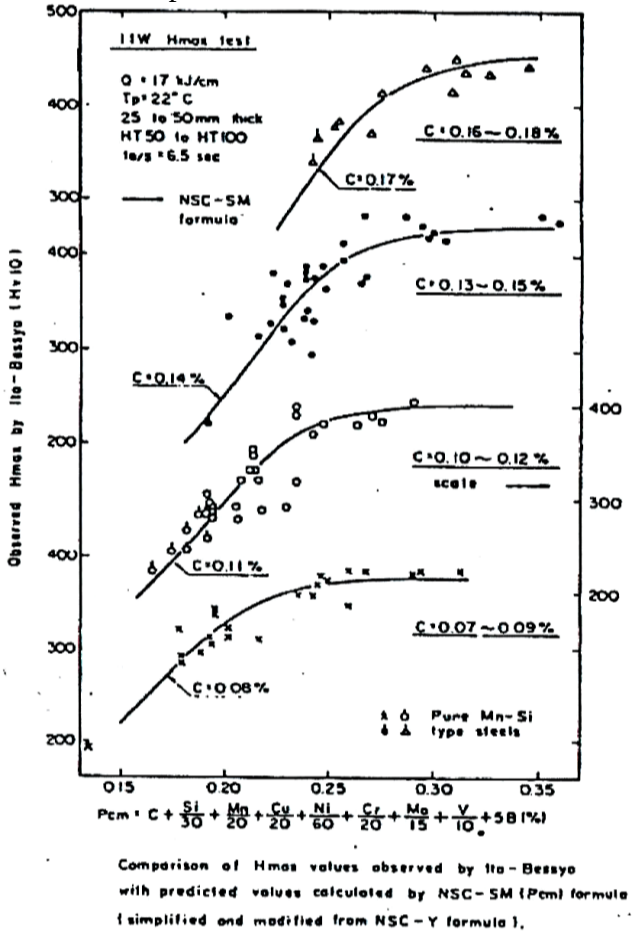

Fig. 11.3 H_{max} as function of P_{cm} observed by Ito-Bessyo

For welding at site a low carbone content is required and in addition the content of V, Nb and S are reduced in order to avoid the so called Hydrogen brittleness.
In addition dried electrodes must be used as well as ciorrect preheating and correct temperature in the melted weld composite.
It should also nbe noted that too high addition of elements for fine grain creation may lead to a narrow brittle zone near the melted zone in the HAZ in the weld.
It is important to be aware of these effect for field welding at site.
The spiral casings for low pressure Francis turbines are normally welded ay site.
Low carbone steel is used due to good weldability whichis normally tested in forhand for safety.
The required value of C and Mn for a bfield welding must fulfil the requirement
C + Mn/6< 0.35.
Finally it should be mentioned that the choise of welding spiral casings at site has lead to a simplified design of the stay ring without any increase in the flow losses.

Based on the development of high stress steel, large Pelton turbines for heads of 800m to 1300 m net head has been built and in Switzerland Pelton turbines for heads close to 2000 m net head has also been built.in one power plant.
By using the well known criterion “LEAKAGE BEFORE RUPTURE” the stress level up to 200 MPa have been used.for all material qualities used in spiral casings and distributors.

An other requirement is that the maximum stress must be limitted to **40%** of $\sigma_{0.2}$.
The conclusion is that safety against yielding in addition to the requirement from the fracture mechanic theory are valid for materials with $\sigma_{0.2} \leq 460$ **MPa** when the stresses have a maximum value of 40% of $\sigma_{0.2}$ or less.
The most important requirement however is to avoid weld defects and brittleness in the heat affected zone.
In order to fulfill this requirement following rule of the thumb may be used: C<0.12%, S<0.010% and V< 0.1. In addition the carbone equivalaent (CE) or tha value of Pcm as presented in the diagram in Fig.18.6.

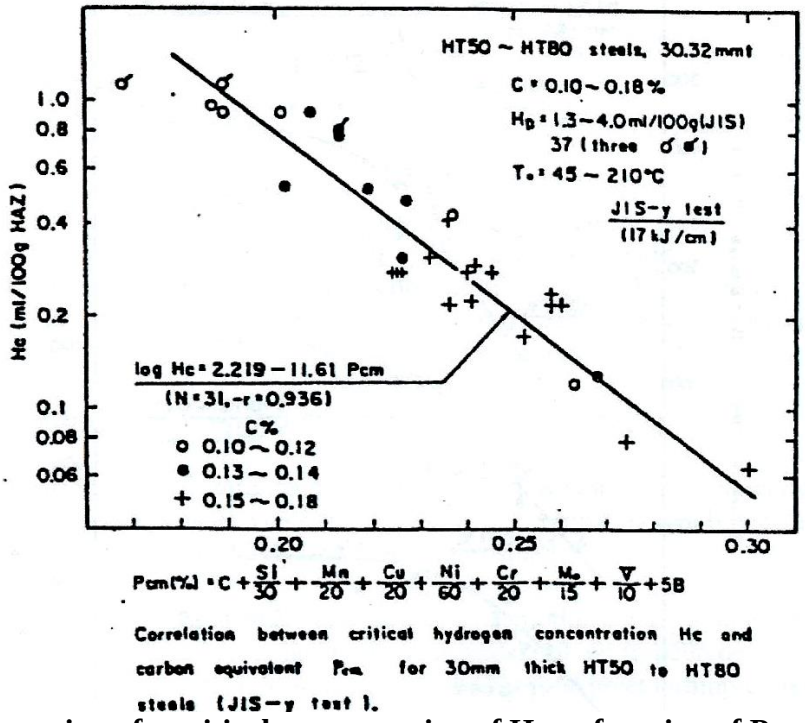

Correlation between critical hydrogen concentration Hc and carbon equivalent Pcm for 30mm thick HT50 to HT80 steels (JIS-y test).

Fig.11.4 A presentation of a critical concentration of Hc as function of Pcm set up according to a Japanese test.

In Japan some formulas for the carbone equivalnt CE and P_{cm} have been expressed as a function of P_{cm}. Both values have been presentated in the empirical diagram illustrated in fig 11.4 in order to find the hardness near the weld after welding with limitation of the content of hydrogen (H_c) in the weld. (See fig. 11.4)

It is important to keep both CE and P_{cm} as low as possible.

The chemical formula of $\mathbf{P_{cm}}$ in digram 11.4 yields:

$$\mathbf{P_{cm}} = C+Si/30 + Mn/20 + Cu/20+ Cr/20 +Ni/60+ M0/15 + V/10 + V/10+ 5B$$

And the formula of CE yields:

$$\mathbf{CE} = C+Mn/6 + Cu/15 + Ni/15 + Cr/5 + Mo/5 +V/5$$

Pcm is valid for C<0.18 in plate materialc before welding while **CE** is valid for **C > 0.18.**
See Maruyoskhi Suzuki.
In fig.(11.3) $\mathbf{H_{max}}$ is plotted against $\mathbf{P_{cm}}$ and in fig.(11.4) the critical value **Hc** is plotted against $\mathbf{P_{cm}}$.

High stress steel with yield point $\sigma_{0.2}$ =460 MPa or higher must normally be prZeheated around 60-80^0 **C**. in order to avoid diffusion of H_2.
Structural parts with large ticknesses must be stress relived at 570-580 ^{0}**C**.wz<<<<<<<
.Special cases be made without post heating if the thickness is below around 40mm.

In a welded stay ring forces from the stay vanes are transferred through the thickness of the stay ring plates. A special fine grain steel with guaranteed Toughness Through the Thickness and good weldability must be used in these plates (TTT steel). (The Toughness Through Thickness is obtained by a low content of sulphur (S_2) and calcium treatment of the liquefied steel which prevents forming of laminated manganize-sulphides in the plates).

The reduced thickness in a shell made of high tensile strength plates compared with a cast design should be noted as illustrated in fig. 11.2.

In some cases parts of the shell may be welded at site in order to transport the stay ring with the main part of the plated shell in one piece and save the cost of expansive flange connection. Highly weldable high tensile steel with $\sigma_{0.2}$ = 460 MPa and low carbon content allowing for welding without heat treatment of thickness up to 50 mm, has been used for such parts welded at site. It is for such steel important to keep the carbon content on a lowest possible value and limit V and Nb and S_2 low. In addition very dry electrodes and preheating to 80□C is recommended in order to prevent hydrogen induced cracking.

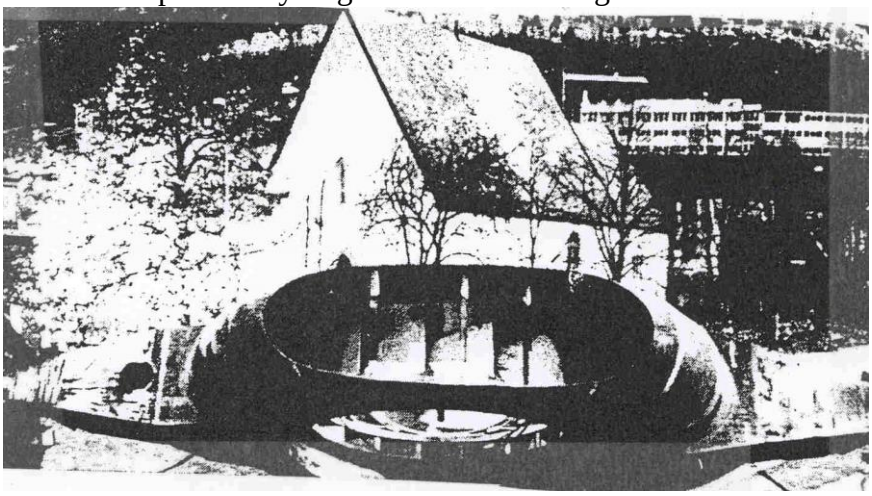

Fig. 11.5 Transport of spiral casing with a one piece stay ring. Note the thin plate transport structure, which will be removed from the spiral casing shelf.

In fig. 11.5 a photo of the transport of a spiral casing on which the thinnest part of the shell will be welded at site without stress relieving by heat treatment.

The shell on the spiral casing of low head Francis turbines are normally completely welded at site of low carbon steel with weldability proven by implant tests. (Requirement: $C+M_n/6 < 0.35$ for material quality with $\sigma_{0.2}$ = 355 MPa)

For large vertical Pelton turbines the development of high tensile steel has allowed for increasing size of turbines for high heads in range of (800-2000 m). Based upon fracture mechanics it is important to design a turbine in order to fulfil the requirement that unstable fracture from a growing crack shall not occur until the crack has penetrated the plate i.e. LEAKAGE BEFORE RUPTURE.

The reason for this is that a crack through the thickness will be easy to detect by the leakage and unstable rupture will be prevented. This requirement will limit the maximum size of the turbine depending on the development of materials with increased toughness i.e. improved Crack Tip Opening Displacement (CTOD) values.

As described in the following the maximum principal stress must be limited to about 200 MPa (N/mm^2) for any material quality developed to day around 2010.

Another requirement is that the safety against yielding will be a nominal maximum "Von Mieses" stress of 40% of $\sigma_{0,2}$.

A conclusion to be drawn from this is that materials of quality $\sigma_{0,2}$ = 460 MPa may be utilised with the required safety against yielding and at the same time fulfilling the requirement "LEAKAGE BEFORE RUPTURE" based upon fracture mechanics. Note: (Materials with higher strength will not give higher safety against unstable fracture unless the CTOD value is increased and such material will normally be more difficult to weld and the danger of brittle heat affected zone HAZ close to the weld is high).

The most important requirement for the production of turbine parts is the weldability in order to avoid defects and brittleness in the heat affected zones of the material. In order to fulfil this requirement limitation in the chemical composition is made. We may put up the following requirement weldability of carbon steel:

$C < 0,13 \quad S < 0.010\% \quad V < 0,09\%$

In addition a carbon equivalent is also containing other components of the chemical elements, but the total weighted sum of the composition must not exceed a given maximum value. By using Quenced and Tempered (QT) or Thermo Mechanical Control Process (TMP) steel quality the chemical requirement is easy to fulfil, but for such materiel the requirement of a good welding procedure is important.

An example of a recommended formula for the carbon equivalent for a micro alloy steel plate with $\sigma_{0,2} \leq 460$ MPa is the P_{cm} together with the absolute content of C. From the value of P_{cm} and C it is possible to calculate the hardness in the HAZ and the limit of H_2 content in the weld where brittleness and hydrogen induced cracking may occur.

It is always important to keep the P_{cm} value as low as possible. The formula for the P_{cm} is very well known in the literature to day. (Ref. paper: CARBON EQUIVALENT AND MAXIMUM HARDNESS, by Maruyoshi Suzuki, IIW Doc IX-1279-83). [Ref. 20]

The formula for P_{cm} yields:

$$P_{cm} = C + Si/30+(Mn+Cu+Cr)/20+Ni/60+Mo/15+V/10+5B$$

P_{cm} is valid for steel with $C < 0,18\%$

High tensile strength steel of quality 460 MPa or higher must normally be welded under slight preheating 60-80 ºC to prevent hydrogen diffusion. Structures with large thickness must be stress relieved at 570-580 ºC. Welding without stress relieving may be done in special cases with thickness less than 50 mm.

In fig. 6.6b chapter 6.2, a site welded manifold for a Pelton turbine is shown before embedment in concrete

11.3 Welding defects, acceptance criteria based on fracture mechanics

Defects will always occur in a weld. Cracks and lack of fusion are the most serious defects because they are two-dimensional and normally they are not detected by X ray examination.

Three-dimensional defects such as slag and gas blows are not so dangerous except if sharp edges of slag are connected to a lack of fusion or a crack. Gas blow pinholes may also indicate hydrogen, which is very dangerous due to micro cracks. (Dry electrodes and preheating should prevent hydrogen problems and porosity of this kind).

Suitable tests for weldability of electrodes and materials will be "TEKEN TEST" and/or "IMPLANT TEST". The last one is a special test for finding the hydrogen cracking in the heat affected zone (HAZ) in the base material, while the first test is a general test of hardening and hydrogen including both weld material and heat effected zone in base material (see fig. 11.4).
As there always will be a number of defects in a weld, it is important to establish acceptance criteria for the sizes of different the defects which will not be dangerous for the operation during the calculated life time of the turbine with a welded structure.
The most dangerous defect is a propagating crack with a very sharp edge denoted as a two dimensional defect or a flaw.

Crack propagation.
As described above defects always occur in a weld or in the base materials. It is therefore important to define the acceptance criteria for defects, which will not grow and lead to a total rupture under the operational condition of the regarded structure.

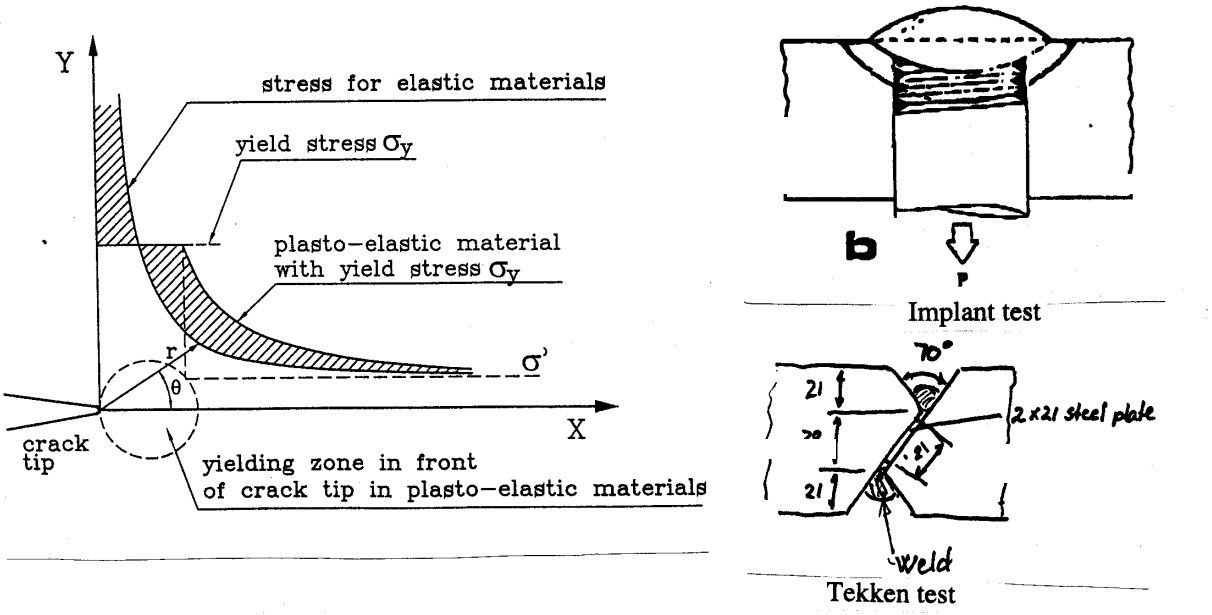

Fig. 11.4 Energy concentration in front of a crack tip and illustration of a "TEKEN TEST" and an "IMPLANT TEST". Note the stress peak of a crack for elastic materials before yielding denoted as the stress for elastic materials in the figure = $\sigma=K/\sqrt{(2\pi r)}$ (K = stress intensity factor and
r = distance to crack tip). Note: Y = direction of the stress = σ_Y and X = distance from the crack tip.)

By means of this theory we will find that the stress at the crack tip will reach an infinite value which indicates that the crack should propagate even for low average stress values = σ in the material surrounding the crack for any small crack with depth = a in a complete elastic material with no ductility.
There will always be weld defects where cracks like inclusions of slag and lack of fusion..
Among these defects lack of fusion is the most serious and common defects.

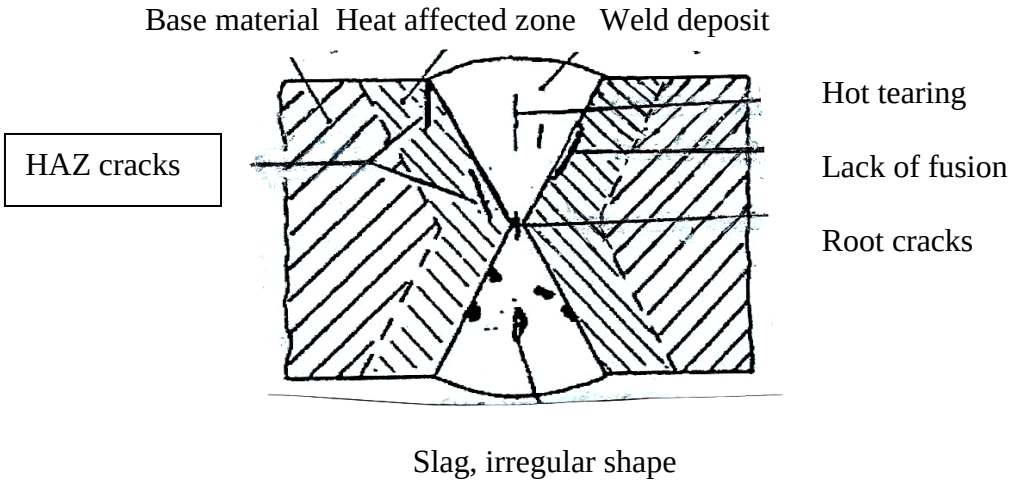

Fig. 11.7 Illustration of different kinds of weld defects.

Three dimensional defects such as slag inclusion is less serious than cracks and lack of fusion unless the edges are sharp that may lead to crack propagation.
Voids caused by gass may be an indication of hydrogen H_2 which is extremely dangerous in connection to micro cracks. (This problem is reduced if dried electrodes and preheating have been used)
As a conclusion we find the most critical defect as an increasing defect with sharp edge i.e. a two dimensional defect.
In fig.11.6 the different types of weld defects are illustrated

Further a description of the definitions of stress concentration in front if a crack is illustrated in fig.11.6.
The use of tests of weldability of different materials are found in the CTOC (Crack Tip Opening Displacement) testing.
The testing of the weldability have as described been TEKEN and/or IMPLANT testing. The test is also made for finding possible cracks caused by H_2 and hardness (Hb) in both welds and basic plate material.
Since we allways have defects in a weld we must have a proper methode to set the standard for welding procedures. Examples of such testings are also given in the pamphlets from International Institute of Welding IIW.

Crack growth based on Fracture Mechanic Theory.

The accept criterion is bases on the present stress = σ and the material defect and the stress intensy factor = K in a in an elastic material as shown earlier. (r = distance to crack tip.) See Fig 11.6.

$\sigma = K/(\sqrt{2\pi}\, r)$

From this equation we find that the sress σ will increase to an infinite value if r is approaching zero. I.e. a crack will increase even for low avrage stress in the material around the weld. However, the assuption of a complete elasic materal is not correct and the material will get a plastic deformation where the stresses exceed the yield point. In fig.11.6 this phenomena is clearly illustrated where $\boldsymbol{\sigma_y}$ is the yield point of the material in question. Even if the value of **r** is decreasing the maximum modified stress will be limitted if the value of $\boldsymbol{\sigma_0} > \boldsymbol{\sigma_y}$ i.e. as long as we have yield stress.
However, if the stress is below $\boldsymbol{\sigma_0}$ the crack propagation will stop and we denotes this phenomena by noting that the material has a certain crack stopping effect.
This is because a crack will grow only if the loss of elasic energy is equal or larger than the energy needed to increase the area of the crack.
The critical elasic energy at the crack tip can be expressed by the stressintensity factor = **K**. If the middle stress in a regarded material without a crack = **σ.** The value of **K** will be defines as follows:

$$\mathbf{K} = \sigma\sqrt{\pi\, a.\, f(\Phi)} \qquad (11.4)$$

In this case an unstable crack growth will only happen if **K** is large enough or equal to $\mathbf{K_C}$ or $\mathbf{K_{IC}}$ for a thick cross section. Here the values $\mathbf{K_C}$ and $\mathbf{K_{IC}}$ are emphirical material constants defined by tests of the material qualities or welds in question.
This phenomena can be compared by punctuation of a rubber balloon compared to a plast balloon. Unstable crack growth is a crack which is penetrating the material with the speed of sound.
A certain plasticity is required in stress loaded parts. Even in the plast balloon the propagation will take place if the elasic energy is exceeding a certain value for creating a new fractured surface.
This theory must be transferred to spiral casings and distributors for turbines.
The possibility of safety can be analysed by evaluation of the given K value or by making a COD or a CTOD test. (COD = Crack Opening Displacement and CTOD = Crack Tip Opening Displacement)
Another very good rule is as follows:
A CRACK MUST NOT LEAD TO AN UNSTABLE CRACK PROPAGATION OR RUPTURE BEFORE THE CRAC IS BIG ENOUGH TO PANATRATE THE PLATES SO THE GROWING CRACK CAM BE DETECTED BY **LEAKAGE BEFORE RUPTURE.**
Tis may be a problem for very large turbines.

Crack growth of a statically stopped crack exposed to dynamic pressur load cycles.

It is possible to measure any crack growth between a relatively large number of load cycles as illustrated in fig.11.6.
In fig.11.6 is shown how an ultimate fracture may occure as a function nof a certain number of cycles N with a stress amplitude $\Delta\boldsymbol{\sigma}$ in a **S-N** diagram for a constant depth = **a** and length = **2C** of a crack.
In this case **R** is given as the ratio between minimum stress $\boldsymbol{\sigma_{min}}$ and maksimumk stress $\boldsymbol{\sigma_{max}}$ where $\mathbf{R}=\boldsymbol{\sigma_{min}}/\boldsymbol{\sigma_{max}}$ based on such measurements, a Paris diagram can be made showing the crack growth ΔK as shown in later in fig. 11.5.

Note that the crack growth is a function of ΔK where $\Delta K = \Delta\sigma\sqrt{a\pi\Phi}$ as shown in fig.18.11.

In this case $\Delta\sigma$ is calculated from $\Delta\sigma = (\sigma_{max} - \sigma_{min})$ and not from $\mathbf{K_{max}}$..which is valid in region II in a Paris diagram as shown in fig 11.8.

In the litterature many books are printed describing fracture mechanic. Some of these books should be recommended such as Almar Næss (METALLISKE MATERIALER (TAPIR 1981) and other more modern books and articles adited by International Institute of Welding.
The theort presented in this chapter is also presented in the recommended litterature.
The basic theory is based on the fact that in front of a weld a stress peak will be formed in an elastic material. This stress peak is also denoted in fig. 11.6 in previous chapter and yields.

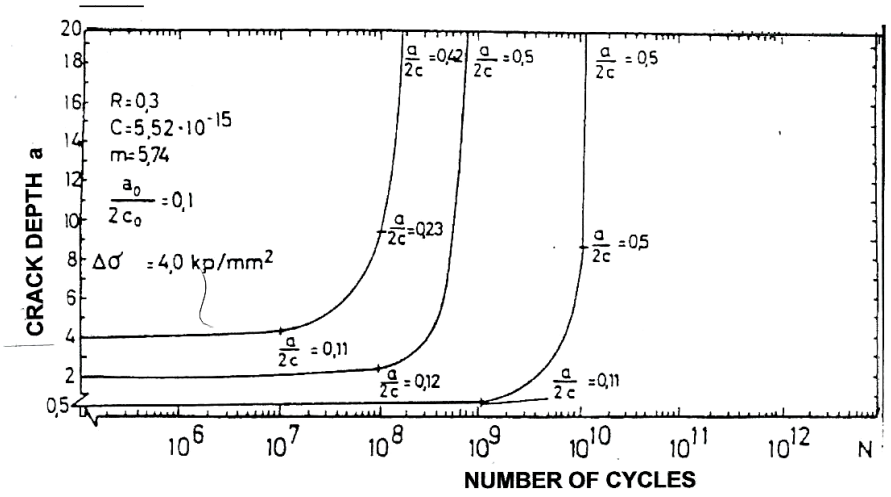

Fig.11.6 Material tests where the crack propagation is obtained by testing.

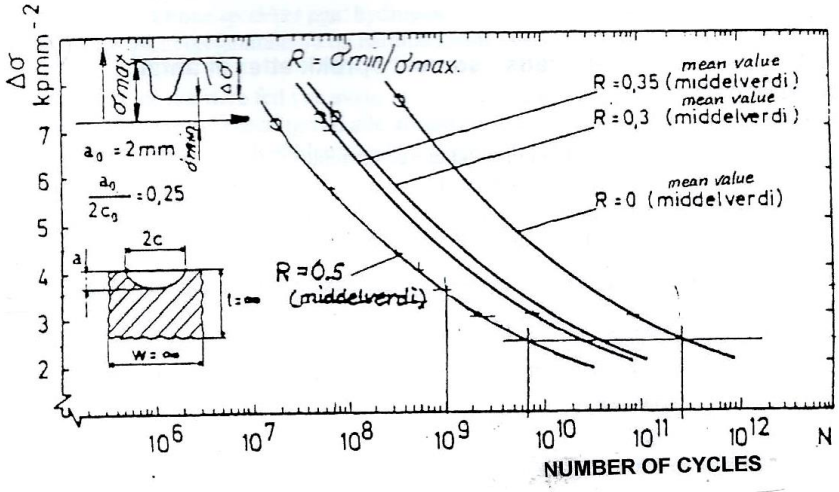

Fig.11.7 Fractures as function of number of loading cycles N and stress amplitudes $\Delta\sigma$.

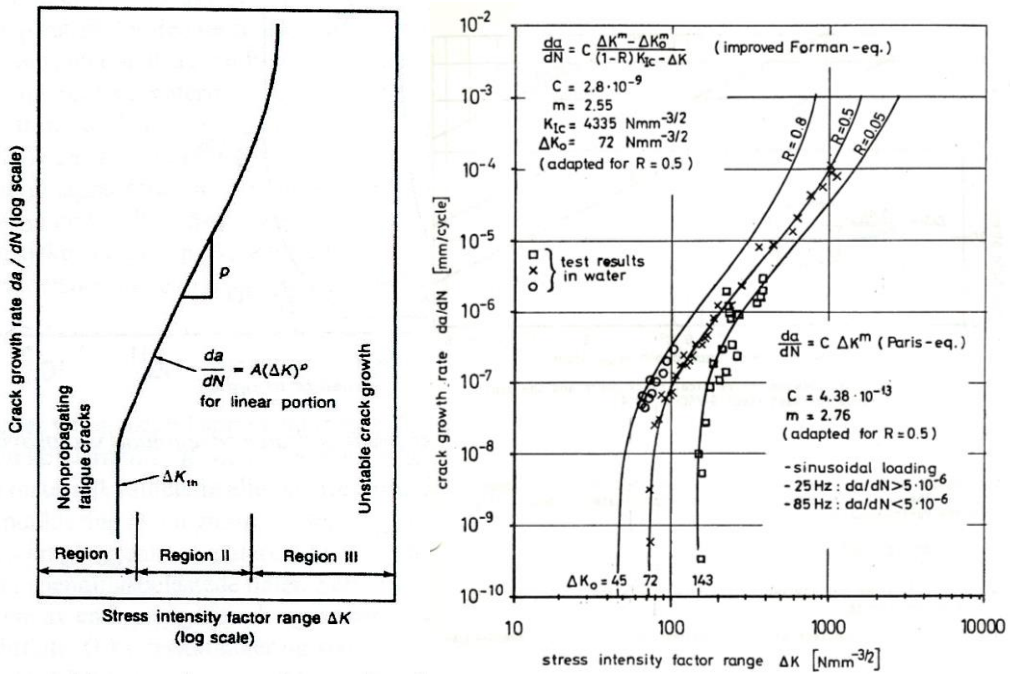

Fig. 11.8 Paris diagram in general version (left) and test results from SULZER by Dr. H. Grain (right). Note that R=$\sigma_{min}/\sigma_{max}$ = stress ratio in the diagram to the right.

In the presented diagrammes the constants C and m are depending on the material quality and can be found in diagrammes presented in Paris diagrammes presented by various authors.

For fatigue of materials we find a threshold value ΔK where no crack growth occures for Martenittic steel as shown in Fig.11.8.

It should be noted that the threshold value where no crack prpagation occures even for infinite number of cycles, is depending on the altitude of the stress amplitudes as shown in Fig 11.8 to the right.

According to experience a fine grain steel quality shows a high resistance against unstable fracture as shown in region III as shown in Fig 11.8 to the left.

However, the crack propagation both for fast stress variations and low frequency stress variations show equal values for low stress design steel and high density micro alloy steel.

It has also been proven that the trash hold value =ΔK_{th} seems to be higher for materials with lower values of $\sigma_{0.2}$ than for qualities with higher values of $\sigma_{0.2}$.

For rotating turbines and pumps the number of load cycles on the runner blades during a life time will be above $N = 10^{10}$ fast oscillating load cycles, while for low cycle cases the fatigue will problems will be in the range of $N < 5*10^4$ cycles.

For $N < 10^3$ the approval criterion regarding defects and stresses should be based on statical loading i.e the K_{IC} and **COD** values.

The reason for the given definition of safety may be based on following statement:

There is no significant difference in the crack propagation speed in high density strong martencitic materials and low stresss materials for oscillating loads in the range of frequencies $10^4 < N < 10^8$.

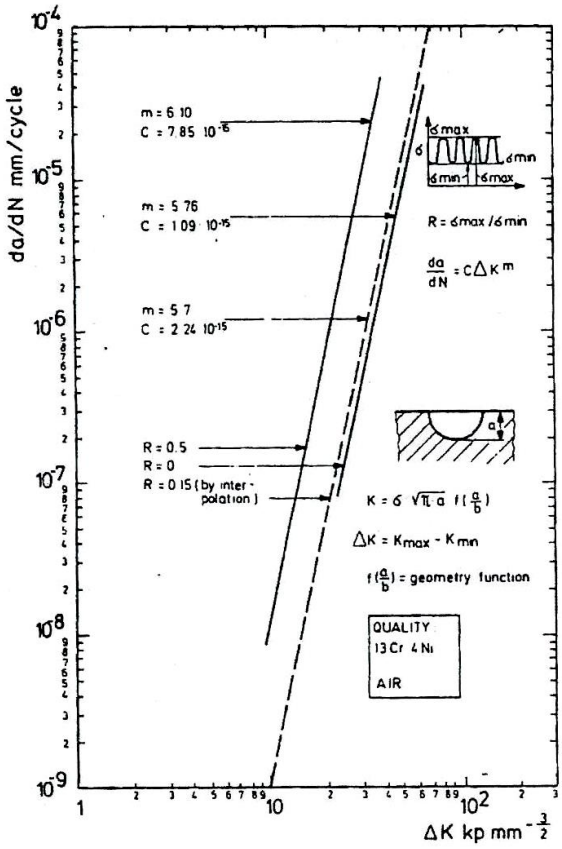

Fig. 11.9 Paris diagram for the steel quality 13Cr4Ni steel

For illustration the fatigue for the different materiales will occure for the number of cycles higher than 10^8 cycles. The fatigue tests of steel $10^4 < N < 10^8$ in the middle region expressed in the Paris diagram is available for illustration based on numerious tests and such results are presnted in the diagram in fig.11.8.

The same criterion for the sressintencity factor, K must be used in order to avoid crackpropagation for parts exposed to high cycle pressure or load changes.
I.e. the maximum level of stress msat not exceed 200 Mpa. The chosen level is referring to accepted defects in welds and is independent of a possible increase in the level of $\sigma_{0.2}$.
Because of this materials with $\sigma_{0.2} > 460$ M Pa are not recommended because of possibility to stop a growing crack before rupture.
For a practical study the publications of IIW (Inteernational Institute of Welding) is recommended.

18.2.2 **Kay words from production of turbines**.

The runner for a Francis tyrbine produced in Norway is made by runner blades cut from plates of 16Cr5Ni martensite – austenite quality.
The blades are then thinned towards the outlet to requested thickness and shped in a pressing machine to the required shape durig a temperature of 900-1000 ^{0}C . After this process the blades are welded to the hub and finally to the band which is normally splitted for access. High specific speed runners may have anotther welding procedure because of easier access for welding.
It should be noted that the design of KVAERNER now RAIN POWER has a double number of blades at the inlet because the use og splitter blades for low specifuc speed runners in order to obtain a smooth operation on the whole range of operation.
Due to the wakes downstream of the guide vanes and difference in velocity from suction side and pressure side pressure pulsations occures in the blade channels causein the sound of turbine you allways can hear in a power house.
The stress amplitudes will normally be around 40 Mpa or in turbines without problems. (Aklso values of stress ampli\tudes of 120 Mpa has been recorded at the blade outlet by strain gauge measurements in turbines with problems.)
The welding quality is in this case important, and a strict procedure for welding must be made. I modern production the runne may be produced excavated in 2 halves from machined the finished design of blades in order to get the weld notches away from the high stress region at band and hub.
At the time being all runners are made by so called stainless materiales such 13.4 CrNi steel or 16.5 CrNi steel as shown in Fig. 11.10.

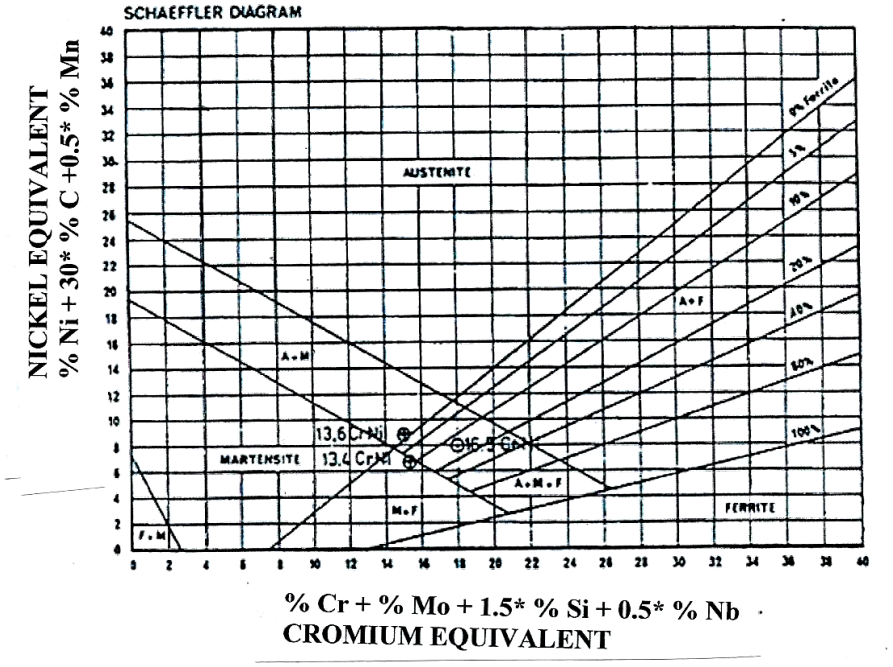

Fig 11.10. Schaeffler diagram showing the most commonly used qualities of steel in Francis runners.

11.4 Toughness testing and critical crack size and fatigue of materials

The crack arresting ability of materials with a high degree of plasticity may be determined by the Crack Tip Opening Displacement (CTOD). For any material used in a stress carrying part there will be a critical crack size which leads to unstable fracture depending on its size. This crack size can be calculated by formulas based on the fracture mechanic theory and the measured CTOD value determined experimentally for the material and welds deposit in question [Ref. 14] and [Ref. 15]. It should be noted that the influence from residual stresses and stress concentration around the area where the defect is located, also has a strong influence on the crack arresting ability i.e. the crack stopping ability.

Materials for turbines are as mentioned of the ductile type and include both elastic and plastic deformation in front of the crack tip before propagation, depending on the strength of the material and the level of the working stress.

However, it is proven from small scale CTOD-tests that high tensile strength steel with high working stress level allows for a smaller critical crack size than a low tensile strength steel with a lower stress level. How to calculate the critical crack size based on the critical CTOD value, (CTODC) is very well described in the report presented in Welding Institute report 278/1985 by M.G. Dawes [Ref. 15]. This calculation is based upon several large scale tension tests of different materials where crack tip opening displacement, crack length and the mean stress in the plate have been measured. The crack tip opening is normally measured in the bottom of the crack of a material test piece under bending by a special tool or at the bottom of a short crack in the middle of a test piece made as a flat plate under tension. The measured crack tip opening just before the total rupture of the test piece will be the critical crack tip opening (CTODC).
How to define an unstable or critical crack size is illustrated in fig. 11.11.

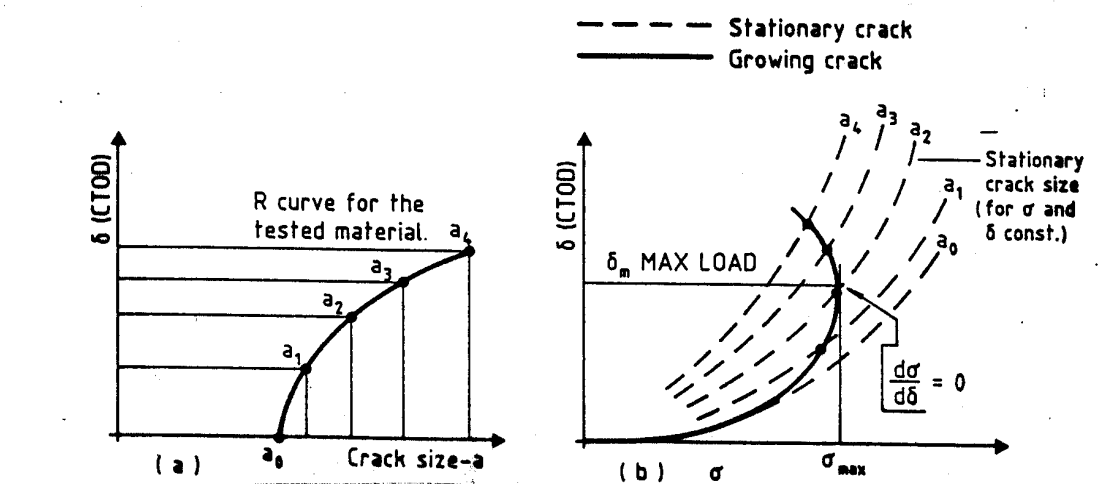

Fig. 11.11 Illustration of crack propagation versus stress and crack size.

Briefly the critical crack size may be defined as follows: A stable crack under static load can only be increased be increasing the working stress in the material where the crack is located. As the crack grows it will finally reach a size where no increase in the stress is necessary to increase the size of the crack opening i.e. $d\sigma/d\delta = 0$. This will be the critical crack size or CTODC value and total rupture occurs even if the stress is not increased (see fig. 11.11).

In fig. 11.12 is shown the design curve for the dimensionless CTODC value φ as a function of applied local stress where the crack is located.

$$\phi = (1/\bar{a}) \cdot (\delta \cdot E/(2\pi \sigma_{0,2})) \cdot (1 - 2\bar{a}/(2w))$$

The dimensionless value φ yields for welded ferritic steel:
When substituting for δ by δ_{cr} (=critical CTODC value which is the value for which the final fracture occur) the second term represents a material constant. The last term in the bracket includes the through plate crack length 2a and the plate width 2W. For a relatively small crack compared to the plate width, this term may be neglected. The σ_1 value in fig. 11.6 represents the working stress including a possible stress concentration and residual stress in the weld.
For post weld hat treated welds:

$$\sigma_1 = \sigma K_{sc} + 0.25\sigma_{0.2}$$

K_{sc} is the stress concentration factor which will be 1.0 in a plane plate with ground weld both for heat treated and not heat treated welds.

$$\sigma_1 = \sigma K_{sc} + \sigma_{0.2}$$

For welds without post weld heat treatment:

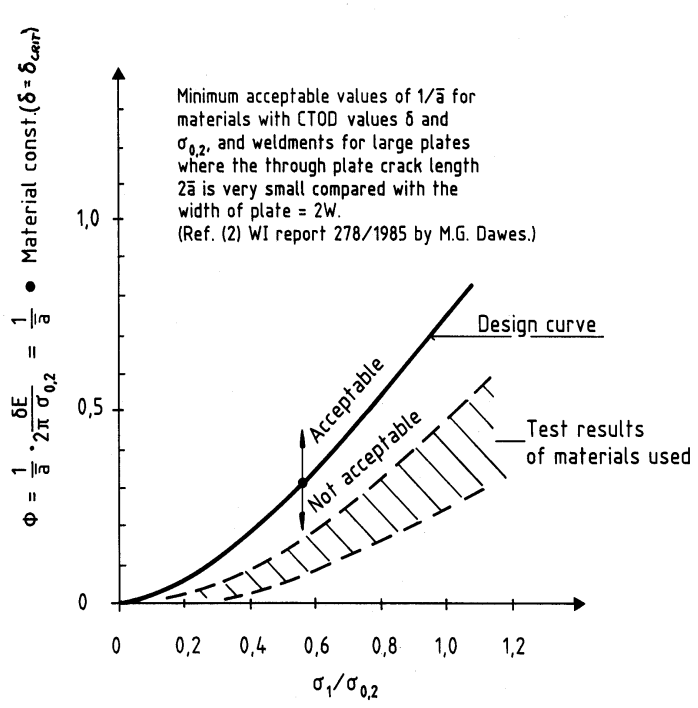

Fig.11.12 design curve vesus crack size $\bar{a}$

By means of σ_1 and the known values of $\sigma_{0.2}$ (or yield stress), the elasticity modules (Young's modules) E (E =2.1*10^5 N/mm^2 for steel) and the critical crack tip opening displacement of the material $\delta = \delta_{cr}$ = CTODC (δ_{cr} = 1 mm for very good materials). The critical value of a through plate crack length = â may then be found by means of the value of $\varphi = f(\sigma_1/\sigma_{0.2})$ taken from fig. 11.6. (The material constants $\sigma_{0.2}$, δ and E can be found for the material in question.)

Then we find by reading the value of ϕ from fig.11.12.

$$\bar{a}_{max} = (1/\phi)\,\frac{\delta_{cr} E}{2\pi\,\sigma_{0.2}}$$

Because a short through plate crack used in a material test is not a normal shape of defect, corresponding values of surface- and sub surface crack must be found. Such corresponding values of crack depths -a- for different crack depth/length ratios (a/2c for surface crack and 2a/2c for buried cracks) have been found by means of fracture mechanical theory and experiments and are presented in fig. 11.13a and fig. 11.13b according to WI report 278/1985 (Ref. 14).

By means of the presented procedure it is possible to determine the statical working stress which allows for a crack depth through the plate thickness for given values of the critical CTOD in plate material and weld deposit used (Ref.. LEAKAGE BEFORE RUPTURE).

It should also be noted that very low values of CTODC in a narrow heat affected zone (HAZ) for high tensile strength fine grain steel with $\sigma_{0.2} > 355$ MPa has been detected (For this reason QT and TMCP quality with less micro alloy elements have been used (see footnote chapter 11.1)). It should be noted that CTODC values down to $\delta_{cr} = 0.02$ mm have been measured in the HAZ in K welds in small test samples for plate qualities with $\sigma_{0.2} = 460$ MPa also after post weld heat treatment. However, CTODC tests of wide plate specimens with welds made according to normal work shop standard have indicated that the tougher material adjacent to the heat affected zone stops the crack and increases the δ_{cr} values close to the values for the weld deposit and plate.

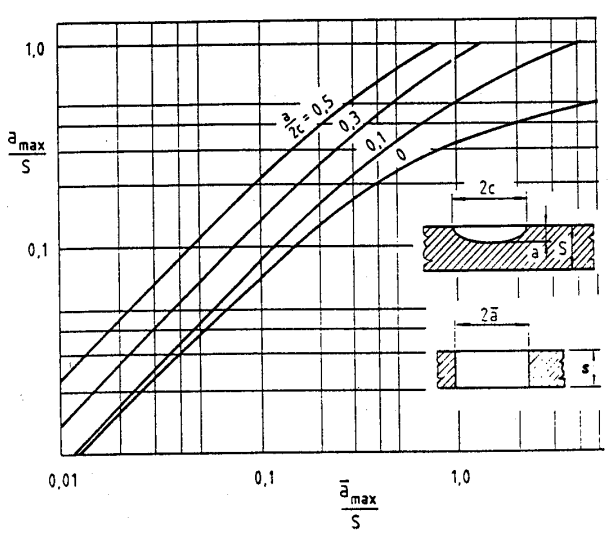

Fig. 11.13.a Semi elliptic surface cracks compared with through plates cracks.

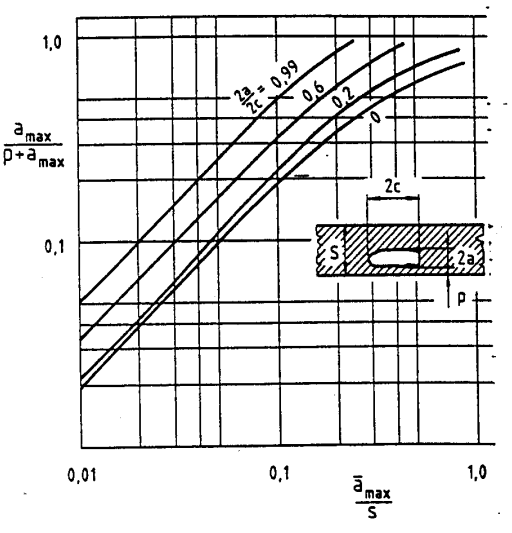

Fig. 11.13.b Elliptic buried cracks compared with through plate cracks.

11.5 Accept criteria for material defects in new machines exposed to fatigue due to periodic hydraulic load.

Parts exposed to low cycle fatigue

Defects of critical sizes rarely occur in a new turbine or pump. Such defects will in any case be detected by a leakage or rupture during the pressure test which is a very important test with pressure 50% higher than maximum operational pressure. However, smaller defects in a new machine may grow to a critical size during lifetime due to fatigue propagation caused by a certain number of loading cycles. (Ref. 26)

Basically the stress carrying parts in a Francis turbine are statically loaded. However, a turbine in typical peaking operation may be stopped and started i.e. depressurized and pressurized 3 times (or more) per. day which for a life time of 50 years leads to about 50 000 cycles totally. This is in the low cycle fatigue domain in modern fracture mechanic theory based on the fatigue law as expressed by Paris' law (see Paris diagram fig. 11.9). In addition minor (about 10% - 20%) stress amplitudes with a much higher number of cycles caused by pressure oscillations from the turbines regulating, will be superimposed.
For this reason the nominal principle stresses must be limited to avoid small material defects such as cracks and other sharp edged defects which may grow to critical size during life time. Safety margin to yield stress or ultimate stress is not sufficient as safety criteria if high tensile strength steel is used.
The following criteria should be fulfilled for a welded spiral casing of a Francis turbine or a distributor of a Pelton turbine made of high tensile strength plates:

1. The static working stresses must be limited to a value which gives a critical crack size large enough to obtain LEAKAGE BEFORE RUPTURE.
2. An acceptable defect shall not grow to a size, which leads to unstable fracture (rupture) within 20 000 - 50 000 loading cycles.
3. A not acceptable defect must not be so small that it may be overlooked during inspection by Ultrasonic-, X-ray-, Magnaflux-, Penetrant liquid or other methods.
4. Residual stresses, must be limited to a level which makes it possible to fulfil 1,2 and 3.

Unfortunately the fatigue crack propagation speed has not decreased by the development of high tensile strength steel even if the toughness and strength have increased. On the contrary some research works have indicated a slight improval of the fatigue lifetime for high cycle fatigue in materials with low yield stress. On the other hand the crack propagation speeds in brittle materials and tougher materials show only negligible differences for high cycle fatigue.
No direct connection between impact tests and crack propagation speed has been proved. However, CTOD value and the ultimate fracture are greatly influenced by the brittleness.
The fatigue crack propagation may be presented in a Paris diagrams based upon an increasing number of measurement of different base materials and weld deposits.

In fig.11.8 and fig. 11.9 the Paris diagram is shown qualitatively. The Paris equation for crack propagation per load cycle = N yields:

$$da/dN = C\,\Delta K^m \qquad (11.6)$$

In equation 11.6, $\Delta k = k_1 - k_2 = (\sigma_1 - \sigma_2)\sqrt{a}\,\phi$, a = crack depth and **m** and **C** are constants based upon tested material quality in question. For welded steel plates including HAZ and weld deposit the values of **C** and **m** in equation 11.6 may be chosen to be $C=10^{-11}$and m = 3.0. (Note: For casted Pelton runners $C = 2.8*10^{-9}$ and m = 2.55, See fig.11.8)

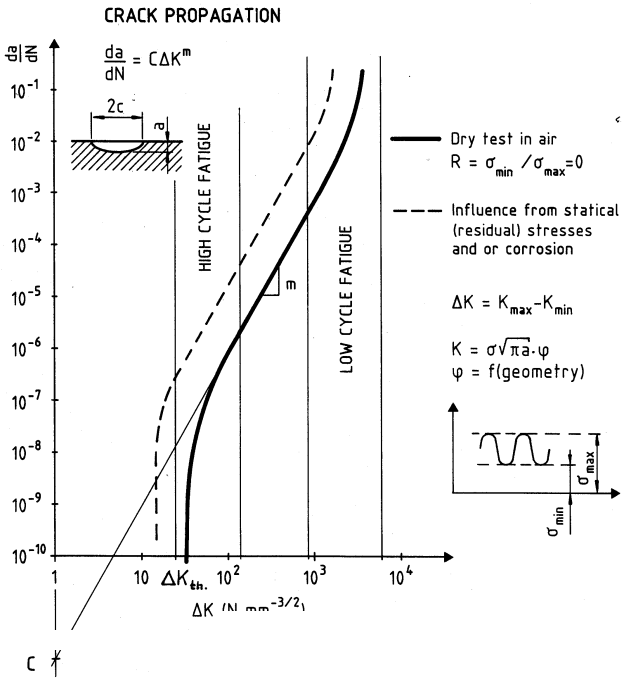

Fig.11.14 Paris diagram. Principal illustration.(Detailed measuring result is shown in fig.11.8)

In fig. 11.15 calculated acceptable defects for a number of cycles up to 50 000 and stresses up to σ_{max} = 180 MPa are shown where the critical crack size is assumed to have a depth of a_{cr} = 100 - 150 mm. for ductile materials with the critical crack tip opening displacement CTODC = δ_{cr} > 1.0 mm. (A furter discussion is given in the next section "Parts exposed to high cycle fatigue".)

Following conclusion may be drawn:
It will be very difficult to increase the maximum working stresses above 200 MPa for turbine parts exposed to a number of loading cycles above 20 000 in the lifetime because acceptable defects then will be too small to be detected.

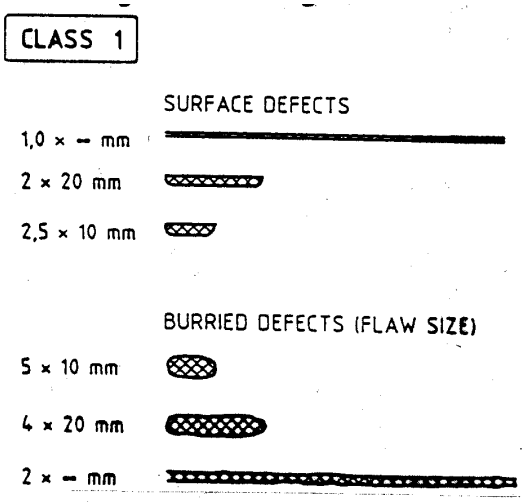

Fig.11.15 Accept criteria for defect sizes in spiral cases of welded high tensil stress steel plates.

Leakage before rupture may be fulfilled if the CTODC values of the HAZ can be improved or if large specimen tests show that the growing crack will be arrested in the ductile material beside the heat effected zone. However, it should be noted that for very large turbines the plate thickness will be too large for fulfilment of the criterion leakage before rupture. Further weldes in stay vanes in spiral casings will not give any leakage before rupture.

Due to the residual stresses and the hardening effect of high tensile strength steels, welds should be post-weld heat treated for all thick plates. Otherwise crack growth may lead to unstable fracture from a not through thickness cracks after a certain number of years in operation.

(Special welding procedures by heat treatments of each welding layer by the next layer may be used for welding of QT (Quenched and Tempered) steel plates. For the last layer good accuracy to locate the edge of the last layer - by 0.5-1.0 mm - to the base material in order anneal the hardened HAZ from the last layer of welding).

Critical high stressed areas in a spiral casing will be the joint between the shell and the stay ring where both the stress and wall thickness have the maximum value. For Pelton turbine manifolds the bend joint on the inside will be the critical point besides joints in the bifurcations.
The peak stress in the stress concentration area of a bend fabricated from cylindrical pipe sections may be expressed by a simple empirical formula based upon theoretical analysis verified by straingauge measurements:

$$\sigma = (pD/(2s))(1 + 3.8 \tan(\alpha/2)) \qquad 11.7$$

In the equation p = pressure, D = diameter of the pipe sections, s = plate thickness and α = angle between the cylindrical bend sections. (See fig. 11.10)

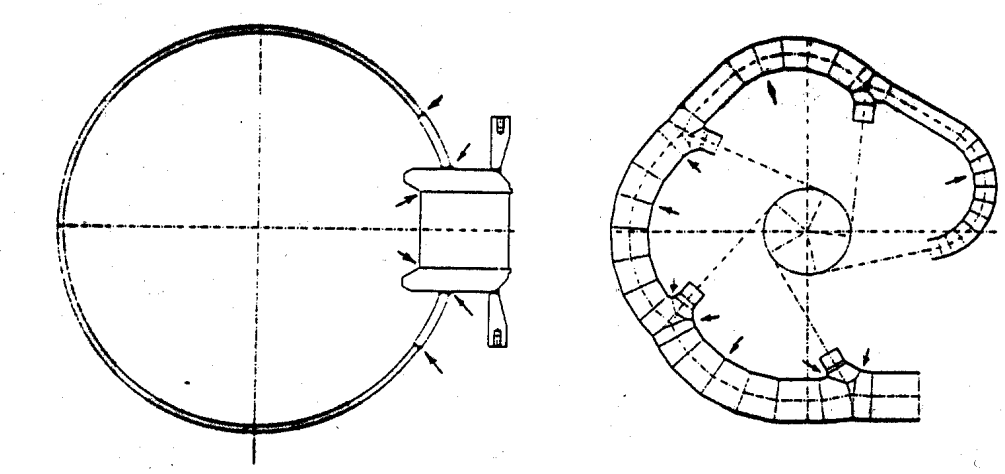

Fig. 11.16 Critical high stress points in spiral cases and distributors

Parts exposed to high cycle fatigue.

Runners for Francis turbines and reversible pump turbines will be exposed to high cycle fatigue with number of cycles up to the range of 10^{11} normally with relatively low stress amplitudes. Casted Pelton runners in 13% Cr 4% Ni alloy steel are examples of of turbine

parts exposed to high cycle fatigue even if the number of cycles will be lower than for the blades in a Francis turbine runner. However, the number of cycles will normally exceed 10^9 cyles in the guaranty period and then no further crack propagation will occure unless grinding and welding on the runner has changed the material or geometry. (After repair welding during maintenance the runner must be treated like a new runner with frequent inspections until the number of cycles has passed $5*10^8$ cycles.)
For fabricated Francis runners also the 16% Ni 5% Cr steel has been used especially in Norway. This steel shows a somewhat better cavitation and erosion resistance than the 13% Cr 4% Ni steel and may be welded with a lower preheating than for 13% Ni 4% Cr steel. A preheating of 50 ^{0}C during welding is sufficient in order to keep the material well above the dew point for drying reason during welding. The low temperature is also convenient when welding runner blades with narrow openings.
The values of crack sizes and crack growth documented by the test results from castings for Pelton runners shovn in fig.11.11, can also be used for weld defects in Francis runners according to the authors experience.

Because the runners for Francis turbines are exposed for high velocities and dynamic load it is important to make the finished runner with lowest possible recidual stresses from production. This can be obtained only if the casting or material for forging have the same chemical composition and the subtraction by cooling of weld deposit and basic materials have only negligible differences.
Also the amount of separated δ-ferrite is of interest because a too high content may lead to long streched zones with low srength. (Look at the Schaeffler diagramme in fig 11.10 to find which composition that gives the highest content of δ ferrite. We also find that the CrNi 16.5 steel has a higher risk than CrNi 13.4 steel.) (Note also that the Swedish quality CrNi 13.6 no longer are in production even if it was a better composition than the quality CrNi 13.4 steel.)
The amount of Nitrogen (N) in the material has a major influence on the portion of stable Austenite in the structure and with a too high content of N the material may be austenitic when the Ms point is pushed to a very low temperature. See fig 11.18 where an increasing content of N will push the Ms point to the left.
Also a study the Schaeffler diagram should be made where the regarded composition is pushed towards the Austenitic domain with an increased content of Ni. The content of Austenite must be under control.

By means of the dilatometer diagram in fig.11.18 where the contraction or expansion of 16Cr5Ni steel is shown by cooling of weld or melted material with a following heating and cooling to create a tough structure.
Normally the austenitic material will decrease in voloume by cooling until the point Ms is reached normally at 150 deg C.
For a 16Cr5Ni steel with correct composition nearly all Autenite will be transformed to Martensite by 30^0 C.

However if the content of Nitrogen, N is too high the values of Ms (Start point) and M_f (Finished point) will be lower. (M_f point is the temperature where all Austenite is transformed to Martensite.) In extreme cases this point may be far below room temoerature like -50 deg C.) The following anealing temperature of about 580 ^{0}C will the then have no effect.
In the litterature, formulas are given to find the this temperature which is depending of the chemical composition of the regarded steel.
If the chemical composition in a 16Cr5Ni steel is correct all austenite will be transformed to Martensite at room temperature after a normalisation of the steel. This Martensite will be

heated to about 580 - 590 ^{0}C to get the correct tough composition.before the final cooling as illustrated in fig.11.18.

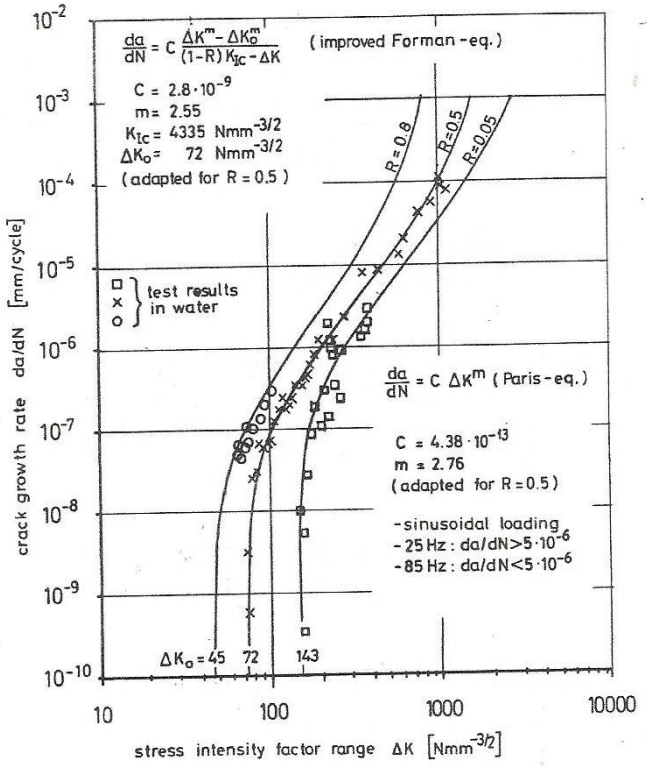

Fig.11.17 Result from material test of 13/4 Cr/Ni steel casings. (Ref. 28 H. Grain)

The Paris and improved Forman equations confirmed through material tests are illustrated in fig 11.17. SULZER made this large scale material test in order to confirm the "Stress Intensity Factor" ΔK_0 also denoted as threshold value $\Delta K_{th} = \Delta K_0 = \Delta\sigma\sqrt{a}\,\varphi$ where no crack propagation occure for the steel quality EN 10283, GX4CrNi 13-4 +QT1 (i.e 13/4 Cr/Ni alloy). The test was made with different values of prestressing expressed by $R = \sigma_{min}/\sigma_{max}$. The geometry factor was set to $\varphi = 1.26$ when used for Pelton buckets. The start defect was set to a semi elliptic surface crack and values for elliptic submerged crack were also confirmed as described by Dr. Grain in (Ref. 28). A fatigue threshold limit for a number of cycles higher than 10^{11} indicates infinite lifetime for a stress amplitude $\Delta\sigma \leq 45$ MPa and a surface crack less than 1 mm. depth and length 2 mm for a 13%Cr 4%Ni steel.
Fatigue cracking and lifetime for Pelton turbines is described in (Ref. 4 and ref. 28).

11.6 Key words on material defects in turbine new turbine production.

Because Francis runners are exposed to high not stationary flow velocities with pressure differences from pressure side to suction side of the blades, the quality and inspection of welds are very important.
It is also very important that the recidual stresses on the runner blades are as low as possible. A strict requirement and inspection of the welds as well as well as a requirement of the welding procedure and thermal stress relieving are important to avoid high residual stresses and possible Austenite in the welds.
In fig.18.14 the heating and cooling of the welds made of 13.4 CrNi or 16.5CrNi steel is illustrated.

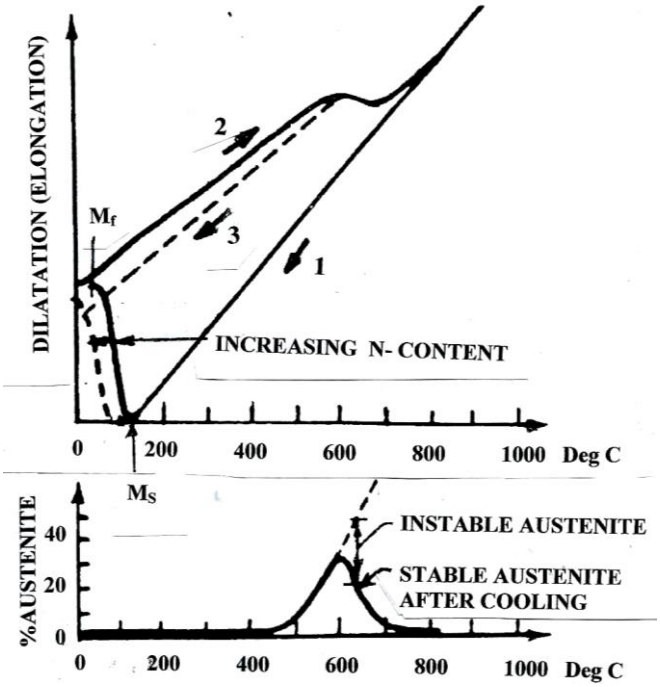

Fig. 11.18 Dilatometer expansion – heating diagram for weld deposit of 13.4 CrNi and 16.5 Cr Ni steel in principple. Note that by exceeding 600 ^{0}C the weld deposit material will be brittle and not suitable for runners.

Because the runners for Francis turbines are exposed for high velocities and dynamic load it is important to make the finished runner with lowest possible recidual stresses from production. This can be obtained only if the casting or material for forging have the same chemocal composition and the subtraction by cooling of weld deposit and basic materials have only negligible differences.

Also the amount of separated δ-ferrite is of interest because a too high content may lead to long streched zones with low strength. (Look at the Schaeffler diagramme in fig 11.10 to find which composition that gives the highest content of δ ferrite. (We find also the CrNi 16.5 has a higher risk than CrNi 13.4 steel. (Note that the Sweedish quality CrNi 13.6 which no longer is in production was a better composition than CrNi 13.4 steel.)

Because the amount of Nitrogen (N) in the material has a major influence on the portion of stable austenite in the structure and with a too high content of N_2 the material may be Austenitic when the Ma point will be pushed to a very low temperature below normal room temperature. See diagram 11.18 where an increasing content of N will push the Ms point to the left and study the Schaeffler diagram pushing the point towards austenite. The content of Austenit must be under control and with a content of N the requirement of Ni will increase in order to decrease the amount of austenite.

By means of the dilatometer diagram in fig. 11.18 where the contraction or expansion of 16Cr5Ni steel is shown by cooling of weld or melted material with a following heating and cooling to create a tough structure.

Normally the austenitic material will decrease in voloume by cooling until the point Ms is reached normally at 150 deg C.

For a 16Cr5Ni steel with correct composition nearly all autenite will be transformed to Martensite by 30^0 C. However if the content of N_i and/or Nitrogen, N_2 is too high the values of Ms (Start point) and M_f (Finished point) will be lower. (M_f point is the temperature where

all Austenite is transformed to Martensite.) In extreme cases this point may be far below room temperature like – 50 deg C.)
The following anealing temperature of about 580 ^{0}C will the have no effect.
In the litterature formulas are given to find the this temperature which is depending of the chemical composition of the regarded steel. If the chemical composition in a 16Cr5Ni steel is correct, all austenite will be transformed to Martensite at room temperature after a normalisation of the steel. This Martensite will be heated to about 580 - 590 ^{0}C to get a correct tough composition.before the final cooling as illustrated in fig. 18.14.

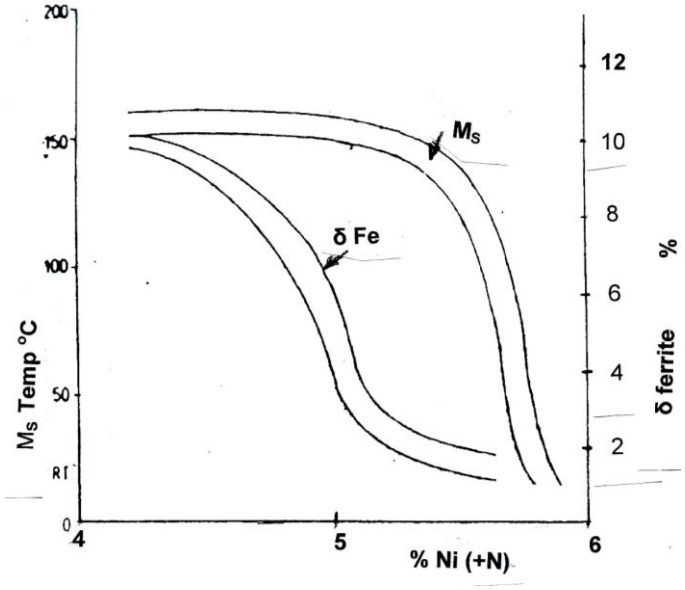

Fig. 11.19 Temperature for creating Martensite Ms as a function of Ni + N content in the steel.

In Fig. 11.19 is shown the importance of getting the correct composition of Ni and δFe inbetween the values of Ms and δFe to get an optimum steel without Ms an δ Ferrite.
This composition is important for all stainless parts in a turbine i.e. both for Francis and Pelton runners an other stainlees parts exposed to cyclic loading.

11.7 Defects and life time of runners exposed to high frequency fatigue.

Stresses in Pelton runners can easily be measured by strain gauge measurements.
These measuring results can be compared to Finite Element analyses made for comparision.
The max stress amplitudes on a Pelton bucket may be set at 45 Mpa peak to peak.
However, much higher stresses may occure if the fillets between the buckets if they are not correctly made. Examples of improvements was made by the Norwegian company KVÆRENER 40 years ago and still minor changes may improve the design.
However, defects especially in casted runners may occure and fatigue cracks have from time to time been detected in casted Pelton runners.
It is important to stop and inspect the runners frequently the first year in operation in order to detect growing fatigue cracks started from defects above acceptable size at an early stage requiring a minor weld repair with anealing of the runner.
After a couple of years in operation passing 10^{10} cycles with no observed fatigue cracks the runner will have an infinite life.

Example of runner that have neen in operation om 30-40 years without repair is a prove of this theory.
The discovered errors is normally caused byMnS inclusions and growing deffects were detected in a Pelton Turnbine operating at 1130 m net head in Norway even if the stress amplitudes were as small as 45 MPa which was measured after the repair.
It is important that a full heat treatment of the runner is made after the repair and the inspection periodes must be as for a new runner i.e. a frequent inspection the first year in operation.
To be on the safe side a crack close to the surface must be smaller than or equal to 2*2 mm in order to be on the safe side.

General conclusion on material defects - inspections and safety

As a conclusion following points may be listed for safe operation of hydraulic machinery.

PRESSURIZED STRESS CARRYING PARTS

- The risk of catastrophic failure in hydraulic machinery increases if the theoretical life time is out and no thoroughly inspection and repair work is done.

- The risk for not detecting a fatigue crack before the critical size is reached by LEAKAGE BEFORE RUPTURE is largest in large units with thick high tensile strength steel plates. For very large units the plate thickness is too large for using this criterion.

ROTATING PARTS

- The risk for fracture in rotating parts should be under control by periodic inspection and careful fabrication and casting procedure. Cheap low quality foundries should be avoided for production of rotating parts for modern machines with high specific speed runners.

11.8. Resistant materials for cavitation, corrosion and sand erosion.

The turbine parts exposed to cavitation are the runner and and top of the draft tube cone for reaction turbines (Francis and Kaplan) and the needle, nozzle and the jet entrance in the buckets of the runner for impulse turbines (Pelton).

Traditionally the austenitic steel 18% Cr 8% Ni with Mo content > 2% has been regarded to have a very good resistance against corrosion and cavitation. However, the fatigue resistance is traditionally regarded to be very poor. No threshold value with acceptable stress level for fatigue has to the author´s knowledge been proven in the Paris diagram except for very low stress amplitudes. From experience with Pelton runners the life time due to fatigue is very short by using Austenitic materiales in Pelton buckets. Also the creep limit is very low and not cold deformed hardened large bolts of 18% Cr 8% Ni may loosen after some time in operation. Further, long small bolts of 18.8 Cr/Ni quality broke due to small periodic stress oscillationsin in a cover plate for the balancing weight in a Reversible Pump Turbine in California in 2010.

Another disadvantage is the self hardening effect of Autenitic steel caused by mechanical abrasion which may cause severe galling if this material is in contact with movable parts.

Conclusion: In runners, and guide vanes, needles and other movable parts the 18% Cr 8% Ni material should not be recommended.

The first material to substitute for the 18% Cr 8% Ni after the introduction of Martensitic stainless steel was the martensitic material 13% Cr 1% Ni which has been successfully used in runners and movable parts during many years after the mid 50ties.

However, the corrosion resistance and resistance against sand erosion and also cavitation resistance was limited due to not sufficient hardness combined with low toughness and low Ni content. The weldability was also poor for the 13%Cr 1%Ni steel which requires a necessary preheating temperature of 200 ^{0}C and a high stress relieving temperature of 680 ^{0}C.

In the late 60-ties the Swedish quality 13% Cr 6% Ni was developed and patented.

The patent resulted in the development of 13% Cr 4% Ni and 17% Cr 4% Ni and 16% Cr 5% Ni alloy which resulted in the ruling qualities to day consisting of 13% Cr 4% Ni on one side and 16% Cr 5% Ni on the other side of the patented alloy. The patent of the 13% Cr 6% Ni steel from Bofors lost the competition due to limited production.

Both 13% Cr and 4% Ni and 16% Cr 5% Ni are austenitic martensitic steel with a limited fraction of δ-ferrite and about 20-25% stable austenite which creates a tough structure combined with the martensite after normalization followed by an annealing to 580 ^{0}C.

The corrosion resistance is satisfactory as well as the cavitation resistance. However, the 16% Cr 5% Ni seems to be slightly better than 13% Cr 4% Ni, but the differences are marginal.
Electrodes with improved cavitation resistance for cladding welding of cavitation eroded places has been developed by substituting the chromium by cobolt in the electrodes.

Good results have thus in some cases been obtained for cavitation repair. Another interesting material which so far has not been very much used in water turbines are the Ferrite Austenitic DUPLEX steel which have proven good qualities in offshore oil exploration as a corrosion, cavitation and erosion resistant material.

However, not sufficient information of high cycle fatigue is so far presented for this material i.e. Paris diagrams with more than 10^9 cycle fatigue tests.

As a conclusion following statement may be drawn: Among the existing materials used in runners it seems that the 13% Cr 4% Ni and 16% Cr 5% Ni behaves satisfactory for a well designed turbine operating in clean water.

For sand erosion no stainless steels show acceptable resistance.
The stellite and also Titanium show improved resistance, but only by a factor of 2-3. However, promising work is going on in developing coating processes of ceramic materials like Tungsen Carbides and others. For Pelton turbines coatings of needle tip and nozzle ring by ceramic materials has showed results that increases the life time with a factor of 10 before repair compared with hardened steel.

It should also be emphasized that sand erosion even from silt with grain size less than 60 μm made severe damage of needles and nozzles in a 800 m head Pelton turbine in Norway while the runner buckets had a negligible damage. Similar results of fine grain sand erosion has been reported from Paute power plant in Equador.

By a ceramic coating of needles and nozzles the sand erosion problems was in this case solved satisfactory by annual replacement of nozzles and needles. However, if coarse sand is present the Pelton buckets are severely eroded while the damage of the nozzles may be less serious. The reason for this may be explained by the extreme acceleration of a particle passing the Pelton bucket. By means of flow analysis an acceleration of 100 000 (m/sec^2)(equivalent to 9.800□g) may occur for small buckets in a high head machine.

Because of this, largest possible buckets and lowest possible number of jets should in general be used for Pelton turbines operating in sand laden water.

The following formula may be established for comparison of the sand erosion in the buckets of a turbine with 4 jets compared with an alternative with 6 jets.

The bucket size as a function of the number of jets [jet number = Z_n (n=1,2,3, ... 6).]

$$B_n = B_{n+1}/(Z_n/Z_{n+1})^{0.5}$$

The difference in life time of a runner (or the time between repair of sand erosion) will be depending on the acceleration which is inverse proportional to the radius of the curvature i.e. the bucket size. Then the amount of sand in contact with the wall will be inverse proportional to the hydraulic radius of the curvature i.e. bucket size. Then the amount of sand in contact with the wall will be inverse proportional to the hydraulic radius or wetted area divided by the cross section.

Finally the erosion must be proportional to the number of jets which is proportional to the number of flushes of a bucket per revolution.

Then the erosion life time ratio formula yields for a 4 jets turbine versus a 6 jets turbine.

T4/T6 = (K-acceleration) x (K-size) x K-(jet number)

or

$$T4/T6 = \sqrt{6/4}\,x\sqrt{6/4}\,x6/4 = 2.25$$

i.e. the life time of a 4 jet machine is 2.25 time longer than a 6 jet machine for the same head and total flow in sand laden water.

So far ceramic coating of the Pelton runners is not commercialized with sufficient success, but runners have been coated and showed some improvement, but surface roughness has decreased the efficiency.

Neither is the coating of facing plates of Francis turbines commercialized while the guide vanes may be treated in the same way as the nozzles and needles of a Pelton turbine. (Ion Nitration have also been used on Francis runners and facing plates on head and bottom covers).

However, work is going on world wide and at the Norwegian University and SINTEF a project is going on to find methods to protect the guide vane facing plate system in Francis turbines.
The coating of the facing plates of covers in Francis turbines is of great importance because the sand erosion in this place creates a leakage flow that decreases the efficiency dramatically.

In fig. 11.20 is shown a comparison of the efficiency before and after refurbishment of a sand eroded guide apparatus at DRIVA power plant in Norway in order to illustrate the importance of reducing sand erosion in the guide vane apparatus of high head turbines.

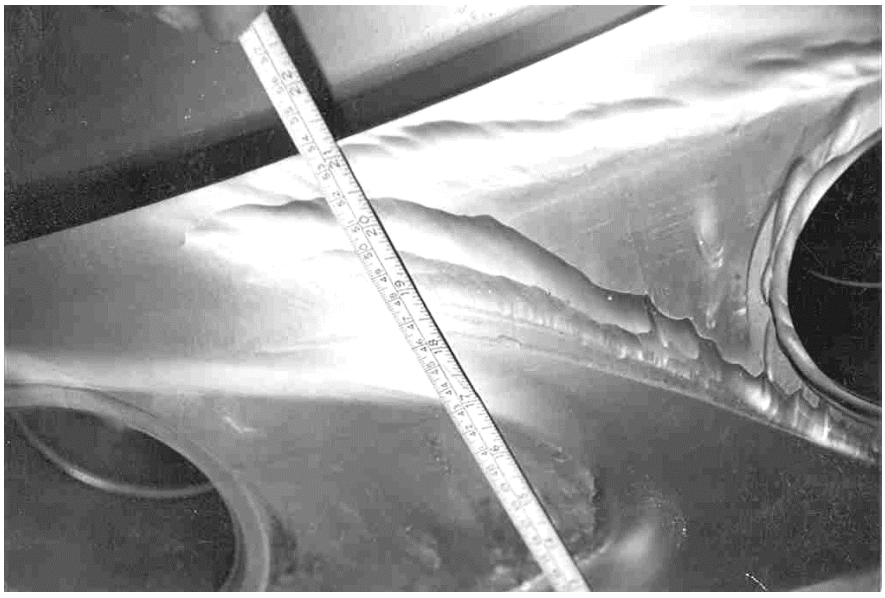

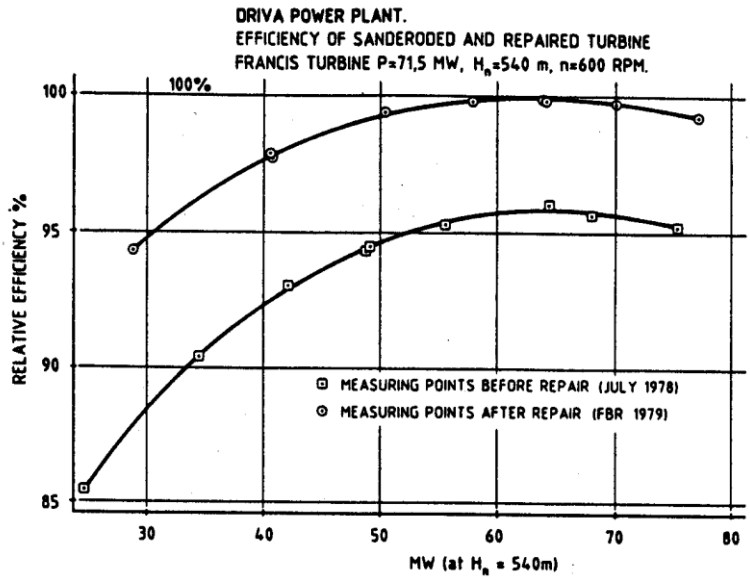

Fig. 11.20 (Top) Result of sand erosion on fasing plates after one year in operation at DRIVA powerplant with net head H = 540 m
(Bottom) Loss in efficiency caused by the sand erosion. Note: The loss due to increased leakage in the labyrinth seals was measured separately to 0.5% only at best efficiency.

.

11.9 Turbine Parts exposed to Sand Erosion.

This chapter will be vey short appointing to the most reliable standard which is CCH 70-3 made for casted turbine runners.
However at the time being more European standards are available included in EU standards which is covering all types of turbines for hydropower.
In addition to fatigue problems, sand erosion and corrosion are the most serious problems for hydro turbines.

In this chapter possible repair and life time of various turbine parts, mainly on Francis and Pelton turbines, will be discussed.

In the dilatometer diagramme in **fig 11.18** is shown expansion and contraction of 16Cr5Ni steel during cooling and heating from melted steel (1) and following heating (2) and final cooling (3) in order to obtain a tough material compostion.
For a 16Cr5Ni steel with correct composition, nearly all Austenite will be transformed to Martensite by 30 ^{0}**C** . However, if the content of **Ni** and/or Nitrogene **N** is too high both **Ms** and $\mathbf{M_f}$ will be lower. (**Mt**=Temperature when all Austenite has been transformed to Martensite is denoted as $\mathbf{M_f}$ in the diagrem in **fig 11.18.**

In order to reduce sand erosion a hard, but tough material is selected. However, the material in guide vanes must have different hardness compared to the head cover and bottom cover surfaces to avoid galling. Minimum clearances between the parts in contact and a difference in hardness is chosen of guide vanes and the plates. The difference in hardness should be 70 HB to avoid galling which was set up after World War II. (A later report has allowed for a difference of 40 HB to avoid galling.) It is very important to avoid Austenitic steel which is vey sencitive for galling.

The guide vanes are normally made of Martensitic steel in quality of 13Cr1Ni steel.
However with higher stresses a somewhat stronger quality 13Cr4Ni has been used and then the fasing plates on head and bottom covers as been covered by a welded layer of 17Cr1Ni steel without any thermal heating in front of or after the final smooth maschining of the surface on head and bottom cover. A hardness of this surface should be HB 350 and then a differnce between head and bottom covers and the guide vanes made of 13Cr4Ni steel should have a hardness equal to or below HB300 which should give a safety against galling..
A rough vear of the fasing plates operating in sand laden water often leads to the final machining to be done in work shops and then the hardness of the surface should be under control.

During the latest years research work agains wear of Francis turbines and Pelton turbines has been made. For Pelton turbines the most critical parts are the nozzles which will be damaged even by very fine grade sand also when minor damage has been made on the buckets.
Hard cheramic covers has been made for nozzles, but cavitation has also in this case given erosion minor rings on the needle tips followed by cavitation damage.
Normally Pelton buckets are exposed to severe sand erosion if more coarce sand is mixed with the water. Due to fatigue problems in Pelton buckets, too hard base materials must be avoyded for Pelton runners.
In order to obtain a sufficient toughness a hardness of HB 250-270 will be the maximum value for the Pelton buckets.

Any damage requires repair welding followed by machining in workshop and normally 13Cr4Ni steel is chosen for Pelton runners which is the best possible quality for weld repair and the highest possible resistance agains sand erosion.
For any repair welding electrodes of the same quality as the base material of the buckets must be chosen in order to avoid residual stresses and fatigue problems after a weld repair. Thermal stress relieving is regarded to be necessary on the repaired areas.

12. TURBINE CONTROL SYSTEMS AND REGULATING REQUIREMENTS OF POWER PLANTS

This chapter deals with the requirements of the dimensions of the conduit system and the generator inertia mass in order to fulfil the guarantees of speed rise and pressure rise as well as regulating stability requirements. (Ref. 25), (Ref.26).

12.1 Dimensioning rules for tunnel systems.

In fig.12.1 a section of the conduit system for a traditional high head Hydro Electric Power Plant is shown.

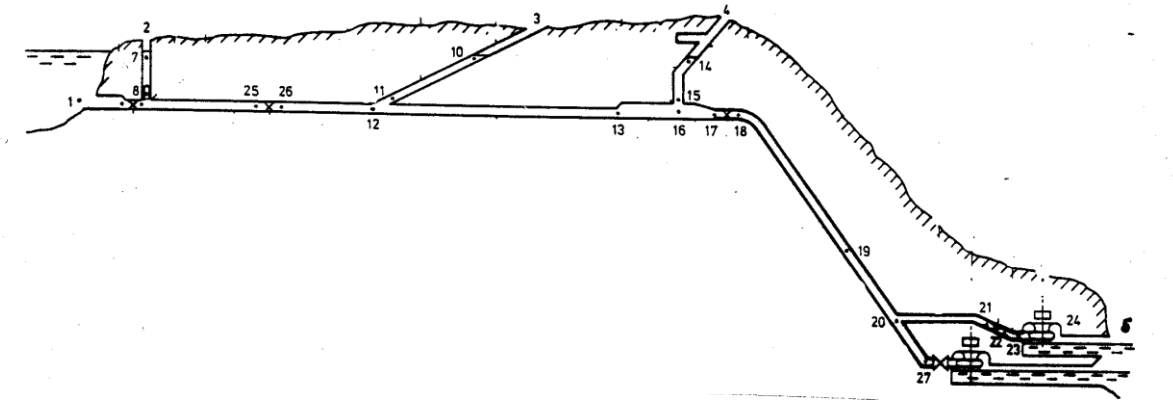

Fig. 12.1 The layout of a high head Hydro Electric Power Plant.

In a traditional power plant the pressure rise and regulating stability can be divided into two main parts.

1. The mass oscillation problem for the tunnels and surge shafts both on the pressure side and the suction side.

2. The water hammer problem of the conduit between the turbine and the water level in the surge shafts on both pressure and suction side.

The mass oscillations
The traditional mass oscillation stability problem was for the first time analysed by Prof. Thoma who established the criterion for the minimum critical cross section of the surge shaft which gave stable mass oscillations.

The criterion is based upon the three following equations:

1. The equation of continuity.

2. The equilibrium of forces (Newton 2. law).

3. The assumption of an ideal turbine governor that is able to fulfil the statement that flow multiplied by pressure is constant. (More advanced theories includes also the turbine efficiency). However, this statement is not fulfilled if the tunnel is short with short surging time because then the turbine governor will be too slow to obtain constant output of the turbine (QH=const.). The margin to the

critical Thoma cross section of the surge shaft, as explained later, must then be increased for short tunnels.

The Thoma criterion is well described in the literature and only the basic equations and the equation for the critical cross section area is included in this volume.

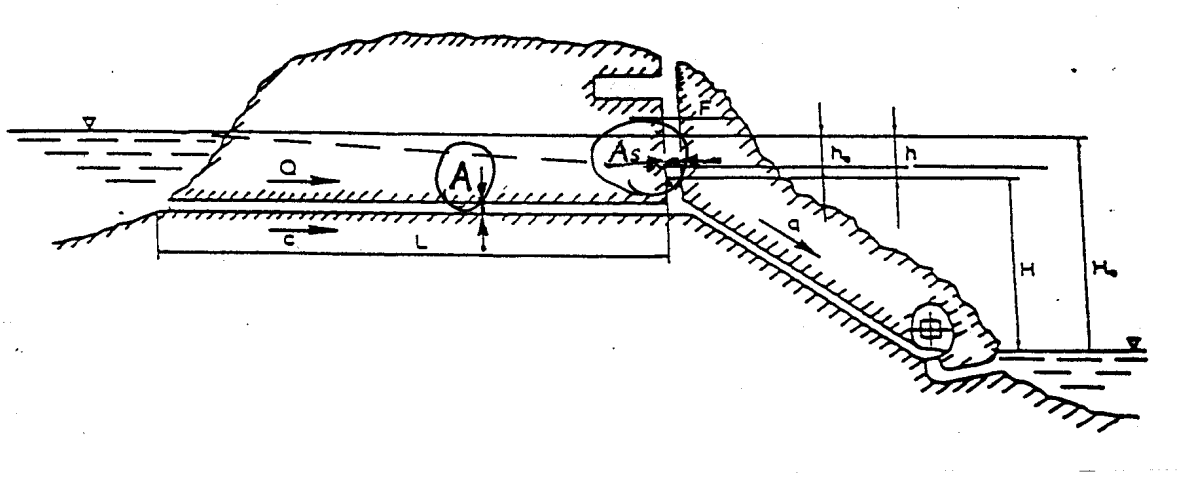

Fig. 12.2 Tunnel and surge shaft with values used for the simple Thoma criterion.

Following equations for developing the Thoma stability criterion my be expressed as follows:

The equation of continuity

$$A_s \frac{dh}{dt} = q - Q \qquad (12.1)$$

The equilibrium of forces

$$\frac{L}{A}\frac{dQ}{dt} = g[h - h_o(\frac{Q}{Q_o})^2] \qquad (12.2)$$

The equation of flow-pressure control of the turbine

$$q(H_o - h) = Q_o(H_o - h_o) \qquad (12.3)$$

By means of the three equations (12.1), (12.2) and (12.3) following critical cross section can be found:

$$A_{scr} = \frac{LAc_o^2}{2g\,h_o(H_o - h_o)} \quad for\ h_o < \frac{1}{3}H_o \qquad (12.4\ a)$$

If substituting for the head loss $h_o = (f/R_h) \square L \square C_o^2/2g$ and $H_o - h_o = H$ = net head equation can be simplified as follows:

$$A_{scr} = \frac{AR_h}{fH_n}$$

where f = Darchy Weissback friction factor. It should be noted that the length L is removed from equation (12.4) if no local throttling exist in the system.

For a tunnel with air accumulator the cross section of the surge shaft = A_s could be substituted for by an equivalent cross section A_{eq}. The equivalent cross section A_{eq} may be calculated for the compression of air and surging of the water level by the equation of polytrophic compression and expansion of the air volume. The equation for A_{eq} yields. (Ref. 6) and (Ref. 7).

$$A_{eq} = 1/(1/A_w + \kappa H_o / V_o)(m^2) \qquad (12.4\ b)$$

(see list of parameters for the parameters in the equation)

Normally we have $1/A_w << \kappa H_o/V_o$ and then the formula may be simplified to:

$$A_{eq} = V_o/(\kappa H_o)\,(m^2) \qquad (12.4\ c)$$

Then the critical air volume can be found by the simplified equation.

$$V_{ocr} = \kappa H_o A_{scr} \qquad (12.4\ d)$$

List of parameters:

L = tunnel length
A = cross section area of tunnel
A_s= cross section of surge shaft
$h = \zeta Q^2/(2gA^2)L$=head loss in tunnel

q = turbine flow
Q = flow in tunnel
$c_o = Q_o/A$ = steady state velocity in tunnel
o = denotes steady state conditions

A_{eq} = equivalent cross section (m^2)
A_w = water level area (m^2)
κ = polytrophic exponent, normally κ =1.3 due to evaporation and freesing of vapour
V_o = air volume in accumulator (m^2)
H_o = air pressure in accumulator (m w.c.)
H = net hed ($H = H_0 - h_0$)

Normally a safety factor to the critical cross section should be 1.3 to 1.5. However, it has been proven that for smooth full profile drilled tunnels a larger margin should be used because of smaller difference between steady state flow friction and friction for flow oscillations (Ref. 7). Further for short tunnels a larger margin is required than for long tunnels because a real turbine governor cannot satisfy eq. 9.3 for short tunnels due the shorter surging time of the pressure. This is also proved during frequency response tests at seven power plants as presented in (Ref. 7).

It should also be emphasized that in the case of a high pressure tunnel the surge shaft will be very long. It has been proven that the width of the shaft must be much bigger than according to the Thoma criterion in order to reduce the effect from the inertia forces of the water in the long shaft. The water hammer wave reflections from the head race tunnel system will because of the inertia mass in the long surge shaft not be damped sufficiently when passing the surge shaft and will reach the turbine.)

As explained later a more economic solution and a better regulating stability will be obtained by building a high pressure air accumulator if the length of the surge shaft exceeds approximately 300 m length.

12.2 Dimensioning criteria based on pressure rise and governor stability requirements.

The general equations

The water hammer problems may be divided into two main areas.

1. The water hammer transient problems causing pressure rises that affects the stresses in penstocks and stress carrying parts of the turbine.

2. The governing stability problems caused by pressure oscillations in the conduit system.

The water hammer problems are based on the equations developed by Allievi (Ref. 19) and various books describe different ways to solve both the governing stability problems and the transient problems. Among the literature the book of Wiley and Streeter, (Ref. 17), shows a general solution of the problems.
A special stability theory for power plants with influence of the frictional damping of oscillations in rough and smooth tunnels as well as the influence from the turbine characteristics is presented in (Ref. 9) and (Ref.8).

The well known equations of dynamics of elastic fluid and conduits were first established by Allievi (Ref 19). Later the frictional term has been included and discussed in the literature (see Ref. 9).

The commonly used dynamic equations of water hammer problems yields:

Equilibrium of forces:

$$\frac{\partial h}{\partial l} = \frac{Q_o}{H_o g A}\left(\frac{\partial q}{\partial t} + Kq\right) \qquad (12.5)$$

The equation of continuity:

$$\frac{\partial q}{\partial l} = \frac{A H_o}{a^2 Q_o}\frac{\partial h}{\partial t} \qquad (12.6)$$

The frictional term K may be expressed by the shear force τ as follows (Ref. 9):

The friction shear force for oscillatory flow is proven to be a function of the flow amplitude q , the frequency of the oscillations and a fictitious roughness of oscillatory flow based on the steady state head loss as explained in (Ref. 9).

$$K = \pi D \tau / (\rho Q_o q) \qquad (12.7)$$

In chapter 12.3 a brief description of the stability analysis will be given.

Equations (12.5), (12.6) and (12.7) are based upon the assumption that the flow is positive out of the pipe end and that rising pressure at the outlet end is positive (see fig. 12.3 and (Ref. 9))

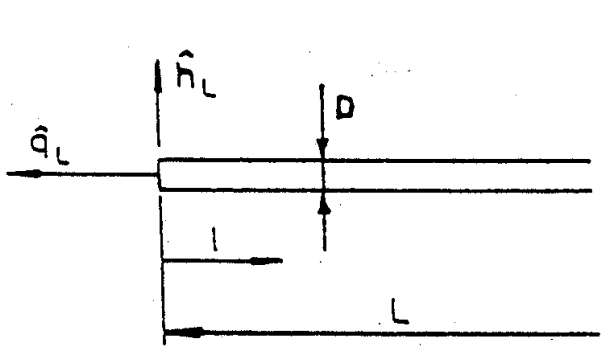

Fig. 12.3 A section of a pipe with diameter=D.

Symbols:

H_o=	steady state pressure or mean pressure before disturbance (mWC)
h =	relative pressure variation $\Delta H/H_o$
Q_o=	steady state flow or mean flow before disturbance (m^3/sec)
q =	relative flow $\Delta Q/Q_o$
l =	distance from pipe outlet along the pipe (m)
L =	length of pipe
D =	diameter of pipe or conduit (m) (Hydraulic radius R_h=D/4 may be used)
A =	cross section of pipe (m^2)
g =	gravity constant
a =	wave propagation speed (m/sec)(also denoted celerity)
K =	head loss friction factor (see eq. (12.7)
τ =	friction shear force per unit length of pipe (N/m)
ρ =	density of fluid (kg/m^3)
o =	denotes steady state conditions

The analysis of pressure rise of the water hammer

During shut down of the turbine-generator aggregate a fast closure of the guide vanes (or needles on Pelton turbines) is required in order to avoid high speed rise. However, a fast closure causes a high pressure rise in the penstock and in addition also the speed rise caused by the loss of generator load has influence on the flow through a reaction turbine.

Of special interest is the high head Francis turbines and in particular the reversible Pump turbines where any speed rise causes a strong reduction of the flow. In fig. 12.4, the speed rise/closure procedure of a high head Francis turbine is illustrated in a characteristic diagram.

Note, the variables along both axes in the diagram in fig. 12.4 include the square root of the pressure ratio. The pressure rise will normally be calculated by means of Allievis equations solved with the characteristic method which is very well described in (Ref. 16). The influence

of the turbine characteristic may be solved as illustrated in fig. 12.4 together with the characteristic method (Ref 10). Another way is to use the so called Suter curves which is a transformation of the turbine characteristic diagram which is shown in fig. 12.4. This method may also be used for calculating speed and pressure rise of Reversible Pump turbines with unstable shape of the turbine characteristics at runaway speed (Ref. 17) and (Ref18).

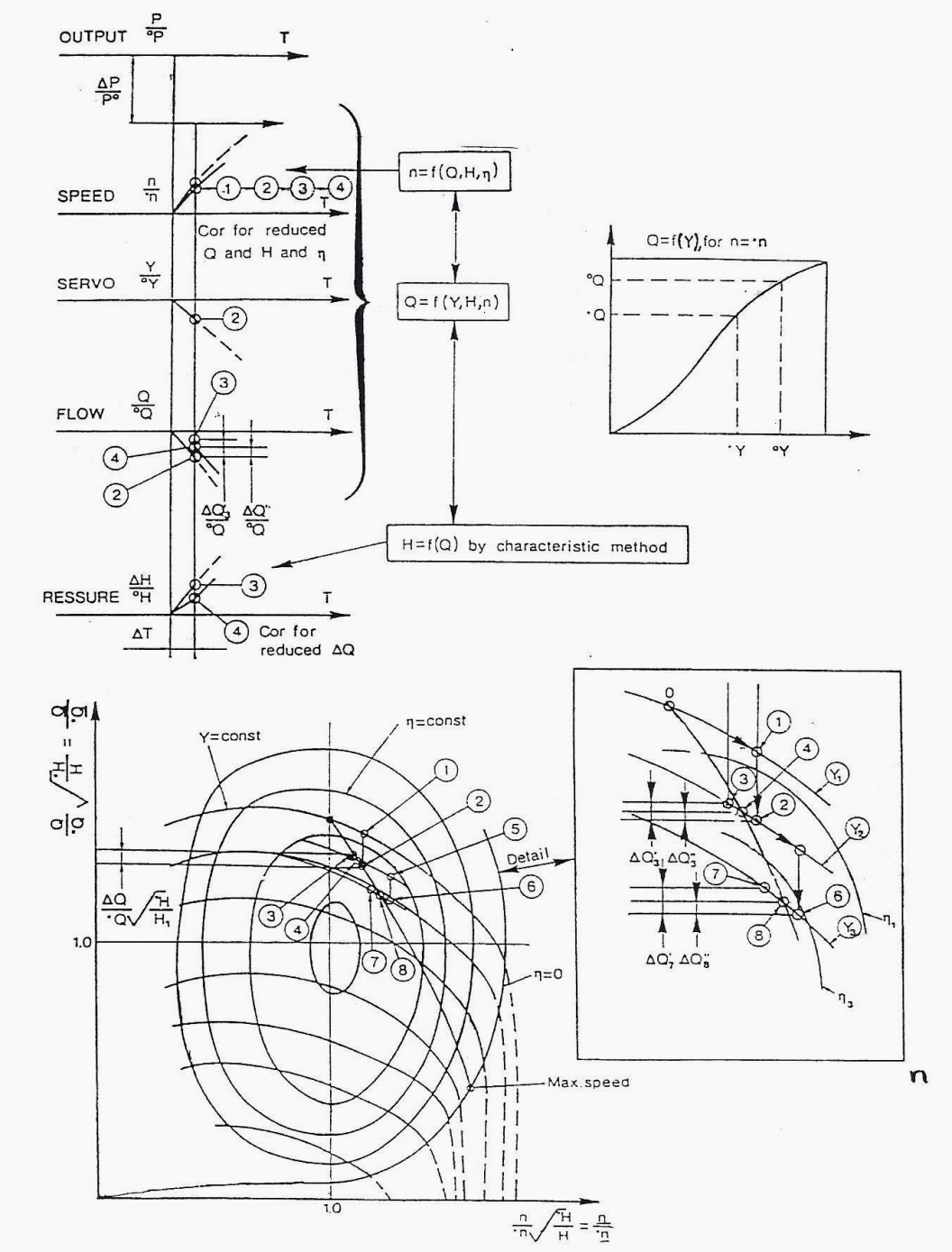

Fig. 12.4 An illustration of the procedure for computing the pressure rise when the turbine characteristics are taken into consideration.

However, simplified formulas may be used in order to calculate the preliminary pressure rise and speed rise. Examples of such formulas which may be developed from Allevis' equations analytically for linear closure with constant speed, will be presented in the following (Ref.10)

Simplified real time calculation of linear closure of turbine gates.

The formulas to be used to determine the closing and opening time for given values of the inertia time constant of the penstock, will be described in the following pages (Ref 10).

Definitions:

$T_w = L^oc/(g^oH)$ (Penstock inertia time), $T_r = 2L/a$ (water hammer reflecting time),
$h_w = a^oc/(2g^oH)$ (Allievi's constant) and $z = 1+\Delta H/^oH$ (Dynamic pressure)

(Here ^{o} a= wave propagation speed denotes nominal full load and H is pressure and ΔH = pressure rise c = steady state velocity and L = length of pipe from turbine to nearest free water level upstream of the turbine.)

The formulas given in the following are developed in detail in (Ref.10) where ΔH is the maximum allowable pressure rise. Note also that the frictional damping is not taken into consideration in the given formulas.

1. Elastic long penstock i.e. $2h_w < (1+z)$
   The closing time for linear closing from 100% opening T_{CL}

$$T_{CL} = Tw\frac{2}{1-z} \qquad (12.8)$$

   Note T_{CL} is negative because $z = \frac{^oH + \Delta H}{^oH} > 1$.

   Also note the maximum value occurs when closing from a small relative opening $(2L/a)/T_{CL}$ after the time = (2L/a) See (Ref.10).

2. The opening time

   Note T_o is positive and $|z|<1.0$. In this case the opening starts from closed gates.

3. "Inelastic" penstock i.e. short penstock $2h_w > (1+z)$

$$T_{c1} = Tw\frac{\sqrt{z}}{1-z} \qquad (12.10)$$

   In this case maximum pressure occurs when closing from largest opening of the turbine governor with closing time = T_{CL}.

* Note that the maximum z value according to eq (12.8) will be obtained with the max. closing speed which is defined 100% closure during the time T_{CL} . However,

maximum pressure occures closure from a small opening with maximum closing speed from which the closing to zero takes the time 2L/a, where L is penstock length and a=wave propagation speed in penstock. The reduction in velocity during this closure will then be $\Delta c = {}^{o}c\ (2L/a)/T_{CL}$.

Then we recognize the following well known formula by substituting for $z=1+\Delta H/{}^{o}H$, $Tw=L\,\Delta c/(g\,{}^{o}H)$ and $T_{CL}=2L/a$ in eq. (12.8).

This formula yields:

$$\Delta H = a\Delta c/g \qquad (12.11)$$

The given simplified formulas may also be used for complex high pressure systems. In such cases the length of the penstock should be regarded from the turbine to the nearest water level in the surge shaft. In case air accumulator is used the nearest water level will be in the accumulator where full reflection of the pressure waves occurs. This will be closer to the turbine than a traditional surge shaft, and excellent regulating conditions will be obtained.

The speed rise of the turbine may also be calculated in a simplified way as follows if the closing time is shorter than the generator inertia time ($T_{CL}<T_a$): Maximum speed will be n and nominal speed is n_n and the following formula may be developed (P_t=relative turbine output, P_g relative generator load and T_a = generator inertia time constant. See (Ref.10).

(Newton's 2. law for rotation)

$$P_t = \frac{\Delta P_t + {}^{o}P}{{}^{o}P} \quad and \quad P_a = \frac{\Delta P_a + {}^{o}P}{{}^{o}P} \quad where \ {}^{o}P = nominal\ \ full\ load$$

$$\frac{n}{n_n} d\left(\frac{n}{n_n}\right) = \frac{P_t - P_g}{Ta} dt$$

$$\varepsilon' = \frac{1}{2}\left(\frac{n^2 - n_n^2}{n_n^2}\right) = \int_0^{T_{CL}} \left(\frac{P_t - P_g}{T_a}\right) dt \qquad (12.12)$$

I.e. by introducing the speed rise constant ε' and after integrating the area as indicated in fig. 12.5 is obtained.

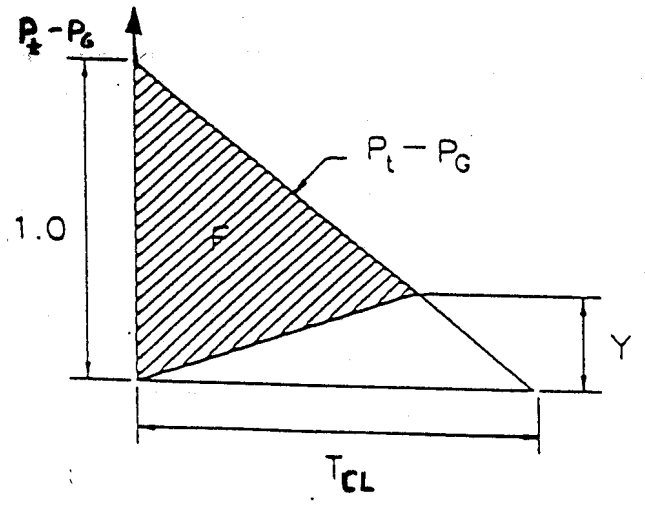

Fig. 12.5 Illustration of the integration of the accelerating torque versus time.

In fig. 12.5 is illustrated the area of the integrated torque=A where the zero efficiency point is taken into consideration in a simplified way. By regarding fig. 12.4 and correcting eq. (12.12) for the influence of zero efficiency, which occurs before total closure of the guide vanes, the following expression is obtained:

$$\varepsilon' = \frac{A}{Ta} = \frac{\frac{1}{2} T_L (1 - Y) ({}^{o}Pa - {}^{o}Pt)}{Ta} = \frac{A}{Ta} \qquad (12.13)$$

Here A = the shaded area in fig.12.5.

The value of Y may be found as follows:

High head turbines H_n>300 m Y = 0.3
Mean head turbines 150m < H_n < 300 m Y = 0.2
Low head turbines H_n < 150 m Y = 0.15

It should be noted that eq (12.13) should be used only if the closing time T_{CL} is equal or less than the generator inertia tima T_a.

Further $Ta=2.74 \cdot 10^{-5} GD^2 n_n^2/P_n$ where P_n=kW, GD^2=kg m^2 and n=RPM

the pressure rise is taken into consideration by multiplying the expression for ε' by $z^{3/2}$, $z=1+\Delta H/H_n$ (eq. 12.8 - 12.11).

Then:

$$\varepsilon' = \frac{A}{Ta} z^{\frac{3}{2}} \qquad (12.14)$$

To calculate the maximum speed=n, from (eq. 12.12).

$$2\varepsilon' = \frac{n^2 - n_n^2}{n_n^2} = \left(\frac{n}{n_n}\right)^2 - 1$$

i.e.

$$\frac{n}{n_n} = \sqrt{1+2\varepsilon'} \quad \text{and} \quad n = n_n + \Delta n$$

then

$$\frac{\Delta n}{n_n} = \sqrt{1+2\varepsilon'} - 1$$

The described theory for a simple analytical analysis of pressure- and speed rise is based upon (Ref. 9) and is described in (Ref. 10).

This chapter has dealt with the traditional lay out. However, in Norway the high head pressure tunnel systems has been introduced due to difficult access for excavating tunnels in our rough mountains were access roads will be expensive and work may be stopped by snow storms in winter.

The high-pressure system will be described in the next sub chapter which contains some examples of our modern high pressure tunnel plants.

12.3 Governor stability analysis

In Norway high pressure tunnels have been excavated for increasing pressure and as a consequence the surge shaft length has increased. Because of the increased length and inertia mass of the water in the surge shaft a relative large portion of travelling water hammer waves passes the shaft junction and will be reflected from the head race tunnel which in turn leads to unstable turbine governing, as mentioned in chapter 12.1. In order to solve this problem the excavated air accumulator surge chamber also denoted as air cushioned surge chamber has been introduced. By means of such surge chambers the distance from the tunnel to the free water level will be short and the water hammer waves from the turbine will be reflected from the surge shaft with only negligible reflection from the upstream tunnel. Also the distance from the turbine to the nearest water level will be short with the air cushioned surge chamber, and an excellent governing stability is usually obtained with such system. In addition fast closure i.e. short closing time of the turbine governor can be obtained with low speed rise without a high-pressure rise. The development of the lay out of high head power plants with the traditional type and the air accumulator or air cushion surge chamber alternative is shown in fig. 12.6.

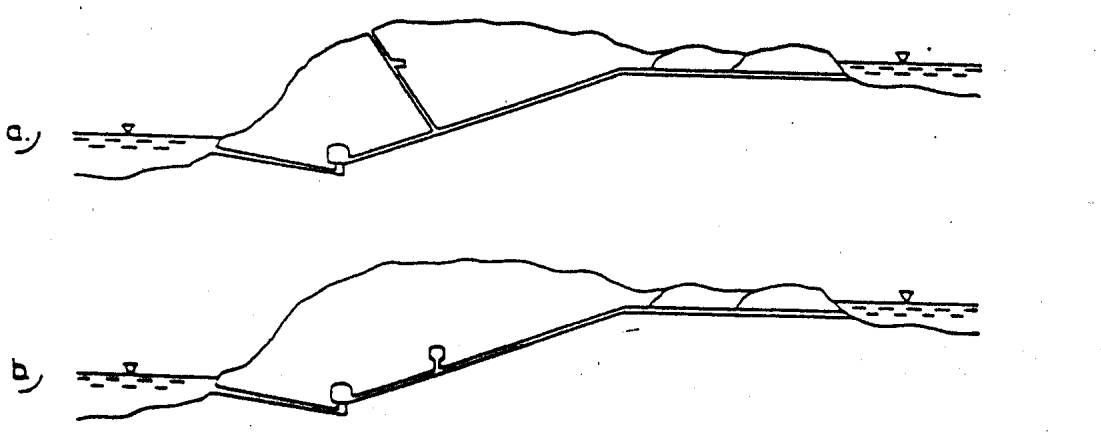

Fig. 12.6 The development of modern high head pressure tunnel plants with a long surge shaft (a) and with air cussioned surge chamber (b)

During the development of the high pressure tunnel systems extensive research work was made on the stability analysis of hydropower plants (Ref. 9).

For the purpose of stability analysis the equations (12.5) and (12.6) have been Laplace transformed and the frictional shear force has been found to be a function of the flow oscillations and the frequency of the oscillations. Such analyses are very complex and will not be described in this book. A full description of such analyses of conduits systems also valid for rough tunnels by using the STRUCTURE MATRIX METHOD is described in (Ref. 9).
The computer programme STABANA was developed for na thotough stability analysis of all kind of Power Plants and the theory has been confirmed by Frequency Response Tests at different types of Power Plants. Other methods are described in (Ref. 16).
It should also be emphasised that the influence from the turbine characteristics must be included to find the correct stability margins (see Ref. 9). However, some rules of the thumb may be established in order to make a brief judgement of the governing stability based on the water inertia constant of the conduit = Tw and the generator inertia constant = Ta with the elasticity constant for the conduit = hw (also denoted as Allievis constant) as a parameter.

The rules of the thumb are:

$$
\begin{array}{ll}
2 \leq hw & Ta/Tw \geq 2.5 \\
1 < hw < 2 & Ta/Tw \geq 3.0 \\
0.7 < hw < 1 & Ta/Tw \geq 3.5 \\
0.5 < hw < 0.7 & Ta/Tw \geq 4.0 \\
0.3 < hw < 0.5 & Ta/Tw \geq 4.5
\end{array}
\qquad (12.15)
$$

These rules are conservative and governing stability on isolated resistive grid could be obtained even by smaller ratios of Ta/Tw if the voltage governor is furnished with a limited adjustable voltage/frequency droop for operation on isolated grid. Also with the pressure feed back system as described in chapter 12.4 stable operation can be obtained with smaller ratios than shown in the formulas given in eq (12.15).

One of the most efficient tests for proving the governing stability is the frequency response test because the frictional damping of oscillatory flow is of great importance and it is difficult to verify the theoretically established frictional term shown in eq. (12.7) by other methods. Results from such test of a complex system are shown in (Ref.9) where complex high pressure conduit systems have been analysed.

The hyperbolic equations (12.5) and (12.6) are functions of q and s = jω. The Laplace transformed equations are (Ref 9) solved by means of the so called STRUCTURE MATRIX method by iteration due to the nonlinear friction factor K = f (q,ω). The basic matrix for a conduit section is shown in eq. (12.16) where the flow direction and pressure are positive as shown in fig. 12.7.

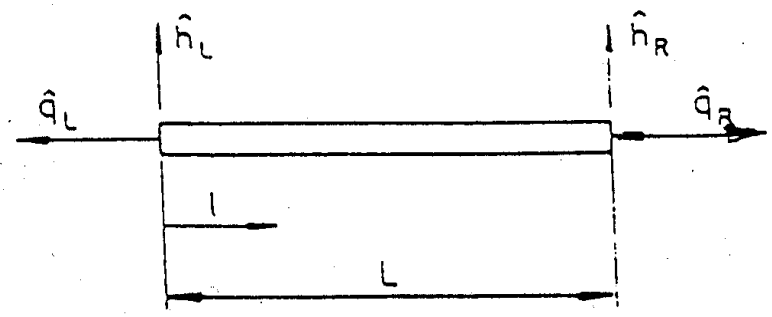

Fig. 12.7 A pipe sections showing the direction of positive flow with positive rising head.

In addition connecting matrices for joints and variation of cross sections have been established together with a matrix for surge shafts and the 7x7 matrix including the turbine characteristics valid for Pelton, Francis and double regulated Kaplan turbine (Ref. 9).

$$\begin{bmatrix} \dfrac{-s}{2h_w z \tanh(Lz/a)} & \dfrac{s}{2h_w z \sinh(Lz/a)} \\ \dfrac{s}{2h_w z \sinh(Lz/a)} & \dfrac{-s}{2h_w z \tanh(Lz/a)} \end{bmatrix} \begin{bmatrix} h_L \\ h_R \end{bmatrix} = \begin{bmatrix} q_L \\ q_R \end{bmatrix} \qquad (12.16)$$

In eq. (12.16) $z = (s^2+Ks)^{0.5}$ where s=jω=Laplace operator

List of parameters for the stability analysis:

K=f(Q_t, A_2, f, ω, Q_o, q)
Q_t= steady flow in regarded conduit
A = cross section
f = Darchy Weissbach friction factor
s = Laplace operator
ω = frequency of oscillation
Q_o= steady state turbine flow
q = _Q/Q_o=dimensionless relative turbine flow amplitude

By means of this briefly described computational analysis system, stability margins of complex power plants can be found and the system can be optimized. In fig. 12.8 the lay out of

the high pressure tunnel system of Kolsvik Power Plant in Norway is shown. In the Kolsvik Power House two 64MW Francis turbines with 600 RPM for 495 m net head have been installed.

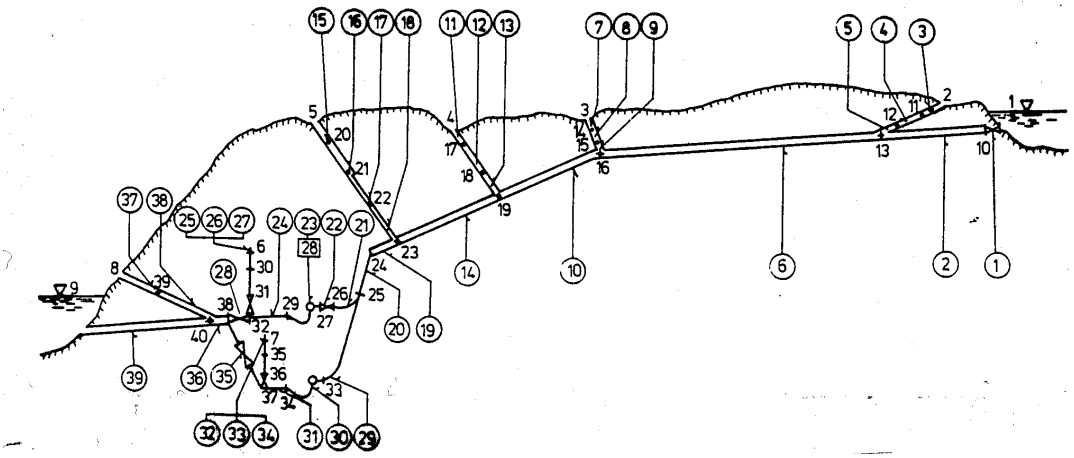

Fig. 12.8 Lay out of Kolsvik Power Plant.

The Kolsvik Power Plant has a high pressure tunnel system with an approximately 700 m long surge shaft. The result from the frequency response test of the pressure/guide vane ratio compared with the computed result (full line curves) is shown in fig. 12.9. In the same fig. is shown the stability analysis to the right where the stability margin is found to be insufficient for operation on isolated load at full load on one machine. (Operation with two machines will decrease the stability margin). The computation is shown in (Ref.9).

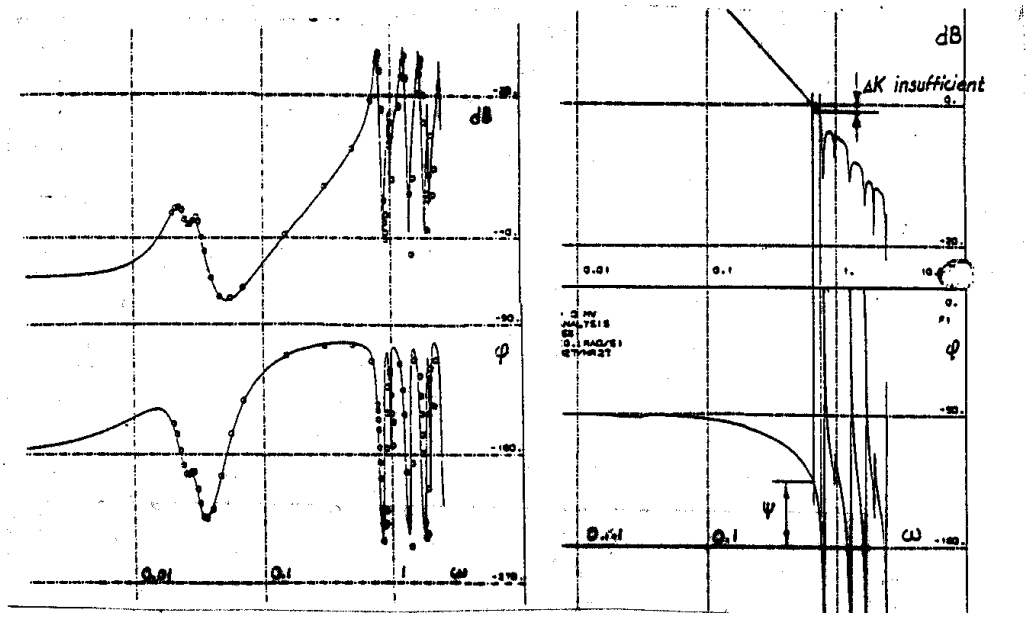

Fig. 12.9 Result from Kolsvik power plant of pressure response of one machine at full load compared with computed result left and the stability analysis right.

For comparison stability analysis and frequency response test from Bratset Power Plant is shown in fig. 12.10 in order to illustrate the advantage of the air accumulator surge chamber. The Bratset high pressure tunnel system has been furnished with an air accumulator surge

chamber with 6000 m^3 compressed air under a pressure of 238 m. W.C. In this plant one 40 MW Francis turbine with speed 600 RPM operating at a net head of 225 m has been installed.

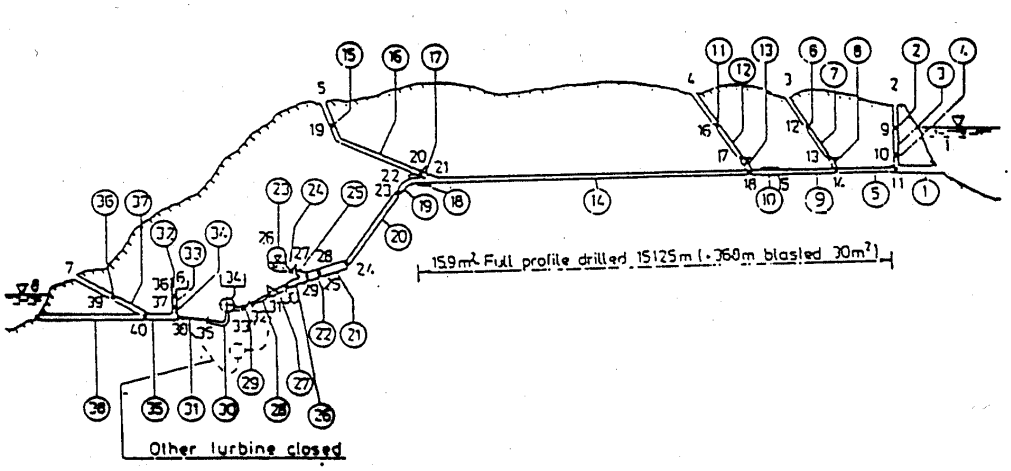

Fig. 12.10 The lay out of Bratset Power Plant.

In fig. (12.11) is shown the result of the frequency response test compared with the computation, left, and the stability analysis based on the same computation parameters to the right shows excellent stability.

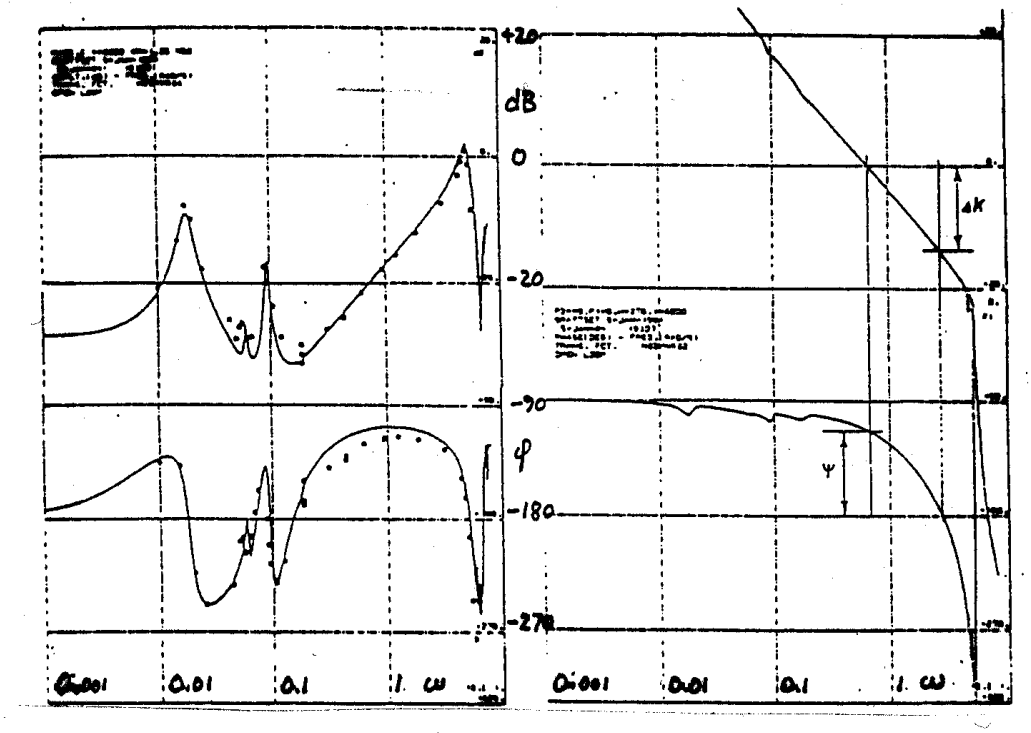

Fig. 12.11 Frequency response test compared with computed result left and stability analysis right.

From the result of Bratset power plant it can clearly be seen that the stability margin is excellent compared with the high pressure system of Kolsvik with the long surge shaft. It should be emphasized that the Thoma mass oscillation stability is very good for Kolsvik. The poor stability is caused by the long surge shaft leading to reflections of the water hammer

waves in the tunnel from the short shafts with surfaces in node no. 3. and 4. in fig. 12.10. In Bratset water hammer reflections are only found from the water level of the air accumulator surge chamber which is in a short distance from the turbine and excellent governing stability is obtained.

The dimension of the air volume can be transformed to an equivalent cross section for a surge shaft by means of eq. (12.17) for small oscillations which is valid for determining the Thoma criterion and the general stability analysis shown in this chapter.

The equation for the equivalent cross section yields:

$$A_{eqv} = \frac{1}{\frac{1}{A_w} + \kappa \frac{H_a}{V_a}} \qquad (12.17)$$

The value of A_{eqv} can now be determined by means of the Thoma criterion by simply using the value of the criterial cross section multiplied by the margin as has been explained earlier.

In eq. (12.17) A_w= water level in surge chamber
κ = polytrophic exponent (1.3 for cold water)
H_a= air pressure in m WC
V_a= air volume in m

12.4 The pressure feed back signal governor.

The development of direct pressure feed back systems has improved the stability of the governing systems. In fig. 12.12 a block diagram is shown for a pressure feed back system of a turbine governing system with the generator connected to a resistive load (e_n = 0). The influence from the turbine efficiency is neglected in this diagram, but is included in the computer program used for the stability analyses.

In the diagram $\varphi = 2h_w \tanh(Ls/a)$ by omitting the friction term K used in eq. (12.5) and eq. (12.16, for comparison of a system with a pressure feed back system and a system without any pressure feed back system . [$h_w = aQ_o/(2gH_oA)$]. The pressure feed back algorithm is denoted by θ. As an example for comparison a system with and without a pressure feed back system, the Pelton turbine power plant (Skjaak) is used (i.e. Q_n = 0 in fig. 12.12) (see also (Ref.9) and (Ref.13)). In this plant a single turbine is connected to a 0.9 m. diameter, 2355 m. long penstock connected to the reservoir via a 5.5 m^2, 1387 m. long tunnel with short 4.8 m^2 surge shaft at downstream end.

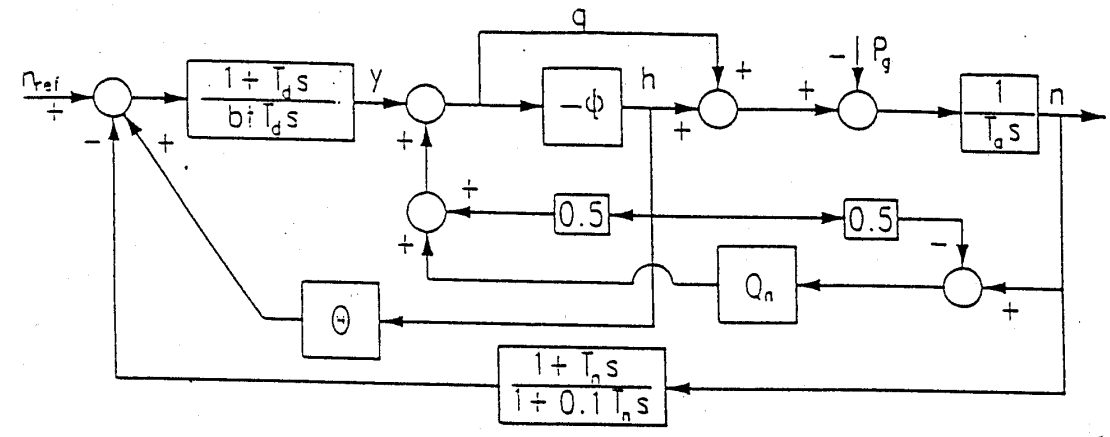

Fig. 12.12 Block diagram including the turbine flow characteristic and pressure feed back system on isolated resistive load for one turbine.

For $Q_n = 0$ the block diagram in fig. 12.12 can be written for the speed response:

$$\frac{n}{n_{ref}} = \frac{(1+T_d s)(1-\phi)}{b_t T_d s[1+0.5\phi[1-2\theta(1+T_{ds})/(b_t T_d s)]]T_a s} \qquad (12.18)$$

By introducing: $0.5[1-2\theta(1-T_d s)/(b_t T d s)] = b$

$$\frac{n}{n_{ref}} = \frac{(1+T_d s)(1-\phi)}{b_t T_a T_d S^2(1+b\phi)} = \frac{1+T_d s}{b_t T_a T_d S^2}\left(\frac{p}{y}\right) \qquad (12.19)$$

The power/guide vane response function my be rewritten as follows [$\varphi = 2h_w \tanh(Ls/a)$]:

$$\frac{p}{y} = \frac{1-\phi}{1+b\phi} = -\frac{1-b}{2b} + \frac{(1+b)}{2b}\frac{(1-2bh_w \tanh(Ls/a))}{(1+2bh_w \tanh(Ls/a))} \qquad (12.20)$$

By using a so called DT1 (derivate one time const.) a pressure feed back element proposed by Prof. G. Lein (Ref. 11) may be used by introducing a constant K as shown in the following equation:

$$\theta(s) = 0.5T_d s/(1+T_H s) = 0.5KT_H s/(1+T_H s) \qquad (12.21)$$

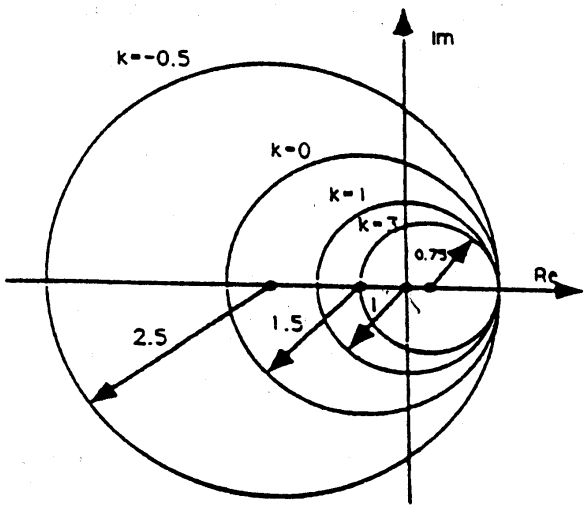

If T_H in Leins model = T_d = the integrating time of the turbine governor, we obtain that b = 0.5(1-K) = const. which allows for an interesting study of the influence from K on the well known transfer function (p/y) obtained for K = 0 i.e. no pressure feed back signal. (See block diagram fig. 12.12)
In fig. 12.13 is illustrated that for increasing values of K > 0 the complex plane plot circle decreases in size, but will always go through the value + 1.0.

Fig. 12.13 (p/y) circle as function of K.

However, by testing the DT1 element with $T_H = T_d$ one will find that the stability margin of the governing system will decrease with increasing values of K in the case of Skjaak power plant, even if the (p/y) circle is reduced in size (see fig. 12.13). Because of this the author of this book and his colleague Dr.ing. **Li Xin Xin** made an improvement of the pressure feed back element as follows: (Ref. 12) and (Ref. 13). Note that $T_N = 0$ i.e.

The improved formula yields:

$$\theta(s) = \frac{K\,T_1 s}{(1+T_1 s)(1+T_d s)(1+0.5s)} \qquad (12.22)$$

For the Pelton turbine at Skjaak power plant T_d = 10 sec, and T_1 = 500 sec. and the result of the (n/n_{ref}) for a DT1 pressure feed back element with variation of the constant K and T_d. From fig. 12.15 it can clearly be seen that the stability margins according to the Nyquist criteria has been improved. The distance to the -1.0 point has increased by the new pressure feed back system when the parameters are optimised.

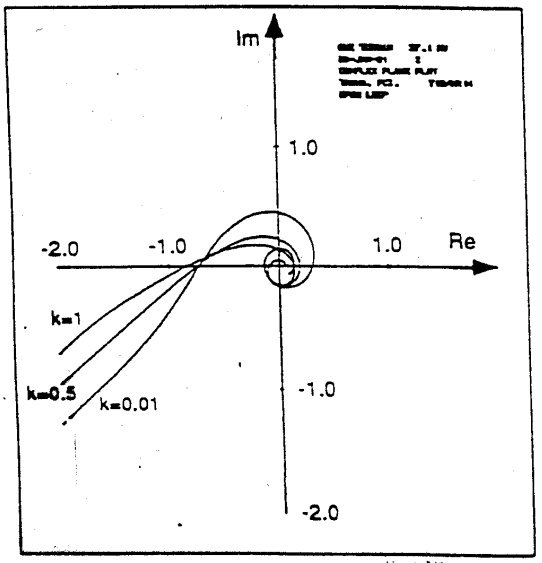

Fig. 12.14 Nyquist diagram for pressure feed back with DT1 element.

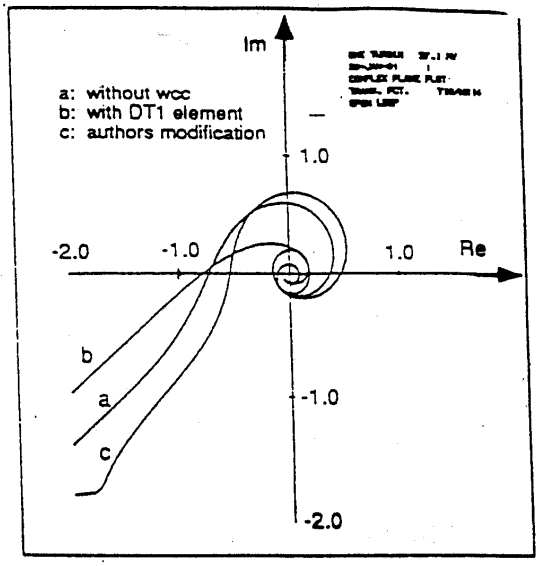

Fig. 12.15 Nyquist diagram for comparison with K=1

For the reader of this chapter it may be of interest that the described pressure feed back system has been installed in SVARTISEN power plant in Norway where the air pressure surge chamber could be omitted due to the improved stability margins obtained saving the cost for excavation of an air cushion surge chamber.

12.5 Pressure reduction by pass system and lay out of deflector control system for Pelton turbines

For a high head Power Plant with long conduit system a by pass system which opens up and by-passes water when the guide vane close, may be necessary to allow for a fast closure of the guide vanes. By means of such system the speed rise may be reduced.

In fig. 12.16 such pressure relief by pass system of Kværner Design is shown. This system is safe and prevents the guide vane servomotor to close fast in case the by pass valve should be stuck and cannot open. The philosophy is that on increased speed rise of the aggregate is less dangerous than a very high pressure rise. However, the hydraulic oil pipe between the servomotor system and the servomotor on the by pass value is vital and must be over dimensioned for safety reason.

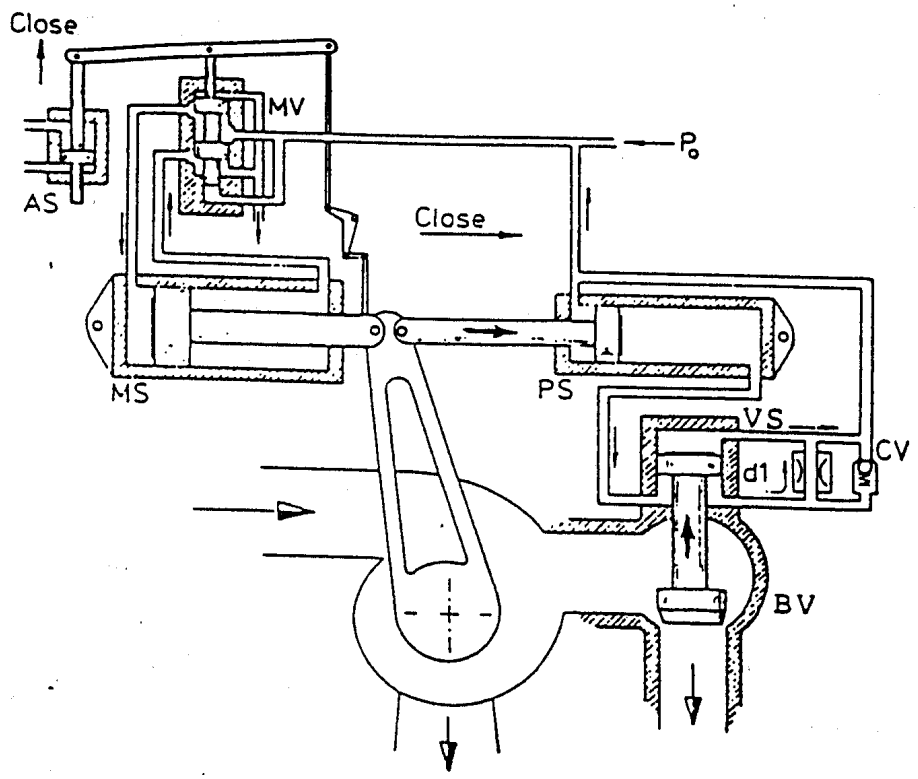

Fig. 12.16 The governor system with by pass valve for a Francis turbine. The energy dissipater sustem of the bypass valve is not shown.

In fig. 12.17 is the influence of the bypass valve is illustrated. It shold be noted that the flow in the bypass valve is influenced by the enrgy dissipater system for the water entering the tailrace system for the turbine. This influence, will not occure if the bypass valve has the outlet as a jet towards an open lake, but that is not the case for a cavern power house. Further the influence from the turbine characteristic is also not included in the principle diagram shown in fig 12.17.

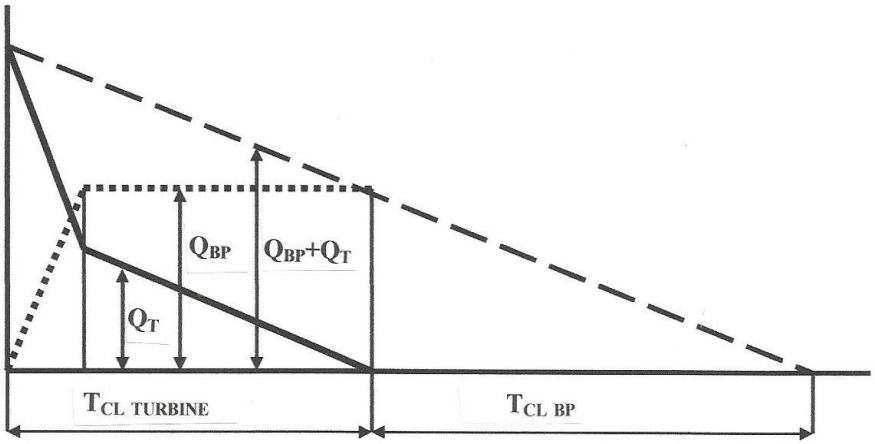

Fig. 12.17 Principple flow charge for a Francis turbine with by pass valve. Note that the reduction in flow of a high head Francis turbine caused by overspeed is not included in the principle diagram shown in this figure.

In fig. 12.18 is shown the double regulating system of a vertical Pelton turbine with deflector control which prevents high speed rise even if the needles are closing slowly. Closing time of Pelton needles may be 20-30 sec. and even longer for extreme lengths of penstock in order to avoid pressure rise above 10%.

It should, however, be emphasized that speed control for minor speed variations at operations on isolated load by using the deflector or cut in type deflector must be avoided. The reason for this is the danger of cavitation damage on the runner and loss in power production due to poor efficiency.

In cases where by pass systems are required a system with energy dissipators must be installed.
In the Pelton turbine power plant BORGUND in Norway, such system has been installed because of the salmon in the river downstream of the cavern power house where a continous flow in the downstream river must be fulfilled also if the power plant is shut down. Such system has been described in chapter 14.4.

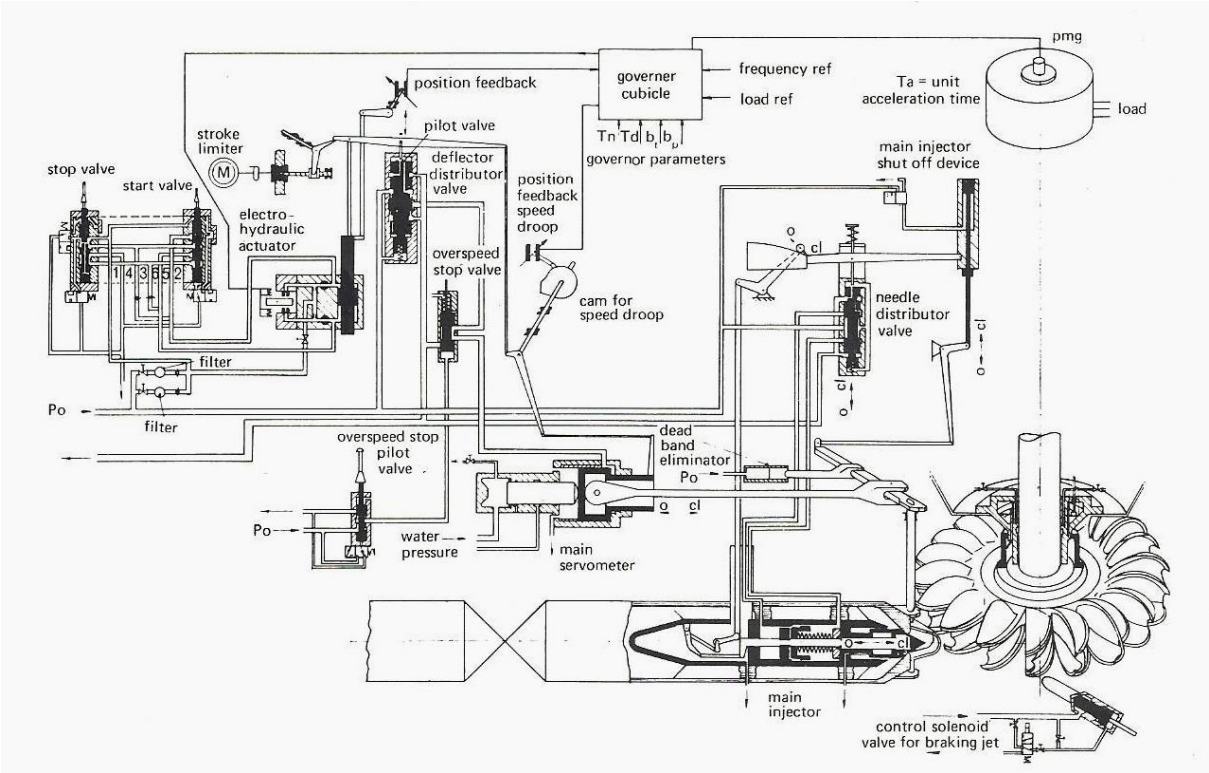

Fig. 12.18 The control system for Pelton turbines. A possible by pass system is not shown in the figure.

13. PERFORMANCE TESTS

Introduction

Performance tests of mechanical equipment for hydro power plants are normally a part of the commissioning of the delivery to the power plant. The equipment (turbine, governor and valves) must be tested functionally so the owner is sure that the performance is in accordance with the guarantee. The field tests should be made in accordance with the IEC recommendation as well as model tests of turbine if the prototype is a low head machine and efficiency test on prototype is difficult to carry out with acceptable measuring tolerances.

Shut down test of inlet valves is also a part of the acceptance tests when required. However, such test should be made after some time of commercial operation when the water has been cleaned from gravel and debris from the construction work.

The reason for this is that the possibility of getting debris, gravel, spikes, welding electrodes etc. jammed in the valves seal is largest in the first period of operation if a valve shut down test with open guide vanes (or needles) on the turbine, is made.

In the following chapter some of the most important performance tests of prototypes and models will be described. Detail information is also available in the IEC recommendation for field acceptance tests and model tests for turbines.

13.1 Field acceptance tests on prototype turbines.

A prototype turbine has normally an efficiency guarantee for certain range of flow or output and head.

Further there is always given an output guarantee for a turbines as a function of the net head. The operation within a given range of head and flow shall be without any damage of the equipment such as cavitation or fatigue fracture. In addition pressure surges and/or speed variations for the governor test shall not be outside the given guarantees. Also noise guarantees for turbines have been discussed. However, such guarantee can not be given by the turbine manufacturer alone, because of possible resonance effects in the supporting structures, and rooms surrounding the turbine which may increase the noise level.

If a machine is noisy (i.e. above 95 dB) a joint venture between civil work contractor, generator manufacturers, consultants and owner should solve problem by insulation if the machine is running safely without any mechanical problem. It should be noted that the noise from generator fans alone normally exceed 90 (dB-A) underneath the rotor i.e. below the roof in the turbine pit.

However, the most important field test for a turbine delivery which always can be measured with sufficient accuracy and calculated tolerances are the turbine output and turbine efficiency* and the load rejection test of the governor.
*(for low head turbines model test are normally used instead of prototype test because of problems with large measuring tolerances of the prototype).

Turbine output versus head

The output of the generator can easily be measured by reading the standard KWh instrument in the power house over a period of time by a stop watch if precision instruments are not available.

The generator efficiency as function of reactive effect cos φ and load can always be obtained from the generator manufacturer or measured at site as part of the generator performance test.

The net head of the turbine can be found by reading the pressure in front of the turbine with precision manometers. Then the velocity head can be calculated by integration by means of following equation using the static pressure or the reading of the hydraulic pressure on the manometer in the first step of calculation.

This equation yields:

$$P = \rho g Q H \eta_t \ [W]$$

or

$$Q = P/(\rho g H_R \eta_t) \ [m^3/sec] \qquad (13.1)$$

ρ = density [Kg/m^3], g = 9.81 [m/sec^2], H_g = [mWC] = reading of manometer or gross head.
η_t = turbine efficiency, P_t = turbine output ($P_t = P_G/\eta_g$ where P_G = generator output and η_g = generator efficiency).

For calculation of the output of the turbine the efficiency guarantee should be used if the efficiency is not measured at site.

A preliminary value of Q can be found by means of the registered generator power and efficiency guarantee of both generator and turbine and the measured pressure at the turbine inlet with the cinetic energy added by means of an approximation of the flow. Furter a correction must be made for the distance from the manometer to tail race level = Z [m].
The velocity can now be found by using the calculated value of Q and the cross section of the pipe at the measuring point by formulas as follows. By repeated calculation three times using the value of Q to find the velocity head C/(2g), a sufficient accuracy will be obtained even for low head plants as shown below.

$$C = Q/(\pi D_p^2/4)$$

The measured head shall then be used to calculate the corrected flow by using

$$H_{RCor} = H_R + Z + C^2/(2g) \ [mwc] \qquad (13.2)$$

By using the corrected value H_{RCor} , a new value of the flow = Q_{cor} can be found.

Then the output of the turbine should be corrected to the head valid for the guaranty of maximum output for the turbine.

$$P_t = \rho g Q_{cor} H_{Rcor} \eta_t (H_n/H_{Rcor})^{1.5} \qquad (13.3)$$

Turbine efficiency

For efficiency measurements following methods are available as listed with remarks as follows:

1. Traditional method with flow measured by current metres
   [Expensive method not practical for large machines with big diameters].

2. Gibsons method or pressure time method.
   [Large inaccurancy, many uncertainties for large diameters and short pipes].

3. Winter/Kennedy methode.(Pressure difference methode.)
   [Large inaccuracy by using the pressure difference for example on the inside and outside the bend in a spiral casing for calculating the flow. In some cases measuring of the flow as a function of the guide vane opening for Francis turbines or needle opening for Pelton turbines gives a better result based on model test results.]

4. The acoustic method.
   [Method under development.]

5. Thermodynamic method.
   [This is the best and cheapest method for measurements of turbine efficiency for heads down to 100 m and with accuracy of +- 0.5% for high head poer plants measurements and +- 1.5% at 100 m head if the temperature is stable. More than 400 measurements have been made in Norway since 1960].

However, it should be emphasised that the price and accuracy of the Thermodynamic method is so favourable that all prototype turbines operating at heads above 100 m should be measured in order to collect data for improved scale effect formulas from models efficiency to prototype measurement.

The only difficulties for the thermodynamic method is if the intake of the conduit system of the plant is shallow or there is a long penstock exposed to sunshine. Especially in tropical countries care should be taken and it is recommended to measure during the night to reduce the temperature variations in the water caused by sunshine.

The principle of the thermodynamic method is the change in specific energy in the water in front of the turbine compared to the downstream side. The difference in specific energy is measured by measuring the temperature difference in the water at the upstream and downstream side of the turbine.
Alternatively the indirect method may be used by bypassing water from the upstream side of the turbine through a throttle, which is adjusted to give the same temperature after the throttle as the discharge water from the turbine. The throttled head compared with the available head then show the lost specific energy in the turbine and the efficiency can be calculated.
The measuring results for the turbine efficiency must be corrected and for leakage losses and mechanical bearing losses etc.
The thermodynamic method and the theory for this method is described in [IEC 41, 1991-11].

Rejection test of the governor

Rejection test is actually a governor test, but the turbine characteristic has also an influence on the result as described in chapter 12.
The governor system and turbine performance will always be tested in a shut down test for each machine normally at 25%, 50%, 75% and 100% load. If overload has been guaranteed a rejection test must also be made at the guaranteed overload.

It should in this chapter be emphasized on high head in power stations with more than one turbine, where part load rejection simultaneously with all machines normally gives higher pressure rise than full load rejection of all machines. [See also chapter 12.]

During the rejection test the maximum pressure should be recorded by fast pressure transducers with short connecting pipes with minimum inside diameter of 8 mm in order to record the real pressure peaks with no unknown damping.
Besides the maximum pressure peak, the maximum speed of the unit must be recorded.

During the shut down test also the minimum pressure in the draft tube should be recorded and special attention should be paid if the distance from the turbine to the water level outside the draft tube gate is long.

The surging of the water level in the draft tube surge shaft of the tail race tunnel in a cavern power house should be carefully analysed. The reason for this is that in some cases a quick uploading following after a full load rejection followed by a repeated rejection, may cause overflow of a cavern power house from the surge chamber. This happend in a cavern power house in Sweeden durig a generator testing some years ago.
In some poerhouses in Norway there are restrictions on the starting up procedure after a full shut down of the turbines. The reason for this is the results from calculations of surgings in long tailrace tunnels showing the possibility for overflooding the power house by starting up all machnes simultaniously a certain time after a full load rejection.

The regulating stability may be tested by means if a frequency response test simply by feeding a small sine wave signal to the governor while the generator is connected to the main electric grid in order to keep the rotating speed constant. The theory is described briefly in chapter 12.

Dynamic performance of the turbines

During commissioning, shaft vibrations and vibrations of guide vanes, head and bottom cover and draft tube cone may be recorded if the dynamic performance is regarded to be poor. Noise level is also often recorded, but as mentioned in the introduction a mutual agreement must be made to include noise the level in the guarantee.

For pressure pusations in a turbine an IEC code somewhat similar to the ISO norms for pumps have been under progress. For low head turbines with large variations in head and load, pressure pulsations may also be part of the guarantee. Runners like the X blade runners which waere developed for Three Gorges Power Plant in China, described in Appendix A1, have proven low pressure pulsations over the whole load domain with large variation in head and flow.

Cavitation

Cavitation may be observed during commissioning as noise. Hydrophone indications seem to be a tool for the future for indication of severe cavitation in an early stage.

The cavitation pitting performance guarantee of the prototype is normally quantified by formulas giving the volume or weight of removed material during a given time of operation. Such guarantee are given in international and national standards (such as IEC or SEN Swedish standard) as the weight or volume of lost material stated in the contract. It should be noted that sometimes cavitation pitting is caused by sand erosion which forms waviness on the surface. However, it is not difficult to distinguish between sand erosion and cavitation in an early stage of damage. Sand erosion gives a sand blasted wavy surface while cavitation starts with pinholes and develops to a sponge like surface in grave stages. A simplified test to recognize the difference between cavitation and sand erosion is to press a finger on to the eroded surface and pull it along the surface. If you are bleeding it is cavitation. In the initial stage, however, the cavitation changes also a shiny polished steel surface to a dark grey surface similar to a shadow with little reflection of light while sand erosion looks like a sand blased surface and you are not normally bleeding after the "finger test".

The cavitation noise is normally not limited in a cavitation guarantee. However, if cavitation noise is observed also cavitation pitting will normally occur which is guaranted.

The cavitation guarantee given by volume of removed material deeper than a certain depth f.ex. 0.5 mm (or weight often calculated by measured volume) will normally be linked to 8000 hours of operation with turbine operation within the guaranteed range of output of the turbine. Recommendation for cavitation guarantee is given in the IEC codes or national codes like the Swedish (SEN) norm or the (IEC TC4) norm.

The turbine load is normally limited not to exceed 100% load and not lower than a given minimum load in many cases. Operation outside the given load limits will normally be limited to a few hundred hours.

13.2 Model test of efficiency and cavitation performance

Background for model testing.

The turbine characteristic diagram with the overall efficiency is normally established by means of model turbine test with flow and efficiency as a function of speed and guide vane openings for Francis turbines and needle stroke for Pelton turbines at constant test head (see fig. 13.1). For Pelton turbines the flow is independent of the speed.

For Kaplan turbines the efficiency must be measured at different combinations of guide vanes angels and blade angels on the runner. Further, both flow and speed will also be a function of head i.e. Q = const.* $\sqrt{H}$ and n = const.* $\sqrt{H}$ and a systematic variation of all parameters must be made during the model test.

It is also convenient to introducing the the so called reduced speed to a head of of 1 m i.e. $\underline{n} = n/\sqrt{2gH}$ and the reduced flow $\underline{Q} = Q/\sqrt{2gH}$ with dimension m^2 also indicating the size of the turbine. Tese use reduced values will be explained later in chaptervalues w
We will then have the influence of the head in a $\underline{Q}$, $\underline{n}$ diagram. (These dimensionless values were introduced by Professor Sundby at the Water Power Laboratory at The Technical University of Norway and presented in reports 1918.)

Further dimensionless velocities $\underline{\mathbf{C}} = \mathbf{C/(2gH)^{0.5}}$ (dimesionless) and reduced flow to 1 m net head giving the size $\underline{\mathbf{Q}} = \mathbf{Q/(2gH)^{0.5}}$ (m^2) have been explained in chapter **16.2** in this book.

Physically we may explain the behaviour of a turbine as follows:

If the speed is increasing above or decreasing below best efficiency speed the efficiency will drop.
In the same way if the head is decreasing at constant speed the efficiency will also drop because the rotational speed is too high for the flow velocity which is proportional to the square root of the head.

The same analysis can be made for the flow.

Further it is convenient to introduce the reduced relative speed and flow as values relative to the best efficiency speed and flow at design head denoted by asterix.

Then we will have on the horizontal axes when knowing $\mathbf{n_{11}}$ is the speed at 1 m net head:

$$\frac{n/\sqrt{H}}{{}^{*}n/\sqrt{{}^{*}H}} = \frac{\underline{n}}{{}^{*}\underline{n}} = \frac{n_{11}}{{}^{*}n_{11}} \qquad (13.4)$$

and on the vertical axis when knowing that $\mathbf{Q_{11}}$ is the flow at 1 m net head:

$$\frac{Q/\sqrt{H}}{{}^{*}Q/\sqrt{{}^{*}H}} = \frac{\underline{Q}}{{}^{*}\underline{Q}} = \frac{Q_{11}}{{}^{*}Q_{11}} \qquad (13.5)$$

The value for the best efficiency point where n = *n and Q = *Q will then be 1.0 on both axes.

In fig. 13.1 are shown four characteristic diagrams for a Pelton turbine, 2 different types of Francis turbines with different specific speed and 1 Kaplan turbine operating at best combination of runner guide vane positions.

The differences in the characteristic diagrams show that for a constant gate opening, the relative reduced flow $\underline{Q} = Q\sqrt{2gH}$ will be constant for variation in speed only for Pelton turbines. Further $\underline{Q}$ will decrease for increasing speed for high head Francis turbines and $\underline{Q}$ shows a slight increase up to best efficiency speed for low head Francis turbines for constant guide vane openings below nominal load. For maximum load the low head Francis turbine show increasing flow up to maximum flow. For Kaplan turbines the flow show a significant increase of $\underline{Q}$ for increasing speed if the runner blades are in fixed position as shown in fig. 13.1 bottom right.

In the diagrams the value Q_{11} and n_{11} have as mentioned above, been used. Q_{11} refers to a turbine with the diameter runner outlet of 1 [m] operating at 1 [m] net head and n_{11} is the speed at 1 m net head.

Then the equations for Q_{11} and n_{11} yield:

$$\mathbf{Q_{11}=Q/(D_1^2\sqrt{H}} \qquad \text{where } D_1 = 1 \text{ [m] and } H_1 = 1 \text{ [m]}$$

And

$$\mathbf{N_{11}=nD/\sqrt{H}} \qquad (13.7)$$

This means that by using relative flow referring to best efficiency i.e. $Q_{11}/{}^{*}Q_{11}$ and relative speed $n/{}^{*}n = N_{11}/{}^{*}N_{11}$ we can use the diagrams obtained by model tests shown in fig. 13.1 also with the head as variable parameter.

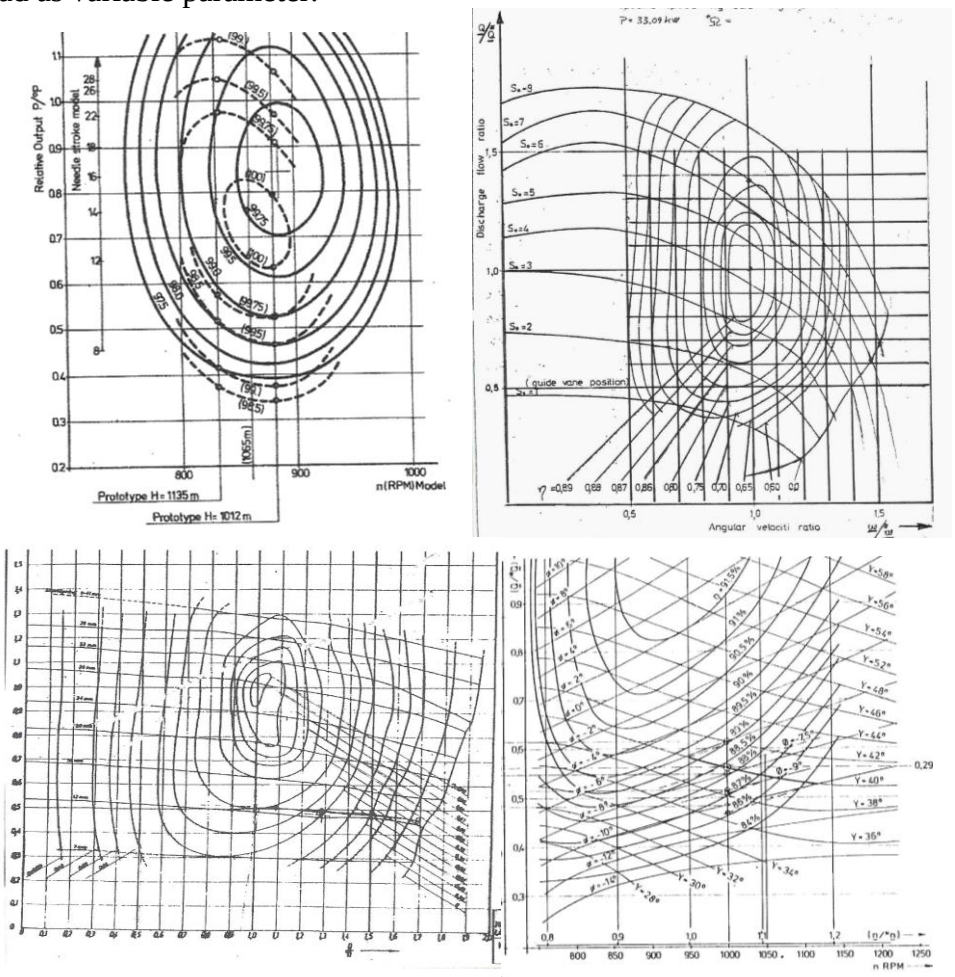

Fig. 13.1 Turbine characteristic diagrams for 4 Norwegian model turbines with Pelton turbine top left compared with prototype measurement at 1012 m and 1135 m, top right shows the efficiency for a low specific speed Francis turbine and bottom right shows the diagramme for a high specific speed Francis turbine and finally bottom right shows the diagramme for a Kaplan Bulb turbine.

By means of model measurements complete diagrams for head variations and flow variations can be made for operational conditions outside what is possible in steady state operation for prototypes. Such diagrams are very useful for determining runaway conditions and the behaviour of the turbines during rejection tests (see chapter 13.1).

[It should be noted that during load rejection tests the correction of the head will be the same along both axes and if no movement of the guide vanes is made the lines for constant position of guide vanes or needles is valid as shown in the diagrams are valid.

However, if the swirl flow of the water in the draft tube may changes the pressure difference from inlet to outlet of the runner. These changes are normally not very large in high head turbines compared to the conduit system and from experience the steady state characteristics can be used with sufficient accuracy for small variations valid for stability analysis around a steady state pint of operation without head corrections.
For computing speed variations during rejection, however, corrections for energy conserved and released from the rotating water should be made for low head turbines and the pressure should be measure just after the runner for very low head turbines like Kaplan and Bulb turbines where the inertia forces from water in draft tube and spiral casings must be taken into concideration.
Research on this problem was presented (Ref 9) where a pressure response test of a Bulb turbine was presented and analysed.

Description of typical laboratory facilities and model testing

Model test are primarily used for development of water turbines in laboratories owned by the industry in order to develop turbines with increased efficiency and cavitation performance. Even if powerful computer programs for CFD flow analysis have been developed, details about non stationary flow in the runner behind the guide vane cascade and draft tube flow are still to be examined experimentally.

Laser Doppler methods, high speed video technique and micro pressure transducers located on the runner blades gives valuable information which may be used for determination of boundary conditions for computation. Further the effect of minor changes in geometry may be found for improvement of the efficiency.
However, performance test of models should be made in a neutral laboratory to prove guarantees given for the user of turbines to be delivered to power plants or model tests carried out as a competition between manufacturers in order to select the best turbine.

At SINTEF/NTNU in Trondheim, Norway a new laboratory was built in 1985 and in fig. 1.2 the test loop in this laboratory is shown*.
The technical data for this laboratory listed below represent a typical modern laboratory:

Pump capacity:	H_{max} = 160 [m], Q_{max} = 1.5 [m^3/sec]
Dynamometer:	P = 320 [kW], N_{max} = 1500 [RPM]
Traceable calibration range:	H : 0-153 [m]
	Q : 0.05-1.5 [m^3/sec]
Water reservoir:	650 [m^3]

*This laboratory has been rented by KVAERNER ENERGY in 1995 and to day by RAINPOWER. The old laboratory at NTNU has be upgraded and is used for student research. In fig. 13.2 the test loop at the laboratory rented by RAINPOWER is shown.

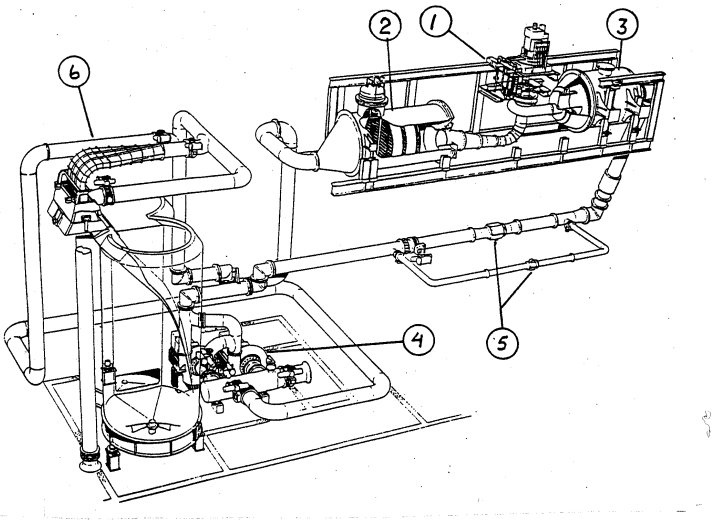

1. Model turbine and dynamometer
2. Pressure tank
3. Low pressure tank
4. Circulation reversible pump turbines for two ways flow
5. Flow metres, high capacity and low capacity loop
6. Flow calibration tank

Fig. 13.2 Test loop at the turbine laboratory, own by the research organization at the Norwegian University of Science and Technology.

For model testing the pressure difference across the model turbine is kept constant by speed regulation of the pumps, which may run in parallel or series according to requirement of pressure and flow.

The suction pressure is controlled by the water volume in the system and the air volume in the suction side low pressure tank.

The turbine speed is normally kept constant for each measuring point by torque control of the generator/motor. [Pump models may also be measured by running the generator/motor in motor mode. In such case the reversible pump turbines in the pump section (4) are running as turbines in order to have a controlled throttling of the pump pressure].
The efficiency is calculated by reading the torque and speed versus the flow and pressure difference across the turbine. Then following equation yields

$$\eta = \frac{T\,\omega}{gHQ} \tag{13.8}$$

where the measured values are:

T = torque [Nm]
ω = speed [rad/s]
gH = specific energy [Joule/kg]
Q = flow [m^3/sec]
ρ = density [kg/m^3]

[Temperature and air content in the water is controlled and measured for determining the density ρ]

The torque is automatically registered by stresses in a thin filament which is calibrated by dead weight. The speed is registered by digital reading consisting of a notched rotating disk and an electromagnetic gap indicator.

The pressure differential transducer is calibrated by a dead weight manometer.

Finally the flow is measured by the electromagnetic flow metres which are calibrated in a weighing tank with a flow diverter, operated by a fast pneumatic servo system controlling the filling time of the tank.

All tolerances of the calibrating units are traceable by international standards.

Cavitation testing facilities

The cavitation tests are made by lowering the system pressure so the pressure on the low pressure side is decreased towards vacuum. The efficiency is measured for each step by decreasing the pressure for fixed guide vane position, speed, flow and pressure drop across the turbine. The pressure must be lowered until critical pressure is passed and the efficiency drops.

In order to compare the nominal positive suction head NPSH of model and prototype it is convenient to use the ratio between NPSH and the net head which is denoted the Thoma cavitation number σ. The σ value for the model can then be calculated from the measured pressures at the turbine inlet and draft tube outlet referred to the reference height on the model according to the IEC standard (see also chapter 9.2).

$$\sigma = \left(\frac{NPSH}{H} \right)_{model} \qquad (13.9)$$

With the measured σ value the critical setting H_s for the prototype can be calculated as shown in fig. 13.3.

However, the nuclei content and content of air in the water has a great influence on the measured value of σ in a model.

Further the contents of silt in the water at site for the prototype has also an influence because the nuclei content is increased by the silt. The lowest value of σ will be obtained in the laboratory if the water is degassed.

For safety reason it has been recommended to use degassed water and then inject nuclei into the water with until the highest σ value is obtained. However,to the authors knowledge the experts on cavitation have so far not agreed upon a standard which includes nuclei injection. Thus the majority of the laboratories have no nuclei injection systems. Then natural air saturated water has been regarded to be the best alternative by many laboratories for model tests so far. This is because degassed water gives a lower value of σ and less margine for the prototype if plant σ is based on the model test.

A scale effect of the Thoma cavitation number σ has so far not been proved, then the σ value for the prototype is regarded to be the same as for the model. For real cavitation test the

Froudes number should be the same both for model and prototype. However, this requirement may lead to an unrealistic low head for the model turbine, so in many practical cases the Froude requirement is not fulfilled.

A general description of cavitation testing in laboratory

The cavitation requirements are, besides the efficiency requirement, the most important requirement for the turbine design.

The cavitation performance may be divided into two different main parts

- Cavitation test on model turbine where the cavitation is indicated visually and measured qualitatively by the influence on efficiency as a function of the draft tube pressure.

- Cavitation pitting measured as loss of materials on prototype turbine (see chapter 13.1).

Cavitation test on model turbine

Cavitation tests on model turbines forms the basis for the cavitation guarantee for turbines. In turbine contracts a model test to prove both efficiency and cavitation is often required. Because the runaway speed is also influenced by the cavitation, runaway speed test of the model with draft tube pressure adjusted to the minimum pressure at site is also required in order to prove the maximum runaway speed guaranteed.
The draft tube outlet pressure is measured at the draft tube outlet and the kinetic energy is calculated based on the measured flow and cross-section area of the draft tube at the measuring point. The Nominal Positive Suction Head (NPSH) is defined as described in chapter 9.2 and in the IEC code.

The measured value of NPSH of the model which will be valid as the $NPSH_R$ for the prototype can be used for calculation of the necessary submergence Hs_o of the prototype as follows:

The equation for NPSH yields:

$$NPSH = h_b - h_{va} - H_s \text{ and } NPSH = H \cdot \sigma_{model} \qquad (13.10)$$

For the model tests however, the value h_b is decreased below atmospheric pressure in the model test loop and thus the value of NPSH can be decreased until cavitation occurs and the Thoma cavitation constant σ can be calculated by keeping the net head H=const.:

$$\sigma_{model} = NPSH/H \qquad (13.11)$$

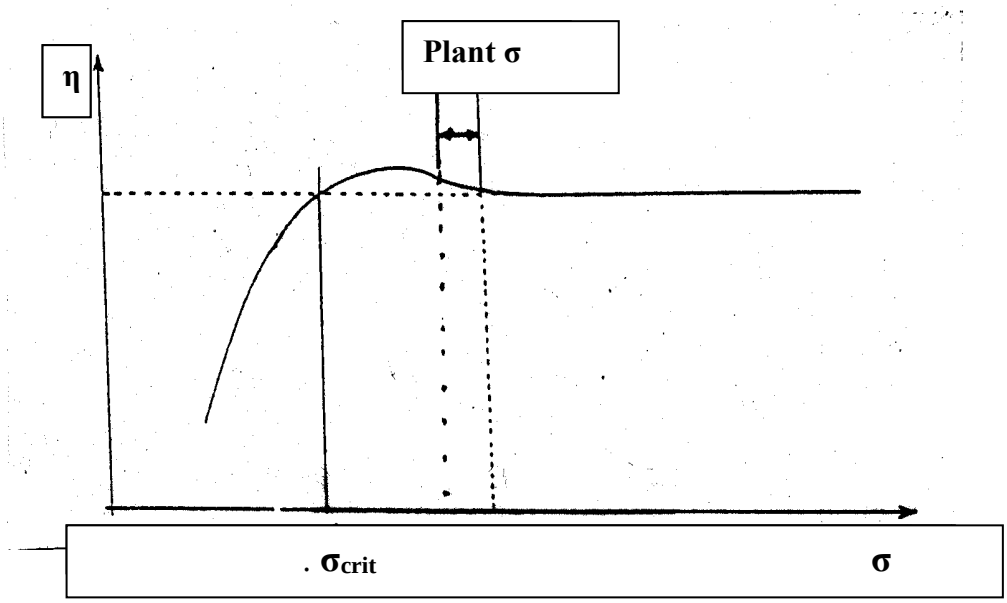

Fig. 13.3 Illustration of the critical value of $\sigma=\sigma_{crit}$ and example of choice of σ plant.

The critical value of σ is defined to be the value where the efficiency drops below the efficiency measured with large values of σ where no changes in efficiency occurs for a variations in σ (see fig. 13.3). If σ is decreased below the critical σ_{cr} the efficiency will drop sharply. (σ_{crit} may also be defined as the value where 1% efficiency is lost (see IEC codes)).

It should be noted that the initial cavitation often leads to a slightly increased efficiency for values of σ slightly larger than σ_{cr}. The reason for this may be found in the tiny initial gas bubbles from the cavitation formed on the blade is serving as a lubrication on the blade surfaces in the turbine and thus reduce the friction loss.

If cavitation is starting near the blade outlet with no cavitation near the leading edge an increase of efficiency may not occur for values of σ close to σ_{cr}.

The safe value of σ and NPSH for a turbine will be a value larger than the value where no increase or decrease in efficiency is measured by decreasing σ. It should be emphasized that even if an increased efficiency is measured for values of σ a little bit large than σ_{crit} serious cavitation pitting may occur especially for high head machines with high velocities. The safety margins must be chosen by studying the values of the velocities in the turbine runner and observe where the cavitation occurs. If the cavitation occur just on the outlet edge of the blades or in the draft tube cone below the runner smaller margins to the critical value of σ may be used.

<u>Cavitation requirements on the model turbine calculated from power house data of the prototype in the water.</u>

The cavitation performance requirements on the prototype is found by calculating the value of $NPSH_A$ of the plant. Note: If the power house is located at high level for example 2000-3000 m above sea level the barometric pressure may be in the order of 2-3 m lower than at sea level where h_b □ 10 m W:C. The variation of the vapour pressure h_{va} is less than 0.5 m for the normal range of temperatures.

The plant σ must be calculated from the planned submergence of the prototype turbine in the power house in order to decide the requirement for the model turbine. The submergence of the turbine is often decided by asking various turbine manufacturers for preliminary cavitation guarantees or by the judgement of technical advisors from experienced consulting engineers.

Runaway testing

Runaway test with zero torque should be measured during a normal model performance test. It should be noted that the runaway speed normally increases with low values of σ. Because of this runaway tests should be run at the lowest values of plant σ.

Pressure surge testing of model

Some contracts contain requirements of dynamic tests of model. In such case a free water level is required on upstream side of the penstock which must be built in the same scale as the model. Also the draft tube outlet of the model must end in a tank with constant pressure and with free water level.

However, in a model testing it will normally not be possible to obtain a correct generator inertia and the electric grid with voltage governor homologous to the prototype. Thus a dynamic surge test of a model built with different relative lengths and flexibility in the conduit system and different inertia of generator and electric load cannot be valid for the possible surging in the prototype.

Conclusion

The model test is valid for following performance tests:

Efficiency test.

Runaway test.

Cavitation test.

[Further test may be discussed, but it is doubtful about the validity of other tests].

13.3 Efficiency scale effect from model to prototype

The efficiency guarantee is one of the most important guarantees of performance. For high head turbines it is possible to measure the efficiency by means of the Thermodynamic method with an accuracy of less than plus-minus 1%. In some cases the efficiency on the model turbine is also guaranteed.

Between the model and the prototype there will be an increase in efficiency because of the decreased friction due to increased dimensions and pressure i.e. increased Reynolds number (Re). The increase in efficiency or scaling up effect of the efficiency has been discussed and is

expressed in the new IEC code for hydraulic machinery valid for Francis turbines and reversible Pump Turbines.

By installing new runners in old turbines the rough surfaces in the old parts of the prototype must be taken into cocideration.
The model should have a smooth surface in all parts.
For a new Francis turbine the different losses may be presented as shown in fig. 13.4

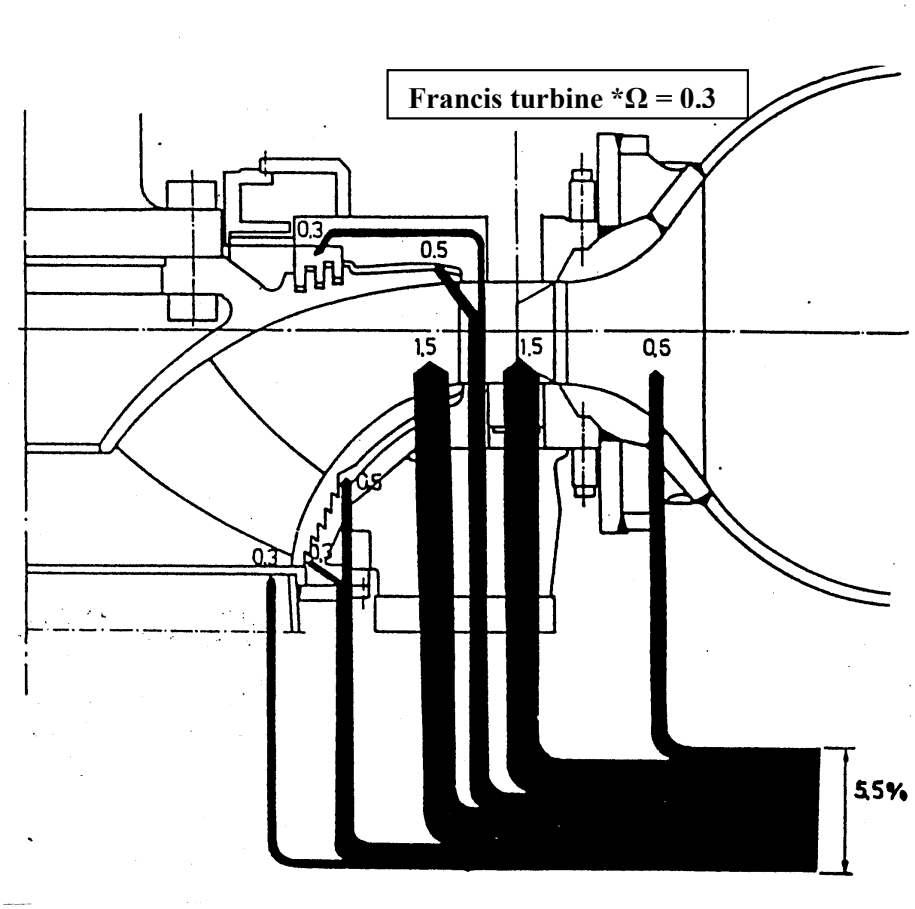

Fig. 13.4 Loss distribution for a high head Francis turbine at best efficiency operation. Losses are partly measured and partly calculated based on the measured total efficiency.

When comparing the efficiency of a prototype with the efficiency of a very well polished model strict tolerances and geometric similarity between model and prototype is required. In fig. 13.5 is shown result of around 20 measurements of prototypes compared with model turbines. The results show a larger scale effect of prototypes (from small to large) than from model to prototypes. The reason for this may be found in a rougher finish and larger clearances and geometric inaccuracy of prototypes than of model turbines made for efficiency acceptance tests.
The scale effect formula in the old IEC Publication 193 and 497 yields:

$$\Delta\eta_\eta = (1 - \eta_{\eta OPTM})V_M(1-(Re_{uM}/Re_{uP})^{\alpha}) \qquad (13.12)$$

Fig. 13.5 also shows a difference in the efficiency and scale effect depending on the end-clearance between guide vanes and the facing plates of upper and lower turbine cover. A difference in efficiency of approximately 1% may be expected with differences in clearances found in turbines made with normal workshop variation in production. This can be seen from fig. 13.5 and (Ref. 5).

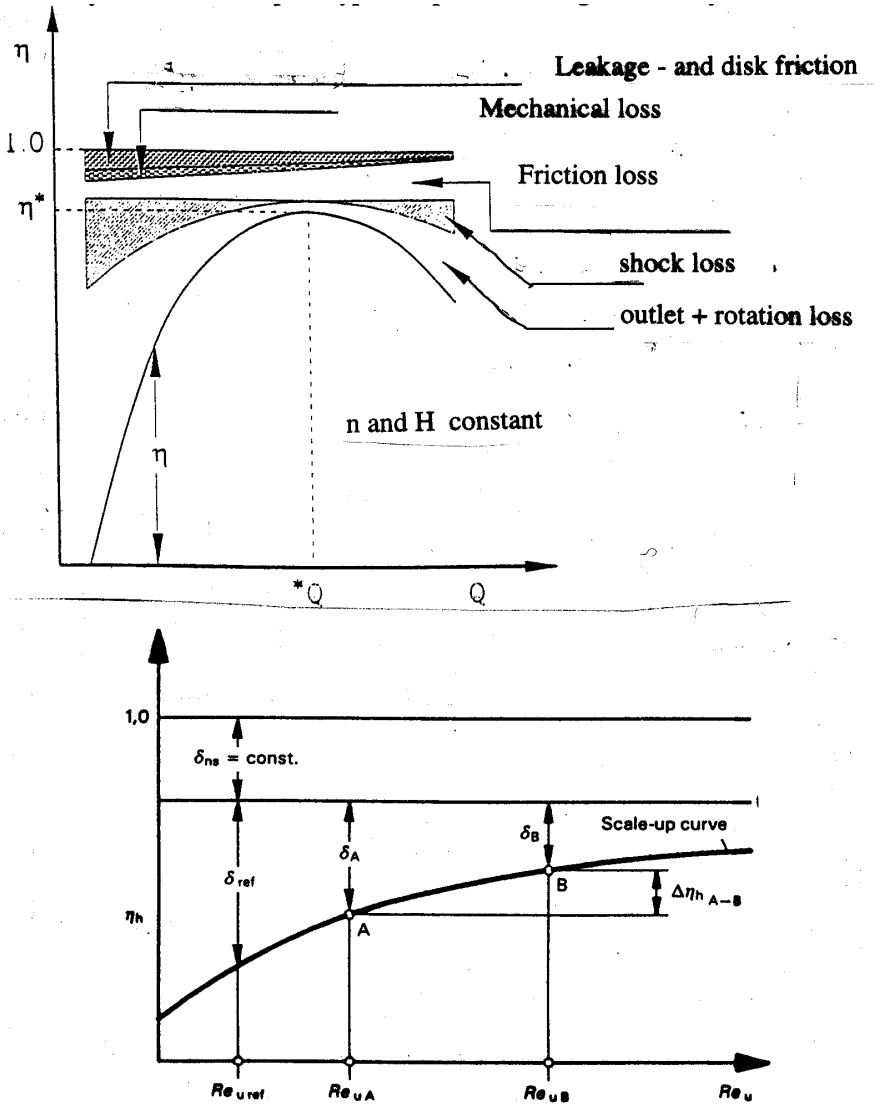

Fig 13.5 Loss distribution (top) and relative scalable losses as function of Reynolds number Re. δ_{ns} = non scalable loss and δ_{ref}, δ_A and δ_B are scaleable losses which are depending on Re. referring to $Re_{u\,ref}$ value and A and B values of Re respectively.

The deviation in scaling up test of splitter blade runners compared with the measured efficiency of model and prototype was the reason for not accepting the scale effect equation. 13.12 from the standard for runners of special design. In the TC4 Work Group 18 (WG 18) the work was aiming at a development of formulas for a scale effect formula based on scaling the separate losses in reaction turbines. The new scale effect formula will then be depending on specific speed and geometric parameters for the turbine design such as blade length. In addition runners with low efficiency shall not get the high weight of scaling up the

efficiency as in the old IEC 995 where a bad runner has a larger scaling up of the efficiency than a good runner. In addition the influence from roughness of old parts with rough surfaces in an old turbine with a new runner installed was not taken correctly into concideration in the old IEC Scale effect code.

The draft for a new scale effect formula has been in progress and was published 2011 with a final correction at the IEC meeting in 2012. As mentioned above the new formula is based on calculating separate losses and thus the scalable friction loss is divided in flow friction loss (denoted as specific energy (J/kg)) E_{lf} and Kinetic energy loss E_{lk} and the disk friction loss (loss in power (W)) P_{Ld} etc. as illustrated in fig 13.6.

The flow friction loss can be calculated as a function of Re for different parts of the turbine with the roughness of both model and prototype taken into consideration. The disk friction loss can also be calculated separately as a function of Re.
The main advantage with the new formula is that the scalable friction loss is calculated separately depending on the roughness on the different parts on both model and prototype.
In fig. 13.6 an illustration is given in flux diagram showing the different losses which are the base for calculation of the different losses in model and prototype depending on scale and roughness IEC 62256. It should also be noted that some losses are not depending on the turbine flow.

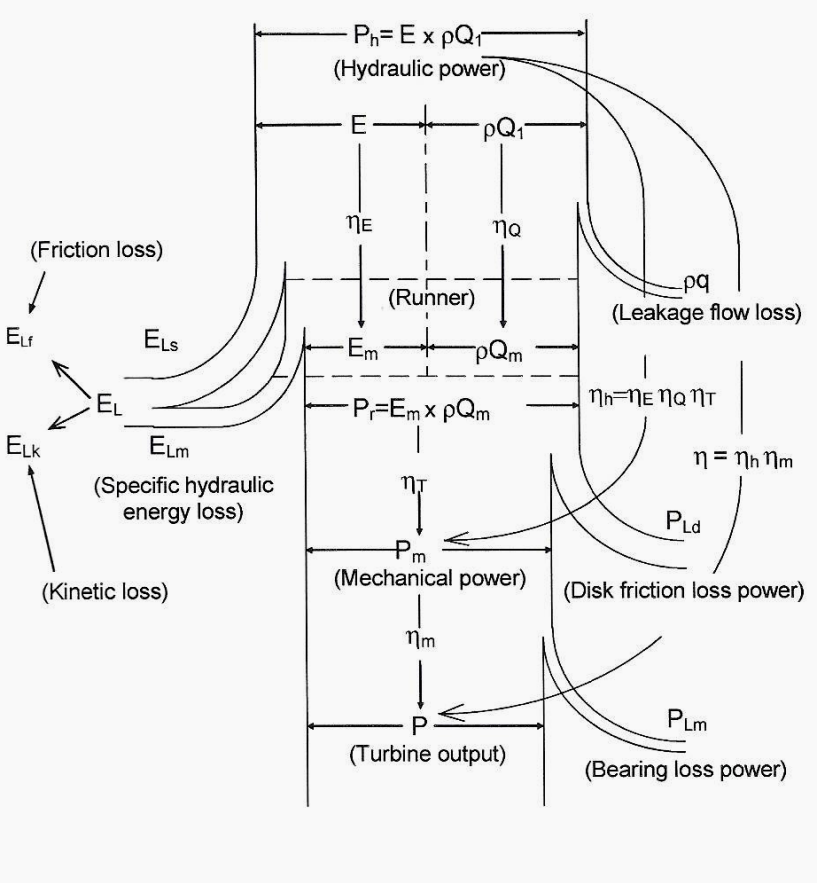

Fig.13.6 Diagramme illustrating the separate losses used in the new IEC code for Step-up of the efficiency from Model to Prototype. (Ref. IEC 62097 code.)

14. INLET VALVES AND BY PASS VALVES

14.1 Introduction

SPHERICAL VALVES are normally installed in front of Pelton turbines and high head Francis turbines inside the machine hall in Norway and Sweden. For low head Francis turbines BUTTERFLY VALVES are used for heads down to 30-50 m. For very low heads where Kaplan- or Francis turbines are used inlet valves will not be installed in front of the turbine. Instead the intake gates are designed for rapid emergency closures.

Before about 1960 SLUICE VALVES were used for high head turbines. Nowadays sluice valves are rearly used except for very small mini turbines in cases were this type of valve is the cheapest choice among mass produced valves. The draw back of large sluice valves is high price and high loss of specific energy compared to losses in the spherical valves.

For by pass systems HOLLOW JET or annular valves are normally used for large capacity flow. NEEDLE VALVES are used for drainage of penstocks. A small needle valve is also installed in a by pass line of the main inlet valve of high head plants for pressurizing the spiral casing before opening the main valve. Normally a sluice valve is also installed bolted on the flange on the main inlet pipe in series of the needle valve to be operated for maintenance of the needle valve and bypass line. Bypass systems are installed for the purpose of balancing the pressure on upstream and downstream side of the main valve before the opening. For low head plants sluice valves without any needle valve are normally used for drainage and bypass systems because this type of valves have the smallest leakage problems and are normally drop tight. In addition the danger of cavitation damage is small at low head during opening and closing.

In addition to the valves mentioned above, specially designed automatically controlled valves for the by pass system of the main inlet valves, have been designed. As an example SEAT VALVES are formed as the valves in a car engine with spread outlet flow are installed at the turbine inlet in the by pass system of high head turbines. The reason for using seat valves instead of needle valves is that a concentrated jet from a needle valve may lead to erosion and cavitation damage. Such bypass valves are used for Pelton turbines and high head Francis turbines. The outlet of the bypass system is normally located near the outlet of the main valve upstream of the expansion joint at the spiral case inlet.

In the following chapter a brief description will be given of different types of inlet valves and by pass valve systems for a high head plants.

14.2 Spherical valves

Normally the spherical valves consist of a split valve body bolted together with heavy flanges enveloping the valve rotor.

However, the valve body may also be made in one piece by joining two halves by welding after premachining of the rotor and the valve body halves as explained in the following description. The advantage of this design is that seals in a split between two halves are avoided. Then the problems with the joint between the split seal and the seals around the end flange connections are avoided. In addition this design leads to an improved stress distribution which is important for valves operating at high pressures.

The spherical valves for high head turbines, produced by KVAERNER before 2002 when nthe company was bought by GE, are usually of the fully welded type as shown in fig. 14.1 and fig. 14.2.
In the following a description will be given of the fully welded “one pice valve” because this type of valve is not often described in the literature.

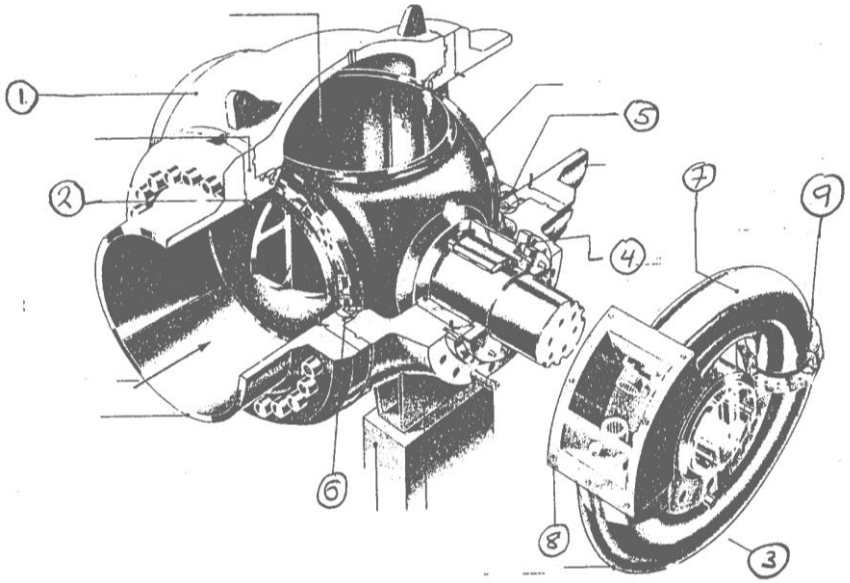

1. Valve body
2. Rotor
3. Servomotor (annular type)
4. Trunnion bearing
5. Main valve seal
6. Maintenance seal
7. Servomotor annular piston
8. Servomotor lever
9. Servomotor seal

Fig. 14.1 Split view of a one piece spherical valve.

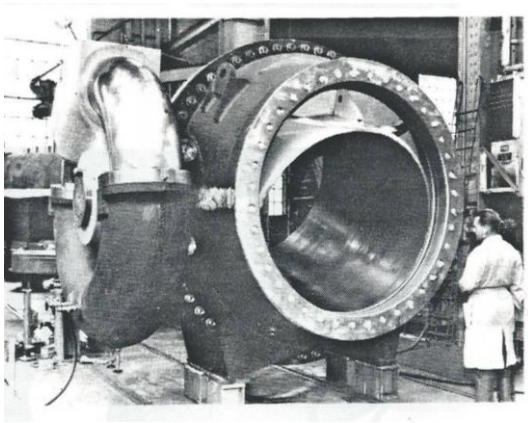

Fig. 14.2 Photo of a spherical valve in the workshop.

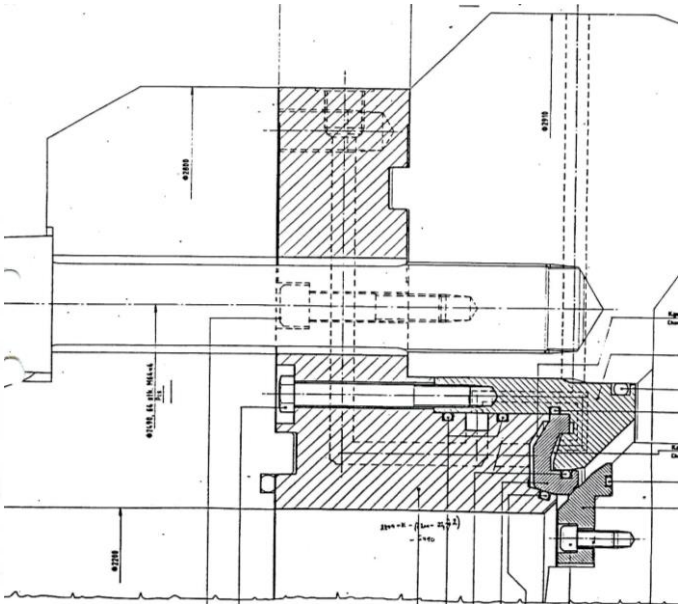

Fig. 14.3 A flexible steel seal will compensate for possible eccentricity of the valve rotor in open position. (Mesitas Power Plant in Colombia)

The one piece valve body is as described made of two pre-machined sphere halves welded together to one piece as shown in fig. 14.1 and fig. 14.2. The halves of the main body are welded together enveloping the rotating member which is locked in correct fixed position relative to the valve body by distance pieces in the trunnion bearing housing during welding. After welding and stress relieving the rotating member is rotated to half open position for sand blasting and painting before the final machining. (For a complete repainting of the inside surface of the valve the rotor also has to be rotated to a half open position).

The final machining after welding starts with machining of the trunnion bearing support in the valve body and the trunnions of the rotating part. The rotating part is held in fixed position by welded studs on the outlet and inlet of the valve during this machining process.

Before machining of the seal supports on each end of the main body, the trunnion bearings have been mounted and the valve rotor is locked in open position by the annular servomotors that must be mounted before this machining process starts. (See fig. 14.1)

For heads higher than 400 m for Pelton turbines the valves may be furnished with a flexible steel seal ring actuated by water pressure. Compared to an ordinary sliding rigid steel seal the flexible seal will adjust itself in case of eccentricity or wear of the seat ring on the rotor. Possible danger of cavitation damage is then reduced. (See fig. 14.3). For Francis turbines the pressure in the spiral casing will not be zero during closure of the valve seal due to the rotating runner during the stopping procedure. Even if the turbine governor does not close the guide vanes the pressure in the spiral casing will be maintained at approximately 50% by the rotating runner at rated speed dropping gradually as the speed drops. Then a rubber seal can normally be used for high head Francis turbines with no damage of the seal. The maintenance seal on the upstream side may also be a rubber seal for both Pelton turbines and Francis turbines. This seal is closed only during maintenance and inspection of turbine and the valve.

The water pressure actuated rubber seal is shown in fig. 14.4.

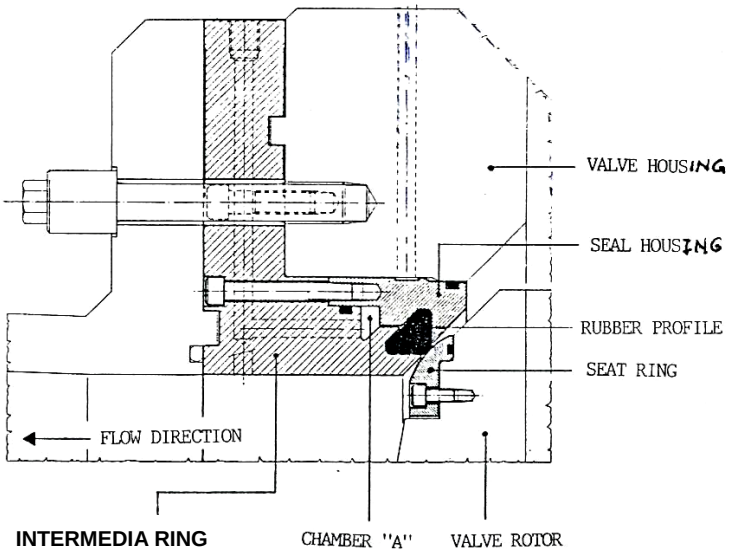

Fig. 14.4 Rubber valve seal for spherical valve. (Inflatable with water pressure)

The control system for a high head spherical valve is normally actuated by water pressure from the penstock. The water is carefully filtered by a filter system with a stand by filter for redundancy. Very good reliability has been obtained.

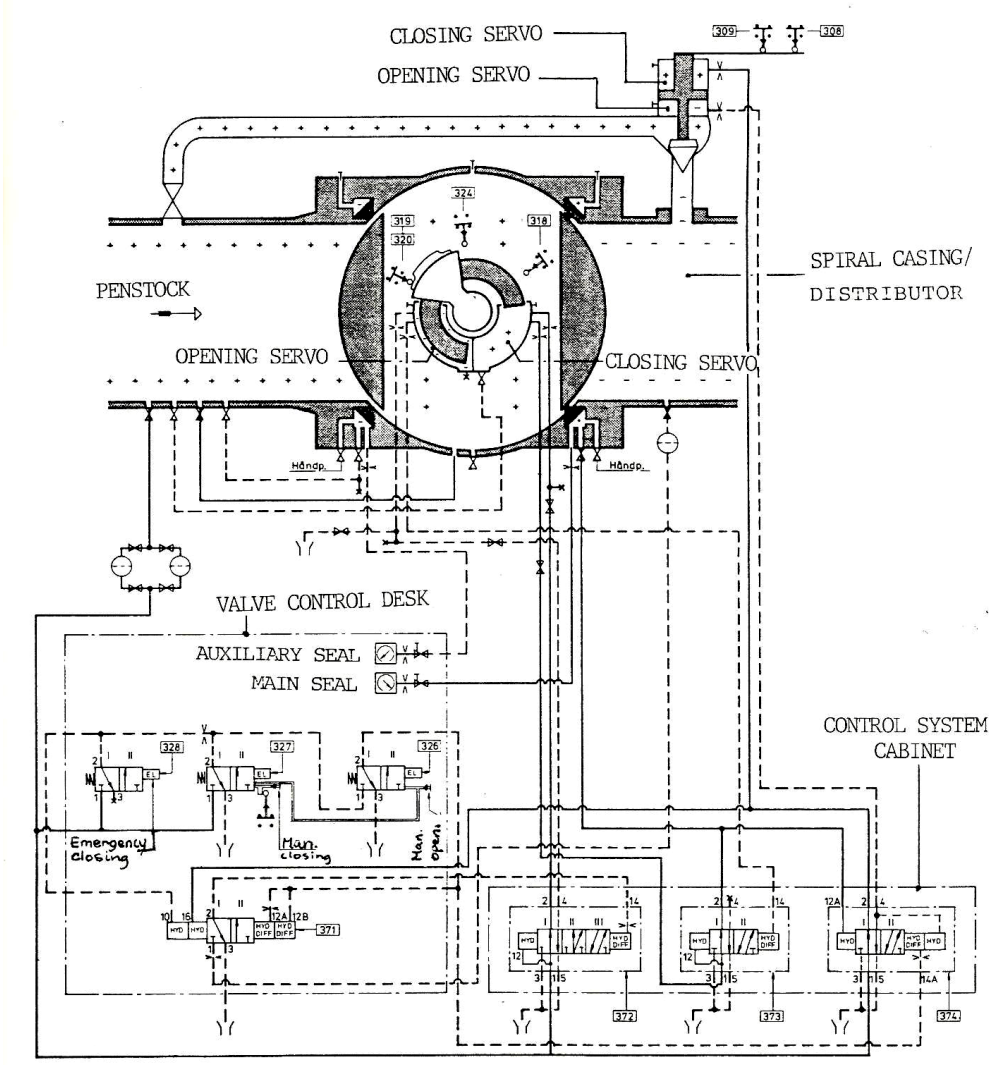

Fig. 14.5 Control system for a spherical valve actuated by water pressure from the penstock

14.3 Butterfly valves

The butterfly valves have gradually been developed for increasing head with increasing thickness of the blade. However, during the last 35 years the casted hollow streamlined thick blade has been substituted by a design with an open frame supporting a thin blade disk. This design has been called LATTIC BLADE BUTTERFLY VALVE. The development of the LATTIC BLADE butterfly valves compared with the thick hollow blade valve for high head up to 200 m is illustrated in fig. 14.6.

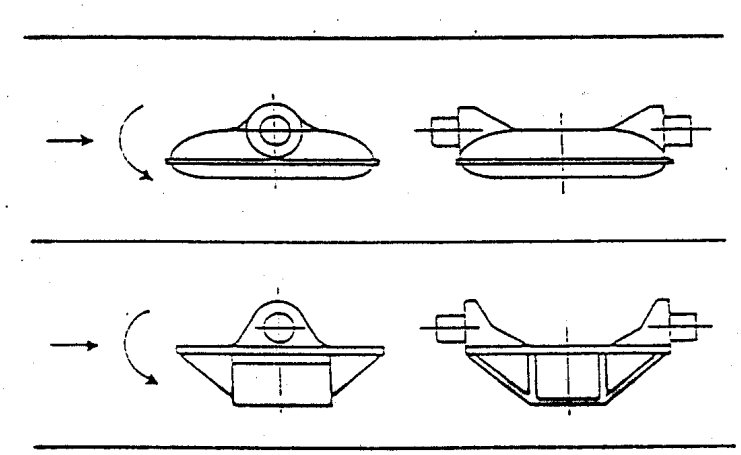

Fig. 14.6 Casted blade design compared with fabricated open frame blade of the Lattic blade butterfly valve

In fig. 14.6 is shown a design of a butterfly valve with integrated trunnions, which requires a split valve housing. However, valve blades with bolted trunnions and nonsplitted valve housing has also been introduced, but this design will not been described in this book. In fig. 14.7 a split view of a high head butterfly valve is shown.

The servomotors for butterfly valves are operated by oil pressure because of the low penstock pressure where these valves are used.

For a safety closure a prolonged servomotor lever is always furnished with a dead weight in case of lost oil pressure supply. The torque from the lever is transferred to the disk trunnion by shear pins. This design of shear pin joint is also normally used for spherical valves.

The total load from the water pressure in closed position is transferred through the trunnions in the same way as for spherical valves. The bearings may be grease lubricated or furnished with a Teflon lined bearing shell which is self lubricated or water lubricated.

The trunnions are positioned eccentric to the disk in order to obtain self-closure of the valve driven by hydraulic forces towards closed position and towards the valve seal seat during the last movement towards closure.

The servomotor system and the eccentricity of the trunnions must be carefully balanced for safe operation and to prevent an accelerating closure towards closed position caused by too strong hydraulic forces. In addition a throttling of the the servomotor control valve towards closed position to reduce the closing speed, is necessary to prevent high water hammer pressure waves. Butterfly valves are also normally used mounted near the inlet of the penstock operated as isolating valvees equipped with a flow velocity sensing control system designed for automatic closure by abnormal high water flow in case of penstock rupture. (See description in chapter 2.)

1. Valve housing
2. Valve disk
3. Rubber seal with support ring
4. Stainless valve seat ring
5. Stopping support
6. Bearing
7. Servomotor lever
8. Servomotor
9. Dead weight for closing

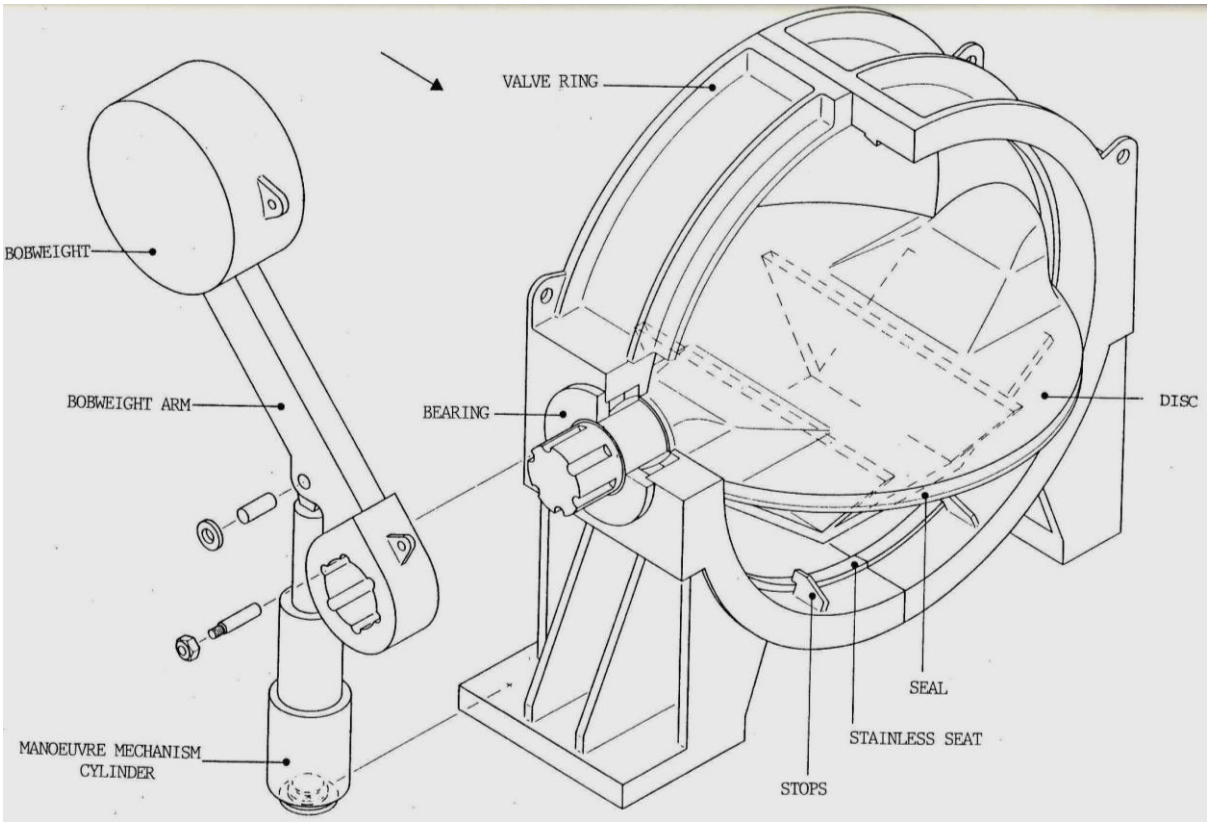

Fig. 14.7 Split view of a fabricated lattic blade butterfly valve.

14.4 By pass valve systems

The most commonly used valve type for by pass systems are the hollow jet type (also named annular valve).

(Similar type of valves has also been used as inlet valves in front of high head Pelton turbines and has also been built integrated with and in front of the straight flow injectors for multi nozzle vertical Pelton turbines. (Ref. Mauranger Power Plant in Western Norway manufactured by CHARMILLE 1970)

For low pressure power plants the hollow outlet jet from these valves may be directed into a tail race tunnel or directed out of the power house along the outlet channels with protected areas closed for admission in open air power plants.

However, for high head plants a throttling system must be mounted downstream of the valve in order to build up pressure downstream of the valve seat in order to avoid cavitation damage, noise and vibration.

A hollow jet valve with a multihole multistage throttling system mounted on the downstream side of the valve is shown in fig. 14.8. This by pass system is able to operate at 1000 m pressure or higher depending on the number of stages. However, it is important that the diameters of the holes through the throttling plates are increased for each stage in flow direction in order to avoid clogging with full pressure over the last stages. Nevertheless even the last stage should be designed for the total pressure drop in "filthy" water for safety reason.

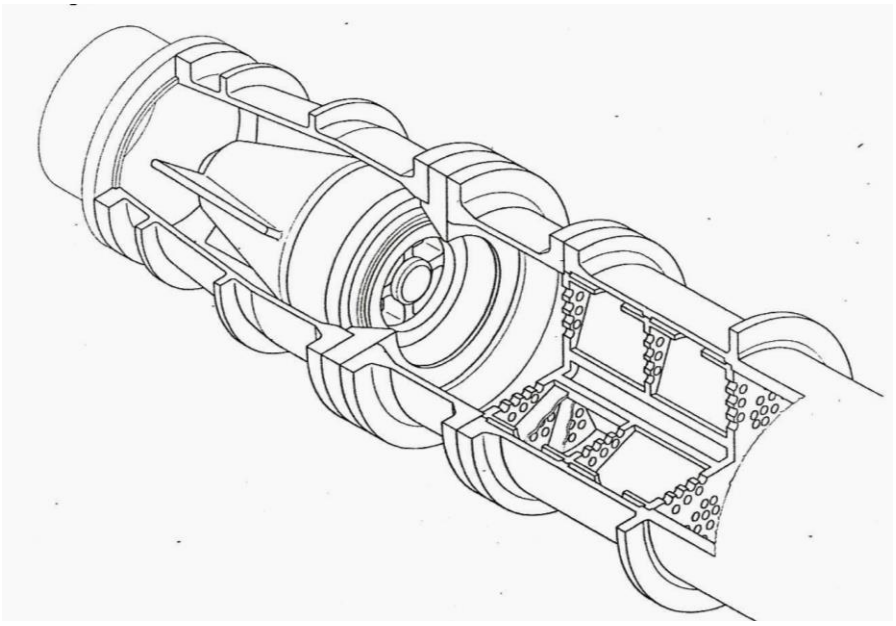

Fig. 14.8 Hollow jet valve with multihole, multistage throttling system for high head operation

The design of a high pressure hollow jet valve consists of a servomotor valve body with the movable cylindrical valve body with a flexible steel seal ring which in closed position forms a drop tight seal against the stationary stainless valve seal (see fig. 14.9)

The valve seal ring is bolted to the outer valve body consisting of a cylindrical and conical shaped outer pipe. Fins connect the servomotor valve body to the outer pipe by welded joints. Oil supply is lead from outside to inside through drilled holes in one of the fins.

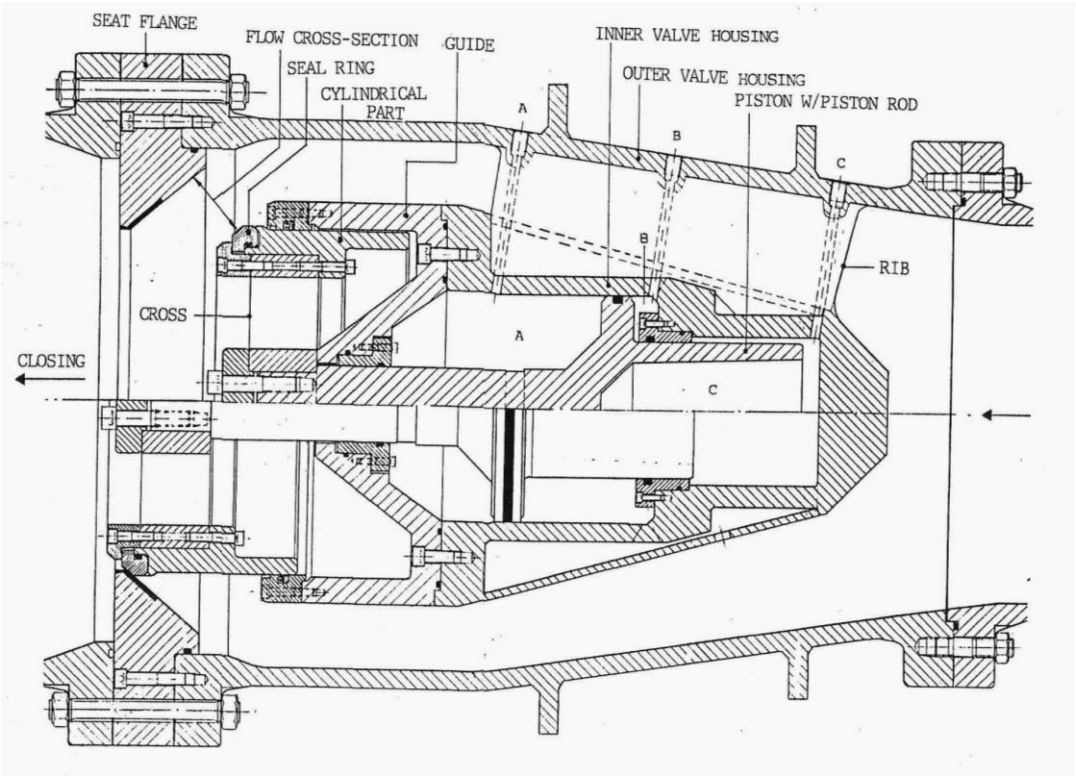

Fig. 14.9 Hollow jet valve for high pressure operation.

The hollow jet valve shown in fig. 14.9 is a typical high-pressure valve with thick walls.

The low pressure valve design is in principle similar to high pressure valves, but the wall thickness will be decreased and the dimensions will increased. For low pressure valves the deformations caused by the water pressure will be the dimensioning factor. Special attention must therefore be taken for the clearance of the seals between pos (4) and (5) in fig. 14.9. The cylinders (4) and (5) must also be designed for buckling due to external pressure and care must be taken during design to avoid buckling
for valves with large dimension and thin plates.

Other remarks should be that all movable parts in the seal system must be made of stainless steel or bronze. The seal rings and seats must also be made of stainless steel of different hardness to avoid galling. The difference in hardness should be 70 BH to be on the safe side. Austenitic steel quality should be avoided.

For low pressure valves the movable seal ring may be made of rubber while the seal seat ring will be of stainless steel also in this case.

14.5 Self excitating pressure oscillations caused by flexible valves and flexible seals.

(Note! A detailed theoretical development of the presented equations in this chapter is given in Chapter 17 in this book.)

Self excitated pressure oscillations may occur in valves or in needles in Pelton turbines or guide vanes for pump turbines during starting in pumping mode caused by flexibility in the structure.

Such oscillations may be very dangerous and they may occur caused by the flexibility in valves or gates both located upstream and downstream of penstocks or tunnel systems.

A simple analysis in the frequency domain may be used to find the criterion where self-excitated oscillations occur.

By means of a block diagram shown in fig. 14.10 following equation (including the flexibility of the valve opening as a function of the pressure variation $[\, d(\Delta A/A)/d(\Delta H/H)\,]$) yields:

$$\hat{h}/\hat{A} = \frac{-j2\,h_w \tan(L\omega/a)}{1 + j(\frac{1}{2} + \partial\hat{A}/\partial\hat{h})2\,h_w \tan(L\omega/a)} \qquad (14.1)$$

(The theory is further developed in chapter 17 where the basic theory for pressure responses in the frequency domain is explained.)

Here $\hat{h} = \frac{\Delta H}{H}$ *and* $\hat{A} = \frac{\Delta A}{A}$ where H = the pressure difference from upstream side to downstream side of the valve and A = the cross section of the opening which gives the leakage flow and H = the steady state pressure.

$\partial\hat{A}/\partial\hat{h}$ = the relative increase in leakage opening versus relative increase in pressure.

From eq.(14.1) we find that if:

$$(\partial\hat{A}/\partial\hat{h}) \rightarrow -0.5 \text{ then } (\Delta H / H) \rightarrow \infty \text{ for } (L/a)\omega = \pi/2, 3\pi/2, 5\pi/2, ...$$

This can simply be expressed as follows:

IF THE LEAKAGE OPENING IS <u>DECREASED</u> BY 50% OR MORE FOR 100% <u>INCREASED</u> PRESSURE DIFFERENCE ACROSS THE VALVE, DANGEROUS SELF EXCITATED PRESSURE OSCILLATIONS MAY OCCUR.

Because of the frictional damping the critical value may be $\partial\hat{A}/\partial\hat{h} \leq -0.55$ or -0.6 instead of the value -0.5 for frictionless flow as shown in eq. (14.1). See also fig. 14.1.
Experiments at the Water Power Laboratory at The Norwegian University of Science and Technology have proved the theory.

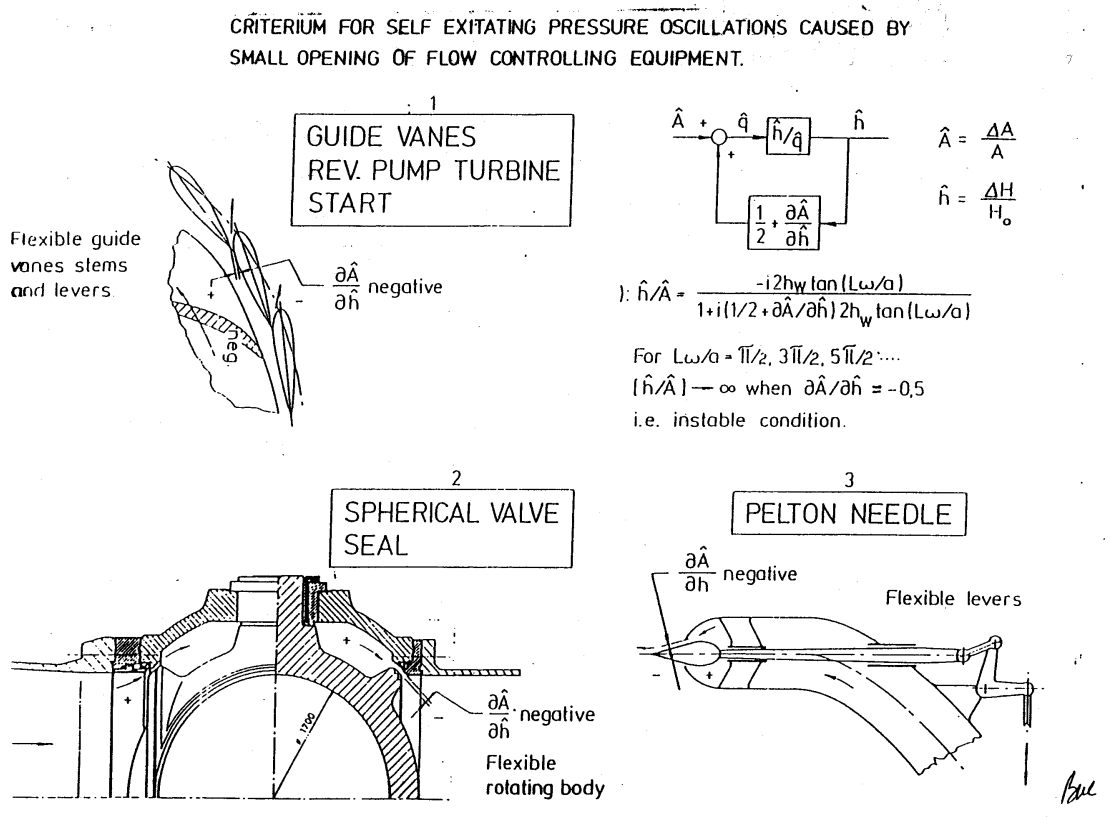

Fig. 14.10. Various criteria for self excitating pressure oscillations.

To prove the criterion for self exitared oscillations a 300 m long 90 mm diameter pipe was intalled in the Water Power Laboratory at the Norwegian University of Science and Technology in 1992.

A flexible valve with closing tendency for increasing pressure was designed for the MSc. work of student Morgan Rydell and tests were made with the valve connected to the end of the 300 m long pipe. (Later Li Xin Xin and Blørnar Svingen included tests with with the flexible valve in their PhD work.
In fig. 14.11 the flexible vlave designed with a flexible plate to obtain decreasing opening for increasing pressure from upstream side to downstream side. At small openings self exitated pressure oscillations occurred at $\partial A \partial h \leq$-o.55 in all tests of the valve connected to the described pipe.

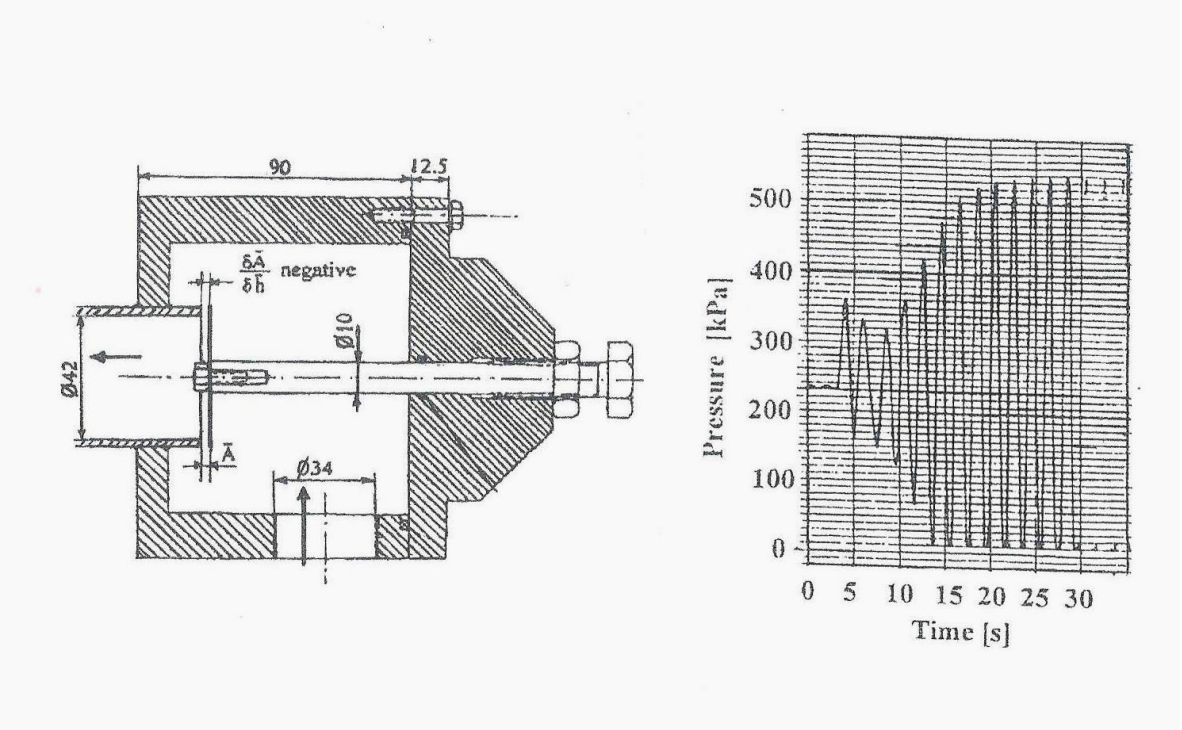

Fig. 14.11. Left: Principle drawing of the described flexible valve where the valve disk will be bent towards the valve seat by the pressure difference between upstream and downstream side and thus reducing the opening at increasing pressure.
Right: Recordied pressure oscillations when the valve opening is decreased to critical opening.

15. POWER HOUSE ARRANGEMENTS AND HYDRAULIC FORCES TRANSFERRED TO THE FOUNDATION.

15.1 General arrangement for Pelton, Francis, Kaplan- and Kaplan Bulb turbine power plants.

This chapter deals mainly with the layout of cavern Power Plants for high head turbines, but examples of Kaplan and Kaplan Bulb turbines are also described.

Inside the high head cavern power houses in Norway there are normally an expansion dismantling joint in front of the turbines downstream of the inlet valve so the hydraulic force from the valve is transferred to the pressure shaft via the penstock flange. Both vertical multi nozzle Pelton turbines and vertical Francis turbines are normally designed with the distributor or spiral case respectively, embedded in concrete.

By this design the hydraulic pressure force on the inlet cross section of each turbine is transferred to the rock walls in the downstream side of the powerhouse through the concrete which are reinforced specially towards the inlet flange of the turbine.

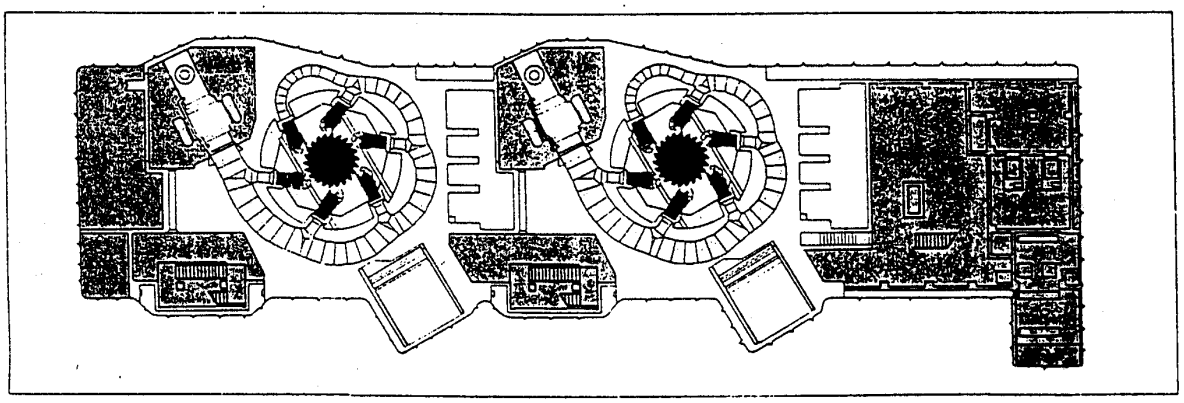

Fig. 15.1 Arrangement for Aurland I power house where 3 identical units are installed.
The turbine data are: P = 243 MW, H_n = 840 m,n = 428.7 RPM (The last unit was installed 20 years after the two first units. This unit is not shown, but is located in the extension of the power house excavated in a later stage to the left).

In fig. 15.1 an arrangement for vertical Pelton turbines is shown and in fig. 15.7 detail for the inlet supporting collar is shown (see chapter 15.2).

The arrangement of the turbines with the penstock branching pipes in an angle different from 90° on the length direction of the excavated powerhouse allows for a minimum width of excavation. This design also reduces the span of the overhead crane rails. This design is favourable specially in difficult rock where it is important to keep the width of the power house on a minimum.

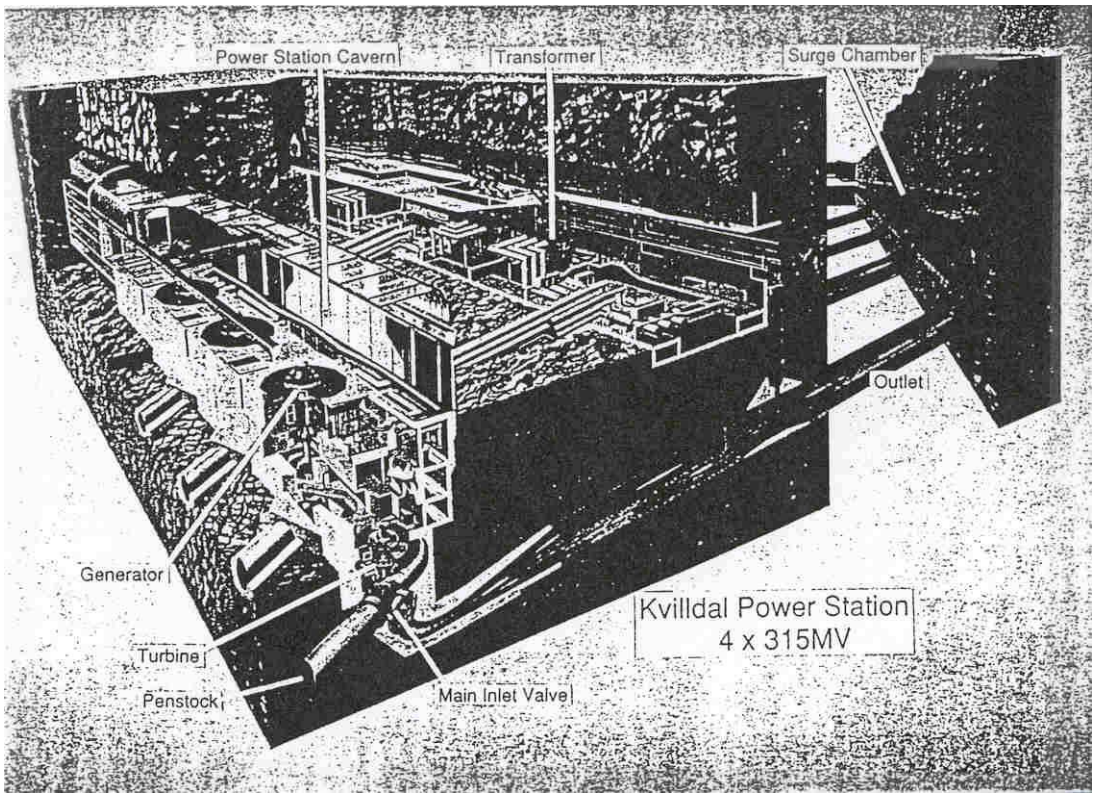

Fig. 15.2 The Kvilldal Cavern power house with 4 high head Francis turbines with following data:
P = 315 MW, H_n = 520 m., n = 333.3 RPM.

In fig. 15.2 a typical underground power plant with high head Francis turbines is shown. For safety reason the transformers are located in a separate cavern instead of in-between the generators in cavern power houses for Francis turbine and Reversible pump turbine.

However, in Pelton turbine powerhouses the transformers may be located between the generators in the main powerhouse. The reason for this is that shock waves from possible transformer explosions may be directed through weak "blow out" walls in the transformer cell towards the free surface tail race tunnel outside a Pelton power house. Such free way shock wave blasting tunnel is difficult to arrange in Francis turbine powerhouses due to the submergence of the tail race tunnel and the turbines.

For low head plants it is often convenient to locate the power plant in the dam. In that case the Kaplan Bulb turbines are used for heads up to about 15 m instead of vertical Kaplan turbines. The reason for this choice is illustrated in fig.15.3 and and fig.15.4. It is clearly illustrated that the deep excavation of the draft tube bend and the much vider space needed for Kaplan turbines will be a more expensive solution than if Bulb turbines are located inside the dam.

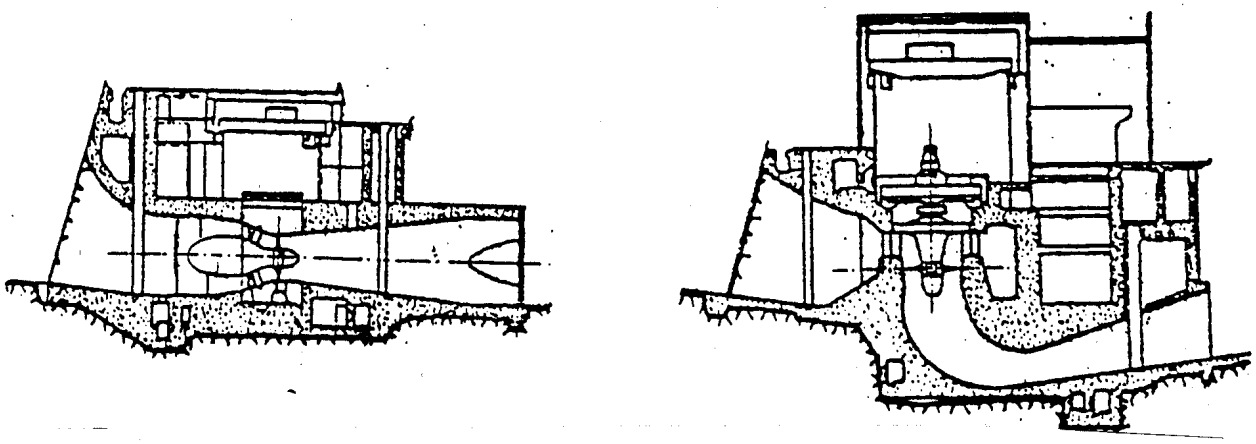

a - Bulb turbine b - Vertical Kaplan turbine.

Fig. 15.3 Comparison of a vertical section of a Kaplan turbine and a Kaplan Bulb turbine

However, the major differences in cost can be found in the differences in width of the vertical Kaplan alternative compared with the Bulb turbine, which is shown in fig. 15.4a and 15.4b.

Because of the large axial forces from the turbine to the bulb supporting structure and external hydraulics forces on the bulb, which will be exposed to buckling, the limit of head for this type of turbines will normally be approximately 15 m for economical reasons.

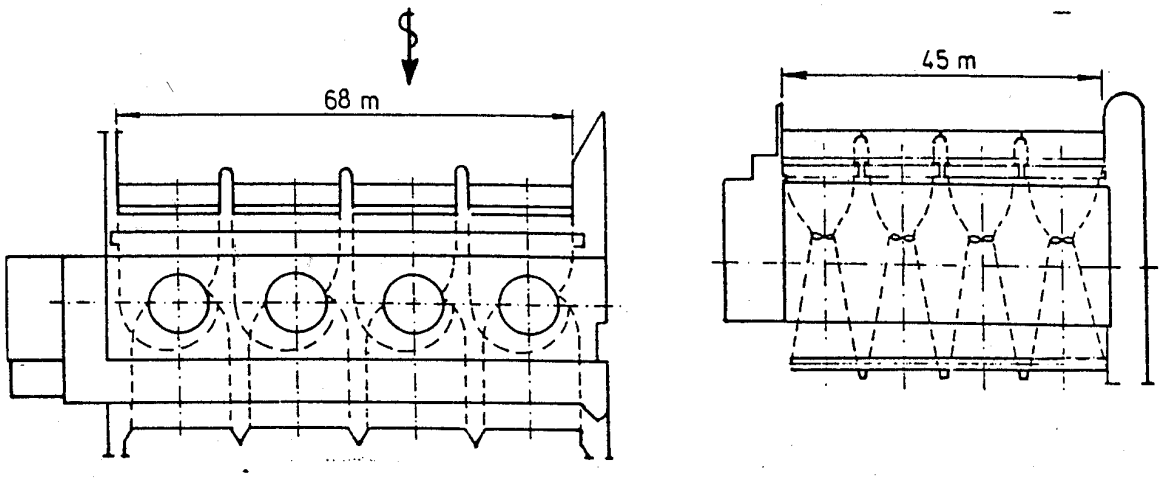

a - Kaplan turbine b - Kaplan Bulb turbine

Fig. 15.4 Comparison between a horizontal section of a Kaplan turbine and a Kaplan Bulb turbine.

For Kaplan units the powerhouse is normally located in rock besides the dam on the river bed for power houses with a small number of units. However, in large rivers as in China, Russia and South America and other places with wide large rivers also vertical Kaplan turbines will be located in the dam as well as low head and medium head Francis turbines.

An example of a Kaplan turbine located besides the dam the turbine for Solbergfoss delivered by KVAERNER in Sweden (see fig. 15.5) A typical example of a Bulb turbine plant is the

turbines for Kongsvinger power plant in Norway also delivered by KVAERNER (see fig. 15.6).

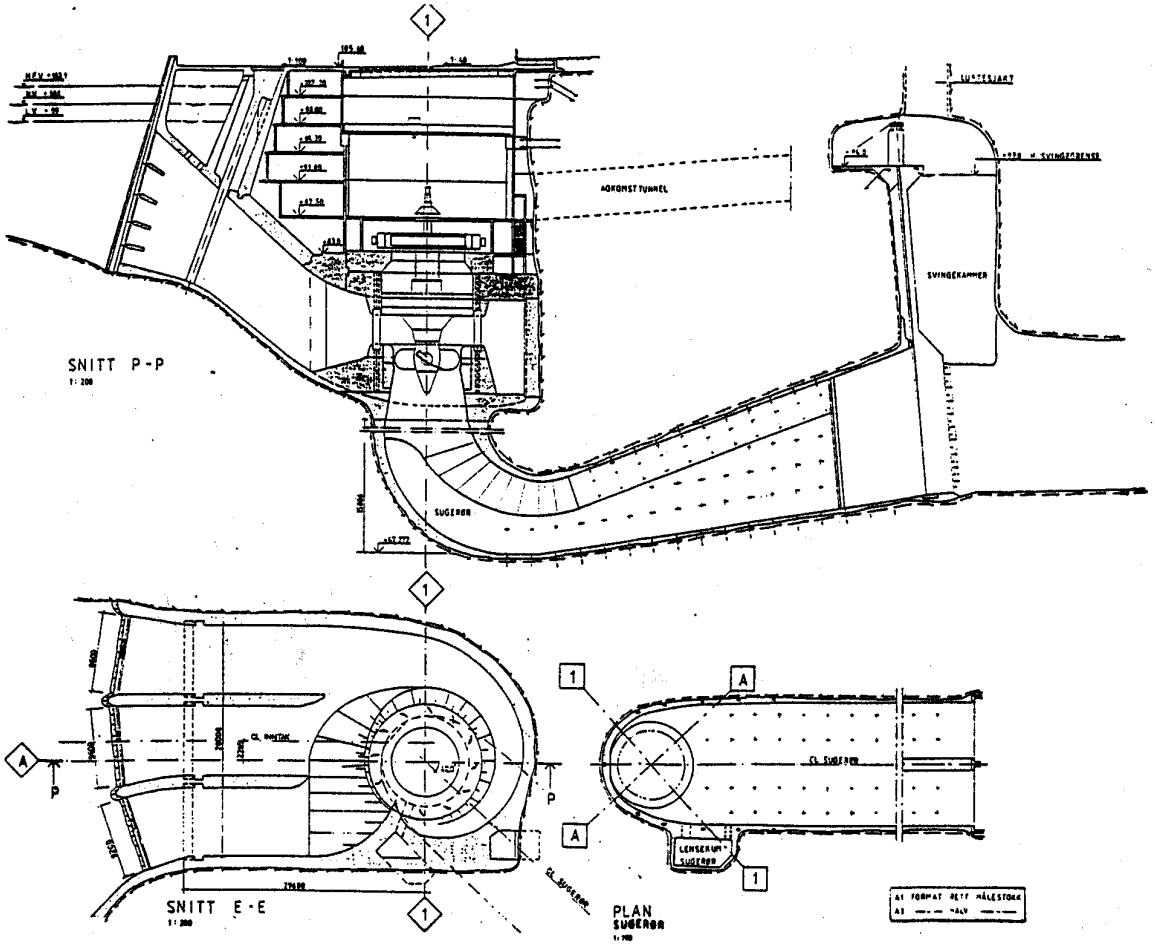

Fig. 15.5 The arrangement of the Kaplan turbine in Solbergfoss power plant

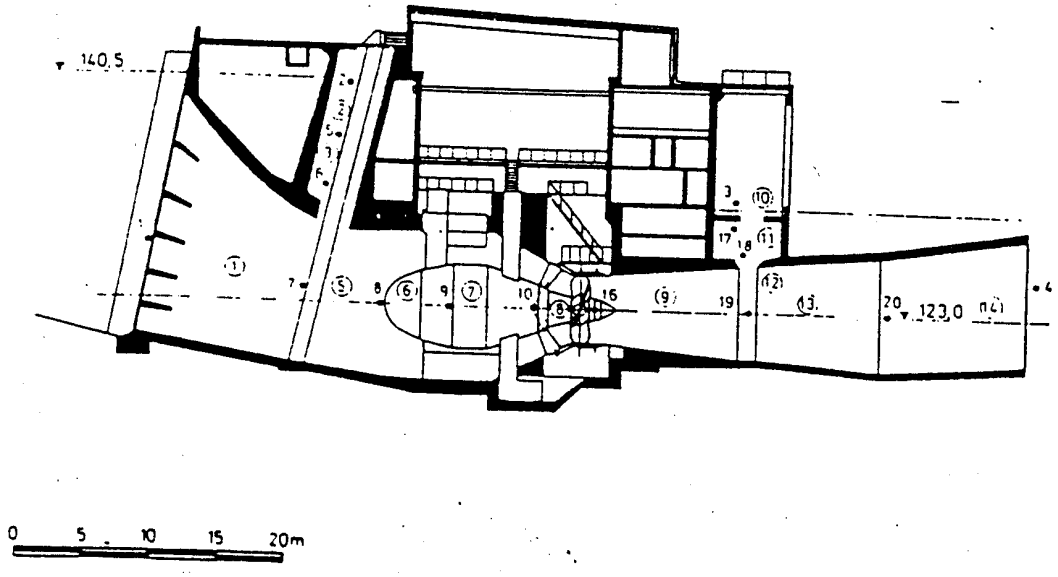

Fig. 15.6 Kongsvinger power plant with a Kaplan Bulb turbine

15.2. Hydraulic forces transferred to power house.

This chapter gives a brief summary of the hydraulic forces transferred through the turbine to the power house foundations.

The main forces from a turbine installed in a power house are transferred through the spiral casing for Francis and Kaplan turbines with steel spiral casing. For vertical Pelton turbines the forces are transferred through the manifold to the concrete.

The horizontal hydraulic force, which is the dominating force of a Kaplan Bulb turbine, is transferred to the concrete via the outer cone and the main struts which transfer the axial hydraulic forces from the turbine. The torque from the generator stator is transferred through the generator support. The axial hydraulic force on the runner is transferred through the thrust bearing via the bulb through the stress carrying structure to the concrete.
Going back to the high head turbines and starting with the vertical Pelton turbines we can summarise the following dimensioning forces from the turbine to the powerhouse:

The hydraulic forces from the horizontal turbines like SKJAAK (fig 4.1 chapter 4.2) are normally transferred to the penstock inlet flange via a ridged connection through a spherical inlet valve. Thus only minor reaction forces from the jets and momentum forces from the deflectors during rejection are transferred to the turbine housing. The jet forces on the runner will be transferred to the radial bearing of the generator, which is bolted to the concrete foundation. These forces are transferred to the surrounding concrete.

For the vertical Pelton turbines located in cavern powerhouses the axial hydraulic forces are normally transfered from the manifold through the concrete to the rock wall on downstreaside of the power- house as shown in fig. 15.7. The maximum magnitude of this force can be expressed by eq. 15.1

$$F = \rho g H_{max} \cdot \pi D_S^2/4 \qquad (N) \qquad (15.1)$$

D_S is the outer diameter of the seal ring of the telescope type dismantling pipe located at the downstream end of the spherical inlet valve and H_{max} is maximum operating pressure.

The reaction forces from the jets are negligible compared to the static hydraulic forces on the manifold. The forces are transferred through the runner and balanced by the turbine bearing and the torque is transferred to the generator stator anchored in the concrete. For horizontal one and 2 jets turbines the jet forces are transferred to the concrete via the radial bearing. During rejection the jets are deflected by the deflectors and the force is transferred to the concrete via the manifold. The maximum reaction force from each jet can be calculated by following expression:

$$F_j = 2\rho g \cdot H_{max} (\pi d_j^2/4) \ \ (N) \qquad (15.2)$$

Here d_j is the maximum jet diameter.
However, in order to transfer the large axial forces from the inlet of a manifold or spiral casing of Francis turbines to the power house an extension of the inlet flange must be welded to the inlet. This flange extension must be dimentioned to reduce the specific pressure on the concrete to maximum 7 MPa to avoid crushing and cracking of the concrete quality which is normally used. The arrangement is illustrated in fig. 15.7, where also the location of the

necessary reinforcement bars surrounding the manifold and locatet on the outside of the turbine casing are shown.

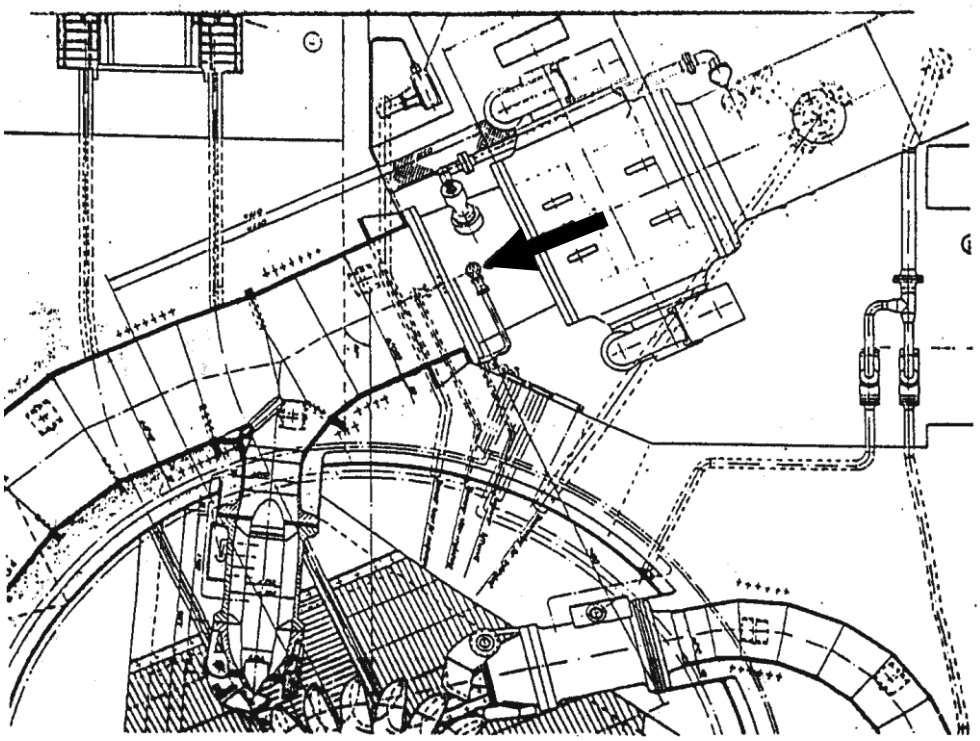

Fig. 15.7 Reinforcement collar on a Pelton turbine manifold inlet for transfer of axial forces.

Note! The hydraulic forces carried by the tangential stresses in a Pelton turbine manifolds or spiral cases of high head Francis turbines are so large that only a negligible part of the hydraulic load can be carried by the concrete. Reinforcement bars are only placed to avoid cracking of the concrete surrounding the steal plates. To avoid local increases of the stresses in the steel plates of the manifold by contact to the concrete, 5 mm soft materials are glued to the steel plates where the maximum deformations occure i.e. at the bifurcations.

The spherical inlet valve is normally free to slide horizontally on its foundation plates on top of the concrete foundations, but is anchored vertically to avoid vibration during valve closure with open needles caused by cavitation during emergency operation.

For high head Francis turbines the hydraulic forces transferred to the concrete is similar to the forces from a vertical Pelton turbine, but the movement of the inlet flange in axial direction is smaller because the inlet part and outlet part in a spiral case are joint in a closed loop.

Reinforcement bars, which are located at each bifurcation in a manifold, will of course not be used for a Francis spiral case.

IT SHOULD ALSO BE EMPHASIZED THAT NO WELDING OF REINFORCEMENT BARS IS ALLOWED ONTO THE HIGH TENSILE STRENGTH STEEL PLATES IN THE STRESS CARRYING PARTS OF HIGH HEAD FRANCIS OR PELTON TURBINES. THE REASON FOR THIS IS THAT DANGEROUS LOCAL HARDENING AND CRACKS MAY OCCUR IN THE STEEL PLATES.

The desribed forces transferred to the powerhouse from vertical turbines described in the previously is valid only for cavern power plants with solid rock on the downstream side.

For open air power houses the horizontal axial forces must normally be transferred to the penstock flange by a rigid connection through the inlet valve as described for the horizontal Pelton turbine. Also for horizontal Francis turbines the axial forces must normally transfer to the penstock flange.

For Kaplan turbines with steel plate spiral casing there is normally no inlet valve and the axial forces will be transferred to the penstock.
The vertical hydraulic forces transferred from the spiral casing will, because of large dimensions and flexible design of low head turbines, partly be transferred to the concrete balance by the weight of the generator. The generator weight is thus utilised to balance the forces from the hydraulic load on the concrete.

For Kaplan turbines with unlined concrete spiral cases, a large support from the generator weight may be utilised in addition to the anchoring of the stay ring. (see fig. 6.15 chapter 6.4).

The thrust bearing is also in some cases located in the turbine pit below the generator, where the weight of the rotating parts is transferred via the turbine head cover to the stay ring. The alternative will be to locate the bearing on top of the generator and transfer the forces by cross beams through the generator support.

For Kaplan Bulb turbines the axial forces are transferred via the main struts to the concrete which must be heavily reinforced in the area surrounding the struts. From experience this part of the foundation is the most critical place in a Kaplan Bulb turbine power plant. The dimension and strength of the concrete, limits the maximum head of operation of this type of turbines to approximately 15m (see fig. 6.23, chapter 6.5).
A picture of the anchoring the stay ring of a Kaplan turbine is shown in fig. 15.8 for illustration of a concrete spiral casing where all hydraulic forces are transferred to the concrete.

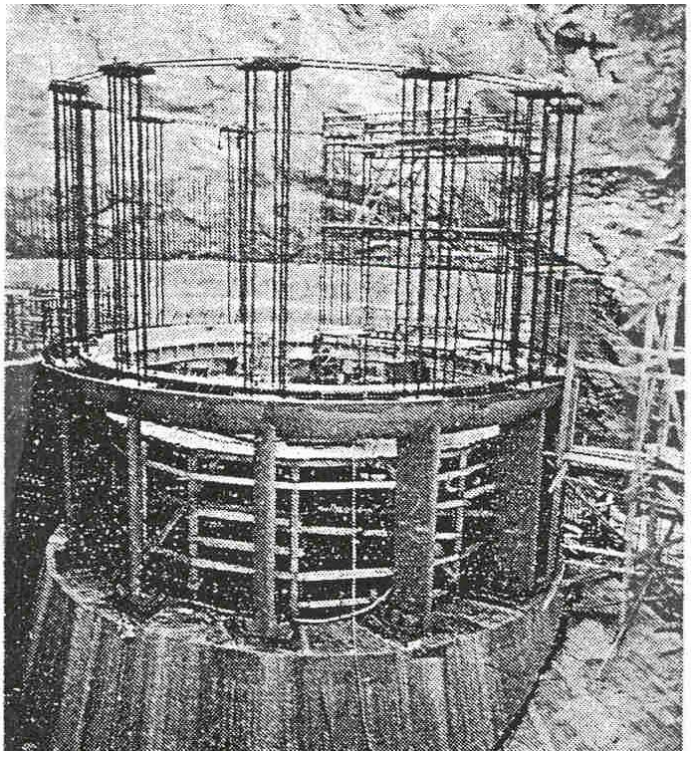

Fig. 1 Concrete spiral casing and stay ring with anchoring bars.

16. CLASSIC TURBINE THEORY FOR RUNNER DESIGN.

INTRODUCTION

The presented basic theory of flow in a Francis turbine runner is based upon the energy equation, the Eulers turbine equation and the equation of continuity for potential flow, but the displacement from the blade thickness of the existing finite number of blades has been taken into account. This analysis has been derived from the basic theory made by professor Sundby at NTNU 1911 – 1952. The equations have been further developed by Chief eng. H.Christie and T.Sømming, employed by the turbine manufacturer KVÆRNER through 1935 – 1960. Finally the equations have been rearranged by the author in order to use the blade lean angle Θ as a dimensioning parameter for cross flow and the pressure distribution between crown and band in a Francis runner.

The theoretical analysis is based on an assumption of infinite the number of blades i.e.we have a potential flow field which is not correct.
However, for a study of a mean pressure gradient between crown and band the theory gives a clear indication of the influence from the blade lean angle and the curvature of crown and band.
No frictional influence is included in the theoretical analysis, which is meant to be used as a simplified analysis for the preliminary shaping of the blades. The resulting geometry should be analysed by a CFD computation for a fine-tuning of the blade lean and outlet and inlet shape before a model is built for testing. It should also be mentioned that the presented theory formed the base for the Authors work during the design of the X blade runners, which were selected for 8 of the first 14 units for Three Gorges Plant in China in 1997. The author worked at that time as advisor for runner design for the turbine manufacturer Kværner.

16.1 Basic theory and governing equations for reaction turbine design.

The relation between pressure and absolute acceleration for frictionfree flow can be expressed by Eulers' turbine equation which is valid for both compressible and incompressible flow. (See S.W.Yan, Foundations of Fluid Mechanics, Prentic Hall Int. Inc. London, p. 181 and p.148).
The Euler equations yields:

$$a_a = \frac{Dc}{dt} = \frac{\partial \vec{c}}{\partial t} + \left(\vec{c} \cdot \nabla\right)\vec{c} = \vec{X} - \frac{\nabla p}{\rho} \qquad (16.1)$$

For stationary flow in a runner $\partial c / \partial t = 0$ and further for incompressible flow $\rho = \text{const.}$

Assuming that a runner has an infinite number of infinite thin blades, the blade itself will form a stream surface in a rotational symmetric potential energy field expressing the blade forces.
This can be seen from Newtons 2.law for a fluid element of size, $\Delta\times, \Delta y, \Delta z$ in x direction which yields:

$$\frac{D}{Dt}(\rho\, \Delta x\, \Delta y\, \Delta z \cdot c_x) = \frac{\partial p}{\partial x}\, \Delta x\, \Delta y\, \Delta z + \vec{X}_x \rho\, \Delta\, x\, \Delta y\, \Delta z$$

Definitions of variables:

X_x is the body force and (D/Dt) $(\rho\,\Delta x\,\Delta y\,\Delta z\,c_u) = \rho\,\Delta x\,\Delta y\,\Delta z\,(Dc_u/Dt)$ is the momentum (ρ = constant for incompressible flow).

Thus we get in x direction

$$\frac{Dc_u}{Dt} = \frac{\partial c_u}{\partial t} + c_u\frac{\partial c_u}{\partial x} + c_n\frac{\partial c_u}{\partial y} + c_m\frac{\partial c_u}{\partial z} = \frac{1}{\rho}\frac{\partial p}{\partial x} + \vec{X}_x \qquad 16.2)$$

or in general

$$(\vec{c}\cdot\nabla)\vec{c} = -\frac{\nabla p}{\rho} + \vec{X} \qquad \text{(Steady state flow } \frac{\partial c}{\partial t} = 0\text{)} \qquad (16.3)$$

The body force $\vec{X}$ may be derived from a potential flow function ϕ as follows:

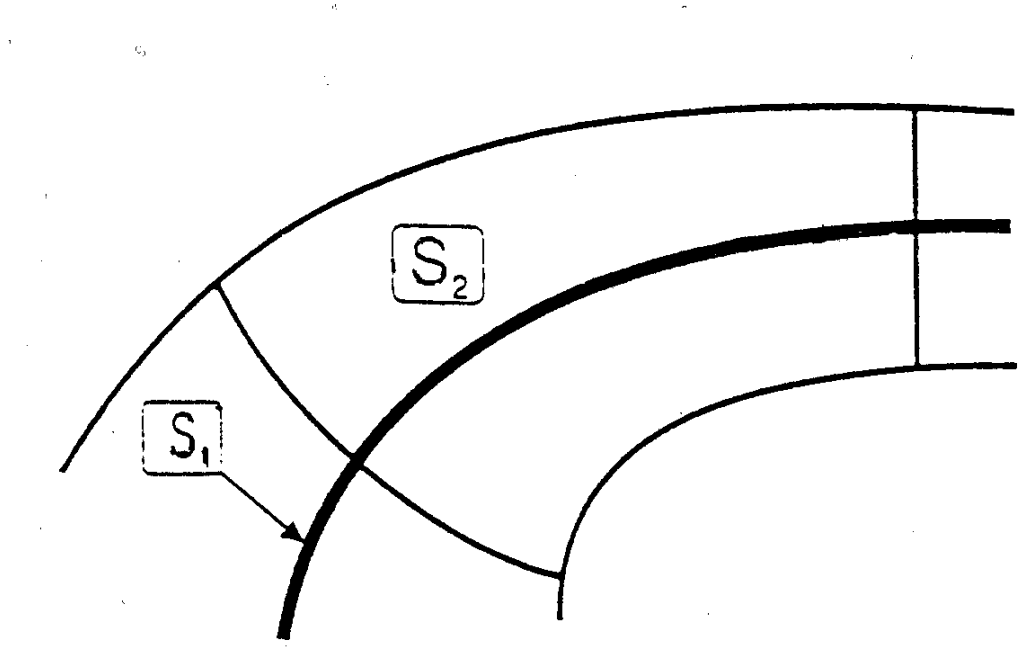

Fig. 16.1. Illustration of the blade surface S_2 on the rotational symmetric blade to blade stream surface S_1.

$$\vec{X}_x = -\frac{\partial\phi}{\partial x}, \qquad \vec{X}_y = -\frac{\partial\phi}{\partial y} \quad \textit{and} \quad \vec{X}_z = -\frac{\partial\phi}{\partial z}$$

A potential flow may be represented by the blade force in a runner with an infinite number of infinite thin blades forming formed by the blade stream surface S2 identical to the real blade surface while the blade to blade S1 stream surface will be a rotational symmetric surface with a potential energy field ϕ similar to a gravity field g-z in the vertical z direction which may be neglected for a runner (or included as a constant contribution in the ϕ field).

Thus the blade force may be represented by the potential field ϕ and thus the equation for $\vec{X}$ yields:

$$\vec{X} = \nabla\phi \qquad (16.4)$$

Note, with infinite number of blades there will be no pressure difference from pressure side to suction side of the blade, but we will still obtain a pressure gradient on the blade surface by the potential ϕ.

The statement of a rotational symmetric stream surface and a blade stream surface then yields. For a runner with a high number of long blades, the analysis of the pressure and velocity distribution on the blade based on this basic theory gives valuable information to the designer of a runner as the first approach.

However, also for high specific speed runners the theory described in following chapter may be used as a tool for the preliminary shaping of the runner. Special attention should be paid on the influence from the blade lean angle Θ as described in the next chapters.

For steady state flow: $(\partial c / \partial t) = 0$ and then the absolute acceleration $\frac{Dc}{dt} = a_a$ in the Euler equation yields:

$$a_a = (\vec{c} \cdot \nabla)\vec{c} = \nabla(\frac{c^2}{2}) - \vec{c} \times (\nabla \times \vec{c}) \qquad (16.5)$$

Substituting in the Euler equation eq (16.3) and rearranging:

$$\vec{c} \times (\nabla \times \vec{c}) = \nabla(\frac{p}{\rho} + \frac{c^2}{2} + \phi) \qquad (16.6)$$

This equation expresses the differentiation of the nominal specific energy of the system. For a turbine the absolute total stagnation energy will be:

$$E = gH_n = \frac{p}{\rho} + \frac{c^2}{2} + \phi \qquad (16.7)$$

By introducing the relative acceleration a_r expressed by the relative velocity w and the angular velocity ω and the radius r of the system for a stationary flow i.e. $\partial w / \partial t = 0$ the following expression is obtained:

$$\vec{a}_r = (\vec{w} \cdot \nabla)\vec{w} = \nabla(\frac{w^2}{2}) - \vec{w} \times (\nabla \times \vec{w}) \qquad (16.8)$$

Further, the relation between the absolute acceleration and relative acceleration yields

$$\vec{a}_a = \vec{a}_r + 2\vec{\omega} \times \vec{w} + \vec{\omega} \times (\vec{\omega} \times \vec{r}) \qquad (16.9)$$

Eq. (16.1) has also proven that:

$$a_a = \vec{X} - \frac{\nabla p}{\rho} = -\nabla\phi - \frac{\nabla p}{\rho}$$

From the basic vector analysis:

$$\vec{w} \times (\nabla \times \vec{w}) = \vec{w} \times (\nabla \times \vec{c}) - \vec{w} \times 2\vec{\omega} = \vec{w} \times (\nabla \times \vec{c}) + 2\vec{\omega} \times \vec{w} \qquad (16.10)$$

From the vector analysis when substituting for the circumferential speed $|u| = |\omega\, r|$:

$$\vec{\omega} \times (\vec{\omega} \times \vec{r}) = \nabla(\frac{\omega^2 r^2}{2}) = -\nabla(\frac{u^2}{2}) \qquad (16.11)$$

Further, the equation for the relative stagnation energy yields:

$$\nabla \mathrm{I} = \vec{w} \times \nabla \times \vec{c} \tag{16.12}$$

Combining eq. (16.12), eq. (16.10) and eq.(18.8) gives:

$$\vec{a}_r = \nabla(\frac{w^2}{2}) - \nabla \mathrm{I} - 2\vec{\omega} \times \vec{w} \tag{16.13}$$

Then by substituting for a_r by eq. (16.13) in eq. (16.9) and for $(\vec{\omega} \times \vec{\omega} \times r)$ by eq. (16.11) we arrive at:

$$\vec{a}_a = -\nabla \mathrm{I} + \nabla(\frac{w^2}{2}) - \nabla(\frac{u^2}{2}) \tag{16.14}$$

Further, by combining eq. (16.7), eq (16.6) and eq.(16.5) gives:

$$\vec{a}_a = \nabla(\frac{c^2}{2}) - \nabla E \tag{16.15}$$

Then by substituting for a_a by eq. (16.15) in eq. (16.14) and rearranging we arrive at:

$$\nabla \mathrm{I} = -\nabla(\frac{c^2}{2}) + \nabla E + \nabla(\frac{w^2}{2}) - \nabla(\frac{u^2}{2}) \tag{16.16}$$

Further, when substituting for E by eq. (16.7) in eq. (16.16):

$$\nabla \mathrm{I} = \frac{\nabla p}{\rho} + \nabla \phi + \nabla(\frac{w^2}{2}) - \nabla(\frac{u^2}{2})$$

$$\nabla I = \nabla\left(\frac{p}{\rho} + \frac{w^2}{2} - \frac{u^2}{2} + \phi \right) \tag{16.17}$$

Further, from fig. (16.2) and (fig.(16.2b) in Chapt. 16.2 ($c_u = c \cos \alpha$.)

$$w^2 = u^2 + c^2 - 2\,\vec{u} \cdot \vec{c} = u^2 + c^2 - 2\,uc_u \tag{16.18}$$

Then after substitution for w^2 by eq. (16.18) in eq. (16.17):

$$\nabla I = \nabla\left(\frac{p}{\rho} + \frac{c^2}{2} - u\ c_u + \phi \right) \tag{16.19}$$

Further, it is known that the relative stagnation energy is constant along a streamline if the friction force is neglected. Then we get from eq. (16.19):

$$\nabla\left(\frac{p}{\rho} + \frac{c^2}{2} - uc_X + \phi \right) = 0 \tag{16.20}$$

Note that u c_x is the energy transferred to the blades and $\nabla\phi$ represents a fictious body force from the runner to the fluid particles expressed by a potential ϕ produced by infinite number

of blades or infinite number of stream surfaces (S2) in fig.(16.2) and (16.2b) formed by the blades with streamsurfaces which will be rotational symmetric:
Thus:

$$uc_u = \phi \tag{16.21}$$

and then

$$\frac{p}{\rho} + \frac{c^2}{2} = const. \tag{16.22}$$

This means that no energy exchanges occur except for the energy absorbed by the fictitious potential flow field set up by the runner i.e. the absolute energy is uniform in the complete domain and we have a so called Beltrami flow which is a rotational symmetric flow.

16.2. Two dimensional flow in a stream surface, which may be regarded to be the suction side of the blade for an infinite number or a high number of blades in a Francis runner.

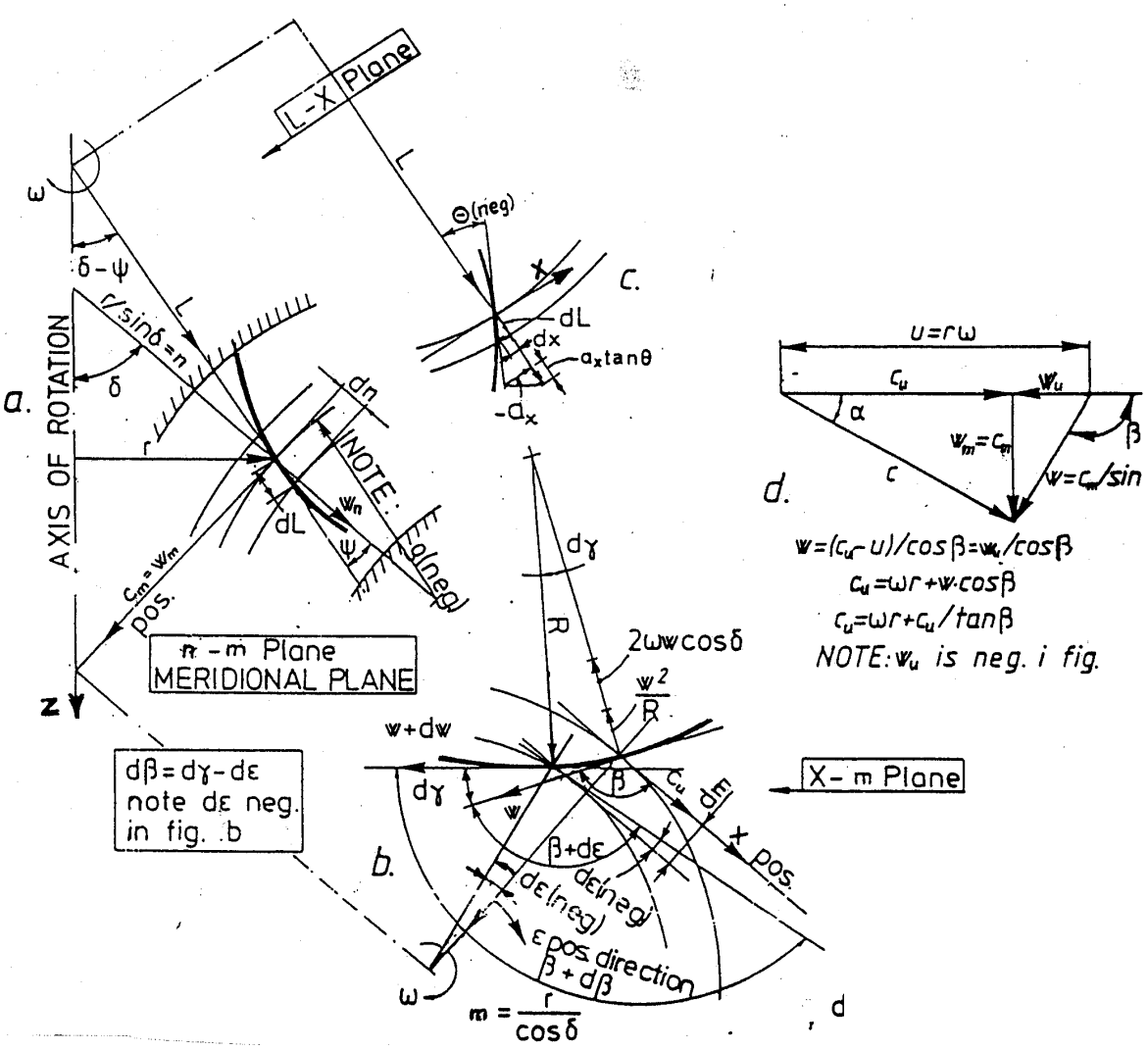

Fig. 16 2. Illustration of parameters in a turbine runner.

In fig. 16.2 x, n, m are orthogonal and m is the streamline direction.

Statements: x, n, m are orthogonal where m is the streamline direction i.e. $w_n = c_n = 0$ for flow in stream line direction.

The velocity diagram in the x,m-plane is valid for flow in stream line direction.

u -The runners peripherical velocity (u is in x direction)
c -The absolute velocity of a fluid element
c_u -The absolute velocity in the same direction as the runners peripherical velocity
c_m -The absolute velocity along the streamline
w -The relative velocity of a fluid element
w_u -The relative velocity in the same direction as the runners peripherical velocity
w_m -The relative velocity along a streamline (Note: $w_m = c_m$)
H - Net head

For a steady state flow we can write $\frac{\partial w}{\partial t} = \frac{\partial c_m}{\partial t} = \frac{\partial w_m}{\partial t} = 0$ when regarding the flow along the stream lines.

Further $\frac{\partial r}{\partial x} = 0$ and $\frac{\partial \beta}{\partial x} = 0$ for an assumed infinite number of blades, i.e. rotational symmetry.

Rearranging eq. 16.22 from Chapt. I and introducing p = $\rho g h$

$$\rho\, g\, h + \rho\, c^2/2 = \rho\, g\, h + (\rho/2)\,(c_u^2 + c_n^2 + c_m^2) = Const.$$

Differentiation after introducing dimensionless variables i.e. dimensionless head and flow:
$h/H_n = \underline{h}$ *and* $c/\sqrt{2gH} = \underline{c}$ *and* $a/(2gH) = \underline{a}\ (m^{-1})$

$$d\underline{h} + 2(\underline{c}_u d\underline{c}_u + \underline{c}_n d\underline{c}_n + \underline{c}_m d\underline{c}_m = 0,$$

When introducing $\underline{c}_u = \frac{dx}{dt}, \underline{c}_n = \frac{dn}{dt}$ *and* $\underline{c}_m = \frac{dm}{dt}$

or: $$d\underline{h} = -2\frac{d\underline{c}_u}{dt}dx - 2\frac{d\underline{c}_n}{dt}dn - 2\frac{d\underline{c}_m}{dt}dz = -2\underline{a}_x dx - 2\underline{a}_n dn - 2\underline{a}_m dm \qquad (16.23)$$

In fig. 16.2 is shown the acceleration as function of the absolute velocity = c and the relative velocity = w [See velocity diagram fig. 16.2]

$$\underline{a}_x = \frac{d\underline{w}}{dt}\cos\beta - \left(\frac{\underline{w}^2}{R} + 2\,\underline{\omega}\,\underline{w}\cos\delta\right)\sin\beta$$

$$\underline{a}_n = -\frac{\underline{c}_u{}^2}{r}\sin\delta - \frac{\underline{c}_m{}^2}{\rho} \qquad \text{(Note negative direction of } \rho \text{ as shown in fig. 16.2).}$$

$$\underline{a}_m = \frac{d\underline{w}}{dt}\sin\beta + \left(\frac{\underline{w}^2}{R} + 2\,\underline{\omega}\,\underline{w}\cos\delta\right)\cos\beta + \underline{\omega}^2\, r\cos\delta$$

Substituting for $\underline{w} = \underline{c}_m / \sin\beta$

Then $$\frac{d\underline{w}}{dt} = \frac{\sin\beta\dfrac{d\underline{c}_m}{dt} - \underline{c}_m\,\cos\beta\,\dfrac{d\beta}{dt}}{\sin^2\beta}$$

From fig. 16.2 b. [Note $d\varepsilon$ is shown negative $c_u = md\varepsilon = (r/\cos\delta)d\varepsilon$ in fig. 16.2 b.]

$$d\gamma = \frac{\underline{w}dt}{R} = \frac{\underline{c}_m\,dt}{\sin\beta\cdot R}, \quad d\varepsilon = \frac{\underline{w}_u\,dt}{m} = \frac{\underline{w}\cos\beta\cos\delta dt}{r} \quad \textit{and} \quad \underline{w}\cos\beta = \underline{c}_m/\tan\beta$$

and $$d\beta = d\gamma - d\varepsilon$$

Then $$\frac{d\beta}{dt} = \frac{\underline{c}_m}{R\sin\beta} - \frac{\underline{c}_m\cos\delta}{r\,\tan\beta}$$

Further $$\frac{d\underline{c}_m}{dt} = \frac{\partial\underline{c}_m}{\partial t} + \frac{\partial\underline{c}_m}{\partial x}\underline{c}_u + \frac{\partial\underline{c}_m}{\partial n}\underline{c}_n + \frac{\partial\underline{c}_m}{\partial m}\underline{c}_m$$

Remembering $\dfrac{\partial\underline{c}_m}{\partial t} = 0$ for steady state flow

From the following boundary conditions, steady state flow, and noticing that (m) is the meridional streamline direction and assuming infinite number of blades it is possible to show that

$$\frac{\partial\underline{c}_m}{\partial t} = 0, \ \frac{\partial\underline{c}_m}{\partial x} = 0. \ \textit{and} \ \ \underline{c}_n = 0$$

Then $$\frac{d\underline{c}_m}{dt} = \underline{c}_m\frac{\partial\underline{c}_m}{\partial m}$$, note pos. direction of m as shown in fig. 16.2.

Now: $$\frac{d\underline{w}}{dt} = \frac{1}{\sin\beta}\underline{c}_m\frac{\partial\underline{c}_m}{\partial m} - \frac{\cos\beta}{\sin^3\beta}\left(\frac{1}{R} - \frac{\cos\beta\cos\delta}{r}\right)\underline{c}_m{}^2$$

Substituting for $\underline{w}$ and $d\underline{w}/dt$ in the equations of acceleration and further substituting for $\underline{c}_u = (\underline{\omega} r + \underline{c}_m / \tan\beta)$ the following equation for a_x, a_y and a_m is obtained:

$$\underline{a}_x = \underline{c}_m \frac{\partial \underline{c}_m}{\partial_m} \frac{1}{\tan\beta} - \frac{\cos^2\beta}{\sin^3\beta}\left(\frac{1}{R} - \frac{\cos\beta\cos\delta}{r}\right)\underline{c}_m^2 - \left(\frac{\underline{c}_{m^2}}{R\sin\beta} + 2\underline{\omega}\,\underline{c}_m\cos\delta\right)$$

and substituting for:

$$\left(\frac{\cos^2\beta}{\sin^3\beta} + \frac{1}{\sin\beta}\right)\frac{\underline{c}_m^2}{R} = \frac{(\cos^2\beta + \sin^2\beta)}{\sin^3\beta}\frac{\underline{c}_m^2}{R} = \frac{1}{\sin^3\beta}\frac{\underline{c}_m^2}{R}$$

$$\underline{a}_x = \underline{c}_m \frac{\partial \underline{c}_m}{\partial m}\frac{1}{\tan\beta} + \left(\frac{\cos\delta\cdot\cos^3\beta}{r} - \frac{1}{R}\right)\frac{\underline{c}_m{}^2}{\sin^3\beta} - 2\,\underline{\omega}\cos\delta\,\underline{c}_m \qquad (16.24)$$

$\underline{a}_n = (\underline{\omega}\, r + \underline{c}_m / \tan\beta)^2 \sin\delta / r - \underline{c}_m^2 / \rho$ (Note ρ is negative in fig 16.2)

$$\underline{a}_n = \left(-\frac{1}{\rho} - \frac{\sin\delta}{r\tan^2\beta}\right)\underline{c}_m{}^2 - \frac{2\underline{\omega}\sin\delta}{\tan\beta}\underline{c}_m - \underline{\omega}^2 r\sin\delta \qquad (16.25)$$

$$\underline{a}_m = \left(\frac{1}{\sin\beta}\underline{c}_m\frac{\partial \underline{c}_m}{\partial m} - \frac{\cos\beta}{\sin^3\beta}\left(\frac{1}{R} - \frac{\cos\beta\cos\delta}{r}\right)\underline{c}_m^2\right)\sin\beta + \left(\frac{\underline{c}_m^2}{R\sin^2\beta}\right.$$
$$\left. + 2\,\underline{\omega}\frac{\cos\delta}{\sin\beta}\underline{c}_m\right)\cos\beta + \underline{\omega}^2 r\cos\delta$$
$$\underline{a}_m = \underline{c}_m\frac{\partial \underline{c}_m}{\partial m} + \frac{\cos\delta}{r\tan^2\beta}\underline{c}_m^2 + 2\,\underline{\omega}\frac{\cos\delta}{\tan\beta}\underline{c}_m + \underline{\omega}^2 r\cos\delta \qquad (16.26)$$

The accelerations $\underline{a}_x$, $\underline{a}_n$ and $\underline{a}_m$ in the local coordinate system are now known and the pressure gradient dh/dy or dh/dl in an arbitrarily chosen plane intersecting with the x – m plane can be found. (See fig. (16.2)).

The equation for the pressure gradient in l direction yields: (See fig 16.2 and eq. (16.23)).

$$\frac{dh}{d1} = -.2\,\underline{a}_x\frac{dx}{dl} - 2\,\underline{a}_n\frac{dn}{dl} - 2\,\underline{a}_m\frac{dm}{dl}$$

here $\frac{dx}{dl} = \tan\theta$, $\frac{dn}{dl} = \cos\psi$ *and* $\frac{dm}{dl} = \sin\psi$ (see fig.16.2).

When substituting for $\underline{a}_x$, $\underline{a}_n$ and $\underline{a}_m$ in addition in eq. (1) (16.23) we arrive at:

$$\frac{d\underline{h}}{dl} = -2\left\{\left[\underline{c}_m \frac{\partial \underline{c}_m}{\partial m}\frac{1}{\tan\beta} + \left(\frac{\cos\delta\cos^3\beta}{r} - \frac{1}{R}\right)\frac{\underline{c}_m^2}{\sin^3\beta} - 2\,\underline{\omega}\cos\delta\,\underline{c}_m\right]\tan\theta\right.$$
$$+\left[\left(\frac{1}{\rho} - \frac{\sin\delta}{r\tan^2\beta}\right)\underline{c}_m^2 - \frac{2\,\underline{\omega}\sin\delta}{\tan\beta}\underline{c}_m - \underline{\omega}^2 r\sin\delta\right]\cos\psi$$
$$\left.+\left[\underline{c}_m\frac{\partial \underline{c}_m}{\partial m} + \frac{\cos\delta}{r\tan^2\beta}\underline{c}_m^2 + 2\,\underline{\omega}\frac{\cos\delta}{\tan\beta}\underline{c}_m + \underline{\omega}^2 r\cos\delta\right]\sin\psi\right.$$

Remembering: $\sin\delta\cos\psi - \cos\delta\sin\psi = \sin(\delta - \psi)$ we get after rearranging:

$$\frac{d\underline{h}}{dl} = 2\left\{\left[\left(\frac{1}{R} - \frac{\cos\delta\cos^3\beta}{r}\right)\frac{\underline{c}_m^2}{\sin^3\beta} - \frac{\underline{c}_m\dfrac{\partial \underline{c}_m}{\partial m}}{\tan\beta} + 2\underline{\omega}\cos\delta\,\underline{c}_m\right]\tan\theta\right.$$
$$\left.+\left[\frac{\sin(\delta-\psi)}{r\tan^2\beta} + \frac{\cos\psi}{\rho}\right]\underline{c}_m^2 + \left[2\underline{\omega}\frac{\sin(\delta-\psi)}{\tan\beta} - \frac{\partial \underline{c}_m}{\partial m}\sin\psi\right]\underline{c}_m + \underline{\omega}^2 r\sin(\delta-\psi)\right\} \qquad *(6)$$

16.27

Note: i.e. If ψ = 0 i.e. if the (L-x) plane is normal to the streamsurface, i.e. it is identical to the (n-x) plane and the terms containing $\sin\psi = 0$, see eq.(16.27). By using the (n-x) plane normal to the stream surface, we get a simpler, but very important equation (16.28)
The simplification is illustrated in fig.(16.2b) which can be compared to fig.(16.2).

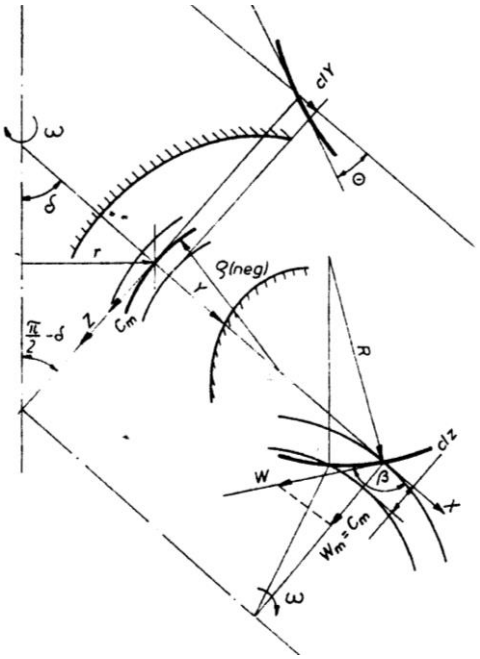

Fig.(16.2b). Simplified illustration of parameters with L-X plain normal to the sream surfaces. (See Fig.(16.2) where the L-X plain had an angle = ψ to the plain normal to the stream surface.)

The equation valid for the pressure field in a plain normal to the regarded stream surface as illustrated in fig. (16.1b) yields:

$$\frac{d\underline{h}}{dn} = 2\left\{ \left[\left(\frac{1}{R} - \frac{\cos\delta\,\cos^3\beta}{r}\right)\frac{\underline{c}_m^2}{\sin^3\beta} - \frac{\underline{c}_m \dfrac{\partial \underline{c}_m}{\partial m}}{\tan\beta} + 2\underline{\omega}\cos\delta\,\underline{c}_m \right] \tan\theta \right.$$

$$\left. + \left[\frac{\sin\delta}{r\,\tan^2\beta} + \frac{1}{\rho}\right]\underline{c}_m^2 + \left[2\underline{\omega}\frac{\sin\delta}{\tan\beta}\right]\underline{c}_m + \underline{\omega}^2 r\,\sin\delta \right\} \qquad (16.28)$$

In order to find the pressure gradient normal to the streamlines in the meridional plane, two more equations are required. That is, the equation for the hydraulic pressure along the stream line and the equation of continuity must be established. The hydraulic pressure along a stream line in the stream surface can be found by means of Euler's turbine equation combined with the energy equation i.e. the ROTHALPHY equation based upon the hydraulic turbine efficiency assuming that the hydraulic efficiency along all streamlines in the stream surface are constant for a runner with infinite number of blades.

THE HYDRAULIC PRESSURE VARIATION ALONG A STREAM LINE

The Euler turbine equation yields: Using reduced non-dimensional variables:

$$\eta_h = 1 - J = 2(\underline{u}_1\underline{c}_{u1} - \underline{u}_2\underline{c}_{u1}) \qquad (16.29a)$$

Here J is reduced loss based upon the reduced dimensional variables $\underline{u}$ and $J = \zeta_1 \underline{c}_1^{2+} \zeta_2 \underline{c}_2^2 + T_s$ where T_s is the reduced inlet shock loss. 1 denotes the inlet conditions and 2 the outlet conditions:

If the turbine efficiency equation is combined with the energy equation also named as the ROTHALPY EQUATION (or Bernoulli's equation for a rotating conduite), the conditions at any point along a stream line may be determined (using "reduced" dimensionless velocities $\underline{C}=(C/(2gH)^{0.5}$ as explained earlier in this book):

Following equation yields, when the energy not transformed to rotational mechanical energy (converted by the runner) is expressed by ($\underline{h} + \underline{c}^2 + J'$) at any place along the stream line: (Note J' is the reduced loss from inlet of the runner to the regarded point).

$$\eta_h = 1 - (J + \underline{h} + \underline{c}^2) = 2(\underline{u}_1\underline{c}_{u1} - \underline{u}\underline{c}_u) \qquad (16.29b)$$

Note that at the inlet $\eta_h = 1 - (J_1 + \underline{h}_1 + \underline{c}_1^2) = 0$ and at the outlet $\eta_h = 1 - (J_2 + \underline{h}_2 + \underline{c}_2^2) = 0{,}98$ or higher for a good runner depending on the total energy loss through the turbine. At the outl $(\underline{h}_2 + \underline{c}_2^2)$ represents part of the total loss J in eq. (8). $J_2 + \underline{h}_2 + \underline{c}_2^2 = \zeta_1\underline{c}_1^2 + \zeta_2\underline{c}_2^2 + T_s$ where $\underline{h}_2 + \underline{c}_2^2 = \zeta_2\underline{c}_2^2$ and $J_2 = \zeta_1\underline{c}_1^2 + T_s$ as explained for eq. (8) (16.29).

After rearranging: eq (8b) (16.29b)

$$\underline{h} = -2\underline{u}_1\underline{c}_{u1} + 2\underline{u}\,\underline{c}_u - \underline{c}^2 - J + 1 \qquad (16.29c)$$

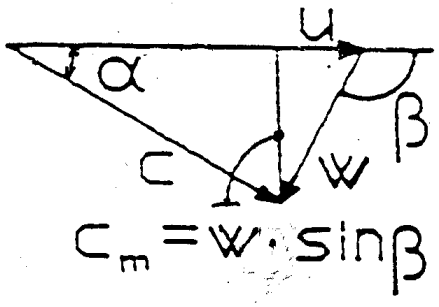

Fig 16.3 Velocity vector diagram

Studying the vector velocity diagram in fig 3 gives:

$$\underline{w}^2 = \underline{c}^2 + \underline{u}^2 - 2\underline{u}\underline{c}\cos\underline{a} = \underline{c}^2 + \underline{u}^2 - 2\underline{u}\,\underline{c}_u \quad \text{i.e.} \qquad 2\underline{u}\,\underline{c}_u - \underline{c}^2 = \underline{u}^2 - \underline{w}^2$$

When substituting for ($2\,\underline{u}\,\underline{c}_u - \underline{c}^2$) in eq. (8c) (16.29c) we get a further substitution for

$\underline{u}^2 = \underline{\omega}^2 r^2$ and $\underline{w} = \underline{c}_m/\sin\beta$

$$\boxed{\underline{h} = \underline{\omega}^2 r^2 - \underline{c}_m^2/\sin^2\beta + (1 - 2\,\underline{u}_1\underline{c}_{u1}) - J} \qquad (16.30)$$

Note that $\underline{1 - 2\,u_1 c_{u1} = const.} = 1 - \underline{\omega}\, r_1 c_{m1}/\sin\beta_1$ and J = 0 at the inlet and

$1\text{-}\eta_h = J \leq 0.04$ at the outlet. Normally the value of J can be judged to be proportional to the length from the inlet to the regarded point varying from 0 to 0.02 – 0.04 from inlet to outlet. An error is not important due to the smallness of this term.

THE EQUATION OF CONTINUITY

In the equation of continuity the influence of the blade thickness must be taken into consideration:

The analysis is based upon the statement that there is no flow across a streamline or across a stream surface defined as the suction side of the blade. (The runner is regarded to having an infinite number of blades for the basic theory as stated earlier, but for the equation of continuity a finite number of blades with real thickness will be used.)

A certain number of stream lines (or stream surfaces) (4-10) should be drawn between crown and band and the analysis should be carried out in the middle between these rotational

symmetric stream surfaces which is regarded to form waterconduits between the blades (because no flow is crossing the stream surface).

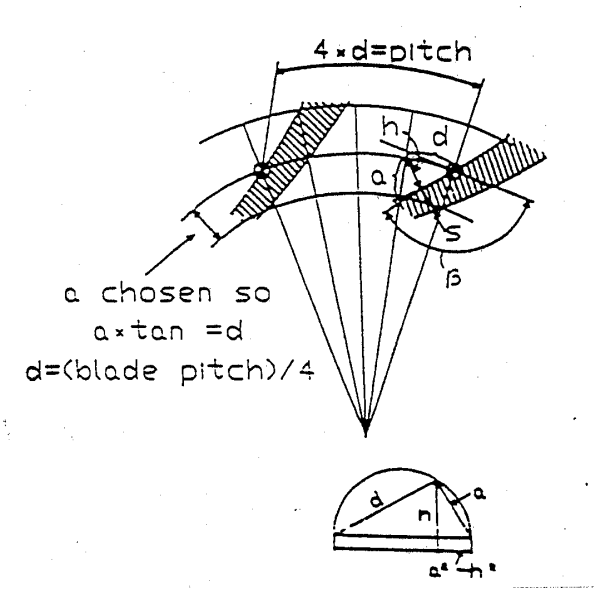

Fig. 16. 4. Illustration of the influence of blade thickness and the parameters a, h, d with the blade thickness = **S** shown in the figure for calculation of the cross section decreasing factor Φ for between the blades.

The equation of continuity can then be established by studying fig. 16.4 as shown in the following:

From basic trigonometry:

$$\frac{a^2}{a^2-h^2}=\frac{d^2}{h^2} \quad \textit{i.e.} \quad h=d/\sqrt{1+d^2/a^2} \quad \text{or } h=d/\sqrt{1+1/\tan^2\beta}$$

Further when N = number of blades and d = blade pitch/4 (see fig. 16.4) then:

$$h=(\pi\, r/2N))/\sqrt{1+1/\tan^2\beta}$$

The decreasing factor ϕ may now be found when the blade thickness = s

$$\phi = 1-\frac{s/4}{h}=1-\frac{s}{4}\frac{2N}{\pi\, r}\sqrt{1+1/\tan^2\beta}$$

or

$$\phi = 1-\frac{sN}{2\pi r}\sqrt{1+1/\tan^2\beta} \qquad (16.31)$$

The distance between the stream lines forming stream tubes with equal flow along its length, in the meridional stream surfaces is denoted by dn (See fig. (16.2) , fig.(16.2b), fig.16.4) and

fig.16.9 as shown later. If the number of stream tubes between crown and band = N, we find the meridional velocity c_m from the equation of continuity as given by eq (16.32) (Note that the distance dn will decrease with increasing value of c_m that is often the case towards the band) (Further N = number of blades that theoretically should be a very high number close to infinite value for the purpose of a very uniform flow field, but for practical cases the number of blades are limited to 15 < N < 32 with the highest number for splitter blade runners).

$$\boxed{c_m = \frac{Q/N}{2\pi\, r\, dn\phi}} \qquad \text{and } \underline{c}_m = \frac{c_m}{\sqrt{2gH}} \tag{16.32}$$

FLOW CONDITIONS BEHIND THE BLADE OUTLETS AND IN FRONT OF THE INLET OF THE RUNNER WHERE THERE IS NO INFLUENCE FROM THE RUNNER BLADES OR ROTATION OF THE RUNNER.

Equation (16.6) gives the equation for the pressure variation across the stream lines behind the blades where no torque is converted when deleting the first term containing the influence from the acceleration in x direction i.e. $a_x = 0$. Further $\underline{\omega} = 0$ outside the rotating runner i.e. Coriolli's and centripital accelerations vanish i.e. all terms including $\underline{\omega}$ shall be omitted. In the velocity diagram $\underline{c}_m/\tan\beta = \underline{c}_u$. Now eq. (16.6) yields for the flow below the runner blades outlet and in front of the runner between the guide vanes and the blades inlet.

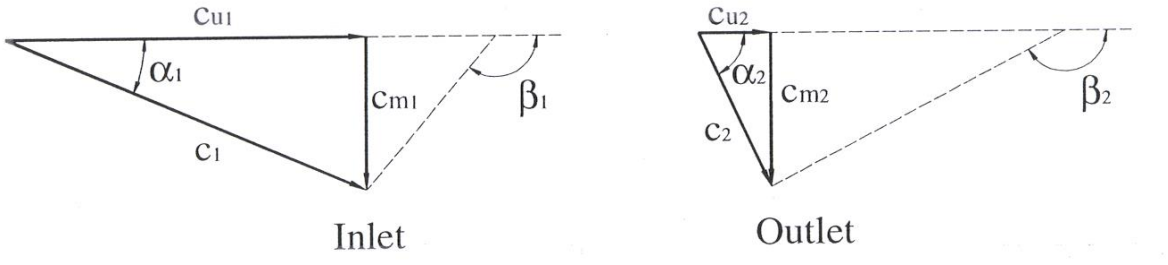

Fig. 16.5. Velocity vector diagram behind the blade outlets in front of the inlet.

When deleting the terms including $\underline{a}_x$ and $\underline{\omega}$ in eq. (16.27) or (16.28), because $\underline{a}_x = 0$ and $\underline{\omega} = 0$, the equation for the flow downstream (or upstream) of the runner can be described by eq. (16.27) or eq.(16.28) which now will be changed as follows:

$$\frac{dh}{dl} = 2\left\{ -\underline{c}_m \frac{\partial \underline{c}_m}{\partial m}\sin\psi + \frac{\sin(\delta-\psi)}{r}\frac{\underline{c}_m^2}{\tan^2\beta} + \frac{\cos\psi}{\rho}\underline{c}_m^2 \right\}$$

Further r/sin (δ - ψ) = l and $\underline{c}_m^2 / \tan^2\beta = \underline{c}_u^2$ and then we arrive at following equation:

$$\underline{dh = 2\left\{ \frac{\underline{c}_m^2}{\rho}\cos\psi + \frac{\underline{c}_u^2}{l} - \underline{c}_m \frac{\partial \underline{c}_m}{\partial m}\sin\psi \right\} d1} \qquad (16.33)$$

Further by introducing the energy equation assuming constant energy across the draft tube.

$$H = \underline{h} + \underline{c}^2 = \underline{h} + \underline{c}_u^2 + \underline{c}_m^2 = \text{constant}$$

After differentiation:

$$d\underline{h} = -(2\,\underline{c}_u d\underline{c}_u + 2\underline{c}_m d\underline{c}_m)$$

By substituting for d$\underline{h}$ in eq.(16.33)

$$\underline{c}_u d\underline{c}_u + \underline{c}_m d\underline{c}_m = \left\{ -\frac{\underline{c}_m^2}{\rho}\cos\psi - \frac{\underline{c}_u^2}{l} + \underline{c}_m \frac{\underline{c}_m}{\partial m}\sin\psi \right\} dl$$

Rearranged

$$\frac{\underline{c}_u^2}{l} dl + \underline{c}_u dc_u + \underline{c}_m d\underline{c}_m = (-\frac{\underline{c}_m^2}{\rho}\cos\psi + \underline{c}_m \frac{\partial \underline{c}_m}{\partial m}\sin\psi) dl \qquad (16.34)$$

Further, when introducing

$$d(r\underline{c}_u) = \underline{c}_u dr + r d\underline{c}_u$$

Then rearranging by multiplying with c_u/r

| $$\frac{\underline{c}_u}{r} d(r\underline{c}_u) = \frac{\underline{c}_u^2}{r} dr + \underline{c}_u d\underline{c}_u$$

Noting from fig.1 that dr/r =dl/l gives:

$$\frac{\underline{c}_u}{r} d(r\underline{c}_u) = \frac{\underline{c}_u^2}{l} dl + \underline{c}_u d\underline{c}_u \qquad (16.35)$$

Combining eq. (13) (16.34) and eq. (14) (16.35):

$$\frac{\underline{c}_u}{r} d(r\underline{c}_u) + \underline{c}_m d\underline{c}_m = \left[-\frac{\underline{c}_m^2}{\rho}\cos\psi + \underline{c}_m \frac{\partial \underline{c}_m}{\partial m}\sin\psi \right] dl$$

Rearranged

$$\frac{d\underline{c}_m}{dl} = -\frac{\underline{c}_m}{\rho}\cos\psi - \frac{\underline{c}_u}{r\underline{c}_m}\frac{d(rc_u)}{dl} + \frac{\partial \underline{c}_m}{\partial m}\sin\psi$$

Further, substituting for

$$d(r\underline{c}_u)^2 = 2r\underline{c}_u d(r\underline{c}_u) \quad or \quad \underline{c}_u d(r\underline{c}_u) = d(r\underline{c}_u)^2/(2r)$$

gives an important equation, i.e.

THE EQUATION FOR THE FLOW BETWEEN GUIDE VANES OUTLET AND RUNNER INLET.

$$\boxed{\frac{d\underline{c}_m}{dl} = -\frac{\underline{c}_m}{\rho}\cos\psi - \frac{1}{2\,\underline{c}_m r^2}\frac{d(r\underline{c}_u)^2}{dl} + \frac{\partial \underline{c}_m}{\partial m}\sin\psi} \qquad (16.36)$$

This equation is valid in a chosen direction l by chosing the angle ψ f.ex. along the inlet or outlet edge of blades or guide vanes.

Eq. (16.36) must be combined with the meridional flow at the guide vanes outlet or any other chosen direction of l as shown later calculated by eq. (16.56) as shown in the last part of this chapter. [Note: If ψ = 0 l-direction will be identical to n-direction].

Eq. (16.36) is the general equation for the flow in front of the runner or behind the runner outlet. If $c_u = 0$ which will be the case in the draft tube at the best hydraulic efficiency $rc_u = 0$ i.e. no rotational flow and eq. (16.36) will be simplified to:

$$\boxed{\frac{d\underline{c}_m}{dl} = -\frac{\underline{c}_m}{\rho}\cos\psi + \frac{\partial \underline{c}_m}{\partial m}\sin\psi} \qquad (16.37)$$

Further if the (l-x) plane is chosen normal to the stream lines $\Psi = 0$ and the following simplified equation can be used for the flow in the draft tube below the runner: (l direction = n direction)

$$\boxed{\frac{d\underline{c}_m}{dn} = -\frac{\underline{c}_m}{\rho}} \qquad (16.38)$$

BLADE LOAD TOWARDS THE OUTLET OF THE BLADES WHERE THE INFLUENCE FROM THE BLADES VANISH AND THE ACCELERATION IS REDUCED TO ZERO.

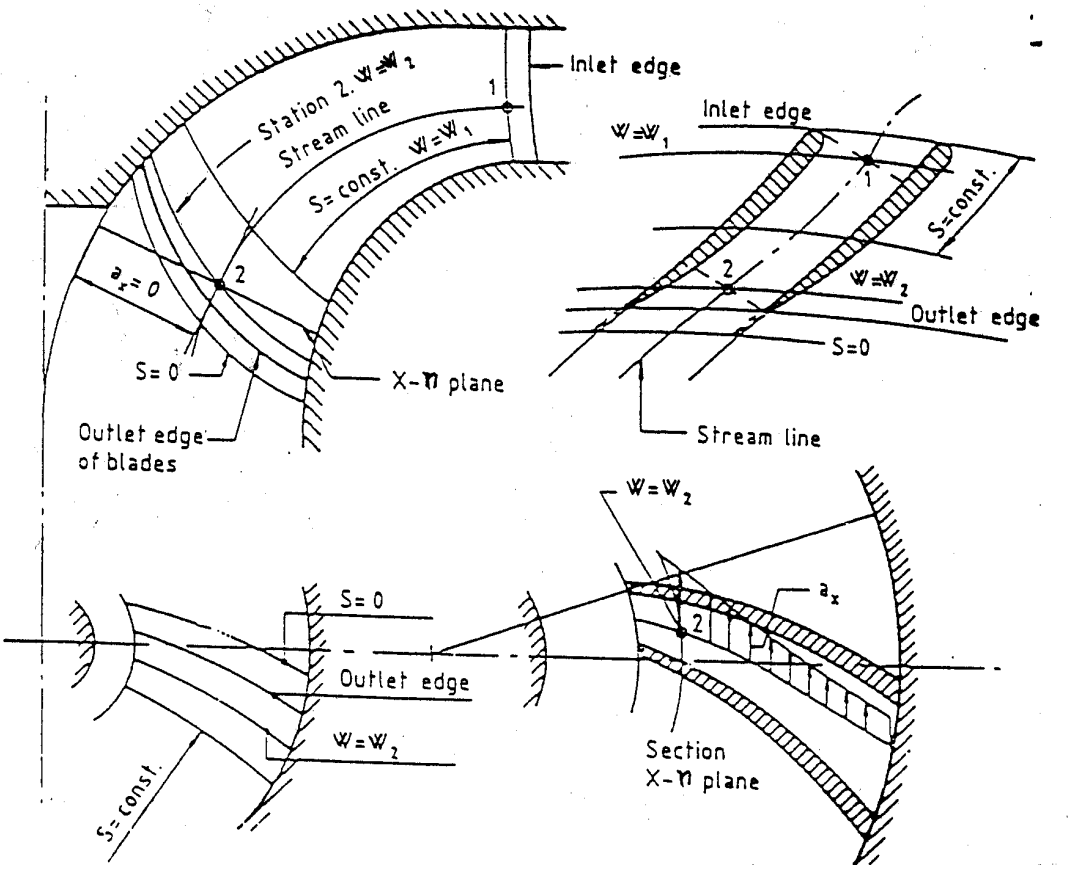

Fig. 16.6. Illustration of blade geometry and acceleration at blade outlet

Following assumption may be made of the decaying of acceleration towards the blade outlet: The influence from the blade is assumed to vanish at the point s = 0, as shown in fig. 16.6, where the prolonged taperedness of the blade ends. (I.e. s = 0, s = blade thickness). (See fig. 16.6).

The stream surface is assumed to be identical to the blades' suction side. The thickness is decreasing towards the outlet tip of the blade with constant taperness and with thickness further prolonged to zero with the same taperedness as shown in Fig.16.6 and in Fig. 16.7.

It may be discussed where the location of point 3 ($w=w_3$ and $a_x = a_{x3}$) is where there is full influence from the blades on the flow according to eq.(16.28) and eq. (16.30) and how the acceleration a_x decreases to zero towards the blades' outlet (see fig. 16.7)

If a sudden decrease of $a_x = a_{x3}$ according to eq (2) to $a_x = 0$ according to eq. (16.37) occurs at a point located between 2 and 3 a discontinuity will occure in the stream lines as the function suddenly shifts from eq.(16.27) to eq. (16.37) for best efficiency point of operation.

However, if a smoothening of the discontinuity is made, the velocity c_m and c_u will be almost correct when the blade thickness s is taken into consideration as well as a wake formed as an elongation of the blades.

Another and may the best approach to the problem is to assume that the acceleration = a_x decreases to zero at the blade tip from a full value according to eq.(16.24) at point 3. That is eq.(16.37) is valid at point 2 (the blade tip) and eq.(16.24) is valid at point 3.

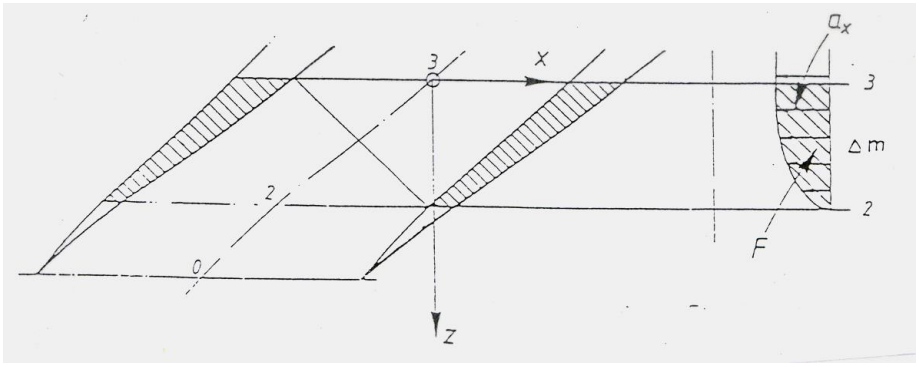

Fig. 16.7. Illustration of the blade outlets and assumed decrease of the acceleration a_x (Note: $\underline{c}_{m3} = \underline{c}_{m2} = \underline{c}_{mo}$ along middle stream surface.)

At point 0 the displacement influence from the blade thickness is assumed to vanish. Between point 3 and 2 in Fig 16.7, the rotational component of $\underline{c}$, $\underline{c}_u$ is assumed to decrease from $\underline{c}_{u3}$ to $\underline{c}_{u2}$ and the acceleration a_x decreases.

Following simplified study may be made in order to find the velocity and acceleration in the outlet region for control of the outlet velocity $\underline{c}_{u2}$.

From the Euler turbine equation the value of c_u in the draft tube may be found

$$\eta_\eta = 2(\underline{u}_1\underline{c}_{u1} - \underline{u}_2\underline{c}_{u2}) \qquad (1 \text{ denotes inlet and } 2 \text{ outlet of blades})$$

Introducing $\underline{u} = \underline{\omega}r$ and rearranging the equation:

$$\underline{c}_{u2} = (\underline{\omega}\, r_1 \underline{c}_{u1} - \eta_h / 2)/(\underline{\omega}\, r_2)$$

Further $\underline{c}_m$ is known in point 3 where eq.(16.28), eq.(16.30) and eq.(16.23) are valid from the analysis described earlier in this chapter and the blade angle or stream surface angle β is known as well as r in point 3. Then we get:

$$\underline{c}_{u3} = \underline{\omega} r_3 - \underline{c}_{m3} / \tan\beta \qquad \text{(note } \underline{c}_m/\tan\beta = \underline{w}_m/\tan\beta = \underline{w}_x\text{)}$$

Further $\underline{a}_x$ can be found from eq.(16.24) when $\underline{c}_m$ is determined in point 3 from the flow analysis in the runner as shown earlier. (See eq.(16.24).

$$\underline{a}_{x3} = \underline{c}_{m3}\left(\frac{\partial \underline{c}_m}{\partial m}\right)_3 \frac{1}{\tan\beta} + \left(\frac{\cos\delta \cos^3\beta}{r} - \frac{1}{R}\right)\frac{\underline{c}_m^2}{\sin^3\beta} - 2\,\underline{\omega}\cos\delta\,\underline{c}_m$$

(See eq.(16.24)).

In addition Δm is known and following simple analysis can be made:

The velocity difference of $\underline{c}_m$ between point 3 and 2 is assumed to be zero i.e. $\underline{c}_m$ = const. and $\partial\underline{c}_m/\partial m = 0$ and then $\Delta t = \Delta m/\underline{c}_m$ where Δm is the meridional distance between point 2 and 3. The variation in $\underline{c}_u$ will be:

$$\Delta \underline{c}_u = \underline{c}_{u3} - \underline{c}_{u2} = \int_{\circ}^{\Delta t} \underline{a}_\chi dt = \int_{\circ}^{\Delta m / c_m} \underline{a}_x / \underline{c}_m dz$$

and $\underline{c}_m = \underline{c}_{m3} = (Q/N) / (2\,\pi\, r\, b\, \phi)$

(See eq. (11)) when assuming $\underline{c}_m$= const. = $\underline{c}_{m3}$ between 2 and 3.

$$\Delta \underline{c}_u = F / \underline{c}_{m3} \; where \; F = \int_{\circ}^{\Delta m / c_m} \underline{a}_x dm \qquad \text{(See fig. 16.7)} \qquad (16.39)$$

For simplification we introduce a value K describing the decrease in acceleration from 3 to 2 as follows, in order to determine $\Delta\underline{c}_u$ and $\underline{c}_{u2}$ for determining the outlet vector velocity diagram where $\underline{c}_u$ should be zero at best efficiency. The value K can then be determined as follows:

$$F = K\,\underline{a}_{x3}\Delta m = 0 \qquad (16.40)$$

Then we arrive at following equation:

$$\Delta \underline{c}_u = \frac{K\ \underline{a}_{x3} \Delta m}{\underline{c}_{m3}} \quad \text{or} \quad K = \frac{\Delta \underline{c}_u\, \underline{c}_{m3}}{\underline{a}_{x3}\ \Delta m} \quad \text{and} \quad \underline{c}_{u2} = \underline{c}_{u3} - \Delta \underline{c}_u \tag{16.41}$$

DETERMINATION OF THE VARIATION OF THE MERIDIONAL VELOCITY c_{m2} IN X DIRECTION BY MEANS OF ANALYTICAL EQUATIONS.

In order to find the variation of c_m in x direction a differentiation of eq. (16.30) may be carried out as follows:

$$\frac{\partial \underline{h}}{\partial x}\, dx = -\frac{2}{\sin^2 \beta}\, \underline{c}_m \frac{\partial \underline{c}_m}{\partial x}\, dx \tag{16.42}$$

Note: All terms except the second term $\underline{c}_m^2 / \sin^2 \beta$ are constant for m= const. in eq. (16.30) (including J ≈ const. for m = const.)

Further from eq. (1) we get for dm = 0: (m = const.)

$$\underline{d\,h} = \frac{\partial \underline{h}}{\partial x}\, dx = -2 \underline{a}_x dx \tag{16.43}$$

By combining eq. (16.42) and eq. (16.43) we get:

$$\underline{a}_x = \frac{1}{\sin^2 \beta}\, \underline{c}_m \frac{\partial \underline{c}_m}{\partial x}\, dx \tag{16.44}$$

Then by substituting for $\underline{a}_x$ by eq. (16.24):

$$\underline{c}_m \frac{\partial \underline{c}_m}{\partial m} \frac{1}{\tan \beta} + \left(\frac{\cos \delta \cos^3 \beta}{r} - \frac{1}{R}\right) \frac{\underline{c}_m^2}{\sin^3 \beta} - 2\, \underline{\omega} \cos \delta\, \underline{c}_m = \frac{1}{\sin^2 \beta}\, \underline{c}_m \frac{\partial \underline{c}_m}{\partial x}\, dx$$

Normally $\partial \underline{c}_m / \partial m$ has a very small value and for simplification the term $\underline{c}_m \frac{\partial \underline{c}_m}{\partial m} \frac{1}{\tan \beta}$ may be neglected and we arrive at the following equation:

$$\frac{\partial \underline{c}_m}{\partial x} = \left(\frac{\cos\delta \cos^3\beta}{r} - \frac{1}{R}\right)\frac{\underline{c}_m}{\sin\beta} - 2\,\underline{\omega}\sin^2\beta\cos\delta \qquad (16.45)$$

After rearrangement and substituting for

$$A = 2\underline{\omega}\sin^2\beta\cos\delta \qquad (16.46)$$

and

$$B = \left(\frac{1}{R} - \frac{\cos\delta\cos^3\beta}{r}\right)\frac{1}{\sin\beta} \qquad (16.47)$$

$$\frac{d\underline{c}_m}{A + B\,\underline{c}_m} = -dx \qquad (16.48)$$

Integration from x = 0 to x where $\underline{c}_m = \underline{c}_{mo}$ increasing to $\underline{c}_m$ which gives following equation:

$$0 - x = -\frac{1}{B}\ln(B\,\underline{c}_{mo} + A) + \frac{1}{B}(B\underline{c}_m + A)$$

or

$$B\underline{c}_m + A = e^{(\ln B\underline{c}_{mo} + A - Bx)}$$

Which may be rearranged to following expression for $\underline{\mathbf{e}}_{\mathbf{m}}$:

$$\underline{c}_m = \frac{e^{\left[\ln\left(B\underline{c}_{mo} + A\right) - Bx\right]} - A}{B} \qquad (16.49)$$

This equation is suitable for controlling the velocity gradient in the field in-between the blades and at the outlet and inlet region where the influence from the blades still fulfil the conditions for eq.(16.30).

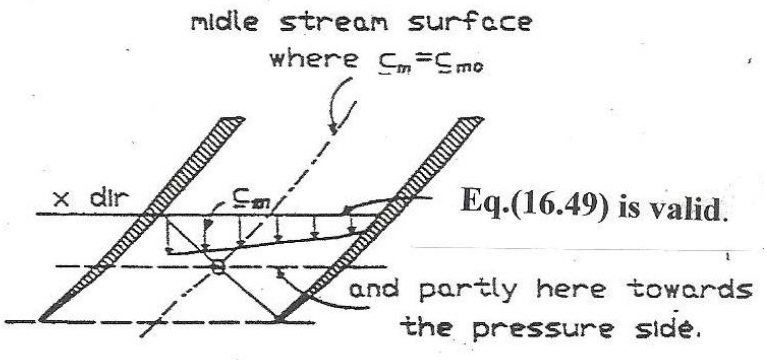

Fig. 16.8 Illustration of the velocity distribution $\underline{c}_m$ at the blade outlets.

(Note: $\underline{c}_{m3} = \underline{c}_{m2} = \underline{c}_{mo}$ along middle stream surface. See fig. 16.7)

The procedure of the graphical iteration process is briefly described for the use of eq. (16.28), eq. (16.30) and eq. (16.32) which must be fulfilled by adjusting the location of the stream lines or stream surfaces in the meridional plane. An example of the graphical procedure is illustrated in fig. 16.9. Normally it is convenient to divide the distance between two blades in 4 sections illustrated on top of fig. 16.9. In this case the number of blades at the inlet is high due to splitter blades i.e. $\Delta\phi = 3^o$ and this value of $\Delta\phi$ will be used through the runner.

Note: In chapter III in this appendix analytical equations for calculation of the angles θ and β are developed for use during blade shaping based on the intersection lines between blades and meridional sections and horizontal section lines of the blades seen from above.

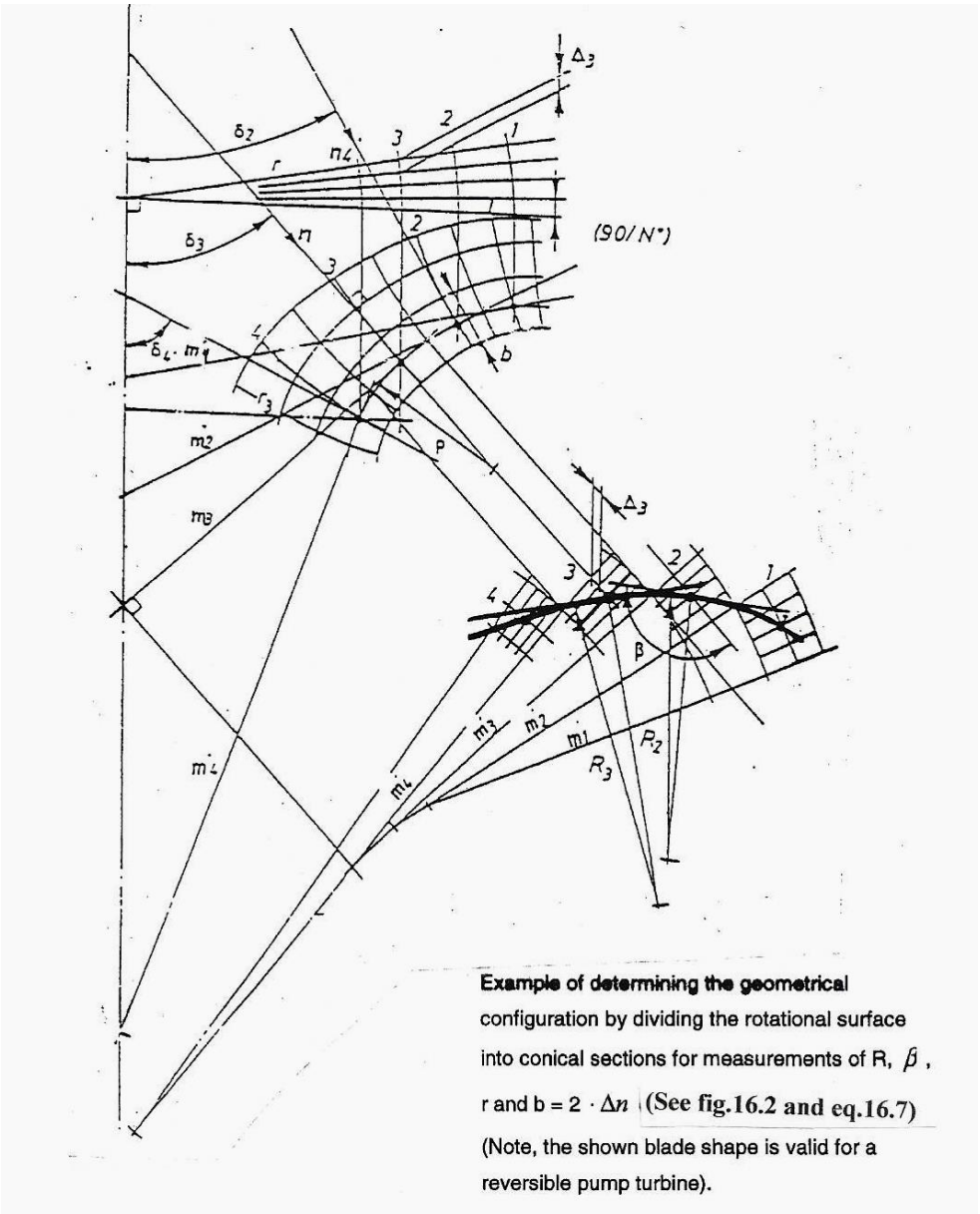

Fig. 16.9. Example of determining the geometrical configuration by dividing the rotational surface into conical sections for measurements of R, β, r and b = 2 Δn (see fig. 1 and eq. (6) (see fig. 16.2 and eq. (16.27))

CALCULATION OF THE FLOW CONDITIONS FROM THE GUIDE VANE OUTLET TO THE RUNNER INLET

The pressure along the L direction in front of the runner can be found by studying the acceleration in m and n direction (see fig. 16.2). The acceleration in n direction can be divided in a contribution from the circumferential velocity component in radial direction $a_r = \underline{c}_u^2 / r$ and from the meridional velocity component caused by the curvature of the stream surface = $\underline{c}_m^2 / \rho$.

The component from $\underline{a}_r$ in n direction yields:

$$\underline{a}_n = \frac{-a_r}{\sin\delta} = \frac{-\underline{c}_u^2}{r\sin\delta} = \frac{-\underline{c}_u^2}{n}$$

Then:

$$\underline{a}_n = -\left(\frac{\underline{c}_u^2}{n} + \frac{\underline{c}_m^2}{\rho}\right)$$

In the same way the acceleration in m direction can be found including the component from the circumferential velocity component = $\underline{c}_u^2 / (r\cos\delta) = \underline{c}_u^2 / m.$

$$\underline{a}_m = \frac{\partial \underline{c}_m}{\partial t} + \underline{c}_m \frac{\partial \underline{c}_m}{\partial m} - \frac{\underline{c}_u^2}{m} \qquad \textit{and} \qquad \frac{\partial \underline{c}_m}{\partial t} = 0 \quad \text{for steady state flow.}$$

From the energy equation:

$$gh + \frac{c^2}{2} = const. \quad \text{with reduced variables } \underline{h} = \frac{h}{H} \textit{ and } \underline{c} = c/\sqrt{2gH} \quad \textit{i.e.} \quad \underline{h} + \underline{c}^2 = const.$$

After differentiation:

$$\frac{d\underline{h}}{dl} = -2\underline{c}\frac{d\underline{c}}{dl} = -2\underline{a}_l$$

or

$$d\underline{h} = -2\underline{a}dl = -2\left(\underline{a}_n\, dn + \underline{a}_m\, dm\right)$$

Substituting for ($\underline{a}_n$) and ($\underline{a}_m$):

$$d\underline{h} = 2\left(\frac{\underline{c}_u^{\,2}}{n}dn + \frac{\underline{c}_{m^2}}{\rho}dn - \underline{c}_m\frac{\partial \underline{c}_m}{\partial m}dm + \frac{\underline{c}_{u^2}}{m}dm\right) \qquad (16.50)$$

From basic geometry study of fig. 16.2

$$\frac{dn}{n} + \frac{dm}{m} = \frac{dl\cos\psi\sin\delta}{r} + \frac{dl\sin\psi\cos\delta}{r} = \frac{dl\sin(\delta+\psi)}{r} = \frac{dl}{l}$$

When substituting for dn=cos ψ dl and dm=sin ψ dl and $\frac{dn}{n}+\frac{dm}{m}=\frac{dl}{l}$ in eq(16.50) :

Then:

$$d\underline{h}=2\left(\underline{c}_u{}^2\frac{dl}{l}+\frac{\underline{c}_m{}^2}{\rho}\cos\psi\ dl-\underline{c}_m\frac{\partial \underline{c}_m}{\partial m}\sin\psi\ dl\right) \qquad (16.51)$$

In addition the energy equation gives:

$$\underline{h}+\underline{c}^2=const$$

and then after differentiation:

$$d\underline{h}=-2\underline{c}\ d\underline{c} \qquad (16.52)$$

Eliminating $\underline{h}$ from eq.(16.51) and eq. (16.52)

$$\underline{c}\ d\underline{c}=-\left(\frac{\underline{c}_u{}^2}{l}dl+\frac{\underline{c}_m{}^2}{\rho}\cos\psi\ dl-\underline{c}_m\frac{\partial \underline{c}_m}{\partial m}\sin\psi\ dl\right)$$

Dividing by dl and substituting for $\underline{c}_u=\underline{c}\cos\alpha$ and $\underline{c}_m=\underline{c}\sin\alpha$:

$$\underline{c}\frac{d\underline{c}}{dl}=-\frac{\underline{c}^2\cos^2\alpha}{l}-\frac{\underline{c}^2\sin^2\alpha\cos\psi}{\rho}+\underline{c}\frac{\partial \underline{c}_m}{\partial m}\sin\alpha\ \sin\psi$$

Then after dividing by $\underline{c}$:

$$\boxed{\frac{d\underline{c}}{dl}=-\underline{c}\left(\frac{\cos^2\alpha}{l}+\frac{\sin^2\alpha\cos\psi}{\rho}\right)+\frac{\partial \underline{c}_m}{\partial m}\sin\alpha\ \sin\psi} \qquad (16.53)$$

or when substituting for $\underline{c}_m=\underline{c}\sin\alpha$:

$$\boxed{\frac{d\underline{c}_m}{dl}=-\underline{c}_m\left(\frac{\cos^2\alpha}{l}+\frac{\sin^2\alpha\cos\psi}{\rho}\right)+\frac{\partial \underline{c}_m}{\partial m}\sin^2\alpha\ \sin\psi} \qquad (16.54)$$

[Note: If ψ = 0 l-direction will be identical to n-direction.]

In addition to eq.(16.54) the value of $\underline{c}_m=\underline{c}\sin\alpha$ can be found by means of the equation of continuity. The equation of continuity yields when assuming the flow between two stream surfaces with distance Δl to be ΔQ: where $\Delta Q=Q/N$ (N = number of spaces between stream surfaces assuming equal flow in all spaces.)

$$\underline{c}_m = \frac{\Delta \underline{Q}}{2\pi\, r \cos\psi\, \Delta l} = \frac{\Delta \underline{Q}}{2\pi\, r \Delta n} \tag{16.55}$$

Along the outlet edge of the guide vanes of a Francis turbine eq. (16.54) may be written as follows when letting l= ∞ i.e. $(\delta + \psi) = 0^\circ$

$$\frac{d\underline{c}_m}{dl} = \underline{c}_m \frac{\sin^2\alpha \cos\psi}{\rho} + \frac{\partial \underline{c}_m}{\partial m} \sin^2\alpha \sin\psi \tag{16.56}$$

In addition the equation of continuity, eq.(16.55), is still valid. (See fig. 16.2 and fig. 16.1).

THE FLOW BETWEEN THE GUIDE VANE OUTLET AND RUNNER INLET

A graphical procedure to solve the flow regime at the guide vane outlet is illustrated in fig. 16.10. Note, between the guide outlet we know that $\underline{u}_o\, \underline{c}_{uo} = \underline{u} \underline{c}_u$ or $r_o\, \underline{c}_{uo} = r \underline{c}_u$.
The value of $\underline{c}_m$ can be found by means of the equation of continuity between the chosen stream surfaces.
The analysis shown in this chapter is made in order to get a physical understanding of the flow in front of the runner inlet expressed by eq. (16.36) which is valid for a free swirl flow.
For a graphical solution it may be convenient to multiply eq.(16.36) by ($2\underline{c}_m$) leading to equation (16.37).

$$\frac{d\underline{c}_m^2}{dl} = \underline{c}_m^2 \frac{2\cos\psi}{\rho} - \frac{1}{u^2} \frac{d(\underline{u}\, \underline{c}_u)^2}{dl} + 2\underline{c}_m \frac{\partial \underline{c}_m}{\partial m} \sin\psi \tag{16.57}$$

Note that the last term may be deleted due to smallness for all practical solutions. The term may be calculated by means of eq.(16.55) by increments of m by Δm when establishing sections with ψ =0, i.e. sections normal to the stream surfaces i.e. in n - direction. Then eq (16.56) and eq.(16.57) will give simplified values of ($d\underline{c}_m/dn$) and (dc_m^2/dn) respectively with the value of ψ =0.

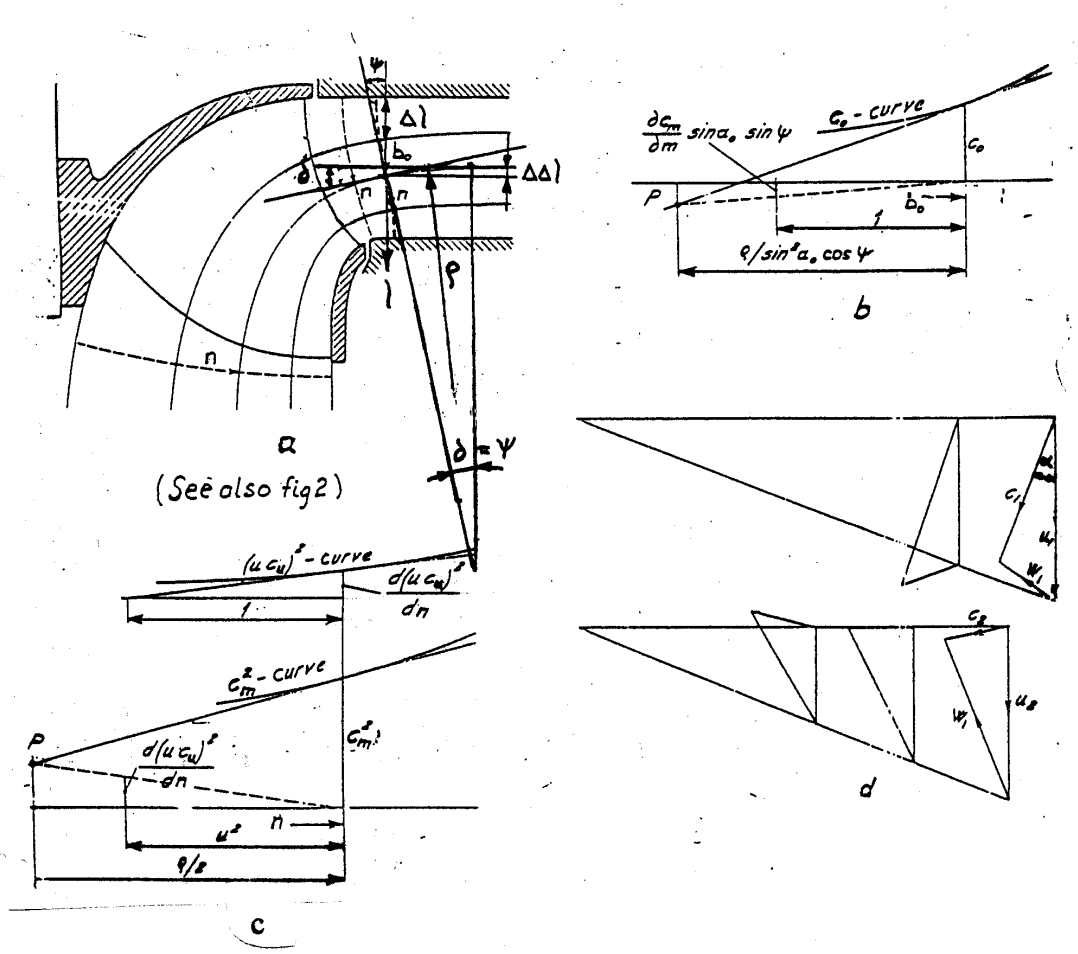

Fig. 16.10 Illustration of the flow at the guide vane outlet egde (see b) and eq.(16.53) and eq.(16.56) with $(\cos^2\alpha\ /l)=0$ for $l=\infty$ and the flow between the guide vane outlet and runner inlet (see c) and eq.(16.55) and eq.(16.57).

CALCULATION OF $\underline{c}_m$, α, ρ and ψ AT THE GUIDE VANE OUTLET AND IN THE VAINLESS SPACE BETWEEN THE GUIDE VANES AND RUNNER INLET

This method is an alternative to the graphical method and is based on an iteration process that can easily be made by a PC.

The governing equations are eq.(16.36) developed earlier for the inlet flow towards the runner and eq.(16.54) and eq.(16.55) for flow condition from conditions between guide vanes and runner inlet. Equation (16.36) is based on equilibrium of forces i.e. Newtons 2. law.

$$\frac{\partial \underline{c}_m}{\partial l} = -\frac{\underline{c}_m}{\rho}\cos\psi - \frac{1}{2\underline{c}_m r^2}\frac{d(r\underline{c}_u)^2}{dl} + \frac{\partial(\underline{c}_m)}{\partial m}\sin\psi \qquad (16.36)$$

(Repeated from earlier development)

Equation (16.55) is based on the energy equation:

$$\frac{\partial \underline{c}_m}{\partial l} = -\underline{c}_m\left[\frac{\cos^2\alpha}{l} + \frac{\sin^2\alpha\cos\psi}{\rho}\right] + \frac{\partial \underline{c}_m}{\partial m}\sin^2\alpha\sin\psi \qquad (16.54)$$

Equation (16.55) is the equation of continuity

$$\boxed{\underline{c}_m = \frac{\Delta \underline{Q}}{2\pi r\cos\psi\,\Delta l}} \qquad (16.55)$$

Here $\Delta Q = Q/N$ where N is the number of spaces between stream surfaces dividing the flow in equal partial flows.
Note, for the outlet edge of the guide vanes $(\delta - \psi) = 0$ and then from fig.16.2 and the development of eq. (16.33) we find $r/\sin(\delta - \psi) = l = \infty$.

Then eq.(16.54) will be simplified to:

$$\frac{\partial \underline{c}_m}{\partial l} = -\underline{c}_m\frac{\sin^2\alpha\cos\psi}{\rho} + \frac{\partial \underline{c}_m}{\partial m}\sin^2\alpha\sin\psi \qquad (16.56)$$

However, it is more convenient to use eq.(16.36), eq.(16.54) and eq.(16.55) for a general solution and let l = ∞ for the special case at the guide vane outlet.

THE SOLUTION

For a start of computation the meridional sections of the stream surfaces must be chosen as a start value (chose 9 or minimum 3 stream surfaces between crown and band.) (See fig. 16.10).

Then start value of $\underline{c}_m$ can be calculated by eq.(16.55).

The parameters ψ, ρ *and* $(r\,\underline{c}_u)$ can be found from the preliminary drawn stream surfaces, runner inlet radius and angular velocity ω.
[ψ and ρ can be found from the drawn meridian section and ($r\,\underline{c}_u$) can be calculated by means of the Euler equation $\underline{\omega}\cdot r_1\underline{c}_{u1} = \eta_h$ because $\underline{\omega} r_2\cdot\underline{c}_{u2} = 0$ ($\omega = *n\cdot\pi/30$ where *n is the turbine speed at best efficiency and $\eta_h = 0.96 - 0.98$.) This is because $r\underline{c}_u = r_0\,\underline{c}_{u0} = r_1\,\underline{c}_{u1}$ = const. between guide vanes and runner inlet].

Then by combining eq (15) (16.36) and eq (33) (16.54) the following equation can be established in order to find $\partial(rc_u)/\partial l = f[\underline{c}_m, (r_1 c_{u1})]$ as follows:

$$-\frac{\underline{c}_m}{\rho}\cos\psi - \frac{1}{2\underline{c}_m r^2}\frac{d(r\underline{c}_u)^2}{\partial l} + \frac{\partial \underline{c}_m}{\partial m}\sin\psi + \underline{c}_m\left[\frac{\cos^2\alpha}{l} + \frac{\sin^2\alpha\cos\psi}{\rho}\right] - \frac{\partial \underline{c}_m}{\partial m}\sin^2\alpha\sin\psi = 0$$

or

$$\underline{c}_m\left[\frac{\cos^2}{l} + \frac{(\sin^2\alpha - 1)\cos\psi}{\rho}\right] + \frac{\partial c_m}{\partial m}\sin\psi\,(1-\sin^2\alpha) - \frac{1}{2\underline{c}_m r^2}\frac{\partial(r\,\underline{c}_u)^2}{\partial l} = 0$$

and finally:

$$\underline{c}_m^2\left[\frac{\cos^2\alpha}{l} - \frac{\cos^2\alpha\cos\psi}{\rho}\right] + \underline{c}_m\frac{\partial \underline{c}_m}{\partial m}\sin\psi\cos^2\alpha - \frac{1}{2r^2}\frac{\partial(r\underline{c}_u)^2}{\partial l} = 0$$

Normally the second term may be omitted due to smallness.

Further $\dfrac{\partial(r\underline{c}_u)^2}{\partial l} = 2(r\underline{c}_u)\dfrac{\partial(r\underline{c}_u)}{\partial l}$ and then

$$\underline{c}_m^2\left[\frac{\cos^2\alpha}{l} - \frac{\cos^2\alpha\cos\psi}{\rho}\right] - \frac{1}{r^2}(r\underline{c}_u)\frac{\partial(r\underline{c}_u)}{\partial l} = 0$$

rearranged and remembering that $r\,\underline{c}_u = r_1\,\underline{c}_{u1} = r_o\,\underline{c}_{uo}$ following two alternatives yields:

$$\boxed{\frac{\partial(r\underline{c}_u)}{\partial l} = \frac{\underline{c}_m^2 r^2}{r\underline{c}_u}\left[\frac{\cos^2\alpha}{l} - \frac{\cos^2\alpha\cos\psi}{\rho}\right]} \text{ or } \boxed{\frac{\partial\left((r\underline{c}_u)^2\right)}{\partial l} = 2\underline{c}_m^2 r^2\left[\frac{\cos^2\alpha}{l} - \frac{\cos^2\alpha\cos\psi}{\rho}\right]} \quad (16.58)$$

For calculation of the swirl variation along the guide vane outlet edge = ($r_o\,\underline{c}_{uo}$) the first term in brackets on right hand side can be omitted as mentioned earlier, because $\sin(\delta - \psi) = \sin o = o$ and $r/\sin(\delta - \psi) = l = \infty$ (see fig. 16.2)

Then

$$\boxed{\frac{\partial(r\underline{c}_u)_o}{\partial l} = -\underline{c}_m^2\frac{r^2}{r\underline{c}_u}\cdot\frac{\cos^2\alpha\cos\psi}{\rho}} \text{ or } \boxed{\frac{\partial\left((r\underline{c}_u)_o^2\right)}{\partial l} = -2\underline{c}_m^2 r^2\frac{\cos^2\alpha\cos\psi}{\rho}} \quad (16.59)$$

Because $r_1 \underline{c}_{u1} = r_o \underline{c}_{uo} = r\underline{c}_u$ = const. the variation of $r_o \underline{c}_{uo}$ i.e. $\frac{\partial (r\underline{c}_u)_o}{\partial l}$ along the guide vane outlet must be calculated in order to find the variation of $r_1 c_{u1}$ at the runner blade inlet.

It is convenient to start with the velocity $\underline{c}_m$ between the middle stream surfaces calculated by means of eq.(16.55). Then $(r_o \underline{c}_{uo})^2 = (r_1 \underline{c}_{u1})^2 = (\eta_h / (2\omega))^2$ must be calculated based on the Euler equation where $\underline{u}_2 \underline{c}_{u2}$ is assumed to be zero.

The value of $(r_o \underline{c}_{uo})_i^2$ between the middle stream surfaces forms the base value for calculation of $\underline{c}_{uo} = \sqrt{(r_o \underline{c}_{uo})^2} / r_o$ which is used for calculation of the correct guide vane angle α_o from the guide vane on the stream surface with angle δ normal to the ψ direction. This angle will be Atan ($\underline{c}_{mo} / \underline{c}_{uo}$) where $\underline{c}_{uo}$ is found by the Euler equation to fit $\eta_h / (2\underline{\omega}) = r_1 \underline{c}_{u1} = r_o \underline{c}_{uo}$.

Then following equation yields for the guide vane angle α_g at the outlet edge if this is parallel to the turbine shaft i.e. $\delta = \psi$: (see fig. 16.10).

$$\tan \alpha_g = \frac{\underline{c}_{mo} \cos \delta}{\underline{c}_{uo}} = \frac{\underline{c}_{mo} \cos \psi}{\underline{c}_{uo}} \qquad (16.60)$$

It must be noted that the guide vane angle α_g is controlling the flow angles α_o as shown in eq (16.60) for all stream lines along the guide vane outlet edge . Then the flow angles α_o must fulfil following equation for all stream surfaces:

$$\tan \alpha_o = \frac{\underline{c}_{mo}}{\underline{c}_{uo}} = \frac{\tan \alpha_g}{\cos \psi} = \frac{\tan \alpha_g}{\cos \delta} \qquad (16.61)$$

By means of the first preliminary drawn stream surfaces the value of $\underline{c}_{mo}$ of the stream lines between the stream surfaces can be calculated by eq (34) (16.55).
The next value $(r_o \underline{c}_{uo})^2_{i+1}$ of between the neighbouring stream surfaces on the outlet edges of the guide vanes can then be found by following equation:

$$\left(r_o \underline{c}_{uo}\right)^2_{i+1} = \left(r_o \ \underline{c}_{uo}\right)^2_i + \frac{\partial\left(\left(r_o \ \underline{c}_{uo}\right)^2\right)}{\partial l}\Delta l \qquad (16.62)$$

Here the last term on right hand side can be found by eq (38) (16.59). (Δl is the distance between the stream surfaces).

Then the value at the runner inlet of $\underline{c}_{u1\,(i+1)} = \sqrt{\left(r_o \ \underline{c}_{uo}\right)^2} / r_1$ can be calculated. The meridian velocity must fulfil eq.(16.55) and following equation after rearranging of eq (40) (16.61).

$$\boxed{\underline{c}_{mo\,(i+1)} = \underline{c}_{uo(i+1)} \tan\alpha_o = \frac{c_{uo(i+1)} \tan\alpha_g}{\cos\delta} = \frac{c_{uo(i+1)} \tan\alpha_g}{\cos\psi}} \qquad (16.63)$$

The value of $\underline{c}_{mo\,(i+1)}$ can now be determined by eq.(16.63), but it must be compared with the value of $\underline{c}_{mo\,(i+1)}$ found by means of eq. (16.55) based on the assumed value of Δl .

If the value of $\underline{c}_{mo\,(i+1)}$ found by eq.(16.55) is larger (or smaller) than the value found by eq.(16.63) the position of the assumed stream surfaces must be corrected i.e. Δl must be increased (or decreased) so $\underline{c}_{mo\,(i+1)}$ will be decreased (or increased) to a value in agreement with eq.(16.63).

However, by doing this the value of $\psi = \delta$ and ρ on the guide vanes outlet may also be changed and thus the value of $\partial\left(\left(r\underline{c}_u\right)^2\right)/\partial l$ determined by eq. (16.59) will be changed according to eq (38) (16.59). (Normally these corrections are minor often within the accuracy of the process. If a CFD analysis shall be made corrections will not be necessary after some

experience with this procedure).
A numerical iteration process may also be established by calculating an approximate value of ρ as a function of the distance $\Delta\Delta l$ below the horizontal stream surfaces at the guide vane outlets as shown in fig.16.10.

However, the following equations (16.64) and (16.65) can only be used for the guide vane outlet edge and other more efficient procedures may also be established and used by means of splaine functions. The presented calculation of ρ should only be regarded as a proposal.

$$\rho = \frac{\Delta\Delta l}{2\sin^2(\psi/2)} = \frac{\Delta\Delta l}{2\sin^2(\delta/2)} \qquad (16.64)$$

Then eq (38) (16.59) may be transformed by substituting for ρ as follows for a preliminar calculation

$$\boxed{\frac{\partial\left(\left(r\underline{c}_u\right)_o^2\right)}{\partial l} = 4\,\underline{c}_m^2\, r^2 \cdot \cos^2\alpha \cos\psi \sin^2(\psi/2)/(\Delta\Delta l)} \qquad (16.65)$$

By means of the presented equation an iteration process could be established by keeping the angle $\psi = \delta$ or the value of ρ growing as a function from band towards crown of the runner. Then adjusted values of $\psi = \delta$ should be introduced in a new iteration process. Where the proposed eq (43) (16.64) may be used or other spline functions combining ρ and $\psi = \delta$ is used. Because this procedure shall be used for a preliminary calculation of the blade angles only, more accurate values of $\psi = \delta$ will not be necessary.

The final result will show a variation of $r_1\,\underline{c}_{u1} = r_o\,\underline{c}_{uo}$ and $\underline{c}_{m1}$ by a calculation along the blade inlet edge of the runner blades leading to a variation of $r_2\,\underline{c}_{u2}$ at the blade outlet if the hydraulic efficiency η_h = const. along each stream surface. For the calculation along the blade inlets eq.(16.55) and eq.(16.58) should be used for control of the curvature radius ρ in a similar procedure as for the guide vane outlet edge.
By means of the values of $(r_1\,\underline{c}_{u1})$ the values for $\underline{c}_{u1}$ can be found by dividing by the known value r_1 from the drawing at each point of calculation. When also $\underline{c}_{m1}$ is found at the blade inlet by means of eq.(16.55) with control of ρ from the drawing andusing eq (16.58), the velocity vector diagram can be found when found by substituting for $\underline{\omega}\, r_1 = \underline{u}_1$. The velocity vector diagram will then give the flow angle α_1 and the blade inlet angle β_1. Further the value of $\underline{u}_1\,\underline{c}_{u1}$ will give a value of $\underline{u}_2\,\underline{c}_{u2}$ by means of the Euler

equation if the hydraulic efficiency is assumed for each stream surface.

The described calculation must only be regarded as a preliminary analysis because it gives only a rough estimate of the outlet swirl from the runner expressed by $\underline{u}_2\ \underline{c}_{u2} = \underline{\omega r}_2 \underline{c}_{u2}$. It should be noted that $\underline{u}_2\ \underline{c}_{u2}$ will not be zero along the total outlet edge of the runner blades in a high specific speed runner as described. However, the mean value should be zero. The values of $\underline{c}_{u2}$ and $\underline{c}_{m2}$ must also be adjusted by the outlet angles β_2 along the outlet edge to fit the Euler equation and the calculation of the pressure on the blade by mean of eq.(16.28), eq.(16.30) and eq.(16.32). [It should also be noted that the hydraulic efficiency η_n will normally not be constant for all stream lines, but for a study of the problem it is recommended to assume η_n = const. as the first approach which gives a better understanding.

It should be noted that a second step in flow analysis by CFD must always be used for fine- tuning of the blades before model test, but the shape of a new runner design should be made by the analysis shown in this chapter.

SUMMARY OF PROCEDURE FOR CALCULATION

(See also chapter V with description of blade shaping)

WHEN CALCULATING THE FLOW FROM THE GUIDE VANES TO INLET OF RUNNER BLADES, FOLLOWING SEQUENCES SHOULD BE FOLLOWED:

1

DRAW OR CALCULATE 9 OR MORE STREAM SURFACES FOR COMPUTER CALCULATION BETWEEN CROWN AND BAND WITH EQUAL CROSS SECTION AREA IN RADIAL DIRECTION AT THE GUIDE VANES INLET AND IN AXIAL DIRECTION BELOW THE RUNNER OUTLET. (FOR GRAPHICAL CALCULATION 3-9 STREAM SURFACES MAY BE USED.)

2

CALCULATE BY ITERATION THE LOCATION OF THE STREAM SURFACES AT THE GUIDE VANES OUTLET EDGES BY MEANS OF EQ (34) (16.55) AND EQ (38) (16.59) IN THE MIDDLE BETWEEN TWO CHOSEN STREAM SURFACES AS A STARTING POINT. IN ADDITION EQ (43) (16.64) AND EQ (44) (16.65) MAY BE USED IF THE VALUE OF ρ IS NOT FOUND BY AVAILABLE SPLINE FUNCTION.

3

CALCULATE BY ITERATION THE LOCATION OF THE STREAM SURFACES AND THE VALUES OF $\underline{c}_{m1}$, $\underline{c}_{u1}$ AND $\underline{u}_1$ AT THE RUNNER BLADE INLET IN ORDER TO DETERMINE THE BLADE ANGLES ALONG THE INLET EDGE. (NOTE $\underline{u}_1\,\underline{c}_{u1}=\underline{u}_o\underline{c}_{uo} = \underline{\omega}\, r_0\, \underline{c}_{uo}$ WHERE $r_o\ \underline{c}_{uo}$ HAS BEEN FOUND PREVIOUSLY AT THE GUIDE VANE OUTLET. THE ANGLE ψ IS THE ANGLE BETWEEN THE DIRECTION ORTHOGONAL TO THE STREAM SURFACES AND THE ANGLE OF THE BLADE INLET EDGE IN THE MERIDIONAL PLANE. THE VALUES OF $\partial(r_1\underline{c}_{u1})/\partial l$ AND $r_1\underline{c}_{u1} = r_0\underline{c}_{u0}$ TO BE USED IN EQ (37) CAN BE FOUND BY ITERATION STARTING FROM THE LOCATION OF THE PRELIMINARY DETERMINED STREAM SURFACES. THE VALUES OF $\underline{c}_{m1}$ CAN BE FOUND BY EQ (34) (16.55).

FINALLY THE EULER TURBINE EQUATION SHALL BE USED TO FIND THE VALUES OF $\underline{u}_2\underline{c}_{u2} = \underline{\omega}\, r_2\, \underline{c}_{u2}$ AT THE BLADE OUTLETS ASSUMING CONSTANT VALUES OF THE HYDRAULIC EFFICIENCY = η_h FOR ALL STREAM SURFACES. (BY A FINAL CFD ANALYSIS IT IS NORMALLY SHOWN THAT THE HYDRAULIC EFFICIENCY MAY NOT BE CONSTANT FOR ALL STREAM SURFACES. A CONTROL MAY BE MADE BY COMPARING THE VALUE OF ($\underline{u}_1\ \underline{c}_{u1}$ - $\underline{u}_2\,\underline{c}_{u2}$) BASED ON COMPUTED VALUES AND THE VALUES FOUND AS DESCRIBED IN THIS CHAPTER).

16.3 Development of the accelerations a_x, a_y and a_z in chapter 16.2 by vector theory.

In this chapter the accelerations in chapter II $\mathbf{a_x}$ (eq.(16.24)), $\mathbf{a_y}$ (eq.(16.25)) and a_z (eq. (16.26)), are developed for use by students and engineers based on vector theory instead of graphical presentation and classic trigonometry.
For steady flow following equations for the absolute acceleration a_a and relative acceleration a_r yield:

$$\vec{a}_a = \nabla\left(\frac{c^2}{2}\right) - \vec{c}\times(\nabla\times\vec{c}) \qquad , \qquad \vec{a}_r = \nabla\left(\frac{w^2}{2}\right) - \vec{w}\times(\nabla\times\vec{w})$$

and

$$\vec{a}_a = \vec{a}_r + 2\,\vec{\omega}\times\vec{w} + \vec{\omega}\times(\vec{\omega}\times\vec{r})$$

$$\vec{a}_a = \nabla\left(\frac{w^2}{2}\right) - \vec{w}\times(\nabla\times\vec{w}) + 2\vec{\omega}\times\vec{w} + \vec{\omega}\times(\vec{\omega}\times\vec{r}) \qquad (16.67)$$

The task will now be to express eq.(16.23) in orthogonal co-ordinates as shown in fig. 16.11 and fig.16.12 in Chapter II.

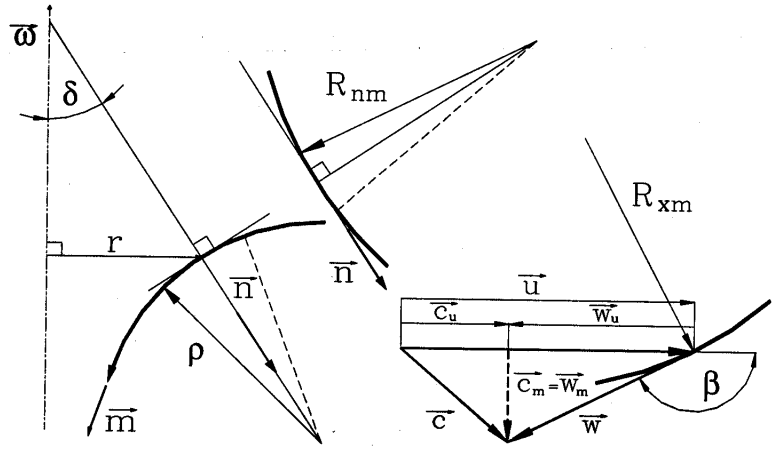

$$W_m = C_m = W\sin(\pi-\beta) \;=\; W\sin\beta$$

$$W_x = \frac{-W_m}{\tan(\pi-\beta)} = \frac{W_m}{\tan\beta} = \frac{C_m}{\tan\beta}$$

$$\textit{i.e.}\quad W_x = -W\cos(\pi-\beta) = W\cos\beta$$

Fig. 16.11. Orthogonal Coordinates

Fig. 16,12 Velocity Diagram

$$d\vec{r} = \vec{i}_x dx + \vec{i}_n dn + \vec{i}_m dm = \vec{i}_x r d\phi + \vec{i}_n dn + \vec{i}_m dm \qquad [\text{NB! } x = r\phi\,]$$

Here, $h_x = r$, $h_n = 1$, $h_m = 1$

$$\frac{\partial r}{\partial n} = \sin\delta\,, \qquad -\frac{\partial r}{\partial m} = \cos\delta. \qquad \frac{\partial r}{\partial \phi} = 0$$

$$\nabla = \frac{\vec{i_x}}{r}\frac{\partial}{\partial \phi} + \vec{i_n}\frac{\partial}{\partial n} + \vec{i_m}\frac{\partial}{\partial m}$$

Substituting for the first term on right hand side in eq.(16.67) by the expression derived as follows:

$$\nabla\left(\frac{w^2}{2}\right) = \nabla\left(\frac{w_x^2 + w_n^2 + w_m^2}{2}\right) = \frac{\vec{i_x}}{R}\left(w_x\frac{\partial w_x}{\partial \phi} + w_n\frac{\partial w_n}{\partial \phi} + w_m\frac{\partial w_m}{\partial \phi}\right) +$$

$$+\vec{i_n}\left(w_x\frac{\partial w_x}{\partial n} + w_n\frac{\partial w_n}{\partial n} + w_m\frac{\partial w_m}{\partial n}\right) + \vec{i_m}\left(w_x\frac{\partial w_x}{\partial m} + w_n\frac{\partial w_n}{\partial m} + w_m\frac{\partial w_m}{\partial m}\right) \qquad (16.67)$$

$V_n = 0$ when moving along a streamline. Further it is assumed that the runner has infinite number of blades 1.e. potential flow as described in chapter 16.1 and then we obtain

$$\frac{\partial}{\partial \phi} = \frac{\partial}{\partial x} = 0$$

From fig. (2) we find $c_m = w_m$

$$\nabla\left(\frac{w^2}{2}\right) = \vec{i_n}\left(w_x\frac{\partial w_x}{\partial n} + w_m\frac{\partial w_m}{\partial n}\right) + \vec{i_m}\left(w_x\frac{\partial w_x}{\partial m} + w_m\frac{\partial w_m}{\partial m}\right)$$

$$\nabla\left(\frac{w^2}{2}\right) = \vec{i_n}\left(\frac{c_m}{\tan\beta}\frac{\partial}{\partial n}\left(\frac{c_m}{\tan\beta}\right) + c_m\frac{\partial c_m}{\partial n}\right) + \vec{i_m}\left[\frac{c_m}{\tan\beta}\frac{\partial}{\partial m}\left(\frac{c_m}{\tan\beta}\right) + c_m\frac{\partial c_m}{\partial m}\right]$$

$$1\nabla\left(\frac{w^2}{2}\right) = \vec{i_n}\left(\frac{c_m}{\tan^2\beta}\frac{\partial c_m}{\partial n} - \frac{c_m^2}{\tan^3\beta}\frac{1}{\cos^2\beta}\frac{\partial \beta}{\partial n} + c_m\frac{\partial c_m}{\partial n}\right)$$

$$+\vec{i_m}\left(\frac{c_m}{\tan^2\beta}\frac{\partial c_m}{\partial m} - \frac{c_m^2}{\tan^3\beta\cos^2\beta}\frac{\partial \beta}{\partial m} + c_m\frac{\partial c_m}{\partial m}\right) \qquad (16.68)$$

(Note: $\tan^3\beta\cos^2\beta = \tan\beta\sin^2\beta$)

It must also be noted that the blade lean angle θ is zero in **fig.16.11** which is valid for a an example of a general vector analysis only.

The second term in eq. (16.67) = $\underline{\vec{w}\times(\nabla\times\vec{w})}$ can be derived as follows:

The curvature of the blades in the direction of the streamlines and normal to the stream lines in the meridional plane as shown in fig. 16.11 yields: (see fig. 16.11)

$$k_m = \frac{1}{\rho}\ , k_n = \frac{1}{R_{nm}}$$

Further we can writefollowing equation when studying fig.116.11 and fig.16.12 and as described in chapter 16.4.

curl w = $\nabla\times\vec{w} = \vec{i_x}\left[\frac{\partial w_m}{\partial n} + w_m k_m - \frac{\partial w_n}{\partial m} - w_n k_n\right] + \frac{\vec{i_n}}{r}\left[\frac{\partial(rw_x)}{\partial m} - \frac{\partial w_m}{\partial\phi}\right] + \frac{i_m}{r}\left[\frac{\partial v_n}{\partial\phi} - \frac{\partial(rw_x)}{\partial n}\right]$

Then by vector multiplication:

$$\vec{w}\times\left(\nabla\times\vec{w}\right)$$

$$\vec{w}\times(\nabla\times\vec{w}) = \begin{vmatrix} \vec{i_x} & \vec{i_n} & \vec{i_m} \\ w_x & w_n & w_m \\ \left(\frac{\partial w_m}{\partial n} + w_m k_m - \frac{\partial w_n}{\partial m} - w_n k_n\right) & \frac{1}{r}\left(\frac{\partial(rw_x)}{\partial m} - \frac{\partial w_m}{\partial\phi}\right) & \left(\frac{\partial w_x}{\partial\phi} - \frac{\partial(rw_x)}{\partial n}\right) \end{vmatrix}$$

$$\left[Note: w_m k_m = \frac{w_m}{\rho} \quad and \quad w_n k_n = \frac{w_n}{R_{nm}} = 0\ because\ w_n = 0\ as\ \text{exp}\ lained\ later\right]$$

$$\left[\vec{w}\times(\nabla\times\vec{w})\right] = \left[\frac{w_n}{r}\left(\frac{\partial w_n}{\partial\phi} - \frac{\partial(rw_x)}{\partial n}\right) - \frac{w_m}{r}\left(\frac{\partial(rw_x)}{\partial m} - \frac{\partial w_m}{\partial\phi}\right)\right]\vec{i}_x +$$

$$\left[w_m\left(\frac{\partial w_m}{\partial n} + w_m k_m - \frac{\partial w_n}{\partial z} - w_n k_n\right) - \frac{w_x}{r}\left(\frac{\partial w_n}{\partial\phi} - \frac{\partial(rw_x)}{\partial n}\right)\right]\vec{i}_n$$
$$+\left[\frac{w_x}{r}\left(\frac{\partial(rw_x)}{\partial m} - \frac{\partial w_m}{\partial\phi}\right) - w_n\left(\frac{\partial w_m}{\partial n} + w_m k_m - \frac{\partial w_n}{\partial m} - w_n k_n\right)\right]\vec{i}_m$$

Considering the vector product $\vec{w}\times(\nabla\times\vec{w})$ in x direction, n direction and m direction:

$$\left[\vec{w}\times(\nabla\times\vec{w})\right]_x = \frac{w_n}{r}\left(\frac{\partial w_n}{\partial\phi} - \frac{\partial(rw_x)}{\partial n}\right) - \frac{w_m}{r}\left(\frac{\partial(rw_x)}{\partial m} - \frac{\partial w_m}{\partial\phi}\right)$$

The following conditions exist along a stream line of a runner as illustrated in fig. 16.11 with infinite number of blades:

$$w_n = 0, \quad \frac{\partial}{\partial\phi} = 0, \quad -\frac{\partial r}{\partial m} = \cos\delta, \quad \frac{\partial r}{\partial n} = \sin\delta$$

Then the expression can be reduced as follows:

$$\left[\vec{w}\times(\nabla\times\vec{w})\right]_x = \frac{w_m}{r}\frac{\partial(rw_x)}{\partial m} = -\frac{c_m}{r}\frac{\partial}{\partial m}\left(r\frac{c_m}{\tan\beta}\right)$$

Finally by substituting for $-\frac{\partial r}{dm} = \cos\delta$ according to fig. 1 after differentiating:

$$\left[\vec{w}\times(\nabla\times\vec{w})\right]_x = \frac{c_m^2}{\tan\beta}\cos\delta - \frac{c_m}{\tan\beta}\frac{\partial c_m}{\partial m} + \frac{c_m^2}{\sin^2\beta}\frac{\partial\beta}{\partial m} \qquad (16.69)$$

The vector product in n direction:

$$\left[\vec{w}\times(\nabla\times\vec{w})\right]_n = w_m\left(\frac{\partial w_m}{\partial y} + w_m k_m - \frac{\partial w_n}{\partial m} - w_n k_n\right) - \frac{w_x}{r}\left(\frac{\partial w_n}{\partial\phi} - \frac{\partial(rw_x)}{\partial n}\right.$$

Remembering: $W_n = 0$ and $\frac{\partial}{\partial\phi} = 0$ *and* $\frac{\partial r}{\partial m} = -\cos\delta$:

$$\left[\vec{w}\times(\nabla\times\vec{w})\right]_n = w_m\frac{\partial w_m}{\partial y} + w_m^2 k_m + \frac{w_x}{r}\frac{\partial(rv_x)}{\partial n} = w_m\frac{\partial w_m}{\partial n} + w_m^2 k_m + \frac{c_m}{r\tan\beta}\frac{\partial}{\partial n}\left(r\frac{c_m}{\tan\beta}\right)$$

Substituting for $\frac{\partial r}{\partial n} = \sin\delta$

$$\left[\vec{w}\times(\nabla\times\vec{w})\right]_n = c_m\frac{\partial c_m}{\partial n} + \frac{c_m^2}{\rho} + \frac{c_m^2}{r\tan^2\beta}\sin\delta + \frac{c_m}{\tan^2\beta}\frac{\partial c_m}{\partial n} - \frac{c_m^2}{\sin^3\beta}\cos\beta\frac{\partial\beta}{\partial n} \qquad (16.70)$$

Finally the vector product of the curl in m direction yields:

$$\left[\vec{w}\times(\nabla\times\vec{w})\right]_m = \frac{w_x}{r}\left(\frac{\partial(rw_x)}{\partial m} - \frac{\partial w_m}{\partial\phi}\right) - w_n\left(\frac{\partial w_m}{\partial n} + w_m k_m - \frac{\partial w_n}{\partial m} - w_n k_n\right)$$

In the same way as for x direction and n direction i.e. $\frac{\partial}{\partial\phi} = 0, w_n = 0$ and from fig. 16.12, $w_x = c_m/\tan\beta$, and $w_m = c_m$ gives:

$$\left[\vec{w}\times(\nabla\times\vec{w})\right]_m = \frac{w_x}{r}\frac{\partial(rw_x)}{\partial m} = \frac{c_m}{r\tan\beta}\frac{\partial}{\partial m}\left(r\frac{c_m}{\tan\beta}\right)$$

Further substituting for $-\frac{\partial r}{\partial m}=\cos\delta$ after differentiating: (see fig 16.11)

$$\left[\vec{w}\times(\nabla\times\vec{w})\right]_m=-\frac{c_m^2}{r\tan^2\beta}\cos\delta+\frac{c_m}{\tan^2\beta}\frac{\partial c_m}{\partial m}-\frac{c_m^2}{\sin^3\beta}\cos\beta\frac{\partial\beta}{\partial m} \qquad (16.71)$$

Then the third term on the right hand side in eq. (1) (16.67) can be developed as follows:

3. $\underline{2\vec{\omega}\times\vec{w}}$

$$2\vec{\omega}\times\vec{w}=2\begin{bmatrix}\vec{i}_x & \vec{i}_n & \vec{i}_m\\ \omega_x & \omega_n & \omega_m\\ w_x & w_n & w_m\end{bmatrix}=2\begin{bmatrix}\vec{i}_\times & \vec{i}_n & \vec{i}_m\\ 0 & -\omega\cos\delta & -\omega\sin\delta\\ w_x & 0 & w_m\end{bmatrix}$$

$$2\vec{\omega}\times\vec{w}=-2w_m\omega\cos\delta\vec{i}_x-2w_x\omega\sin\delta\vec{i}_n+2w_x\omega\cos\delta\vec{i}_m$$

$$2\vec{\omega}\times\vec{w}=-2c_m\omega\cos\delta\vec{i}_x+2\frac{c_m}{\tan\beta}\omega\sin\delta\vec{i}_n+2\frac{c_m}{\tan\beta}\omega\cos\delta\vec{i}_m \qquad (16.72$$

Finally the last term on the right hand side of equation 1 can be developed as shown in the following equation:

4. $\underline{\vec{\omega}\times(\vec{\omega}\times\vec{r})}$

Since $\vec{\omega}$ *and* $\vec{r}$ are perpendicular vectors $\left|\vec{\omega}\times(\vec{\omega}\times\vec{r})\right|=\omega^2 r$ (see Capter 16.4.)

Then the last term can be written as follows; (see fig 1 $\omega^2 r=\left|r\sin\delta\vec{i}_n+r\cos\delta\vec{i}_n\right|\omega^2$)

$$\vec{\omega}\times(\vec{\omega}\times\vec{r})=-\omega^2 r\sin\delta\vec{i}_n+\omega^2 r\cos\delta\vec{i}_m \qquad (16.73)$$

Now, using eq.(16.24), (16.26), (16.26a), (16.27) and (16.28) and express eq. (16.73) in following way:

$$a_x=-\frac{c_m^2}{r\tan\beta}\cos\delta+\frac{c_m}{\tan\beta}\frac{\partial c_m}{\partial m}-\frac{c_m^2}{\sin^2\beta}\frac{\partial\beta}{\partial m}-2c_m\omega\cos\delta$$

$$a_x=c_m\frac{\partial c_m}{\partial m}\frac{1}{\tan\beta}+\frac{c_m^2}{\sin^3\beta}\left[-\sin\beta\frac{\partial\beta}{\partial m}-\frac{1}{r}\sin^2\beta\cos\beta\cos\delta\right]-2c_m\omega\cos\delta \qquad (16.74)$$

According to the geometry condition in fig 16.2 in chapter 16.2

$$d\beta = d\gamma - d\varepsilon$$

(R_{xm}= radius of curvature of the blade in x-m plain denoted R in chapter 16.2)

$$d\gamma = \frac{wdt}{R_{xm}}, \qquad d\varepsilon = \frac{w_x}{m}dt, \qquad \frac{dt}{dm} = \frac{1}{w_m}$$

$$\frac{\partial\beta}{\partial m} = \frac{\partial(\gamma-\varepsilon)}{\partial m} = \frac{\partial\gamma}{\partial m} - \frac{\partial\varepsilon}{\partial m} = \frac{w}{R_{xm}}\frac{dt}{dm} - \frac{w_x}{m}\frac{dt}{dm}$$

$$\frac{\partial\beta}{\partial m} = \frac{w}{R_{xm}}\frac{1}{w_m} - \frac{w_x}{m}\frac{1}{w_m},$$

Here, $m = \frac{r}{\cos\delta}$, $\qquad w_x = \frac{w_m}{\tan\beta}$, $\qquad w_m = w\sin\beta$,

then by substituting for m and w_x and w gives:

$$\frac{\partial\beta}{\partial m} = \frac{w}{R_{xm}}\frac{1}{w\sin\beta} - \frac{w_m}{\tan\beta}\frac{\cos\delta}{r}\frac{1}{w_m} = \frac{1}{R_{xm}}\frac{1}{\sin\beta} - \frac{\cos\beta\cos\delta}{r\sin\beta} \qquad (16.75)$$

Substituting eq. (16.75) into eq. (16.74)

$$a_x = c_m\frac{\partial c_m}{\partial m}\frac{1}{\tan\beta} + \frac{c_m^2}{\sin^3\beta}\left[-\frac{1}{R_{xm}} + \frac{\cos\beta\cos\delta}{r} - \frac{1}{r}\sin^2\beta\cos\beta\cos\delta\right] - 2c_m\omega\cos\delta$$

$$a_x = c_m\frac{\partial c_m}{\partial m}\frac{1}{\tan\beta} + \frac{c_m^2}{\sin^3\beta}\left[-\frac{1}{R_{xm}} + \frac{1}{r}\cos^3\beta\cos\delta\right] - 2c_m\omega\cos\delta \qquad (16.76)$$

Then by means of eq.(16.68), eq.(16.70), eq.(16.71) and eq.(16.73):

$$a_n = \frac{c_m}{\tan^2\beta}\frac{\partial c_m}{\partial n} - \frac{c_m^2}{\tan^3\beta\cos^2\beta}\frac{\partial\beta}{\partial n} + c_m\frac{\partial c_m}{\partial n} - \frac{c_m^2}{\rho} - \frac{c_m^2}{r\tan^2\beta}\sin\delta - c_m\frac{\partial c_m}{\partial n}$$

$$-\frac{c_m}{\tan^2\beta}\frac{\partial c_m}{\partial n} + \frac{c_m^2}{\sin^3\beta}\cos\beta\frac{\partial\beta}{\partial n} + 2\frac{c_m}{\tan\beta}\omega\sin\delta - \omega^2 r\sin\delta$$

If substituting for $\tan^3\beta\cos^2\beta = \sin^3\beta/\cos\beta$ in the second term the equation can be simplified as follows:

$$a_n = -\frac{c_m^2}{\rho} - \frac{c_m^2}{r\tan^2\beta}\sin\delta + 2\frac{c_m}{\tan\beta}\omega\sin\delta - \omega^2 r\sin\delta$$

$$a_n = \left(-\frac{1}{\rho} - \frac{\sin\delta}{r\tan^2\beta} \right) c_m^2 + 2\frac{c_m}{\tan\beta}\omega\sin\delta - \omega^2 r\sin\delta \qquad (16.77)$$

Finally, from eq.(16.68), eq.(16.71), eq.(16.72 and eq.(16.73):
):

$$a_m = \frac{c_m}{\tan^2\beta}\frac{\partial c_m}{\partial m} - \frac{c_m^2}{\tan^3\beta\cos^2\beta}\frac{1}{\partial m}\frac{\partial\beta}{\partial m} + c_m\frac{\partial c_m}{\partial m} + \frac{c_m^2}{r\tan^2\beta}\cos\delta - \frac{c_m}{\tan^2\beta}\frac{\partial c_m}{\partial m}$$

$$+ \frac{c_m^2}{\sin^3\beta}\cos\beta\frac{\partial\beta}{\partial m} + 2\frac{c_m}{\tan\beta}\omega\cos\delta + \omega^2 r\cos\delta$$

Here the second – and sixth term cancel each other because
$\tan^3\beta\cos^2\beta = \sin^3\beta/\cos\beta$. Further first – and fifth term cancel each other and then the following expression for a_m is obtained:

$$a_m = c_m\frac{\partial c_m}{\partial m} + \frac{\cos\delta}{r\tan^2\beta}c_m^2 + 2\frac{c_m}{\tan\beta}\omega\cos\delta + \omega^2 r\cos\delta \qquad (16.78)$$

Equation (16.76), (16.77) and (16.78) are identical to equations (16.24), (16.25) and (16.26) in chapter **16.2**. The radius of curvature in the m, n plane as shown in fig. 16.11 is also denoted ρ in equation (3) (16.25) in chapter II, while the radius R_{xm} in equation (10) (16.76) in this chapter, is identical to the blade curvature radius denoted by R in eq (2) (16.24) in chapter **16.2.**

It should also be noted that the classical theory of trigonometry in chapter **16.2** has been used instead of the vector analysis because of a simpler procedure and because this approach gives a better physical understanding of the problem.

However, for computer analysis the codes must be based on vector analysis and therefore it is useful to prove the validity of the theory by vector analysis as shown in this chapter.

16.4 The relations between the blade lean angle θ and $'\theta$ and the blade angle β and $'\beta$ as illustrated in Fig. 16.12 and Fig. 16.13.

It is convenient to make the representation of a runner blade for an analytical analysis by a vertical view with horizontal plain sections normal to the axis of rotation with constant equidistance and meridional plain sections with constant increment of angle $\Delta\Phi$ illustrated in a horizontal view in a vertical plane.

The vertical section plains can then be drawn by folding the meridional selections into one meridional plain (like folding a Japanese fan) as shown in fig. 16.12.

Such representation of a runner blade is very convenient for the shaping process of a blade. However, the blade angles and blade lean angles is only illustrated indirectly by the blade angle $'\beta$ in the horizontal plain (bottom in fig. 16.12) and by the blade lean angle $'\theta$ in the vertical (folded) plain containing the meridional section with angle increments $\Delta\Phi$

In order to find the relation between the real blade lean angle θ and the angle $'\theta$ in the meridional plain and the real blade angle β and the angle $'\beta$ in the horizontal section plain, a detailed figure of the vertical and horizontal section is illustrated in fig. 16.13.

From fig. 16.13 following equations can be established.

$$\Delta' n = \Delta n - \Delta X \tan(0.5\Delta\phi \sin\delta)$$

$$\Delta X = \Delta' n \tan\theta = [\Delta n - \Delta X \tan(0.5\Delta\phi \sin\delta)]\tan\theta$$

Then

$$\Delta X = \frac{\Delta n}{1/\tan\theta + \tan(0.5\,\Delta\phi \sin\delta)} \qquad (16.79)$$

Further

$$\frac{\Delta' m}{\Delta X} = \tan\beta \quad i.e. \Delta X = \frac{\Delta' m}{\tan\beta} = \frac{\Delta m - \Delta X \tan(0.5\Delta\phi\cos\delta)}{\tan\beta}$$

Then

$$\Delta X = \frac{\Delta m}{\tan\beta + \tan(0.5\,\Delta\phi\cos\delta)} \qquad (16.80)$$

Further

$$\frac{\Delta' r}{\Delta X} = \tan'\beta \, i.e. \Delta X = \frac{\Delta' r}{\tan'\beta} = \frac{\Delta r - \Delta X \tan(0.5\Delta\phi)}{\tan'\beta}$$

Then

$$\Delta X = \frac{\Delta r}{\tan'\beta + \tan(0.5\Delta\phi)} \qquad (16.81)$$

Further

$$\Delta m = \Delta n \tan'\theta \qquad (16.82)$$

Finally

$$\Delta r = \Delta Z \left[\tan\delta - \tan(\delta - '\theta)\right]$$

and

$$\Delta Z = \Delta n \cos\delta$$

Then

$$\frac{\Delta r}{\Delta n} = \cos\delta[\tan\delta - \tan(\ \delta - '\theta\ )] \qquad (16.83)$$

Combining equation (1) (16.79) and equation (3) (16.81)

$$\frac{\Delta r}{\Delta n} = \frac{\tan'\beta + \tan(0.5\Delta\phi)}{1/\tan\theta + \tan(0.5\Delta\phi\sin\delta)} \qquad (16.84)$$

Then combining eq (7) (16.84) and eq (5) (16.83)

$$\frac{\Delta r}{\Delta n} = \cos\left[\tan\delta - \tan(\delta - '\theta)\right] = \frac{\tan'\beta + \tan(0.5\Delta\phi)}{1/\tan\theta + \tan(0.5\Delta\phi\sin\delta)} \qquad (16.86)$$

and

$$\text{cotan}\,\theta = 1/\tan\theta = \frac{\tan'\beta + \tan(0.5\Delta\phi)}{\cos\delta[\tan\delta - \tan(\delta - '\theta)]} - \tan(0.5\Delta\phi\sin\delta) \qquad (16.87)$$

From the basic theory of geometry

$$\tan(\delta - '\theta) = \frac{\tan\delta - \tan'\theta}{1 + \tan\delta\tan'\theta}$$

Then

$$\tan\delta - \tan(\delta - '\theta) = \tan\delta - \frac{\tan\delta - \tan'\theta}{1 + \tan\delta\tan'\theta} = \frac{\tan\delta + \tan^2\delta\tan'\theta - \tan\delta + \tan'\theta}{(1 + \tan\delta\tan'\theta)}$$

after rearrangement:

$$\tan\delta - \tan(\delta - '\theta) = \frac{\cos^2\delta \tan'\theta(\tan^2\delta + 1)}{\cos^2\delta(1 + \tan\delta\tan'\delta)} = \frac{(\sin^2\delta + \cos^2\delta)\tan'\theta}{\cos^2\delta(1 + \tan\delta\tan'\theta)}$$

then

$$\left[\tan\delta - \tan(\delta - '\theta)\right] = \frac{\tan'\theta}{\cos\delta(\sin\delta\tan'\theta + \cos\delta)} \qquad (16.88)$$

Substituting for eq. (16.88) in eq. (16.89)

$$\text{cotan}\,\theta = \frac{\left[\tan'\beta + \tan(0.5\Delta\phi)\right]}{\tan'\theta}\ (\sin\delta\tan'\theta + \cos\delta) - \tan(0.5\Delta\phi\sin\delta) \qquad (16.90)$$

or

$$\tan\theta = \frac{\tan'\theta}{\left[\tan'\beta + \tan(0.5\Delta\phi)\right]\left[\sin\delta\tan'\theta + \cos\delta\right] - \tan'\theta\tan(0.5\Delta\phi\sin\delta)} \qquad (16.91)$$

Note: for $\Delta\Phi \rightarrow 0$ (See fig.16.13)

$$\boxed{\tan\theta \Rightarrow \tan'\theta\,\frac{1}{\tan'\beta(\sin\delta\tan'\theta + \cos\delta)}} \qquad (16.92)$$

<u>Combining eq. (16.79) and eq. (16.80)</u>

$$\frac{\Delta m}{\Delta n} = \tan'\theta = \frac{\tan\beta + \tan(0.5\,\Delta\phi\cos\delta)}{1/\tan\theta + \tan(0.5\,\Delta\phi\sin\delta)} \qquad (16.93)$$

Rearranging

$$\tan'\theta\left[1/\tan\theta + \tan(0.5\,\Delta\phi\sin\delta)\right] = \tan\beta + \tan(0.5\,\Delta\phi\cos\delta)$$

then after rearranging and substituting for 1/tan θ by eq. (16.87)

$$\tan\beta = \tan'\theta\left[\frac{\tan'\beta + \tan(0.5\,\Delta\phi)}{\cos\delta\left[\tan\delta - \tan(\delta - '\theta)\right]} - \tan(0.5\,\Delta\phi\sin\delta) + \tan(0.5\,\Delta\phi\sin\delta)\right] - \tan(0.5\phi\cos\delta)$$

and finally

$$\tan\beta = \tan'\theta\left[\frac{\tan'\beta + \tan(0.5\,\Delta\,\phi)}{\cos\delta\left[\tan\delta - \tan(\delta - '\theta)\right]}\right] - \tan(0.5\,\Delta\,\phi\cos\delta) \qquad (16.94)$$

Substituting for eq (10) (16.88) in eq (16) (16.94) we arrive at following equation

$$\underline{\tan\beta = \left[\tan'\beta + \tan(0.5\,\Delta\,\phi)\right]\left[\sin\delta\tan'\theta + \cos\delta\right] - \tan(0.5\,\Delta\phi\cos\delta)} \qquad (16.95)$$

By combining eq. (16.91) and eq. (16.95) we arrive at eq. (16.96) $\theta = f(\beta,'\theta)$

$$\tan\theta = \frac{\tan'\theta}{(\tan\beta + \tan(0.5\Delta\phi)\cos\delta) - (\tan'\theta\,\tan(0.5\Delta\phi)\sin\delta)/(\sin\delta\,\tan'\theta + \cos\delta)} \qquad (16.96)$$

For $\Delta\,\phi \to 0$ (See fig.16.13)

$$\tan\beta \Rightarrow \tan'\beta\,(\sin\delta\,\tan'\theta + \cos\delta) \qquad (16.97)$$

By means of eq. (16.92) and eq. (16.96) following inverse formula can be established for calculating ‘β and ‘θ based on given values of β, θ and δ.

Rearranging eq. (16.96)

$$\tan'\beta = \tan\beta/(\sin\delta\,\tan'\theta + \cos\delta)$$

Rearranging eq. (16.92) and substituting for tan’β

$$\tan'\theta = \tan\theta\tan\beta \qquad (16.98)$$

Then finally after substituting for tan’θ from eq. (16.97) in the rearranged eq. (16.98)

$$\tan'\beta = \tan\beta/(\sin\delta\tan\theta\tan\beta + \cos\delta) \qquad (16.99)$$

CONTROL OF SPECIAL CASES
FOR $\Delta\,\theta \to 0$ OF EQUATION (14) (16.92) AND EQUATION (19) (16.97)

1. When substituting for ‘θ = 0 = θ
   tanβ = tan’β cosδ or tan’β = tanβ/cosδ

   a) Then for δ = π/2
      tan’β = ∞ if β≠0 and then ‘β = π/2 i.e.
      we have an axial turbine with no blade lean

   b) For δ = 0, tanβ = tan’β i.e. we have a radial turbine (which yields also for ‘θ ≠0)

2. When substituting for $'\theta \neq 0$:

   If $\delta = 0$ i.e. we have a radial turbine:
   then: $\tan\beta = \tan'\beta$
   and $\tan\theta = \tan'\theta/\tan'\beta = \tan'\theta/\tan\beta$

   If $\delta = \pi/2$ i.e. we have an axial turbine. By means of eq. (16.92) and eq. (16.97) we get:
   $\tan\beta = \tan'\beta \tan'\theta$ and $\tan\theta = \tan'\theta/(\tan'\beta\tan'\theta) = 1/\tan'\beta$, then for $'\beta = \pi/2$, $\theta = {}'\theta = 0$.

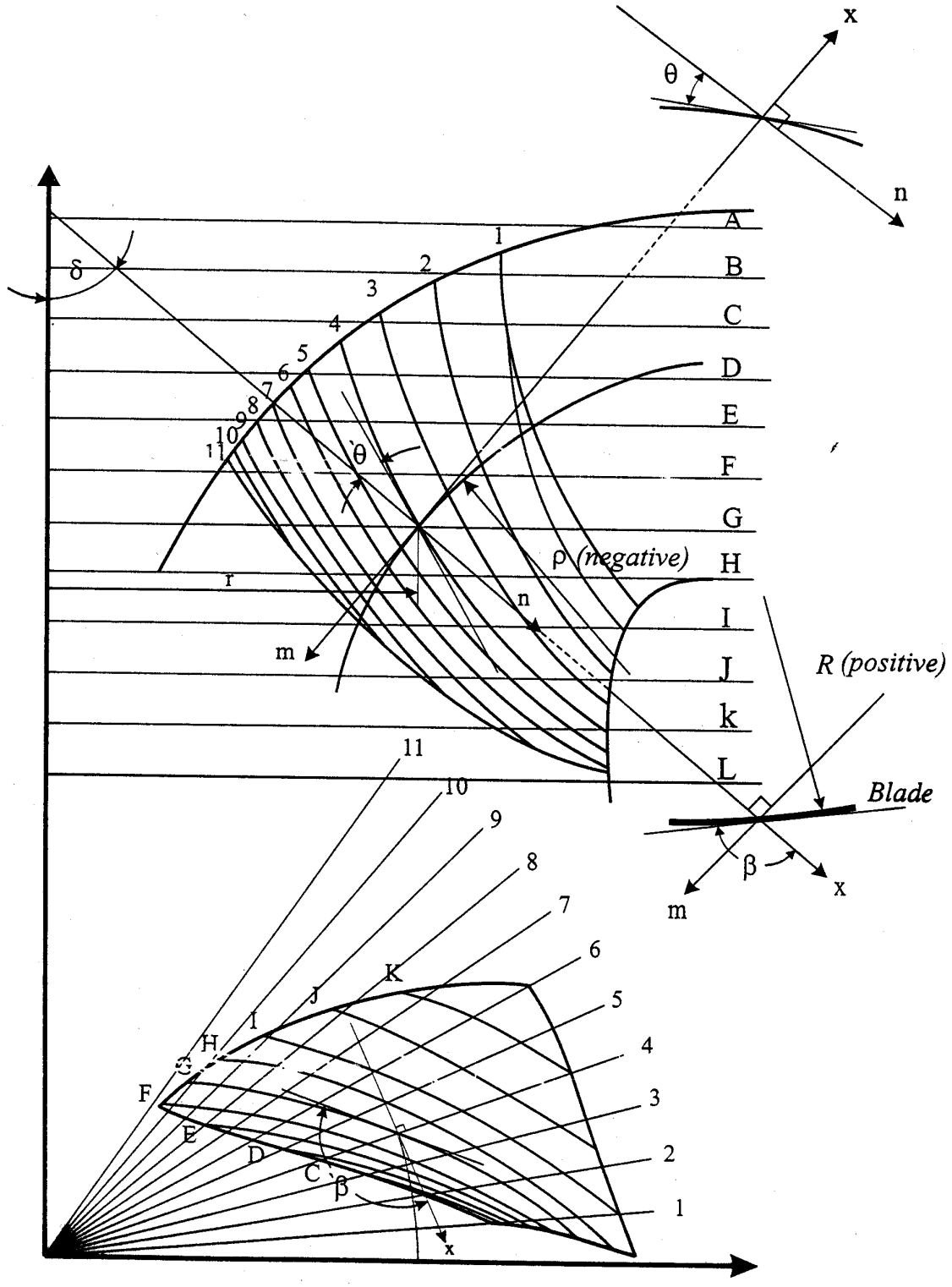

Fig. 16.12. Principle for the preliminary blade design for calculation of β and θ and R for the analysis of the pressure design. (Note the drawing shows a left hand rotating system.)

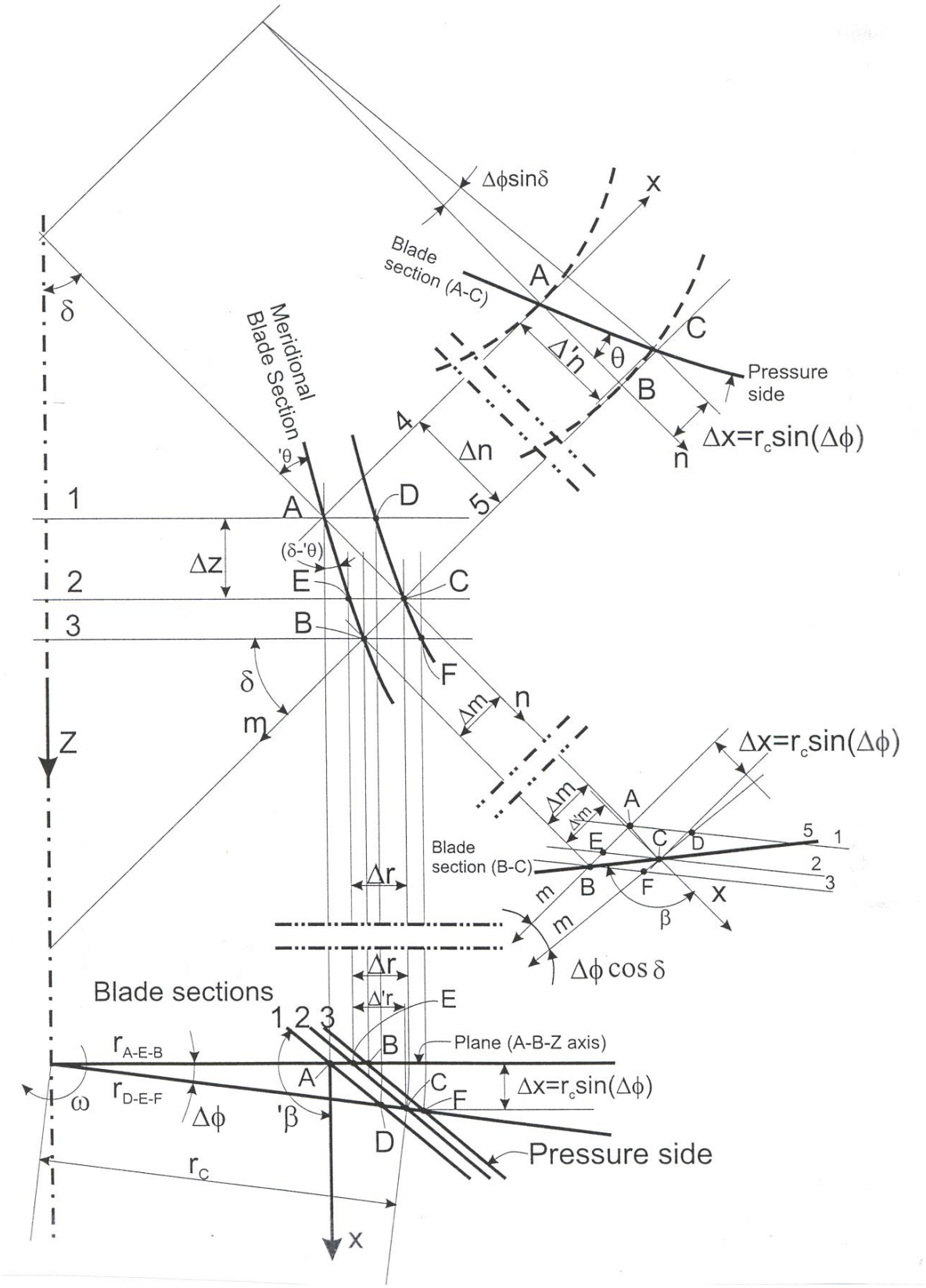

Fig. 16.13. Detailed study of a small section of the blade in horizontal and vertical view as shown in fig. 16.12.

CALCULATION OF THE RADIUS (R) OF THE BLADE CURVATURE BASED ON BLADE ANGLE VERSUS BLADE LENGTH IN THE BLADE DRAWING IN FIG 1 AND FIG 16.14.

From geometry study of fig. 16.14 we obtain (see next page)

$$2\sin(0.5\Delta\gamma) = \frac{\Delta S}{R} \qquad \text{and} \qquad \Delta\gamma = \beta_2 - \beta_1 \div \Delta\phi \cos\delta$$

$$R = \frac{\Delta S}{2\sin(0.5(\beta_2 - \beta_1 \div \Delta\phi\cos\delta))} \tag{16.100}$$

By assuming fixed steps in $\Delta\Phi = 6^o$ (or 3^oC) and ΔZ as shown in fig. 1 and fig 16.13. ΔS can be determined as follows:

$$\Delta S = \sqrt{(\Delta' m^2) + (\Delta X^2)}$$

Where 'm for an angle $\Delta\Phi$ can be expressed by

$$\Delta' m = \Delta X \tan\beta$$

(See development of eq.(16.80) and study also fig 16.13 and fig. 16.14.)

Further from fig.16.13:

$$\Delta X = r_1 \cdot \sin(\Delta\Phi) \tag{16.101}$$

Then by substituting for Δ'm

$$\Delta S = \sqrt{(\Delta X \tan\beta)^2 + (\Delta X)^2} = \Delta X \sqrt{\tan^2\beta + 1}$$

and finally substituting for ΔX by eq. (16.101)

$$\Delta S = r_1 \sin\Delta\phi\sqrt{\tan^2\beta + 1} = r_1 \sin\Delta\phi \ \frac{1}{\cos\beta_1} \tag{16.102}$$

Then the radius of curvature can be found from eq.(16.100) by substituting for ΔS by eq. (16.102) in order to calculate the pressure gradient from crown to band of a runner. It will be convenient to make this calculation by a simple numerical program by calculating values of β by eq. (16.95)by reading $\Delta\Phi$, 'θ, 'β, r_1 and δ from fig. 16.14 and giving suitable increments of
$\Delta\Phi$ and $\Delta r = f(\Delta\Phi)$ and ΔZ with connecting values of δ, 'θ and 'β read from the blade geometry.

The equation for the radius of curvature of the blade suction side along the stream lines:

$$R = \frac{r_1 \sin(\Delta\phi)}{2\cos\beta_1 \cdot \sin(0.5(\beta_1 - \beta_2 - \Delta\phi\cos\delta))} \tag{16.103}$$

Further the radius of curvature of the stream lines in the meridional plane can be found by studying fig. 16.12, fig. 16.13 and fig. 16.14:

$$\rho = \frac{\Delta m}{2\sin(0.5(\delta_1 - \delta_2))} \tag{16.104}$$

From fig. 16.13 we find:

$$\Delta m = \Delta' m + \Delta X \tan(0.5\Delta\phi\cos\delta_1)$$

When substituting for Δ'm = ΔX tan β_1 (see fig. 16.13) and substituting for ΔX by eq. (16.101).

$$\Delta m = r_1 \cdot \sin(\Delta\phi)\left[\tan\beta_1 + \tan(0.5\Delta\phi\cos\delta_1)\right] \tag{16.105}$$

When substituting for Δm by eq. (16.105) in eq. (16.104) we get:

$$\rho = \frac{r_1 \sin(\Delta\phi)\left[\tan\beta_1 + \tan(0.5\Delta\phi\cos\delta_1)\right]}{2\sin(0.5(\delta_1 - \delta_2))} \tag{16.106}$$

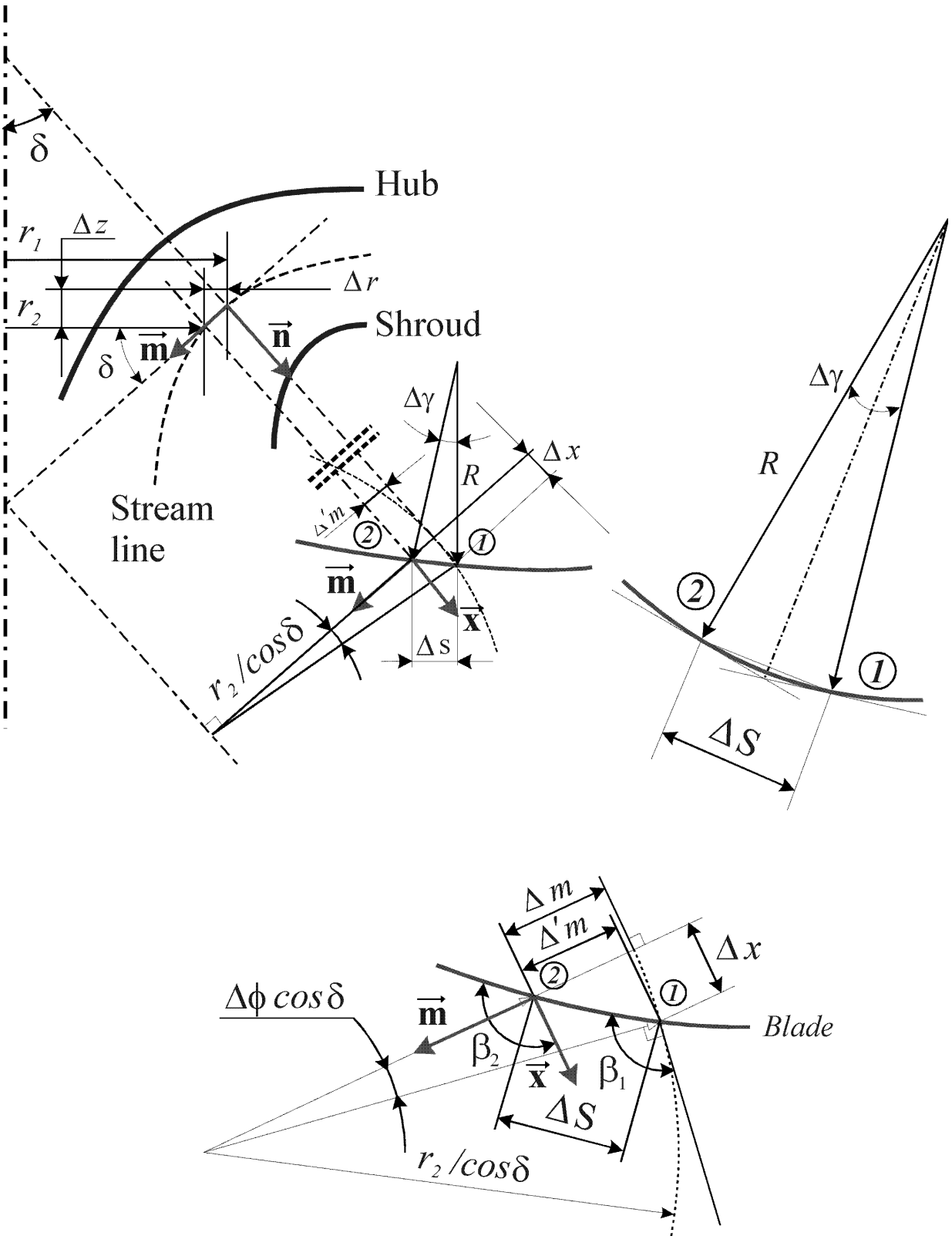

Fig. 16.14. Blade curvature and radius of curvature along a streamline on the blade

ILLUSTRATIONS OF RADIAL- AND AXIAL TURBINES

RADIAL TURBINE

$\delta = 0 \quad \Delta m = \Delta r$ and $\Delta \Phi \rightarrow O$

Eq. (16.97): $\tan\beta = \tan'\beta$

Eq. (16.92): $\tan\theta = \dfrac{-\tan'\theta}{\tan'\beta} = \dfrac{\dfrac{\Delta m}{\Delta n}}{\dfrac{\Delta r}{\Delta x}} = \dfrac{\dfrac{\Delta m}{\Delta n}}{\dfrac{\Delta m}{\Delta x}} = \dfrac{\Delta x}{\Delta n}$

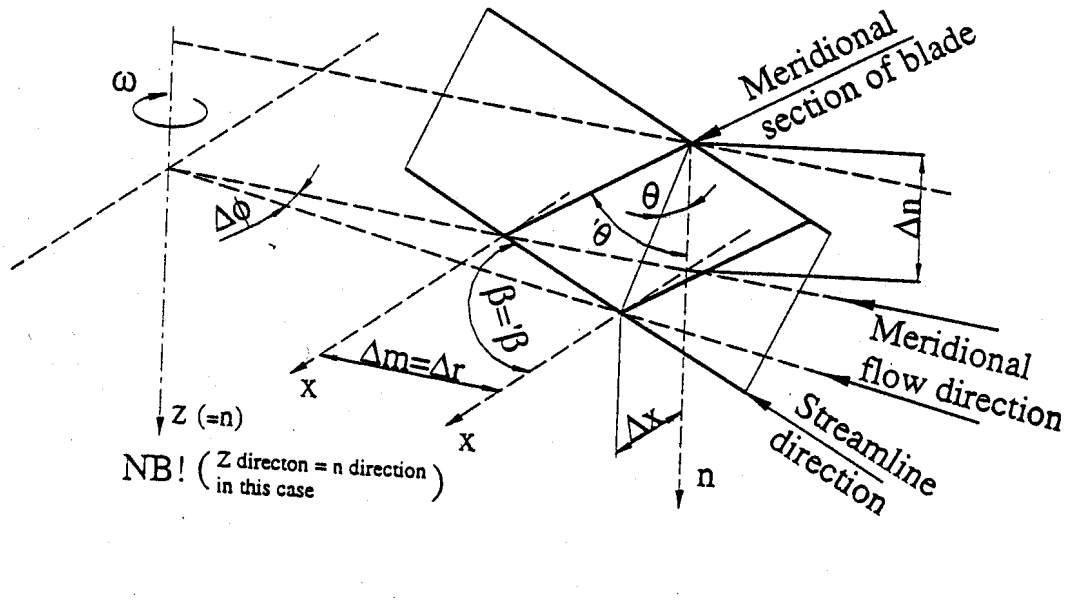

Fig. 16.15. Detail of blade for a radial turbine

AXIAL TURBINE WITH CYLINDERICAL BAND AND HUB WHERE $\delta = \dfrac{\Pi}{2}$

$\delta = \dfrac{\pi}{2} \quad \Delta n = \Delta r$

Eq. (16.97) $\tan\beta = \tan'\beta \tan'\theta = \dfrac{\Delta r}{\Delta x}\dfrac{\Delta m}{\Delta n} = \dfrac{\Delta m}{\Delta x}$

Eq. (16.92) $\tan\theta = \dfrac{-1}{\tan'\beta} = \dfrac{1}{\dfrac{\Delta n}{\Delta x}} = \dfrac{\Delta x}{\Delta n} = \dfrac{\Delta x}{\Delta r}$

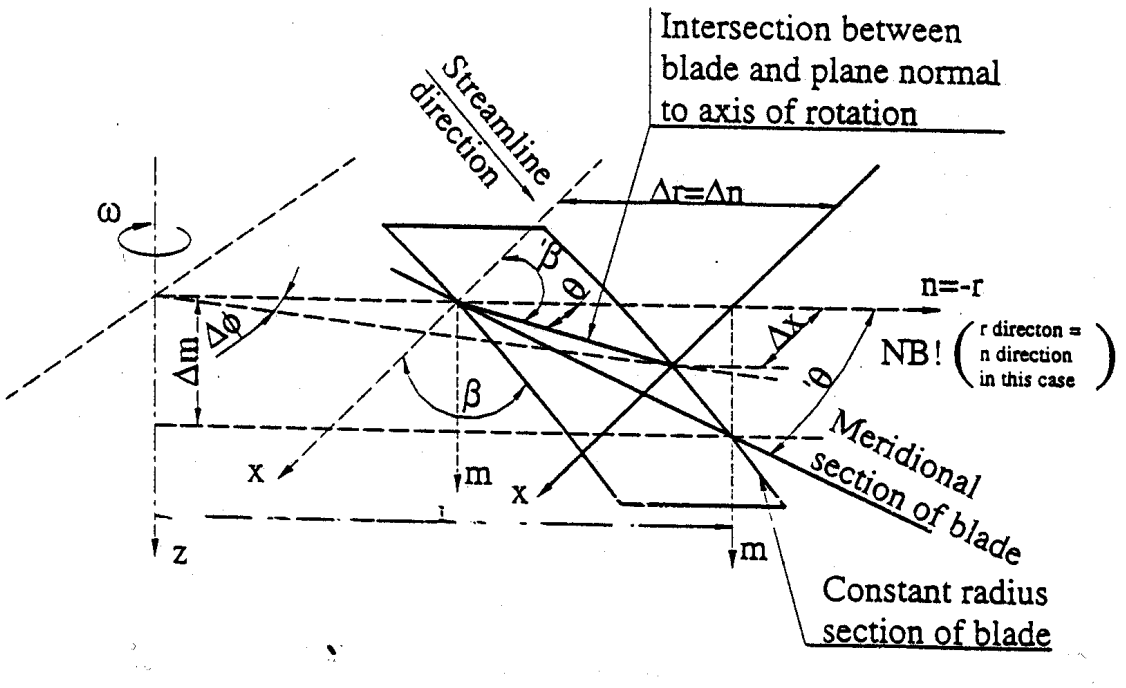

Fig. 16.16. Detail of blade for an axial turbine

16.5 Procedure for preliminary design of runner.

1. Draw estimated contours of crown and band after outlet diameter and guide vane height is determined. Calculated from specific speed and $NPSH_a$ and *Q and *H.

2. Calculate the inlet velocity vector diagrams based on rc_u = const and the flow from the guide vane outlet edge as described in chapter II eq, (16.53) and eq.(16.57) as illustrated in fig. 16.9 if an analytical solution is chosen. Another solution is to make a CFD analyse of the guide vane flow without runner, but with boundary conditions of mean pressure at runner inlet at best efficiency flow *Q. The chosen guide vane angles should fit best efficiency flow *Q, head *H. The inlet blade angles should be chosen to fit best efficiency speed *n in order to fit the absolute velocity from the guide vanes in order to calculated velocity diagrams at crown, at middle stream lines and at band (see fig. 15 chapter III) (chapt. 16.3)?.

   Calculate the meridian velocity at outlet based on $-dc_m / dn = d_n / \rho$ (see eq. (16.38) Chapt 16.2) and behind the blade outlets. (Use mean value c_m = *Q/$\left(\pi D_2^2 / 4\right)$ as a base

and calculate $\pi \int_{r_{hub}}^{r_{band}} c_m' r\, dr = {}^*Q'$ as a control for adjustment of $C_m = C_m' \frac{{}^*Q}{{}^*Q'}$. Draw the outlet velocity diagrams using c_m and $u_2 = r_2 \omega$ for crown middle and band. Draw assumed streamlines in stream surfaces fitting inlet and outlet stream surfaces by regarding stream surfaces as shown in fig. 16.9, chapter 16.2.

(Remember that we shall have the same flow between two neighbouring stream surfaces in middle and at crown and at band.) Start with cylinders formed by the stream surfaces with equal cross section below the runner where $\rho = \infty$ and c_m = constant to fit the inlet stream surfaces from the guide vanes.

PROCEDURE FOR DESIGNING A RUNNER BLADE

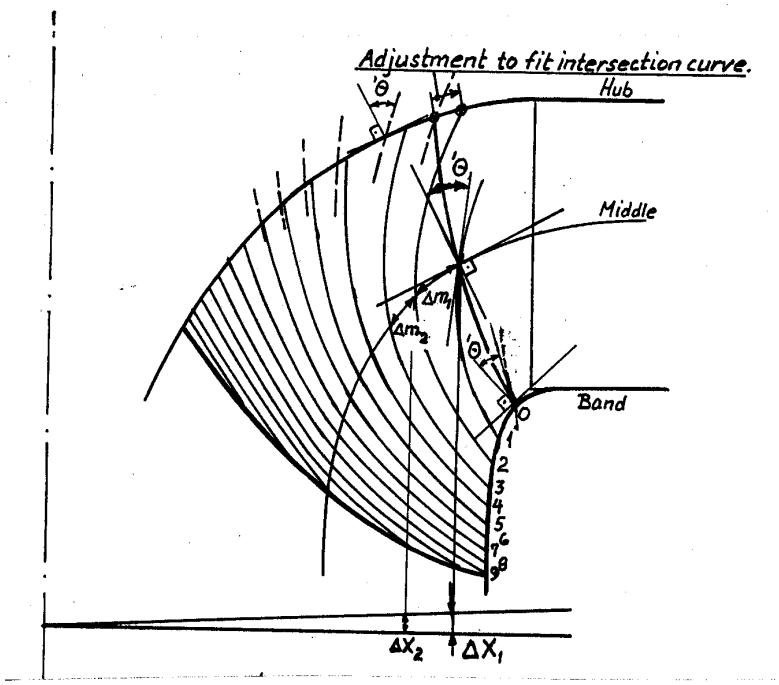

Fig. 16.17 Meridian intersection lines with suction side of blade folded into one plane with chosen hub curvature, and band curvature, with calculated angles for blade outlet and blade inlet and 3 preliminary drawn streamlines. The preliminary intersection lines at hub are also shown before calculation of $'\theta$ angles with adjustment of the blade profile. (Note: The meridian intersection lines are shown only as an illustration and no calculation of $'\theta$ angles to obtain dh/dn = 0 has been made for fig. 16.17 and fig. 16.18).

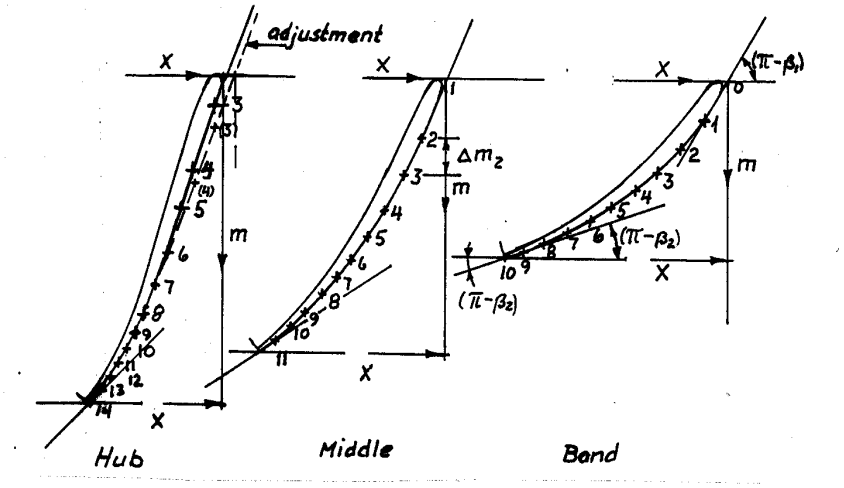

Fig. 16.18 Blade shape for choosing β along the blade by drawing the suction side based on (Δm) and (ΔX) values taken from fig.16.17. An iteration process is necessary for this procedure.

3. After the inlet angle β_1 and outlet angle β_2 has been calculated as described in section 2 for preliminary drawn streamlines as well as for hub and band for a chosen speed number $\Omega = \sqrt{\pi}\,\underline{u}_2^{\,3/2}\sqrt{\tan\beta_2}$, the values for the angle increment $\Delta\text{ø}$ between the meridian sections must be chosen. (Normally $\Delta\text{ø} = 3^\circ$)

4. Then the distance Δm between the sections at the inlet of the blade and the next meridian section with angle increment $\Delta\phi$ along hub, band and along the stream surfaces may be calculated by eq. (16.105), **Chapter 16.5** at the inlet and outlet of the blade. The calculation for ΔX and Δm by following the equations from **Chapter 16.4** for development of the angles $'\beta$ and $'\theta$ yields:

   See fig.(16.13), **chapter 16.4.**

   From fig. 16.14 **chapter 16.4** following equations have been developed:

$$\Delta m = r_1 \sin(\Delta\text{ø}) \cdot \left[\tan\beta_1 + \tan\left(0.5\Delta\text{ø}\cos\delta_1\right)\right] \qquad (16.105)$$

$$\Delta X = r_1 \sin\left(\Delta\text{ø}\right) \qquad (16.106)$$

   further eq. (16.105) can be rearranged explicit on tan β_1

$$\tan\beta_1 = \frac{\Delta m}{r_1 \sin\left(\Delta\text{ø}\right)} - \tan\left(0.5\Delta\text{ø}\cos\delta_1\right)$$

   Note: The values can also be determined by simpler formulas by studying fig.(16.13) and fig.(16.14) in this chapter /16.3) by measuring r_1 at the blade inlet and calculating ΔX which in this case can simply be expressed by following equation:

$$\Delta X = r_1\left(\Delta\phi\right) \approx r_1\left(\Delta\phi\right)\pi/180 \qquad (16.107)$$

(Note: $r_1(\Delta\phi)\ \pi/180 \approx r_1 \tan(\Delta\phi) \approx r_1 \sin(\Delta\phi)$ *for* $(\Delta\phi \leq 3^o)$
Then Δm *on the stream surface can be calculated based on the calculated inlet angle* β_1 *as shown in chapter IV. This is because* $\tan\beta_1 = \Delta m/\Delta X \approx \Delta' m/\Delta X$ *i.e:*

$$\Delta' m \approx \Delta m = \Delta X \tan\beta_1 \qquad (16.108)$$

The same procedure should be used at the outlet edge where β_2 has been calculated, when calculating the main dimensions.
Note from eq. (16.96) tan θ = f $(\beta, '\theta)$ if the runner blades with β is given as shown in fig. (16.18).

5. The inlet and outlet velocity vector diagram for each streamline can be drawn and the suction side of the blade can be drawn in an X-m diagram (see (fig.(16.14)), where $\tan\beta$ and ΔX can be calculated as shown in section (16.4). Then it is possible to draw a blade and read Δm from the drawing of the blade as shown in fig. (16.18) and mark the points of intersection between the meridional planes for each $(\Delta\phi)$ from inlet to outlet as shown in fig. 1. Note the total length of m = $\sum \Delta m$ can be found from fig. 1 and (m) can be used as an aid for the drawing of the blade in m - X plane.

6. After dividing the meridian component of the streamlines in the (Z-r) plane into Δm sections, the values of θ can be calculated from eq. (16.92), Chapter (16.3) for dh/dy=0. The needed value of the streamwise blade curvature radius R can be calculated by eq.(16.103) and δ can be calculated by eq. (16.104), Chapter 16.3. The blade curvature radius R may also be measured on the drawn blade shown in Fig. (16.12) and fig. (16.14). Then the value of $'\theta$ can be calculated by eq. (16.98), Chapter (16.4) for a middle stream line and stream lines along hub and band near the inlet edge of the blades, in order to find the direction of the intersection lines between the meridian plane and the blade suction side.

   The same procedure should be followed by calculation of the direction of the angle $'\theta$ along the blade outlet in order to find the line of intersection between the meridian planes and the blade.

7. Now it will be possible to draw intersection lines in the meridian planes (const. ø) and the blade suction sides by means of the calculated direction of the angles $'\theta$ (which gives (dh/dy)=0) at the chosen middle streamline and at hub and band near the blade inlet and outlet in order to get a pressure balanced blade.

   An adjustment of the position of the blades must finally be made as shown for the blade profile along the hub in fig. 16.18 and fig. 16.17 by bending the blade and correct the streamwise curvature of the blade. This procedure must be made for all stream lines if the meridian intersection lines are corrected. However, the inlet angles β_1 and outlet angles β_2 should not be changed during this adjustment. (Note: the curvature along the blade may give a third order curvature along the hub.
   See fig. (16.17) (fig.16.18).

It may also be convenient to calculate Δm values based on the curvature in fig.(16.17) and (fig.16.18) where the β values can be measured and then calculated the direction of θ and $'\theta$. This is in order to indicate the direction of the intersection line over the total length of the blade. An iteration process may also be convenient to establish on a computer after some experience has been achieved in this process. However, the feeling for making new designs may be lost by a computer system if the process is automatic. Finally the thickness and blade profile must be drawn based on the suction side of the blade.

* After adjustment of the blade by iteration, the blade is ready for a CFD analysis after choosing number of blades and blade profiles. The equation of the acceleration forces, the equation of continuity and the ROTHALPY equation may be transformed to an equation for determination of the velocity gradient from blade to blade. This velocity gradient should be used for optimising the number of blades.

The aim for the preliminary control of the number of blades is to avoid too large difference in the relative velocity between the blades pressure sides and suction sides of the blades at the runner inlet after shaping pressure balanced blades based on a theory valid for an infinite number of blades. The number of blades may be controlled by the simplified equation, which yields:

$$\frac{\partial w}{\partial n} = -\frac{w}{R} - 2\omega \cos\delta$$

See also chapter 16.4 eq (23) to eq (28) in order to study the outlet flow and the influence from the number of blades and the blade geometry at the outlet.

17. RESONANT PRESSURE

17.1 Resonant pressure osillations in conduit systems.

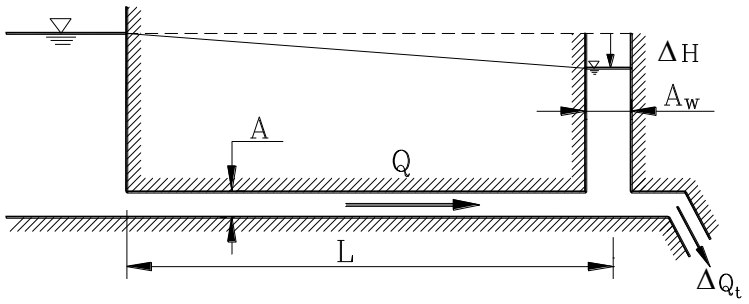

Figure 17.1 Conduit system for a high head hydropower plant.

In the following dimensionless Laplace transformed equations have been used to prove the criterion for resonant pressure oscillations in tunnels where compressibility is neglected and in elastic pipes with compressible water. The pressure response for a tunnel-surge shaft system can be developed by means of block diagrams as shown in the following Figure 17.2.

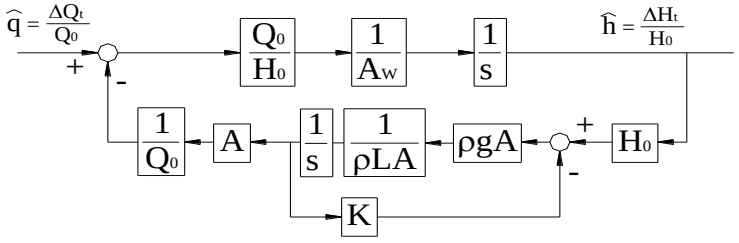

Figure 17.2 Detailed blockdiagram of the system.

Linearized friction

$$k = 22 \cdot \lambda \frac{L}{R_n} \cdot \frac{|c|}{2g}$$

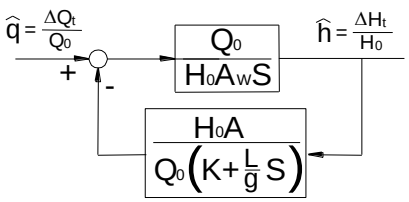

Figure 17.3 Redused blockdiagram.

Note: H_o = static pressure upstream of valve

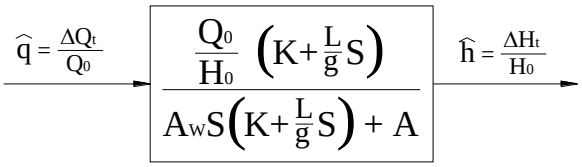

Figure 17.4 Final block diagram for analysis.

Rearranging and substituting for s = j ω

$$\frac{\hat{h}}{\hat{q}} = \frac{(Q_o / H_o)\left(K + \frac{L}{g}S\right)}{\frac{A_w L}{g}S^2 + A_w K S + A} = \frac{\frac{KQ_0}{AH_0}(1 + Tj\omega)}{-\left(\frac{\omega}{\omega_0}\right)^2 + 2\,\xi\; j\left(\frac{\omega}{\omega_0}\right) + 1} \qquad (17.1)$$

Here are

$$\omega_0 = \sqrt{\frac{Ag}{A_w L}} \; and \; \xi = \frac{A_w K}{ZA}\,\omega_0$$

and $$T = \frac{L}{gK}$$

DISCUSSION ON SELF EXITATED OSCILLATIONS

$\hat{q} = f(y)$ y = gate opening

Definition: Rising pressure positive flow out of the pipe is positive.

Rigid valve.

Feed back from pressure

$\hat{y} = \Delta y / y$

$$\hat{h} = \Delta H / H_o$$

$$\hat{q} = \Delta Q / Q_0$$

$$Q = \mu Y \sqrt{2gH}$$

$$dQ = \mu\sqrt{2g}\left(d\mathrm{Y}\sqrt{H} + \frac{\mathrm{Y}}{2\sqrt{H}}\, dH \right)$$

$$\frac{dQ}{Q_o} = \frac{\mu\sqrt{2g}}{\mu\sqrt{2g}}\left(\frac{d\mathrm{Y}\sqrt{H_o}}{\mathrm{Y}_o\ \sqrt{H_o}} + \frac{\mathrm{Y}_o\ \ dH}{2\sqrt{H_o}\,\mathrm{Y}_o\sqrt{H_o}} \right) \qquad (17.2)$$

$$\frac{dQ}{Q_o} = \frac{d\mathrm{Y}}{\mathrm{Y}_o} + \frac{1}{2}\ \frac{dH}{H_o}$$

$$\frac{\Delta Q}{Q_o} \approx \frac{\Delta \mathrm{Y}}{\mathrm{Y}_o} + \frac{1}{2}\,\frac{\Delta H}{H_o}$$

$$\underline{\underline{\Delta \hat{q}_h \approx \hat{y} + \frac{1}{2}\hat{h}}} \qquad (17.3)$$

Flexible valve or gate (see fig. 14.10 Chapter 14.5)

Substituting for the turbine flow in fig. 17.2 by a valve flow wich is reduced for increasing pressure by a by flexible movement of the valve creating a throttling proportional to the increasing pressure, creating a negative feed back system leading to increasing pressure oscillations. (See Fig. 14.10 in chapter 14.5)

$$\hat{q}_Y = \frac{\Delta q_Y}{Q_o} = \frac{\Delta A}{A_G} = \hat{A} = \hat{h}\left(\frac{\Delta A / A_o}{\Delta H / H_o} \right)$$

The total valve flow variation due to pressure variation and flexibility of the valve yields:

$$\hat{q} = \hat{q}_h + \hat{q}_\mathrm{Y} = -\hat{h}\left(\frac{1}{2} + \frac{\Delta A / A_o}{\Delta h / H_o} \right) + \hat{y} = -\hat{h}\left(\frac{1}{2} + \frac{\partial \hat{A}}{\partial \hat{h}} \right) \qquad (17.4)$$

The block diagram for the total system with a valve movement $\hat{y}$ can now be established. See also fig.**(**14.10), chapter 14.5.

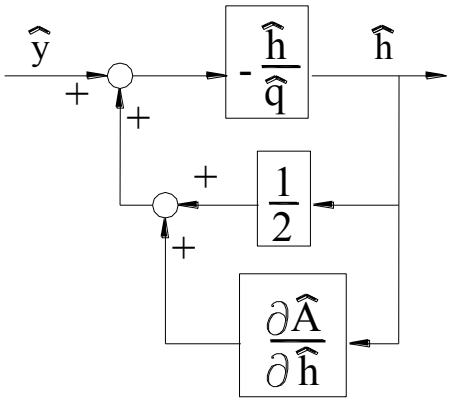

Figure 17.5 Block diagram with a flexible element δA/δh.

Rearranged:

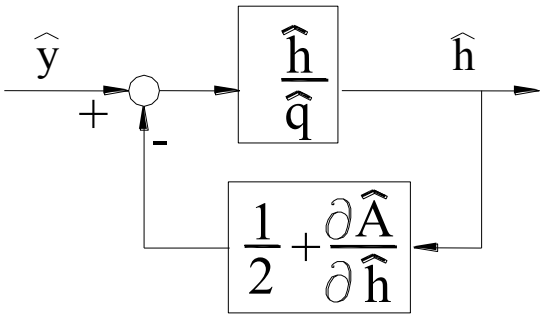

Figure 17.6 Reduced block diagram.

or
$$\frac{\hat{h}}{\hat{y}} = \frac{\frac{\hat{h}}{\hat{q}}}{1+\left(\frac{1}{2}+\frac{\partial \hat{A}}{\partial \hat{h}}\right)\frac{\hat{h}}{\hat{q}}} \qquad (17.5)$$

This equation is also shown in fig (14.10), chapter 14.5 proving the possibility for selfexitation from a positive feed back system of a valve where the opening is decreased with increasing pressure..

For $\frac{1}{2}+\frac{\partial \hat{A}}{\partial \hat{h}} \le 0$ *i.e.* $\frac{\partial \hat{A}}{\partial \hat{u}} \le -\frac{1}{2}$ unstable system i.e. self exitated oscillations will occur if the function $\left(\hat{h}/\hat{q}\right)(j\omega)$ has infinite value for a negative value of δA/δh <-0.5.
Substituting for $\left(\hat{h}/\hat{q}\right)$ by the transferfunction for a tunnel with surge shaft according to eq. (17.1).

When friction is ignored i.e. k = or $\xi = 0$ following equation yields:

$$\frac{\hat{h}}{\hat{q}} = \frac{\frac{Q_o}{H_o}\frac{L}{g}}{-\left(\frac{\omega}{\omega_o}\right)^2 + 1} \tag{17.6}$$

For $\frac{\partial \hat{A}}{\partial \hat{h}} \to -\frac{1}{2}$ in eq. (17.5) $\frac{\hat{h}}{\hat{y}} \to \frac{\hat{h}}{\hat{q}}$

ant then

$$\frac{\hat{h}}{\hat{y}} = \frac{\hat{h}}{\hat{q}} = \frac{\frac{Q_o L}{H_o g}}{-(\omega/\omega_o)^2 + 1} \to \infty \quad \text{for} \quad \omega \to \omega_o = \sqrt{\frac{Ag}{A_w L}}\,(rad/\sec) \; or \; f = \frac{1}{2\pi}\sqrt{\frac{Ag}{A_w L}}\,(Hz)$$

If friction is included in eq.(17.1) then $(\hat{h}/\hat{q}) \to \infty$ for $\left(\frac{1}{2} + \frac{\partial \hat{A}}{\partial \hat{h}}\right) < 0$. The negative value for self-oscillating condition is depending on the frictional damping. This problem may be studied in the time domain by converting eq.(17.1) to the time domain that can easily be done for a system with finite number of zeros and poles as shown in fig. (17.7) illustrating eq (17.6) valid for mass oscillations in a tunnel.

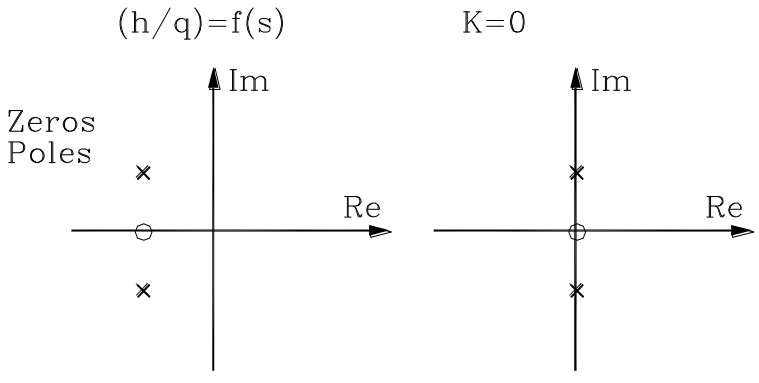

Fig. (17.7). Locations of zeros and poles for eq.(17.1) with friction left and without friction right.

However, it is more convenient to illustrate the problem in the frequency domain as shown in fig. (17.8).

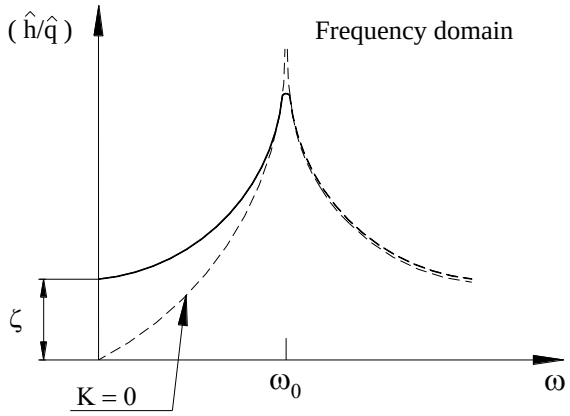

Fig. (17.8). Frequency response for $\hat{h}/\hat{y}$ for a tunnel with surge shaft with a flexible valve or a gate with leaking seal.

If substituting for $\left(\hat{h}/\hat{q}\right)$ in eq. (17.5) by the transfer function for a flexible penstock or a pipe with friction (see also chapter 12.3 and 14.5). Note that for the theory developed for pressure oscillations in a pipe $\left(\hat{h}/\hat{q}\right)$ is positive for increasing pressure instead of decreasing pressure as shown in fig. 1 valid for eq. (17.1).

Then:

$$\frac{\hat{h}}{\hat{q}} = +2h_w \frac{z}{s} \tanh\left(\frac{L}{a} z\right) \text{where:} \qquad z = \sqrt{s^2 + Ks}, \; s = j\omega \qquad (17.7)$$

$$K = f(\omega, q, \lambda)$$

If friction is ignored i.e. K= 0: Z = s

$$\underline{\frac{\hat{h}}{\hat{q}} = +2h_w \tanh\left(\frac{L}{a} s\right)} \qquad (17.8)$$

Then the equation for the system yields when substituting for s = j ω and

$$\tanh\left(j\frac{L}{a}\omega\right) = j\tan\left(\frac{L}{a}\omega\right) \qquad \text{(See also chapter 14.5.)}$$

Then following equation yields:

$$\frac{\hat{h}}{\hat{y}} = \frac{-j2h_w \tan\left(\frac{L}{a}\omega\right)}{1 + j\left(\frac{1}{2} + \partial\hat{A}/\partial\hat{h}\right)2h_w \tan\left(L\omega/a\right)} \qquad (17.9)$$

We now find that $\hat{h}/\hat{y} \Rightarrow -j2h_w \tan\left(\frac{L}{a}\omega\right)$ for $\partial\hat{y}/\partial\hat{h} \Rightarrow -\frac{1}{2}$

i.e. $\partial\hat{y}/\partial\hat{h} \to \infty$ *for* $\frac{L}{a}\omega = \frac{\pi}{2}(1+2n)$

or

$$\omega_c = \frac{a}{L}\frac{\pi}{2}, \quad \frac{a}{L}\frac{3}{2}\pi, \quad \frac{a}{L}\frac{5}{2}\pi, \ldots\ldots$$

The number of poles and zeros in the complex plane is infinite for

$$\left(\hat{h}/\hat{y}\right) \Rightarrow \left(\hat{h}/\hat{q}\right) = j2h_w \tan\left(\frac{L}{a}\omega\right)$$

In fig. (17.9) the locations of poles and zeros for eq.(17.9) with friction and without friction is illustrated in a complex plain plot for $\left(\hat{h}/\hat{y}\right) = \hat{h}/\hat{q}$.

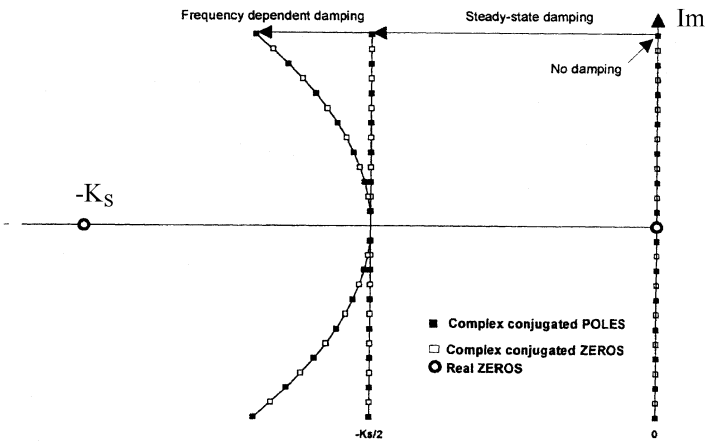

Fig. (17.9) Location of poles and zeros for eq. (17.9) right and for the same equation with friction according to eq. (17.7) left.

An approximation in the time domain can be found by using a finite number of zeros and poles. However, it is also in this case more convenient to study the problem in the frequency domain as shown in fig. (17.10) where $\left(\hat{h}/\hat{y}\right)(j\omega) \to \left(\hat{h}/\hat{q}\right)(j\omega)$.

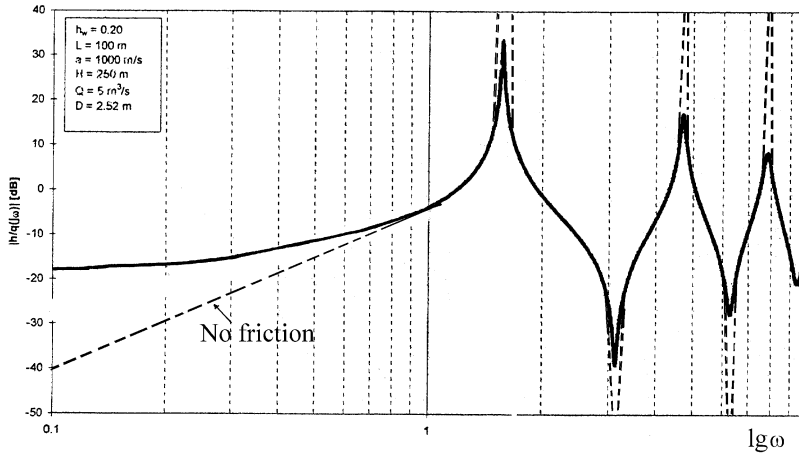

Fig. (17.10) Frequency response result for flexible pipe with a flexible valve

If the load is suddenly disconnected from the generator connected to a high head Francis turbine, the speed, will increase and the turbine governor will start the closing.
I this chapter we will study the changes during the first time intervals after a disconnection = Δt.
Because of the increase in speed, the flow in a high head Francis turbine will decrease and this phenomena can be explained by the efficiency diagram for the turbine by means of the lines for constant guide vane openings versus speed rise.
During the same time intervals the guide vanes are closing from the starting point to a smaller opening.
The total reduction in flow will on the other hand lead to a pressure rise which can be calculated by means of the method of characteristic – or by the analytical method by means of the equation $\Delta H=\alpha\Delta Q/(gA)$ during the first interval in time.

It should be noted that even if the guide vanes do not move a reduction of the flow will occur if the speed is increased for a high head turbine or a centrifugal pump in reversed speed operation. This may happen by disconnection from the grid.
It is of importance that the acceleration time is not too short so the speed rise is not too large for such machines because this may lead to very high pressure rises.
In order to avoid such problems for small units, fly wheels are often installed.
Pressure variations which can be computed based on the relative reduction in flow (Q/*Q) will lead to a correction of the value found in the diagram from point 2 to point 3 in the diagram shown in Fig. 17.11.
The corrected flow will reduce the pressure rise as finally shown in the characteristic diagram from point 3 to 4.
During this iteration process between the values in the characteristic diagram and the pressure rises found by the characteristic method, an increase in speed should be kept constant until an agreement occurs between Q and H for flow and pressure.
In the next time interval a consideration of the influence from speed correction should be made based on $((Q - \Delta Q) (H + \Delta H) \rho g \eta)$ during a time interval.
In the pages307 - 309 is shown a manual analysis of the pressure rise during runaway for a high head Francis turbine.
Analysis of this type is valid only if $h_w < (1 + \sqrt{z})/2$, i.e. for a high pressure plant.

17.2 The influence from the turbine characteristic on speed and pressure pulstions in the pipe line.

If the load is suddenly diaconnected from the generator connected to a high head Francis turbine, the speed will increase and the turbine governor will start closing.
In this chapter we will study the change ΔT during the first time intervals after a disconnection.
Because of the increase in speed the flow in a high head Francis turbine will decrease and this phenomena can be explained by the efficiency diagram for the turbine by means of the lines for constant guide vane openings versus speed rise.
During the same time intervals the guide vanes are closing from the starting point to a smaller opening.
The total reduction in flow will on the other hand lead to a pressure rise which can be calculated by means of the methode of characteristic – or by the analyttical methode by means of the equation $\Delta H=\alpha\Delta Q/(gA)$ during the first interval in time.
It should be noted that even if the guide vanes do not move, a reduction of the flow will occur if the speed is increased for a high head Francis turbine or a centrifugal pump in reversed operation. This may happen by disconnection from the grid.
It is of importance that the acceleration time must not be too short and the speed rise not too high for such machines because this may lead to a very high pressure rise.
In order to reduce such problems for small units, fly wheels are often onstalled.
Pressure variations can be calculated based on on the relative reduction in flow (Q/*Q) as shown in Fig 17.11 on next page by a correction of the value from point 2 to point 3 in the diagram.

During an iteration process between the values in the charcteristic diagram and the pressure rise found by the characteristic methode, an increase in speed should be be kept constant until an agreement occurs between Q and H for the flow and pressure.
In the next time interval consideration of the influence from speed correction is based on $((Q - \Delta Q)*(H+\Delta H)\rho g\eta)$ during a time interval.
In addition a manual analysis of the pressure rise during ruaway for a high head Francis turbine is shown in the following pages 307 – 309..
It should be noted that the highest value occures after a time interval $\Delta t=2L/a$ and in this time interval a calculation can be made in a simple way by a one time interval only when the highest increase on speed occures.
Analysis of this type is valid only if $h_w < (1+\sqrt{z})/2$, i.e. for a high head Francis turbine or a high head pump in reverse operation.

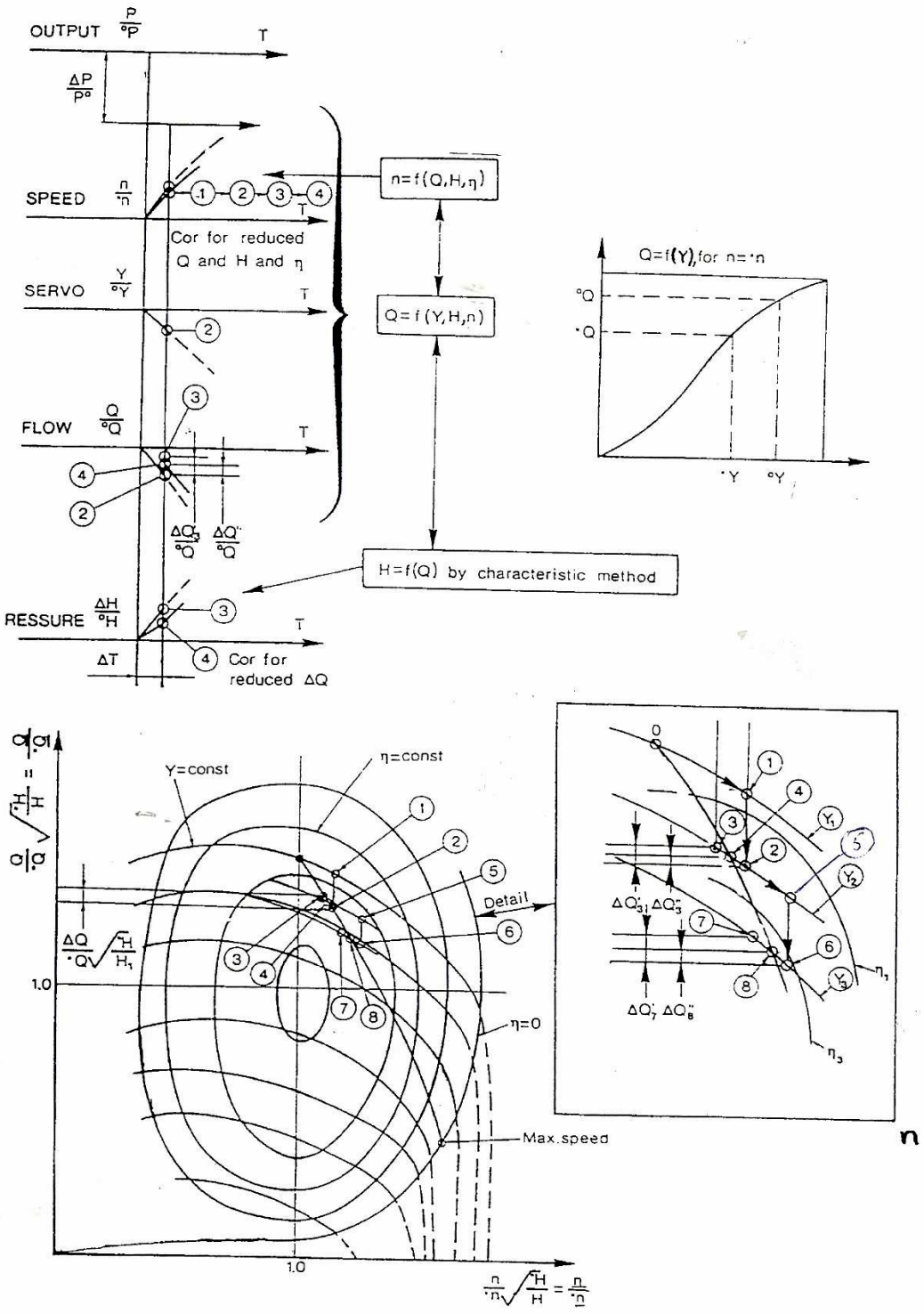

Fig. 17.11. The influence from the turbine characteristic expressed by the model test,

Illustration of the iteration steps in computation.

Study of speed rise and pressure rise caused by runaway of the turbine with guide vanes in fixed position can be made as illustrated below.
Iteration is made by simplifying the formula for pressure rise $\Delta H = a\Delta C/g$ in addition to the characteristic diagram shown at the end of this chapter. (See Fig. 2)

$$\Delta Q = \Delta n_{11} \delta Q/\delta n_{11} + \Delta y$$

$$\Delta H = a\Delta C/g = C_0 \Delta Q_{11} a/(Q_{11} g) \quad \text{for } 0 < t < 2L/a = T_w/h_w$$

For this case following values are chosen: $T_w = 3.06$ (sec), $h_w = 2.3$ (m), a=1300 (m/sec) (Normally a > 600 and a < 1300)
The procedure will be as follows for a runaway analysis.
If $T_a = 7$ sec, the maximum runaway speed will occur after 8 -10 sec and the speed rise will be approximately a linear function of time in the first 4 -5 sec with a speed rise of 100% during a time $t = T_a = 7$ sec, according to the definition of T_a.
Now the reflection time will be as follows when using a = 1300 m/s.

$$\Delta T = 2L/a = T_w/h_w = (LC/gH)/(aC/(2gH)) = 3.06/2.3 = 1.3 \text{ sec}$$

Then the following procedure can be followed.

Iteration step 1:

Time $\Delta T = 2L/a = 1.3$ sec, Ta = 7 sec and $C_0 = 7.42$ m/sec.

Step in speed:

$$\Delta n/n_0 = ((2L/a)/Ta)100 = (1.3/7)100 = 18.6\ \%$$

This value is constant, but n_{11} is not constant.

$$n_{110} = 55$$

and then

$$\Delta n_{11} = 55*0.186 = 10.21$$

I.e. $n_{11} = n_{110} + \Delta n_{11} = 55. + 10.21 = 65.21$

Further iteration can be made when ΔH and ΔQ are determined by correcting $\Delta n/n$ as a function of $Q + \Delta Q$ and $H + \Delta H$.

From the characteristic diagram we will find:

$$Q_{11} = 0.5 \quad \text{for} \quad \alpha_{max} = 15 \text{ deg.}$$

Further $Q_{11} = 0.533$. Then the pressure rise can be found as follows when a ≈ 1300 m/sec.

$$\mathbf{\Delta H_1 = 7.42*(0.533 - 0.5)\ 1300/(0.533*9.81) = 60.9\ m}$$

By regarding the characteristic diagram for the turbine, we find that the decrease in Q_{11} is not correct combined with the pressure rise.
(The corrected value will be $Q_{11} = 0.5((H_0 + \Delta H)/H_0)^{\wedge}0.5 = 0.562$)

To find the correct value an iteration procedure as shown in the following, must be used.

Iteration step 2.

$$n_{11*c1} = n_{110}\sqrt{(H_0/(H_0 + \Delta H_1)} = 65.21(230/(230 + 60.9)) = 58.0$$

$$\mathbf{Q_{11c1} = 0.522}$$

$$\mathbf{\Delta H_2 = C_0\ (C_{110} - C_{11c1})*a/Q_{110g} = 7.42*(0.533 - 0.522)*1300/(0.533*9.81) = 20.3\ m}$$

Corrected: $Q11c1 = 0.522\sqrt{(H_{otb}/H_o)} = 0.522*\sqrt{((230+20.3)/230)} = 0.54454$

Iteration step 3.

$$n_{11*c2} = n_{110}\ \sqrt{}\ (H_0/(H_0 + \Delta H_2)) = 65.21\sqrt{(230/(230 + 20.3))} = 62.5$$

$$\mathbf{Q_{11c2} = 0.509}$$

$$\mathbf{\Delta H_3 = C_0\ (C_{110} - C_{11c3})*a/Q_{110g} = 7.42*(0.533 - 0.509)*1300/(0.533*9.81) = 44.3\ m}$$

Iteration step 4.

$$n_{11*c3} = n_{110}\sqrt{}\ (H_0/(H_0 + \Delta H_3)) = 65.21\sqrt{(230/(230 + 44.3))} = 59.7$$

$$\mathbf{Q_{11c3} = 0.519}$$

$$\mathbf{\Delta H_4 = C_0\ (C_{110} - C_{11c3})*a/Q_{110g} = 7.42*(0.533 - 0.519)*1300/(0.533*9.81) = 25.8\ m}$$

Iteration step 5.

$$n_{11*c4} = n_{110}\sqrt{}\ (H_0/(H_0 + \Delta H_4)) = 65.21\sqrt{(230/(230 + 25.8))} = 61.8$$

$$\mathbf{Q_{11c4} = 0.511}$$

$$\mathbf{\Delta H_5 = C_0\ (C_{110} - C_{11c4})*a/Q_{110g} = 7.42*(0.533 - 0.511)*1300/(0.533*9.81) = 40.6\ m}$$

Iteration step 6.

$n_{11*}c_5 = n_{110}\sqrt{(H_0/(H_0 + \Delta H_5))} = 65.21\sqrt{(230/(230 + 40.6))} = 60.1$

$Q_{11c5} = 0.518$

$\Delta H_6 = C_0 (C_{110} - C_{11c5})*a/Q_{110g} = 7.42*(0.533 - 0.518)*1300/(0.533*9.81) = 27.7$ m

Iteration step 7.

$n_{11*}c_6 = n_{110}\sqrt{(H_0/(H_0 + \Delta H_5))} = 65.21\sqrt{(230/(230 + 27.7))} = 61.6$

$Q_{11c6} = 0.512$

$\Delta H_7 = C_0 (C_{110} - C_{11c6})*a/Q_{110g} = 7.42*(0.533 - 0.512)*1300/(0.533*9.81) = 38.7$ m

Iteration step 8.

$n_{11*}c_7 = n_{110}\sqrt{(H_0/(H_0 + \Delta H_6))} = 65.21\sqrt{(230/(230 + 38.7))} = 60.3$

$Q_{11c6} = 0.516$

$\Delta H_8 = C_0 (C_{110} - C_{11c7})*a/Q_{110g} = 7.42*(0.533 - 0.516)*1300/(0.533*9.81) = 31.4$ m

Final iteration on ΔH instead of n.

$\Delta H = (38.7 - 31.4)/2 = 35.$ (m)

$n_{11c8} = n_{110}\sqrt{(H_0/(H_0 + \Delta H))} = 65.21\sqrt{(230/(230 + 35))} = 60.75$ m
$Q_{11c8} = 0.514$

CONTROL: Q_{11} Corrected $= 0.514\sqrt{((230+35)/230)} = 0.53$

$\Delta H = C_0 ((C_{110} - C_{11c8})\, a)/Q_{110g} = 7.42(0.533 - 0.516)1300/(0.533*9.81) = 35.0$ m

In the diagram in last page the starting value of n_{11} can be found without correction for pressure rise and the final values of n_{11} and Q_{11} .
The final values of n_{11} and Q_{11} after T = (2L/a) are**:** $n_{11} = 60.75$, $Q_{11} = 0.514$ and the pressure rise $\Delta H = 35$ m.
Because $h_W > 1.$, the maximum pressure occurs for $t > 2L/a = 1.3$. Then the iteration requires that the pressure is calculated for steps in time for $t > 2L/a$ either by the characteristic method or a graphic method or by analytical way by the functions $F(t) - f(t-2L/a)$
This problem is normally solved by means of computers.
However, for $\Delta H > 35$ (m) it may be assumed to be $\Delta H \approx 50$ (m) without friction based on experience from plants like the diagram for Porce II.
Also the friction term my be included in the computer program.

The friction term is according to the term used by Streeter and Wylie for the time domain analyses, i.e. $\Delta H = DQ^2$. It should also be emphasized that the friction term in the stability analysis in the frequency domain is also containing an additional frictional term caused by the acceleration of the flow.

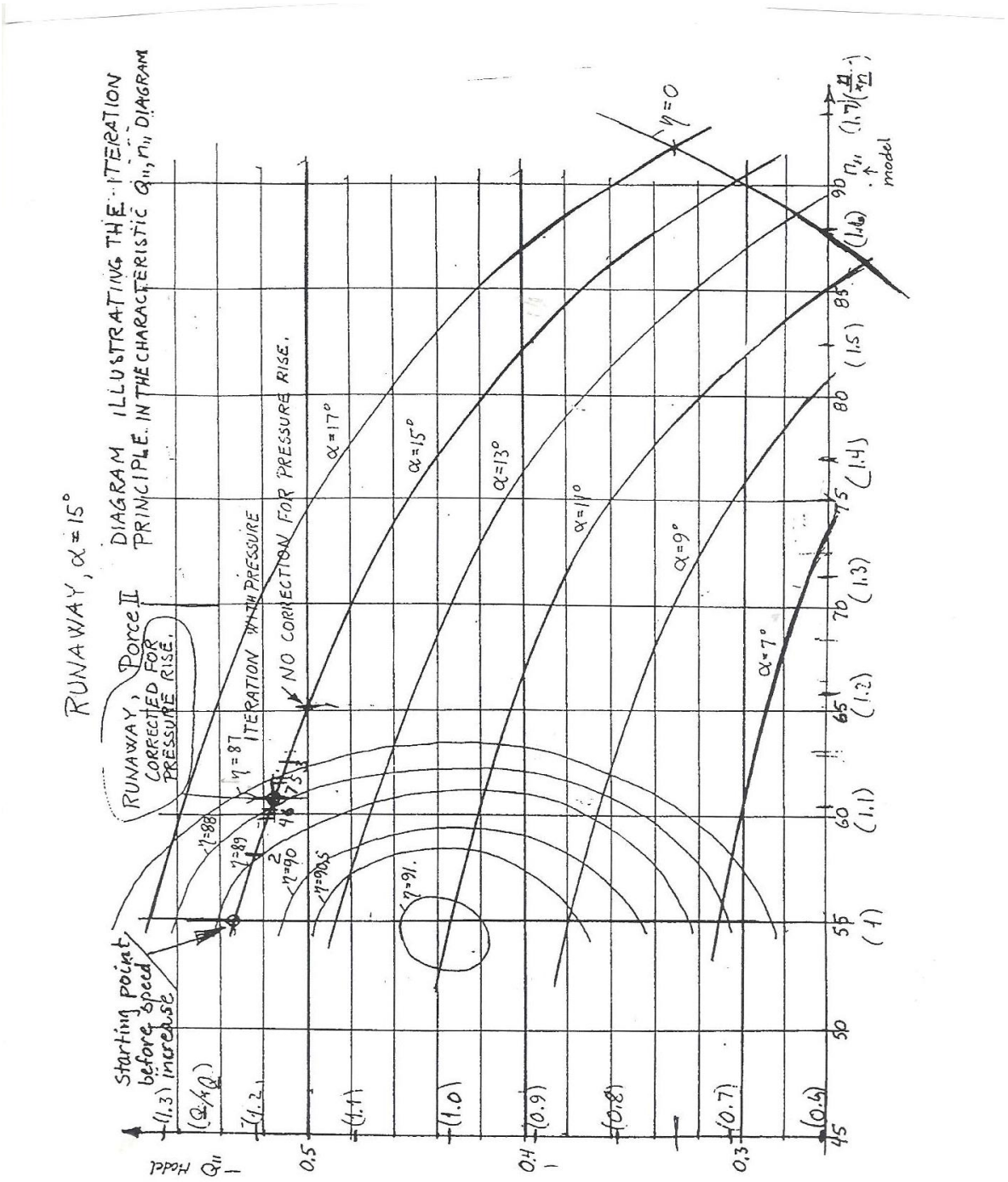

Fig. 2 Diagram for illustration of the iteration during runaway

18. MATERIALS AND FRACTURE MECHANICS.

18.1 Geometry, material quality and loading.

Pumps and turbines are of quite different design depending on pressure and flow.
For large values of flow and pressure and lower than 50 m head Kaplan turbines have been used.
For higher pressure up to around 500 m and middle and large flow values Francis turbines are used. For very high heads and relatively lower flow per unit, Pelton turbines are used.
The choice of turbines is in fact more complicated than given is this guide line, because the way of operation and the quality of the water will make an influence on the choice of turbine type.
For the choice of pumps the geometry will be towards Kaplan turbines for large flow compared to the operational head while a pump for high head will be designed in direction of a Francis turbine.
Because of this the different types of turbines will be described in different sections in this chapter.

18.2 Kaplan turbines and Bulb turbines.

In fig. 18.1 a cross section of a Kaplan Bulb turbine is shown. For this type of turbine the length of the conduite system is short. As usual we have a trash rack at the intake. The turbine is connected to the concrete structure through a hollow steel plate design. The conical guide vane system is located close to the runner. The runner consist of a certain low number of movable blades (normally 4.) which are connected to the hub.
From the runner the water flows through a horizontal draft tube which is equipt with a covered opening for inspection and gates for draining the turbine for inspection of the turbine during stand still.
Normally the runner will be made of stainless steel, while the other parts of the turbine will be made of painted plates of carbone steel.
The guide vanes for a Bulb turbine is normally arranged on a slightly conical surface. This design requires spherical joints in the connections between the guide vanes.
For large turbines separate servomotores are made for each guide vane because of the requirement in different planes for the different guide vanes. The movement of the servomotores is syncroniced by a control nsystem
Further the movement of the runner blades are controlled by one servomotor normally located on the hub of the turbine.
The linked guide vanes and the control of the runner blades require a strict requirement for turbines that are operating from 3 m to close to 15 m as a maximum. The same requirement is used for Kaplan turbines where the number of blades may be as high as 6.
.
The basic requirement is normally the allowable deformations because of large dimensions and a minimum of allowable clearances.
Also the requiremeny of allowable amplitudes of vibrations and stresses are very important. The main design for fulfilling the requirement is based on conical parts stiffened by necessary ribs.

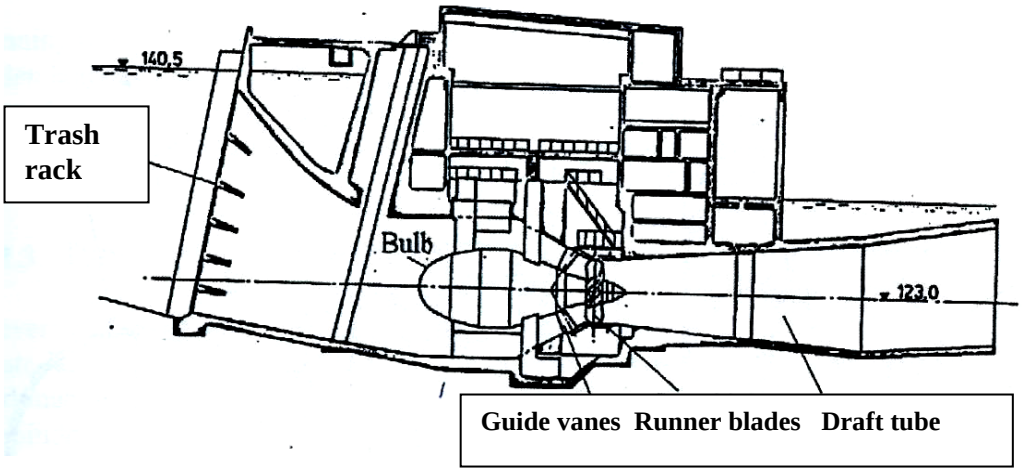

Figure 18.1 Cross section of a Kaplan Bulb Turbine

By analysing forces, dimensions and requirement of deformations a design base on requirements deasribes above is chosen.
The desing is also based on welding at site of low carbone, not stainless steel, for the main structure and it is important to chose weldable low carbone steel because any stressrelieving by heating is impossible at site and any hardness in the welds must be avoided to avoid fatigue problems.
The fine grain steel used should fulfil following requirement for this reason.'

C+ Mn/6 < 0.35 .

The runner blades are normally made by the quality 13Cr1Ni or 13Cr4Ni steel for a higher resistance against cavitation and corrosin.
The hub has parts inside in addition to control systems which is normally made by cast steel. However, in some turbines made from around 1990 and later the main parts have been made from thick plate.
It is important is that these parts in the hub are not exposed to water.

18.3 Francis Turbines

In fig 18.2 a cross sction of Francis turbine is shown.
The turbine is normally baed on pressure loaded parts which consists of spiral casing wiyh stay sing and head and bottom covers and draft tube and other parts not exposed to pressure.
We will find movable guide vanes and labyrinth seal rings against the rotating parts on head cover and lower cover and seal ring and shaft. Note that the regulating ring connecting equal movement for all guide vanes, are among the parts not in contact with water.

The head cover and bottom cover are dimensioned for a small deformation in order to reduce the clearance in the labyrinth seals as much as possible and the stresses are normally low.

The head cover and bottom cover are made by fine grain carbon steal with low content of carbon as well as the part of the draft tube towards the turbine. These parts are stress relieved by heating even if the stresses are low in order to avoid deformation on parts that shall be machined.
The outlet part of the draft tube and other parts that shall be welded at site are all made of low carbon steel to be welded without thermal stress relieving.
The tolerances are more strict than for Kaplan turbines and we will find maximum deviations of 0.1 mm even for large parts.

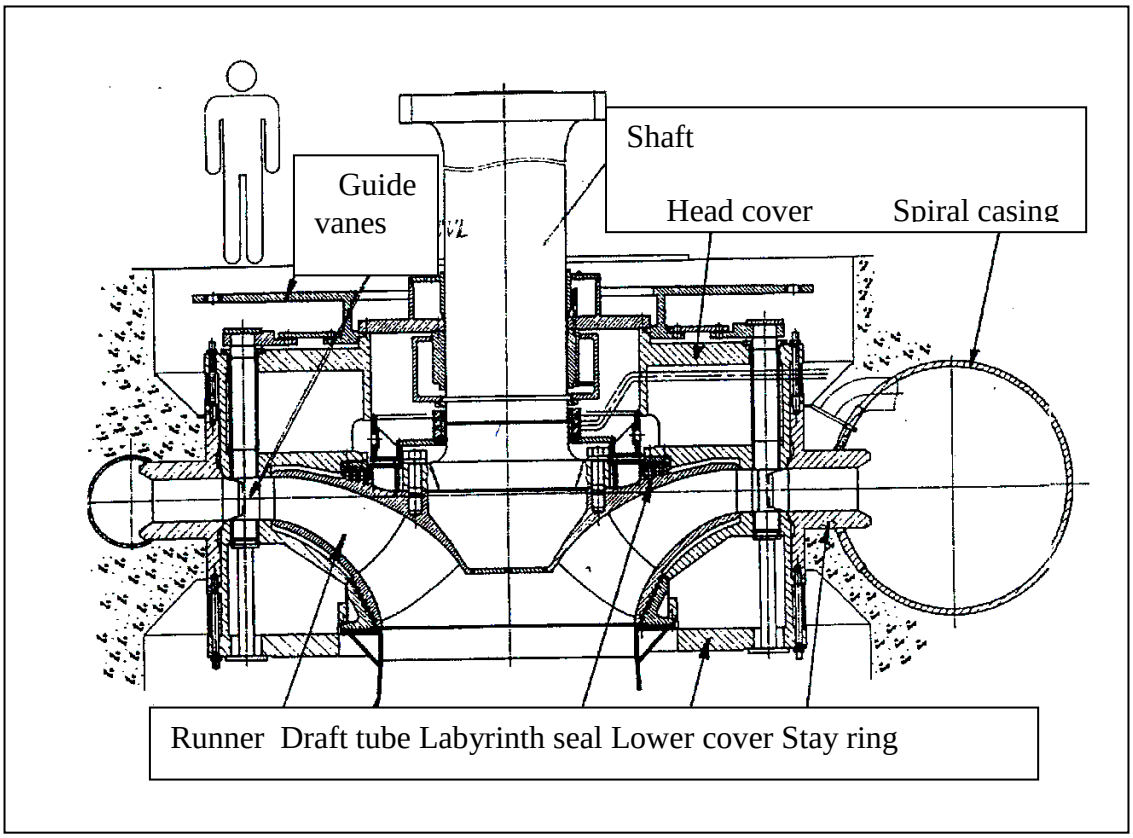

Fig. 18.2 Cross section of a Francis turbine

The shell in the spiral casing of a high head Francis turbine is normally as desribed, made by fine grain steel.
Then the maximum stresses and the axepted size of defects during welding must have a practical size so all critical sizes of defects can be detected and possibly repaired for an infinite life of the spiral casing and head and bottom covers. To obtain such criterion the stresses must be limited to be 200 MPa even if the yield point $\sigma_{0.2}$ for the material used is above 460 MPa.(See discussion later in this chapter.)

The guide vanes and the runner with the rotating labyrinth- seal ring are exposed to high flow velocities and possible cavitation and turbulence erosion damages. Because of this these parts are normally made by stainless steel qualities like 13Cr4Ni or 16Cr5Ni steel. 16Cr5Ni quality is used in runners due to a good weldability without pre heating.
The upper part of the draft tube closest to the runner outlet is also normally made by 16Cr5Ni steel in order to reduce cavitation damage where the velocity is so high that any painting will be damaged.

The surfaces on the head and bottom covers in contact with the guide vanes is covered by a welded layer of 16Cr5Ni or 17Cr1 Ni steel with hardness above 300-400 HB on the surface. This is done to obtain difference in hardness between guide vanes and head cover and bottom cover and thus avoid tearing during movement of the guide vanes especially when moving the guide vanes without water pressure on the turbine.
The difference in hardness should be higher than 70 HB.
The stationary part of labyrinth sealing against the runner should be made of NiAl bronce which is harder than the material in the rotating runner.
This bronce has also shown a good recistance against turbulence erosion, sand erosion and also corrosion. Also possibility of tearing by direct metallic contact is reduced.
The seal ring around the turbine shaft is normally made as a labyrinth ring in turbines made in Norway.
Thye stationary part is made by Babitt metal which is a soft material based on Tin with harder Antimony (Sb) crystals for wear protection. Because an efficient pumping system causes the shaft to run dry without water during operation. Then the seal ring will not be exposed to sand erosion if there is sand in the water.

Aksial forces and balancing axial hydraulic forces by upper and upper and lower axial seals yields as follows:

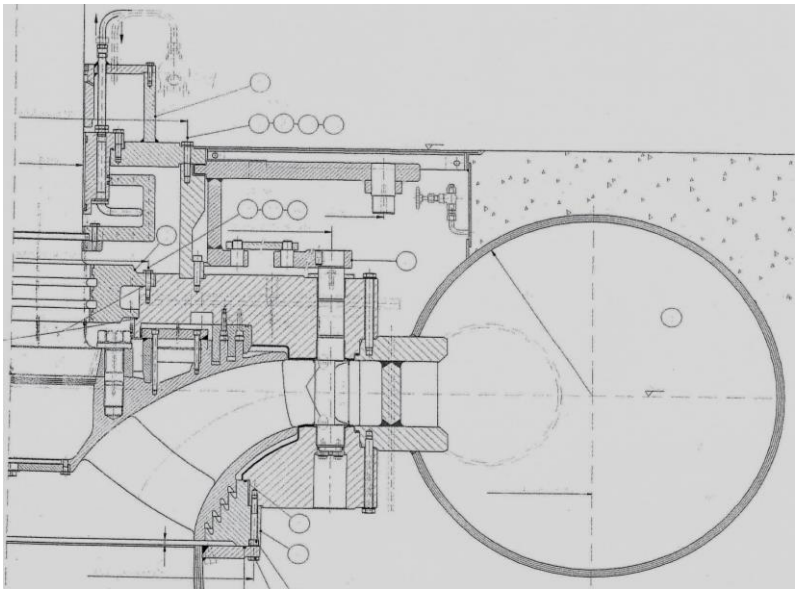

Fig 18.3 Cross section of runner with upper and lower labyrint seals.

For the labyrinth seals on Francis turbines and reversible pump turbines following dimensions could be followed;
The clearance gaps are in genearal for upper and lower seals except for the last outlet step on the lower seal towards the draft tube:
2S = 0.7D/1000 + 0.2 mm (**S** = radial gap) (Arne Bjørnsgaard multiplied by 0.7 which have been added because it was introduced for older turbines.)
For the last step at the outlet at the band you shall take away **0.2 mm** so the clearance shall be: **2S = 0.7D/1000.**

On the upper side i.e on the hub side all steps shall have the same clearance
i.e. **2S = 0.7D/10000 + 0.2 mm**.
NB! For smaller turbines the term **0.7** may be substituted by **1.0.**

18.4 Reversible Pump turbines.

The operation regime of reversible Pump turbines is similar to the regime of Francis turbines. The only difference is that the reversible Pump turbines is operation both as a pump in oposite rotational direction compared to the direction of the turbine.
Then the requirement of the bearing is however that the unit must be designed for operation in both directions.
I order to obtain an operational head in pump direction higher than for operation in turbine direction the runner must be built as a pump impeller which gives a larger diameter than the runner for an ordinary Francis runner.

18.5 Pelton Turbines.

In Fig.18.4 a cross sction of a vertical multijet Pelton turbine is shown.
A Pelton turbine can be devided in the pressure loaded part which is the distributor designedfor pressure up to about 2000 m WC. In addition we have nozzles, deføllectors, runner and turbine casing.
The distributor is normally made by welded fine grain steel plates in order to have a smallest possible thickness of the pressure loaded parts. The stresses are normally like or below 200 MPa in order which allows an unstable crack to penetrate the plate and cause leakage which will be detected before an unstable rupture. I.e. LEAKAGE BEFORE RUPTURE as a safety factor for the design.
A dilemma occurs if the turbine is very large and the plate thickness increases so the safety of leakage before rupture can not be used.
In order to solve such problem a manifold made by two parts in order to reduce the plate thickness can be designed as described in articles in WATERPOWER & DAM CONSTRUCTION November 1987 and Hydropower & Dams March 1994.
For information an unstable rupture will lead to an explosive crack propagation where the crack tip in the plate wall increase with speed of sound.
It should also be emphasized on the fact that if the safety margine of leakage before rupture so the crack can be detected and repaired is not fulfilled, an unstable rupture may occure without any varning for necessary repair.
The accept criteria for defects caused by production is normally smaller than the cracks that my lead to rupture as described abow. However, even minor material defects caused by production will grow during cyclic load during operation which may be as large as 10 000 time during a life time leading to the size which is giving unstable ruptures.
In the turbine casing low carbone steel is normally used for parts made for welding in the field without any heat stress relieve after welding. Such parts are the turbine casing which is welded before embedment in concrete.
The main purpose for the turbine casing is to guide the outlet flow from the runner and down to the outlet canal.

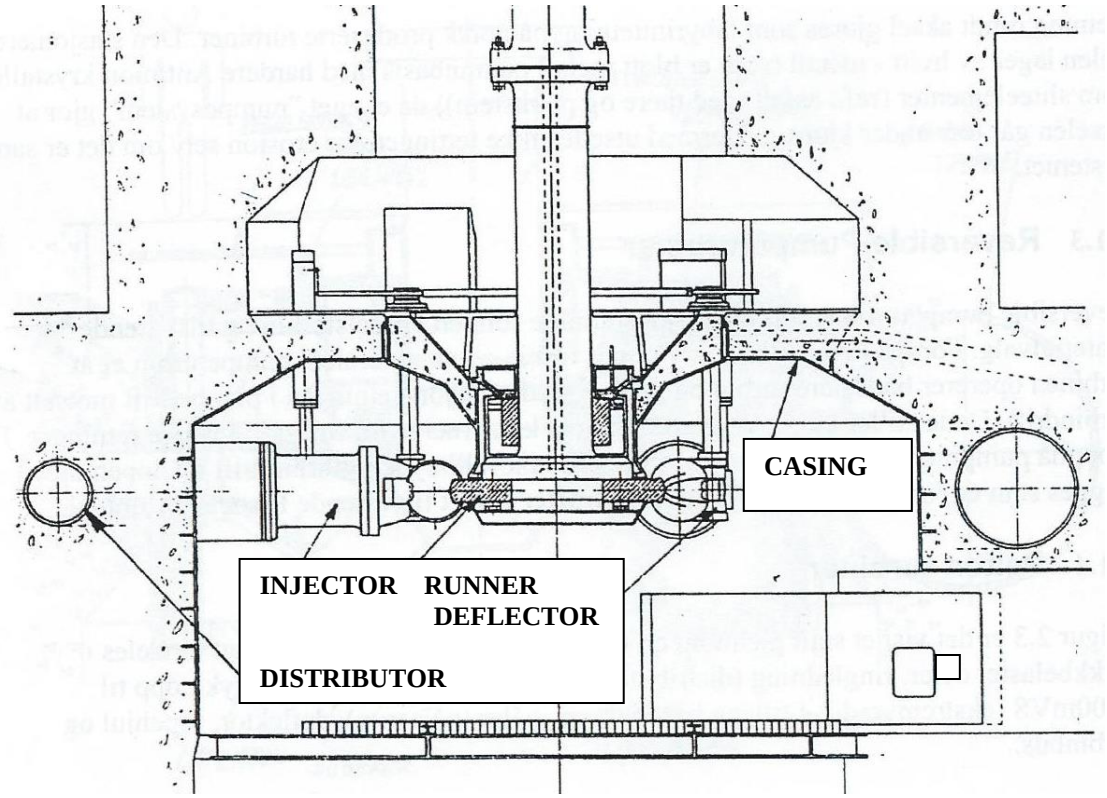

Fig 18.4 Cross section of a vertcal Pelton turbine.

Accept criteria for production defects are normally much smaller than the defects which leads to unstable ruptures. The danger vis that vthe bsmall defects crated during production as described previously will grow a little bit each btime the distributor is pressurized and after a certain start stops as for example 10 000 times during the blife span even small cracks may breach the sice of unstable rupture where the stresses are highest. Then the last safety margine mey be useful i.e." LEAKAGR BEFORE RUPTURE".
In the turbine casing low carbone steel have been used for production ans later weld repair if necessary. This bis because the rigidity snd not the stresses is the design criteria for bthese parts.
The main purpose for bthe turbine casing is conduction of the outlet flow from the runner and being the support for the turbine bearing.
The stationary parts exposed to the highest speed of flow are the needle tips and the nizzles normally made of hardened 12Cr4Ni or 16Cr5Ni steel.
If wear from sand inbthec water is expected the vsurfaces may bbe coated by STELLITE (or ceramical coating). Sych hard surface coating requires spacvial competence of the company.
For the needle stem made of stainless steel the surface should normally be coated by hard cromium on the surface because the support is bronce bearing and especially the stem is carrying plate springs for balancing the hydraulic forces.
(Note that the base material for the needle stem should be stainless steel to avoid corrosion in possible crack on the coating.)
The Pelton runner is normally made of 13Cr4Ni steel quality.
Due to danger of fatigue from the pulsating load, a heat treatment should be made after all milling and grinding of the buckets and due to the danger of fatigue a moderate value of $\sigma_{0.2}$ should be shosen. It is important that the content of Sulphur and Nitrogen are kept to a lowest possible value. (S<0.008% and N<0.0002%).

It should be noted that MnS creates the most dangerous defects because the defects are formed as flakes i.e. two dimensional defects. Because of the danger from high frequency stress loading the calculated stress level should have a maximum level of 45 MPa.

10.12.2014

REFERENCES

1. Brekke, H. "THE INFLUENCE FROM THE GUIDE VANE CLEARANCE GAP ON EFFICIENCY AND SCALE EFFECT FOR FRANCIS TURBINES". IAHR Symposium on Hydraulic Machinery and Cavitation, June 1998. Proceeding.

2. Chen Xin, Brekke H: "FLOW VISUALIZATION AND LDV MEASUREMENT IN THE DOUBLE CASCADE OF A FRANCIS TURBINE. IAHR Symposium on Hydraulic Machinery and Cavitation, Sept 1992, Sao Paulo. Proceedings.

3. Gindroz, B., Avellan, F., Henry, P. "GUIDELINES FOR PERFORMING CAVITATION TESTS". IAHR Symposium on Hydraulic Machinery and Cavitation, Sept 1990. Proceedings.

4. Brekke, H. "A DISCUSSION ON PELTON TURBINES VERSUS FRANCIS TURBINES FOR HIGH HEAD PLANTS". Proceedings. Symp. ASCE-IAHR/ASME Colorado State Univ. USA 1978

5. INTERNATIONAL STANDARD, IEC 41. "FIELD ACCEPTANCE TEST TO DETERMINE THE HYDRAULIC PERFORMANCE IF HYDRAULIC TURBINES, STORAGE PUMPS AND PUMP TURBINES". Third edition 1991-11.

6. Brekke, H. "A GENERAL STUDY OF THE DESIGN OF VERTICAL PELTON TURBINES" Proceedings 25 Anniversary Symposium Turbo Institute Ljublana 1984.

7. Brekke, H. "EXPERIENCES FROM LARGE PELTON TURBINES IN OPERATION" Proceedings IAHR Symposium on Hydraulic Machinery, Amsterdam 1982.

8. Brekke, H. "SURGE TANK STABILITY AND TURBINE GOVERNING STABILITY ANALYSED WITH AN IMPROVED APPROACH TO THE FRICTIONAL DAMPING OF OSCILLATORY FLOW IN ROUGH TUNNELS AND PENSTOCKS" Paper IAHR Work Group on Behaviour of Hydraulic Machinery under steady oscillatory conditions, Mexico City, 1985

9. Brekke, H. "A STABILITY STUDY ON HYDRO POWER PLANT GOVERNING INCLUDING THE INFLUENCE FROM A QUASI NONLINE DAMPING OF OSCILLATORY FLOW AND FROM THE TURBINE CHARACTERISTICS" Dr.techn dissertation, The Norwegian Institute of Technology, May 22, 1984.

10. Brekke, H. "REGULERING AV HYDRAULISKE STRØMNINGSMASKINER" Compendium for students in Norwegian language.

11. Lein, G and Maurer, W. "ADVANCE IN CONTROL OF HYDRO POWER PLANTS" Will be published in book series for Hydraulic Machinery. Vol 9, Gover.

12. Brekke, H. and X.X.Li. "A REVIEW OF MODERN TURBINE CONTROL SYSTEM FOR HYDROPOWER PLANTS WITH HIGH PRESSURE TUNNELS". Proceedings Hydropower 92, Balkema, Edited by Broch & Lysne.

13. Xin Xin Li, "STABILITY ANALYSIS AND MATHEMATICAL MODELLING OF HYDROPOWER SYSTEMS" Dr.ing. Dissertation 1989. The Norwegian Institute of Technology

14. Andersen, T.L. “ELASTIC PLASTIC FRACTURE ASSESSMENTS BASED ON CTOD” Welding Institute G.B. WI report 276/1985.

15. Dawes, M.G. “THE CTOD DESIGN CURVE APPROACH LIMITATION, FINITE SIZE AND APPLICATION. WI report 278/1985.

16. Hirsch, C. “NUMERICAL COMPUTATION OF INTERNAL AND EXTERNAL FLOW” vol 2, J.Wiley & Sons 1990.

17. Wylie, B.E. Streeter, L.V. “FLUID TRANSIENTS” Mc Graw-Hill, New York

18. Pejovic, S, Boldy, A.P. and Obradovic D. “GUIDELINES TO HYDRAULIC TRANSIENT ANALYSIS”

19. Allievi, L. “THEORY OF WATER HAMMER” Translated from Italian by E.E. Halmos Ricardo Garoni, Rome 1925.

20. Suzuki, M. “CARBON EQUAIVALENT AND MAXIMUM HARDNESS” IIW Dec IX-1279-83.

21. Brekke, H. “STATE OF THE ART IN PELTON TURBINE DESIGN” Journal of Hydropower & Dams, 1994

22. Brekke, H..”RECENT TRENDS IN THE DESIGN AND LAYOUT OF PELTON TURBINES”, 1987

23. Brekke, H. “HYDRAULIC DESIGN STRATEGU FOR FRANCIS TURBINES” Journal of Hydropower and Dams, 3 Issue 1996.

24. Yuan, S.W. “FOUNDATIONS OF FLUID MECHANICS” Prentice-Hall International Inc London 1970.

25 Marchal M., Flech G. and Suter P. “THE CALCULATION OF WATERHAMMER PROBLEMS BY MEANS OF DIGITAL COMPUTER” Proceedings, International Symposium on Waterhammer in Pumed Storage Projects, ASME Chicago 1965.

26 Martin. C, S..”TRANSFORMATIONS OF PUMP TURBINE CHARACTERISTICE FOR HYDRAULIC TRANSIENT ANALYSIS.” IAHR Symposium, Pumps and Power Plants, AMSTERDAM , 1982

27 .
Brekke H.. “PERFORMANCE AND SAFETY OF HYDRAULIC TURBINES.” 25th IAHR Symposium on Hydraulic Machinery and Cavitation. Sept 20-24 Timasuara, Romania

28 H. Grain, R. Anghern, M. Lorenz.l. “INSPECTION PERIODS OF PELTON RUNNERS.” IAHR Symposium Stirling August 27-30. 1984.

29 Joachim Raabe “ HYDRAULISCHE MASCHINEN UND ANLAGEN” VDI-Verlag GmbH1989. German language)

30 Yuanfan Huan, Hermod Brekke ”X-SHAPE BLADE APPLICATION FOR THE THREE GORGES PROJECT.” Article: Water Power & Dam Construction. Jan. 2012